

Electrochemical Benzylic C–H Fluorination and 4d-Metallaelectro-Catalyzed C–H and C–C Functionalizations

Dissertation for the award of the degree
“Doctor rerum naturalium” (Dr. rer. nat.)
of the Georg-August-Universität Göttingen



within the doctoral program of chemistry
of the Georg-August-University School of Science (GAUSS)

Submitted by
Alexej Scheremetjew
from Bernau b. Berlin

Göttingen, 2023

Thesis Advisory Committee

Prof. Dr. Lutz Ackermann

Institut für Organische und Biomolekulare Chemie (IOBC),
Georg-August-Universität Göttingen

Prof. Dr. Shoubhik Das

Organic Synthesis (ORSY) research division, Department of Chemistry, University of
Antwerp, Belgium

Members of the Examination Board

1st Reviewer: *Prof. Dr. Lutz Ackermann*

IOBC, Georg-August-Universität Göttingen

2nd Reviewer: *Prof. Dr. Shoubhik Das*

ORSY research division, Department of Chemistry, University of Antwerp, Belgium

Further Members of the Examination Board:

Prof. Dr. Dietmar Stalke

IAC, Georg-August-Universität Göttingen

Jun.-Prof. Dr. Nadja A. Simeth

IOBC, Georg-August-Universität Göttingen

Jun.-Prof. Dr. Johannes Walker

IOBC, Georg-August-Universität Göttingen

Dr. Daniel Janßen-Müller

IOBC, Georg-August-Universität Göttingen

Date of the Oral Examination: March 02, 2023

In loving memory of my grandmother *Zilja Leschinskaja* ז"ל, who cultivated my strive for critical thinking, morality, commitment and curiosity.

TABLE OF CONTENTS

1	Introduction.....	1
1.1	Transition Metal-Catalyzed Coupling Reactions.....	1
1.1.1	Classical Cross-Coupling.....	1
1.1.2	C–H Activation.....	3
1.1.3	C–C Activation and Functionalization	8
1.2	Carboxylate-Assisted Ruthenium-Catalyzed C–H Activation	11
1.3	Decarboxylative Coupling Reactions	14
1.4	Rhodium-Catalyzed C–C Activation.....	19
1.5	Undirected C–H Functionalization.....	24
1.5.1	General Aspects	24
1.5.2	Benzylic C–H Fluorination.....	25
1.6	Electrochemistry in Organic Synthesis.....	29
1.6.1	Brief History & General Aspects.....	29
1.6.2	Electrochemical Benzylic C–H Fluorination and other Benzylic C–H Functionalizations	33
1.6.3	Electrochemical C–H Activation.....	40
2	Objectives	55
3	Results & Discussion	58
3.1	Electrochemical Fluorination of Benzylic C(sp ³)–H Bonds.....	58
3.1.1	Optimization	59
3.1.2	Scope.....	62
3.1.3	Mechanistic Insights	68
3.1.4	Mechanistic Proposal.....	69
3.2	Ruthena-Electro-Catalyzed Decarboxylative Alkenylation of Anisic Acids.....	70
3.2.1	Rationale	71
3.2.2	Optimization	72

TABLE OF CONTENTS

3.2.3	Scope.....	88
3.3	Rhoda-Electro-Catalyzed C–C Activation	93
3.3.1	Optimization	93
3.3.2	Scope.....	97
3.3.3	Mechanistic Studies	102
3.3.4	Mechanistic Proposal	109
4	Summary and Outlook	111
5	Experimental Part.....	114
5.1	General Remarks.....	114
5.1.1	Materials	114
5.1.2	Analytical and Experimental Methods.....	115
5.2	General Procedures	119
5.2.1	General Procedure A for the Electrochemical Fluorination of Benzylic C(sp ³)–H Bonds	119
5.2.2	General Procedure B for the Ruthena-Electro-Catalyzed Decarboxylative Alkenylation of Anisic Acids.....	119
5.2.3	General Procedure C for the Rhoda-Electro-Catalyzed C–C Activation.....	120
5.3	Electrochemical Fluorination of Benzylic C(sp ³)–H Bonds.....	120
5.3.1	Characterization Data.....	120
5.3.2	Gram-Scale Reaction	145
5.3.3	H/D Exchange Experiment	148
5.3.4	Kinetic Isotope Effect Studies	150
5.4	Ruthena-Electro-Catalyzed Decarboxylative Alkenylation.....	154
5.4.1	Characterization Data.....	154
5.4.2	Electrolyte Activation Study.....	174
5.5	Rhoda-Electro-Catalyzed C–C Activation	177
5.5.1	Characterization Data.....	177
5.5.2	Gram-Scale Reaction	192

TABLE OF CONTENTS

5.5.3	C–C Alkenylation by Aerobic Oxidation	193
5.5.4	Competition Experiment.....	193
5.5.5	H/D Exchange Experiment	194
5.5.6	Rhodium Complex 190b-Catalyzed C–C Alkenylation and Product Release 196	
6	References.....	197
	Acknowledgements.....	211
	Curriculum Vitae	213
	Personal Information.....	213
	Education	213
	Fellowships	214
	Publications.....	214
	Zusammenfassung.....	215
	NMR Spectra	217

ABBREVIATIONS, SYMBOLS AND UNITS

In this thesis, the mentioned physicochemical properties/quantities and natural constants are reported with symbols, units and conversion factors, that are recommended by internationally accepted standard references.^[1]

List of abbreviations, descriptors and coefficients

Ac	acetyl	C _q	quaternary carbon
acac	acetylacetonate/acetylacetonato	CV	cyclic voltammetry
ACE	alternating current electrolysis	Cy	cyclohexyl
Ad	1-adamantyl	δ	chemical shift
add.	addition	d	doublet (spectral)
ADME	absorption–distribution–metabolism–excretion	DAST	(diethylamino)sulfur trifluoride
AG	activating group	DCB	dichlorobenzene
Alk	alkyl	DCE	1,2-dichloroethane
Am	amyl	DCM	dichloromethane
AMLA	ambiphilic metal ligand activation	DDQ	2,3-dichloro-5,6-dicyano-1,4-benzoquinone
aq.	aqueous	DG	directing group
Ar	aryl	dmaan	2,6-dimethylacetanilide
ATR	attenuated total reflection	DME	1,2-dimethoxyethane
BDE	bond dissociation energy	DMF	<i>N,N</i> -dimethylformamide
BIES	base-assisted internal electrophilic-type substitution	DMPU	<i>N,N'</i> -dimethylpropyleneurea
Bn	benzyl	DMSO	dimethylsulfoxide
BQ	1,4-benzoquinone	dppe	1,2-bis(diphenylphosphino)ethane
br	broad signal/singlet (spectral)	dtbbpy	4,4'-di- <i>tert</i> -butyl 2,2'-dipyridine
BPE	bipolar electrolysis	<i>e</i>	fundamental charge
Bu	butyl	<i>e</i> ⁻	electron
calc.	calculated	ECF	electrochemical fluorination
cat.	catalytic	EDG	electron-donating group
CCE	constant current electrolysis	EI	electron ionization
CDC	cross-dehydrogenative coupling	elim.	elimination
chd	cyclohexadiene	equiv.	equivalent(s)
CMD	concerted metalation-deprotonation	ESI	electrospray ionization
cod	1,5-cyclooctadiene	Et	ethyl
Cp*	1,2,3,4,5-pentamethylcyclopentadienyl	ET	electron transfer
CPE	constant potential electrolysis	EWG	electron-withdrawing group
CPET	concerted proton-coupled electron transfer	F	Faraday constant
		Fc	ferrocene
		FCC	flash column chromatography

ABBREVIATIONS, SYMBOLS AND UNITS

FG	functional group	NFSI	N-fluorobenzenesulfonimide
GC	gas chromatography, glassy carbon	NHPI	N-hydroxyphthalimide
GF	graphite felt	NMP	<i>N</i> -methylpyrrolidone
GPC	gel permeation chromatography (also SEC)	NMR	nuclear magnetic resonance
GVL	γ -valerolactone	<i>o</i> -	<i>ortho</i> -
Hal	halogen	Oct	octyl
HAT	hydrogen atom transfer	OVAT	one variable at a time
HSP	<i>Hansen</i> solubility parameters	Ox.	oxidation/oxidized
BPIn	pinacolboronyl	<i>p</i> -	<i>para</i>
Het	heteroatom	PCET	proton-coupled electron transfer
Hex	hexyl	pcp	[2.2]paracyclophane
HFIP	1,1,1,3,3,3-hexafluor-2-propanol	pdipb	1,4-diisopropylbenzene
HOMO	highest occupied molecular orbital	PEG	polyethylene glycol
HPLC	high performance liquid chromatography	Pent	pentyl
HR-MS	high-resolution mass spectrometry	PG	protecting group
<i>i</i> -	<i>iso</i> -	PGCC	propylene (glycol cyclic) carbonate
IES	internal electrophilic substitution	PINO	phthalimide <i>N</i> -oxyl
IMEs	1,3-bis(2,4,6-trimethylphenyl)- imidazol-2-ylidene	Ph	phenyl
IR	infrared	Phth	phthaloyl
<i>J</i>	coupling constant	Piv	pivaloyl
KIE	kinetic isotope effect	PP	polypropylene
L	ligand	ppm	parts per million
LED	light-emitting diode	Pr	propyl
LUMO	lowest unoccupied molecular orbital	PEG	polyethylene glycol
LG	leaving group	PTFE	polytetrafluoroethylene
<i>m</i> -	<i>meta</i> -	Py	2-pyridyl
M	molar	q	quartet (spectral)
m	multiplet (spectral)	quint	quintet (spectral)
M ⁺	parent molecular ion	R	organic rest/substituent
mdipb	1,4-diisopropylbenzene	red.	reduction/reduced
Me	methyl	ref.	reference
Mes	mesityl (2,4,6-trimethylphenyl)	RRDE	rotating ring disc electrode
Med.	mediator	r.t.	room temperature
MO	molecular orbital	RVC	reticulated vitreous carbon
M.p.	melting point	s	singlet (spectral)
MS	mass spectrometry, molecular sieves, multi-site	SAR	structure-activity relationship
nbd	norbornadiene	sat.	saturated
<i>n</i> -	linear	SCE	standard calomel electrode
$\tilde{\nu}$	wavenumber	SDS	sodium dodecyl sulfate
		SEC	size exclusion chromatography (also GPC)
		SET	single electron transfer
		SOMO	singly occupied molecular orbital

ABBREVIATIONS, SYMBOLS AND UNITS

SPO	secondary phosphine oxide	tipb	1,3,5-triisopropylbenzene
SPS	solvent purification system	TLC	thin layer chromatography
<i>t</i> -	<i>tert</i> -	TM	transition metal
TBA	tetra- <i>n</i> -butylammonium	<i>TON</i>	turnover number
TEMPO	(2,2,6,6-tetramethylpiperidin-1-yl)oxyl	TosMIC	<i>p</i> -toluenesulfonylmethyl isocyanate
Tf	trifluoromethanesulfonyl	Ts	<i>p</i> -toluenesulfonyl
TFA	trifluoroacetic acid	TS	transition state
TFE	2,2,2-trifluoroethanol	UV	ultraviolet
THTD	tetrahydrothiophene dioxide (sulfolane)	X	(pseudo)halide
THF	tetrahydrofuran	<i>y_F</i>	Faradaic yield/efficiency

Table I Physical quantities and their commonly used units.

quantity	unit	quantity	unit
<i>l</i> (length)	m (meter), Å (Ångström)	<i>V</i> (volume)	L (liter)
<i>m</i> (mass)	g (gram), Da (dalton)	<i>Q</i> (charge)	C (coulomb), e (fundamental charge)
<i>t</i> (time)	s (second), h (hour)	<i>W</i> (Energy/work)	J (joule), cal (calory)
<i>n</i> (amount of substance)	mol	<i>E</i> (Electrostatic potential)	V (volt)
<i>I</i> (electric current)	A (ampere)	<i>ν</i> (frequency)	Hz (hertz), rpm (rounds per minute)
<i>T</i> ([reaction] temperature)	K (kelvin), °C (degree Celsius)	<i>p</i> (pressure)	bar, atm (atmospheric pressure)

Table II Unit prefixes for conversion factors.

prefix	name	conversion factor
G	giga	$\times 10^9$
M	mega	$\times 10^6$
k	kilo	$\times 10^3$
c	centi	$\times 10^{-2}$
m	milli	$\times 10^{-3}$
μ	micro	$\times 10^{-6}$
n	nano	$\times 10^{-9}$
p	pico	$\times 10^{-12}$

1 INTRODUCTION

During the past decades, the awareness about the finiteness of crucial raw materials, such as crude oil, gas, and precious metals raised significantly due to multiple economic and environmental crises, many of which were caused by limitedly predictable political tensions in the first place. Hence, the necessity of sustainability in all areas of trade and industry became evident and a shift towards renewable energies and raw materials, as well as general hazard minimization has been globally encouraged by scientists and politicians.^[2] A generally accepted sustainability guideline for chemical production was summarized by *Anastas*,^[3] with the key tasks being:

- waste prevention by implementing atom- and step economical syntheses,^[4] thereby minimizing the amount of by-products.
- hazard prevention by substitution of dangerous and pollutive components with less harmful alternatives and working at ambient conditions.
- avoidance of processes requiring large amounts of auxiliary chemicals, especially if they are not renewable or recyclable.

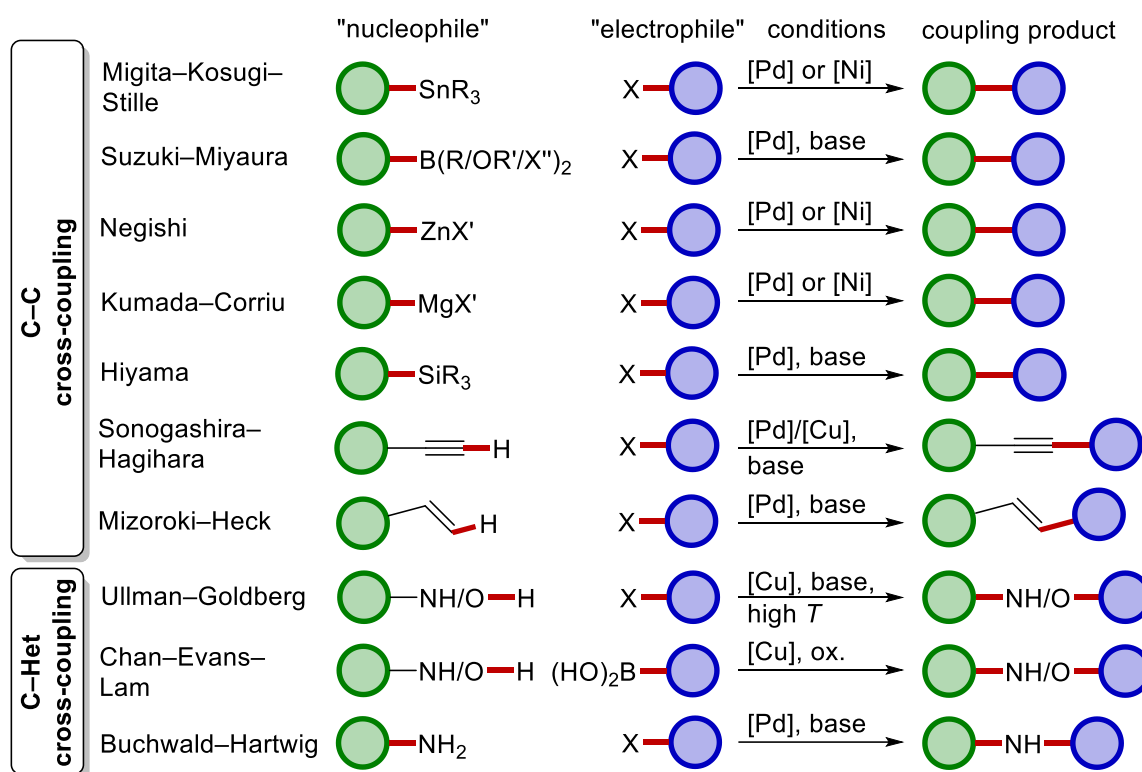
Naturally, catalytic processes play a key role in achieving these goals, since the concept of catalysis is the facilitation and thereby acceleration of a reaction by mechanistic alteration. While some catalysts, such as simple *Brønsted* or *Lewis* acids and bases, can catalyze myriads of reactions, other catalysts can be highly chemo-, regio-, site- and even enantio-selective. With their help, syntheses of complex structures^[5] can be streamlined by the selective targeting of desired positions, avoiding the use of protecting groups and other economy-diminishing detours.^[6]

1.1 Transition Metal-Catalyzed Coupling Reactions

1.1.1 Classical Cross-Coupling

The construction of previously hardly accessible arene motifs, as ubiquitously encountered among natural products, biologically active compounds and pharmaceuticals,^[7] was significantly facilitated with the implementation of transition metal catalysis into organic synthesis. Arguably the most significant breakthrough was the discovery of the concept of palladium-, nickel- and copper-catalyzed C–C and C–Het coupling reactions (**Scheme**

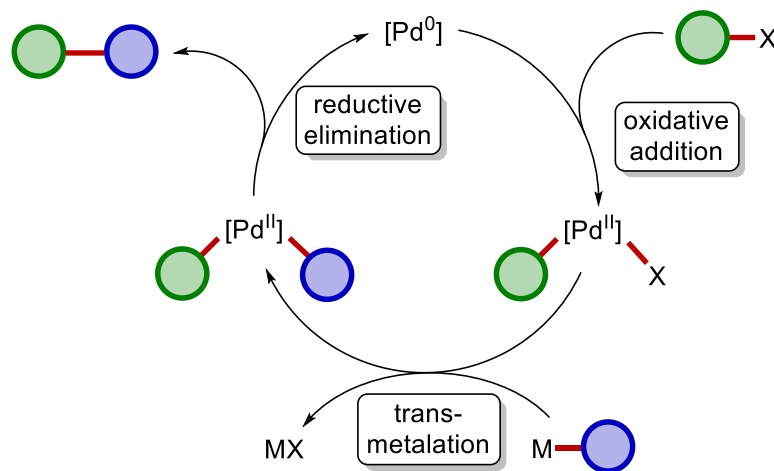
1-1),^[8] with the most prominent systems developed by *Mizoroki/Heck*,^[9] *Migita/Kosugi/Stille*,^[10] *Suzuki/Miyaura*,^[11] *Kumada/Corriu*,^[12] *Hiyama*,^[13] *Sonogashira/Hagihara*,^[14] *Negishi*,^[15] *Chan/Evans/Lam*^[16] and *Buchwald/Hartwig*.^[17] Their mechanistic principles can be backdated to the fundamental discoveries in copper-catalyzed bond formation by *Ullman, Hurtley and Goldberg*.^[18]



Scheme 1-1 Overview on popular transition metal-catalyzed cross-coupling reactions.

The low strength of organometallic bonds is the basis for the facile achievement of new connectivities by transition metal mediation.^[19] In most cases, one of the coupling partners has an electrophilic character due to a nucleofuge substituent, and the other component has nucleophilic character provided by a metal or main group center substituent. This constellation implies that the catalytic cycles mostly consist of the same elementary steps. Exemplified with palladium (**Scheme 1-2**), a representative cycle starts with the oxidative addition of the C–X bond onto the palladium(0) species, followed by a transmetalation between the resulting palladium(II) intermediate and the nucleophile, and is terminated by the reductive elimination of the active catalyst. The coupling conditions vary in harshness,

but the trend is that the mildest conditions and lowest catalysts loadings can be achieved when expensive palladium catalysts are employed.



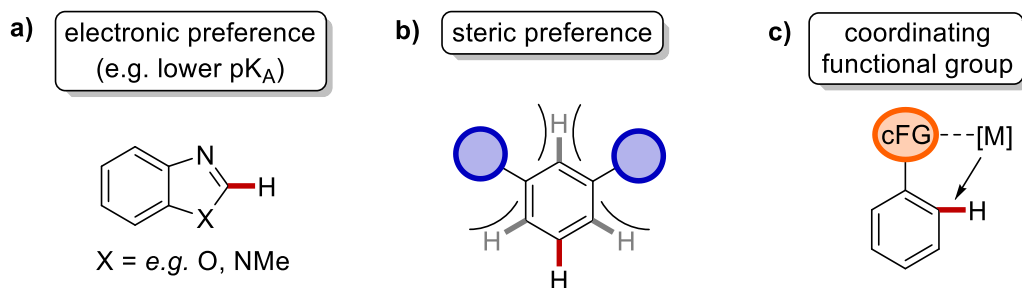
Scheme 1-2 General mechanism for palladium-catalyzed cross-coupling reactions.

These methods nowadays belong to the standard repertoire of organic synthesis and their importance can be hardly overrated, since the production of an enormous number of life-saving drugs relies on cross-coupling chemistry. These monumental achievements were honored with the Nobel Prize, awarded in 2010 to *Akira Suzuki*, *Ei-ichi Negishi* and *Richard F. Heck*,^[20] and the Wolf Prize 2019, awarded to *Stephen L. Buchwald* and *John F. Hartwig*.^[21] Despite these advances, catalysis in general and coupling reactions in particular remain an attractive research area due to multiple challenges that are still associated with the atom- and step-economy of the envisioned transformations.

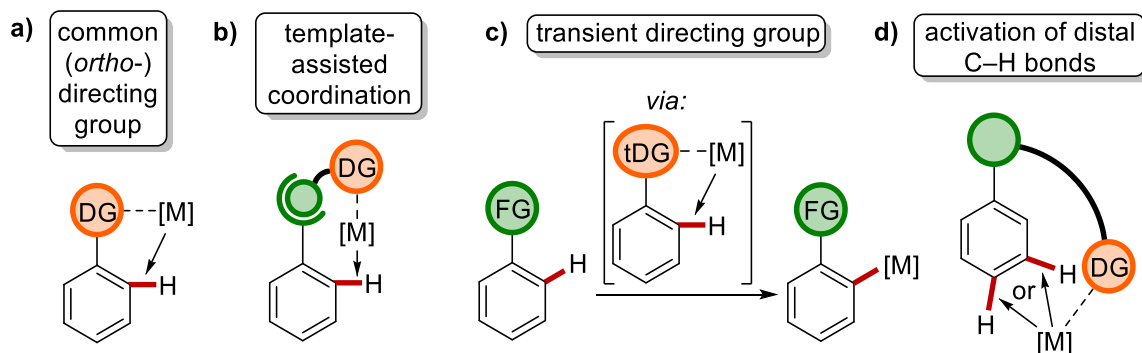
1.1.2 C–H Activation

The prefunctionalization of substrates towards the nucleophile/electrophile pair, that is needed for traditional cross-coupling, causes chemical waste during each synthetic step (**Scheme 1-3, a**). Moreover, many organometallic reagents call for special handling precautions due to their toxicity and/or hydrolytic sensitivity. An arguably more direct approach is reductive cross-coupling of two electrophiles (**Scheme 1-3, b**).^[22] However, in addition to the innate challenge of overcoming undesired homocoupling, the waste balance is similarly problematic. In this context, C–H activation emerged as a powerful approach to unlock expedient reactivities of ubiquitously occurring C–H bonds while circumventing

other available C–H bonds.^[32] Such features can be electronic singularity (**Scheme 1-4, a**),^[33] steric preference (**Scheme 1-4, b**) or the assistance of proximal functional groups (**Scheme 1-4, c**). Unfortunately, the reactivity in the first two cases is generally substrate-specific and therefore the applicability is rather limited. By contrast, certain substituents can either act as reactivity directors^[34] by themselves (**Scheme 1-5, a**), or provide an anchor for a directing template or a transient^[35] directing group (**Scheme 1-5, b and c**). The variety of possibilities led to the establishment of directing groups as the gold standard in C–H activation chemistry. The principle of operation is the coordination of the *Lewis*-basic moieties to the *Lewis*-acidic metal center of the catalyst and thereby keeping it on average in close proximity to the aromatic ring.^[36] Consequently, the kinetic probability of the metal to interact with a particular C–H bond is increased, since the process is effectively intramolecular. As a general rule, the strength of a directing group correlates with the inherent ligand strength of the coordinating moiety, and the denticity, with bi- and tridentate directing groups fixating the metal by chelation.^[37] Most directing groups have an *ortho*-directing effect, since geometrically favored five- and six-membered metallacycles are intermediately formed. Remote functionalization in *meta*- and *para*-position by directing group assistance is also possible, yet highly challenging, and mostly involves the use of carefully designed spacers or templates (**Scheme 1-5, d**).^[35d,38]

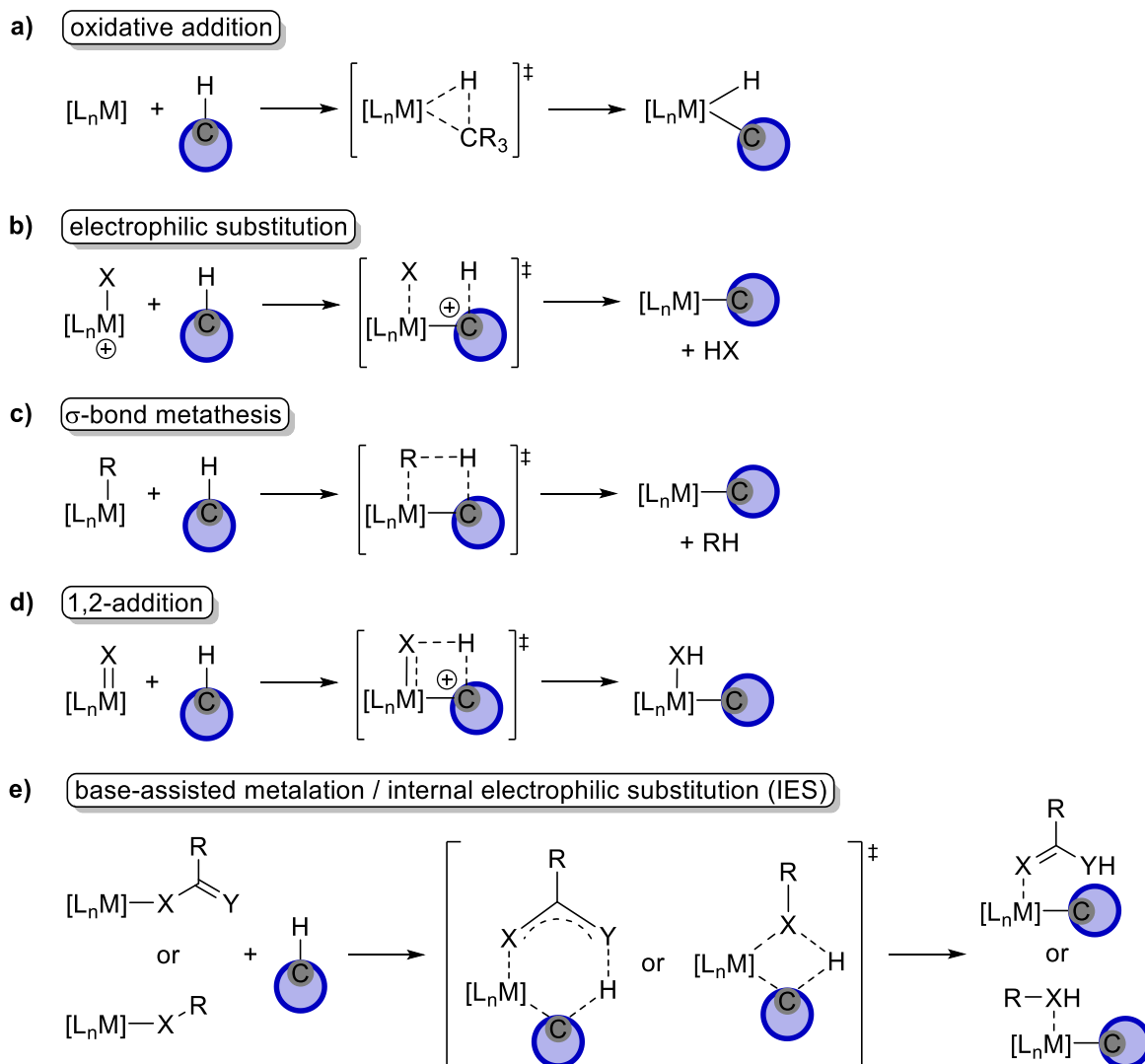


Scheme 1-4 Differentiation strategies for C–H bonds.



Scheme 1-5 Different directing groups.

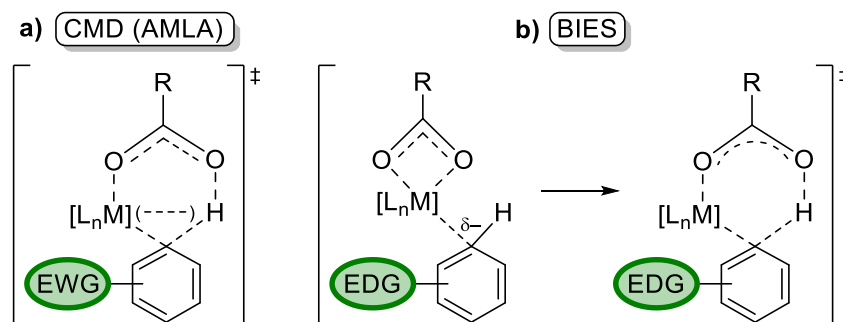
The activation of the C–H bond can occur by several means.^[39] For inner-sphere processes, that are characterized by the formation of an organometallic M–C bond, the common ground is that electron density is donated from the σ -C–H molecular orbital (MO) into a vacant d_z orbital of the metal complex, while π -backdonation occurs from an occupied d_{π} -MO of the metal into the antibonding σ^* -C–H, resulting in the synergistic weakening of the C–H bond. This process, regardless of its exact nature, requires a vacant site on the metal. When coordinatively unsaturated complexes of late transition metals are involved, oxidative addition in a mostly concerted manner is a common metalation pathway (**Scheme 1-6, a**). Typical examples are ruthenium(0), rhodium(I), iridium(I) and palladium(0). The oxidation state of the metal is thereby formally increased by two units and the complex geometry is changed upon the accommodation of the new ligands. Whereas high-valent or cationic complexes of late transition metals preferably react in a redox-neutral electrophilic substitution (**Scheme 1-6, b**). Other redox-neutral metalation pathways are the mechanistically related σ -bond metathesis (**Scheme 1-6, c**) and 1,2-addition (**Scheme 1-6, d**), both of which occur through a four-membered transition state. These reactions are observed mainly with early transition metals, including actinides and lanthanides. Lastly, many C–H functionalizations involving the assistance of a basic ligand were realized (**Scheme 1-6, e**). The C–H acidity is elevated by the coordination of the electron-deficient metal center. Due to the concurrent protonation of the basic ligand, the electrophilicity of the metal center further increases, resulting in a facile internal electrophilic substitution (IES) by the carbon moiety through a four- or six-membered transition state.



Scheme 1-6 Mechanisms for C–H bond activation.

Among the base-assisted mechanisms, the ones involving a bifunctional carboxylate group are arguably the most prominent.^[40] Two distinct operational modes are widely accepted, that can be accounted for different substrate preferences. On the one hand, a concerted metalation-deprotonation^[41] (CMD, **Scheme 1-7, a**) is accelerated by electron-withdrawing substituents on the aromatic ring, therefore leading to a higher kinetic C–H acidity and a more facile proton abstraction. In an independent study, an additional agostic interaction between the hydrogen atom and the metal center was proposed, that was described as an ambiphilic metal-ligand activation (AMLA).^[42] On the other hand, when the proton transfer is preceded by a coordination of the metal at the *ipso*-position, electron rich substituents accelerate the reaction (**Scheme 1-7, a**). This sequence can be qualified as a base-assisted internal electrophilic substitution (BIES).^[43] In other discussions, this distinction is

questioned due to different selectivities observed with kinetic *vs.* thermodynamic control of the cyclometalation.^[44]



Scheme 1-7 Mechanistic variants of carboxylate-assisted C–H activation.

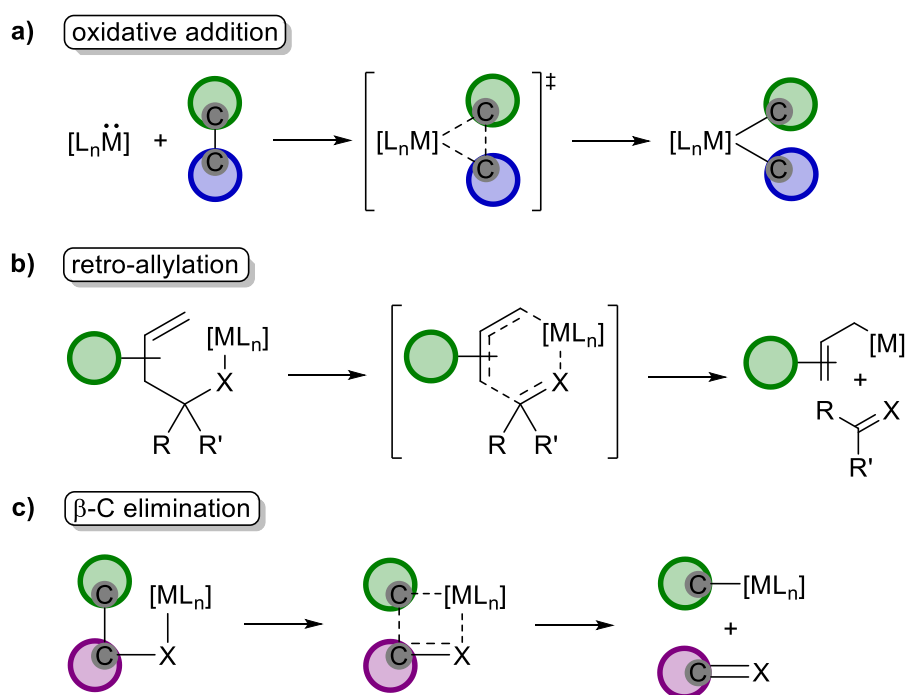
The tremendous value of the directed activation of C–H bonds is universally acknowledged and applied in complex synthetic tasks, such as the functionalization of C(sp³)–H bonds,^[45] enantioselective transformations,^[46] total synthesis^[47] and late-stage diversification^[48] of biomolecules^[49] and active pharmaceutical ingredients^[47c,50]. Nevertheless, the development of complementary approaches is remains important (*vide infra*).

1.1.3 C–C Activation and Functionalization

Efficient synthesis involves the minimization of synthetic steps, which is determined by the utilization of readily available starting materials. Naturally, expanding the range of bond activation methods towards C–C bonds^[51] is highly desirable, since their natural occurrence is likewise ubiquitous. Consequently, the advantage of C–H activation over traditional cross-coupling chemistry, namely that the substrate reactivity does not rely on the existence of a nucleophilicity-inducing main group center, is kept, while the eligibility of alternative substrates could prevent otherwise potentially necessary defunctionalization^[35a,52] and therefore enable new retrosynthetic partitions.

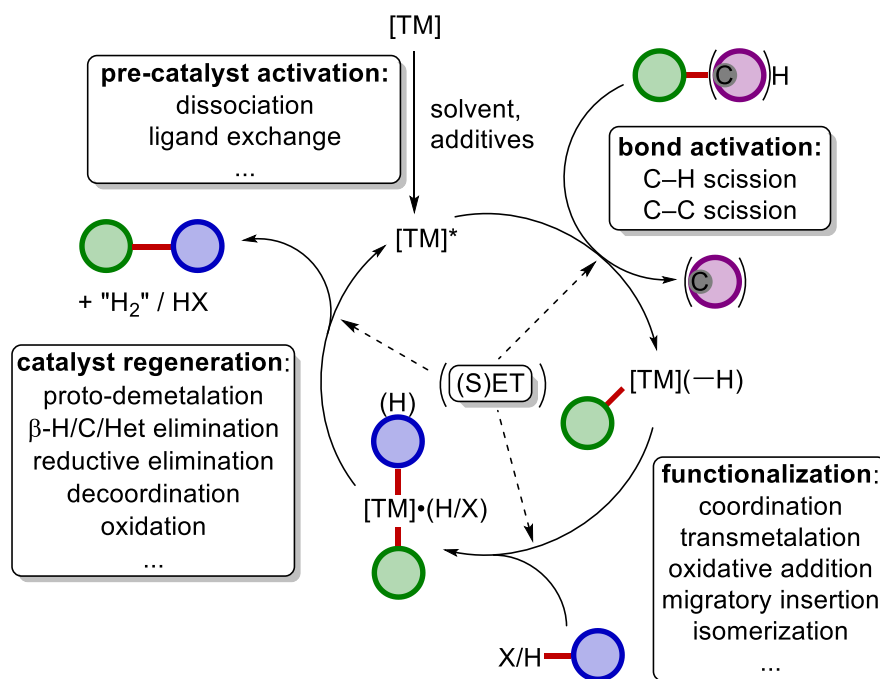
Although aromatic C–H bonds are generally stronger than structurally unbiased C–C single bonds, the activation of the latter is aggravated by several factors.^[53] First, the attachment of up to three additional substituents per carbon atom can significantly restrict the steric availability of the cleavable C–C bond. Second, the strictly directional C–C- σ -bond does not possess domains with a well-accessible spherical electron density, as opposed to a C–H bond with an exposed s-orbital. Hence, a significant overlap with metallic d-orbitals is

geometrically unfeasible, unless a heavy distortion of the bond is enforced. Accordingly, the discrete event of C–C bond activation in many cases is assumed to be endergonic, and the realization is therefore mostly bound to thermodynamically or kinetically supporting processes, such as the relaxation of ring strain, coordinative or chelating assistance, an aromatization or the release of small low-energy molecules. The activation of C–C bonds by transition metals mainly occurs *via* three mechanisms: oxidative addition (**Scheme 1-8, a**),^[51h] retro-allylation (**Scheme 1-8, b**)^[54] and β -carbon elimination (**Scheme 1-8, c**). As in the case of C–H activation, the oxidative addition is viable for low valent, electron-rich complexes of late transition metals, while the redox-neutral activation pathways are predominantly observed with electron-deficient complexes thereof. Retro-allylation is achieved with homoallylic substrates *via* a 6-membered transition state. Likewise, the β -carbon elimination, formally being the reverse of a migratory insertion, is accompanied by the extrusion of a molecule containing a multiple bond as the stoichiometric byproduct. Many C–C *ipso*-substitutions are reported with tertiary alcohols as starting materials, which consequently release a ketone. Other substrate classes can, for instance, be activated *via* transition metal-mediated decarboxylations, decarbonylations and decyanations.^{[[51a,51e]}



Scheme 1-8 Mechanisms for transition metal-assisted C–C bond activation.

Overall, the transition metal-assisted activation of abundant C–H and C–C bonds provides an expedient starting point for a wide range of functionalizations in a catalytic manner (**Scheme 1-9**). The upkeep of catalytic activity depends on the modality of the functionalization. The catalyst can be released in its active state, directly entering the next catalytic turnover, or retained in an inactive state, which in the case of oxidative coupling requires reoxidation. Importantly, the oxidation step is not cardinally limited to the termination of the catalytic cycle. Oxidative (single) electron transfers can occur at almost any stage of the catalytic cycle and be crucial for the triggering of consecutive elementary steps, such as the oxidation-induced reductive elimination.^[55] Often, the electron transfer occurs in an “inner-sphere” process, which is characterized by a major reorganization of the coordination sphere during the transition state and resulting in a concomitant transfer of an atom or atom groups.^[56]

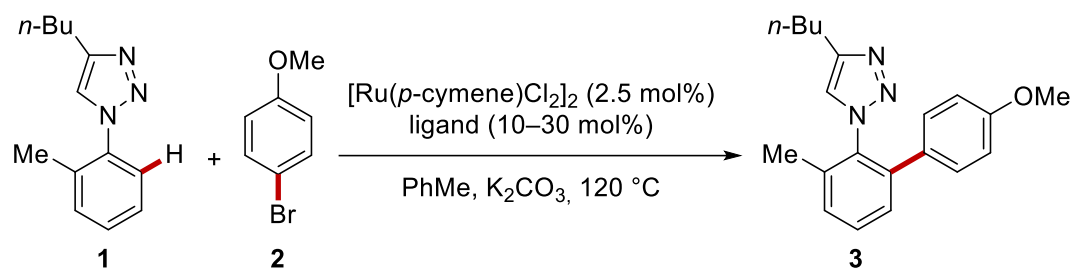


Scheme 1-9 General catalytic cycle for transition metal-catalyzed C–H and C–C functionalizations.

1.2 Carboxylate-Assisted Ruthenium-Catalyzed C–H Activation

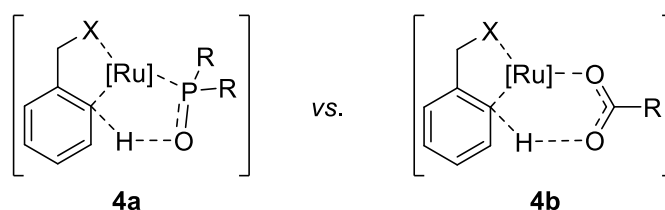
Ruthenium has gained widespread popularity in the field of C–H functionalization. Compared to rhodium (41.88 €/mmol), palladium (6.13 €/mmol) and iridium (23.2 €/mol), ruthenium (1.47 €/mmol) is less expensive,^[57] and therefore an attractive alternative when similar reactivities can be accomplished. The ability of the metal to undergo directed metalations and functionalize C–H bonds with catalytic turnover was unlocked in 1986 by pioneering work from *Lewis/Smith*.^[58] The authors observed the *ortho*-alkylation of phenol by ethylene, when a cyclometalated ruthenium phosphite complex was used. Years later, *Murai/Kakiuchi/Chatani* reported on a catalytic alkylation of phenones.^[59] The system stood out due to low catalyst loading and generality, being also suitable for heteroaromatic ketones, as well as for olefin coupling partners of different substitution grades. In 2005, the first ruthenium-catalyzed *ortho*-arylation with aryl chlorides was developed by *Ackermann*. The reaction was both air- and moisture-stable, and worked with different *N*-directing groups.^[60] In a later study, the applicability of this approach was extended to aryl tosylates.^[61] Key to the robustness and efficiency of these transformation was the use of bulky secondary phosphine oxide (SPO) preligands. The *P,O*-bifunctional nature of the ligands allowed for an efficient deprotonation assistance in a five-membered transition state (**Scheme 1-10, b**).^[62] This principle served as a gateway for the development of C–H activations assisted by the likewise bifunctional carboxylate group. In a 2008 study, *Ackermann* could demonstrate that this inexpensive ligand class matched and mostly outperformed the phosphine ligands in direct arylations of arenes **1**, with bulky substituents being the most effective (**Scheme 1-10, a**).^[63]

a) ligand optimization



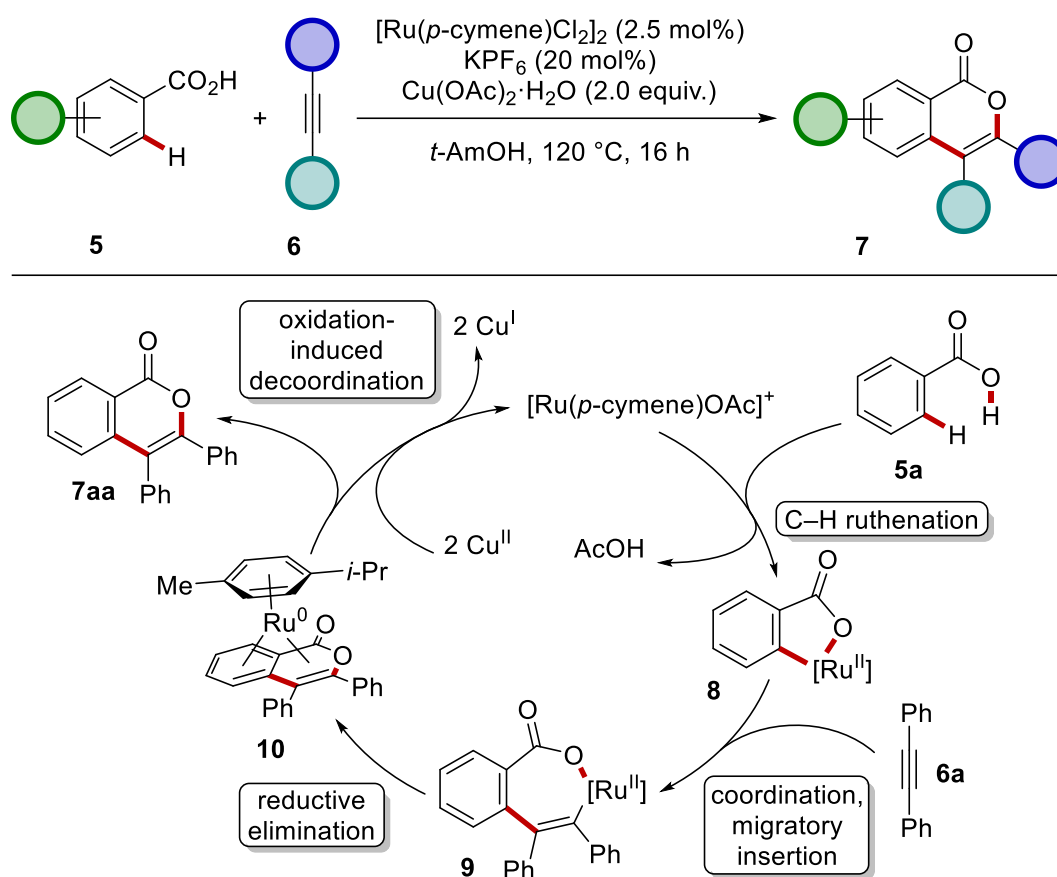
ligand	(PhO) ₂ P(O)OH	<i>i</i> -PrCO ₂ H	(1-Ad) ₂ P(O)H	1-AdCO ₂ H	MesCO ₂ H
yield (%)	50	69	85	85	93

b) postulated transition states



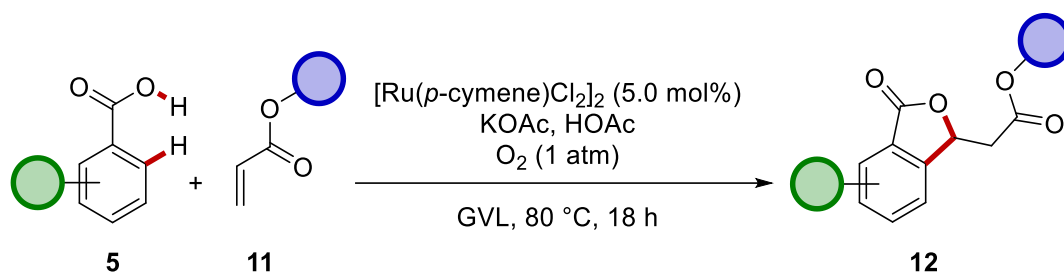
Scheme 1-10 Bifunctional ligand assistance for ruthenium-catalyzed C–H activation.

In the following years, many versatile and robust protocols for different types of functionalization by carboxylate-assisted *via* ortho-ruthenation have emerged.^[40a,62a] Annulations *via* twofold C–H/Het–H activation, mostly with acetylenes as the reaction partners, gave access to a large variety of heterocyclic motifs.^[64] In these reactions, the directing group becomes a part of the scaffold, thereby leading to excellent atom economies. In the case of *Ackermann's* isocoumarine synthesis,^[64i] the catalytic cycle commences with C–H activation of benzoic acids **5**, followed by the coordination of the alkyne **6**, its migratory insertion into the Ru–C bond of intermediate **8** and a reductive elimination to form the product **7**. Reoxidation of the ruthenium intermediate is carried out by the copper(II) salt. In a subsequent approach of 2015,^[65] molecular oxygen could be employed as the terminal oxidant and mechanistic studies identified that the reductive elimination leads to an isolable ruthenium(0) sandwich complex **10**, which releases the product upon oxidation (**Scheme 1-11**).



Scheme 1-11 Mechanism of ruthenium-catalyzed isocoumarin formation.

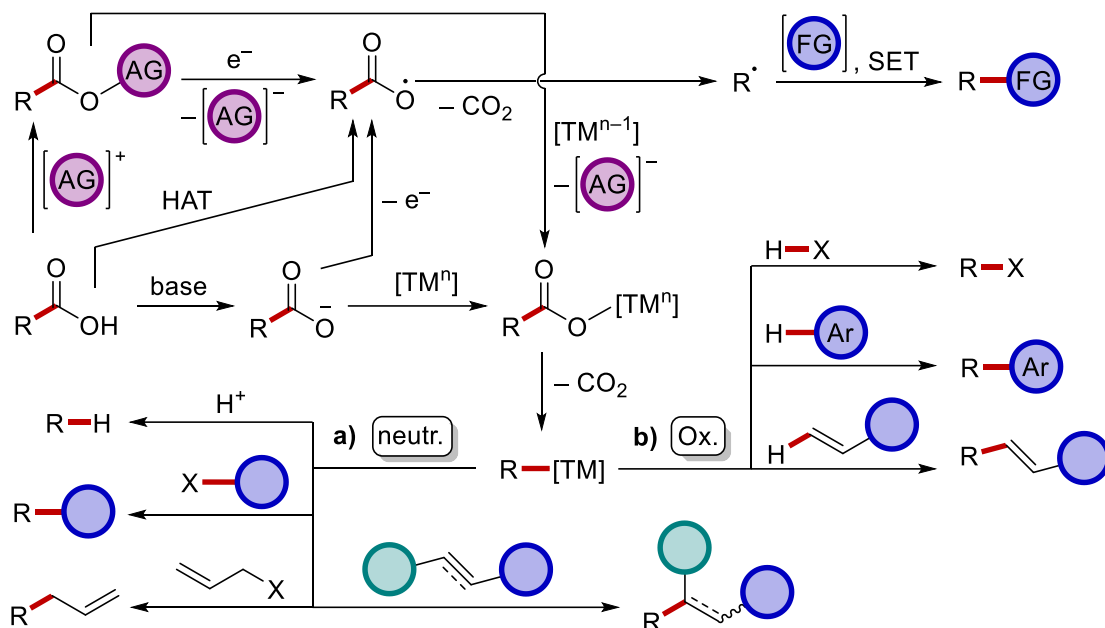
Moreover, alkenylations,^[66] arylations,^[67] benzylations,^[68] alkylations^[69] and allenylations^[70] were developed. A valuable addition to the versatility of carboxylate-assisted ruthenium catalysis is the possibility to also form C–O^[71] and C–N^[71b,72] bonds. The ability to catalyze this multitude of transformations mostly with weak directing groups^[73] turned out to be a salient characteristic of carboxylate-assisted ruthenium catalysis. One particularly important scaffold that could be obtained by ruthenium-catalyzed alkenylation is the phthalide motif **12** (**Scheme 1-12**).^[66h] The cyclization of the alkenylated product is favored due to the utilization of electron-deficient alkenes **11** as coupling partners, which after the functionalization act as acceptors for an intramolecular *oxa-Michael* addition. The robust nature of this regime allowed for further optimization towards sustainable synthesis,^[74] leading to a protocol that used GVL as green solvent and molecular oxygen as oxidant at ambient pressure.^[75]



Scheme 1-12 Phthalide synthesis under “green” conditions.

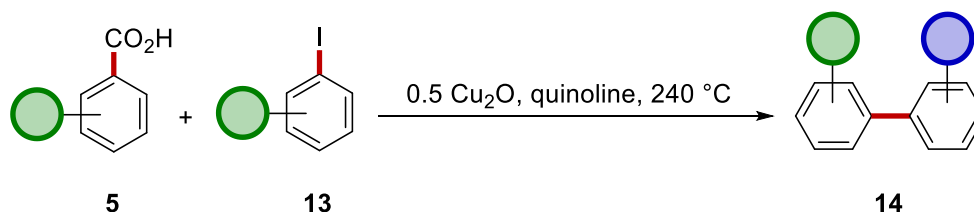
1.3 Decarboxylative Coupling Reactions

A highly transformation-specific directing group is oftentimes installed for the fulfillment of its synthetic purpose – directing a metalation – and not to serve as an integral component of the target structure. Therefore, removability of these moieties is highly desired. A directing group is usually declared as “removed”, when it has been deconstructed up to a small and easily diversifiable functional group as a residue.^{[[35a,35e,52,76]} A typical example is the hydrolytic cleavage of amide-bridged heterocycles to yield an amine. By contrast, a traceless removal is achieved, when the directing group-bearing position is defunctionalized to a proton as substituent. As such, directing groups that can undergo de-insertions or eliminations as small molecules are the ideal candidates for this task. In particular, decarboxylation can serve as a key step in both, the activation of the *ipso*-position for homo- and cross-coupling reactivity,^[77] and the defunctionalization of the highly popular carboxylate directing group in C–H activation.^[78] Aside from radical pathways and sequences starting from activated acid derivatives,^[79] the *ipso*-coupling of a carboxylic acid is initiated by the coordination of the transition metal and the subsequent C–C activation by means of β -C elimination, leading to carbometalation and the extrusion of CO₂ as byproduct. On the one hand, the carbometalated species can undergo reactions in a redox-neutral fashion (**Scheme 1-13, a**), leading to classic cross-coupling products with (pseudo-)halides,^[80] or addition and allylation products with typically alkynes and olefins, respectively. On the other hand, oxidative couplings in a formally dehydrogenative manner can deliver halogenated and arylated products, as well as olefins in a decarboxylative *Mizoroki-Heck* reaction (**Scheme 1-13, b**).



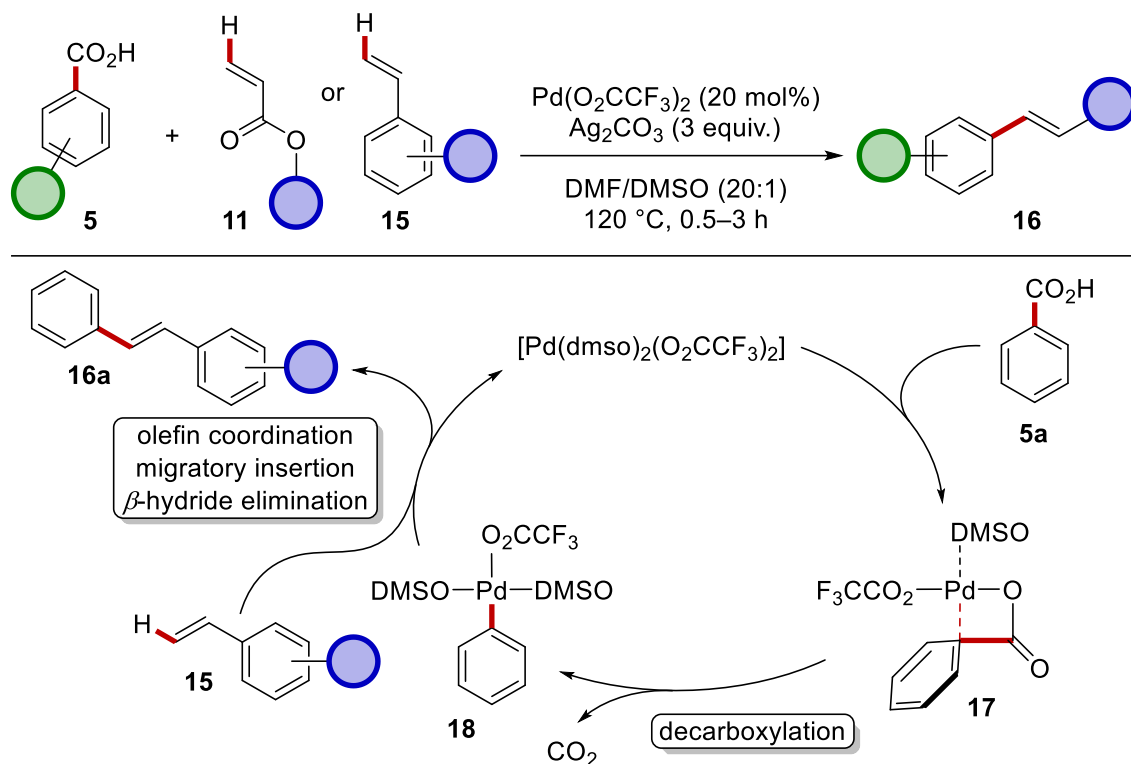
Scheme 1-13 General pathways of decarboxylative couplings by *ipso*-substitution.

The finding of a variant of the *Ullmann* coupling between a benzoic acid derivative **5** and an aryl halide **13** pioneered the field of decarboxylative cross-coupling. In the report of 1966 by *Nilsson*,^[81] a stoichiometric amount of Cu_2O was used (**Scheme 1-14**).



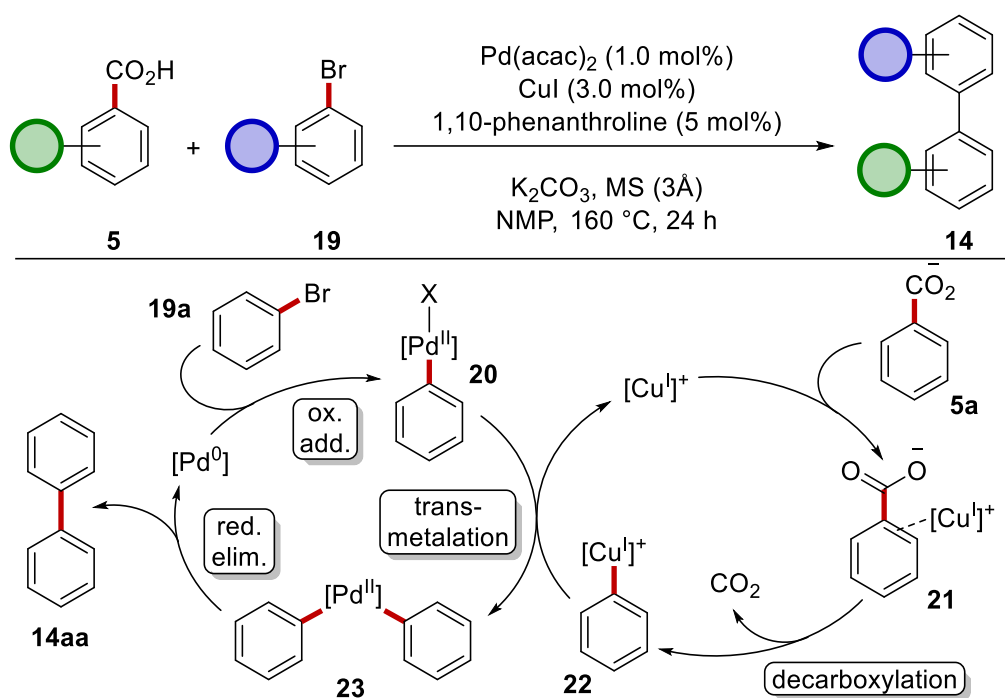
Scheme 1-14 Nilsson's biaryl coupling.

The next landmark contribution was achieved by *Myers*,^[82] who developed a palladium-catalyzed oxidative *Mizoroki-Heck*-type alkenylation (**Scheme 1-15**). The reaction had an ample scope, but was compromised by a high catalyst loading and the addition of six equivalents of silver(I) ions. In a subsequent mechanistic study, several key intermediates, such as an analogue of complex **18**, could be analyzed by X-ray crystallography, leading to a fundamental mechanistic proposal, that the rate-determining decarboxylation step proceeds through a four-membered transition state.^[83]



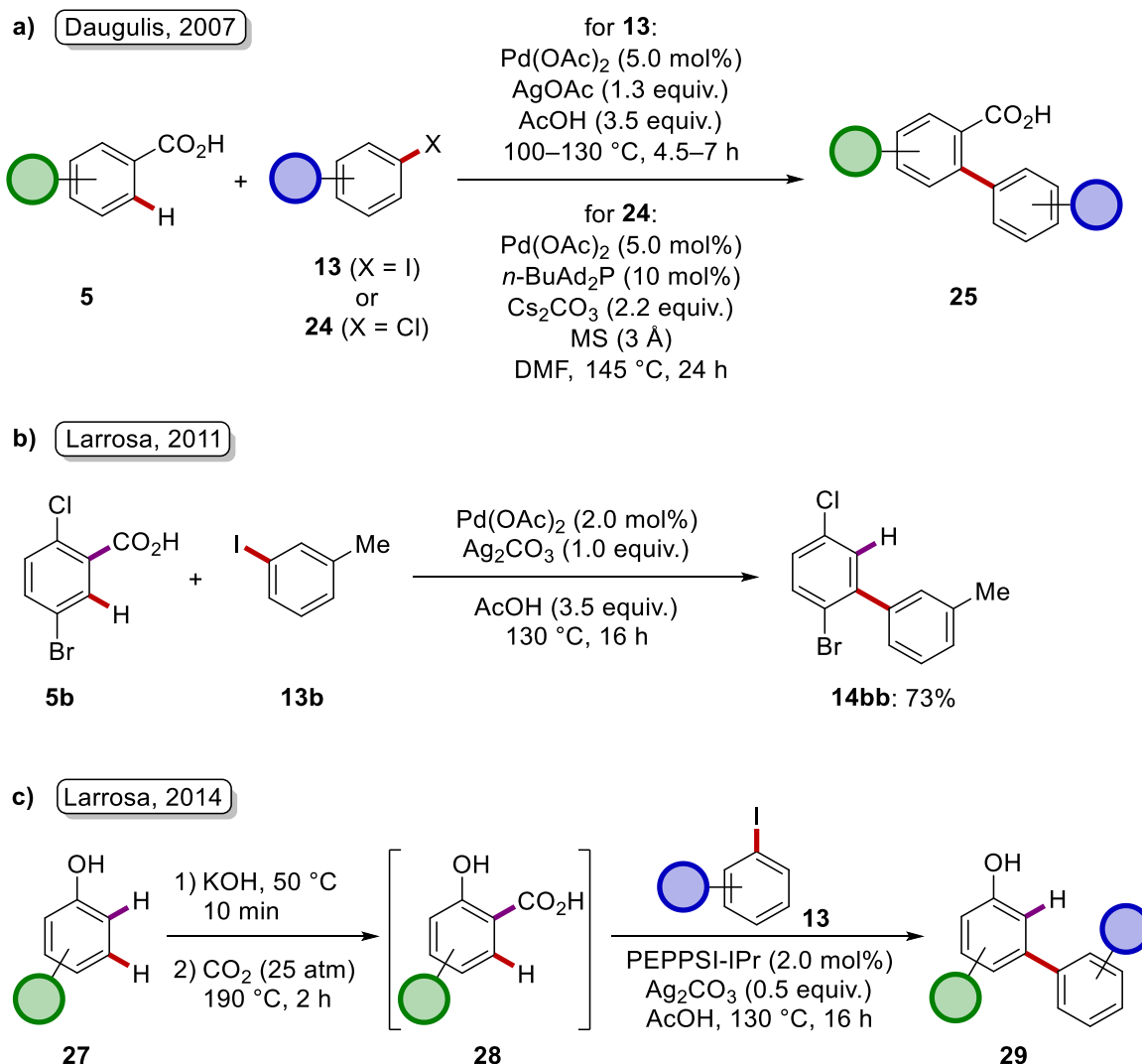
Scheme 1-15 Myers' palladium-catalyzed alkenylation.

In 2006, *Goossen* developed a highly efficient biaryl coupling of benzoic acids **5** and haloarenes **19** by dual catalysis. The addition of 3 mol% of copper salt and an appropriate ligand allowed for a reduction of the palladium loading to 1 mol% (**Scheme 1-16**).^[84] The idea was to combine two catalytic cycles of different transition metals that are known to be particularly effective in different elementary steps: copper salts for the decarboxylation and palladium for the classic cross-coupling sequence.



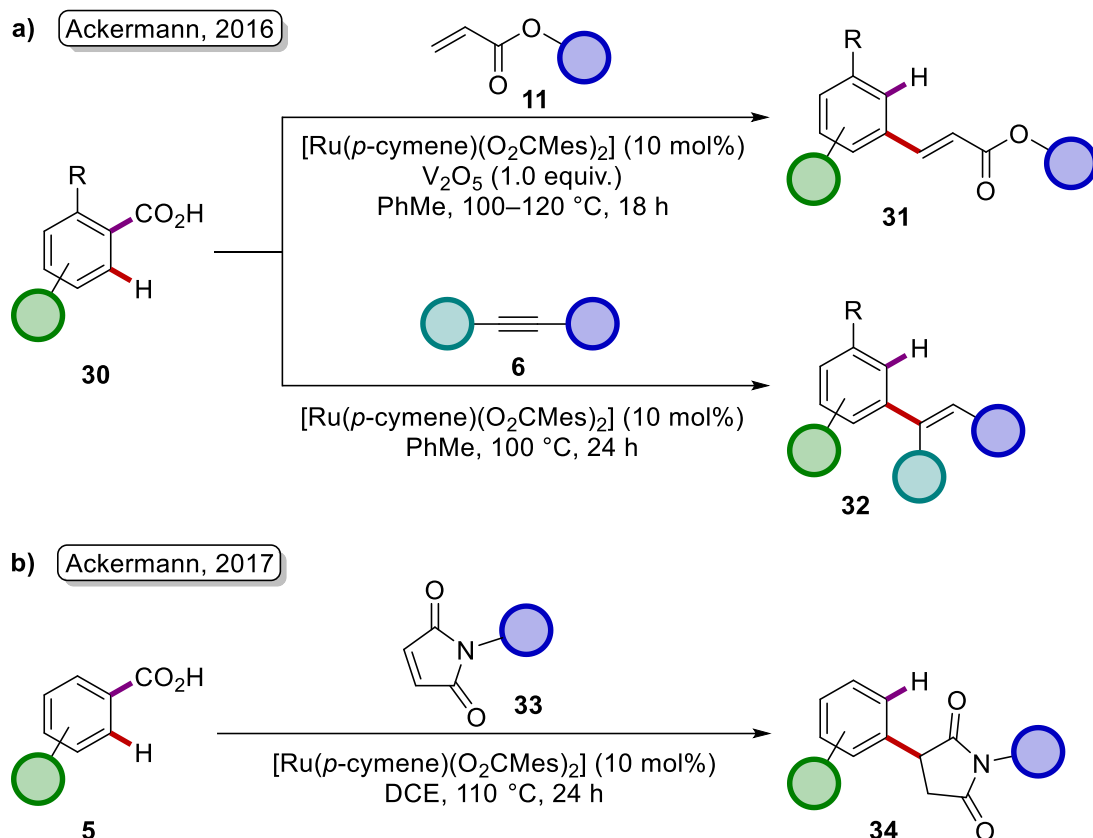
Scheme 1-16 Pd/Cu-catalyzed biaryl coupling by Goossen.

As stated before, the carboxylic acid moiety can not only act as an efficient halogen-free leaving group alternative for cross-coupling transformations, but also as a tracelessly removable *ortho*-directing group for C–H functionalization. The first report on *ortho*-arylation of benzoic acids **5** by *Daugulis*^[85] (**Scheme 1-17, a**), and studies on copper- and silver-mediated proto-decarboxylations^[86] served as the basis for the development of a decarboxylative arylation sequence, introduced by *Larrosa* in 2011.^[87] The method used Pd(OAc)₂ as the catalyst and despite the redox-neutrality of the transformation, substantial amounts of silver salt were required to facilitate the proto-decarboxylation step (**Scheme 1-17, b**). The method was extended to phenols **27** as starting materials for a one-pot sequence, that commenced with a *Kolbe-Schmitt* carboxylation^[88] with CO₂ to form the corresponding salicylic acid derivative **28** *in situ* (**Scheme 1-17, c**).^[89]



Scheme 1-17 One-pot *ortho*-arylation/proto-decarboxylation sequences by Larrosa. PEPPSI-IPr = *trans*-dichloro(1,3-bis-(2,6-diisopropylphenyl)imidazolylidinium)(3-chloro-pyridine)palladium(II).^[90]

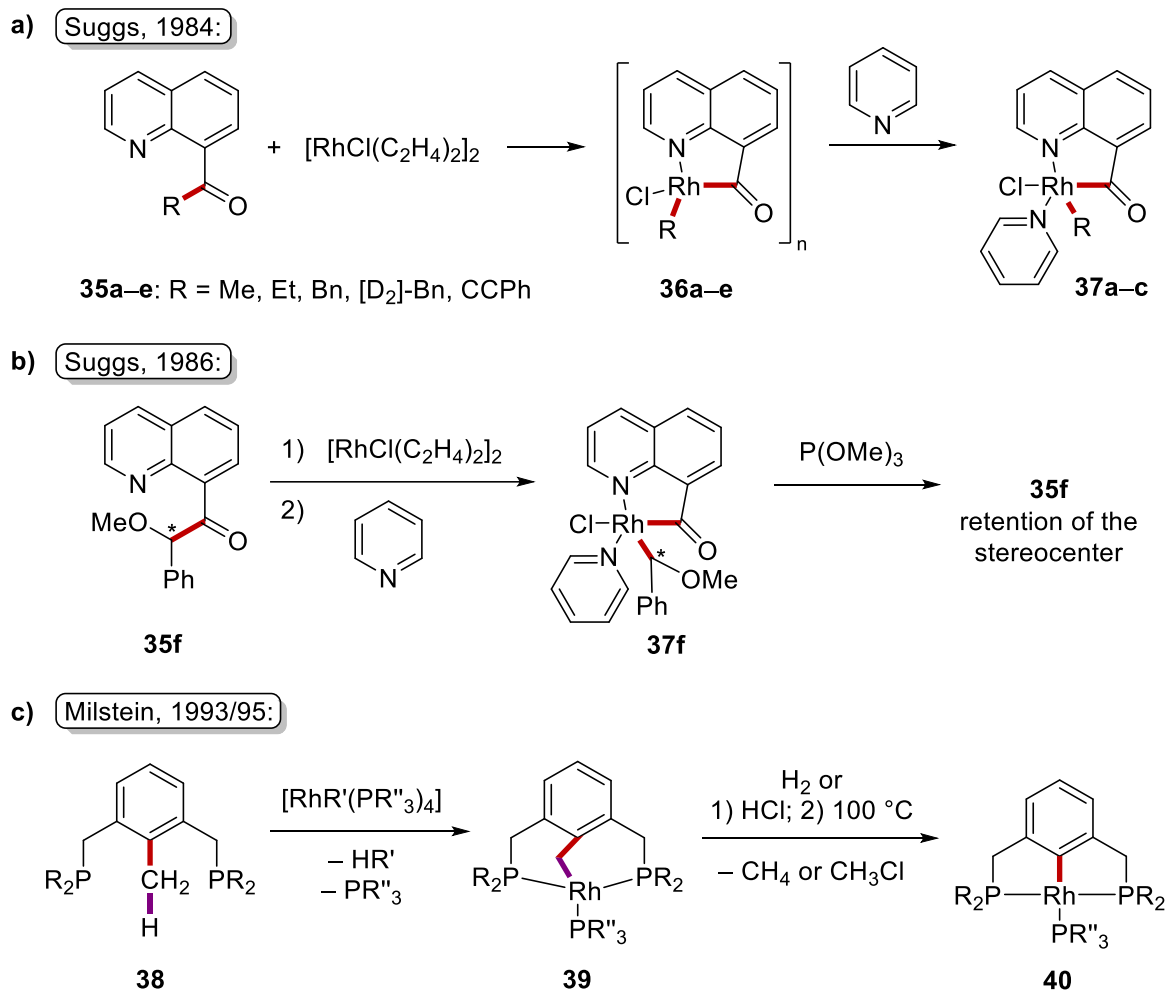
A few years later, *Ackermann* disclosed several robust protocols for decarboxylative *ortho*-functionalizations, catalyzed by less cost-intensive ruthenium complexes. Redox-neutral additions of maleimides^[91] **33** and alkynes **6**,^[66c] as well as the oxidative alkenylation with activated olefins^[66c] **11** were achieved without the use of silver salts as decarboxylation-fostering additives. For the catalyst regeneration in the oxidative alkenylation, vanadium pentoxide was employed (**Scheme 1-18**).



Scheme 1-18 Ruthenium-catalyzed decarboxylative *ortho*-functionalizations.

1.4 Rhodium-Catalyzed C–C Activation

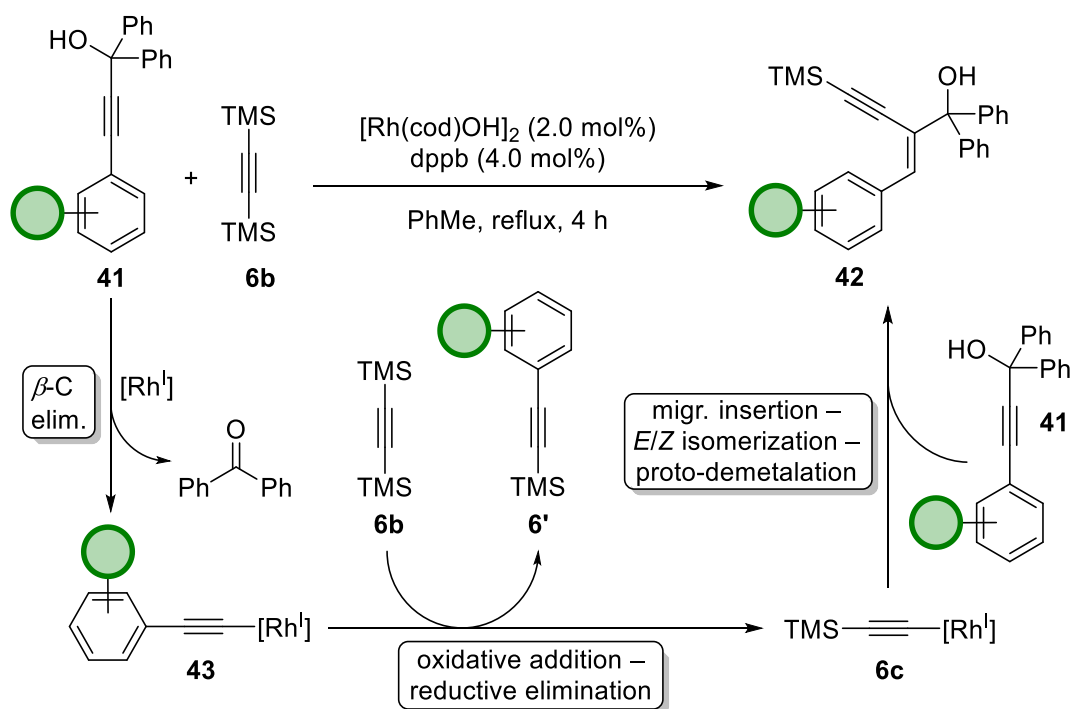
The first reports on directed insertion of a transition metal into a C–C bond are from the mid-80-s from *Suggs*, who observed the formation of polymeric acylrhodium complexes **36**, when quinoline-substituted ketones **35** were treated with a rhodium(I) complex (Scheme 1-19, a, b).^[92] When the soluble pyridine-ligated derivatives **37** were converted to the starting materials by phosphine ligand-promoted reductive elimination, a retention of the stereocenters was observed. Later, *Milstein* showed that PCP-rhodium(III) pincer complexes **39** and **40** could be obtained from the methyl-substituted ligand precursors **38** (Scheme 1-19, c).^[53c,93] Whether C–C activation was favored over C–H activation, strongly depended on the substituents both on the rhodium ligands and the pincer ligand precursor **38**, despite the general thermodynamic preference of the C-arylated complex **40**. This illustrates the importance of the kinetic facilitation in C–C activations. The study was eventually extended to include PCN-pincer complexes.^[94]



Scheme 1-19 First reports on directed transition metal insertion into C–C bonds.

Among the early examples of catalytic C–C activations is the rhodium(I)-catalyzed hydrogenolysis of strained cyclobutanones.^[95] The transformation was developed by *Ito* on the basis of a stoichiometric reaction that resulted in decarbonylative ring contractions. The bond activation occurred by means of oxidative addition. Catalytic coupling reactions proceeding through β -C elimination were first reported with palladium catalysts. Tertiary propargyl alcohols, which are the most facile substrates to get activated by this mechanistic means, in combination with aryl bromides **19** as electrophile, formed a C–C bond with almost no homocoupling byproducts, thereby overcoming a general selectivity challenge of the *Sonogashira-Hagihara* reaction.^[96] Analogous reactivity was achieved with tertiary benzylic alcohols.^[97] Moreover, oxidative coupling with alkenes to form enynes was achieved with molecular oxygen as sole oxidant.^[98] The first rhodium-catalyzed cross-coupling, that involved a β -C elimination, was achieved by *Miura*, and was likewise

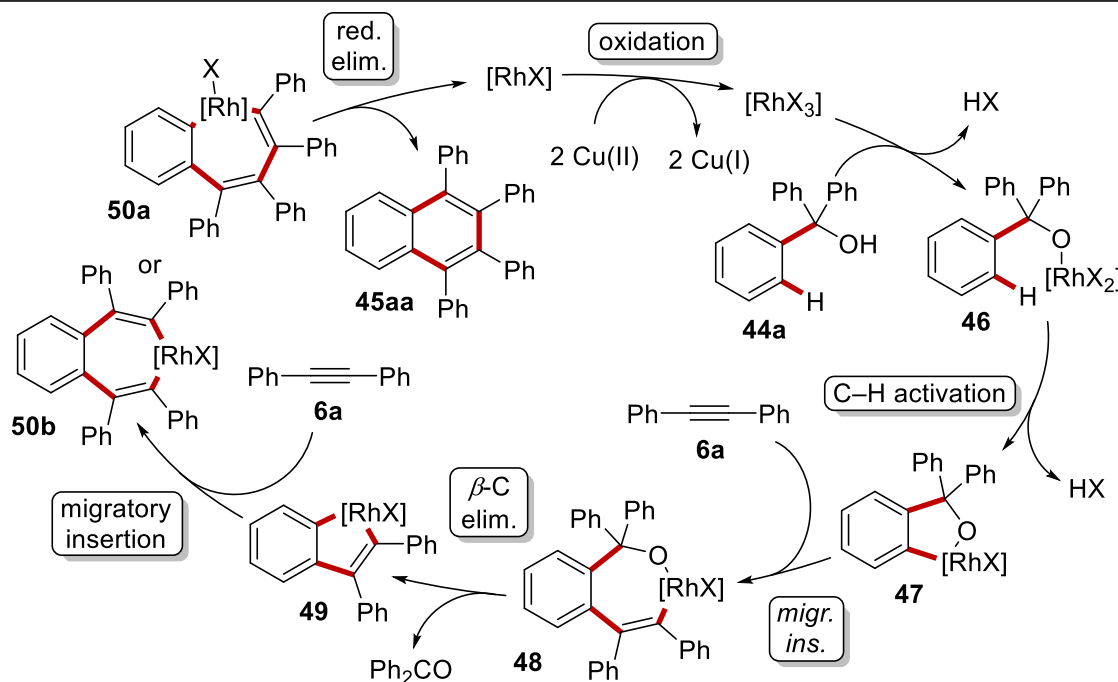
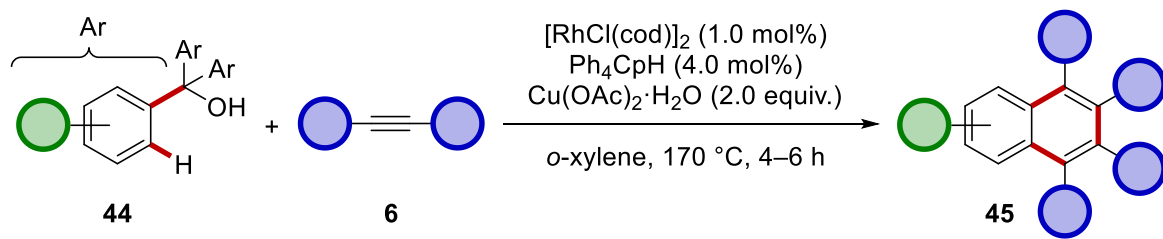
accomplished between propargyl alcohols **41** and alkynes **6b** (Scheme 1-20).^[99] The key to avoid homocoupling, which was previously reported by the same group,^[100] was the slow addition of the alcohol. Thereby, the concentration of the coupling partner **6b** was kept in great excess which fostered the exchange of alkynyl residues on the metal. Unfortunately, this meant that only half of the limiting reagent **41** was actually available for product formation.



Scheme 1-20 Rhodium-catalyzed cross-coupling of propargyl alcohols **41** by C–C activation.

In 2008, *Sato* and *Miura* published an oxidative oxidative annulation of triarylmethanols **44** towards highly substituted naphthalenes **45** (Scheme 1-21).^[101] The reaction is remarkable for the formation of three new bonds and the dual function of the leaving group, which in the beginning of the sequence acts a directing group for C–H activation. The leaving group is expelled from the 7-membered cyclometalated intermediate **48**, which is formed after the migratory insertion of the first equivalent of alkyne **6**. The second insertion can occur into both available Rh–C bonds of **49** to form intermediates **50a** or **50b**, which upon reductive elimination release the desired product **45**. The reoxidation of the catalyst is carried out by the copper(II) salt. The system has two apparent disadvantages. First, high temperatures are required, which is likely to be attributed to the weak and flexible alcohol

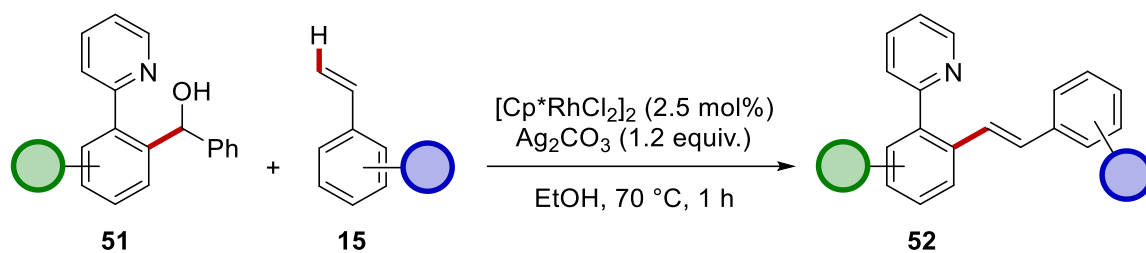
directing group. Second, the starting material has to carry three equal arene moieties, which is especially uneconomical if expensive substituents are installed.



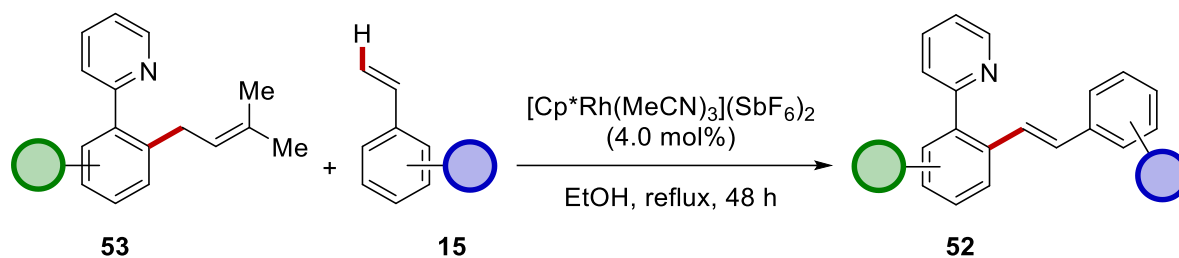
Scheme 1-21 Oxidative annulation of triarylmethanols **44**.

The beneficial effect of a strong directing group for atom-economy and milder reaction conduct was demonstrated by *Shi*, who developed an efficient alkenylation protocol of *N*-heterocycle-substituted diarylmethanols **51** (**Scheme 1-22, a**).^[102] The reaction was conducted in environmentally benign ethanol at only $T = 70$ °C and gave very good yields after short reaction time even with atom-economic benzaldehyde as leaving group. A silver-free modification for the synthesis of the same product class **52** was developed by *Kakiuchi*, using a retro-allylation as activation mechanism of the substrates **53** to achieve redox-neutrality (**Scheme 1-22, b**).^[103] The transformation requires longer reaction times in comparison to *Shi*'s approach, which is likely to be caused by the weaker interaction of the catalyst with an olefinic moiety as opposed to an alcoholic one.

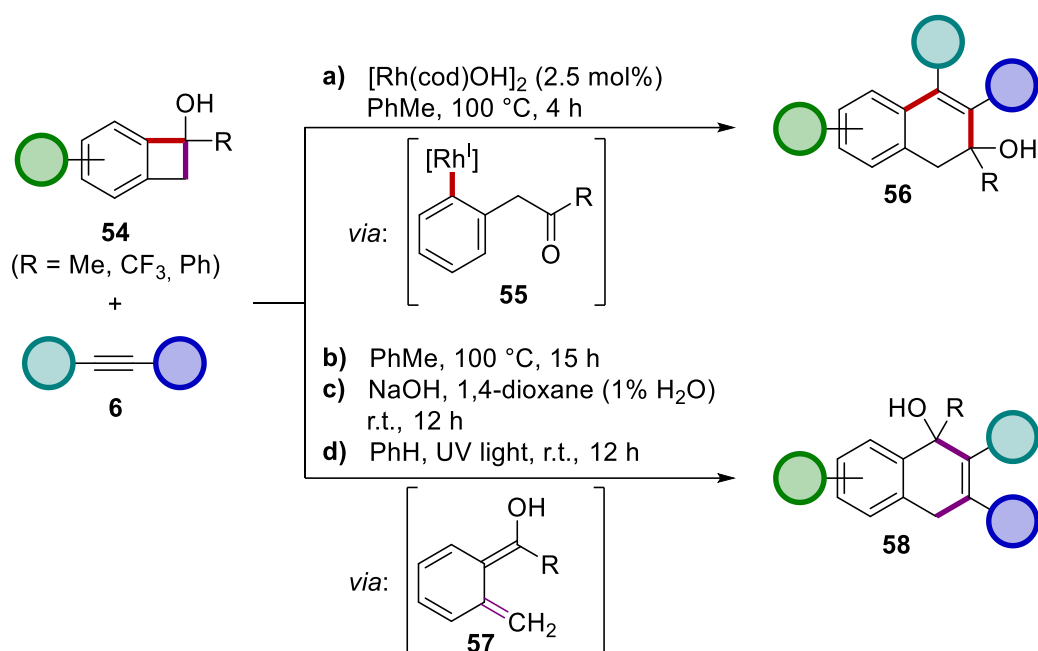
a) Shi, 2011:



b) Kakiuchi, 2018:

**Scheme 1-22** Directed alkenylation approaches by *Shi* and *Kakiuchi*.

An interesting example, where the complementary selectivities of transition metal-catalyzed reactions *vs.* metal-free transformations were demonstrated, was published by *Murakami*. Therein, the opening of benzocyclobutanone **54**, subsequent alkyne **6** insertion and cyclization led to a net ring expansion by two units, forming a dihydronaphthalene isomer **56** (**Scheme 1-23, a**). This disconnection is not accessible through thermal, basic or photochemical conditions, since they all lead to the cleavage of the C–C bond distal to the arene moiety to form a ketone **58** (**Scheme 1-23, b–d**).^[104]



Scheme 1-23 Selectivities of metal-free vs. rhodium-catalyzed benzocyclobutanol ring opening.

1.5 Undirected C–H Functionalization

1.5.1 General Aspects

With the aid of directed metal-catalyzed C–H functionalizations, syntheses under mild conditions towards a large variety of molecular scaffolds were unlocked. Nevertheless, this approach is not free of drawbacks and inherent limitations. First, the ideal directing group for the envisioned transformation is not necessarily present in the substrate molecule *a priori*. Hence, a derivatization of the available precursor functionality is sometimes necessary to install the desired directing group. Moreover, the removal of the directing group, after it fulfilled its purpose, is also often times needed. Second, certain molecule geometries or substitution patterns cause some C–H bonds to be virtually inaccessible for directed metalations with existing methods. Third, transition metal catalysis can be disadvantageous from an economical perspective. Some metals are rare and therefore expensive, and on top of that might entail extensive purification procedures for the products to meet legal regulations for trace metal impurities.^[105] Therefore, methods for undirected and optionally metal-free C–H bond functionalization are likewise desirable.^[106] As indicated before, C–H bonds can be also differentiated by stereo-electronic parameters. Due to the lack of a directing group, the interaction of the reagent or catalyst is intermolecular and mostly follows an outer-sphere mechanism for bond activation –

typically involving radical processes,^[107] in particular HAT,^[108] or reactions with metal carbenes or nitrenes.^[109] One of many outstanding examples for the undirected activation of generally inert C(sp³)-H bonds was contributed by *Davies*, where the C-H bond of the desired substitution grade could be targeted by highly site-selective dinuclear rhodium catalysts.^[110]

1.5.2 Benzylic C-H Fluorination

An evident illustration of the efficiency of undirected C-H functionalizations is the functionalization of benzylic C-H bonds. Together with allylic C-H bonds, they are inherently weaker than structurally unbiased C-H bonds of the common C atom hybridization states (**Figure 1.5-1**).^[1b] In combination with their good steric accessibility, this makes benzylic positions particularly suited for outer-sphere bond cleavage.



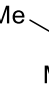
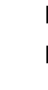


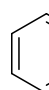


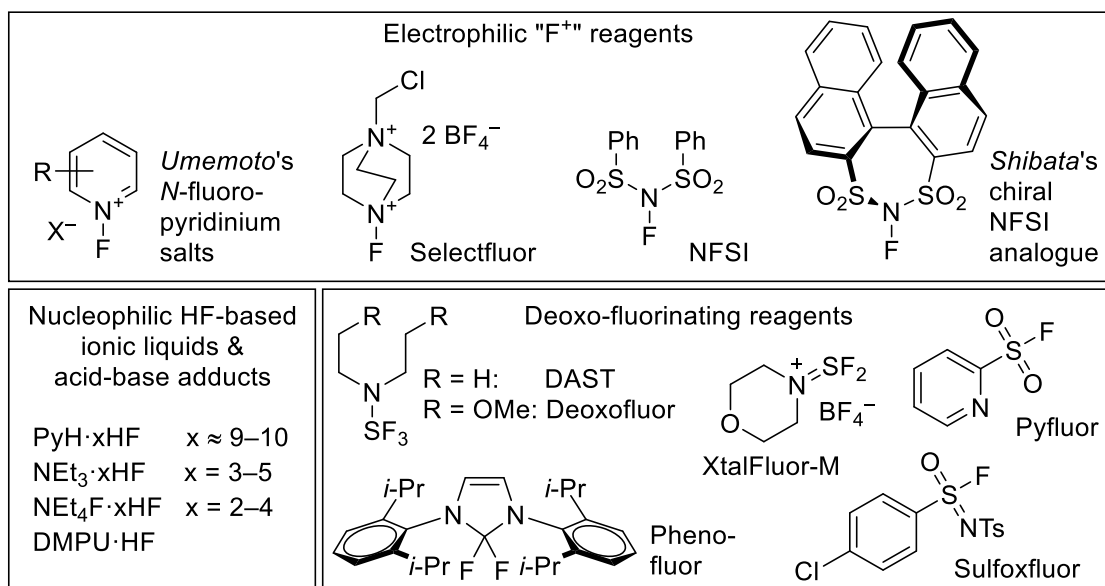
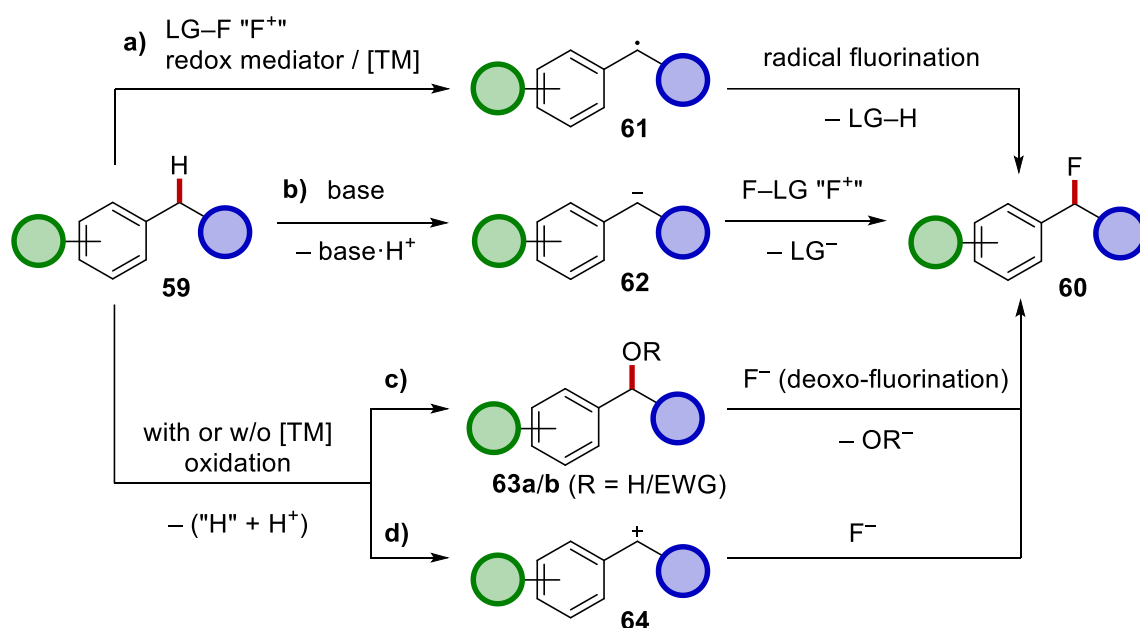
C-H bond									
≈ BDE (kcal/mol)	105	101	98	96	90	88	111	111	133

Figure 1.5-1 BDEs of different C-H bonds.

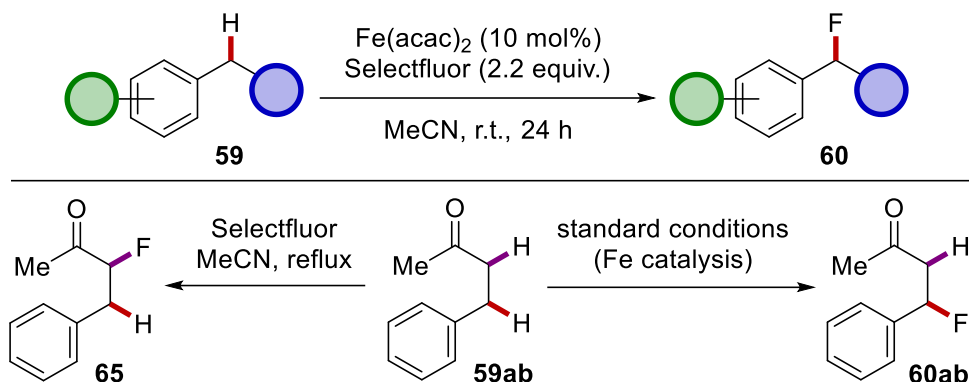
Facile homolytic scission of the benzylic C-H bond by means of PCET, (MS-)CPET,^[111] or HAT yields a conjugation-stabilized sp²-hybridized benzylic radical, which upon further oxidation leads to a benzylic cation. The latter is an excellent electrophile, equally stabilized by conjugation. Both intermediates can be intercepted by amenable reaction partners, namely SOMO-philic reagents, or nucleophiles, respectively. The outstanding reactivity can be utilized for a convenient access of selectively functionalized chemicals with challenging coupling partners. Among the most effortful transformations is the fluorination of organic molecules,^[112] since the fluoride ion is a weak nucleophile on the one hand, and on the other hand, due to the fluorine atom's high electronegativity, it connotes an energetically demanding polarity switch towards becoming an electrophile. Benzyl fluorides are highly electrophilic. From a synthetic perspective, they are themselves valuable substrates for their ability to benzylate electron-rich arenes in the mere presence of strong H-bond donors such as HFIP; a task normally accomplished by a strong *Lewis* acid when other alkyl halides are employed.^[113] The finding by *Paquin* was integrated into

reaction sequences where the intermediary generated benzyl fluoride was used without isolation to accomplish the benzylation.^[114] Generally, the substitution of a H atom by fluorine is a net oxidative processes. Therefore, two major alternatives are conceivable for the fluorination of C–H bonds (**Scheme 1-24**). First, electrophilic fluorine surrogates^[115] can be used to introduce fluorine at electron-rich centers. These reagents have in common that the fluorine atom is covalently bound to an excellent leaving group, thereby becoming the only position for nucleophilic attack. Due to the often harshly basic conditions required for carbanion formation (**Scheme 1-24, b**), electrophilic fluorination is preferably performed *via* a radical pathway (**Scheme 1-24, a**), sometimes mediated by transition metal catalysts. Second, nucleophilic fluoride can attack on electrophilic positions. For this purpose, the C–H bond has to be first oxidatively transformed into an electron-deficient center bearing an oxygen-based leaving group (**Scheme 1-24, c**). The substitution step is in this case termed deoxo(deoxy)-fluorination. Alternatively, a vacant cationic site can be created for a fluorination *via* S_N1 by means of HAT/PCET or electrochemical oxidation (**Scheme 1-24, d**). For health and safety reasons, anhydrous HF is disfavored as nucleophilic fluoride source, while metal fluorides are unpractical due to their often times poor solubility and competing basicity. In this context, nitrogen bases proved advantageous for the creation of easier-to-handle alternatives to HF, the prototype of which is *Olah's* pyridine/HF reagent.^[116] A relatively new development is the DMPU-HF reagent:^[117] a combination that was deduced from the acquisition of relevant parameters for the enhancement of fluoride nucleophilicity. Among the deoxo-fluorinating agents, for decades, DAST was used as a reliable reagent, despite its thermal instability.^[118] Over the years, many stable and selective alternatives were developed,^[119] many of which are based on the sulfonyl fluoride moiety.



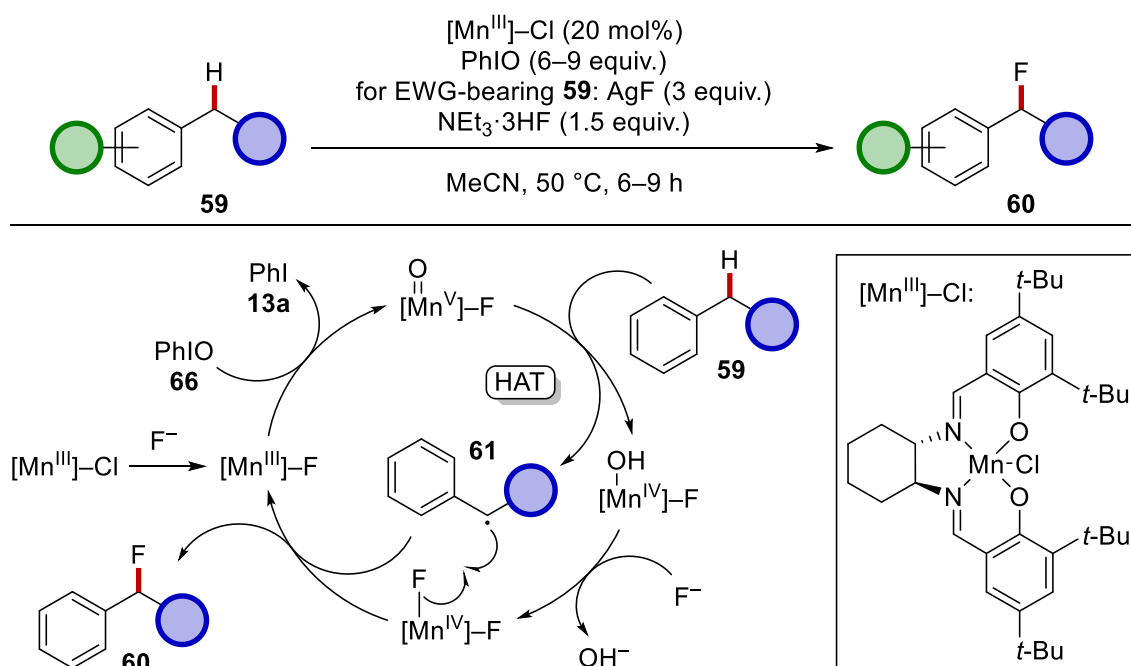
Scheme 1-24 General fluorination strategies and common fluorinating reagents.

Among the first transition-metal catalyzed benzylic C–H fluorinations, the system of *Lectka*^[120] should be mentioned (**Scheme 1-25**). It uses an inexpensive redox-active iron catalyst and Selectfluor as the fluorine source, and operates at room temperature. This example also illustrated the different selectivity in comparison to metal-free electrophilic fluorination, where the functionalization typically occurred at the more acidic C–H bond (**65**). Other metal-mediated systems employed silver,^[121] copper,^[122] and tungsten cluster^[123] catalysts. The latter method uses photoexcitation to activate the redox-catalyst. This principle has also been used in several metal-free approaches.^[124]



Scheme 1-25 Iron-catalyzed benzylic C–H fluorination.

In the same year, *Groves* reported a protocol employing $\text{NEt}_3 \cdot 3\text{HF}$ as an inexpensive nucleophilic fluorine source and an *in-situ*-formed manganese-salen complex as catalyst.^[125] Although electrophilic fluorinating reagents could be avoided, the economic aspect was compromised by the use of overstoichiometric amounts of iodosobenzene **66** and, in case of electron-deficient substrates, additional AgF . The reaction is sustained by the terminal oxidant, which generates a high-valent manganese(IV) species, that abstracts a hydrogen atom from the benzylic substrate **59** to form the radical **61**. The radical fluorine abstraction from the manganese(IV) complex terminates the catalytic cycle, leading to the formation of the fluorinated product **60**.



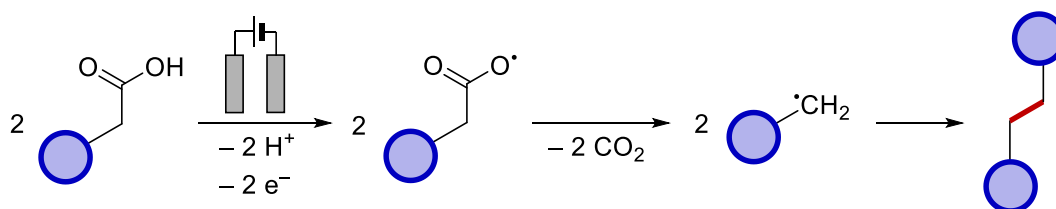
Scheme 1-26 Manganese-catalyzed nucleophilic fluorination.

Despite the economic appeal of chemo-oxidative nucleophilic fluorinations, reports on them are scarce.^[126] Alternative approaches for nucleophilic fluorinations by means of atom-economic electrochemical activation will be discussed in chapter 1.6.2 (*vide infra*).

1.6 Electrochemistry in Organic Synthesis

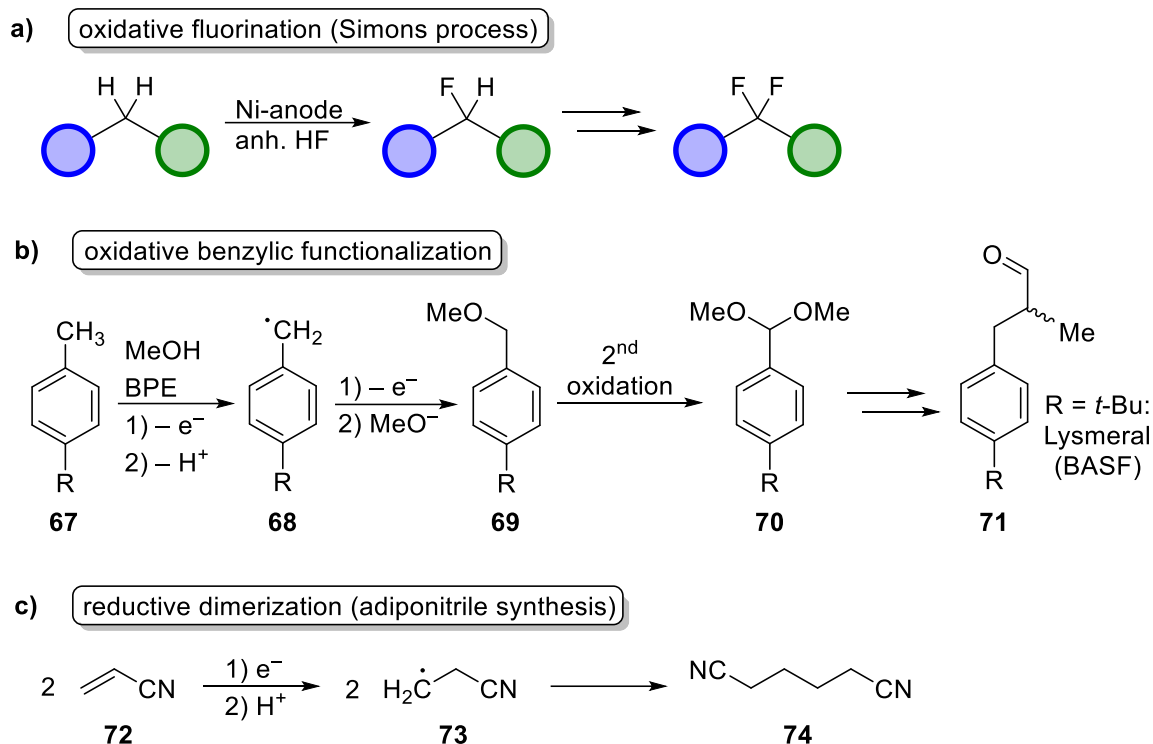
1.6.1 Brief History & General Aspects

Electrochemistry dates back to the early 19th century. Pioneering work by *Volta*^[127] *Petrov*,^[128] *Faraday*,^[129] and the Göttingen scholar *H. Kolbe*^[130] revealed the capability of electric current to enable unprecedented reactivities. The oxidative electro-decarboxylation of aliphatic carboxylic acids to form the corresponding dimeric alkanes *via* radical recombination became the first well-documented organic electrolysis (**Scheme 1-27**).^[131]



Scheme 1-27 Kolbe electrolysis.

The potency of electrolysis was demonstrated in many still indispensable industrial applications.^[132] Inorganic base material electrosyntheses include the chloralkali process^[133] and the Hall-Hérault process^[134] for the production of metallic aluminum. While in the organic section, the oxidative (per)fluorination of organic materials (**Scheme 1-28, a**),^[135] the benzylic oxidation (**Scheme 1-28, b**)^[136] and the reductive adiponitrile synthesis (**Scheme 1-28, c**)^[137] shall be mentioned as methodic milestones. The appeal of electrochemical reactions is justified by the low cost of electrons as a reagent and the possibility to obtain electricity from sustainable energy sources, thereby making electrosynthesis an inherently “green” synthetic method.^[138]

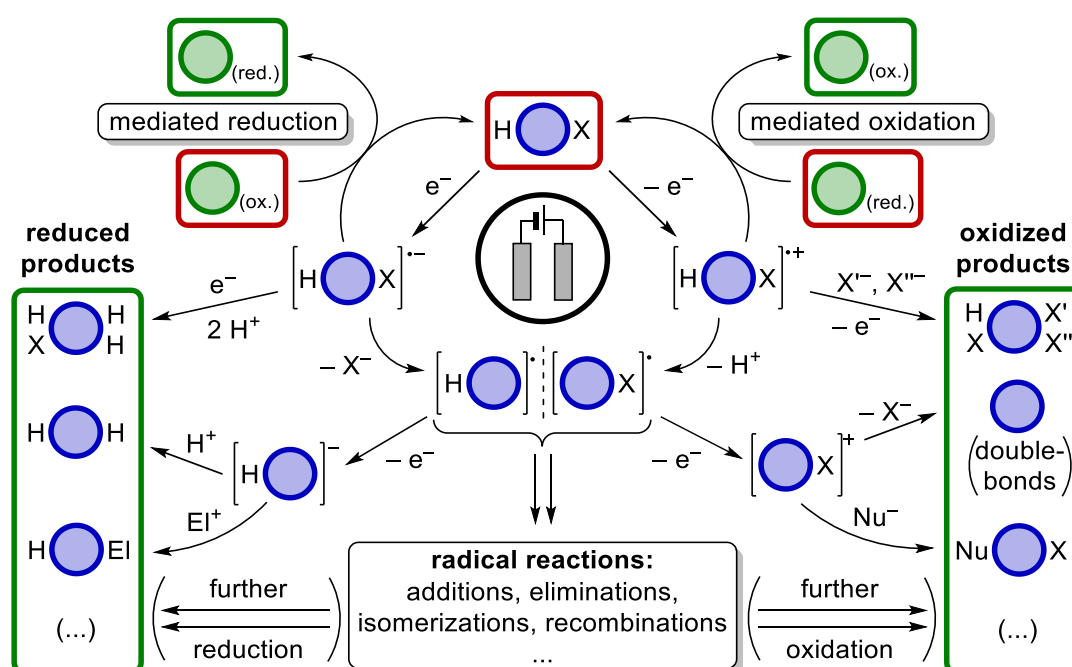


Scheme 1-28 Electroorganic syntheses applied in industry.

Nevertheless, organic electrochemistry has remained a peripheral academic research area until a recent renaissance, which is also reflected in a large number of recent electrosynthesis and -analysis tutorials for organic chemists^[139] and the launch of the first commercial laboratory-scale electrolysis kit as late as in 2017 by IKA.^[140] Otherwise, electrosynthesis is mostly performed with unstandardized equipment, at times leading to poor reproducibility.^[141] The largely untapped potential inspired many researchers to investigate new electrochemical reactivities and apply them in the syntheses of complex molecules and materials.^[136,142]

In electrosynthesis, electrons from an external power source are utilized to induce a chemical reaction. Since the underlying principle is the interconversion of electrical and chemical energy, a polarized conductive surface with adequately tuned potential is to some extent able to mimic the redox activity of chemical reactants in a homogeneous phase. The direction of the electron transfer is dictated by electrode's *Fermi* level,^[143] and the HOMO-, LUMO- and SET-generated SOMO levels of the species in solution. The oxidation or reduction power of an electrode can be manipulated almost unrestrictedly to the precise

needs of an amenable reaction partner. After an initial electron transfer has taken place, the primary products are mostly highly reactive intermediates, that undergo follow-up reactions with nucleophiles, electrophiles, acids, bases, and further electron transfers (**Scheme 1-29**).^[144] Importantly, these elementary steps can in principle be undertaken by any suitable species in a given system. Therefore, reactions can be designed with an emphasis on the electrochemical activation of the substrates, a reagent, or the catalyst.^[145] In recent years, considerable attention was devoted to the additional photo-irradiation of electrochemical systems. The combination of two orthogonal electron excitation methods can enable or facilitate electron transfers that are not achievable by only one of the techniques or only under highly forcing conditions.^[146]



Scheme 1-29 General reaction pathways in organic electrochemistry.

Compared to the execution of classic syntheses, electrolyses need to be carried out in electrically conductive reaction media due to the spatially separated buildup of electric charge and the necessity for their compensation. The anodic oxidation of the electron donor with the lowest oxidation potential and the cathodic reduction of the electron acceptor with the least negative reduction potential are the thermodynamically favored reactions to close the electric circuit. However, energy barriers, that manifest themselves as overpotentials, can kinetically disfavor certain electron transfers and therefore lead to different selectivities. Conversely, electrolyses conducted at excessive overpotentials can trigger

undesired reactions that otherwise would be kinetically and/or thermodynamically discriminated. The overpotential at an electrode is largely a consequence of the underlying electron transfer (ET) mechanism. An ET (also between two particles in homogeneous solution) can take place either in terms of a reactant proximity-enabled outer-sphere mechanism,^[147] or an inner-sphere mechanism,^[148] that is characterized by strong orbital interactions in an activated complex between donor and acceptor. Inner-sphere ETs are therefore dependent on the suitability of the electrode surface material. Typical examples of the importance of the choice of electrode materials are the use of platinum electrodes for efficient proton reduction or the obtainment of carbocations instead of radicals (*Kolbe* reactivity) from carboxylic acids in the *Hofer-Moest* reaction, when the platinum anode is replaced by a carbon-based material.^[131] Overoxidation or overreduction can nevertheless take place, despite a careful evaluation of the electrode materials.^[149] A general strategy to increase the stability of the substrate is to perform an indirect electrolysis, using a mediator that is able to selectively shuffle the electrons between the substrate and the electrode.^[150] Sometimes, in avoidance of counterproductive electron transfers, a separation of the anodic and the cathodic compartment is needed, complemented by a semi-permeable diaphragm or salt bridge to allow charge balancing. Naturally, this division increases the total resistance of an electrochemical cell. In order to minimize resistivity-caused overpotentials and thermal energy losses, in most cases, conductivity-supporting salts are added, the majority of which reach their highest activity in polar solvents. Alternatively, high resistivities can be compensated by special reactor designs, such as flow cells.^[151] Apart from less common contactless bipolar electrolyses (BPE)^[152] and alternating current electrolyses (ACE),^[153] there are two operational modes mainly employed by organic electrochemists.^[154] On the one hand, constant potential electrolysis (CPE, **Figure 1.6-1, a**) with variable current offers ideal selectivity, but is compromised by a more complicated setup including a reference electrode, and often longer reaction times. On the other hand, in constant current electrolysis (CCE, **Figure 1.6-1, b**), the potential is automatically adjusted to sustain the kinetically most feasible combination of reduction and oxidation in the system, thereby operating at minimum overpotential as long as the mass transport does not fall below the set electrolysis rate due to substrate depletion. Consequently, CPE is the method of choice for challenging reactions that require careful control of chemoselectivity over their whole course, while CCE is the convenient alternative for less sensitive transformations.

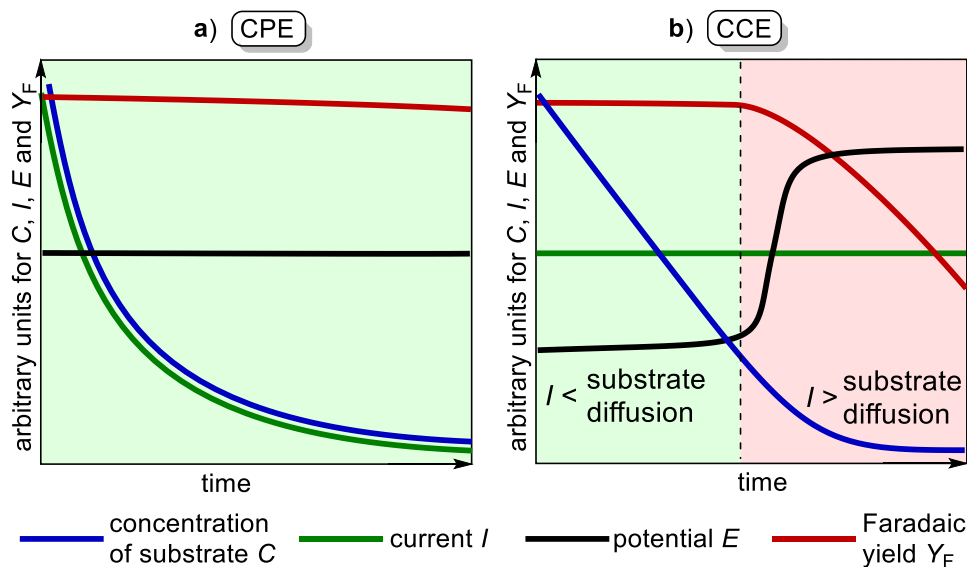


Figure 1.6-1 Time course of a) CPE and b) CCE.

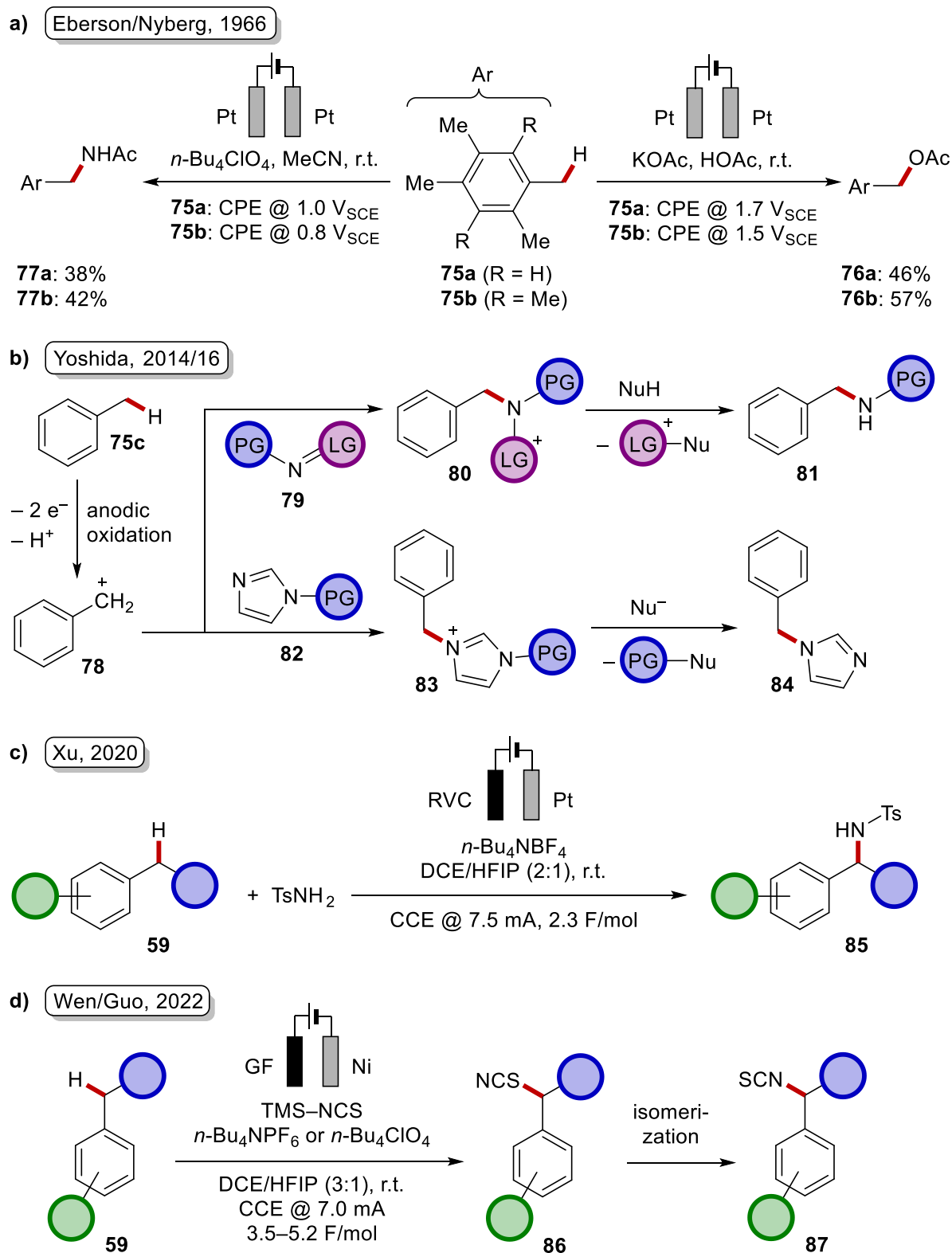
For the successful outcome of electrochemical reactions, the electricity-related parameters must be optimized in addition to the purely chemical ones, thereby adding to the dimensionality of the problem. Moreover, these parameters are often interdependent and an orthogonal treatment is hardly possible in these cases. In this regard, examining one variable at a time (OVAT) is limitedly productive, and the implementation of high-throughput techniques and machine learning becomes especially attractive.^[155]

1.6.2 Electrochemical Benzylic C–H Fluorination and other Benzylic C–H Functionalizations

The role of electricity in electrochemical reactions can be diverse (*vide supra*, chapter 1.6.1). A self-evident strategy for the initiation of a reaction cascade is the conversion of a reagent into a reactive state by oxidation or reduction. This concept was applied by *Simons* (*vide supra*),^[135] enabling the efficient (per)fluorination of organic molecules by electricity in inexpensive anhydrous HF. To this day, this landmark reaction remains essential. There are several theories that try to pin down the mechanism leading to the tremendous reactivity, but it is majorly believed that the NiF₂ passivation layer releases molecular or radical fluorine upon the further oxidation of the nickel centers at highly positive electrode potentials.^[156] Unsurprisingly, these harsh reaction conditions do not allow for selective fluorination and usually all available C–H bonds in a molecule get fluorinated. A more

selective approach is matching the oxidation or reduction power of the working electrode to the potential that is needed for the execution of the most facile electron transfer of the valuable substrate or a suitable mediator. When the innate electronic structure of a molecule allows for site-selective electrochemical bond activation, the employment of metal catalysts and directing groups can be avoided, adding to the overall sustainability of the transformation.

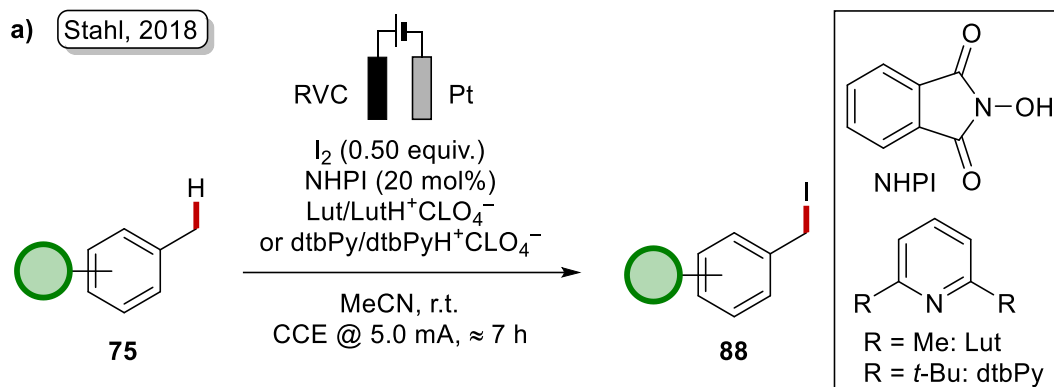
As stated earlier, oxidative benzylic radical and consecutive cation formation is in general comparably facile. The intermediates can be also accessed by electrochemical oxidation of the neighboring aromatic core, since the restoration of the aromatic π -system to form the benzylic radical upon deprotonation is favored. The first studies on the functionalization of anodically generated benzylic cations in terms of C–H acetoxylation^[157] and acetamidation^[158] were conducted in the 1960s by *Ebersson* and *Nyberg* (**Scheme 1-30, a**). Since then, numerous reliable protocols for diverse C–Het bonds formations were elaborated. Several amination reactions were developed by *Yoshida* using the cation-pool strategy (**Scheme 1-30, b**)^[159] with protected amines **79** to prevent the amine coupling products **80** from overoxidation. Inspired by these pioneering studies, *Xu* developed a more atom-economic direct amination that omitted the deprotection (**Scheme 1-30, c**).^[160] Very recently, an isothiocyanation was developed that takes advantage of the isomerization of benzylic thiocyanates **86** as the primary products of the transformation (**Scheme 1-30, d**).^[161]



Scheme 1-30 Electrochemical benzylic C–N bond formations.

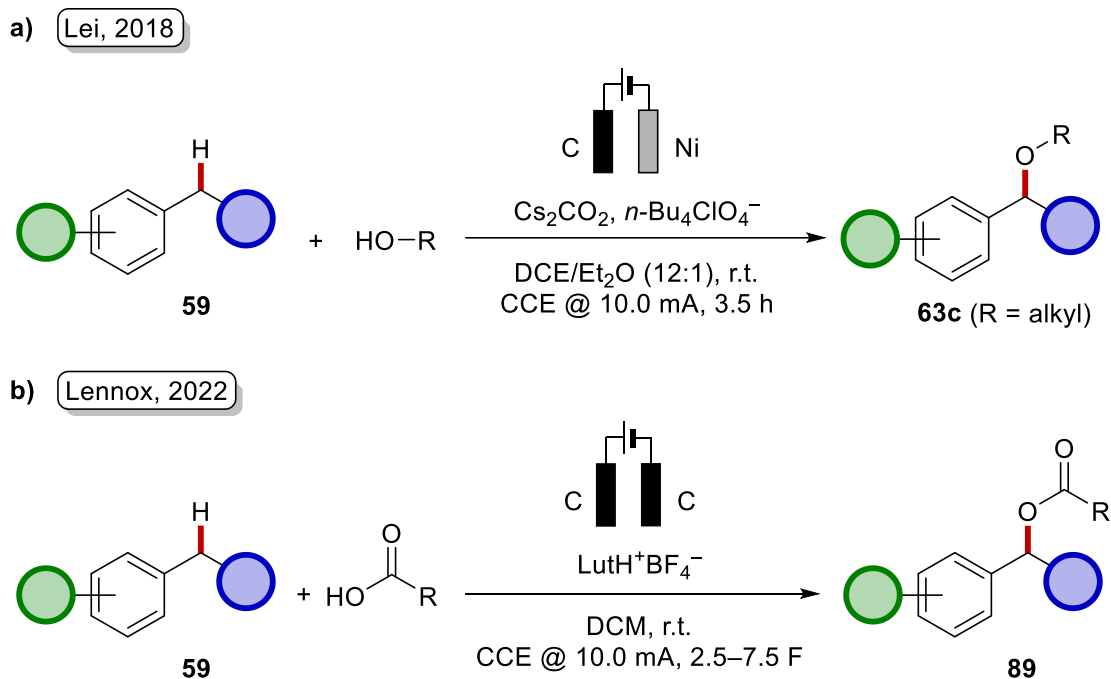
In 2018, *Stahl* reported a *N*-hydroxyphthalimide (NHPI)-mediated iodination (**Scheme 1-31**).^[162] The benzylic radical was generated by HAT to the oxidized counterpart of NHPI:

phthalimide-*N*-oxyl (PINO). The iodine radical abstraction from molecular iodine led to the desired product.



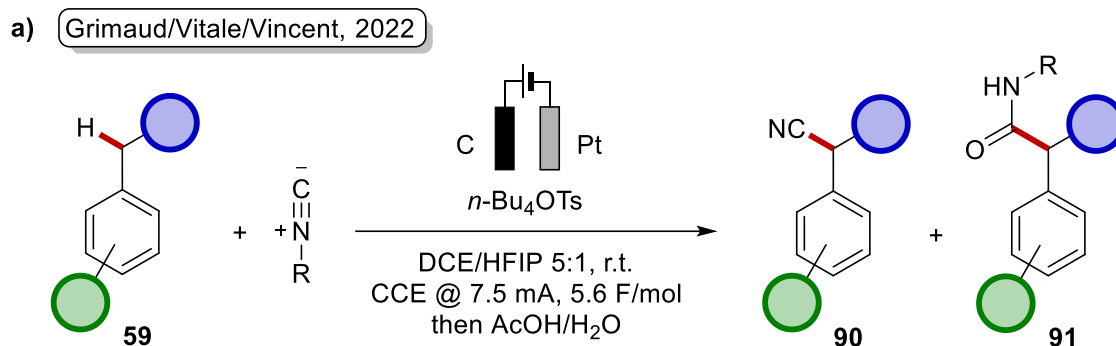
Scheme 1-31 Electrochemical benzylic iodination.

Regarding the utilization of *O*-nucleophiles, etherifications were reported in 2018 by the *Lei* group (**Scheme 1-32, a**).^[163] While many oxygenation protocols rely on (co-)solvent quantities of the corresponding alcohol, *Lei*'s method displayed a satisfactory performance with only few equivalents. A similarly effective C–O bond formation reaction was recently reported by *Lennox*,^[164] using free carboxylic acids as the acyloxylating reagents (**Scheme 1-32, b**).



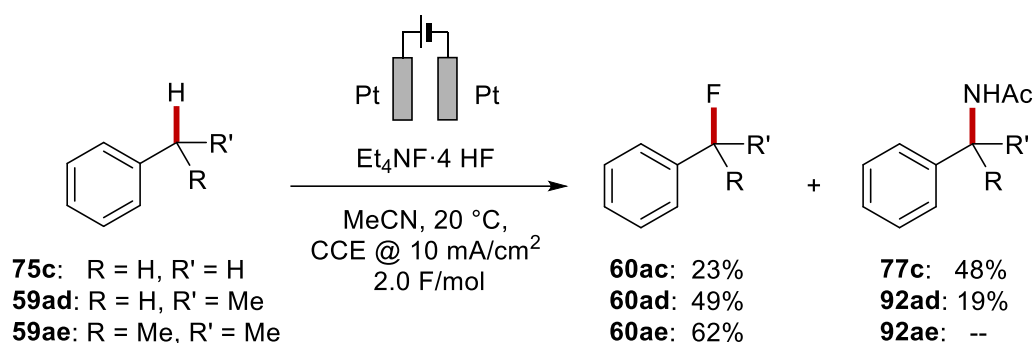
Scheme 1-32 Electrochemical benzylic oxygenations.

A recent study by *Grimaud/Vitale/Vincent* also disclosed the construction of benzylic C–C bonds in terms of carbamoylation and cyanation by employing isocyanates as C-nucleophiles (**Scheme 1-33**).^[165]



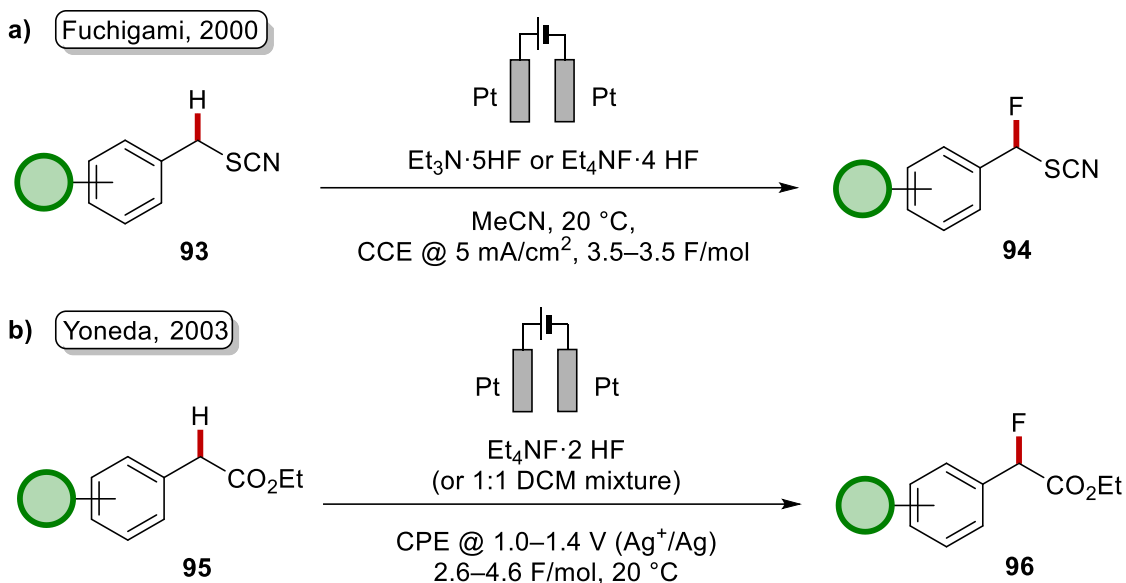
Scheme 1-33 Electrochemical benzylic C–C bond formation.

While in the abovementioned transformations the interception of the benzylic carbocation was accomplished by moderate-to-good nucleophiles, the extension of this principle towards fluoride is highly challenging. The high electronegativity of the fluorine atom as accountable for the fluoride anion's poor nucleophilicity,^[166] which is crucial for the interception of the benzylic cation. This weakness remained an issue throughout decades of developments of electrochemical fluorination reactions, where MeCN has been almost invariably the solvent of choice.^[167] MeCN forms highly conductive electrolytes due to its high polarity and low viscosity. Moreover, it is inert towards radicals and possesses good anodic stability. In practice, the application of MeCN in benzylic fluorination revealed itself as being far from ideal due to competing *Ritter*-type nucleophilic attack at the benzylic carbocation, forming acetamidated products. In a 2002 and follow-up 2005 study, *Fuchigami* specified that acetamidation is favored with a decreasing substitution pattern in the benzylic position, while fluorination is preferred at positions generating more stable benzylic cations (**Scheme 1-34**).^[168]



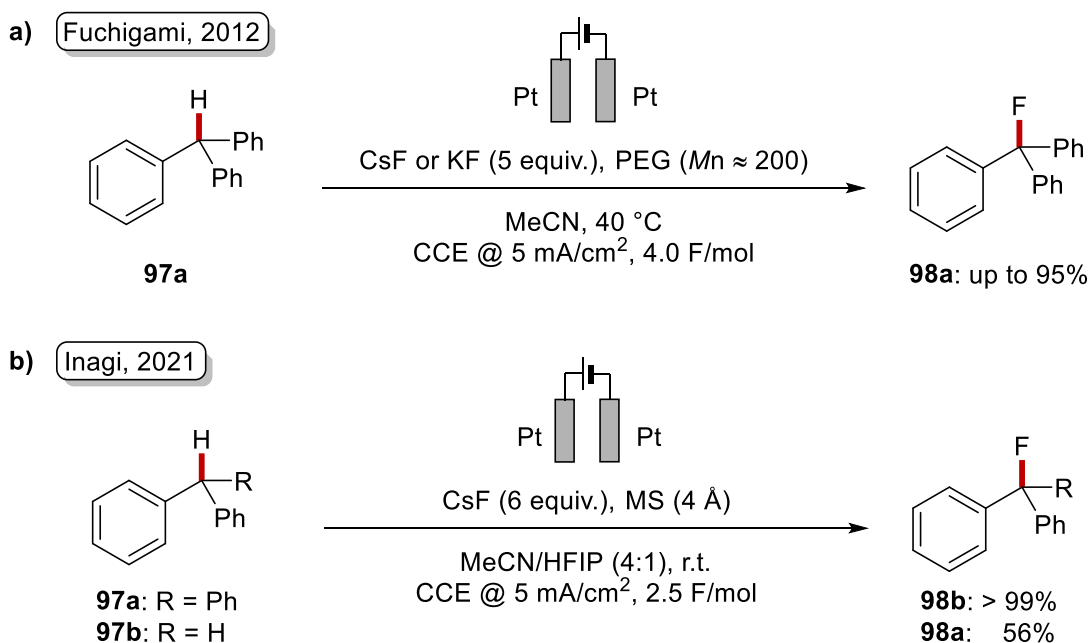
Scheme 1-34 Fuchigami's study on fluorination/acetamidation selectivity depending on the benzylic substitution grade.

To prevent the formation of these solvent-caused byproducts, other solvents, that do not possess pronounced *Lewis*-basicity, were tested. In particular, tetrahydrothiophene dioxide (THTD, sulfolane) did not show any nucleophilic reactivity, but caused fluorination of the aromatic core as a side reaction.^[169] Subsequently, the selectivity in ammonium/HF-based ionic liquids as solvents for the fluorination of unactivated benzylic substrates was studied by *Middleton*^[170] and *Morita*^[171] and it was found that substantial amounts of other fluorinated byproducts was inevitable. A feasible protocol for the fluorination of benzylic substrates was developed by *Fuchigami*, where ionic liquids with high HF content, such as Et₄NF·4HF and Et₃N·5HF were used.^[172] These electrolytes with excellent anodic stability^[173] proved powerful fluorine sources, preventing the acetamidation by MeCN (**Scheme 1-35, a**). The employed substrates were benzyl thiocyanates **93**, which due to the electron-withdrawing substituent have a greater acidity and facilitate the deprotonation in the overall acidic system. Phenylacetic acids **95** as another class of activated substrates were selectively fluorinated with HF-based ionic liquids as the electrolyte or with DCM as the cosolvent, thereby excluding the possibility to form acetamidated byproducts (**Scheme 1-35, b**).^[174]



Scheme 1-35 Electrochemical benzylic fluorinations of activated substrates with ionic liquid fluoride sources.

In search of a better selectivity, interesting concepts were revealed, namely that metallic fluorides could be used instead of HF-based fluoride sources, that can be activated either by the use of PEG (**Scheme 1-36, a**)^[175] or fluorinated alcohols (**Scheme 1-36, b**)^[176]. However, the applicability of these approaches were severely limited, displaying appreciable reactivity only with highly stabilized benzylic cations, such as triphenylmethane **97a**.



Scheme 1-36 Benzylic electrochemical fluorination (ECF) with metallic fluoride.

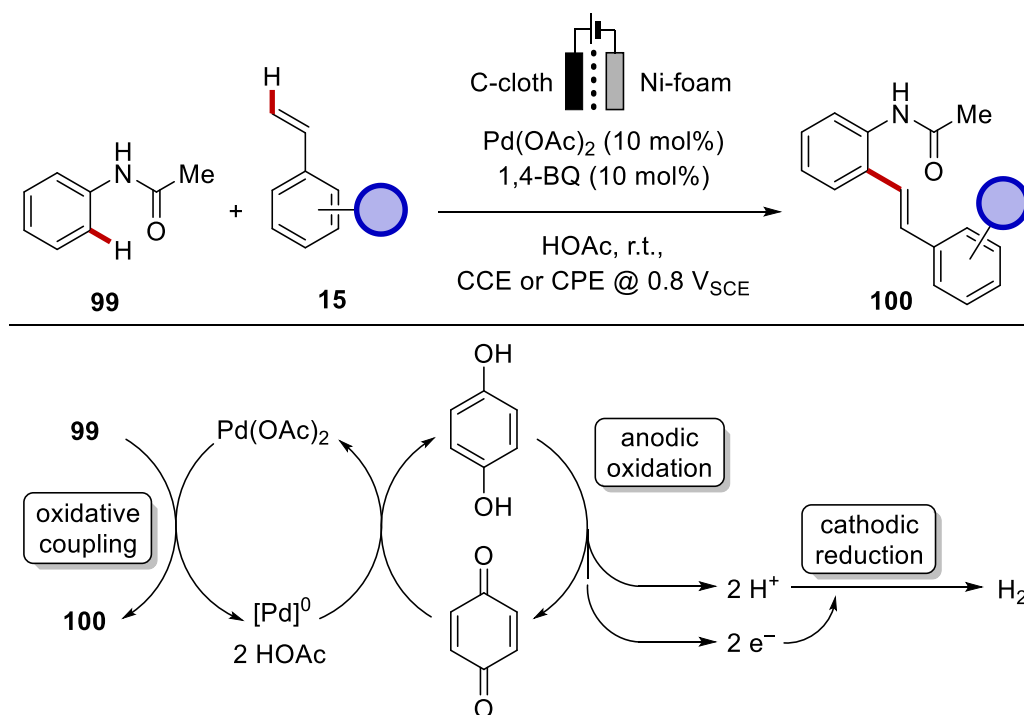
1.6.3 Electrochemical C–H Activation

Transition metal-catalyzed C–H activation is an inherently sustainable method to initiate a functionalization sequence on a molecule. However, in oxidative couplings, the need for stoichiometric amounts of oxidants is an environmental and financial burden. In view of the possibility to obtain electricity from green sources at costs that are several magnitudes lower than chemical oxidants, the idea of combining both methods emerged, leading to the concept of metalla-electrocatalysis.^[142d,177] Therein, electron transfers are mostly used for catalyst regeneration or the triggering of other oxidation state-dependent elementary steps of metalated intermediates.^[145]

1.6.3.1 With Noble 4d and 5d Late Transition Metals

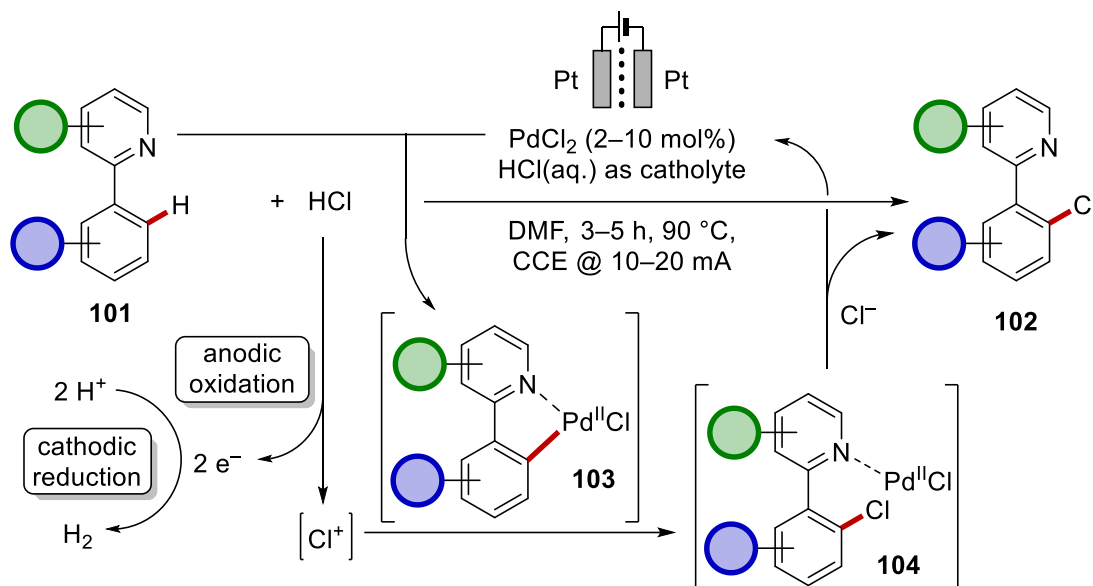
1.6.3.1.1 Palladium

The first catalytic C–H activation, that was promoted by means of electricity, was reported by *Amatore* and *Jutand* in 2007^[178] as a modification of a *Fujiwara-Moritani*-type reaction^[179] on benzamides **99** (Scheme 1-37). Catalytic amounts of 1,4-benzoquinone (1,4-BQ) were necessary to mediate the reoxidation of palladium(0) to palladium(II). Since palladium(II) is prone to cathodic deposition, the reaction was carried out in a divided cell.



Scheme 1-37 First electrochemical C–H activation with benzoquinone mediation by *Amatore/Jutand*.

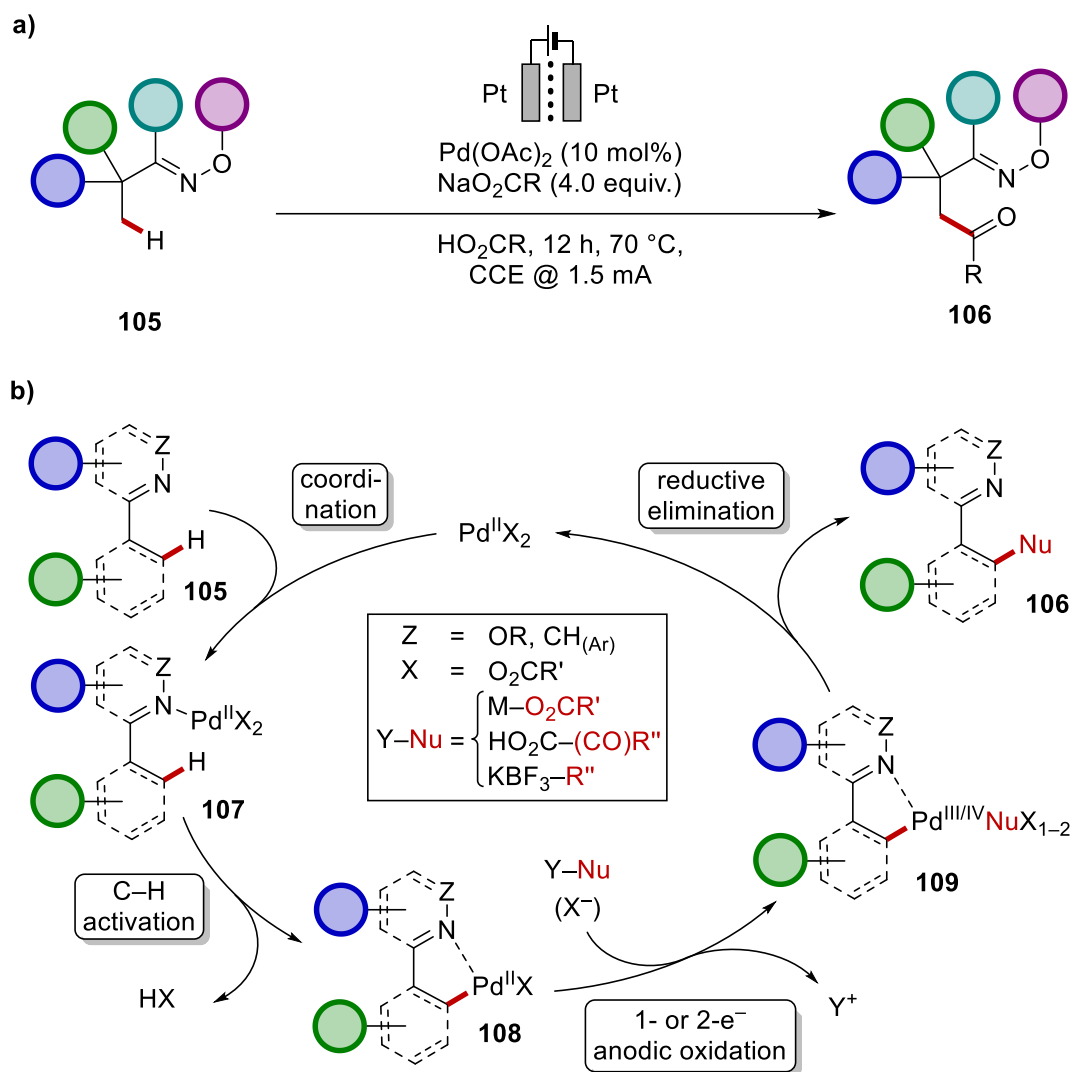
The next milestone was accomplished by *Kakiuchi* in 2009, reporting a pallada-electro-C–H chlorination of phenylpyridines **101** (Scheme 1-38).^[180] In contrast to *Jutand*'s work,^[178] where the catalyst was regenerated by mediated anodic oxidation, the electricity was instead used to oxidize the inexpensive aqueous hydrogen chloride coupling partner to a reactive chloronium electrophile, which enters a net-redox-neutral catalytic cycle. With a cross-dehydrogenative balance, the atom economy of conventional coupling with NCS was substantially improved. The method was extended to brominations and iodinations.^[181]



Scheme 1-38 *Kakiuchi*'s seminal study on electrochemical C–H halogenation.

Later, *Mei* disclosed an oxime-directed acyloxylation of C(sp³)–H bonds by palladium catalysis (Scheme 1-39).^[182] The carboxylic acid coupling partner is employed as solvent, while the corresponding sodium salt is used as base. The reaction proceeds through carboxylate-assisted C–H activation of the pre-coordinated substrate **107**, followed by anodic oxidation of intermediate **108**, to generate a high-valent palladium(III) or palladium(IV) species **109** that undergoes facile reductive elimination to form the desired product **106**. This study is an exemplary case of the facilitation or induction of elementary steps by the change of the oxidation state. In a mechanistically similar fashion, the same group achieved C(sp²)–H acetoxylation,^[183] as well as acylations with glyoxalic acids and alkylations with alkyl trifluoroborates,^[184] while the groups of *Budnikova* and *Lei* developed protocols for a pyridine-directed C(sp²)–H phosphonation,^[185] and an

intramolecular C(sp²)-H amination towards the synthesis of pyrido[1,2-a]benzimidazoles,^[186] respectively.

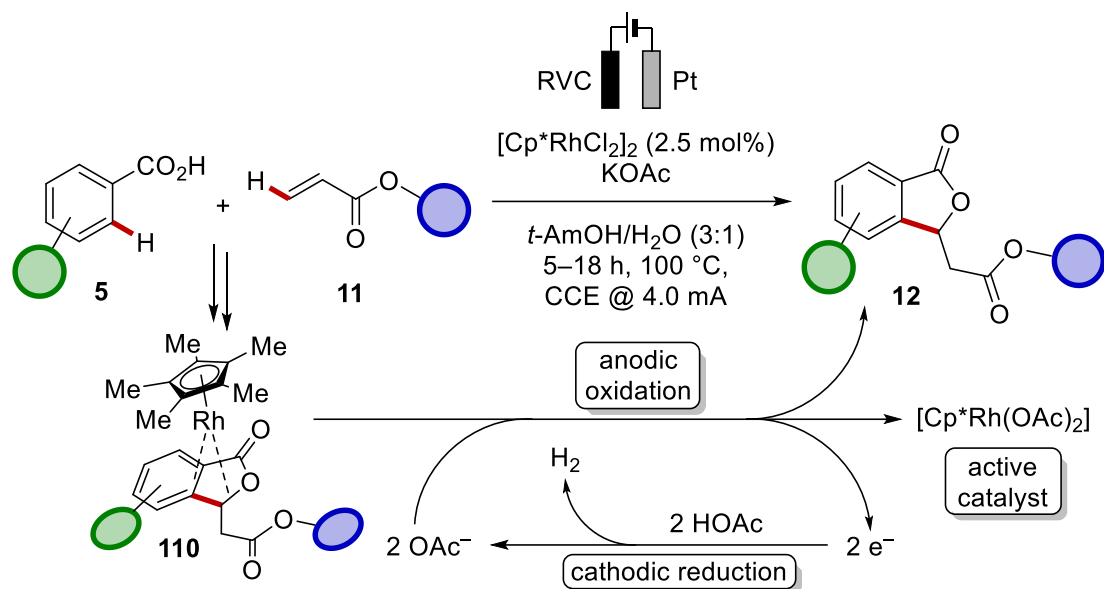


Scheme 1-39 a) Pallada-electro C-H oxygenation by *Mei* and b) general catalytic cycle for oxidation-induced reductive elimination-type functionalization with strong *N*-directing groups.

1.6.3.1.2 Rhodium & Iridium

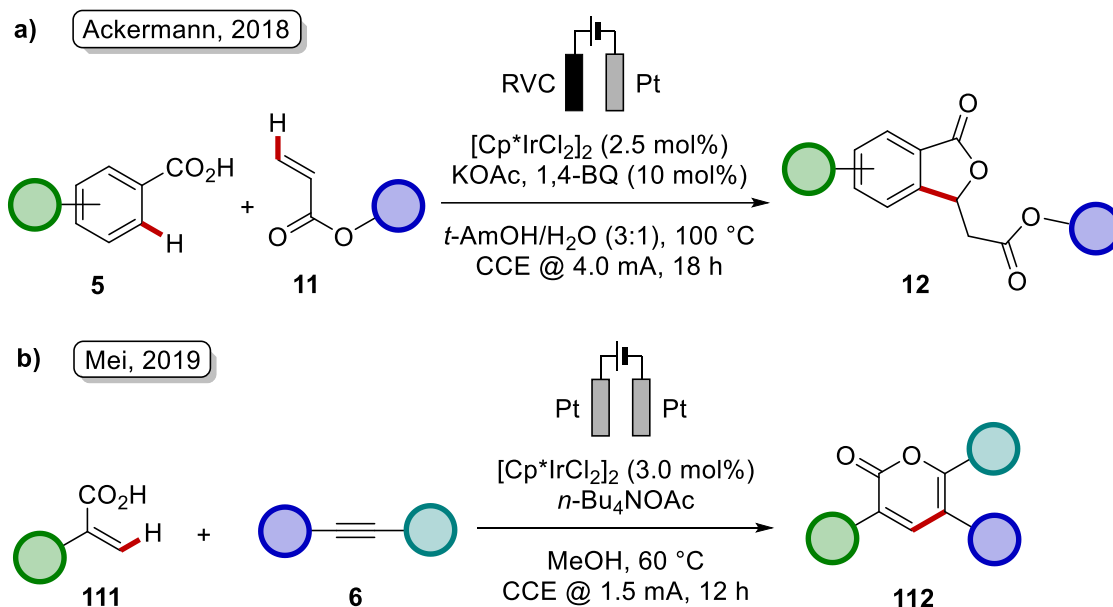
Considering the multitude of highly efficient rhodium-catalyzed oxidative couplings by C-H activation, it is rather surprising that the first report on an electrochemically-driven transformation of this type was issued as late as in 2018 by *Ackermann* (**Scheme 1-40**).^[187] In this protocol, benzoic acids **5** and acrylates **11** were coupled in a twofold C-H activation with subsequent intramolecular *oxa-Michael* addition to form a phthalide scaffold **12**. A slight preference of electron-rich benzoic acids was observed in competition experiments, being suggestive of an activation of the arene C-H bond in a BIES-type mechanism. The

electricity triggers an oxidation-induced decoordination of the product from a proposed rhodium(I) sandwich complex **110**, thereby restoring the active rhodium(III) catalyst. The reaction conditions were rather mild, giving optimal results in a non-toxic *t*-AmOH/water mixture. Molecular H₂ was formed as only byproduct.



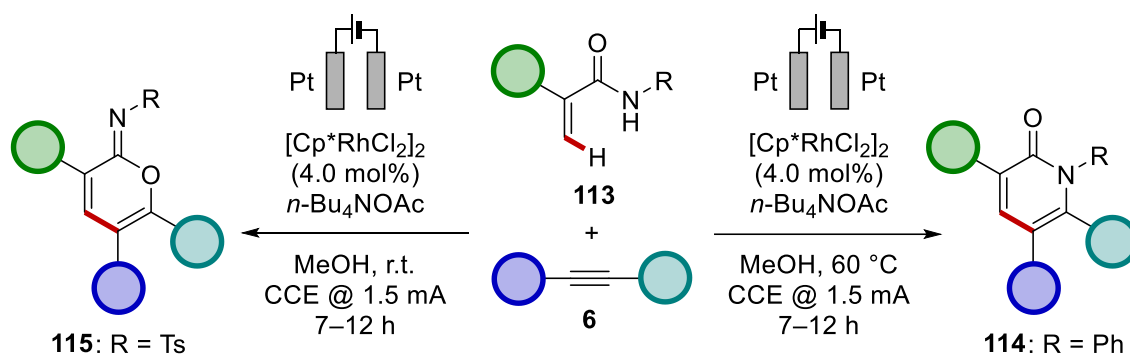
Scheme 1-40 First report on rhoda-electro-catalyzed C–H activation by *Ackermann*.

An analogous reactivity was also achieved with iridium catalysis (**Scheme 1-41, a**).^[188] However, the oxidation-induced product release from the iridium analogue of intermediate **110** was aided by 1,4-BQ as redox mediator. Another notable irida-electro-catalyzed transformation was achieved by the *Mei* group, who were able to construct α -pyrones **112** from acrylic acids **111** (**Scheme 1-41, b**).^[189]



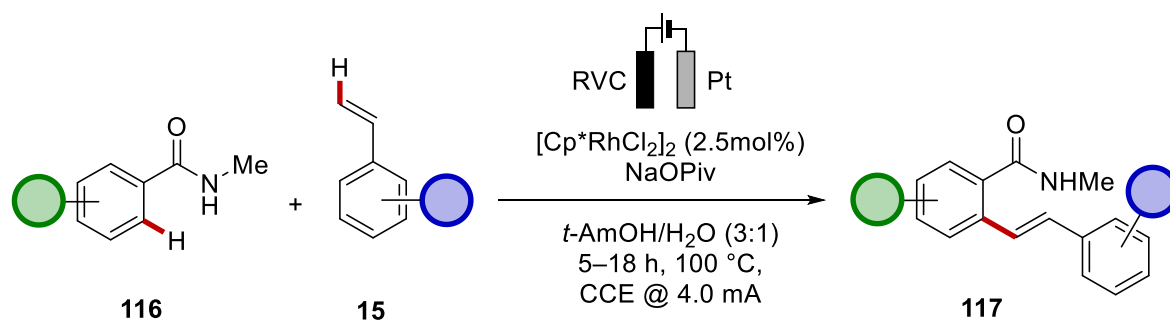
Scheme 1-41 Irida-electro-catalyzed C–H activation.

In a later study, *Mei* could show that acrylamides **113** undergo similar transformations with rhodium catalysis, forming either α -pyridones **114** or cyclic imidates **115**, depending on the substitution pattern and with slightly different conditions (Scheme 1-42).^[190]



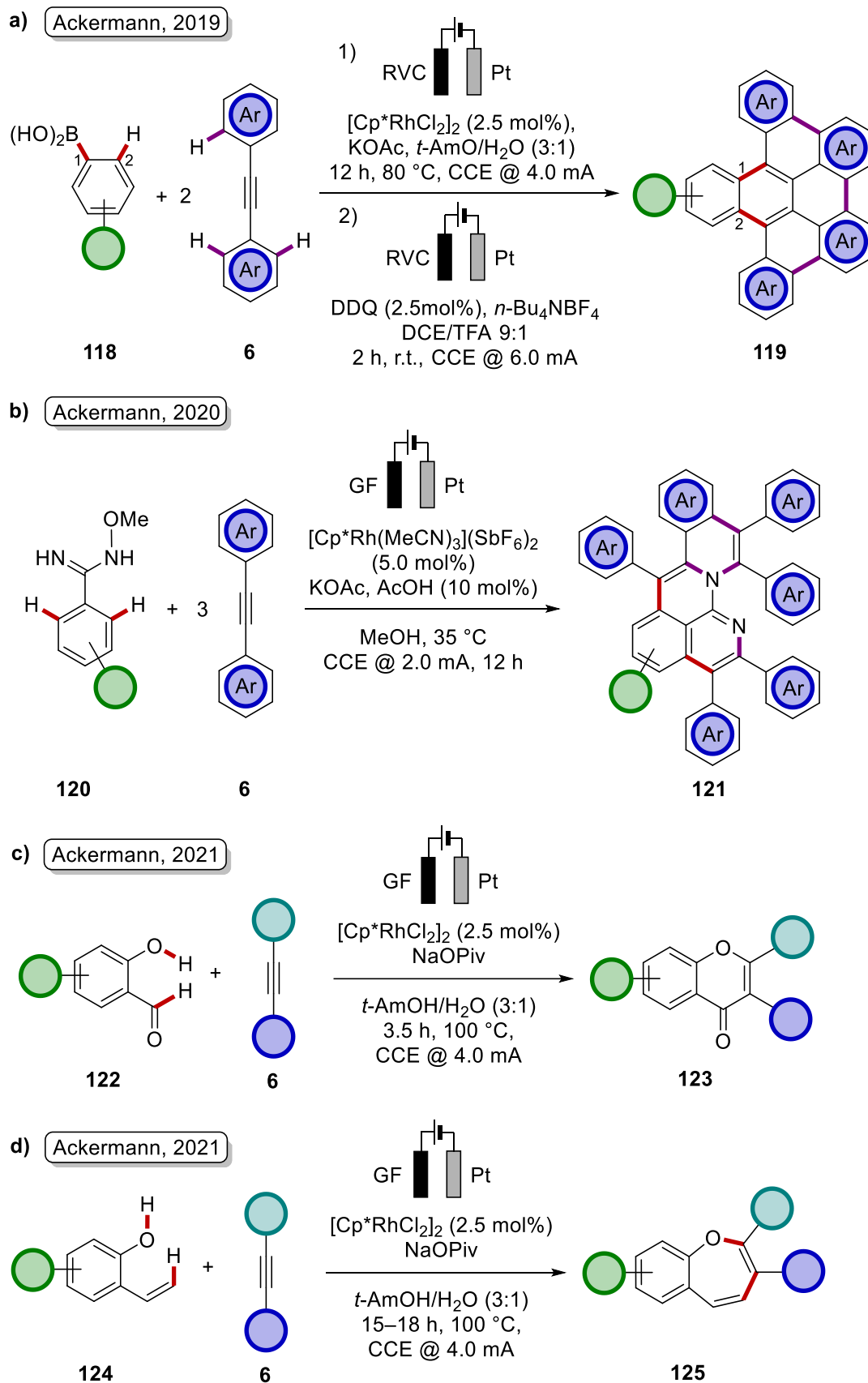
Scheme 1-42 Annulation of acrylamides **113** with alkynes **6** by rhoda-electrocatalysis.

After these studies and the development of an electrochemical alkenylation *via* C–C bond activation (discussed in chapter 3.1),^[191] the *Ackermann* group revealed a rhoda-electrocatalyzed alkenylation of benzamides **116** (Scheme 1-43).^[192] Notably, intramolecular *aza-Michael* addition to afford cyclized products was not observed.



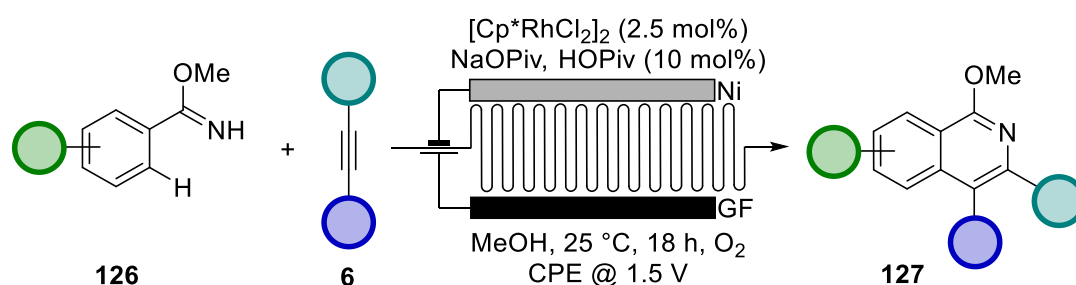
Scheme 1-43 CH Alkenylation of benzamides **116** by rhoda-electrocatalysis.

Rhodium catalysis has proven a powerful tool in various annulation reactions. In 2019, a [2+2+2] cyclization *via* C–B/C–H activation was developed to furnish tetra-arene-substituted naphthalenes **45**.^[193] The arene substituents could be further annulated by means of DDQ-mediated electro-oxidation to yield polycyclic aromatic hydrocarbons (PAHs) **119** (**Scheme 1-44, a**). The study served as basis for a domino alkylation of *N*-methoxy benzimidamides **120** to form polycyclic *aza*-hydrocarbons **121** (**Scheme 1-44, b**).^[194] Other structural motifs, that were assembled by rhoda-electro-catalyzed alkyne annulations with cost-effective starting materials, include chromones **123** (**Scheme 1-44, c**)^[195] and benzoxepines **125** (**Scheme 1-44, d**).^[196]



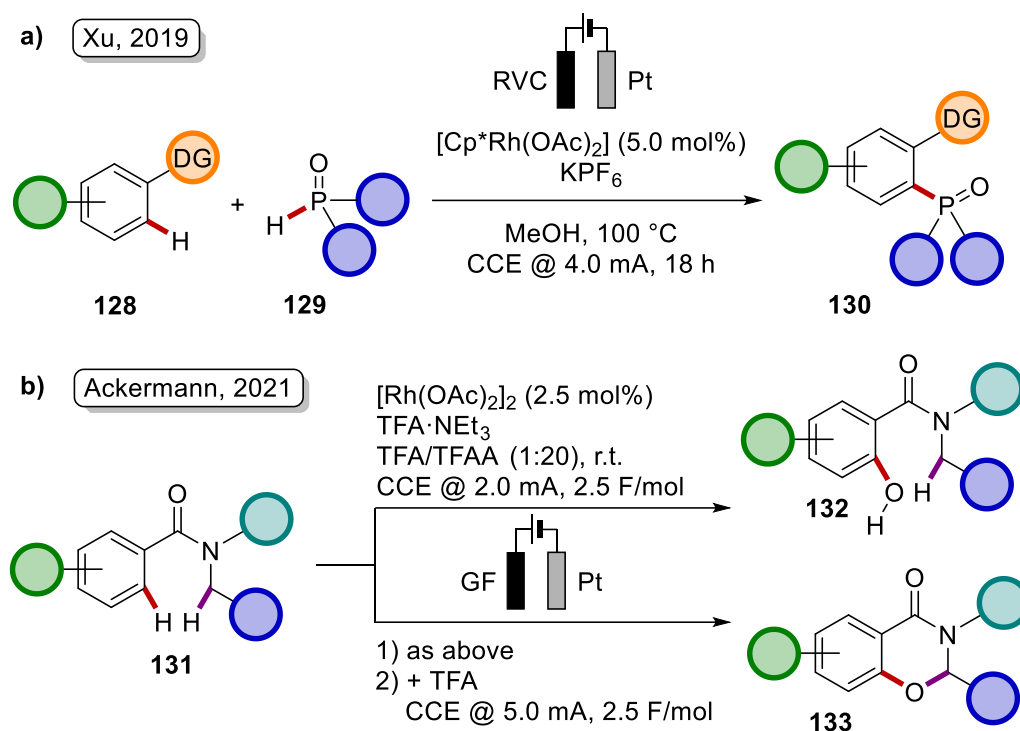
Scheme 1-44 Alkynylnative annulations by rhoda-electrocatalysis developed by *Ackermann*.

Rhoda-electrocatalysis was also demonstrated to proceed efficiently in flow setups, exemplified with benzimidate **126** annulations by alkynes **6** to afford isoquinolines **127** (Scheme 1-45).^[197]



Scheme 1-45 Rhoda-electro-catalyzed assembly of isoquinolines **127** in flow.

Besides the multiple varieties of C–C bond formations, the use of rhoda-electrocatalysis was extended towards the $\text{C}(\text{sp}^2)\text{--H}$ functionalization with heteroatoms. *Xu* achieved a scalable *N*-heterocycle-directed phosphorylation of arenes **128** with secondary phosphine oxides **129** (Scheme 1-46, a).^[198] More recently, the *Ackermann* group reported an oxygenation protocol with bimetallic rhodium catalysis (Scheme 1-46, a).^[199] Interestingly, the base assisted C–H activation step was determined to be induced by the oxidation of the bimetallic rhodium species, thereby increasing its *Lewis*-acidity and electrophilicity of the active catalyst. The amide directing group of the product **132** could be further functionalized in a consecutive a *Shono*-type oxidation^[200] at higher current densities, leading to cyclized products **133**. This bifunctional reactivity impressively illustrated the different selectivities of metalla-electrocatalysis and metal-free C–H functionalization in electrochemical reactions.

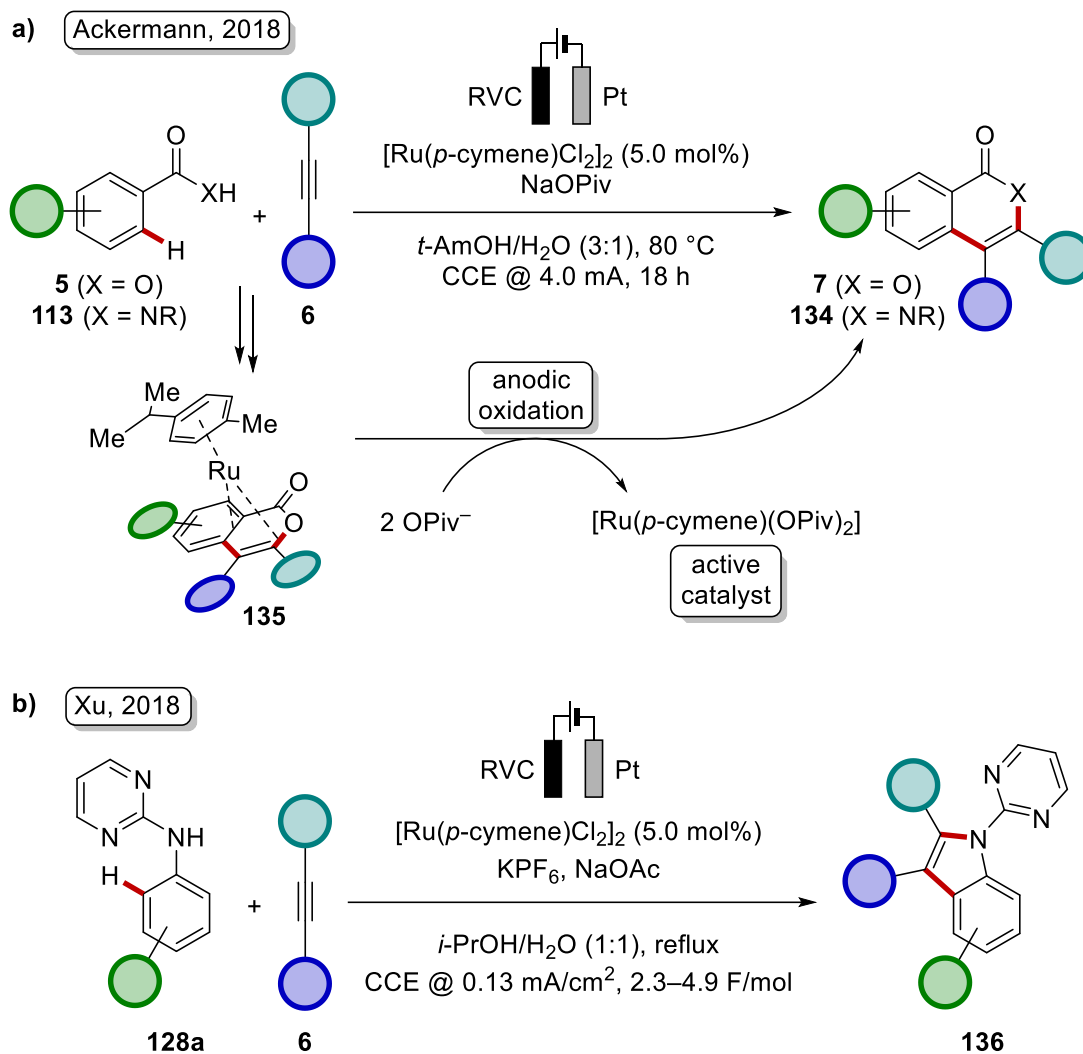


Scheme 1-46 C–H functionalization with heteroatoms by rhodium catalysis.

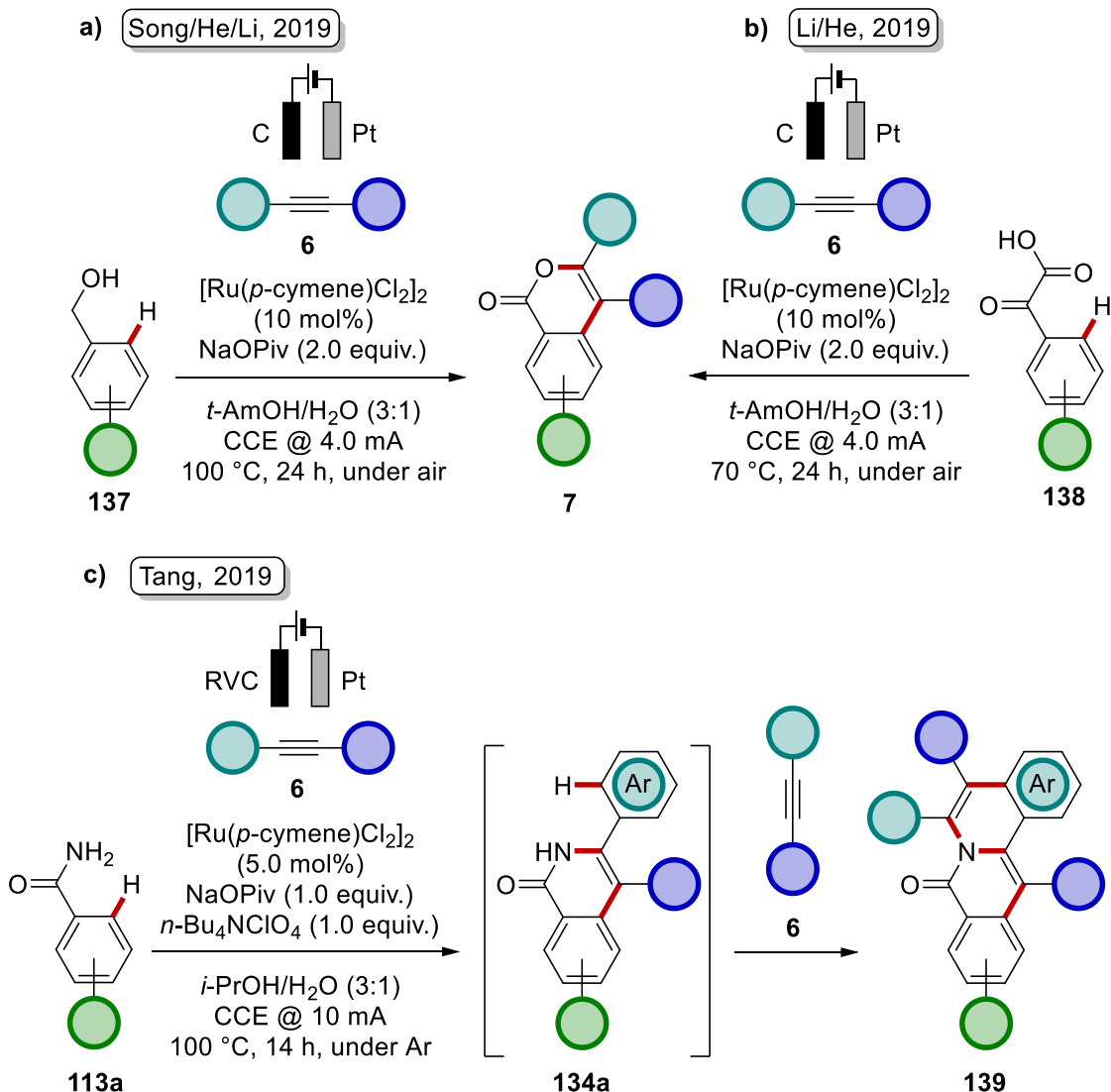
1.6.3.1.3 Ruthenium

The potential of electrochemically-driven ruthenium catalysis was independently unlocked by *Ackermann* and *Xu* in 2018, showcased with the alkynylative annulation towards isocoumarin **7** or isoquinolone **134** (Scheme 1-47, a),^[201] and indole motifs **136** (Scheme 1-47, b),^[202] respectively. Both approaches employed a ruthenium(II) catalyst, that is regenerated by anodic oxidation from a ruthenium(0) intermediate. In the study of *Ackermann*, C–H activation likely occurs by means of BIES, as suggested by the faster reaction of electron-rich benzoic acids. Moreover, the key sandwich intermediate **135** was isolated and oxidation-induced product decooordination was confirmed experimentally. Several other methods were subsequently developed to construct the isocoumarin scaffold **7** by ruthenium electrocatalysis. In a study by *Song*, *He* and *Li*, benzylic alcohols **137** undergo ruthenium-mediated anodic oxidation to the corresponding coordinated benzoic acids, which then followed the catalytic functionalization pathway disclosed by *Ackermann* (Scheme 1-48, a).^[203] A similar protocol by the *Li* and *He* groups utilized glyoxalic acids **138** as the starting material,^[204] which prior to entering the abovementioned benzoate functionalization sequence, undergo ruthenium-mediated oxidative decarboxylation

(Scheme 1-48, b). Ackermann's isoquinolinone synthesis was further extended by Tang towards the synthesis of polycyclic arenes **139** (Scheme 1-48, c).^[205] When *N*-unsubstituted benzamides were used, the initially formed isoquinolinone motif **134a** acted as a directing group to activate the *ortho*-C–H bond of its 3-aryl substituent, thereby initiating a second annulation with the given alkyne **6**.

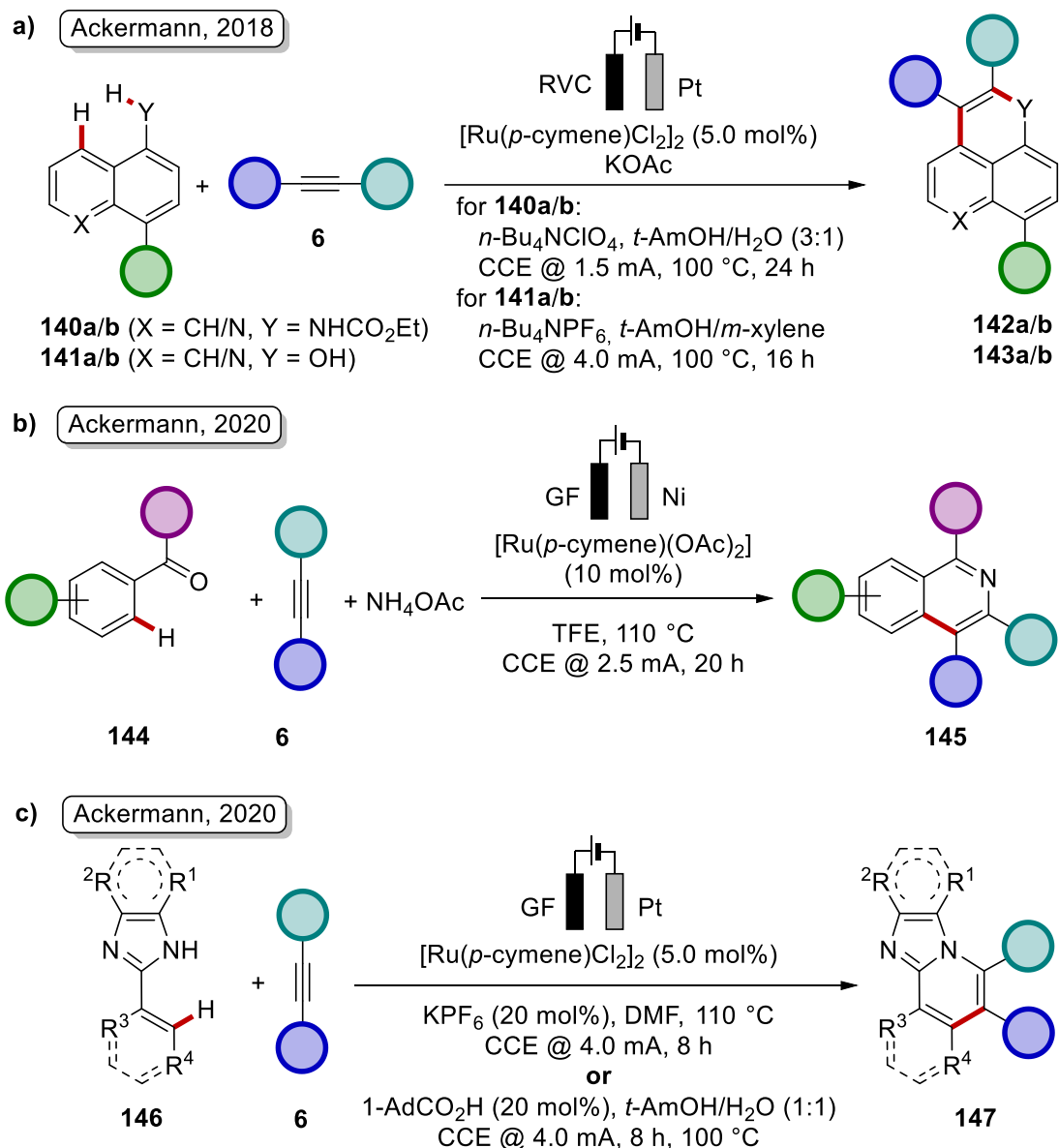


Scheme 1-47 First reports on ruthena-electro-catalyzed C–H activation.



Scheme 1-48 Variants of ruthena-electro-catalyzed access to isocoumarins **7** and the construction of isoquinolinones **139** from unsubstituted benzamides **113**.

The outstanding performance of ruthenium complexes in electro-catalyzed alkyne annulations was further demonstrated by *Ackermann* in the activation of the *peri*-C–H bonds in naphthalene derivatives **140** and **141** (**Scheme 1-49, a**),^[206] the synthesis of isoquinolines **145** in a three-component reaction with aryl ketones **144** and ammonium acetate (**Scheme 1-49, b**),^[207] and in the synthesis of bridgehead *N*-fused bicyclic heteroarenes **147** (**Scheme 1-49, c**).^[208]

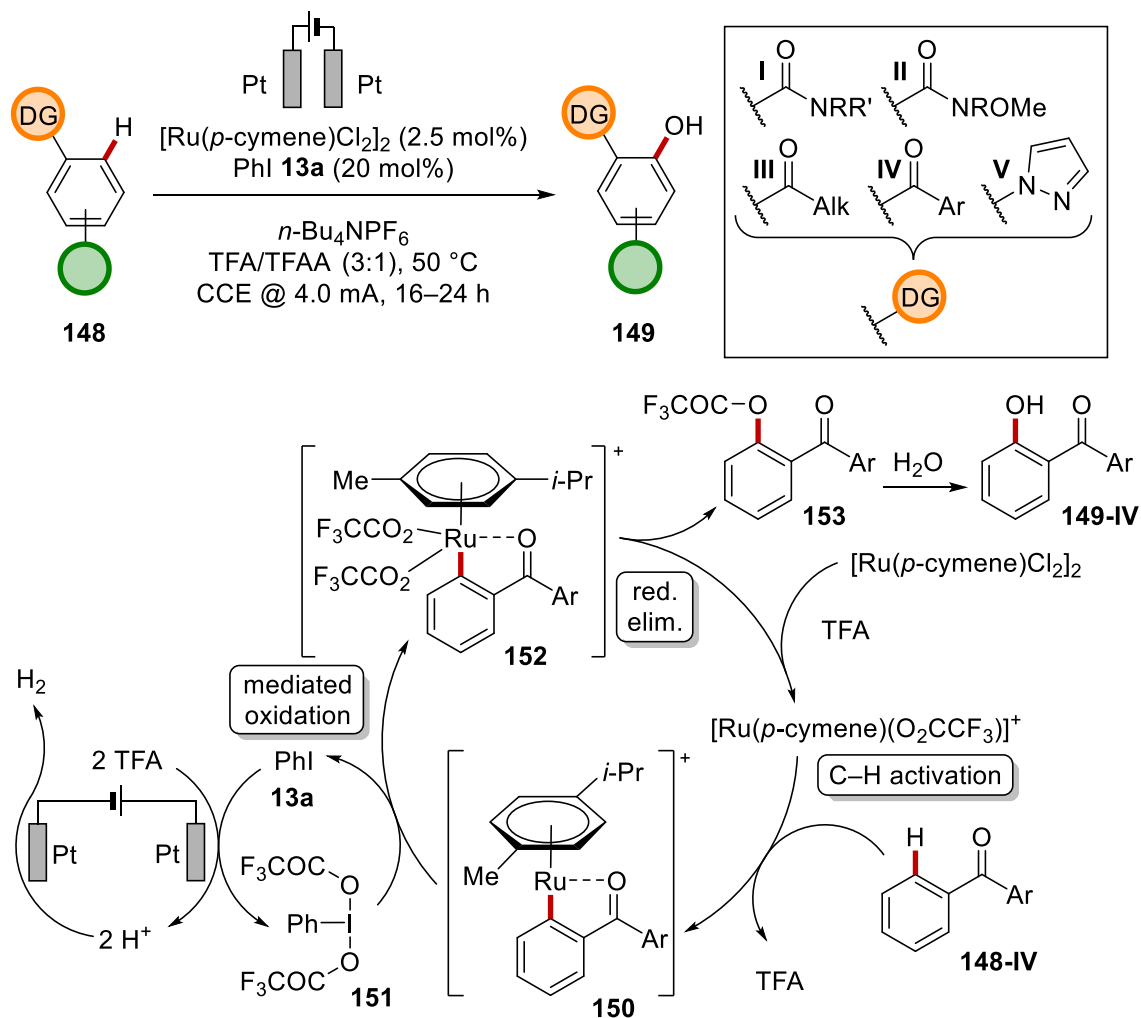


Scheme 1-49 Other ruthena-electro-catalyzed annulations.

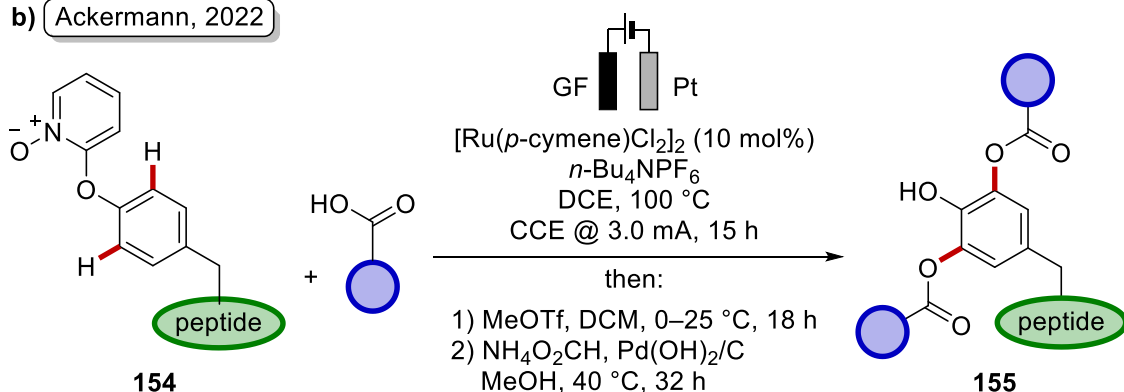
Ruthenium catalysis also proved effective in the electrochemical formation of C–O bonds. In 2019, the Ackermann group disclosed a method to functionalize arenes **148** bearing weakly-coordinating directing groups I–V (**Scheme 1-50, a**).^[73,209] The metalated intermediates **150** and **151** were determined to be of cationic nature and the functional group is introduced during the oxidation from ruthenium(II) to ruthenium(IV), accomplished hypervalent iodine species **151**. The thus-formed phenyl iodide **13a** could be electrochemically reoxidized at the platinum anode to sustain the redox mediation by hypervalent iodine. In another study, a general acyloxylation protocol of phenol derivatives

154 was developed.^[210] The removability of the pyridine-*N*-oxide directing group allowed for the late-stage diversification of tyrosine moieties in peptides.

a) Ackermann, 2019



b) Ackermann, 2022

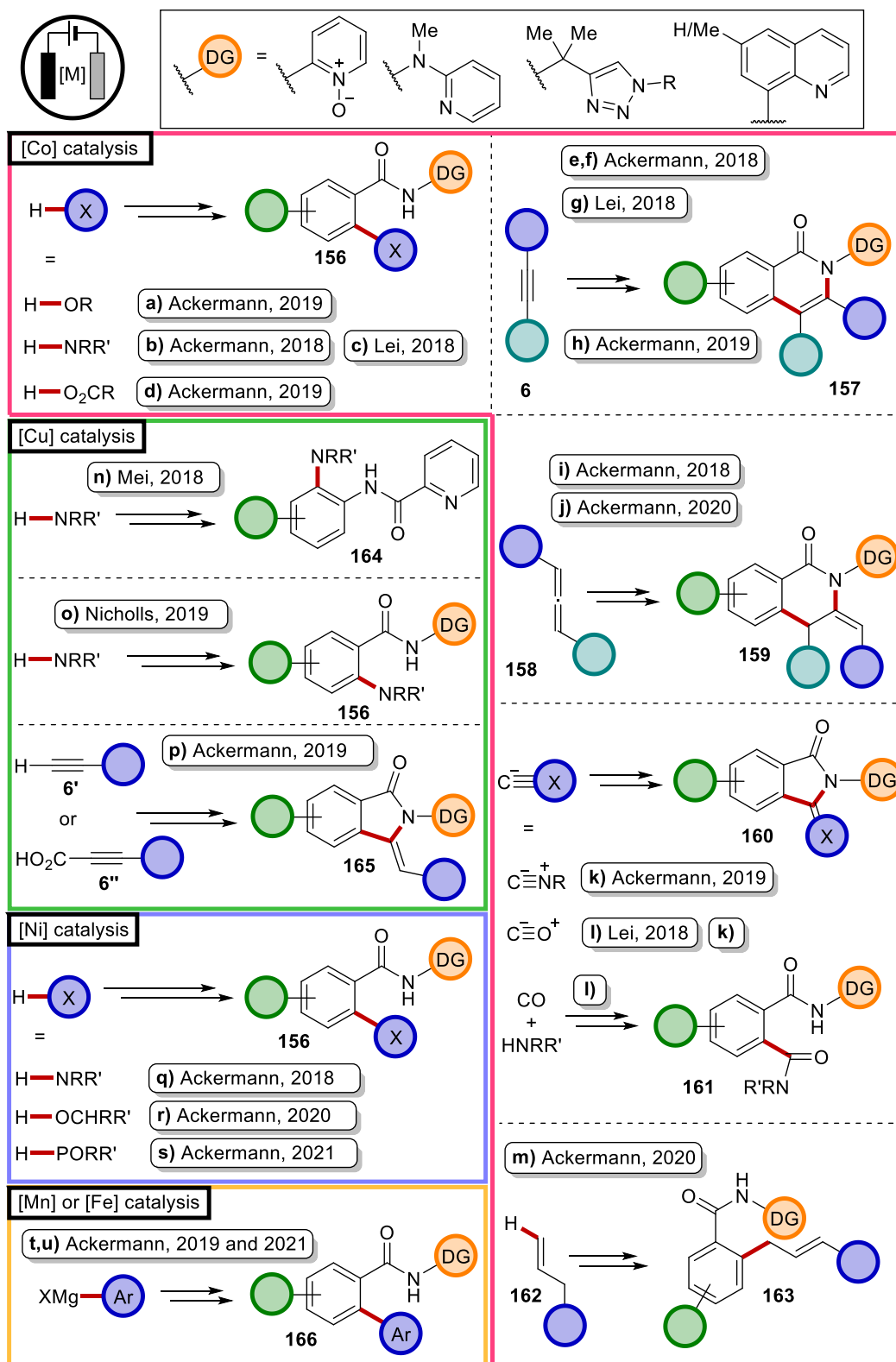


Scheme 1-50 Ruthena-electro-catalyzed C–O bond formation.

1.6.3.2 With Earth-Abundant 3d Transition Metals

Several functionalizations that were achieved by electrochemical C–H activation using precious 4d and 5d metals^[211] (*vide supra*) could also be realized with abundant, inexpensive and generally less toxic 3d metal homologues.^[142d,177b] Most of the transformations catalyzed by 3d metals required strong bidentate directing groups, which coordinate the metal center by chelation. Although their use implies a lesser atom economy when compared with monodentate and weakly coordinating directing groups,^[73] the benefit of avoiding rare metals arguably prevails. Moreover, the often employed heterocycle-connecting amide moiety allows for various cleavage strategies, thereby providing multiple options for further derivatization. In 2017, *Ackermann* reported the first 3d-metalla-electrocatalyzed C–H activation using inexpensive cobalt(II) acetate for the alkoxylation of arenes (**Scheme 1-51, a**).^[212] Over the following years, cobalt became the most explored 3d metal for electrochemical C–H activation thus far. Further C–Het bond formations by cobalt catalysis include aminations^[213] and acyloxylation^[214] (**Scheme 1-51, b–d**). For alkynylations, procedures utilizing terminal^[215] and internal^[216] alkynes, as well as 1,3-diyne^[217] and acetylene gas^[218] have been optimized (**Scheme 1-51, e–h**). Notably, the N–N bond of the pyridylhydrazide directing group employed in *Ackermann*'s protocol^[216] was found to be tracelessly removable by electro-reductive cleavage. Moreover, allenes were transformed into *exo*-methylene isoquinolone scaffold **159** (**Scheme 1-51, i,j**).^[219] Annulation reactions yielding isoindolones **160** with CO were independently achieved by *Lei*^[220] and *Ackermann*^[221] (**Scheme 1-51, k,l**). *Ackermann*'s conditions are also applicable to isoelectronic isocyanides. When CO was used in combination with an amine, non-cyclized amidated arenes **161** were accessible with *Lei*'s conditions. Furthermore, in 2020 the *Ackermann* group developed an allylation with terminal olefins **162** (**Scheme 1-51, m**).^[222] Copper complexes proved efficient in aminations (**Scheme 1-51, n,o**) and alkynylations (**Scheme 1-51, p**). In those reports by *Mei*,^[223] *Nicholls*^[224] and *Ackermann*,^[225] mechanistic studies by cyclic voltammetry unanimously suggested that the functionalization step was triggered by a Cu(II)→Cu(III) single electron oxidation, and a second SET takes place at the end of the catalytic cycle to regenerate Cu(II) from the terminal Cu(I) intermediate. The cross-dehydrogenative formation of C–Het bonds was also achieved with nickel-electrocatalysis. Versatile amination,^[226] oxygenation^[227] and phosphorylation^[228] protocols were developed by the *Ackermann* group (**Scheme 1-51, q–s**). Admittedly, for iron and manganese, reports are thus far scarce. In 2019, *Ackermann* could proof the concepts of ferra- and mangana-electro- C–H activation by arylations with

Grignard reagents (**Scheme 1-51, t**).^[229] Manganese catalysis could be extended to the use of benzamides with monodentate coordination (**Scheme 1-51, u**).^[230]



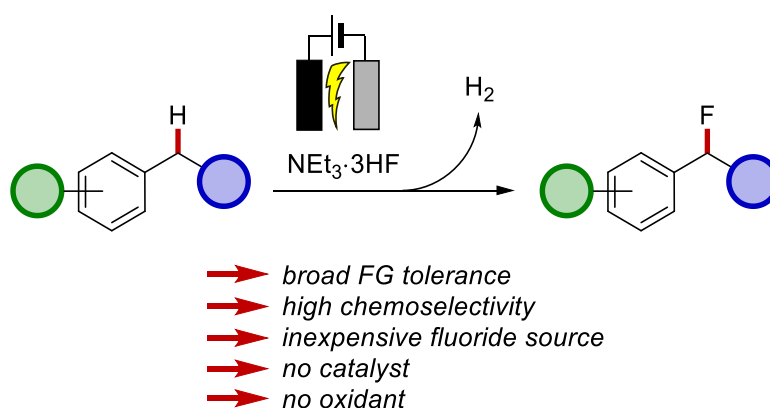
Scheme 1-51 Product classes achievable by electrocatalysis with Earth-abundant 3d metals.

2 OBJECTIVES

Direct functionalizations of C–H and C–C bonds exhibit multiple advantages in comparison with their historic methods predecessor; cross-coupling reactions. The required nucleophiles are mostly obtained *via* metalation of the parent (pseudo-)halides, which for their part are mostly products of a preceding halogenation, due to the inherent scarcity of naturally occurring C–(pseudo)Hal bonds. Hence, the time- and step-economic direct utilization of abundant C–H and C–C bonds translates to the reduction of solvent and metal halide byproduct waste. Naturally, for oxidative couplings, stoichiometric amounts of oxidants are needed. While for many reactions harsh and/or expensive oxidants such as peroxides and noble metal salts could be replaced with abundant and non-polluting molecular oxygen,^[231] many transformations rely on the use of these environmentally and economically disadvantageous reagents. Since the oxidase catalysis is mostly balanced by protons, the oxidation power of molecular oxygen is pH-dependent, and there is no guarantee that for a particular system this parameter can be matched accordingly in order to design an aerobically driven reaction. Moreover, the activity and therefore the reaction rate is limited by the often times poor solubility of the gas in the reaction mixture.^[232] That being said, reactions conducted under air let alone under pure oxygen atmosphere on large scale are dangerous, when a flammable solvent is used, especially at elevated temperatures, which are often required for the activation of C–H bonds.^[233] The risk of ignition due to static electric discharge entails operation at depleted oxygen levels of few volume per cent.^[30a,234] In this context, electrochemistry offers a viable alternative, since the power of reductive electron donation or oxidative electron withdrawal can be steplessly adapted to the needs of the designated reaction partner under the given reaction conditions. The precise potential control could ideally also contribute to a broader applicability of a selected reaction towards redox-sensitive substrates, that would normally suffer overoxidation with chemical oxidants. In addition, the electrochemical setup allows to avoid the use of combustion-supporting molecular oxygen, which in combination with the well-documented scalability^[138b,235] is especially attractive for industrial application. In view of these advantageous characteristics, the implementation of electrolysis into the field of C–H and C–C functionalization is studied in three different projects, namely for two metal-catalyzed transformations and one metal-free approach. For each of the reactions, we intended to reduce the overall negative ecological impact by replacing harmful and expensive chemical oxidants with inexpensive, readily available, and environmentally

sound electricity. A particular focus was set on the investigation of the functional group tolerance, since both working and counter electrode are intended to operate at minimal overpotentials with respect to the terminal ET processes, thereby also minimizing the probability of undesired side reactions.

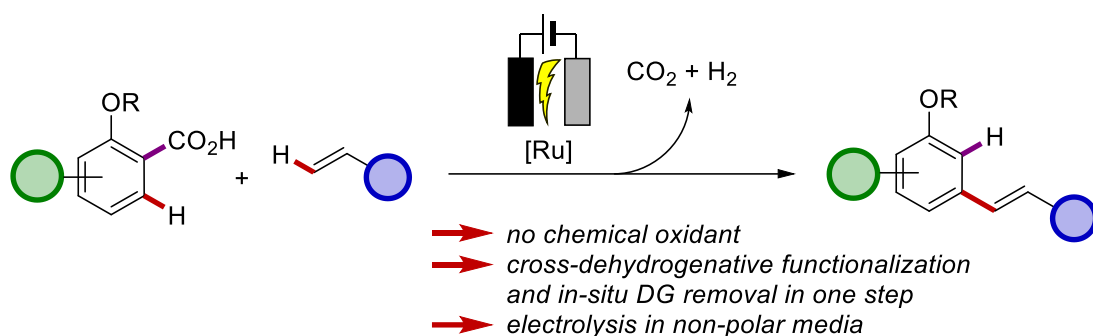
First, the development of a metal-free electrochemical benzylic C–H fluorination will be discussed (**Scheme 2-1**). Fluorinated compounds are of universal interest in many industrial branches. However, contemporary fluorination methods continue to lack the combination of being atom-economic, selective, versatile and inexpensive. Commonly, either the reactions depend on the use of metal catalysts and large amounts of oxidant, or expensive F^+ surrogates instead of abundant fluorides are employed, or electrochemical methods are used. However, the latter either have compromised efficiency due to competing functionalization by the solvent molecule or they lack generality. Herein, these drawbacks were addressed, leading to a broadly applicable electrochemical fluorination protocol that uses an inexpensive source of nucleophilic fluoride.^[236]



Scheme 2-1 Electrochemical benzylic C–H fluorination.

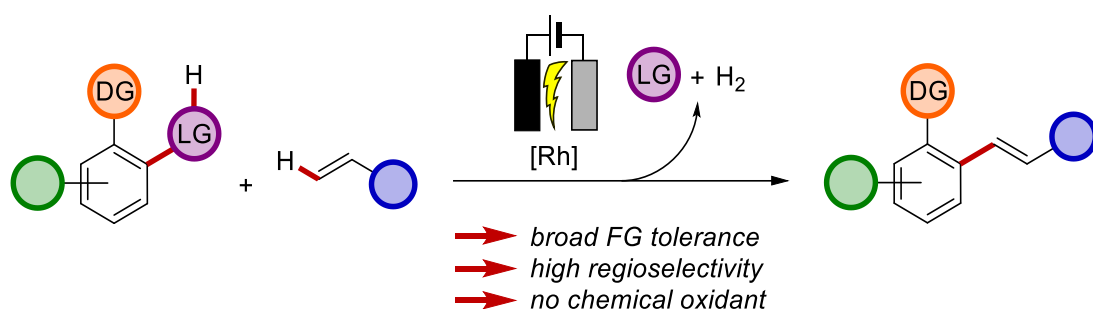
Second, a ruthenium-catalyzed decarboxylative C–H alkenylation of abundant anisic acids was selected for its electrification (**Scheme 2-2**).^[66c] The power of this transformation lies in the twofold action, accomplishing the functionalization and the removal of the directing group in one step. However, this pathway was shown to be taken predominantly when non-polar solvents were used which are inherently disadvantageous for electrolysis. Besides the general goal of improving the sustainability of the reaction by obviating the harmful vanadium oxidant,^[105] we intended to identify a general approach to the challenging electrification of reactions in non-polar solvents.

OBJECTIVES



Scheme 2-2 Ruthena-electro-catalyzed decarboxylative C–H alkenylation.

Third, a rhodium-catalyzed C–C alkenylation is studied (**Scheme 2-3**).^[191] Previous reports showed high positional selectivity originating from chelation assistance of the leaving group.^[102] The initial evidence of the excellent compatibility of this method with electrochemical catalyst activation raised our intention to design a protocol with highly improved catalyst performance, devoid of expensive chemical oxidants, which is moreover easily scalable and highly atom-economic by producing only H₂ and a small organic molecule as byproducts.



Scheme 2-3 Rhoda-electro-catalyzed C–C alkenylation.

3 RESULTS & DISCUSSION

3.1 Electrochemical Fluorination of Benzylic C(sp³)-H Bonds

Fluorinations of organic compounds are of great interest to major industrial branches, such as pharmaceuticals,^[237] materials sciences^[238] and agrochemicals.^[239] The introduction of fluorine atoms into molecules can dramatically change their chemical and mechanical properties.^[240] In comparison with the hydrogen atom, to which the fluorine atom is often considered as isosteric, the latter is distinguished by high electronegativity – the highest of all elements – and therefore a low polarizability. Hence, the interchange of both atoms usually has a profound effect on electron density distribution, lipophilicity, pK_A values of neighboring groups, and many other parameters. Therefore, a single substitution offers a powerful handle to modify both the structure-activity relationship (SAR) and the absorption–distribution–metabolism–excretion (ADME) profile of the respective molecule.^[241]

The fluorine atom can be incorporated nucleophilically as a fluoride ion, or electrophilically by providing a formal F⁺ source. Although the latter approach is regularly employed for its good selectivity, the use of the respective reagents, especially on large scale, is compromised by high cost and poor atom economy. The high natural abundance of fluoride and the resistiveness of its oxidation state makes nucleophilic fluorination the inherently more sustainable choice. In addition, for applications requiring ¹⁸F-labeling, the utilization of nucleophilic fluorination agents is especially desirable, since the most effective radionuclide generation method provides the ¹⁸F as aqueous fluoride solution.^[242] For the highly interesting benzyl fluoride motif, however, established nucleophilic fluorination protocols suffer from the requirement of additional expensive metal catalysts and oxidants.^[126] These drawbacks were addressed in attempts to employ electricity as the oxidant and substrate activator. Unfortunately, electrochemical fluorinations (ECF) in several cases are impaired by the usage of specific and cost-intensive ionic liquids, and generally by suboptimal selectivities due to the relatively weak nucleophilicity of the fluoride ion. For instance, MeCN has proven a vital solvent in many protocols, but causes undesired acetamidation as side reaction due to the non-negligible nucleophilicity of the nitrile group towards highly reactive cationic intermediates. Therefore, we envisioned to develop a method that combines all the advantages of the abovementioned approaches

(Figure 3.1-1), leading to a versatile and selective metal- and oxidant-free electrochemical benzylic fluorination with an inexpensive fluoride source.

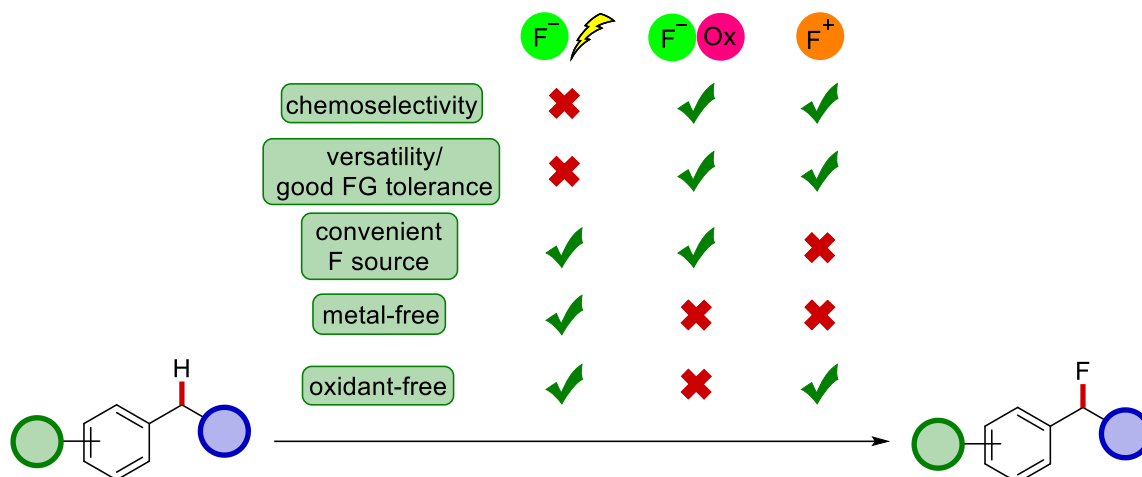


Figure 3.1-1 Advantages and disadvantages of current benzylic fluorination methods.

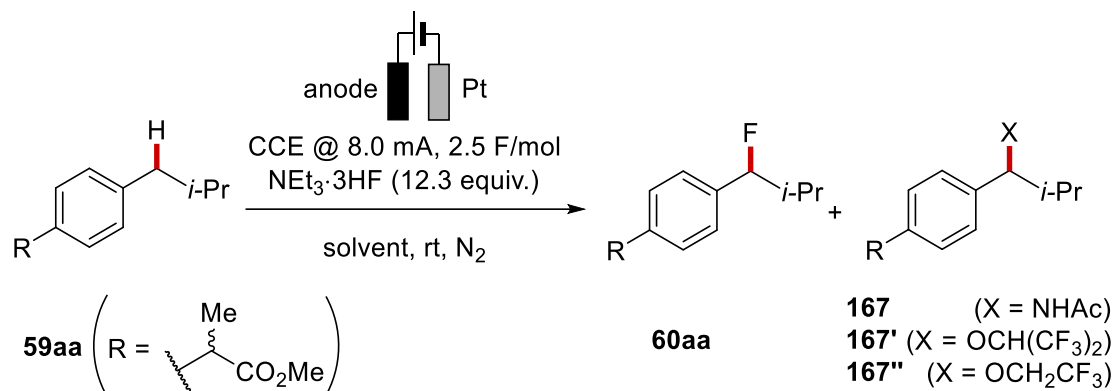
3.1.1 Optimization

The optimization was carried out by *Dr. Maximilian Stangier* in the *Ackermann* group (Table 3.1-1) using the methyl ester of ibuprofen **59aa** as model substrate, bearing a secondary and an electron-deficient tertiary benzylic position.^[243] A convenient undivided-cell-two-electrode setup was chosen and the initial reactions with MeCN as solvent and inexpensive $NEt_3 \cdot 3HF$ as fluoride source showed the formation of equal amounts of fluorinated and acetamidated products **60aa** and **167** (19% each, entry 1). The functionalization took place at the secondary carbon. Although the addition of HFIP increased the yield of the desired product **60aa** up to 28%, which can be attributed to the strong donation of nucleophilicity-enhancing hydrogen bonds by the cosolvent,^[244] the additional formation of oxygenated side product **167'** was observed here (entry 2). When CsF was used as the fluoride source, the oxygenated species was formed as main product, with only trace amounts of the fluorinated product formed (entry 3). A switch of the solvent mixture to DCE/HFIP revealed a substantial increase in yield (85%, entry 4). Carbon-based anode materials delivered the product **60aa** in comparable yields, with inexpensive GF having proved most efficient (entries 5–6). Notably, by the addition of a quaternary ammonium salt supporting electrolyte, the amount of fluoride source could be reduced by 75%, albeit with a 26% decrease in yield. In view of the recently enforced restrictions on the use of DCE as a solvent,^[245] DCM was tested as an alternative and proved only slightly

RESULTS & DISCUSSION

less effective. Finally, less expensive TFE was probed to substitute HFIP. However, 23% of the substrate **59aa** were converted to the corresponding oxygenated side product **167''**, likely due to the higher nucleophilicity of TFE as compared to HFIP.

Table 3.1-1 Optimization studies of Electrochemical Benzylic C(sp³)-H Fluorination.^[a]



Entry	Anode material	Solvent	Further deviations	Yield (%) of	
				60aa	167/'/'
1	Pt	MeCN		19	19/--/--
2	Pt	MeCN/HFIP (4:1)		28	14/6/--
3	Pt	MeCN/HFIP (4:1)	CsF (1.8 equiv.) instead of NEt ₃ ·3HF	<5	--/49/--
4	Pt	DCE/HFIP (2:1)		85	--/--/--
5	RVC	DCE/HFIP (2:1)		82	--/--/--
6	GF	DCE/HFIP (2:1)		92	--/--/--
7	RVC	DCE/HFIP (2:1)	NEt ₃ ·3HF (3.1 equiv.), <i>n</i> -Bu ₄ NBF ₄ (0.6 equiv.)	66	--/--/--
8	GF	DCM/HFIP (2:1)		90	--/--/--
9	GF	DCE/TFE (2:1)		37	--/--/23

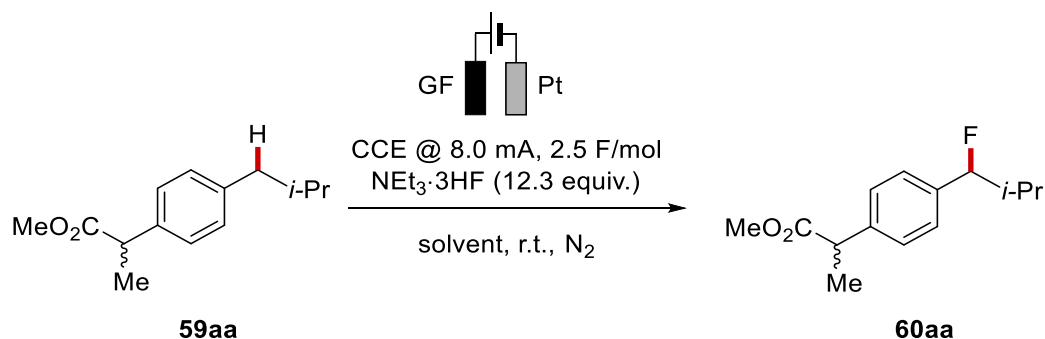
[a] Reaction performed by *Dr. Stangier*. Reaction conditions: Undivided cell, GF anode, Pt cathode, **59aa** (0.50 mmol), NEt₃·3HF (1.0 mL, 12.3 equiv.), solvent (3.0 mL), under inert atmosphere. NMR yields with CH₂Br₂ as the internal standard are given.

The electrolyte of the optimized conditions (entry 6) features good conductivity and solubilization properties^[246] due to the high polarity and polarizability, as well as the low viscosity of the individual solvent components. Moreover, the electrolyte possesses a reasonable redox window, allowing on the one hand a facile proton reduction at the platinum cathode, and on the other hand offering high anodic stability, as confirmed by

RESULTS & DISCUSSION

cyclovoltammetric studies performed by *Dr. Stangier*.^[236,243] However, despite these important properties for efficient electrolysis and the generally easy handling of the developed setup, the hazardous nature of halogenated solvents remains an issue and efforts to at least partly replace them with less problematic components^[247] were made. Polar, weakly-coordinating solvents were tested as 2:1 mixtures with HFIP (**Table 3.1-2**). The reactions carried out in propylene carbonate (PGCC) and sulfolane (THTD) mixtures formed the product **60aa** cleanly, without solvent-caused side reactions, albeit in unsatisfactory yields (entries 1–2). DME and bio-derived CyreneTM failed to deliver the product (entries 3–4). The best result of non-halogenated co-solvents was achieved by nitromethane (entry 5). However, the outstanding performance of the DCE/HFIP mixture has not been matched. Moreover, due to the high polarity of the nitromethane-based mixture, solubility problems of highly non-polar substrates are expected. Therefore, the scope of the reaction was explored with the established DCE/HFIP mixture. Conveniently, the setup did not require additional drying of the solvents. Hydroxylation products were not observed despite the use of bench top-stored commercial chemicals, including the fluoride source, whose purification due to its ionic liquid nature is time-consuming.^[248]

Table 3.1-2 Screening of alternative solvents^[a]

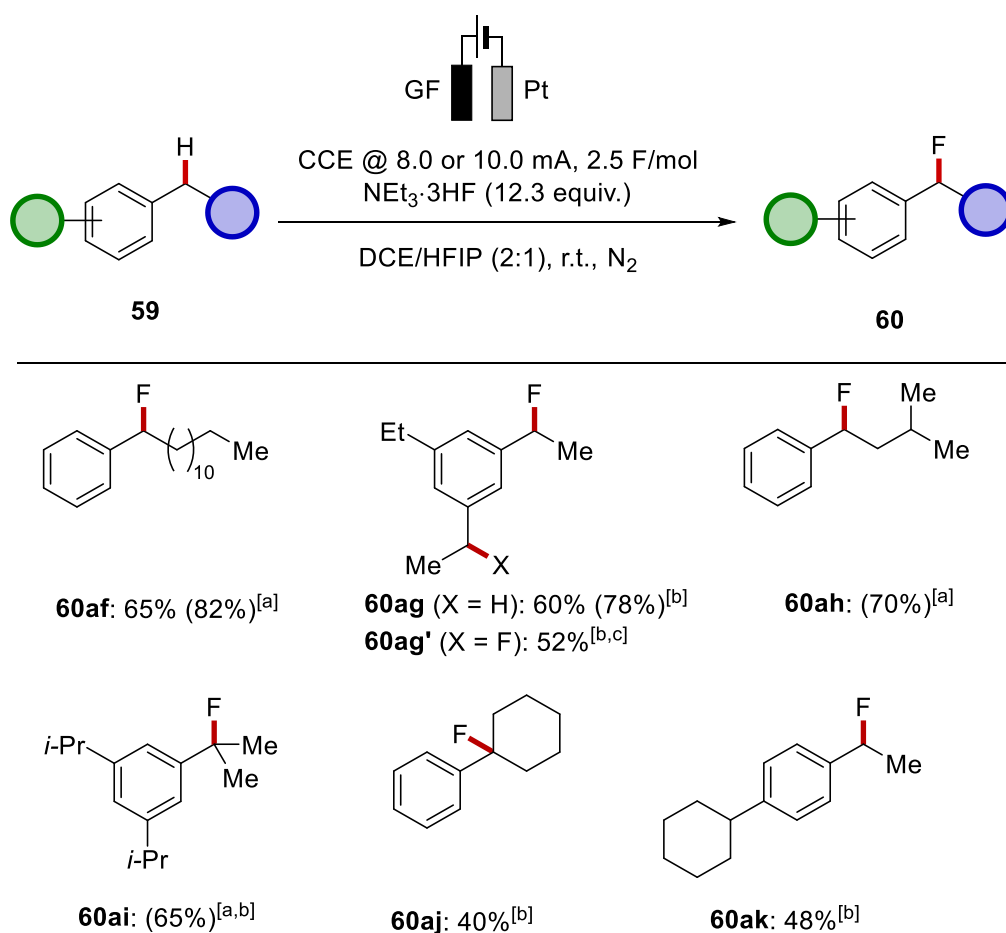


Entry	Solvent	Yield of 60aa [%]
1	PGCC/HFIP (2:1)	36
2	THTD/HFIP (2:1)	19
3	Cyrene TM /HFIP (2:1)	--
4	DME/HFIP (2:1)	--
5	MeNO ₂ /HFIP (2:1)	68

[a] Reaction conditions: Undivided cell, GF anode, Pt cathode, **59aa** (0.50 mmol), NEt₃·3HF (1.0 mL, 12.3 equiv), solvent (3.0 mL), under inert atmosphere. NMR yields with CH₂Br₂ as the internal standard are given.

3.1.2 Scope

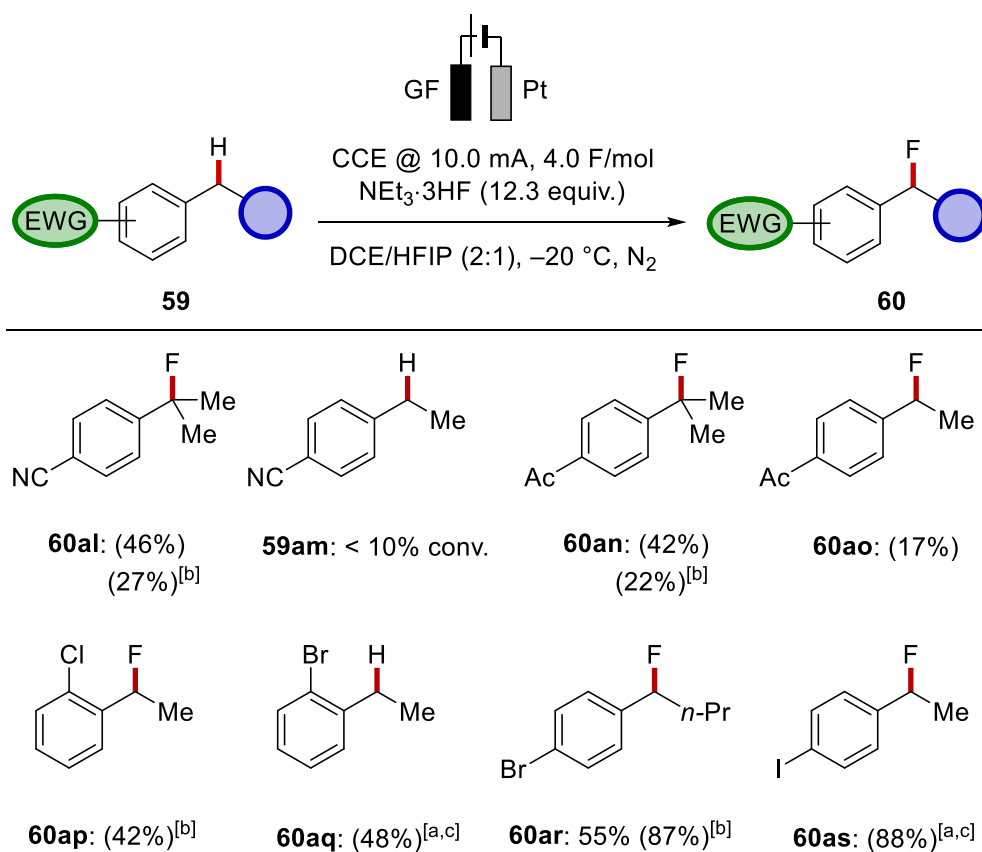
We began exploring the scope by testing alkylarenes **59af–59ak** (Scheme 3-1). Substrates **59af–59ah** with secondary benzylic positions bearing linear and branched side chains were smoothly converted to the corresponding fluorinated products **60af–60ah** in yields of up to 82%. Notably, by doubling the equivalents of passed electrons, a consecutive fluorination of **60ag** was achieved at the unfunctionalized position to deliver **60ag'** in 52% yield. Tertiary benzylic positions were also efficiently functionalized (**60ai, 60aj**). In accordance with previous reports for benzylic C–H functionalizations, secondary positions are favored over tertiary ones, as demonstrated with substrate **59ak**, where both functionalities are present electronically unbiased in one molecule.



Scheme 3-1 Scope of alkylarenes **60**. NMR yields in parentheses. [a] Reaction performed by *Dr. Stangier*. [b] Reaction conducted at $T = 0$ °C. [c] 5.0 F/mol passed.

In contrast, for substrates bearing strongly electron-withdrawing substituents *para* to the benzylic position (Scheme 3-2), tertiary positions were functionalized more readily (**60al**,

60am), likely due to the additional positive inductive effect, which consequently would lower the oxidation potential as compared to secondary substrates **59an** and **59ao**, that were converted to the corresponding products in less than 20% yield. Notably, these substrates also required higher current densities and lower reaction temperatures. At ambient temperature, **60al** and **60an** were only obtained in 27% and 22% yield, respectively. Haloarenes displayed a similar trend. At $T = 0\text{ }^{\circ}\text{C}$, more electron-deficient chloro-substituted product **60ap** was formed less efficiently than bromo-substituted **60ar** (42% vs. 87%, respectively). Likewise, bromo-substituted **60aq** was obtained at ambient temperature in lower yield (48%) than iodo-substituted **60as** (88%) and **60ar** at $T = 0\text{ }^{\circ}\text{C}$ (87%).

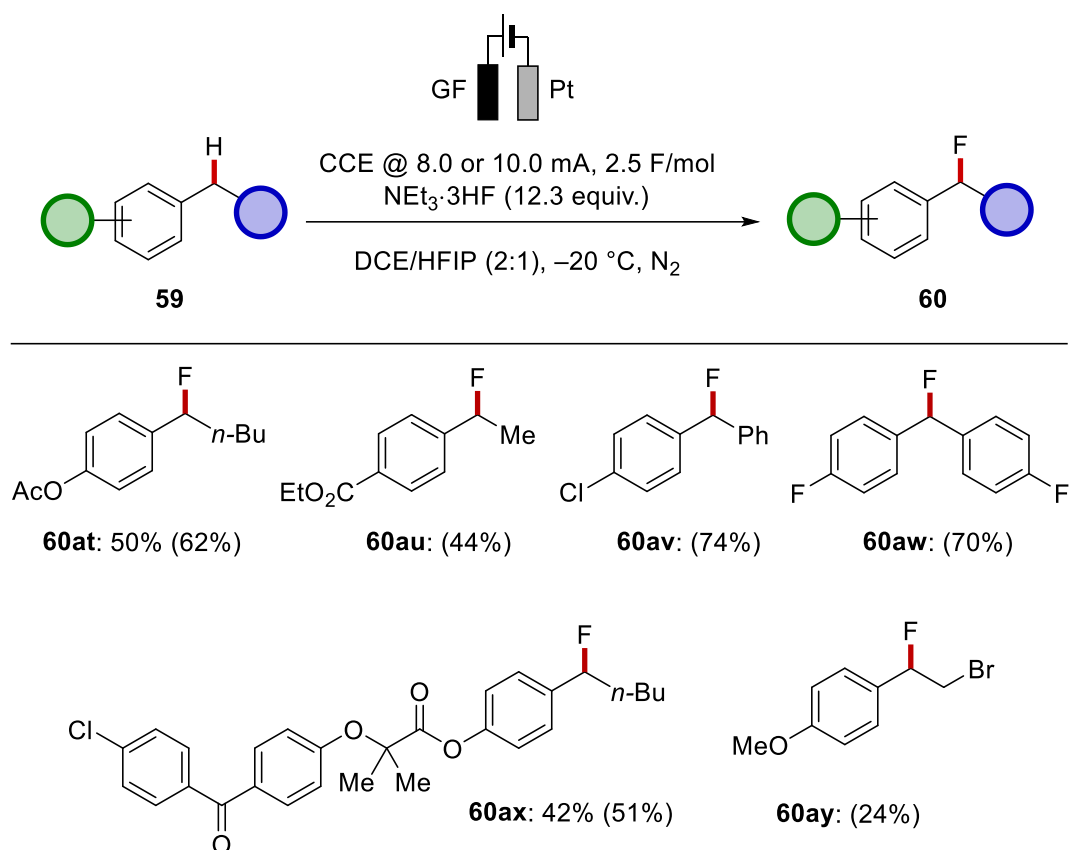


Scheme 3-2 Scope of fluorinated alkyl arenes **60** with electron-deficient groups. NMR yields in parentheses. [a] Reaction performed by *Dr. Stangier*. [b] Reaction performed at $T = 0\text{ }^{\circ}\text{C}$. [c] Reaction performed at r.t.

Next, we turned our attention to substrates bearing moderately electron-donating and electron-withdrawing groups **59at–59ay** (Scheme 3-3). The fluorination occurred with moderate efficiency to furnish benzyl fluorides decorated with acetoxy (**60at**) and ester

RESULTS & DISCUSSION

(**60au**) groups. Halogen-substituted diarylmethanes **59av** and **59aw** were converted in good yields of 74% and 70% to the corresponding products **60av** and **60aw**. We were also impressed to observe that fenofibrate derivative **59ax** was selectively functionalized without affecting the multiple functional groups present in this drug analog. However, **60ay** which bears a strongly electron-donating alkoxy substituent, could only be obtained in poor yield.

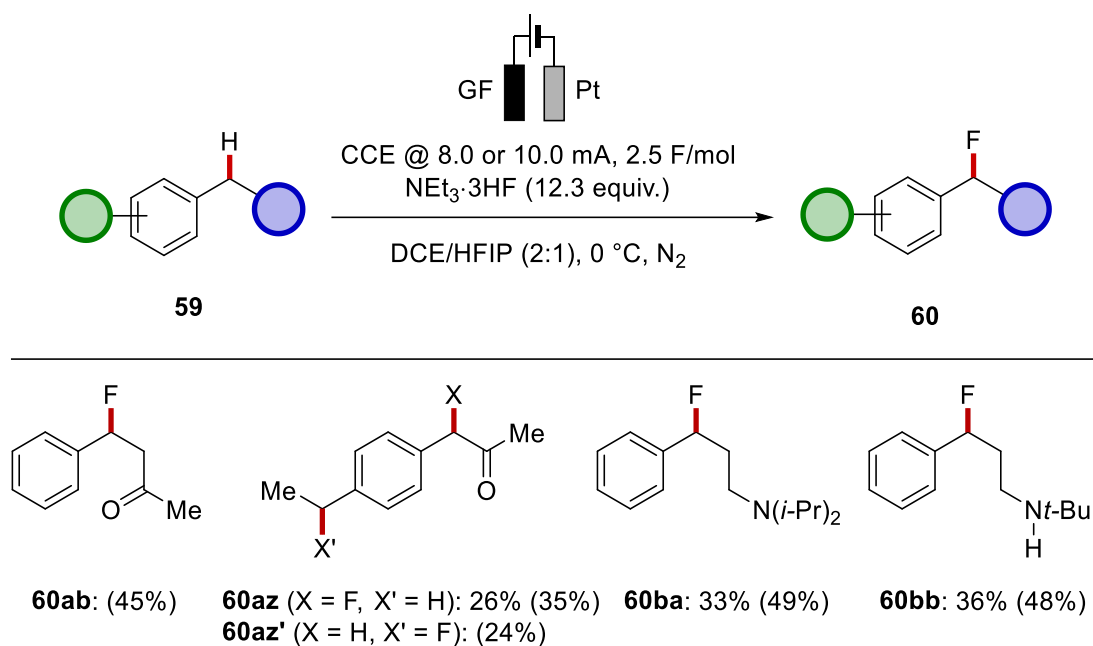


Scheme 3-3 Scope of moderately electron-deficient and electron-rich substrates. NMR yields in parentheses.

We then decided to explore the compatibility of different side chain functionalities with our electrochemical fluorination (**Scheme 3-4**). The carbonyl groups of substrates **59ab** and **59az** proved amenable for the reaction conditions, albeit the products were obtained only in moderate yields of 45% (**60ab**) and 59% (**60az/60az'**, mixture of regioisomers). Interestingly, a slight preference for the *alpha*-carbonyl benzylic position was observed for substrate **59az**, which is indicative of an increased acidity and an additional mesomeric stabilization of the sp²-hybridized intermediates due to the neighboring carbonyl group. In addition to electrophilic moieties, we became curious to test the applicability of nucleophilic free amines. For many examples we observed close-to-quantitative Faradaic

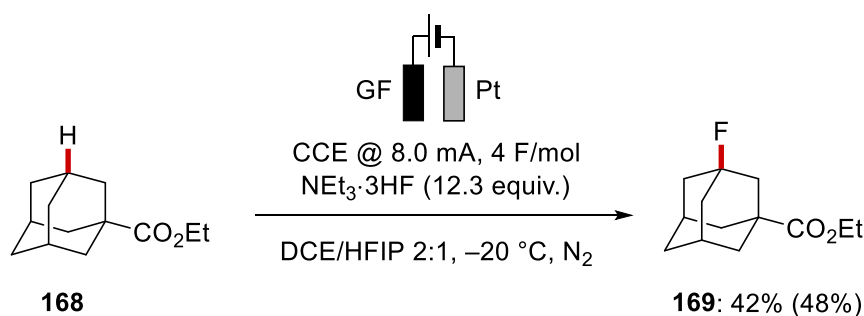
RESULTS & DISCUSSION

efficiencies over the most course of the electrolysis. Hence, we could conclude that triethylamine does not undergo electro-oxidative degradation, or at least not to a notable extent. Furthermore, we have not observed any side products that could originate from nucleophilic attack of triethyl amine. Therefore, we were pleased to confirm the expected compatibility of our system with free secondary and tertiary amines by synthesizing target compounds **60ba** and **60bb** in moderate yields.



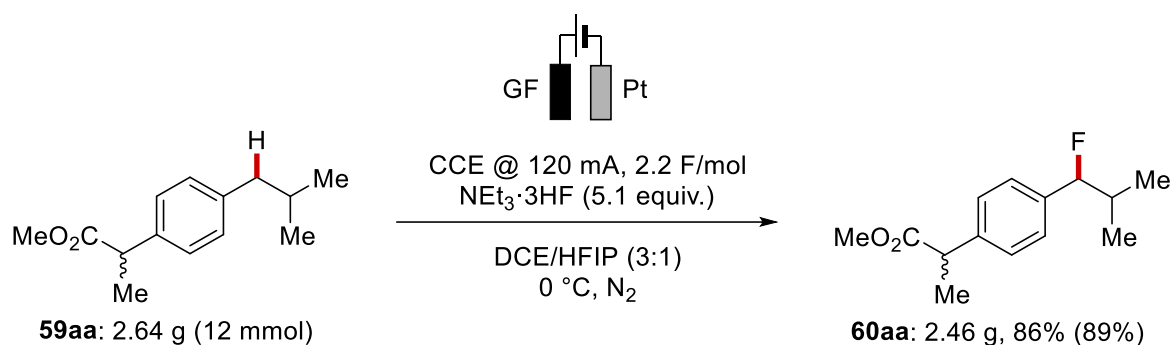
Scheme 3-4 Exploration of side chain compatibility. NMR yields in parentheses.

In addition to the fluorination of benzylic positions, we also investigated the applicability of our system towards adamantane, which is a lead structure in drug design.^[249] We were pleasantly surprised that despite previous reports, which required expensive ionic liquid HF sources,^[250] we could obtain the bridgehead C-fluorinated adamantane derivative **169** in moderate yield using inexpensive $\text{NEt}_3 \cdot 3\text{HF}$ (**Scheme 3-5**).



Scheme 3-5 Fluorination of adamantane **168**. NMR yield in parentheses.

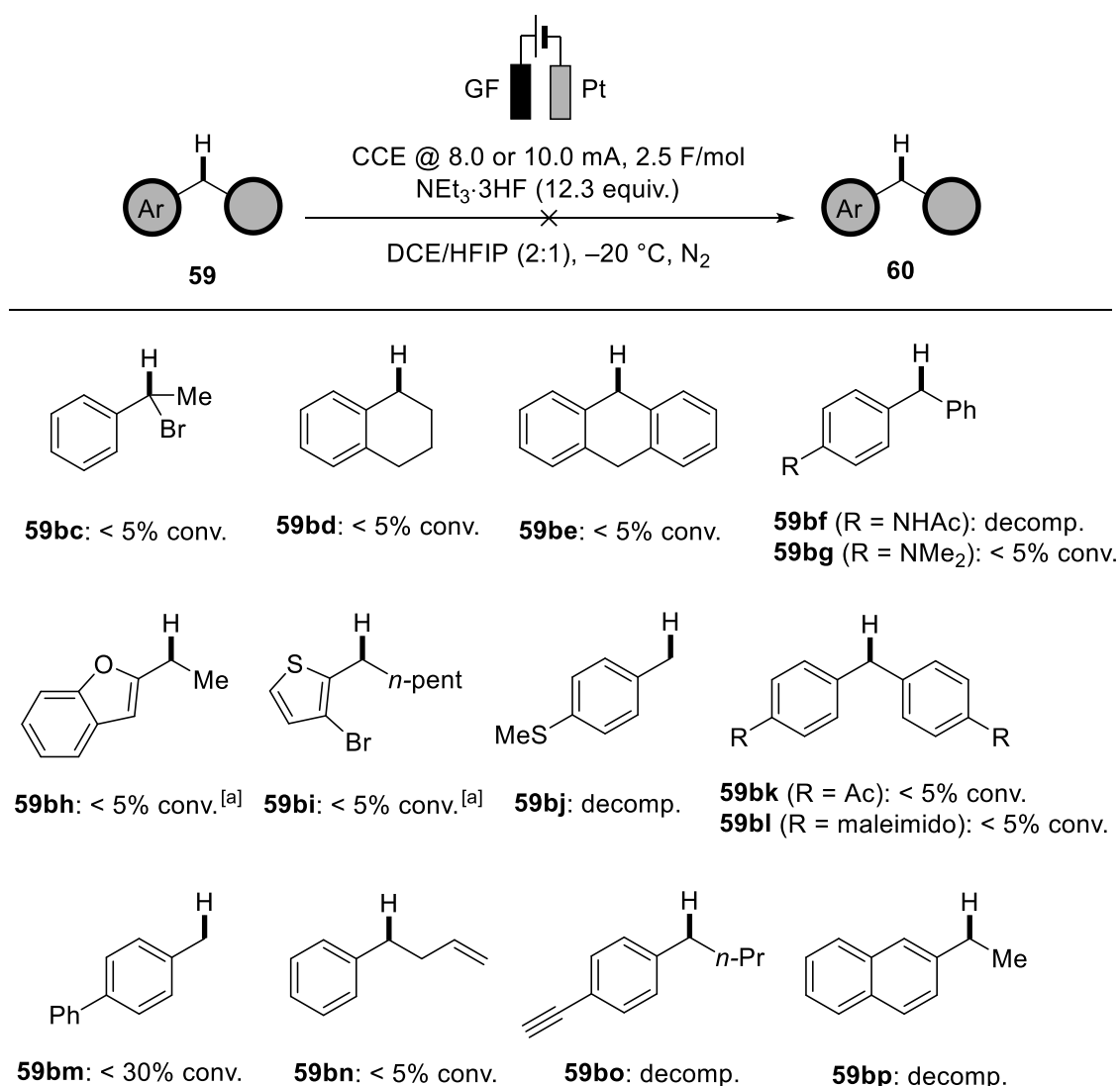
Next, we probed the scalability of our system by employing the substrate **59aa** on a 12 mmol scale (**Scheme 3-6**). We have obtained the product **60aa** in 86% isolated yield. Notably, the amount of the fluorinating agent could be significantly reduced to 5.1 equiv. instead of 12.3 equiv. without a negative effect, further highlighting the practicality and adaptability of the reaction. The robustness of the electrochemical setup was further demonstrated by an experiment conducted by *Dr. Stangier* who showed that the reaction could be run using solar energy, that is prone to temporary fluctuations.^[236,243]



Scheme 3-6 Gram-scale electrochemical C–H fluorination of **59aa**. NMR yield in parentheses.

During the exploration of the substrate scope we also found motifs that were not compatible with our electrochemical fluorination (**Scheme 3-7**). Most of the findings are in accordance with previous studies on benzylic functionalizations^[160,251] The fluorination does not occur with substrate **50bc**, which bears a bulky benzylic bromo substituent. We assume that this is caused by the difficulty to align the C–H bond with the aromatic π -orbitals (*i.e.* 90° to the aromatic plane). This is the preferred conformation for efficient C–H deprotonation due to the electron donation into the π -system. Substrates with annulated side chains **59bd** and **59be** were also not functionalized, as opposed to literature precedence.^[114b,163,174] We assume here, that their lesser flexibility disfavors the adoption of a planar conformation of the sp^2 -hybridized reactive intermediates.^[252] In addition to cyclic substrates, no reactivity was observed with aniline and anilide derivatives **59bf** and **59bg**. A plausible explanation for this finding is the protonation of the functional groups by the acidic environment, thereby significantly elevating the oxidation potential of the aromatic core. Furthermore, the positive charge of the cationic intermediates is likely to have a higher tendency to be centered at the electron-donating hetero atom instead of the benzylic position. Heterocycles

59bh and **59bi** probably did not undergo efficient functionalization for the latter reason. Thioanisole **59bj** formed mainly the corresponding sulfone. Substrates with multiple electron-withdrawing substituents, such as diarylmethanes **59bk** and **59bl** remained unfunctionalized, likely due to exceedingly high oxidation potentials. Although methyl biphenyl **59bm** did react with admittedly impracticable Faradaic efficiency, the isolation of the compound has not been achieved. The presence of a terminal alkene moiety in substrate **59bn** shut the reaction down, while phenylacetylene and naphthalene derivatives **59bo** and **59bp** underwent side reactions to form several unidentified products.

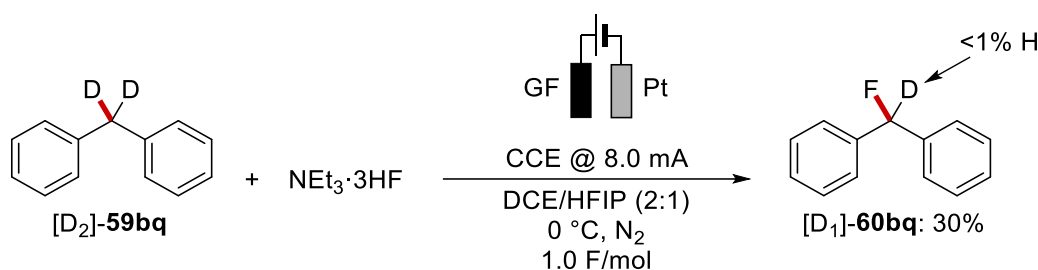


Scheme 3-7 Limitations of the electrochemical fluorination method. [a] Reaction performed by *Dr. Stangier*.

3.1.3 Mechanistic Insights

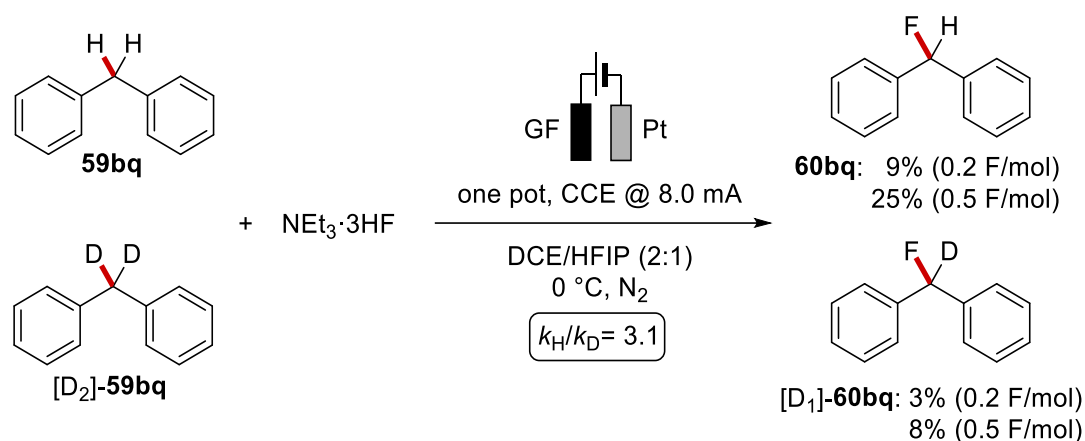
Cyclovoltammetric studies performed by *Dr. Stangier* revealed several key points which rationalize the efficiency of the reaction conditions.^[236,243] HFIP was found to significantly lower the oxidation potential of the investigated substrate, giving rise to two discrete irreversible oxidation events for the substrate, being indicative for the crucial role of HFIP in the stabilization of the radical species. Both effects were documented in other transformations involving radical and radical-cationic intermediates with HFIP as cosolvent.^[253] The second oxidation event was more pronounced in presence of $\text{NEt}_3 \cdot 3\text{HF}$. This finding might be attributed to its buffer character. $\text{NEt}_3 \cdot 3\text{HF}$ is known to be in a non-negligible equilibrium with the free amine, thereby providing arguably the more efficient proton acceptor than HFIP and consequently accelerating the deprotonation.^[254] Furthermore, the oxidation potential of the monofluorinated reaction product was found to be substantially higher as compared to the starting material, which is decisive for achieving good selectivities.

Additionally, a H/D exchange experiment (**Scheme 3-8**) on deuterated substrate $[\text{D}_2]$ -**59bq** confirmed the irreversible nature of the electron transfer and deprotonation sequence, since no proton incorporation was observed in the deuterated product $[\text{D}_1]$ -**60bq**.



Scheme 3-8 H/D exchange experiment. NMR yield given.

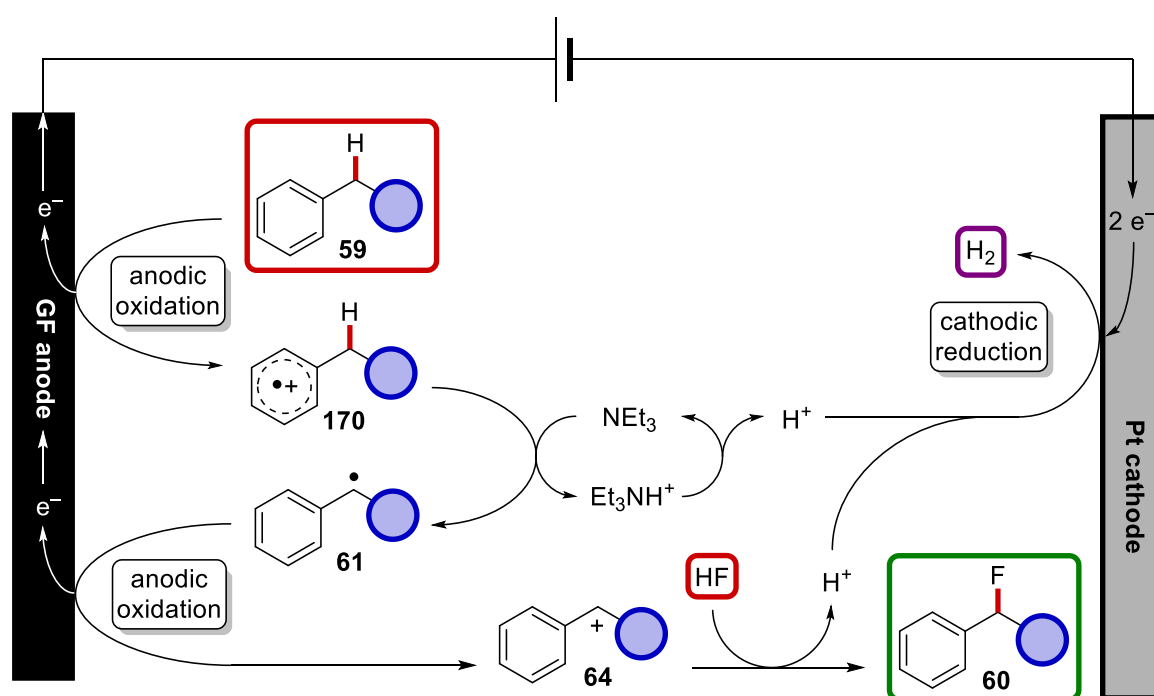
In an intermolecular KIE experiment using the substrates **59bq** and $[\text{D}_2]$ -**59bq**, a value of $k_{\text{H}}/k_{\text{D}} \approx 3.1$ was obtained (**Scheme 3-9**). These results indicate that the deprotonation step is rate-limiting and product-determining. Hence, unless the reactivity of the substrates **59** is impaired by the presence disadvantageous functional groups (*vide supra*), the position selectivity, as observed in **Scheme 3-1**, is governed by the kinetic C–H acidity.



Scheme 3-9 Intermolecular KIE experiment. NMR yields given.

3.1.4 Mechanistic Proposal

Based on our mechanistic findings, a plausible mechanistic sequence is proposed in **Scheme 3-10**. At the anode, a SET from the aromatic core of **59** furnishes the radical cation **170**, stabilized by a solvate shell of HFIP. Upon rate-limiting heterolytic C–H cleavage, likely aided by free triethyl amine, a radical **61** is formed, which undergoes a second anodic SET to form the benzylic cation **64**. This species is then nucleophilically intercepted by fluoride to yield the fluorinated product **60**. Hydrogen evolution by proton reduction was identified as the cathodic counter reaction by headspace-GC.



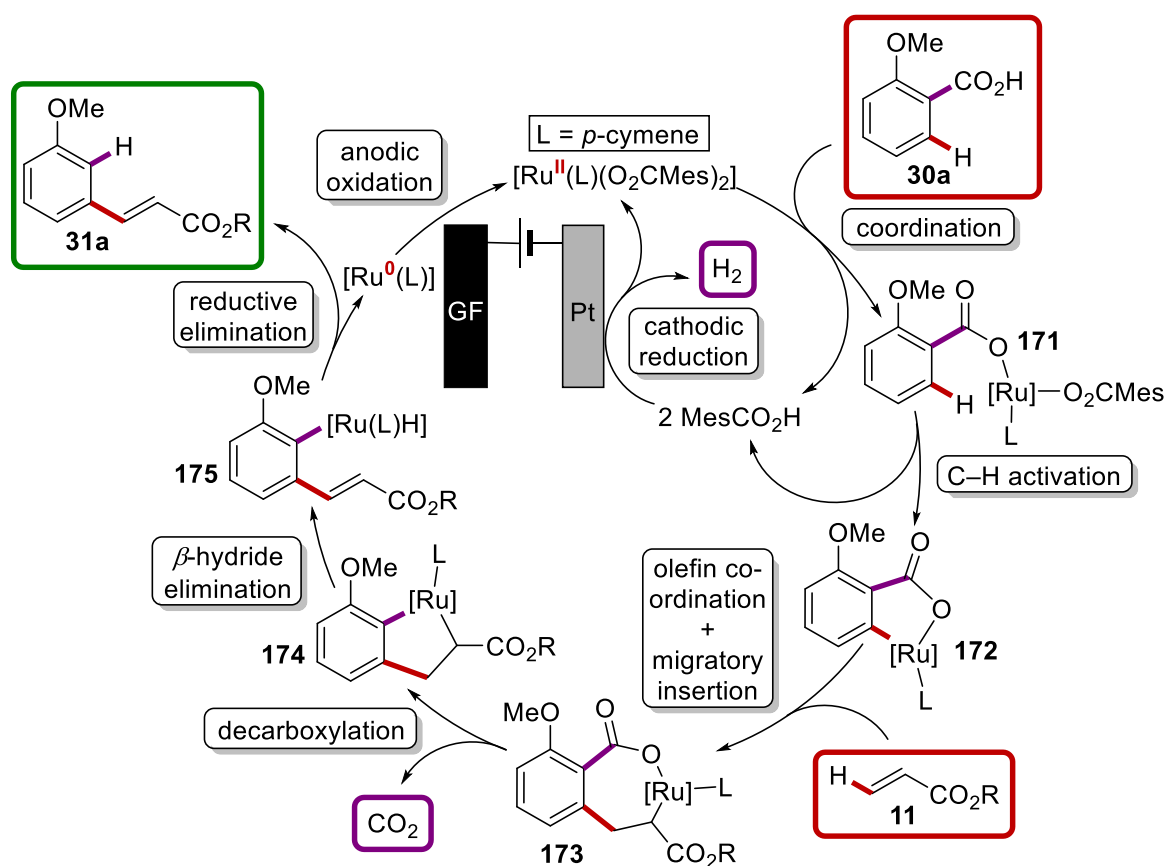
Scheme 3-10 Mechanistic proposal.

3.2 Ruthena-Electro-Catalyzed Decarboxylative Alkenylation of Anisic Acids

Among the natural feedstocks for organic molecules, oil and gas are still the most exploited ones despite their finiteness. The fact, that their main components are small molecules, ready to be functionalized or fragmented in homogenous and heterogenous catalytic processes, and subsequently separated, is of great convenience.^[255] In contrast, biomass-derived and therefore renewable lignocellulose as a raw material does require pre-treatment in the form of depolymerization, which for one of its main components, lignin, is particularly challenging due to the complex and at the same time robust structure.^[256] However, lignin is the most abundant source for valuable aromatic building blocks on the Earth's surface, and recent advances in lignin degradation promise to notably facilitate their high-volume access. The primary products are mostly electron-rich phenols and anisols. On the one hand, these molecules can be defunctionalized towards fuels and bulk chemicals. On the other hand, their direct functionalization is an attractive concept for the efficient production of value added chemicals. Structurally related anisic acids are therefore key starting materials for this transformational platform. Ruthenium complexes have shown great capabilities in the direct functionalization of aromatic compounds by means of C–H activation.^[29c,40a,257] Remarkably, various scaffolds were constructed utilizing rather weak oxygen-containing directing groups.^[37d] These reactions are of great interest due to the ubiquitous occurrence and easy access of carbonyl- and hydroxyl-group-based substituents, and their more facile modification, as compared to strongly coordinating *Lewis*-basic *N*-heterocycles. In particular, the carboxyl group has been employed for centuries as a strategic fragment due to its facile installation and removability *via* the release of CO₂ under orthogonal conditions, such as thermal treatment, acid-base catalysis or electrochemistry. The resource- and time-saving factor is maximized when both the functionalization and the removal of the potentially dispensable directing group occur in one step. In 2016, a decarboxylative alkenylation of anisic acid derivatives was developed by the *Ackermann* group.^[66c] However, the efficient one-step access to *meta*-substituted anisoles was dependent on stoichiometric amounts of chemical oxidants, such as V₂O₅, which in view of its generally hazardous assessment and possible carcinogenicity, undermines the positive balance of this approach. We therefore intended to enhance the sustainability of this impactful protocol by incorporating it into an electrochemical framework.

3.2.1 Rationale

In order to outline our electrification approach, we considered a plausible *modus operandi* for an electro-oxidative decarboxylative alkenylation of C(sp²)-H bonds in a cross-dehydrogenative fashion. For that purpose, the mechanistic investigations in related works were considered, leading to a conceivable scenario with an anticipated sequence of generic elementary steps, including the C-H activation, the migratory insertion and the decarboxylation. (**Scheme 3-11**) The electric current is expected to come into play in the last step of the catalytic cycle, namely the regeneration of a ruthenium(II) species by an anodic oxidation of a ruthenium(0) intermediate, that could be stabilized by solely the η⁶-arene ligand, or as a sandwich complex, analogous to **135** (not shown). Hydrogen evolution by proton reduction is presumed as a viable counter reaction.



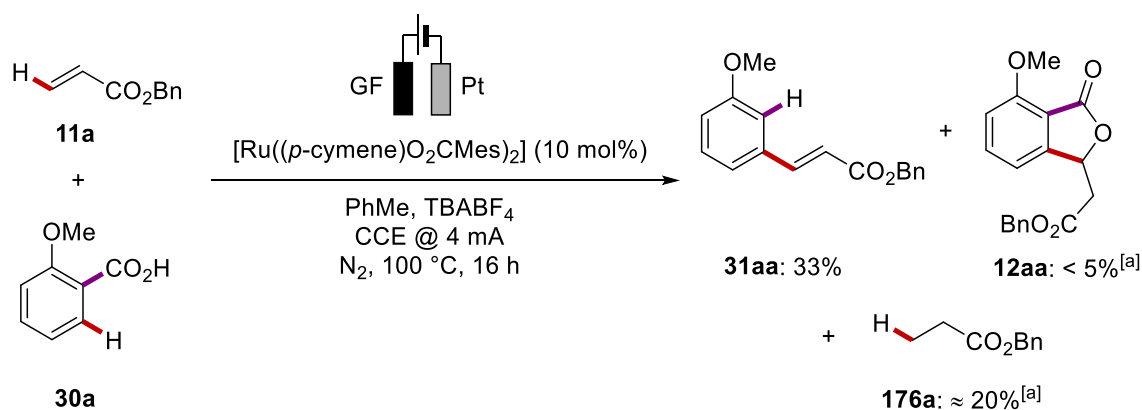
Scheme 3-11 Mechanistic hypothesis.

The mechanistic hypothesis served as a guiding principle for the systematic optimization of the reaction parameters.

3.2.2 Optimization

3.2.2.1 Standard Reaction Parameters

As a reference point for the reaction development, the optimized reaction conditions^[66c] of the elegant transformation developed by *Ackermann* and co-workers were chosen, where PhMe as the solvent gave the best results. The electrification was approached by replacing the oxidant V₂O₅ with a supporting electrolyte and applying a constant current of 4 mA in an undivided cell. In analogy to known ruthena-electrocatalyses (see chapter 1.6.3.1.3), GF was selected as carbon-based anode, and a platinum cathode was designated to execute the proton reduction. The reaction gave 33% of the desired product **31aa** (Scheme 3-12). In addition, small quantities of undecarboxylated phthalide side product **12aa** were formed and considerable amounts of benzyl propionate **176a**.



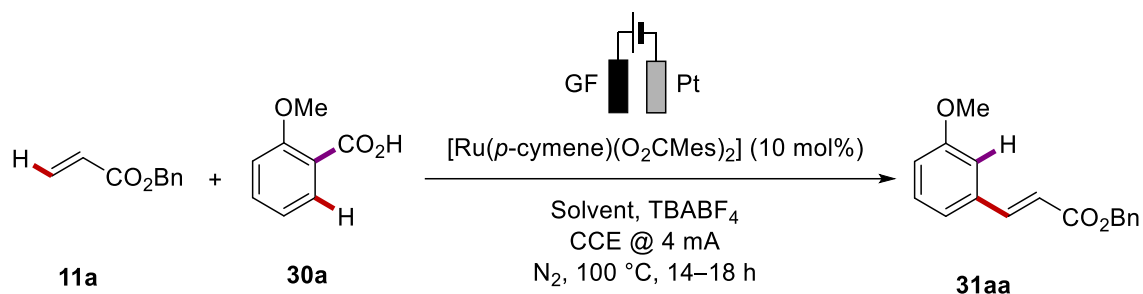
Scheme 3-12 Initial reactivity. [a] Estimated by GC analysis.

An exploration of viable solvents (Table 3.2-1) revealed that in alcoholic (entries 1–3), etheric (entries 4, 5), polar aprotic solvents (entries 6–11) and an ionic liquid (entry 12), the reaction performed either poorly or no product was formed at all, with the starting materials remaining unconsumed for the most part. Therefore, further aromatic solvents were examined next (entries 13–25). Apart from cumene (entry 14), which caused an immediate decomposition of the catalyst, PhCN (entry 17) and PhOCF₃ (entry 21), all solvents allowed for at least two catalytic turnovers. However, with many poorly conductive electrolytes, a current limit in the range of 2–3 mA was reached at 20 V cell potential. When TBAPF₆ was examined as the supporting electrolyte in place of TBABF₄ in order to improve the conductivity, the same result was obtained in the thus far best performing solvent PhOMe (47%, entry 26 vs. entry 16). The further optimization was

RESULTS & DISCUSSION

continued with TBAPF₆, for the superior stability of the hexafluorophosphate anion against anodic oxidation.^[258]

Table 3.2-1 Initial optimization of solvents.^[a]



Entry	Solvent	Yield of 31aa (%)
1	1,4-dioxane	--
2	diglyme	25
3	<i>t</i> -AmOH	< 5 ^[b]
4	Glycerine	--
5	BnOH	< 5 ^[b]
6	GVL	20
7	MeNO ₂	23
8	MeCN	--
9	DMSO	--
10	DMF	--
11	THTD	19
12	BMIM Cl	--
13	<i>o</i> -xylene	26
14	cumene	--
15	cymene	29
16	PhOMe	47 ^[c]
17	PhCN	< 5 ^[b]
18	4-MeC ₆ H ₄ OMe	43 ^[c]

RESULTS & DISCUSSION

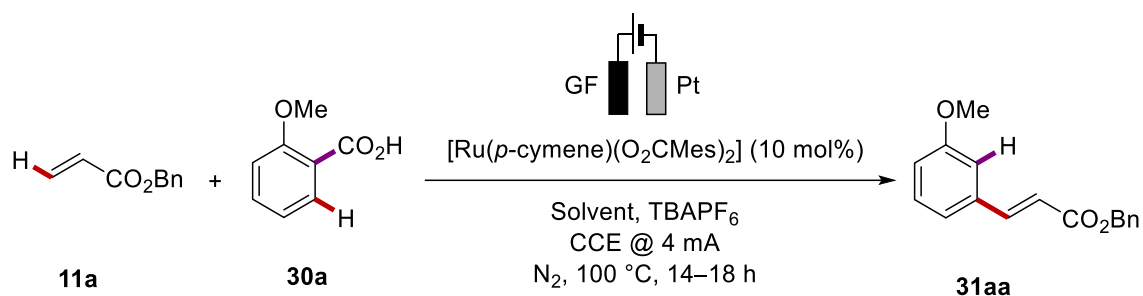
19	<i>o</i> -DCB	46 ^[c]
20	PhCF ₃	36
21	PhOCF ₃	< 5 ^[b]
22	PhSMe	21
23	Ph–Ph	41
24	1-methylnaphthalene	41
25	PhOPh	35
26	PhOMe ^[d]	47 ^[c]

[a] Reaction conditions: Undivided cell, GF anode, Pt cathode, **11a** (0.50 mmol), **30a** (1.50 mmol), [Ru(*p*-cymene)(O₂CMe)₂] (10 mol%), TBABF₄ (0.20 M), solvent (4.0 mL), *T* = 100 °C, under N₂, CCE (4.0 mA) maintained for 14–18 h; yields refer to isolated product. [b] Estimated by GC analysis. [c] Increased amount of **12aa** (approx. 10%) detected by GC-MS. [d] TBAPF₆ as supporting electrolyte. BMIM Cl = 1-butyl-3-methylimidazolium chloride; THTD: tetrahydrothiophene dioxide (sulfolane).

Unfortunately, the most unpolar solvents and therefore least conductive electrolytes led to the best selectivities (entries 13, 15, 23, 24), forming the phthalide side product **12aa** in only trace amounts, while in the moderately conductive PhOMe electrolyte, the GC signal for **12aa** doubled in comparison with the reaction in PhMe (**Scheme 3-12**). Hence, binary and heterogeneous systems were tested to probe whether a tradeoff solution between conductivity and selectivity could be reached (**Table 3.2-2**). With PhMe as the major component, the effect of polar aprotic co-solvents varied severely. While DMSO and formamide had detrimental effects on the outcome (entries 1, 2), weakly-coordinating tetrahydrothiophene dioxide (THTD, sulfolane) and propylene glycol cyclic carbonate (PGCC) improved the yield by more than 20% compared to pure PhMe as the solvent (entries 3, 4), and the cell potential dropped by approximately 80% to 3.5–4.5 V. Interestingly, an equal amount of THTD and PhMe proved disadvantageous (entry 5), and only 24% of the target compound was isolated. Other sulfones (entries 6, 7) did not reach the level of performance of THTD as cosolvent. While small amounts of water were found to be disadvantageous (entry 8), attempts to run the reaction in an aqueous micellar environment failed (entries 9, 10). When PhOMe was employed as 1:1 mixtures with PhMe and *n*-octane, respectively, no appreciable improvement as compared to pure PhMe was registered (entries 11, 12).

RESULTS & DISCUSSION

Table 3.2-2 Screening of binary and heterogeneous solvent systems.^[a]



Entry	Solvent	Yield (%)
1	PhMe/DMSO (5:3)	--
2	PhMe/formamide (5:3)	14
3	PhMe/PGCC (5:3)	46 ^[b]
4	PhMe/THTD (5:3)	48 ^[b]
5	PhMe/THTD (1:1)	24
6	PhMe/Me ₂ SO ₂ (5:3)	40
7	PhMe/Ph ₂ SO ₂ (5:3)	24
8	PhMe/THTD/H ₂ O (5:3:1)	26
9	H ₂ O, SDS (2.5 wt-%)	--
10	H ₂ O, Triton™ X-100 (4 wt-%)	--
11	PhOMe/PhMe (1:1)	35
12	PhOMe/ <i>n</i> -octane (1:1)	43

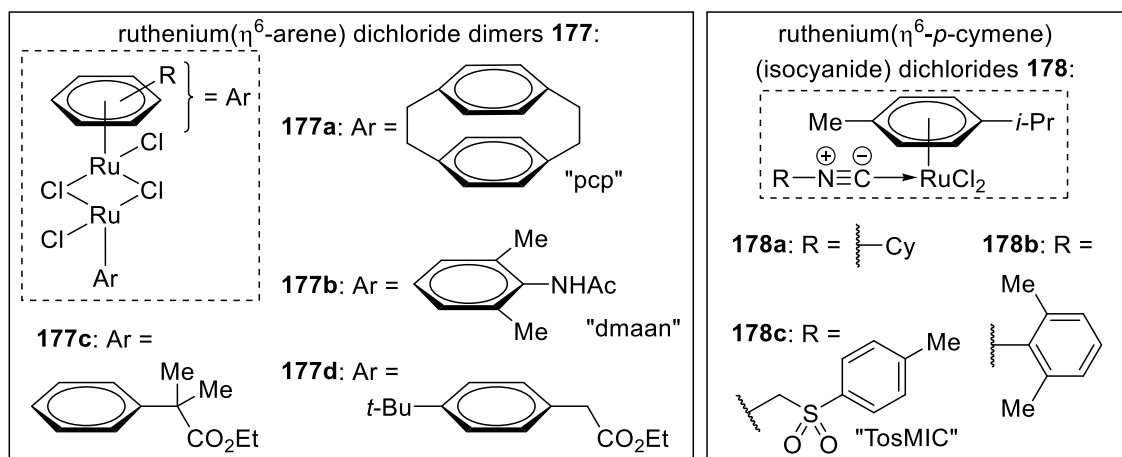
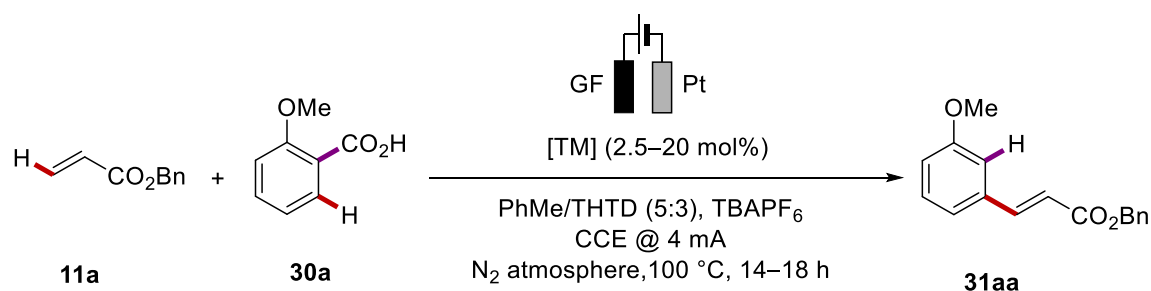
[a] Reaction conditions: Undivided cell, GF anode, Pt cathode, **11a** (0.50 mmol), **30a** (1.50 mmol), [Ru(*p*-cymene)(O₂CMes)₂] (10 mol%), TBAPF₆ (0.20 M), solvent (4.0 mL), *T* = 100 °C, under N₂, CCE (4.0 mA) maintained for 14–18 h; yields refer to isolated product. [b] Increased amount of **12aa** (approx. 10%) detected by GC-MS.

Thereafter, an extensive screening of ruthenium and other metal catalysts was performed (**Table 3.2-3**). Various carboxylate anions and hydroxamate proved less effective (entries 1–3). However, they are expected to influence mostly the C–H activation step, which is presumed to be mechanistically equivalent with various robust ruthenium-catalyzed transformations (see chapter 1.2 and 1.6.3.1.3). In view of the observation that the better the reactions worked, the later they visibly darkened, it is plausible that the major disruptive

factor was the decomposition of the catalyst at the end of the catalytic cycle, which is likely to be terminated by the release of a poorly stabilized ruthenium(0) species. In contrast, the isocoumarine **7** synthesis by ruthena-electro catalysis^[201] was found to proceed through a stable ruthenium(0) sandwich complexes with the product (**135**), which liberated the catalytically active ruthenium(II) *via* oxidative de-coordination. In the present case, an insufficient coordinative stabilization would lead to the collapse of the complex and to the formation of small ruthenium particles, which likely caused the dark coloration towards the end of the reaction. This hypothesis is supported by the consistent detection of free *p*-cymene in the GC-MS analysis of the crude reaction mixtures, indicating the lability of the arene ligand under the given reaction conditions. Therefore, we continued to vary the neutral ligands with the perspective to stabilize the coordination sphere of the presumed final intermediate. Hence, we replaced the *p*-cymene ligand by other η^6 -arene ligands (entries 5–14). Highly electron-rich arenes (entries 7–10) were expected to facilitate the reoxidation by lowering the oxidation potential. However, the catalytic activity was poor. Although aromatic, cyclophanes are known to have partial diene character due to the distortion of the aromatic ring. Since multiple diene-coordinated ruthenium(0) complexes are known, we anticipated that the [2.2]paracyclophane (pcp) ligand would have a stabilizing effect on the putative transient ruthenium(0) species. Unfortunately, the catalyst **177a** visibly decomposed within minutes in the reaction mixture (entry 11). Acetanilide (entry 12) or ester substituents (entries 13–15) could potentially contribute with additional weak coordinations.^[259] Unfortunately, no reactivity was observed in this case either. Additional ligands, such as SPOs (entries 16, 17), phosphine (entry 18), NHC (entry 19) and isocyanides (entries 20–22) also lowered the reactivity. The reaction did also not work with other common ruthenium(II) and ruthenium(III) complexes (entries 23–29), the osmium homologue (entry 30) and 3d metal catalysts (entries 31–35).

RESULTS & DISCUSSION

Table 3.2-3 Catalyst optimization.^[a]



Entry	TM catalyst (mol%)	Additives(s) (mol%)	Yield of 31aa (%)
1	[Ru(<i>p</i> -cymene)(OAc) ₂] (10)	(2,4,6-(MeO) ₃ C ₆ H ₃)CO ₂ H	28
2	[Ru(<i>p</i> -cymene)Cl ₂] ₂ (5)	(30) K ₂ CO ₃ (30)	37
3	[Ru(<i>p</i> -cymene)Cl ₂] ₂ (5)	(Me ₃ Ph)CO ₂ H (30) K ₂ CO ₃ (30)	17
4	[Ru(<i>p</i> -cymene)Cl ₂] ₂ (5)	PivNHOK (30)	< 5
5	[Ru(PhH)Cl ₂] ₂ (5)	MesCO ₂ K (30)	23
6	[Ru(<i>t</i> -BuPh)Cl ₂] ₂ (5)	MesCO ₂ K (30)	31
7	[Ru(C ₆ Me ₆)Cl ₂] ₂ (5)	MesCO ₂ K (30)	< 5
8	[Ru(mdipb)Cl ₂] ₂ (5) ^[260]	MesCO ₂ K (30)	< 10
9	[Ru(pdipb)Cl ₂] ₂ (5) ^[260]	MesCO ₂ K (30)	< 10
10	[Ru(tipb)Cl ₂] ₂ (5) ^[260]	MesCO ₂ K (30)	--
11	[Ru(pcp)Cl ₂] ₂ 177a (5) ^[261]	MesCO ₂ K (30)	--

RESULTS & DISCUSSION

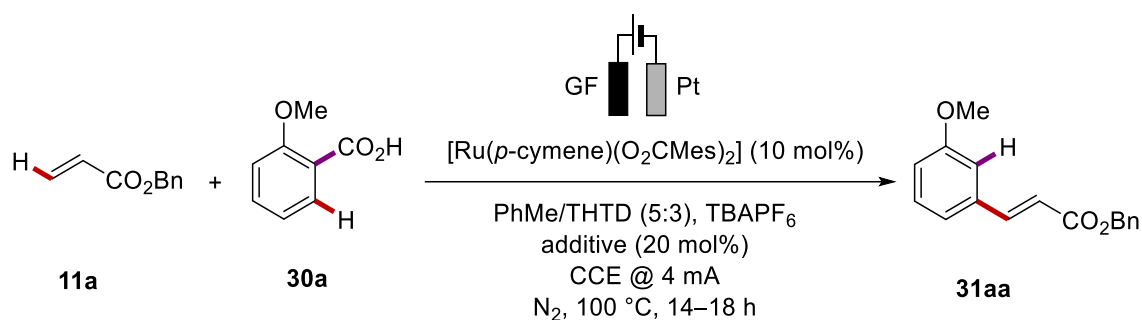
12	[Ru(dmaan)Cl ₂] ₂ 177b (5)	MesCO ₂ K (30)	--
13	[Ru(PhCH ₂ CO ₂ Et)Cl ₂] ₂ (5) ^[262]	MesCO ₂ K (30)	--
14	177c (5)	MesCO ₂ K (30)	--
15	177d (5)	MesCO ₂ K (30)	--
16	[Ru(<i>p</i> -cymene)(<i>t</i> -BuPhPHO)Cl ₂] (10) ^[263]	MesCO ₂ K (30)	--
17	[Ru(<i>p</i> -cymene)(Ph ₂ PHO)Cl ₂] (10) ^[263]	MesCO ₂ K (30)	--
18	[Ru(<i>p</i> -cymene)(PPh ₃)Cl ₂] (10)	MesCO ₂ K (30)	--
19	[Ru(<i>p</i> -cymene)(IMes)Cl ₂] (10) ^[264]	MesCO ₂ K (30)	--
20	[Ru(<i>p</i> -cymene)(CyNC)Cl ₂] 178a (10)	MesCO ₂ K (30)	--
21	178b (10)	MesCO ₂ K (30)	--
22	[Ru(<i>p</i> -cymene)(TosMIC)Cl ₂] 178c (10)	MesCO ₂ K (30)	--
23	[Cp*RuCl ₂] _n (10)	MesCO ₂ K (30)	--
24	[Ru(cod)Cl ₂] _n (10)	MesCO ₂ K (30)	--
25	[Ru(nbd)Cl ₂] _n (10)	MesCO ₂ K (30)	--
26	RuCl ₃ ·3H ₂ O (10)	MesCO ₂ K (30)	--
27	[Ru(dmsO) ₄ Cl ₂] (10)	MesCO ₂ K (30)	--
28	Ru(acac) ₃ (10)	MesCO ₂ K (30)	--
29	[Ru(dtbbpy) ₂ Cl ₂] (10)	MesCO ₂ K (30)	--
30	[Os(<i>p</i> -cymene)Cl ₂] ₂ (5)	MesCO ₂ K (30)	--
31	[Mn(CO) ₅ Br] (10)	MesCO ₂ K (15)	--
32	Fe(acac) ₃ (20)	--	--
33	Co(OAc) ₂ (20)	--	--
34	[Cp*CoCl ₂] ₂ (5)	KOAc (15)	--
35	[Ni(dme)Cl ₂] (10)	KOAc (30)	--

[a] Reaction conditions: Undivided cell, GF anode, Pt cathode, **11a** (0.50 mmol), **30a** (1.50 mmol), catalyst (5–20 mol%), TBAPF₆ (0.20 M), additive, PhMe/THTD (5:3, 4.0 mL), *T* = 100 °C, under N₂, CCE (4.0 mA) maintained for 14–18 h; yields refer to isolated product.

RESULTS & DISCUSSION

Since the initially employed mesityl carboxylate complex was still the best catalyst (**Table 3.2-2**, entry 4; 48%), a series of additives was tested, which could modify the catalyst or the regeneration pathway *in situ* (**Table 3.2-4**). In particular, we intended to test, whether a beneficial effect in terms of the mediation of the oxidation step could be achieved. Several studies confirmed the strong cooperation of oxidants^[30b] during the reductive elimination step rather than after product liberation.^[56a-c] The best oxidant for the chemo-oxidative decarboxylative alkenylation was V₂O₅.^[66c] Neither V₂O₅ nor VO(acac)₂ or other metallic oxidants improved the outcome of the reaction (entries 1–5). In contrast to counterproductive DDQ, the presence of benzoquinone, which among other quinones is often employed as redox mediator^[265] and has also demonstrated ligand cooperation with iridium,^[188] did not affect the reaction outcome (entries 6,7). Iodide ions inhibited the catalytic activity (entry 8).

Table 3.2-4 Additives screening.^[a]



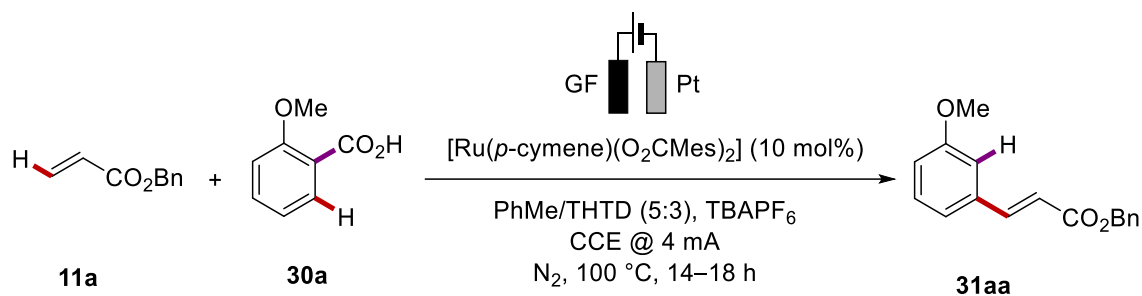
Entry	Additive	Yield of 31aa (%)
1	V ₂ O ₅	33
2	VO(acac) ₂	30
3	Cu(OAc) ₂	31
4	AgNTf ₂	< 5
5	Fc	< 5
6	BQ	46
7	DDQ	--
8	KI	--

RESULTS & DISCUSSION

[a] Reaction conditions: Undivided cell, GF anode, Pt cathode, **11a** (0.50 mmol), **30a** (1.50 mmol), [Ru(*p*-cymene)(O₂CMe)₂] (10 mol%), TBAPF₆ (0.20 M), additive (10 mol%), PhMe/THTD (5:3) (4.0 mL), 100 °C, under N₂, CCE (4.0 mA) maintained for 14–18 h; yields refer to isolated product.

Attempts to foster the oxidation efficiency by conducting the reaction in a divided cell (**Table 3.2-5**, entry 1) or employing a higher current (entry 2) did not lead to the desired result. The addition of silica in order to absorb the ruthenium decomposition products and thereby possibly counteract the further aggregation, was unsuccessful (entry 3). The variation of electrode materials (entries 4–7), reaction temperature (entries 8, 9), a lower catalyst loading (entry 10) and the continuous slow addition of the catalyst *via* a syringe pump (entry 11) did not prevent a rapid halt of the reaction either.

Table 3.2-5 Variation of other key parameters.^[a]



Entry	Deviations from standard reaction conditions	Yield of 31aa (%)
1	Divided cell setup; only solvent and conducting salt in cathodic compartment	< 5 ^[b]
2	$I = 8\text{ mA}$	40
3	Silica (1.00 g) added	10
4	Electrodes: Pt(+) Pt(-)	--
5	Electrodes: GF(+) Ni-foam(-)	27
6	Electrodes: GF(+) GF(-)	< 5 ^[b]
7	Electrodes: graphite rod(+) Pt(-)	17
8	$T = 80\text{ }^\circ\text{C}$	20
9	$T = 120\text{ }^\circ\text{C}$	44
10	Catalyst loading: 5 mol%	27

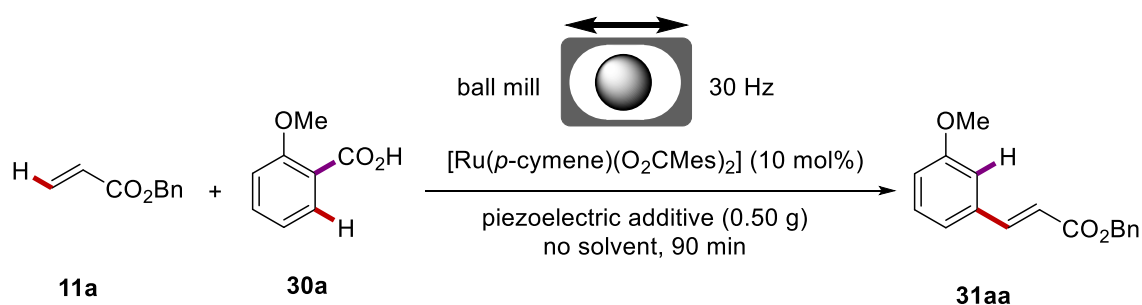
RESULTS & DISCUSSION

11	Continuous addition of catalyst ^[c] over 8 h	23
----	---	----

[a] Reaction conditions: Undivided cell, GF anode, Pt cathode, **11a** (0.50 mmol), **30a** (1.50 mmol), [Ru(*p*-cymene)(O₂CMe)₂] (10 mol%), TBAPF₆ (0.20 M), additive (10 mol%), PhMe/THTD (5:3, 4.0 mL), *T* = 100 °C, under N₂, CCE (4.0 mA) maintained for 14–18 h; yields refer to isolated product. [b] Estimated by GC analysis. [c] Dissolved in 1 mL of the solvent mixture.

As a matter of interest, we explored the possibility to achieve reactivity under neat conditions by means of a piezoelectro-mechanochemistry manifold (**Table 3.2-6**).^[266] In addition to the substrates and the catalyst, piezoelectric materials were added to a ball mill apparatus. We speculated that the necessary electron transfers could occur at the particles' surface upon impact-induced polarization. Unfortunately, no product formation was observed neither in the additive-free reaction (entry 1) nor in the presence of the additives (entries 2–5).

Table 3.2-6 Attempts for piezoelectric mechanochemical activation.



Entry	Piezoelectric material	Yield
1	none	--
2	Sodium potassium L-(+)-tartrate	--
3	Poly(vinylidene difluoride), <i>M_w</i> ≈ 10 ⁶ g/mol	--
4	BaTiO ₃	--
5	NaNbO ₃	--

[a] Reaction conditions: ZrO-coated grinding jar and milling ball, **11a** (0.50 mmol), **30a** (1.50 mmol), [Ru(*p*-cymene)(O₂CMe)₂] (10 mol%), piezoelectric additive (0.50 g), no solvent, no heating/cooling, under air, milling at 30 Hz maintained for 90 min.

3.2.2.2 Electrolyte Activation Study

Since there was no lead whether the system could be improved by the variation of reagents, we returned to address the still present dichotomy of requirements for the solvent regarding selectivity on the one hand and conductivity on the other. When conducting the reactions in PhMe and other non-polar aromatic solvents, the average applied voltage frequently was in the range of 20–30 V, which reflects a high cell resistance, that is generally counterproductive for the selectivity of the electrolysis and therefore the achievable turnover. A notable improvement in yield was achieved when PhOMe or binary solvent mixtures such as PhMe/THTD were employed, accompanied by a substantial decrease of the applied potential. However, as the polarity of the electrolyte was increased, the GC analysis revealed also an increased formation of the corresponding undesired phthalide side product **12aa**, which is in line with the favorable conditions for its intentional preparation (**Figure 3.2-1**).^[66b]

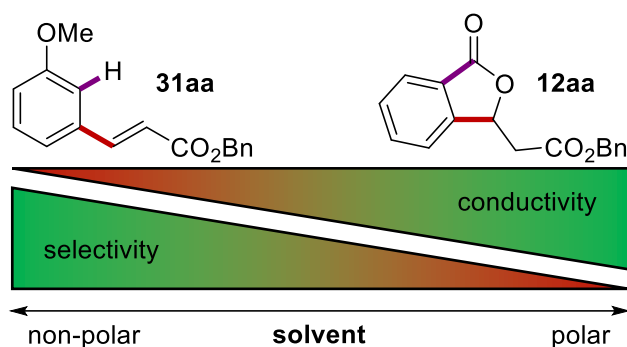


Figure 3.2-1 General effect of the solvent polarity on product selectivity and conductivity.

Generally, in electrochemical reactions, polar solvents are preferred due to their increased ability to form electrolytes by dissociating salt-like substances and solvate the corresponding ions, which are responsible for the conductivity. However, the decarboxylative alkenylation set the challenge to extend the selection of applicable solvents to non-polar ones. As previously indicated, the general answer was highly likely to be found in binary mixtures of polar and non-polar solvents. Specifically, the question was, how much the concentration of the polar component of a homogenous binary solvent mixture could be decreased in order to maintain the conductivity in a favorable range, at the same time keeping predominantly the chemical environment of the non-polar solvent component?

Hence, a series of conductivity tests was performed by recording the constant Faradaic current that could be achieved in the one-electron oxidation of easily oxidizable ferrocene as a model substrate. A reproducible setup was achieved when chronoamperometry was performed at a rotating ring-disc electrode (RRDE) and the steady-state current was measured (see experimental part for details). Accurate control of convection and consistent electrode distance are the crucial benefits of the chosen setup. Initially, the behavior of PhMe as the main electrolyte component was rationalized (**Figure 3.2-2**, red line). Surprisingly, no current was measurable. However, a low current was detected when the solvent contained 6 vol-% of THTD and it increased in a close-to-linear manner up to a THTD percentage of 16 vol-% by almost a factor of 20. The electrolysis rate stayed within a similar range up to a content of 50 vol-%, with a maximum observed at 25 vol-%. The electrolyte formed by pure THTD exhibited a poor conductivity, which can be rationalized by its high viscosity. In sharp contrast, PhOMe revealed a good conductivity, which still could be improved by a factor of approx. 2 with the addition of only 6 vol-% of THTD (**Figure 3.2-2**, black line). However, it should be emphasized that the electrolytic properties of PhOMe, despite being generally considered as a non-polar solvent, are exceptional, as it has been investigated in previous studies.^[267]

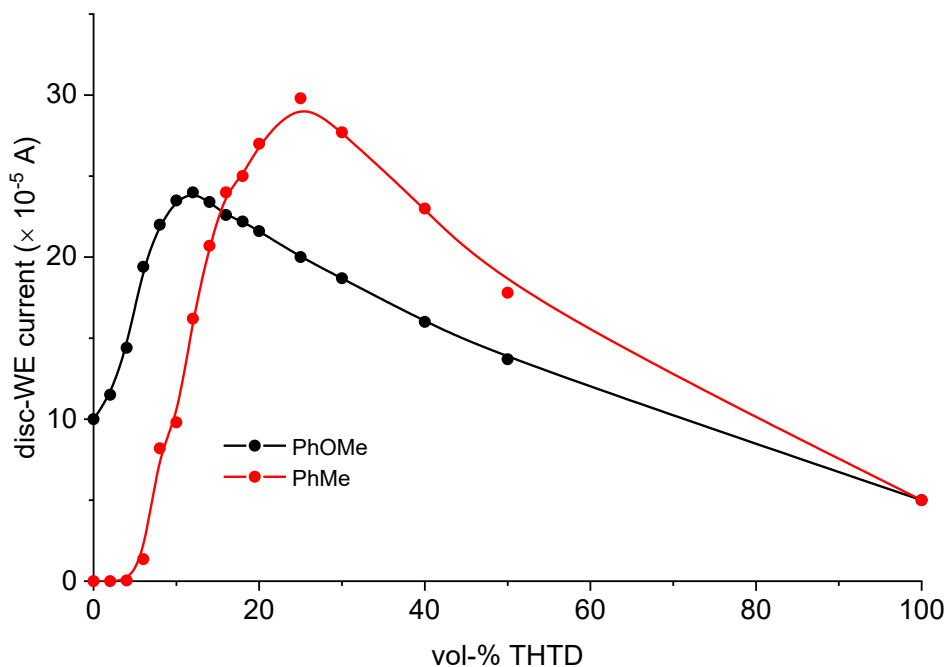


Figure 3.2-2 Conductivity evolution of PhMe (red) and PhOMe (black) in combination with THTD as the cosolvent. Chronoamperometry conditions: RRDE @ 1000 rpm, ferrocene (5 mM), TBAPF₆ (100 mM), 1.3 V vs. Ag/AgCl, 20 °C.

Then, we extended the measurements to several non-polar solvents, commonly employed in transition metal-catalyzed C–H activation reactions. In addition to PhOMe (**Figure 3.2-6**), which gave the best results for the given transformation, PhMe (**Figure 3.2-3**), *t*-AmOH (**Figure 3.2-4**) and 1,4-dioxane (**Figure 3.2-5**) were combined with three highly polar solvents (PGCC, THTD and MeCN; black lines, red lines and blue lines, respectively).

In the case of PhMe and *t*-AmOH, up to a threshold concentration of few vol-% of polar co-solvent, no significant conductivity was observed. Further cosolvent addition resulted in a steep linear rise of conductivity (over an approximately equal range of per cent points) until it stagnated. In slight contrast, the conductivity of the 1,4-dioxane-based electrolyte increased gradually from the beginning. When the volume percentage of added polar co-solvent is converted to the stoichiometric equivalents in relation to the conducting salt (**Table 3.2-7**), the steep rise of the conductivities flattened in the range of 12–15 equivalents for the bulkier PGCC and THTD molecules, and around 19–23 equivalents for the smaller MeCN molecule (estimated by the x-value of the intersection of the tangents of the respective regions). This ratio suggests that up to this point the added cosolvent is almost entirely involved in the buildup of a solvate shell around the cations and anions, with the maximum activity being reached, when there is sufficient polar cosolvent to form typical coordination spheres^[268] with solvent coordination numbers of 6–8 for PGCC and THTD and approximately 12 for MeCN. This behavior also implies that at the threshold percentage for conductivity buildup, most of the conducting salt is dissolved as ion pairs after gradual breakdown of higher-order ionic conglomerates. In the case of PhOMe, lesser amounts of polar co-solvent were required to maximally activate the conductive salt, because as previously stated, it is known to form adequate electrolytes on its own.^[267] With the further addition of the polar co-solvent, the conductivity curve evolves gradually, with the slope likely to be governed by the evolution of the dielectric constant/^[269]viscosity quotient of the solvent system. It shall be noted that for highly non-polar solvents, such as alkanes and long-chain aliphatic ethers, no polar co-solvent (restricted to binary systems) was found to form a homogeneous electrolyte. Interestingly, the progression of conductivity was similar to other studies conducted on electrolytes formed by water and mineral acids.^[270]

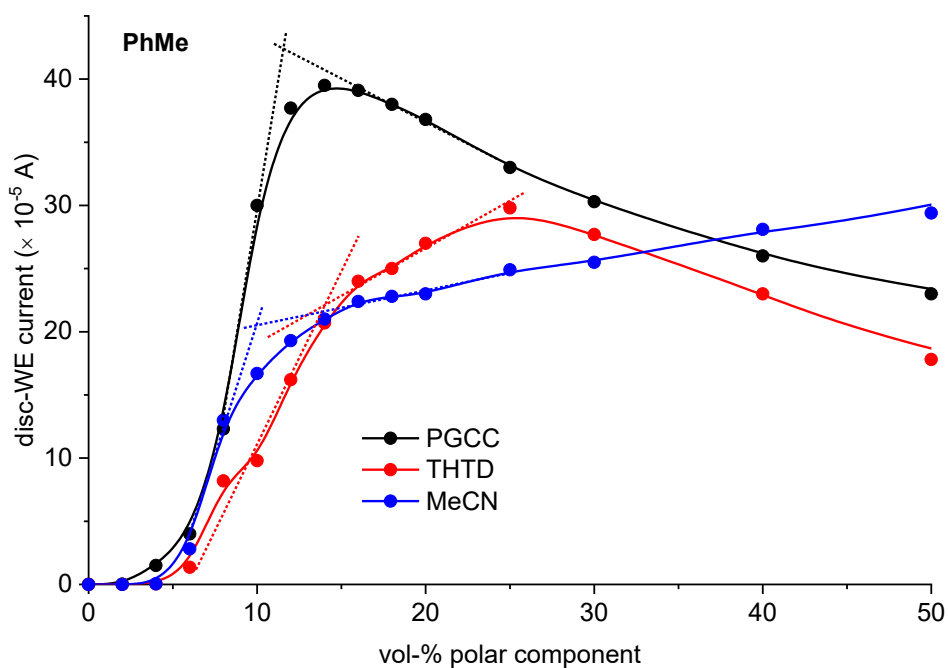


Figure 3.2-3 Conductivity evolution of PhMe. Dotted lines: tangents of activation and stagnation sections (also in following figures). Chronoamperometry conditions: RRDE @ 1000 rpm, ferrocene (5 mM), TBAPF₆ (100 mM), 1.3 V vs. Ag/AgCl, 20 °C.

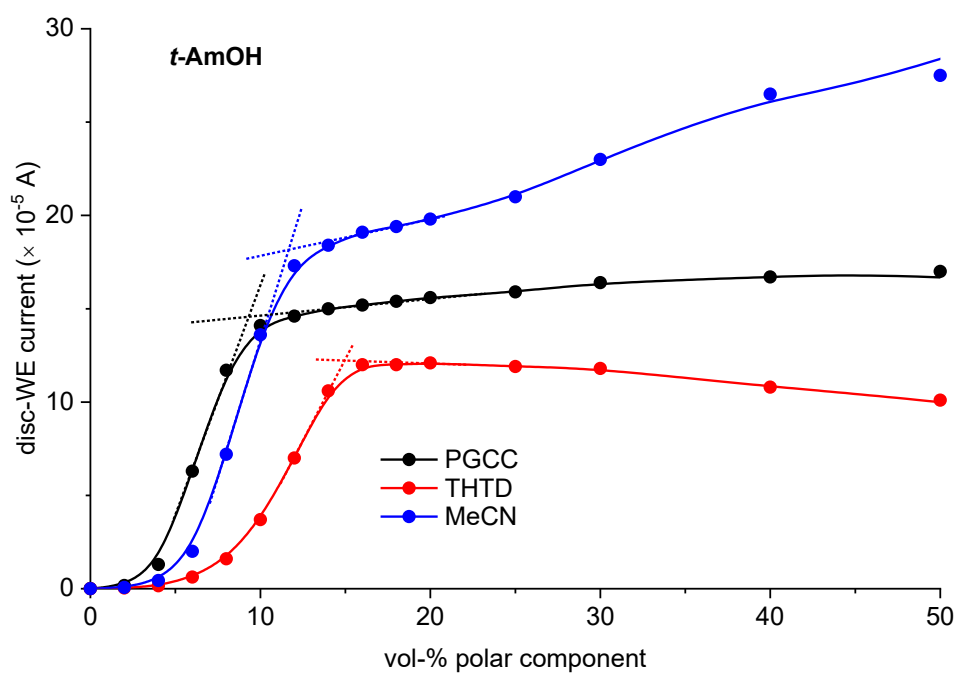


Figure 3.2-4 Conductivity evolution of *t*-AmOH. Chronoamperometry conditions: RRDE @ 1000 rpm, ferrocene (5 mM), TBAPF₆ (100 mM), 1.3 V vs. Ag/AgCl, 20 °C.

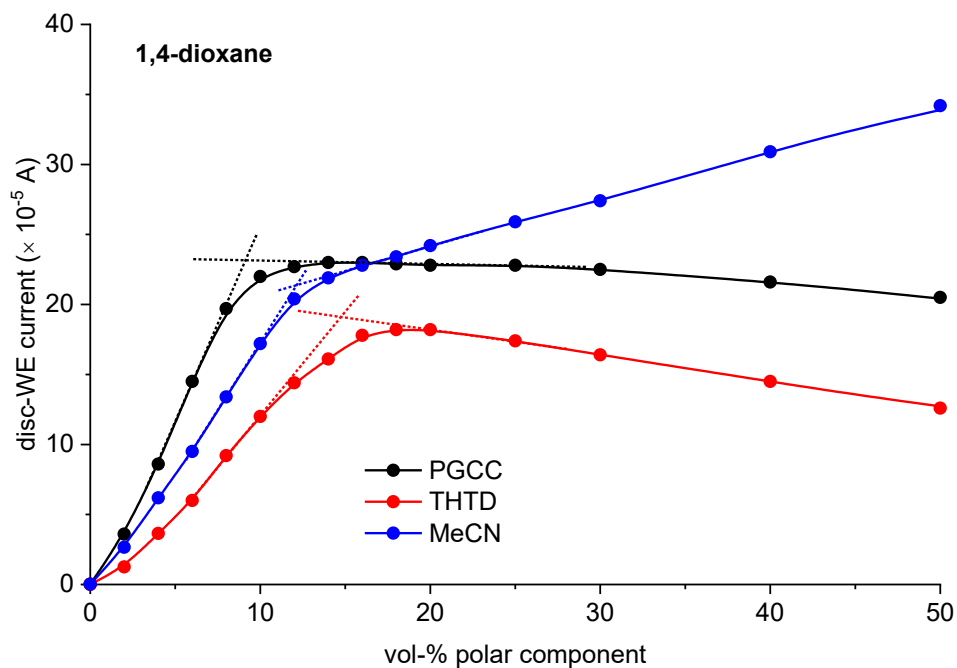


Figure 3.2-5 Conductivity evolution of 1,4-dioxane. Chronoamperometry conditions: RRDE @ 1000 rpm, ferrocene (5 mM), TBAPF₆ (100 mM), 1.3 V vs. Ag/AgCl, 20 °C.

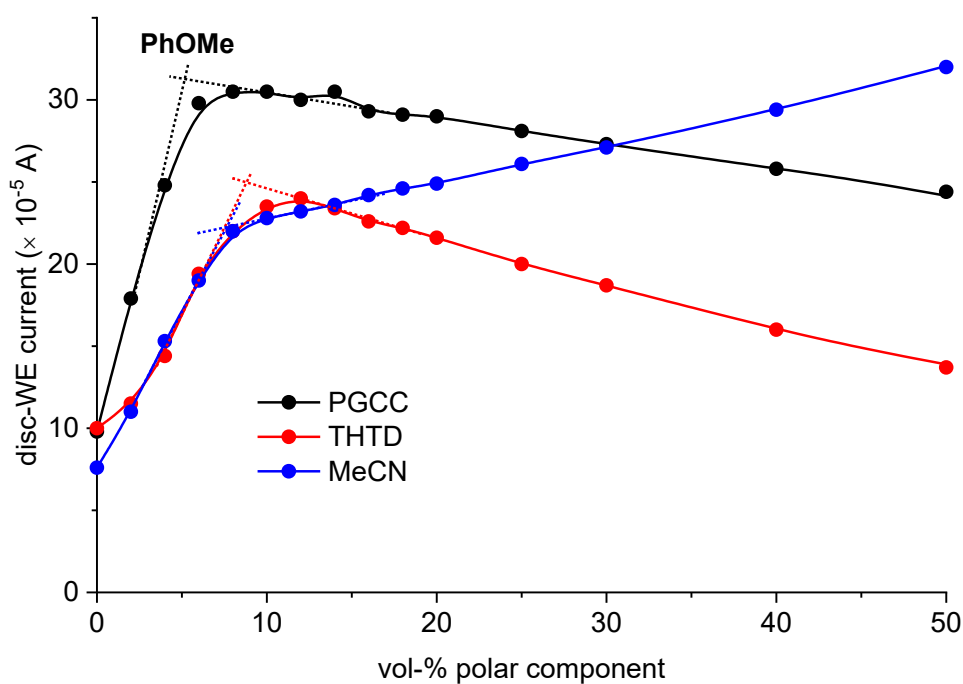


Figure 3.2-6 Conductivity evolution of PhOMe. Chronoamperometry conditions: RRDE @ 1000 rpm, ferrocene (5 mM), TBAPF₆ (100 mM), 1.3 V vs. Ag/AgCl, 20 °C.

RESULTS & DISCUSSION

Table 3.2-7 Volume (and stoichiometric equivalents based on TBAPF₆) of the polar co-solvent at the intersection of activation and stagnation regions.

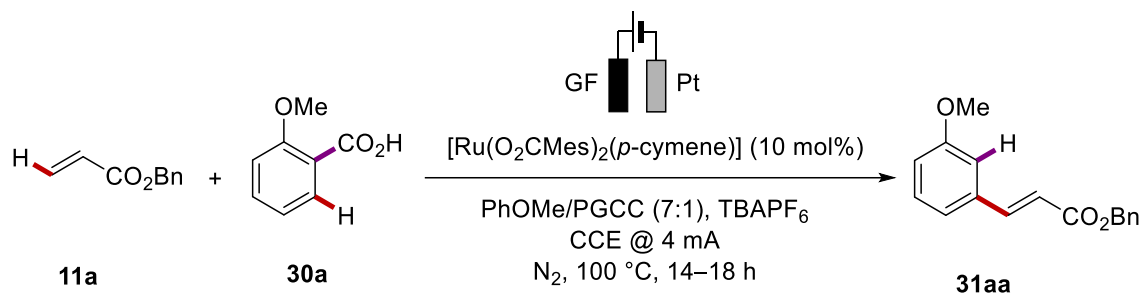
	<i>t</i> -AmOH	1,4-dioxane	PhMe	PhOMe
THTD	15.0 (≈ 16)	14.7 (≈ 15)	14.1 (≈ 15)	8.9 (≈ 9)
PGCC	9.3 (≈ 12)	9.2 (≈ 12)	11.5 (≈ 13)	5.1 (≈ 6)
MeCN	11.6 (≈ 22)	12.2 (≈ 23)	10.0 (≈ 19)	7.7 (≈ 15)

This was just a preliminary study of only few relevant parameters in the field of electrolyte activation in non-polar solvents. Only one conducting salt (TBAPF₆) has been investigated, and it is safe to assume that the solubilities and activities are highly dependent on the nature of both the cation and the anion. The temperature dependence was not investigated, and neither was the concentration dependence of the conducting salt. Nonetheless, the results summarized in **Table 3.2-7** suggest that in order to create conductive homogenous solutions from solvents with low polarity, an addition of 15–20 equivalents based on supporting electrolyte of a polar co-solvent is highly beneficial. This ratio allows the formation of solvated ions within a matrix of the non-polar solvent. On its own, the polar component must be a good solvent for the conductive salt and be well-miscible with the non-polar solvent. Thus, a sufficient proximity in the *Hansen* solubility parameters (HSP) space is required.^[271]

After these insights, the suspicion arose that in many of the previously investigated solvents no actual electrocatalytic turnover was obtained and the undergoing of multiple catalytic cycles was promoted by the acrylate substrates **11** acting as endogenous hydrogen acceptors to form propionates **176** – a behavior that was recently also observed in another ruthenium-catalyzed alkenylation.^[272] This unfortunately also implies that the consumed fraction of the limiting substrate is unavailable for product formation. Indeed, without electricity, the outcome of the CCE reaction in poorly conducting PhMe barely differed from the test runs without current (**Scheme 3-12** vs. **Table 3.2-8**, entry 1). According to **Figure 3.2-6**, out of the investigated cosolvents, the most potent improvement of the performance of PhOMe, which so far was found to be the best individual solvent for the transformation, is expected with the addition of PGCC. Gratifyingly, a PhOMe/PGCC ratio of 7:1 improved the yield up to 60% (entry 2), which corresponds to an almost twofold efficiency improvement as compared to the currentless reaction reported in entry 3. Interestingly, the catalyst performed comparably well with air as the sole oxidant (entry 4)

with in isolated yield of 49%. Rather counterintuitively, the combination of electrical and aerobic oxidation had an adverse effect (entry 5), delivering the target compound **31aa** in only 36% yield.

Table 3.2-8 Test reactions with optimized solvent.^[a]



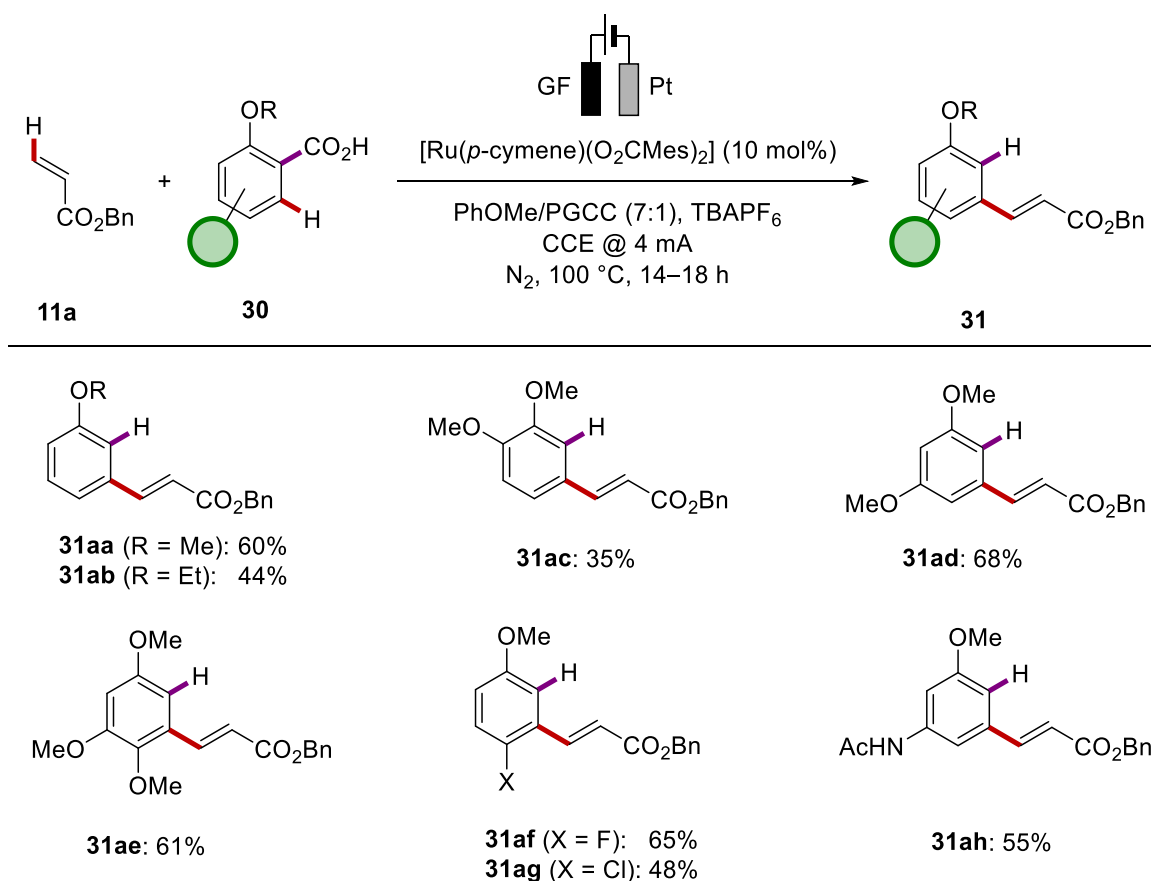
Entry	Deviations from standard conditions	Yield of 31aa (%)
1	No current, no TBAPF ₆ , solvent: PhMe	33
2		60
3	No current, no TBAPF ₆	35
4	Under air, no current, no TBAPF ₆	49
5	Under air	36

[a] Reaction conditions: Undivided cell, GF anode, Pt cathode, **11a** (0.40 mmol), **30a** (1.20 mmol), $[\text{Ru}(p\text{-cymene})(\text{O}_2\text{CMes})_2]$ (10 mol%), TBAPF₆ (0.10 M), PhOMe/PGCC (7:1, 4.0 mL), $T = 100\text{ }^\circ\text{C}$, under N₂, CCE (4.0 mA) maintained for 14–18 h; yields refer to isolated product.

3.2.3 Scope

At this stage, we decided to probe the versatility of the reaction. For this purpose, several anisic acid derivatives **30** were subjected to the optimized conditions with benzyl acrylate **11a** as the coupling partner (**Scheme 3-13**). The manipulation of the *ortho*-alkoxy substituent proved rather limited, allowing to convert only the ethoxy derivative **31ab** in acceptable yield. The reaction efficiency of multiply methoxy-substituted benzoic acids was various, giving the corresponding products **31ac–31ae** in yields between 35% and 68%. Among the halogen-substituted anisic acids, only the fluoro and chloro derivatives **31af** and **31ag** were tolerated by the catalyst, yielding of 65% and 48%, respectively. Moreover, acetanilide-derived product **31ah** was formed in a moderate yield of 55%.

RESULTS & DISCUSSION



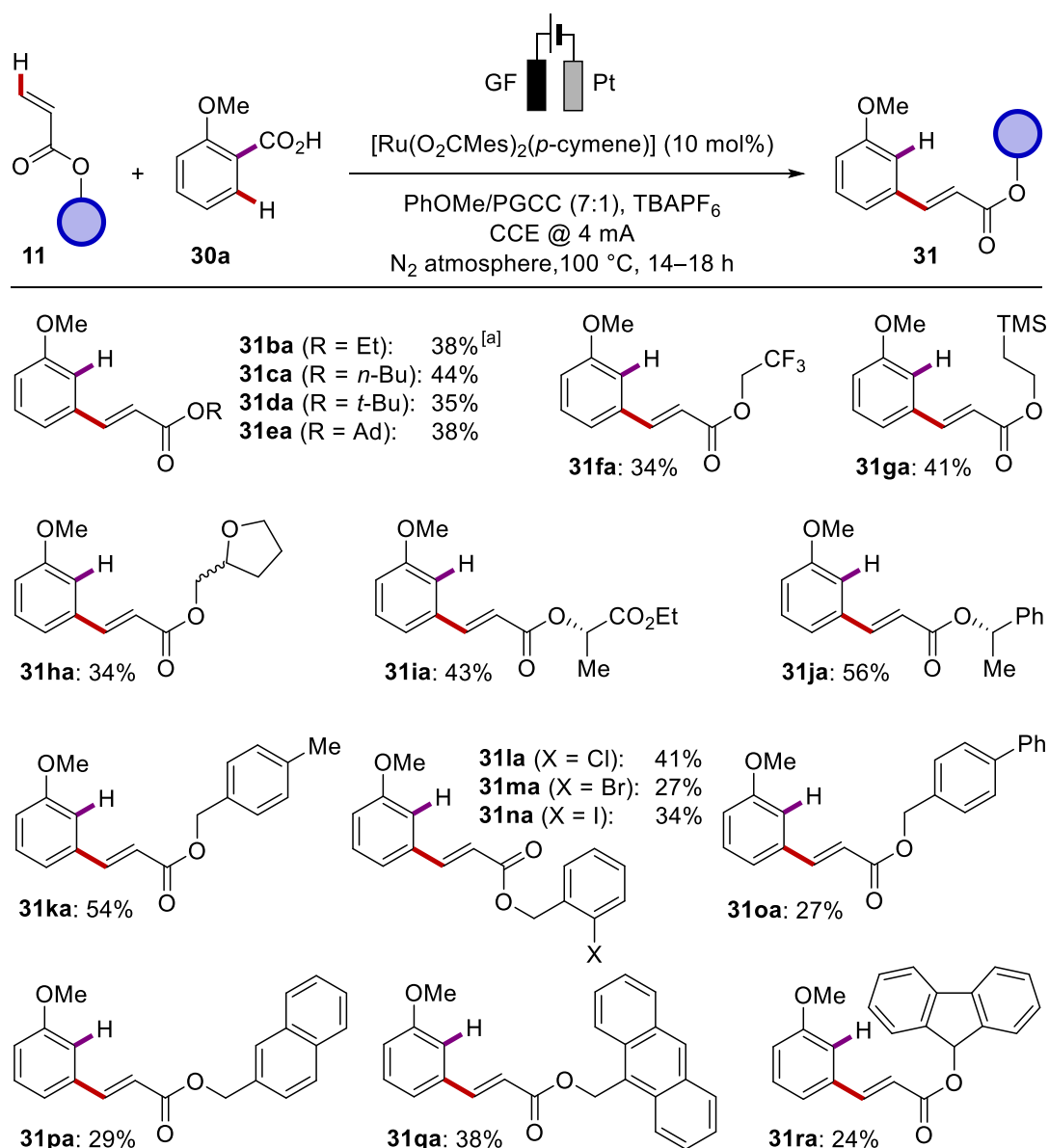
Scheme 3-13 Scope with various alkoxybenzoic acids **30**.

As for the acrylate substrates (**Scheme 3-14**), alkyl esters **11b–11e** reacted only in moderate yields of 35–44%. However, the beneficial role of electricity was confirmed here as well, since ethyl ester **31ba** was formed only in 16% yield without current. The moderate reactivity also prevailed for non-polar heteroatom-containing esters **11f** and **11g**, as well as for polar chains **11h** and **11i**. Compared to the so far most reactive benzyl acrylate **11a** (60% yield), the introduction of an additional methyl substituent in benzylic or *para*-position (**11j**, **11k**) did not alter the yield significantly (56% and 54%, respectively). This finding suggests that a sterically unhindered benzyl substituent on the acrylate coupling partner has a stabilizing effect on the catalyst. Unfortunately, other benzylic substrates, bearing halide substituents in *ortho*-position (**11l–11n**) or larger aromatic moieties (**11o–11r**) hardly exceeded three catalytic turnovers.

Overall, the rather low *TONs* suggest that the conductivity optimization does not fully compensate for the inherently difficult ET, that is needed for the oxidative catalyst regeneration. The unmatched performance of V_2O_5 as terminal oxidant^[66c] is indicative of

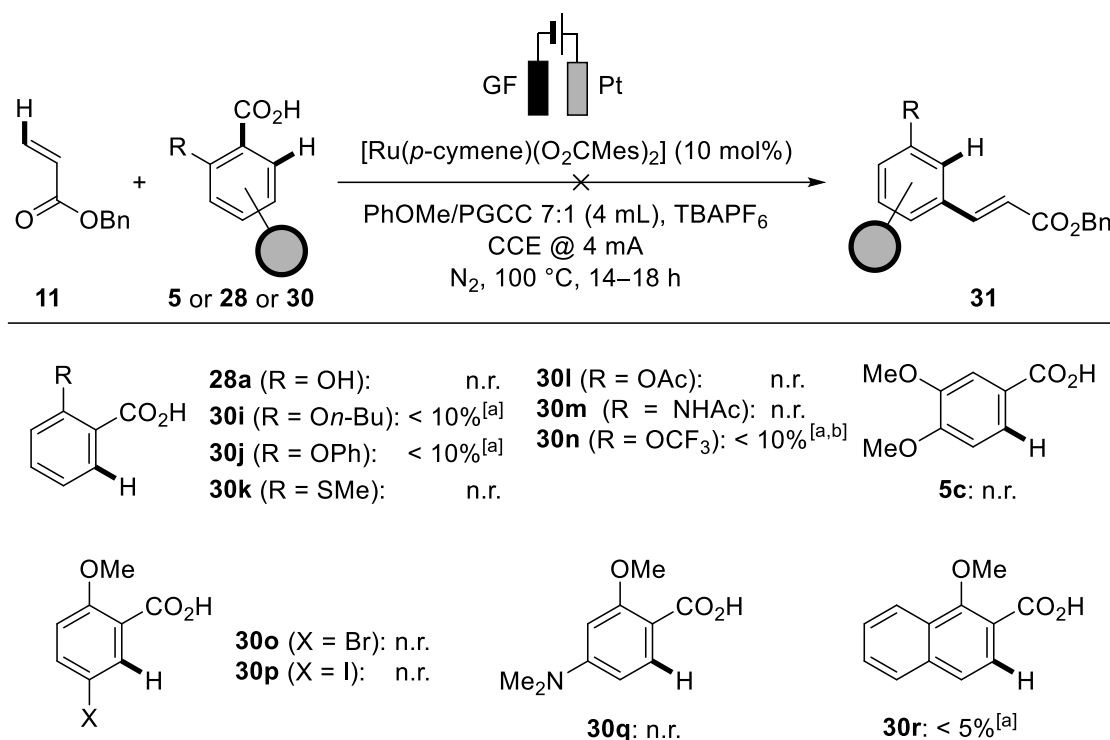
RESULTS & DISCUSSION

an ET, that preferentially occurs through an inner-sphere mechanism, which in turn would require either an adequate mediator or a modified electrode surface in order to provide a favorable orbital overlap by homogeneous or heterogeneous means, respectively. This circumstance illustrates the non-triviality of electrification, meaning that even though potential control is a powerful handle to generate reactivity, its correct adjustment is barely sufficient, when inner-sphere ETs are part of the equation, and the lifetime of the key intermediate is so short, that a timely encounter with the heterogeneous electrode surface is hardly achievable.



Scheme 3-14 Scope with various acrylates **11**. [a] 16% yield was obtained when the reaction was performed without electric current.

In addition to the generally challenging nature of the electrified decarboxylative alkenylation, we also discovered several specific limitations of the system. For the aromatic acid substrates (**30** or **5**, **Scheme 3-15**), we evidenced an outright dependence on the *ortho*-effect.^[273] Due to the repulsive interactions between the carboxyl group and the *ortho*-substituent, anisic acids **30** are inherently destabilized, which aids the decarboxylation step through. The *ortho*-methoxy group proved vital for the alkenylation, since neither salicylic acid **28a** nor substrates carrying bulkier ether (**30i**, **30j**), thioether (**30k**), ester (**30l**) or amide (**30m**) substituents could form the desired products in acceptable yield. More electron-deficient anisic acid derivative **30n** mainly led to the phthalide side product **12an**. Without *ortho*-substituent (**5c**), also no product was formed. Bromo, iodo and amino substituents (**30o–30q**) were incompatible with the reaction, as well as naphthoic acid derivative **30r**.



Scheme 3-15 Limitations of the aromatic acids within the ruthena-electro-catalyzed decarboxylative alkenylation. [a] Estimated by GC-MS. [b] Phthalide side product **12an** (approx. 30%) detected by GC-MS.

The given transformation was thus far not extendable to other activated vinyl derivatives (**Scheme 3-16**) such as styrene **15a**, acrylic acid **111a**, acrylamide **113a**, acrylonitrile **72**, thioacrylate **179a** and imide **113b**. Highly activated maleimides **33** were previously shown to undergo redox-neutral alkylations under comparable current-free conditions,^[91] which

3.3 Rhoda-Electro-Catalyzed C–C Activation

Despite its rarity and high cost, rhodium has proved indispensable in ton-scale industrial applications due to its unparalleled selectivity and activity.^[274] Moreover, the noble character reveals itself in exceptional turnover numbers (*TON*) and therefore low catalyst loadings. At last, elaborate procedures were developed to recycle the precious metal,^[275] thereby further justifying its employment in essential scenarios. Therefore, the potential of homogeneous rhodium catalysis is still being actively explored,^[276] after having already demonstrated versatile reactivity in the area of oxidative arene functionalization by means of C–H^[29f,277] and C–C^[51,278] activation. Within few decades, a multitude of alkenylation and annulation reactions were developed under remarkably mild catalytic conditions.

In terms of substrates, the utilization of naturally occurring motifs for the construction of envisioned scaffolds is highly desirable, since prefunctionalizations can be avoided. Next to C–H bonds, C–C single bonds are ubiquitously occurring in organic molecules. In contrast to C–H bonds, the targeting of a particular C–C bond is less equivocal due to its specific substitution pattern, which can aid the fixation of the catalyst. In this context, several C–C activation reactions were developed, with particular interest for unstrained motifs. Among others, *Shi* has shown that highly regioselective alkenylations of arenes can be achieved using rhodium catalysis^[102], when the desired position is substituted with an appropriate leaving group, proving superior to an analogous C–H functionalization. One drawback of the system is the employment of stoichiometric amounts of expensive silver salts. We intended to modify the reaction by substituting the oxidant by electricity, thereby dramatically reducing the load of heavy metal and improving the overall sustainability in terms of atom economy and waste prevention.

The discovery and the major part of the optimization of the electrochemical cross-dehydrogenative C(sp²)-C/C(sp²)-H functionalization was accomplished by *Dr. Youai Qiu*. I joined the project at an early stage, contributing mainly to the substrate scope and mechanistic studies.

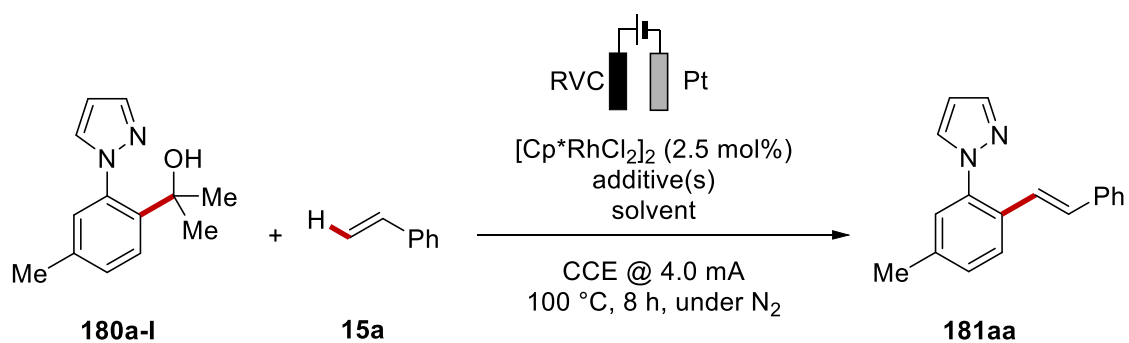
3.3.1 Optimization

The reactivity of model substrates **180a** and **15a** towards an electro-oxidative coupling was tested in presence of a rhodium catalyst and KOAc as the basic additive (**Table 3.3-1**). For this purpose, a convenient undivided cell setup was used, with a platinum cathode and a

RVC anode. This choice of electrode materials proved efficient in various metalla-electrocatalyzed C–H activation reactions. The reaction proceeded in the constant current mode at 4 mA with significant turnover in several highly polar protic solvents, such as H₂O, MeOH and TFE (entries 1–3), while in less polar *t*-AmOH, the catalysis stopped at *TON* = 2 (entry 4), presumably due its poor ability to form conductive solutions (see chapter 3.2.2.2). Aprotic PhMe and MeCN failed to deliver the desired product **181aa** (entries 5 and 6). The best result was obtained when a 3:1 mixture of *t*-AmOH and H₂O was used (entries 7 and 8), and the desired compound **181aa** was isolated in 82% yield, irrespective of which substrate was used as limiting reagent. Variation of the solvent ratio did not improve the outcome (entries 9 and 10) and the starting material was quantitatively recovered. Without electric current, only 9% of the desired product **181aa** were formed (entry 11), whereas in the absence of catalyst the reaction did not proceed at all (entry 12). The rhodium catalyst was also proven superior to less costly ruthenium-based catalyst (entry 13). The homologue iridium complex did not display any catalytic activity (entry 14). In the absence of a basic additive, the reaction did not proceed efficiently (entries 15 and 16). The performance observed with KOAc was not matched by other additives, such as NaOPiv and K₂CO₃ (46% and 61%; entries 17 and 18, respectively). Due to the biphasic nature of the solvent system, the contact area of the electrode with the highly conductive aqueous layer was fluctuating, thereby causing fluctuations in the potential. Therefore, homogenized systems were tested, using *i*-PrOH as a water-miscible alternative to *t*-AmOH (entry 19), a ternary solvent system with EtOH as additional co-solvent (entry 20), and a surfactant as additive (entry 21). Indeed, the average cell potential, usually varying between 3.5 V and 4.5 V, was both stabilized and lowered in all cases to 1.3 V, 1.2 V and 1.7 V, respectively. Although the desired effect was achieved, the overall outcome of the electrolysis could not be improved. Running the reaction at *T* = 85 °C slightly lowered the yield (entry 22). Aerobic atmosphere was well tolerated (82%, entries 7 and 8 *vs.* 78%, entry 23). However, a lower current decreased the efficiency to 45% (entry 24).

RESULTS & DISCUSSION

Table 3.3-1 Optimization studies for the rhoda-electrocatalyzed C–C alkenylation.^[a]



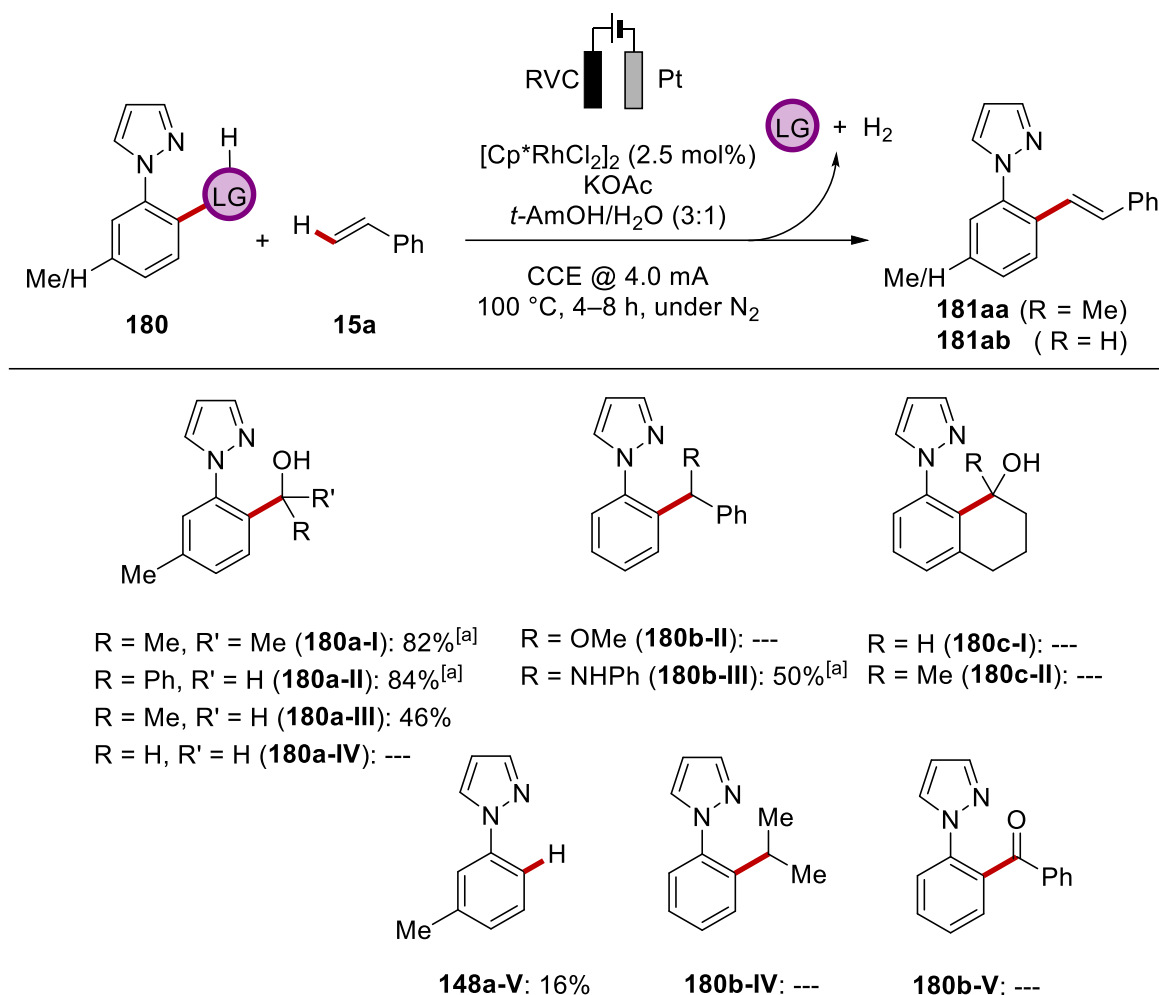
Entry	Solvent	Additive	Deviation from reaction conditions	Yield of 181aa (%)
1 ^[b]	H ₂ O	KOAc		35
2 ^[b]	TFE	KOAc	$T = 70\text{ °C}$	18
3	MeOH	KOAc	$T = 60\text{ °C}$	60
4	<i>t</i> -AmOH	KOAc		10
5	MeCN	KOAc	$T = 80\text{ °C}$	---
6 ^[b]	PhMe	KOAc	<i>n</i> -Bu ₄ NBF ₄ (0.1 M) was added	---
7 ^[b]	<i>t</i> -AmOH/H ₂ O (3:1)	KOAc		82
8	<i>t</i> -AmOH/H ₂ O (3:1)	KOAc	180a-I : 0.375 mmol 15a : 0.25 mmol	82
9 ^[b]	<i>t</i> -AmOH/H ₂ O (1:1)	KOAc		69
10 ^[b]	<i>t</i> -AmOH/H ₂ O (7:1)	KOAc		51
11 ^[b]	<i>t</i> -AmOH/H ₂ O (3:1)	KOAc	without electric current	9
12 ^[b]	<i>t</i> -AmOH/H ₂ O (3:1)	KOAc	without catalyst	---
13 ^[b]	<i>t</i> -AmOH/H ₂ O (3:1)	KOAc	[RuCl ₂ (<i>p</i> -cymene)] ₂	34
14 ^[b]	<i>t</i> -AmOH/H ₂ O (3:1)	KOAc	[Cp*IrCl ₂] ₂	---
15 ^[b]	<i>t</i> -AmOH/H ₂ O (3:1)	KPF ₆		8
16 ^[b]	<i>t</i> -AmOH/H ₂ O (3:1)	---		22
17 ^[b]	<i>t</i> -AmOH/H ₂ O (3:1)	K ₂ CO ₃		46
18 ^[b]	<i>t</i> -AmOH/H ₂ O (3:1)	NaOPiv		61
19 ^[b]	<i>i</i> -PrOH/H ₂ O (3:1)	KOAc	$T = 85\text{ °C}$	72

RESULTS & DISCUSSION

20	<i>t</i> -AmOH/EtOH/H ₂ O (2:1:1)	KOAc		38
21	<i>t</i> -AmOH/H ₂ O (3:1)	KOAc	sodium 2-dodecylbenzene sulfonate (0.05 M) was added	60
22	<i>t</i> -AmOH/H ₂ O (3:1)	KOAc	<i>T</i> = 85 °C	68
23	<i>t</i> -AmOH/H ₂ O (3:1)	KOAc	under air	78
24	<i>t</i> -AmOH/H ₂ O (3:1)	KOAc	1mA, 16 h	45

[a] Reaction conditions: undivided cell, RVC anode, Pt cathode, **180a-I** (0.25 mmol), **15a** (0.50 mmol), catalyst (2.5 mol% of dimer), additive (2.0 equiv), solvent (4.0 mL), *T* = 100 °C, under N₂, CCE (4.0 mA) maintained for 8 h, yields refer to isolated product. [b] Reaction performed by *Dr. Qiu*.

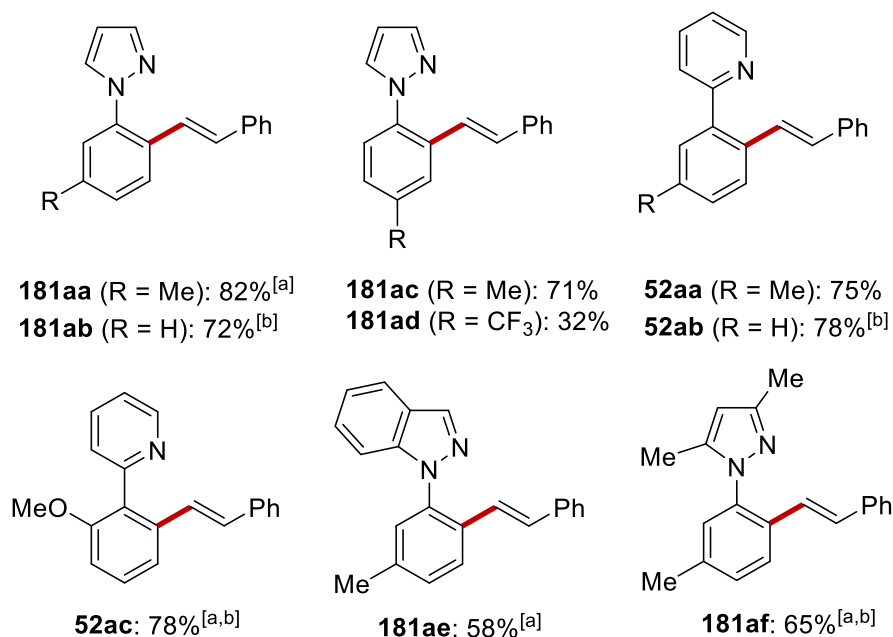
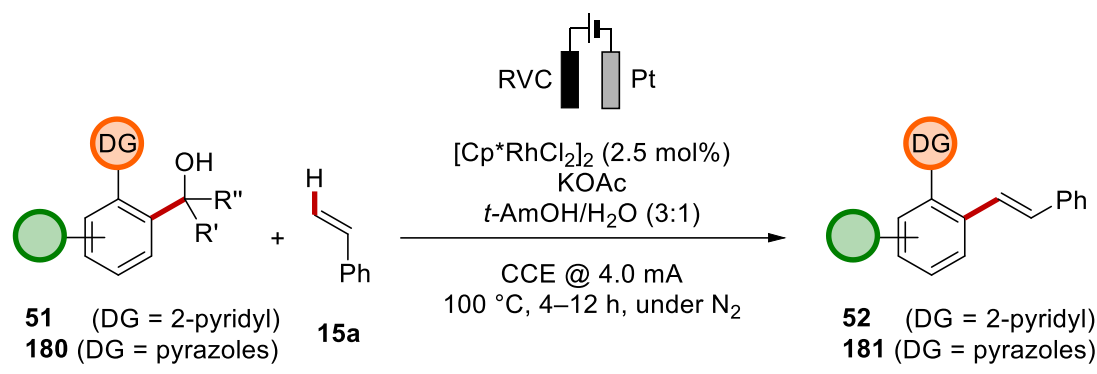
At this point, we examined the leaving group efficiency (**Scheme 3-17**). Several substituted alcohols in the *ortho*-position to the pyrazolyl group displayed good reactivity, furnishing the product **181aa** and the corresponding ketone or aldehyde. Acetone and benzaldehyde leaving groups proved similarly efficient (82% for **180a-I** and 84% for **180a-II**). By contrast, acetaldehyde displayed substantially diminished leaving group ability (**180a-III**), forming the product **181aa** in only 46% yield, while the parent formaldehyde substrate **180a-IV** was unable to form any product. An imine as leaving group (**180b-III**) proved to be a less suited alternative, giving a moderate yield of 50%. Unfortunately, substrates **180c-I** and **180c-II**, which bear an intramolecularly tethered leaving group, did not show reactivity. According to the proposed catalytic cycle (*vide infra*) it seems plausible, that the limited rotational flexibility prevents the catalyst from efficient coordination. Moreover, also aprotic derivatives **180b-II**, **180b-IV** and **180b-V** failed to furnish any product. The leaving group-free substrate **148** delivered the product in poor yield, proving the higher bond activation rate of the leaving group-bearing substrates **180-I** and **180-II**. For this reason, in most cases, an excess amount of arenes **180** was employed (conditions of **Table 3.3-1**, entry 8), despite their usually higher value than alkenes **15**, in order to completely suppress their conceivable partial *di*-functionalization. We also decided to continue the investigation of the substrate scope mainly with substrates bearing the acetone leaving group due to the outstanding combination of reactivity and atom economy.



Scheme 3-17 Investigation of the leaving group efficiency. [a] Reaction performed by *Dr. Qiu*.

3.3.2 Scope

With the optimized conditions in hand, we began to investigate the versatility by varying the directing group (**Scheme 3-18**). Among the substrates with unsubstituted pyrazole (**180a–180d**), the more electron-rich arenes **180a** and **18c** reacted more efficiently (82% and 71% vs. 72% for **180b** and 32% for **180d**, respectively). Substrates with modified pyrazole rings **180e** and **180f** led to slightly decreased yields. Besides the pyrazolyl moiety, the pyridyl group also proved amenable, delivering products **52aa–52ac** in 75–78% yield.

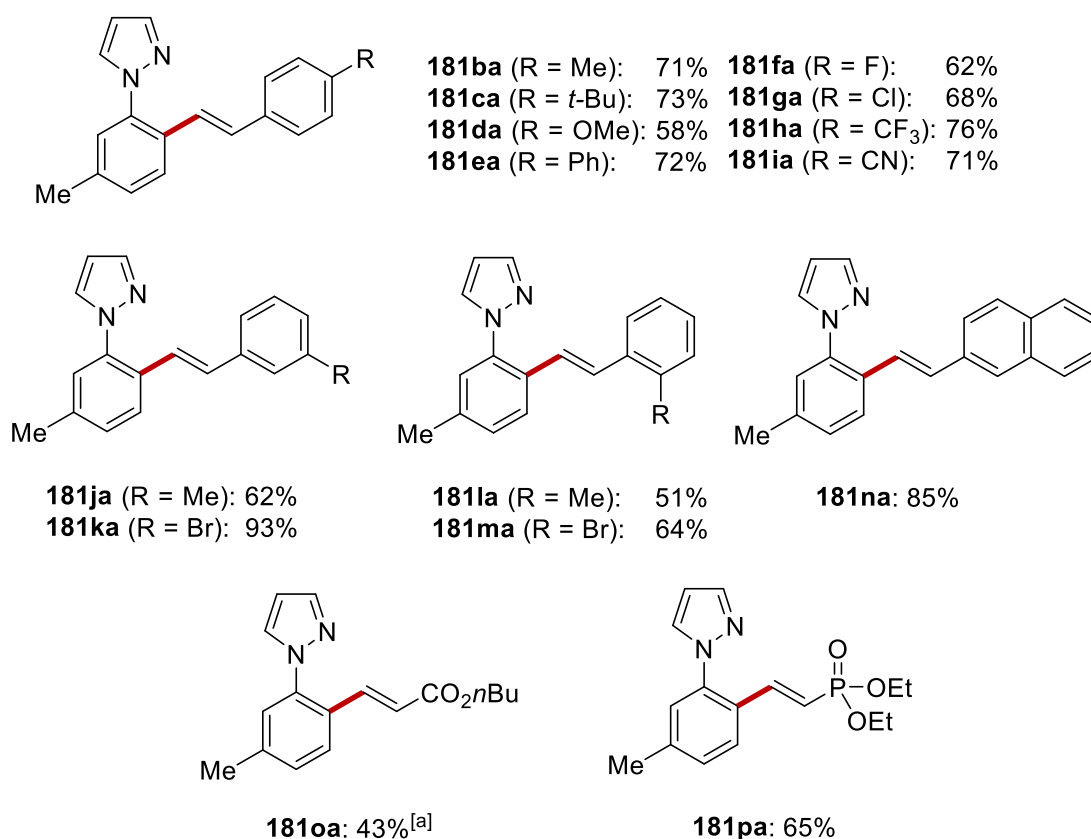
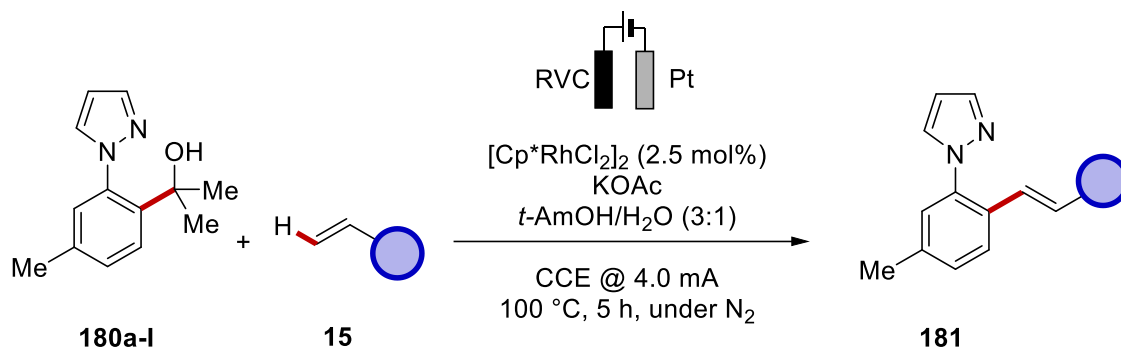


Scheme 3-18 Variation of the directing group and the arene moiety. [a] Reaction performed by *Dr. Qiu*. [b] Substrate with R' = Ph, R'' = H used.

Next, we varied the styrene coupling partners (**Scheme 3-19**). A wide range of substituents in the *para*-position to the vinyl group with various degrees of electron deficiency and electron-richness proved compatible with the reaction conditions and underwent the cross-dehydrogenative coupling (CDC) in similarly good yields (**181ba–181ia**) of 58–76%. Good yields were also obtained when the styrene substrate was substituted in *meta*-position (**181ja, 181ka**). The yields were slightly lower when the same substituents were introduced in *ortho*-position (**181la, 181ma**), thereby potentially creating a steric conflict with the catalytic center. Interestingly, in both cases, a bromo substituent performed better than a methyl substituent, which is suggestive of secondary substrate-substrate or substrate-catalyst interactions by halogen bonding.^[279] The excellent tolerance towards halogens is especially valuable for the feasibility of further functionalization. In addition to styrenes,

RESULTS & DISCUSSION

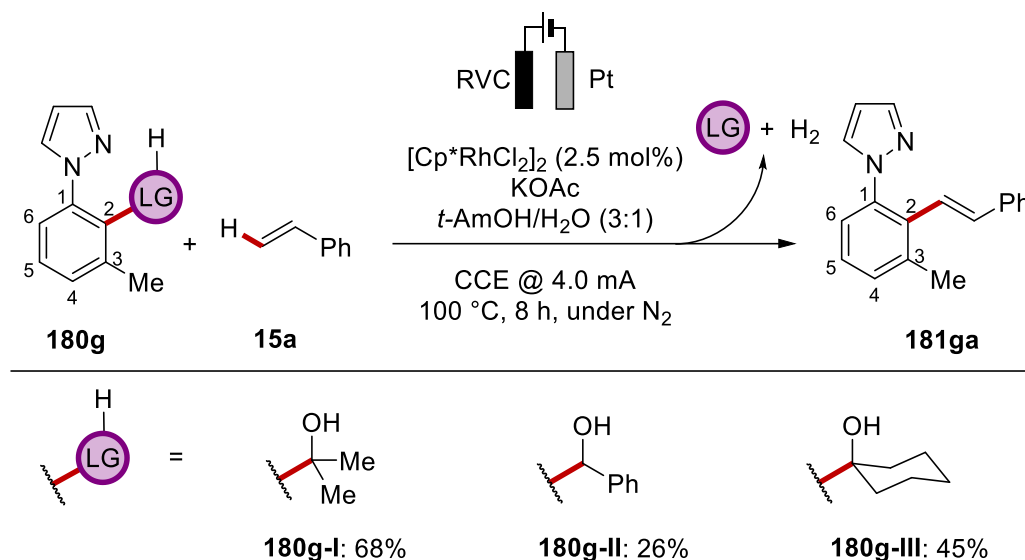
vinyl naphthalene **15n**, vinylphosphonate **15o** and acrylate **11c** proved viable coupling partners.



Scheme 3-19 Scope of olefins. [a] Reaction performed by *Dr. Qiu*.

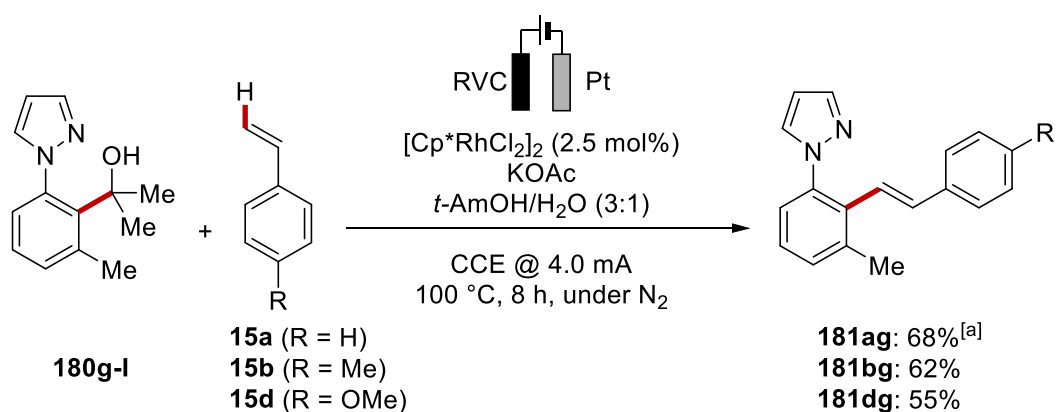
To further demonstrate the utility of our approach, we synthesized sterically congested substrates **180g** (**Scheme 3-20**), which feature a methyl substituent in the *ortho*-position (*C*-3) to the leaving group (*C*-2). As previously shown in **Scheme 3-17**, **148a-V** reacted *via* a C–H activation pathway selectively at the sterically less hindered position. Therefore, without the positional specification, guided by a leaving group, a 1,2,3 substitution pattern

on the arene ring would be inaccessible by conventional C–H activation, when the C-6 position is also available for functionalization. For this substrate class, a reexamination of the leaving groups was undertaken, revealing that once again, acetone was the leaving group of choice.



Scheme 3-20 Re-investigation of the leaving group for the synthesis of 1,2,3-substituted arenes **181g**. Reactions performed by *Dr. Qiu*.

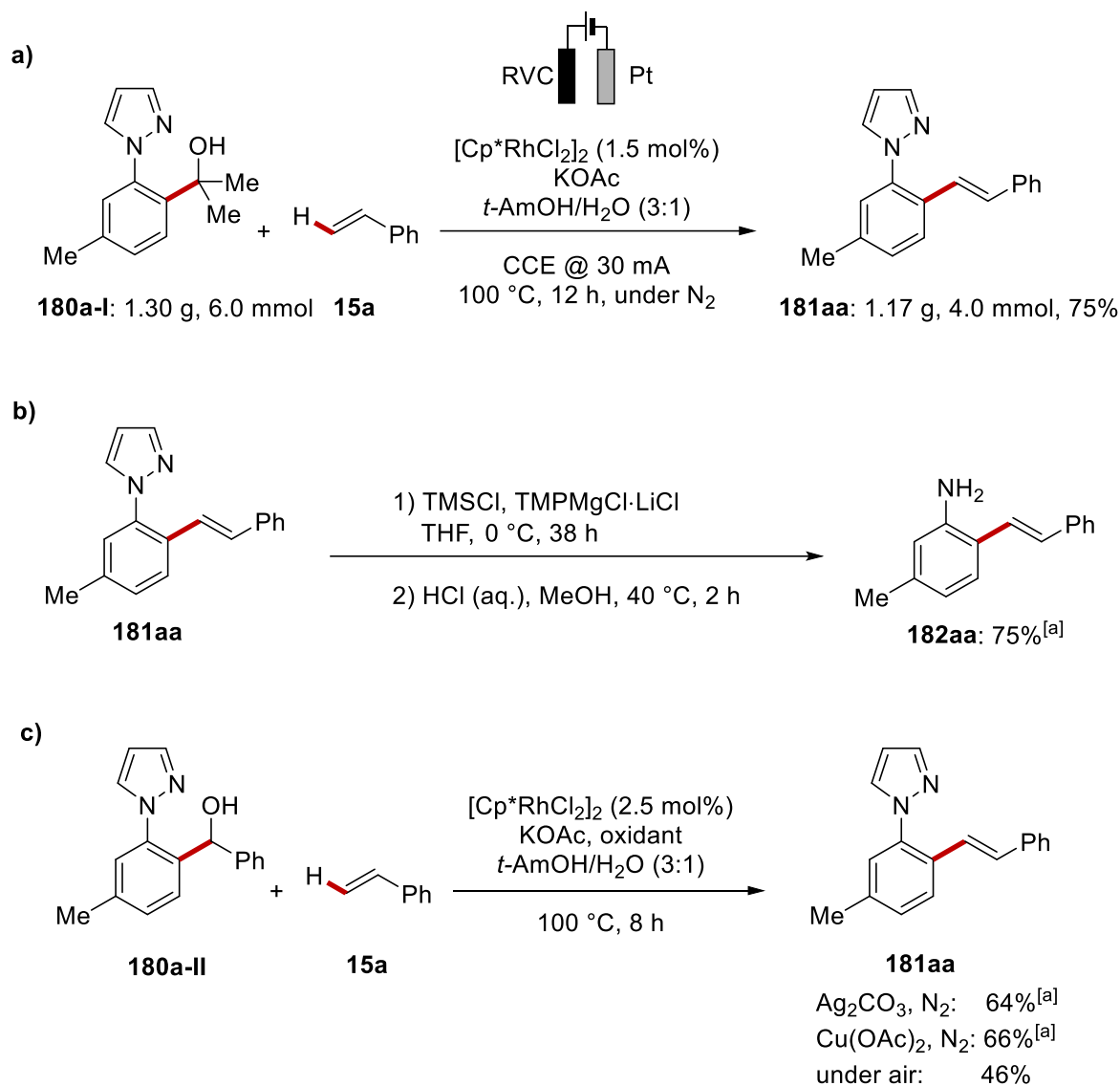
Thus, substrate **180g-I** was converted in moderate to good yields, but excellent positional selectivities to the desired products **181ag–181dg** (**Scheme 3-21**).



Scheme 3-21 Alkenylation towards 1,2,3-substituted arenes **181**. [a] Reaction performed by *Dr. Qiu*.

The practicality of the reaction was showcased by a gram-scale reaction with almost undiminished efficiency, even despite a reduced catalyst loading (**Scheme 3-22, a**), and the

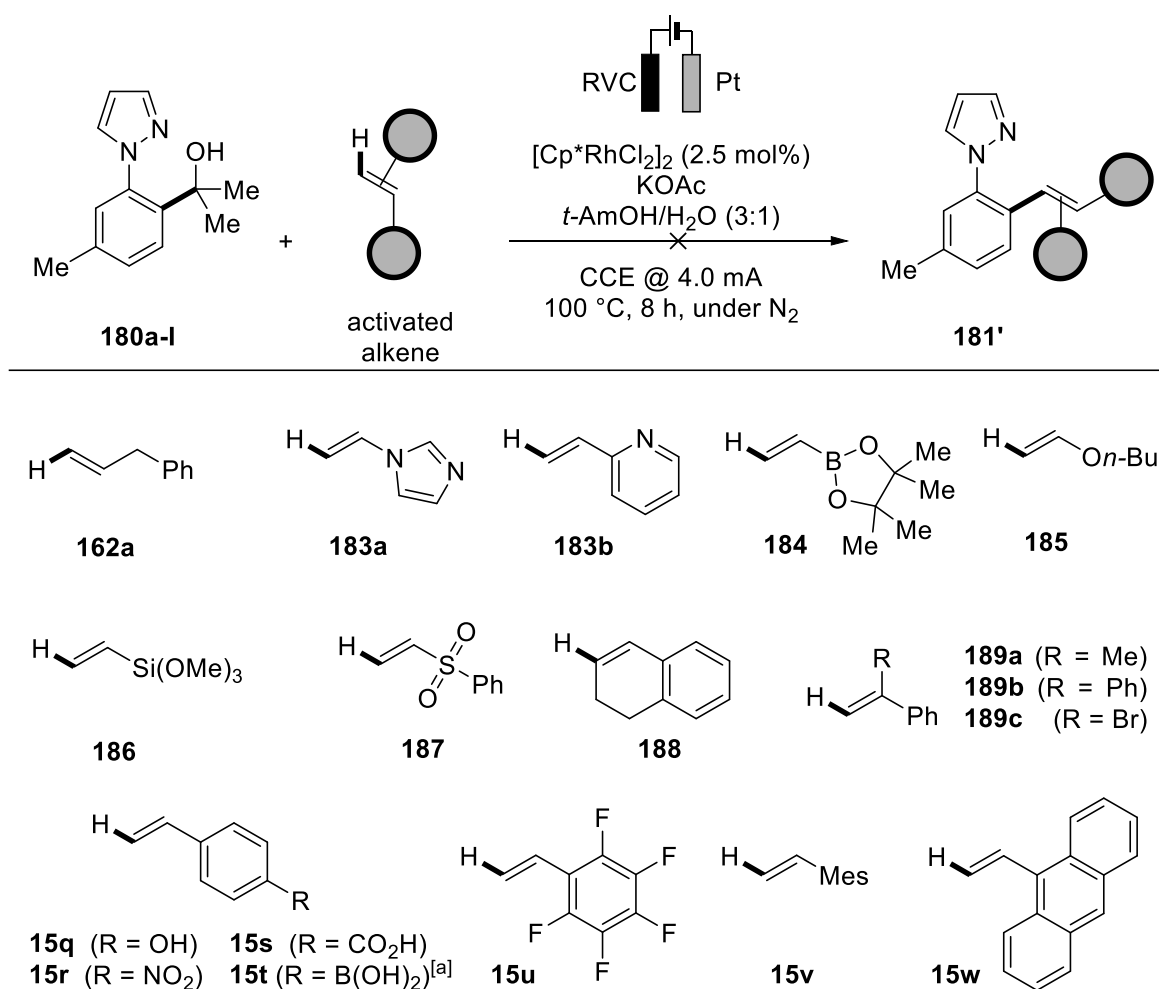
traceless removal of the directing group that presumably proceeds *via* base-mediated ring opening of pyrazole (**Scheme 3-22, b**).^[103] Remarkably, our electro-oxidative protocol outperformed conventionally employed noble metal salts^[102] and aerobic oxygen as oxidants (**Scheme 3-22, c**).



Scheme 3-22 a) Gram scale synthesis of **181aa**. b) Base-assisted cleavage of the pyrazole directing group. c) Comparison of chemo-oxidative coupling. [a] Reaction performed by *Dr. Qiu*.

Many vinyl coupling partners for the aryl alcohols have been tested beyond the styrene motif. Unfortunately, apart from acrylates and phosphonates, further vinyl derivatives were found to be not suitable under otherwise identical reaction conditions (**Scheme 3-23**). In most instances, the incompatible vinyl coupling partners remained unreacted, while arene alcohol **180a-I** degraded to arene **148a-V**. So far, allyl benzene **162a**, heteroarenes **183a**

and **183b**, pinacolborane **184**, vinyl ether **185**, sulfone **186** and siloxane **187** proved elusive substrates. Furthermore, the reaction only proceeded when the vinyl moiety was not multiply substituted (**188–189**). Among the substituents, that were not tolerated on the phenyl ring of styrene, are hydroxyl (**15q**), nitro (**15r**), free carboxylic acid (**15s**) and boronate groups (**15t**). The latter was presumably hydrolytically cleaved, catalyzed by the rhodium complex, furnishing **181aa**. Highly electron-deficient pentafluorostyrene **15u** and sterically demanding substrates **15v** and **15w** also failed to form the corresponding coupling products.

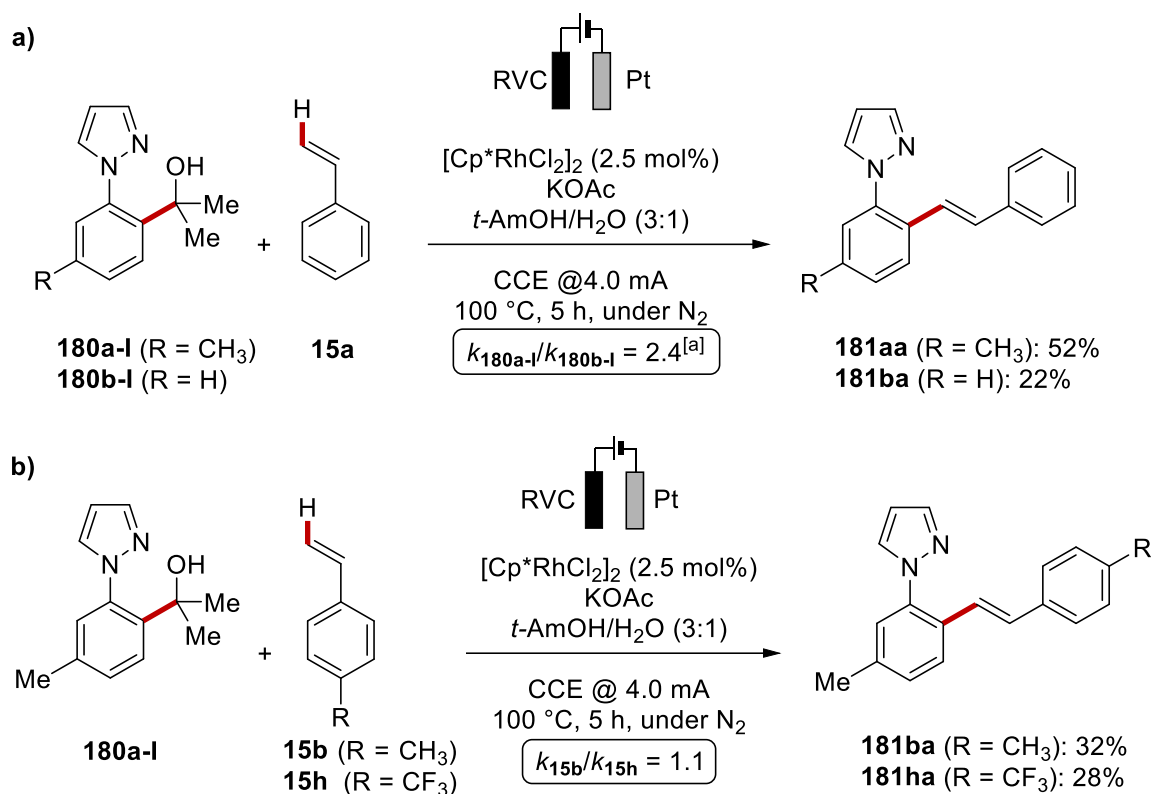


Scheme 3-23 Limitations of the rhoda-electro-C–C alkenylation. [a] **181aa** detected by GC.

3.3.3 Mechanistic Studies

To gain insights into the mode of operation of the rhodium-catalyzed C–C alkenylation, we first performed a series of competition experiments. *Dr. Qiu* showed that more electron-rich arene **180a-I** reacted more efficiently than **180b-I** (Scheme 3-24, a), which can be

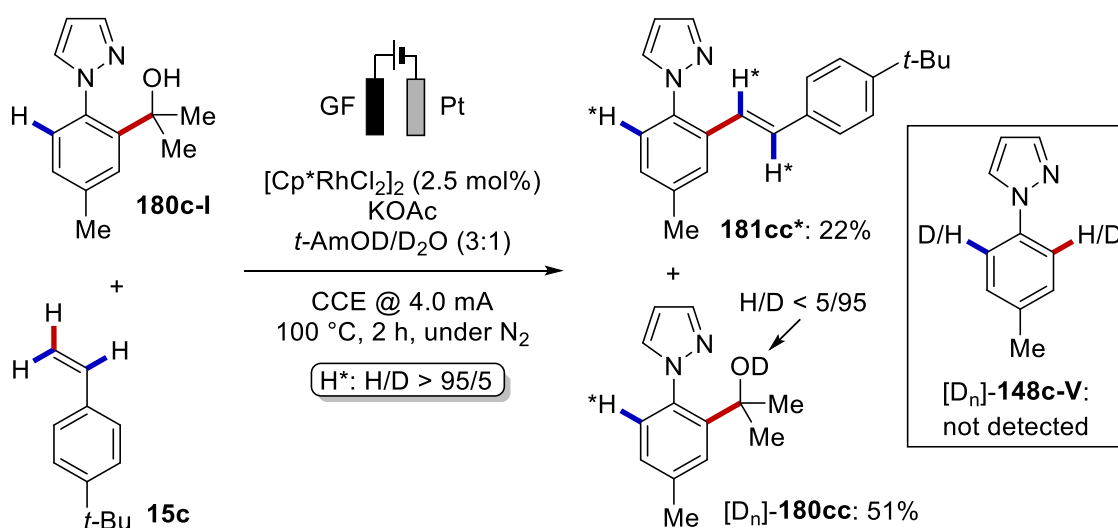
rationalized by the consequentially increased nucleophilicities of the directing group and the C-2 position, that undergoes metalation and functionalization. By contrast, only an insignificant coupling efficiency dependence on the electron density of the olefin substrates **15b** and **15h** was observed (Scheme 3-24, b), which further illustrates the broad tolerance towards electronically diverse alkenes.



Scheme 3-24 Competition between substrates with different electron densities. [a] Reactions performed by Dr. Qiu.

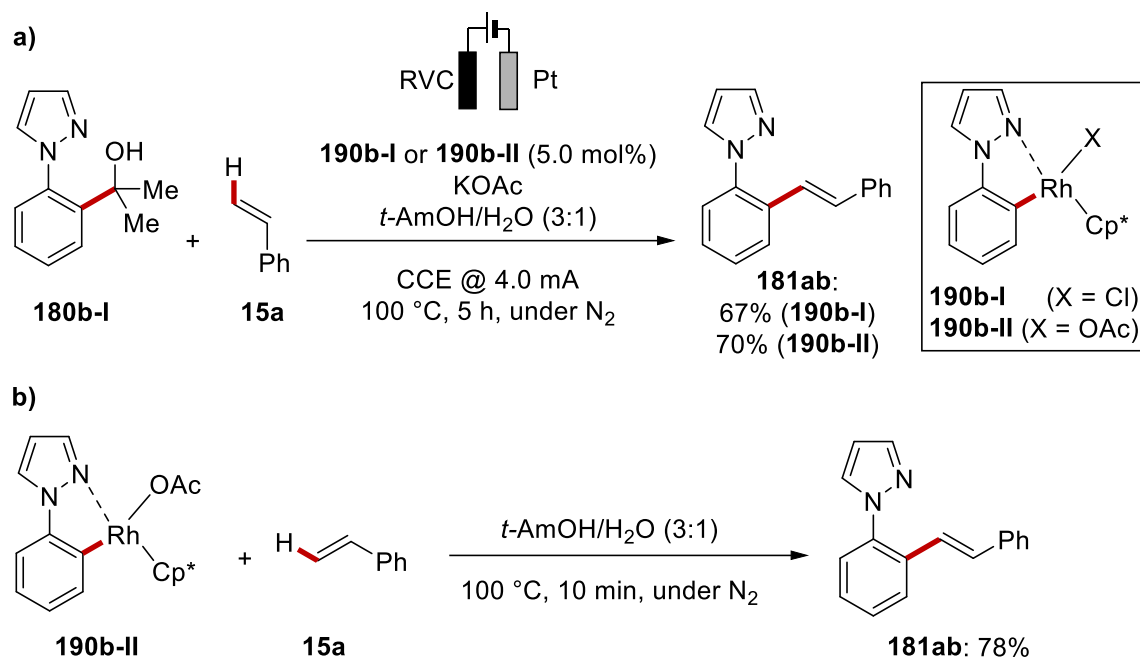
In a deuterated solvent mixture, deuterium incorporation was not observed at any potentially activatable C–H bond in neither the product **181cc*** nor the remaining starting material **15c** (Scheme 3-25). This finding is in line with the previously ascertained preference of C–C activation over C–H activation. Since in this particular experiment, the reaction was halted before completion, almost no **148c-V** was formed as side product, which otherwise would be expected to be deuterated at the *ipso*-position. Normally, **148-V** occurs in considerable quantities, when the reaction was ineffective. This product distribution suggests that after the extrusion of the leaving group, a rhodacycle with a long lifetime is formed. Thus, when the olefin coupling partner is well available, the catalytic cycle likely proceeds to facile coordination and subsequent migratory insertion. Otherwise,

proto-demetalation will eventually occur. Notably, the current efficiency was rather poor ($y_F = 28\%$; first catalytic turnover excluded, compared to $y_F > 40\%$ for most reactions in **Scheme 3-19**), despite stopping the reaction at 1.2 F/mol of charge passed, *i.e.* way before the approach of the substrate diffusion limit. Albeit not studied in detail, a positive H/D-KIE induced by the protic solvent would be indicative of the reductive elimination being the rate-determining step, since metal hydrides are known to form dihydrogen bonds, and the zero-point energy of the interacting pair is lower when the protic bonding partner is substituted with a deuterium.^[280]



Scheme 3-25 Reaction in deuterated solvent.

In order to prove our mechanistic hypothesis, we attempted to isolate putative intermediates and subsequently study their behavior. We were able to synthesize two cyclometalated rhodium(III) complexes **190b-I** and **190b-II**. Both complexes displayed catalytic activity (**Scheme 3-26**), which supports the likelihood of them being reaction intermediates that are formed after C–C activation. Moreover, a stoichiometric reaction between complex **190b-II** and **15a** released the product **181ab** in 78% yield in a short reaction time and without the aid of electricity. This finding suggests that the remaining elementary steps up to the release of the product are facile, and that the anodic oxidation, that keeps the reaction running, occurs at the end of the catalytic cycle on a species that is not bound to the reaction product. Hence, β -hydride elimination and product de-coordination are unlikely to be promoted by an electrochemically induced change of the oxidation state.



Scheme 3-26 Catalytic activity of cyclometalated complexes **190b-I** and **190b-II**.

Finally, we performed cyclic voltammetric (CV) studies to specify the role of electricity in the reaction. Substrates **180a-I** (blue line) and **15a** (red line) did not display any redox activity within the investigated potential window (**Figure 3.3-1**). However, due to the extended π -electron system, the oxidation potential of product **181aa** (black line) is lowered as compared to the starting materials, which is reflected in a pronounced irreversible anodic peak current $E_p = 0.93 \text{ V vs. Fc}^{+/0}$. The products are therefore increasingly prone to oxidative decomposition upon completion of the reaction. Although the presumed intermediate **190b-II** (green line) was shown to be oxidizable, the onset potential of $0.40 \text{ V vs. Fc}^{+/0}$ is considerably higher than the one of a model rhodium(I) species, which makes an oxidation event on **190b-II** within the catalytic cycle improbable (*vide infra*).

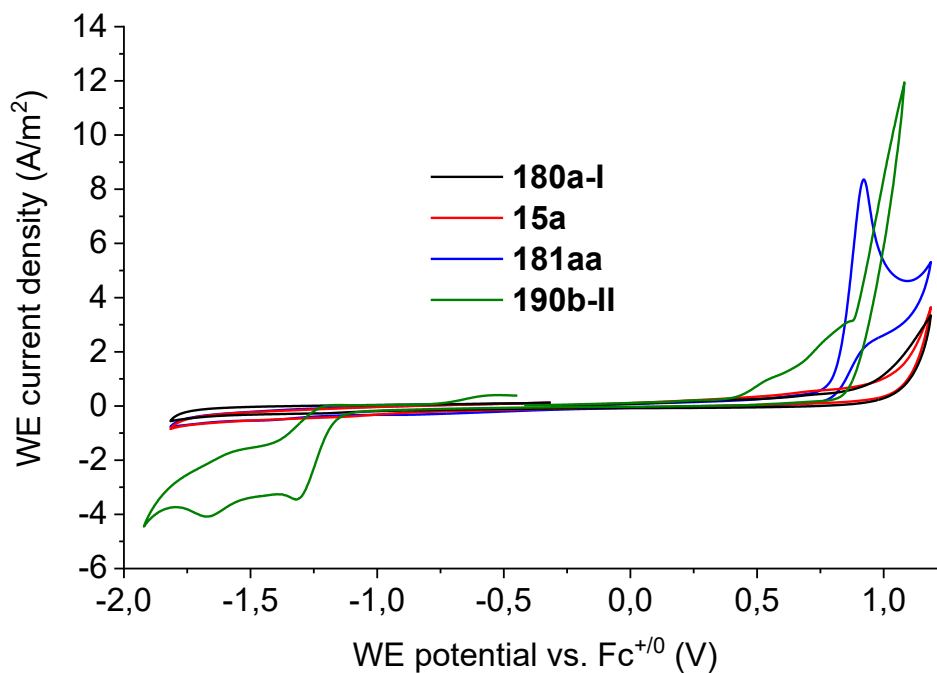


Figure 3.3-1 CV in MeOH, 100 mM TBAPF₆, 100 mV/s. Black: **180a-I** (5 mM); red: **15a** (5 mM); blue: **181aa** (5 mM), green: **190b-II** (5 mM).

Next, we examined the effect of the basic additive (**Figure 3.3-2**). A negative potential shift in the reductive scan of the pre-catalyst [Cp*RhCl₂]₂ (black line) was observed upon addition of KOAc (red line). The resulting voltammogram qualitatively matched the one of [Cp*Rh(OAc)₂] (blue line), which is indicative of a rapid ligand exchange and consequently the acetate-coordinated rhodium being a catalytically relevant species.

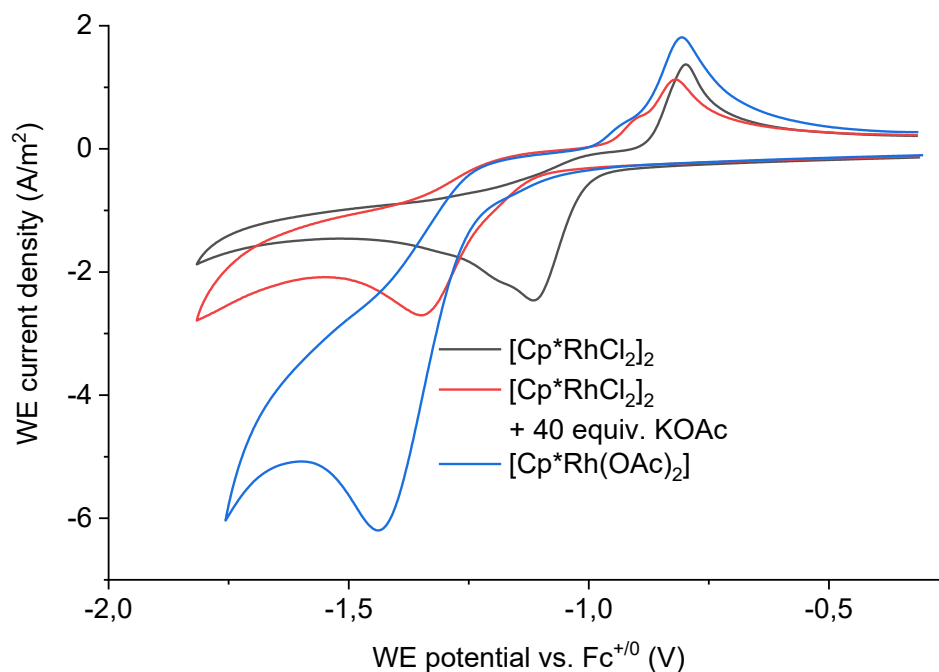


Figure 3.3-2 CV in MeOH, 100 mM TBAPF₆, 100 mV/s. Black: [Cp*RhCl₂]₂ (2.5 mM); red: [Cp*RhCl₂]₂ (2.5 mM) + KOAc (40 equiv.); blue: [Cp*Rh(OAc)₂] (5 mM).

Since the isolation of the putative Cp*-ligated rhodium(I) intermediate has proven elusive, the rhodium(I)→rhodium(III) oxidation was modeled with the well-defined rhodium(I) complex [Cp*Rh(cod)] (**Figure 3.3-3**). At $E_p = -0.16$ V vs. Fc⁺⁰, the complex was irreversibly oxidized (black line). Among all recorded voltammograms, this anodic current appeared at the lowest potential, which supports the selective regeneration of rhodium(III) by anodic oxidation. In view of the increase of the anodic current upon addition of HOAc (**Figure 3.3-4**), we concluded that the oxidation is facilitated by the presence of HOAc, which is formed during the proposed reductive elimination step.

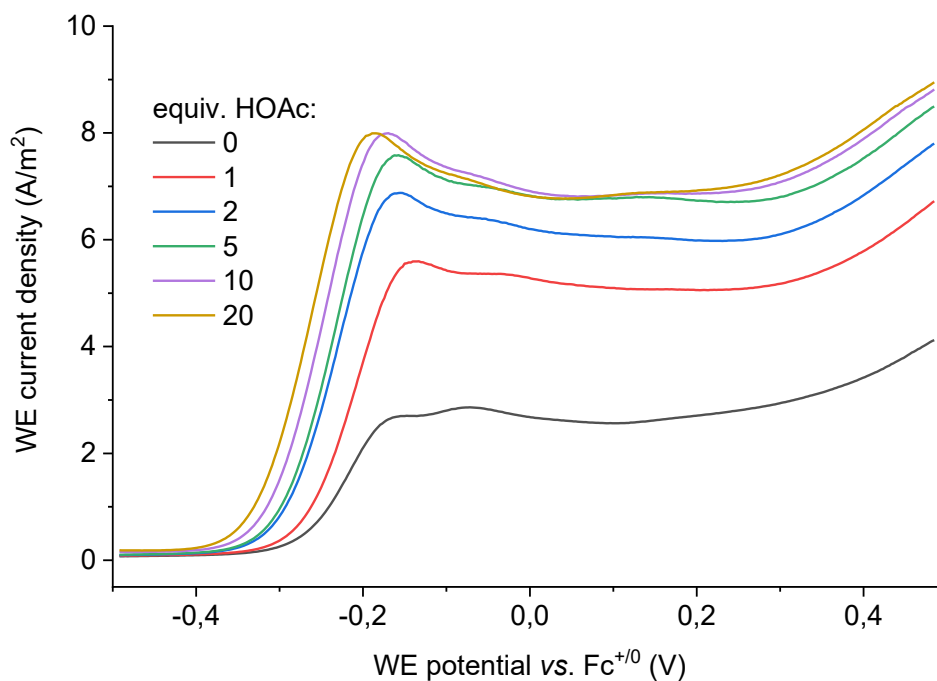


Figure 3.3-3 CV in MeOH, 100 mM TBAPF₆, 100 mV/s, [Cp*Rh(cod)] (5 mM), + X equiv. HOAc. Black: X = 0; red: X = 1; blue: X = 2; green: X = 5; purple: X = 10; yellow: X = 20.

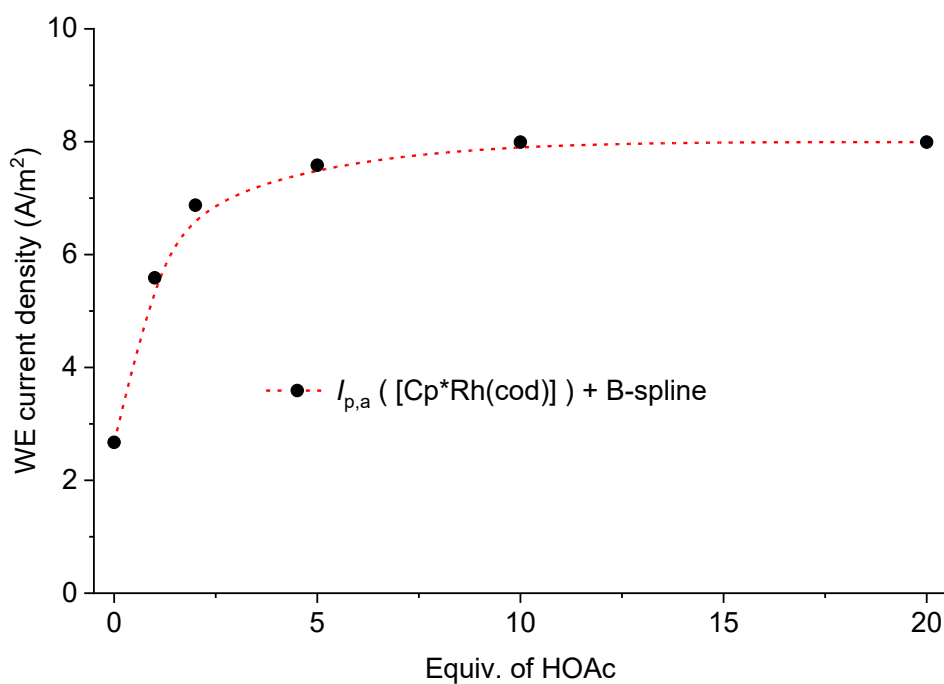
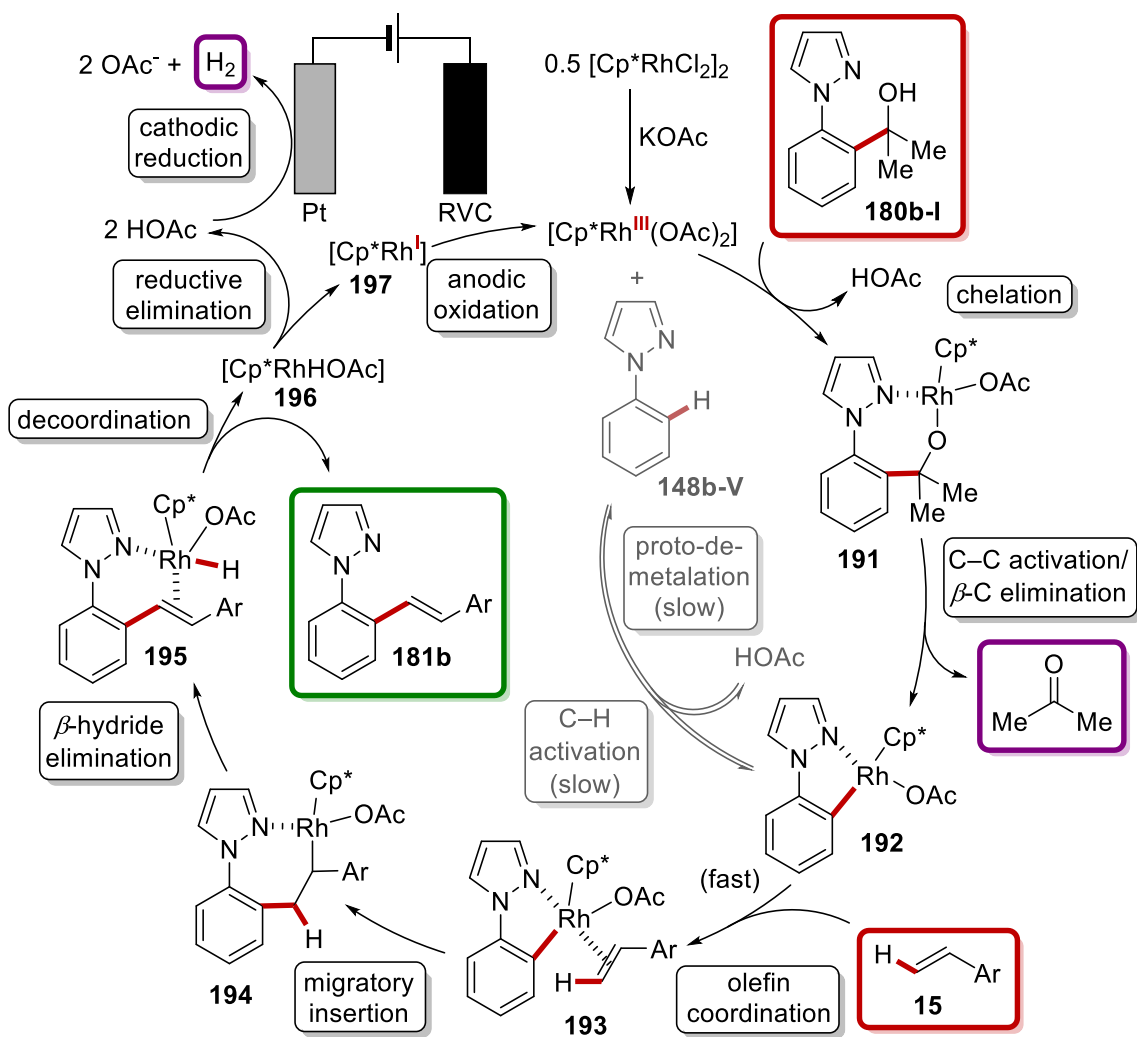


Figure 3.3-4 Anodic peak currents ($I_{p,a}$) from Figure 3.3-3.

3.3.4 Mechanistic Proposal

Based on precedent studies on oxidative couplings by C–H and C–C activation,^[29f,102,277c] and own experimental findings, we propose a catalytic cycle (**Scheme 3-27**) that commences with a bidentate coordination of the catalyst by the pyrazole directing group and the deprotonated alcoholic leaving group, generating intermediate **191**. This strong fixation rationalizes the favorable kinetics of the C(sp²)–C activation pathway over C(sp²)–H activation. The C–C cleavage is accompanied by an irreversible extrusion of a ketone via β -C elimination, forming rhodacycle **192**, that is prone to proto-demetalation as major side reaction. After the coordination of the olefin and its migratory insertion into the C–Rh bond of intermediate **193**, the cycle proceeds through β -hydride elimination on intermediate **194** and the subsequent release of the product **181**. At this stage, rhodium(III) hydride intermediate **195** is most likely formed. For the regeneration of the catalytically active species, a sequence of reductive elimination and two-electron anodic oxidation of rhodium(I) species **196** seems the most plausible. However, the coexistence of an oxidatively induced reductive elimination, initiated and completed by two anodic SETs, thereby going through oxidation states 3→4→2→3, cannot be ruled out, since the model substrate [Cp*Rh(cod)], that was used in the CV measurements, was not structurally equivalent. Hydrogen gas was detected in GC-headspace analysis, thereby confirming proton reduction as the counter reaction at the platinum cathode.

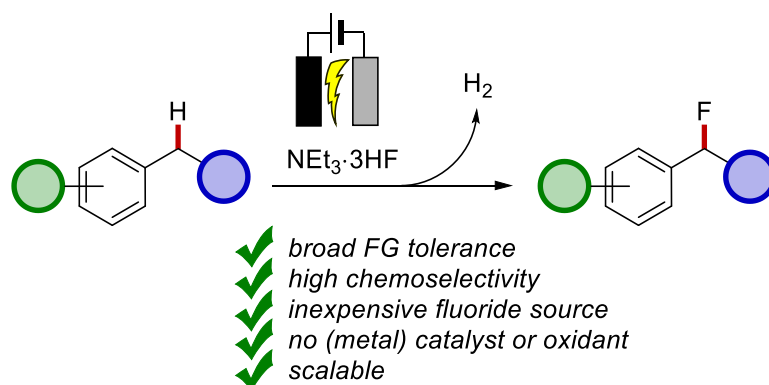


Scheme 3-27 Proposed mechanism of the rhoda-electro-catalyzed C-C alkenylation.

4 SUMMARY AND OUTLOOK

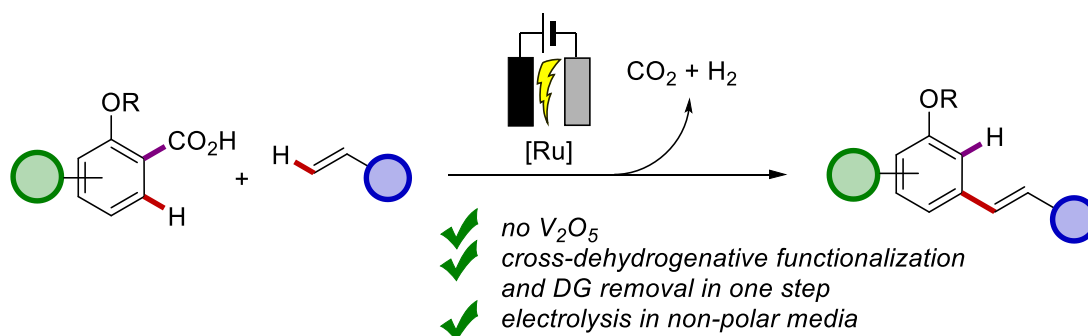
Chemists discovered the transformative capabilities of electrical current more than two centuries ago. The conversion of infinitely variable electrical energy into chemical energy allows the straightforward formation of reactive intermediates that can hardly be realized with chemical energy carriers. To this day, this principle remains relevant. Many electrolytic processes of hitherto unprecedented reactivity were developed and refined to a degree of efficiency, that they became an indispensable part of the chemical industry. In view of imminent resource shortage and environmental awareness, the appeal of using low-cost and sustainably produced electricity instead of chemicals is higher than ever, especially at industrial scale. Thus, over the past years, organic chemists increasingly considered the utilization of electrolysis in order to lessen the ecological impact of existing methods, but also to create new reactivities. In this exciting merging process of methodologies, the heterogenous electron transfer was learned to be carefully harnessed and purposely integrated into the chain of events in reaction mechanisms. Within the described projects, we intended to show that electricity can be implemented as a vastly superior substitute for stoichiometrically employed chemical oxidants in oxidative C–H and C–C functionalization reactions.

In the first project, an electrochemical fluorination of benzylic C(sp³)–H bonds was achieved with the use of inexpensive NEt₃·3HF as a source of nucleophilic fluoride. The reaction does not require any catalyst or directing group, since the innate reactivity of the substrates is used. Key factor for the facilitation of the reaction was the use of HFIP as the cosolvent, which significantly lowered the oxidation potential of the arenes. Much to the convenience for the user, the reaction proceeded in an undivided cell, and standard laboratory glass can be used despite the presence of HF. Moreover, the conductivity was provided by the fluorination agent, thereby obviating the need for an additional supporting electrolyte. The reaction performed most efficiently with secondary benzylic substrates. However, many tertiary benzylic positions were functionalized as well, with even higher yields than the analogous secondary substrates, when the arene was bearing electron-withdrawing substituents. In addition, we also observed the functionalization of adamantane at the bridgehead position. Overall, we evidenced a remarkable functional group tolerance and excellent chemoselectivity, since no more than trace amounts of solvent-caused byproduct were formed.



Scheme 4-1 Electrochemical metal-free C–H fluorination by nucleophilic fluoride.

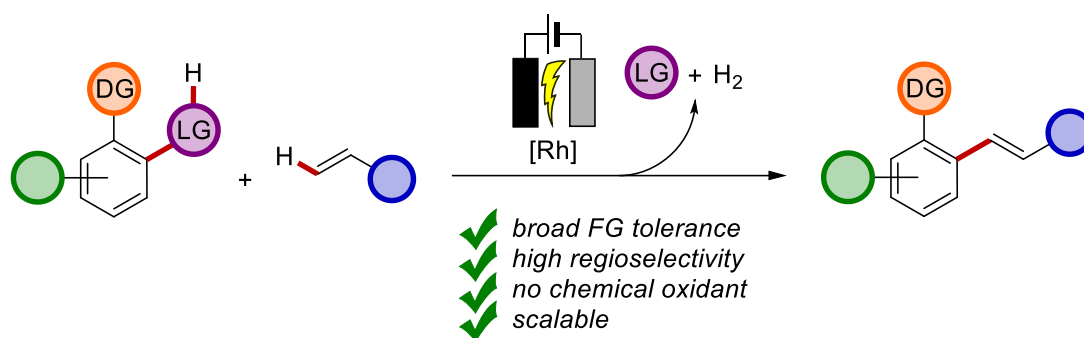
The second project, the attempted electrification of a ruthenium-catalyzed decarboxylative C(sp²)–H alkenylation, proved to be highly challenging. Despite a number of examples with good efficacies, this particular transformation generally provided sub-moderate yields and revealed limited functional group tolerance. The main problem is highly likely to be found in the inherent instability of the ruthenium(0) intermediate. Due to the necessity of non-polar reaction media, that are by default adversarial for electrolysis, since the employed conductive salts remain agglomerated and therefore inactive, the conductivity of binary solvent systems was carefully studied, and the reoxidation efficiency could be substantially improved.



Scheme 4-2 Ruthena-electro-catalyzed decarboxylative C–H alkenylation.

Lastly, an electrochemical cross-dehydrogenative C(sp²)–C/C(sp²)–H coupling was achieved by rhodium catalysis, and aided by a removable directing group. The protocol allowed the synthesis of diaryl-substituted *E*-alkenes in a user-friendly undivided cell setup. The electro-oxidative reaction featured a better performance than analogous setups using silver(I) or copper(II) salts, or air, thanks to highly efficient anodic catalyst regeneration,

as suggested by the undertaken CV studies. Besides the undisputable sustainability advantage, the reaction proved easily scalable. Moreover, we could demonstrate in several experiments the kinetic superiority of C–C activation over C–H activation, which practically reveals itself in excellent regioselectivity, yielding sterically congested 1,2,3-substituted arenes in good yields. The functional group tolerance was comparable with related methods that utilize chemical oxidants.



Scheme 4-3 Rhoda-electro-catalyzed C–C alkenylation.

In conclusion, the field of organic electrochemistry, metalla-electrocatalysis in particular, has grown steadily over the past years for good reason. Many new reactivities were discovered, and established ones were improved in many respects. Thus, a further grow is to be expected, not least because the incorporation of electric current into organic and metalorganic reactions entails an additional set of electricity-related optimization parameters, that need as careful attention as chemical ones, especially since often times they are not independent of one another. These challenges foster the engagement with further methodologies and as a result, the already multidimensional problem set becomes even more complex, but in turn, an inspiring plethora of opportunities arises that calls the researcher for action.

5 EXPERIMENTAL PART

5.1 General Remarks

Air- and moisture-sensitive reactions were carried out under dry nitrogen atmosphere and set up using standard *Schlenk* techniques, with threefold gas exchange and the addition of solids in a counterflow of the protective gas. Glassware, molecular sieves and large stainless steel cannulas for the transfer of air- and moisture-sensitive liquids were stored in a BINDER FD 240 oven at $T = 150\text{ }^{\circ}\text{C}$ for at least 24 h before use. Solutions were concentrated under reduced pressure by rotary evaporation at $50\text{ }^{\circ}\text{C}$ bath temperature. Non-volatile products were dried under oil pump vacuum ($p = 0.1\text{ mbar}$) for 0.5–16 h. Air- and moisture-sensitive substances were stored in a MBRAUN glovebox. Uncommented yields refer to isolated compounds, estimated to be $> 95\%$ pure by $^1\text{H-NMR}$ spectroscopy. Yields of unisolated compounds were estimated by GC-MS analysis, using *n*-dodecane or *n*-tetradecane as the internal standards. For bench-top work-ups, distilled technical grade solvents were used. Ratios of liquids (solvents, eluents) refer to volumetric parts.

5.1.1 Materials

5.1.1.1 Solvents

For electrochemical reactions, commercially available reagent grade-chemicals ($< 99\%$) were used as solvents. Solvents for air- and moisture sensitive reactions were obtained from a solvent purification system (SPS-800 by MBRAUN) and include: DMF, THF, Et_2O , PhMe and DCM. Dry DMSO and MeCN were purchased from THERMO SCIENTIFIC™ in bottles with AcroSeal™ sealing. MeOH was distilled over magnesium methanolate by *Karsten Rauch*.

5.1.1.2 Catalysts, Reagents and Substrates

Commercially available chemicals with purities higher than 95% were used as received. Catalysts and substrates, that were not available from commercial suppliers, were synthesized by following previously reported procedures: 2-(1-Pyrazolyl)-benzyl alcohols **180**,^[281] η^6 -arene ruthenium(II) chloride complexes.^[260,262,264] Following substrate classes were synthesized using standard textbook procedures in 1–2 steps starting from commercially available chemicals: Alkoxybenzoic acids **30** were obtained from the

respective hydroxybenzoic acids by a methylation–hydrolysis sequence. Acrylates **11** were obtained by condensation of acryloyl chloride and the corresponding alcohol. Benzylic substrates were derivatized using standard esterification and S_N2 protocols towards starting materials **59**.

The following chemicals were synthesized and generously provided by the people named below:

Karsten Rauch: [Ru(*p*-cymene)Cl₂]₂, [Ru(*p*-cymene)(OAc)₂]₂, [Ru(*p*-cymene)(O₂CMe)₂]₂, [Cp**Rh*Cl₂]₂, [Cp**Ir*Cl₂]₂

Korkit Korvorapun: [Ru(*t*-BuPh)Cl₂]₂

Svenja Warratz: [Ru(*p*-cymene)(*t*-BuPhPHO)Cl₂], [Ru(*p*-cymene)(Ph₂PHO)Cl₂]

5.1.2 Analytical and Experimental Methods

5.1.2.1 Liquid Chromatographic Methods

Flash column chromatograph (FCC) was employed as the main method for the purification of organic compounds. It was carried out at 0.10–0.15 bar overpressure using glass frit-equipped chromatography columns and distilled technical grade solvents. For the stationary phase, MERCK silica gel, grade 60 (40–63 μm 70–230 mesh ASTM), was used. The crude products were loaded as concentrated solutions of the respective starting eluent. For some acid-sensitive compounds, such as benzyl fluorides, the silica gel was partially neutralized with 4 wt-% (based on silica mass) of NEt₃ prior to use. Thin-layer chromatography (TLC) was used for monitoring the progress of the reactions and the FCC purifications, and performed on silica gel 60-coated aluminum sheets by MACHEREY NAGEL, with fluorescence indicator F-254. Visualization was achieved by either UV light irradiation or by staining with KMnO₄ solution and subsequent gentle heating, when needed. Gel permeation/size exclusion chromatography (GPC/SEC) was performed on a Japan Analytical Industries LC-92XX II Series instrument, equipped with JAIGEL 2HH series column, 4-channel UV-Vis and RI Detector, using HPLC-grade CHCl₃ (stabilized with 0.6% EtOH) as eluent.

5.1.2.2 Gas Chromatographic Methods

Gas chromatographic analysis coupled with mass-spectrometry (GC-MS) was performed on an AGILENT 7890A GC System or AGILENT 7890B GC System equipped with an AGILENT HP-5MS column (30 m × 0.25 mm diameter, 0.25 μm film thickness) and a flame-ionization detector (FID) using hydrogen as the carrier gas. Mass spectra were obtained on a coupled AGILENT 5875C Triple-Axis-Detector or AGILENT 5977B MSD with electron ionization (EI) at 70 eV in positive ion mode. Analysis of the reaction headspace was performed on an AGILENT 7890B GC System equipped with a 5 Å MS column and a thermal conductivity detector, using helium as the carrier gas. Gas samples were taken with a 1.00 mL HAMILTON Gastight™ syringe.

5.1.2.3 Nuclear Magnetic Resonance (NMR) Spectroscopy

NMR spectra were recorded on BRUKER Avance 300, Avance III HD 400, Avance Neo 400, Avance III HD 500; VARIAN Mercury VX 300, Inova 500 or Inova 600 spectrometer at 300 MHz, 400 MHz, 500 MHz, 600 MHz (¹H-NMR), 75 MHz, 100 MHz, 125 MHz (¹³C-NMR) and 282 MHz (¹⁹F-NMR), respectively. Chemical shifts are reported as δ-values in parts per million (ppm) relative to the resonance frequencies of SiMe₄ (¹H-NMR and ¹³C-NMR) or CFCl₃ (¹⁹F-NMR), and are referenced to the residual proton peak or the carbon peak of the deuterated solvent (**Table 5.1-1**).^[282] All measurements were performed at 298 K, unless stated otherwise. The resonance multiplicities are reported by the following abbreviations: s (singlet), d (doublet), t (triplet), q (quartet), quint (quintet), sext (sextet), sept (septet), m (multiplet) and br (broad signal/singlet), and combinations thereof. The coupling constants *J* are reported in Hertz (Hz). Analysis of all spectra until February 2019 was performed with MestReNova v10.0.2 and from February onwards with MestReNova v14.1.0 from MESTRELAB RESEARCH S.L.

Table 5.1-1 Chemical shifts δ of deuterated NMR solvent signals (ppm).

Solvent	¹ H-NMR (residual proton)	¹³ C-NMR (carbon)
Acetone- <i>d</i> ₆	2.05	206.26
CD ₂ Cl ₂	5.32	53.84
CDCl ₃	7.26	77.16
CD ₃ OD	3.31	49.00

EXPERIMENTAL PART

D ₂ O	4.79	--
DMSO- <i>d</i> ₆	2.50	39.51
C ₆ D ₆	7.16	128.06

5.1.2.4 Mass Spectrometry (MS)

High resolution (HR) electrospray ionization (ESI) mass spectra were recorded on a micrOTOF or a maXis from BRUKER DALTONICS or a LTQ Orbitrap XL from THERMO SCIENTIFIC. EI-MS spectra were recorded on a JEOL AccuTOF™ (EI) instrument. The ratio of mass to charge (m/z) is given, intensities relative to the base signal (intensity = 100) are written in parentheses.

5.1.2.5 Melting Point Determination

Melting points were measured on a STUART™ SMP3 apparatus. Values are uncorrected.

5.1.2.6 Infrared (IR) Spectroscopy

Infrared (IR) spectra were recorded on a BRUKER Alpha-P FT-IR spectrometer with an ATR diamond probe for detection in the range of $\tilde{\nu} = 4000\text{--}400\text{ cm}^{-1}$. Analyses of the spectra were performed with the software Opus 6.5 from BRUKER.

5.1.2.7 Electroanalytical Methods

Unless indicated otherwise, electroanalytic experiments were performed as follows. Cyclic voltammetry (CV) measurements were conducted with a Metrohm Autolab PGSTAT204 potentiostat and Nova 2.1 software. All solutions were saturated with N₂ prior to the measurement and an overpressure of N₂ was maintained throughout the experiment. The protective gas was passed through a gas washing bottle with the respective electrolyte solvent in order to minimize concentration changes due to evaporation. The experiments were carried out at ambient temperature (295±5 K) and ambient pressure. The standard electrolyte volume was 2.0 mL and analytes were employed at a concentration of 5 mM. A glassy carbon disc working electrode (diameter: 3.0 mm, ALS Japan Co., Ltd.) and a coiled platinum wire counter electrode (diameter: 1.0 mm, 99.9%, CHEMPUR) were employed,

with a scan rate of 100 mV/s. A AgCl-coated silver-wire (diameter: 1.0 mm, 99.9%, CHEMPUR) in close proximity to the working electrode was used as the pseudo-reference electrode, and the voltammograms were referenced internally vs. $\text{Fc}^{+/0}$. The acquired data was analyzed and plotted and with software from ORIGINLAB. Rotating ring disc electrode (RRDE) experiments were performed using a METROHM Autolab PGSTAT204 workstation and a RRDE-3A Rotating Ring Disk Electrode Apparatus Ver.2.0 purchased from ALS Japan Co., Ltd. For the experiments, a glassy carbon disc (diameter: 4.0 mm) – platinum ring (inner/outer diameter: 5.0/7.0 mm) electrode was used. The disc was connected as the working electrode and the ring was connected as the counter electrode. A AgCl-coated silver wire (diameter: 1.0 mm, 99.9%, CHEMPUR) in close proximity to the rotating electrode was used as the pseudo-reference electrode.

5.1.2.8 Electrosynthetic Setups

Unless specified otherwise, all electrochemical reactions were set up as follows. Electrolyses were carried out in undivided electrochemical cells. For that purpose, 10 mL oven-dried, rubber septum-sealed *Schlenk* tubes, equipped with a PTFE-coated magnetic stirring bar, were employed. The reactions were run under dry nitrogen atmosphere. Other measures towards the exclusion of moisture were not taken. Platinum electrodes (15 mm × 10 mm × 0.25 mm, 99.9%; obtained from CHEMPUR, Karlsruhe, Germany) and graphite felt (GF) electrodes (10 mm × 8 mm × 6 mm, SIGRACELL® GFA 6 EA; obtained from SGL Carbon, Wiesbaden, Germany) were attached to stainless steel holders, separated at the bottom part by a PP or PTFE spacer and the holders were pierced through the septum. The electrode holders were connected to a power supply by METROHM (Multi Autolab/M204), ROHDE&SCHWARZ (HMP4040) or AXIOMET (AX-3003P), set up in constant current mode. The electrodes were adjusted to be plane parallel with a separation of 3–6 mm, depending on the electrode material, and submerged into the electrolyte to a depth of 8–10 mm. Divided cells, separated by a P4 glass frit, were custom-made and obtained from GLASGERÄTEBAU OCHS, LABORFACHHANDEL e.K. (Bovenden, Germany).

5.2 General Procedures

5.2.1 General Procedure A for the Electrochemical Fluorination of Benzylic C(sp³)–H Bonds

Important note: Special precautions are advised for the handling of HF and sources thereof, since these reagents are highly toxic and they easily penetrate biological tissue, leading potentially to irreversible damage. These reagents should be handled only by trained staff, and in addition to the observation of general rules for good laboratory practice, particular attention should be paid to the usage of appropriate impenetrable gloves. Storage of antidote (e.g. calcium gluconate-based ointment) within easy reach is recommended. Glassware should not be exposed to these reagents for unnecessarily long times, as HF etches their surface. Furthermore, due to the reportedly high reactivity of the products,^[283] decomposition upon concentration in glassware or purification on silica gel is possible.^[284] It is therefore recommended (but not mandatory) to use inert polymer-based vessels for the reaction and the workup, and perform the chromatographic purification on (at least partly) deactivated/neutralized silica gel.

Benzylic substrate **59** (0.50 mmol), DCE (2.0 mL), HFIP (1.0 mL), and NEt₃·3HF (1.0 mL) were placed in a standard undivided electrochemical cell. Electrosynthesis was performed, unless noted otherwise, at r.t. with a constant current of 8.0 mA until 2.5 F/mol were passed (4.2 h). After electrolysis, the platinum cathode and the graphite felt anode were washed with DCM (Pt: 1 × 2 mL; GF: 3 × 2 mL). The washings were combined with the reaction mixture and diluted with *n*-hexane (15 mL). The organic mixture was washed three times with water (3 × 15 mL) in a separatory funnel and dried over Na₂SO₄. After adding silica gel (2.0 g), the mixture was filtered over a pad of celite, and the solvents were removed in vacuo. CH₂Br₂ (36 μL, 0.50 mmol) and PhCF₃ (62 μL, 0.50 mmol) were added to the residue and the mixture was submitted for NMR analyses.

5.2.2 General Procedure B for the Ruthena-Electro-Catalyzed Decarboxylative Alkenylation of Anisic Acids

To an oven-dried standard electrochemical cell, acrylate **11** (0.40 mmol, 1 equiv.), *o*-alkoxybenzoic acid **30** (1.20 mmol, 3 equiv.), [Ru(*p*-cymene)(O₂CMe)₂] (22.4 mg, 0.040 mmol, 10.0 mol%), TBAPF₆ (155 mg, 0.40 mmol, 1 equiv.), PhOMe (3.5 mL) and PGCC

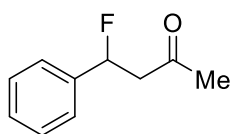
(0.5 mL) were added. The electrocatalysis was performed for 8 h at $T = 100\text{ }^{\circ}\text{C}$ with a constant current of 4 mA. After cooling down to room temperature, the platinum cathode was rinsed with DCM (2 mL) and the GF anode was cleaned by three cycles of rinsing/soaking with DCM (2 mL) and squeezing. The combined washings were added to the reaction mixture. After concentration under reduced pressure, the crude mixture was purified by flash column chromatography (FCC). Concentration and drying in vacuo gave products **31**.

5.2.3 General Procedure C for the Rhoda-Electro-Catalyzed C–C Activation

To an oven-dried standard electrochemical cell, alcohol **180** (0.375 mmol, 1.5 equiv), alkene **15** (0.25 mmol, 1.0 equiv), KOAc (49 mg, 0.50 mmol, 2.0 equiv), $[\text{Cp}^*\text{RhCl}_2]_2$ (3.9 mg, 2.5 mol%) and $t\text{-AmOH}/\text{H}_2\text{O}$ (3/1, 4.0 mL) were added. The electrocatalysis was performed at $T = 100\text{ }^{\circ}\text{C}$ with a constant current of 4.0 mA maintained for 4–12 h. The RVC anode was washed with EtOAc (3×10 mL) in an ultrasonic bath. Evaporation of the solvent and subsequent FCC afforded the corresponding products **3**.

5.3 Electrochemical Fluorination of Benzylic $\text{C}(\text{sp}^3)\text{--H}$ Bonds

5.3.1 Characterization Data



4-fluoro-4-phenylbutan-2-one (**60ab**)

The general procedure A was followed using 4-phenylbutan-2-one **59ab** (74.2 mg, 0.50 mmol, 1.0 equiv) at $0\text{ }^{\circ}\text{C}$.

Benzyl Fluoride C–H Shift: $^1\text{H-NMR}$ (300 MHz, CD_2Cl_2) $\delta = 5.97$ (ddd, $J = 46.9, 8.8, 3.9$ Hz, 1H). Calibrated $^1\text{H-NMR}$ yield from benzylic proton: 42%. **Benzylic Fluoride Shift:** $^{19}\text{F}\{^1\text{H}\}\text{-NMR}$ (282 MHz, CD_2Cl_2) $\delta = -173.9$. Calibrated $^{19}\text{F}\{^1\text{H}\}\text{-NMR}$ yield from

EXPERIMENTAL PART

benzylic fluoride: 45%. **HR-MS** (EI) m/z calc. for $C_8H_8^{35}ClF [M]^+$: 158.0299, found: 158.0293. The spectral data are in accordance with those reported in literature.^[124b]

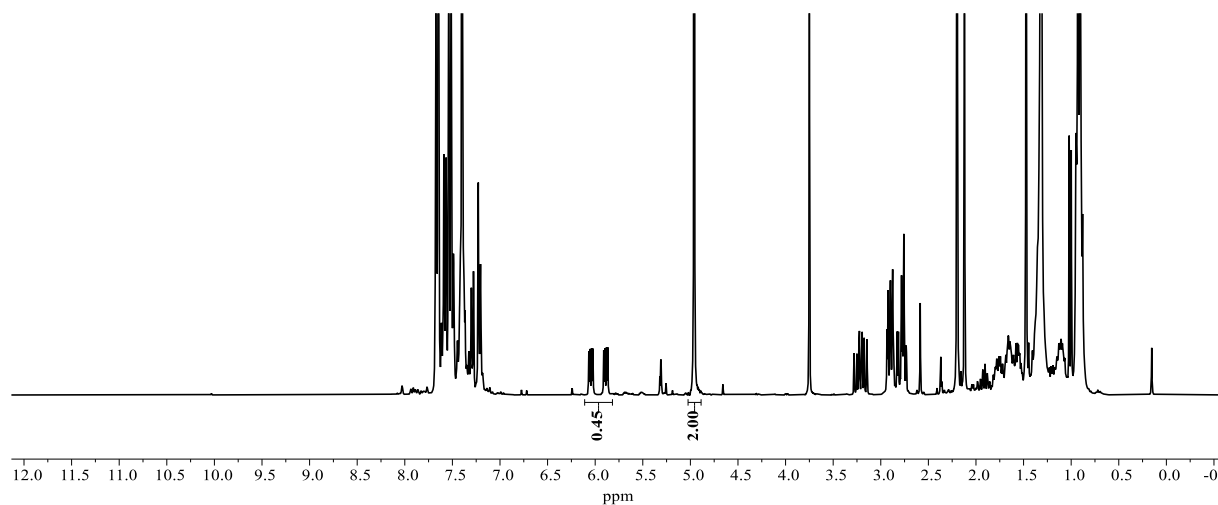


Figure 5.3-1 Crude ¹H-NMR Spectrum (300 MHz, CD₂Cl₂) of the reaction mixture with CH₂Br₂ (36 µL, 0.50 mmol) as the internal standard (4.96 ppm). The signals of the benzylic proton and the internal standard are integrated.

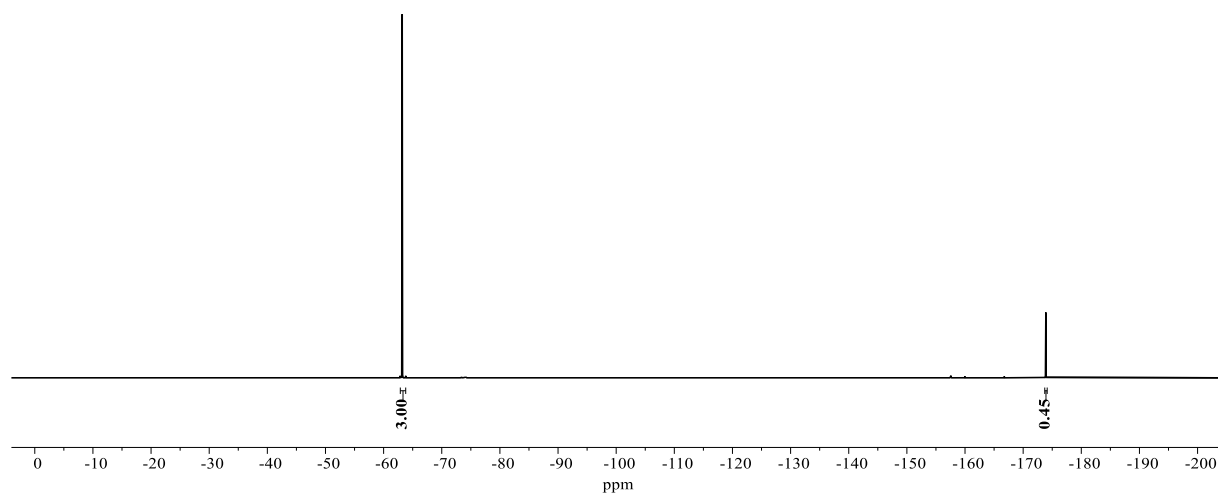
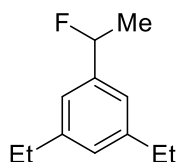


Figure 5.3-2 Crude ¹⁹F{¹H}-NMR Spectrum (282 MHz, CD₂Cl₂) of the reaction mixture with PhCF₃ (62 µL, 0.50 mmol) as the internal standard (-63.2 ppm). The signals of the benzylic fluoride, aromatic fluoride and the internal standard are integrated.



1,3-Diethyl-5-(1-fluoroethyl)benzene (**60ag**)

The general procedure A was followed using 1,3,5-triethylbenzene **59ag** (81.3 mg, 0.50 mmol) at 0 °C. After conducting the NMR analysis, the solvents were removed in vacuo, and the residue was purified by FCC on partially neutralized silica (*n*-hexane/EtOAc = 40:1) to obtain the product **60ag** as a colorless oil (54.4 mg, 0.30 mmol, 60%).

¹H-NMR (300 MHz, CDCl₃): δ = 7.01 (s, 3H), 5.59 (dq, J = 47.8, 6.4 Hz, 1H), 2.65 (q, J = 7.6 Hz, 4H), 1.65 (dd, J = 23.9, 6.4 Hz, 3H), 1.25 (t, J = 7.6 Hz, 6H). Calibrated **¹H-NMR** (300 MHz, CD₂Cl₂) yield from benzylic proton: 78%. **¹⁹F{¹H}-NMR** (282 MHz, CDCl₃) –165.9. Calibrated **¹⁹F{¹H}-NMR** (282 MHz, CD₂Cl₂) yield from benzylic fluoride: 75%. **¹³C{¹H}-NMR** (101 MHz, CDCl₃): δ = 144.7 (C_q), 141.6 (d, $^2J_{C-F}$ = 19.2 Hz, C_q), 127.6 (d, $^5J_{C-F}$ = 2.1 Hz, CH), 122.3 (d, $^3J_{C-F}$ = 6.5 Hz, CH), 91.4 (d, $^1J_{C-F}$ = 166.8 Hz, CH), 29.0 (CH₂), 23.1 (d, $^2J_{C-F}$ = 25.4 Hz, CH₃), 15.7 (CH₃). **IR** (ATR): $\tilde{\nu}$ = 2968, 2934, 2873, 1606, 1460, 1374, 1083, 1060, 870, 847, 710. **HR-MS** (EI) m/z calc. for C₁₂H₁₇F [M]⁺: 180.1314, found: 180.1309.

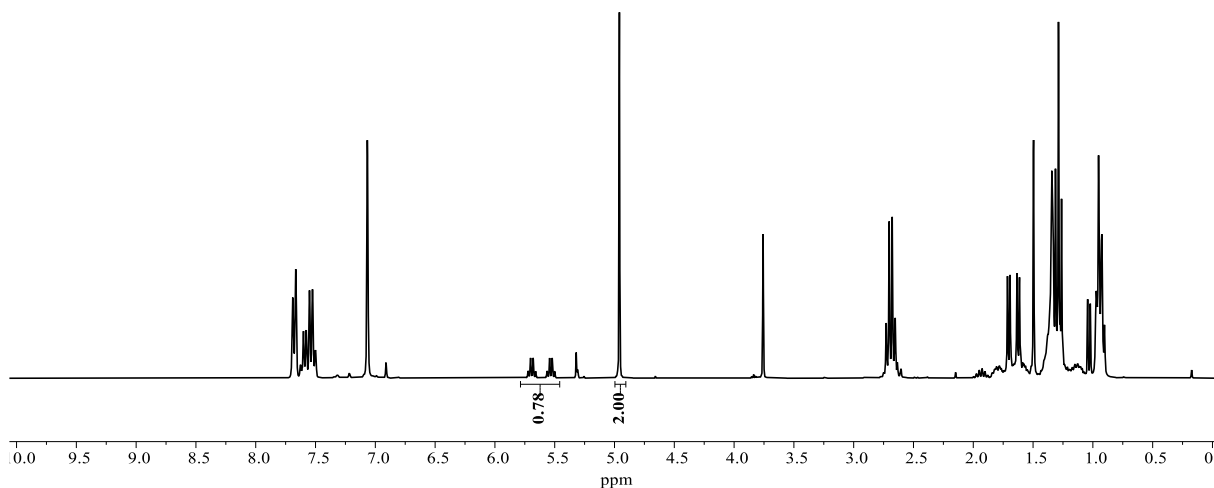


Figure 5.3-3 Crude ¹H-NMR Spectrum (300 MHz, CD₂Cl₂) of the reaction mixture with CH₂Br₂ (36 μ L, 0.50 mmol) as the internal standard (4.96 ppm). The signals of the benzylic proton and the internal standard are integrated.

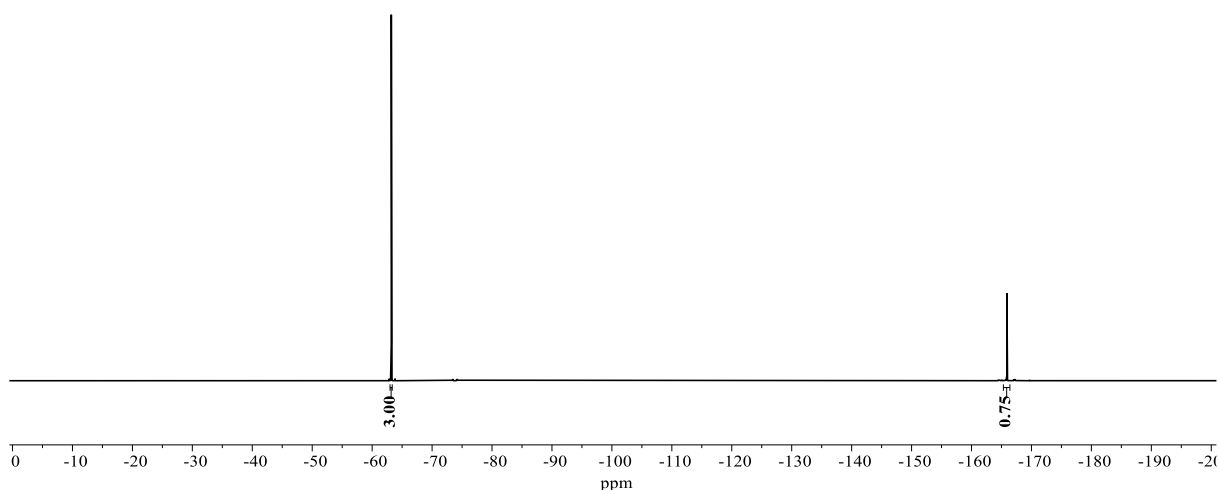
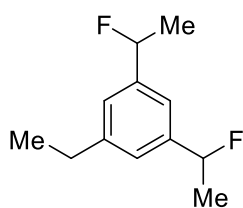


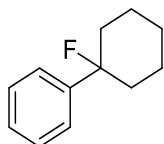
Figure 5.3-4 Crude $^{19}\text{F}\{^1\text{H}\}$ -NMR Spectrum (282 MHz, CD_2Cl_2) of the reaction mixture with PhCF_3 (62 μL , 0.50 mmol) as the internal standard (-63.2 ppm). The signals of the benzylic fluoride and the internal standard are integrated.



1-Ethyl-3,5-bis(1-fluoroethyl)benzene (**60ag'**)

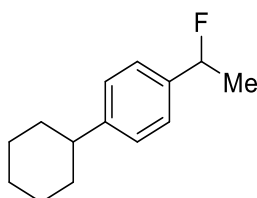
The general procedure A was followed using 1,3,5-triethylbenzene **59ag** (81.3 mg, 0.50 mmol) at 0 °C with 5.0 F/mol total charge. The solvents were removed in vacuo, and the residue was purified by FCC on partially neutralized silica (*n*-hexane/EtOAc = 40:1) to obtain the product **60ag'** as a colorless oil (51.5 mg, 0.26 mmol, 52%).

^1H -NMR (300 MHz, CDCl_3): δ = 7.15 (s, 3H), 5.62 (dq, J = 47.7, 6.4 Hz, 2H), 2.69 (q, J = 7.6 Hz, 2H), 1.65 (dd, J = 23.9, 6.4 Hz, 7H), 1.26 (t, J = 7.6 Hz, 3H). $^{19}\text{F}\{^1\text{H}\}$ -NMR (282 MHz, CDCl_3) -167.06 (d, J = 24.4 Hz). $^{13}\text{C}\{^1\text{H}\}$ -NMR (101 MHz, CDCl_3): δ = 145.1 (d, $^4J_{\text{C-F}}$ = 2.2 Hz, C_q), 142.0 (dd, $^{2,4}J_{\text{C-F}}$ = 19.5, 1.5 Hz, C_q), 124.8 (ddd, $^{3,5}J_{\text{C-F}}$ = 6.5, 1.5 Hz, diastereomer, CH), 119.6 (dt, $^3J_{\text{C-F}}$ = 6.9 Hz, diastereomer, CH), 91.0 (d, $^1J_{\text{C-F}}$ = 167.7 Hz), 29.0 (CH_2), 23.1 (d, $^2J_{\text{C-F}}$ = 25.3 Hz, CH_3), 15.6 (CH_3). IR (ATR): $\tilde{\nu}$ = 2980, 2935, 2876, 1607, 1456, 1376, 1327, 1175, 1079, 878, 840, 713. HR-MS (EI) m/z calc. for $\text{C}_{12}\text{H}_{16}\text{F}_2$ $[\text{M}]^+$: 198.1220, found: 198.1215.

**(1-Fluorocyclohexyl)benzene (60aj)**

The general procedure A was followed using cyclohexylbenzene **59aj** (80.1 mg, 0.50 mmol) at 0 °C. The solvents were removed in vacuo, and the residue was purified by FCC on partially neutralized silica (*n*-hexane) to obtain the product **60aj** as a colorless oil (32.0 mg, 0.20 mmol, 40%).

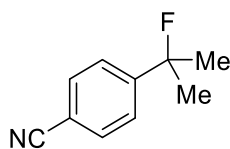
¹H-NMR (300 MHz, CDCl₃): δ = 7.45–7.22 (m, 5H), 2.10–1.95 (m, 2H), 1.92–1.63 (m, 7H), 1.39–1.23 (m, 1H). **¹⁹F{¹H}-NMR** (282 MHz, CDCl₃) δ = –158.9 (broad). **¹³C{¹H}-NMR** (75 MHz, CDCl₃) δ = 146.1 (d, ²*J*_{C-F} = 21.9 Hz, C_q), 128.3 (d, ⁴*J*_{C-F} = 1.3 Hz, CH), 127.3 (d, ⁵*J*_{C-F} = 1.5 Hz, CH), 124.1 (d, ³*J*_{C-F} = 9.2 Hz, CH), 96.2 (d, ¹*J*_{C-F} = 173.7 Hz, C_q), 37.3 (d, ²*J*_{C-F} = 23.8 Hz, CH₂), 25.1 (CH₂), 22.1 (d, ³*J*_{C-F} = 1.7 Hz, CH₂). **IR** (ATR): $\tilde{\nu}$ = 2937, 2963, 1448, 1018, 949, 845, 758, 698, 542. **HR-MS** (EI) *m/z* calc. for C₁₂H₁₅F [M]⁺: 178.1152, found: 178.1153.

**1-Cyclohexyl-4-(1-fluoroethyl)benzene (60ak)**

The general procedure A was followed using 1-cyclohexyl-4-ethylbenzene **59ak** (94.3 mg, 0.50 mmol). The solvents were removed in vacuo, and the residue was purified by FCC on partially neutralized silica (*n*-hexane) to obtain the product **60ak** as a colorless oil (49.6 mg, 0.24 mmol, 48%).

¹H-NMR (400 MHz, CDCl₃): δ = 7.34–7.27 (m, 2H), 7.25–7.21 (m, 2H), 5.61 (dq, *J* = 47.8, 6.4 Hz, 1H), 2.60–2.44 (m, 1H), 1.94–1.81 (m, 4H), 1.80–1.73 (m, 1H), 1.65 (dd, *J* = 23.8, 6.5 Hz, 3H), 1.51–1.34 (m, 4H), 1.33–1.19 (m, 1H). **¹⁹F{¹H}-NMR** (282 MHz, CDCl₃) –164.6. **¹³C{¹H}-NMR** (101 MHz, CDCl₃): δ = 148.4 (d, ⁵*J*_{C-F} = 2.3 Hz, C_q), 138.9 (d, ²*J*_{C-F} = 19.5 Hz, CH), 127.1 (CH), 125.5 (d, ³*J*_{C-F} = 6.2, CH), 91.1 (d, ¹*J*_{C-F} = 166.3,

CH), 44.5 (CH), 34.6 (CH₂), 27.0 (CH₂), 26.3 (CH₂), 22.8 (d, ²J_{C-F} = 25.4, CH₃). **IR** (ATR): $\tilde{\nu}$ = 2982, 2924, 2852, 1449, 1068, 1006, 885, 828, 561. **HR-MS** (EI) *m/z* calc. for C₁₄H₁₉F [M]⁺: 206.1465, found: 206.1465.



4-(2-fluoropropan-2-yl)benzonitrile (60al)

The general procedure A was followed using 4-isopropylbenzonitrile **59al** (72.7 mg, 0.50 mmol) at -20 °C with 4.0 F/mol total charge.

2-fluoropropan-2-yl C-H Shift: ¹H-NMR (300 MHz, CD₂Cl₂) δ = 1.68 (d, *J* = 22.0 Hz). Calibrated ¹H-NMR yield from 2-fluoropropan-2-yl proton: 46%. **Benzylic Fluoride Shift:** ¹⁹F{¹H}-NMR (282 MHz, CD₂Cl₂) δ = -139.8. Calibrated ¹⁹F{¹H}-NMR yield from benzylic fluoride: 46%. **HR-MS** (EI) *m/z* calc. for C₁₀H₁₀FN [M]⁺: 163.0797, found: 163.0792. The spectral data are in accordance with those reported in literature.^[285]

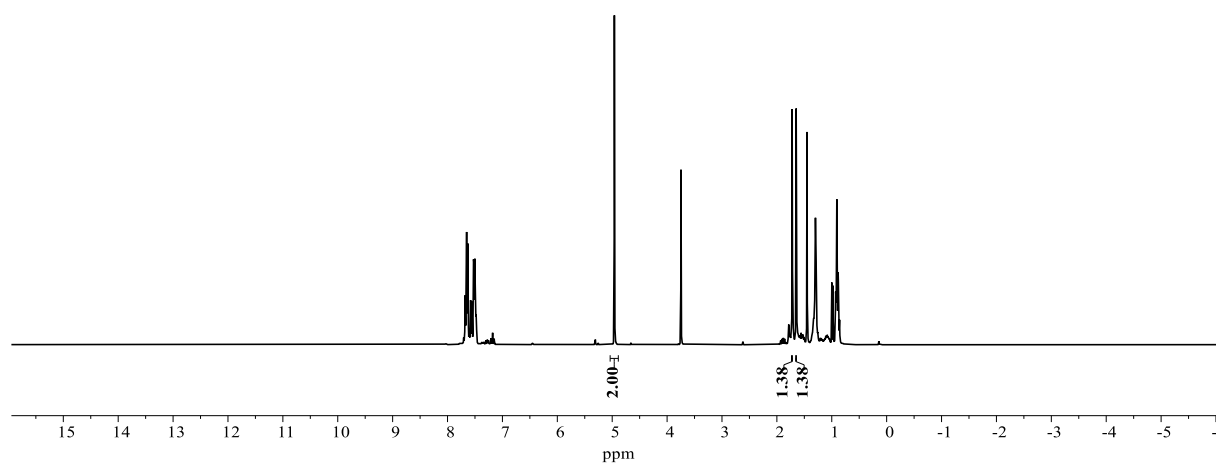


Figure 5.3-5 Crude ¹H-NMR Spectrum (300 MHz, CD₂Cl₂) of the reaction mixture with CH₂Br₂ (36 μ L, 0.50 mmol) as the internal standard (4.96 ppm). The signals of the fluoroisopropyl group and the internal standard are integrated.

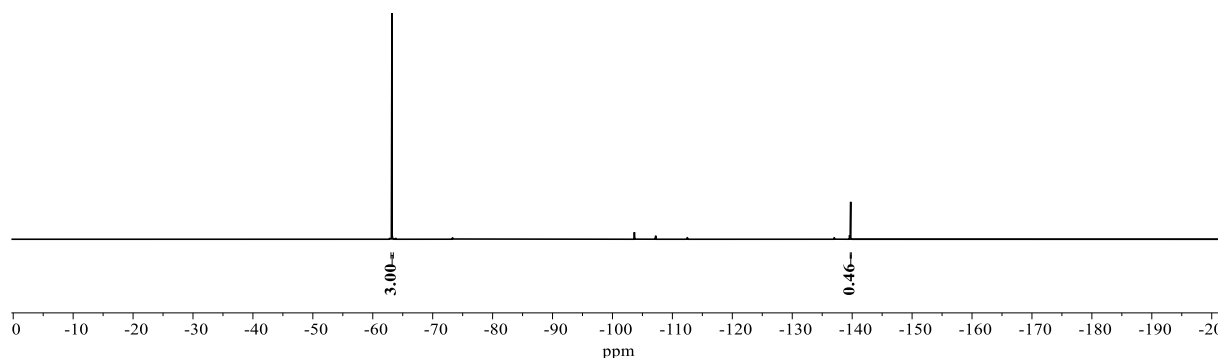
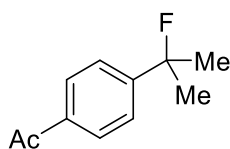


Figure 5.3-6 Crude $^{19}\text{F}\{^1\text{H}\}$ -NMR Spectrum (282 MHz, CD_2Cl_2) of the reaction mixture with PhCF_3 (62 μL , 0.50 mmol) as the internal standard (-63.2 ppm). The signals of the benzylic fluoride and the internal standard are integrated.



4-(2-fluoropropan-2-yl)acetophenone (60an)

The general procedure A was followed using 4-isopropylacetophenone **59an** (81.3 mg, 0.50 mmol) at $-20\text{ }^\circ\text{C}$ with 4.0 F/mol total charge.

2-Fluoropropan-2-yl C-H Shift: ^1H -NMR (300 MHz, CD_2Cl_2) $\delta = 1.72$ (d, $J = 21.9$ Hz). Calibrated ^1H -NMR yield from 2-fluoropropan-2-yl proton: 42%. **Benzylic Fluoride Shift:** $^{19}\text{F}\{^1\text{H}\}$ -NMR (282 MHz, CD_2Cl_2) $\delta = -139.0$. Calibrated $^{19}\text{F}\{^1\text{H}\}$ -NMR yield from benzylic fluoride: 42%. **HR-MS** (EI) m/z calc. for $\text{C}_{11}\text{H}_{13}\text{FO}$ $[\text{M}]^+$: 180.0950, found: 180.0945. The spectral data are in accordance with those reported in literature.^[124b]

EXPERIMENTAL PART

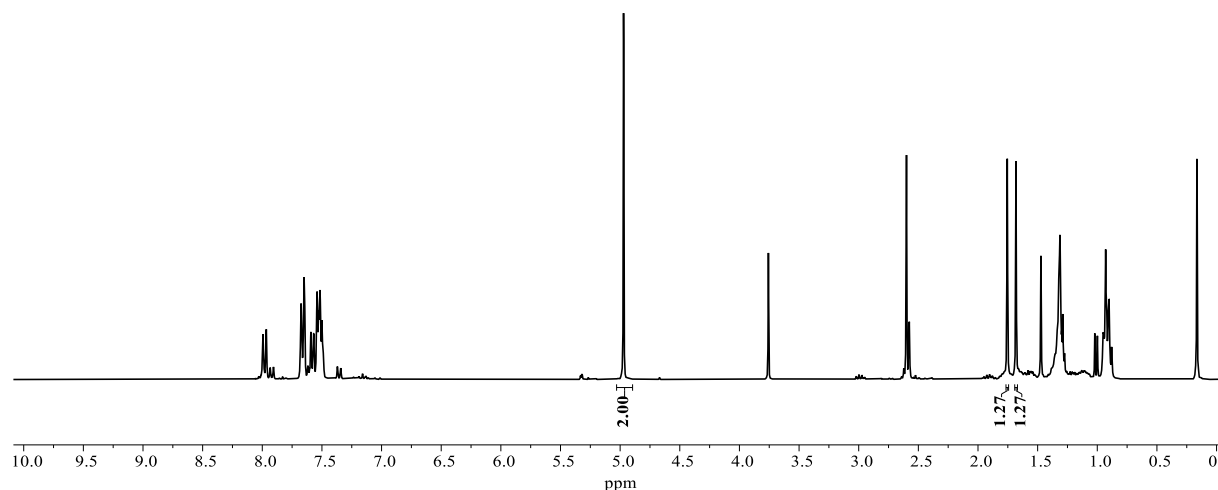


Figure 5.3-7 Crude ^1H -NMR Spectrum (300 MHz, CD_2Cl_2) of the reaction mixture with CH_2Br_2 (36 μL , 0.50 mmol) as the internal standard (4.96 ppm). The signals of the fluoroisopropyl group and the internal standard are integrated.

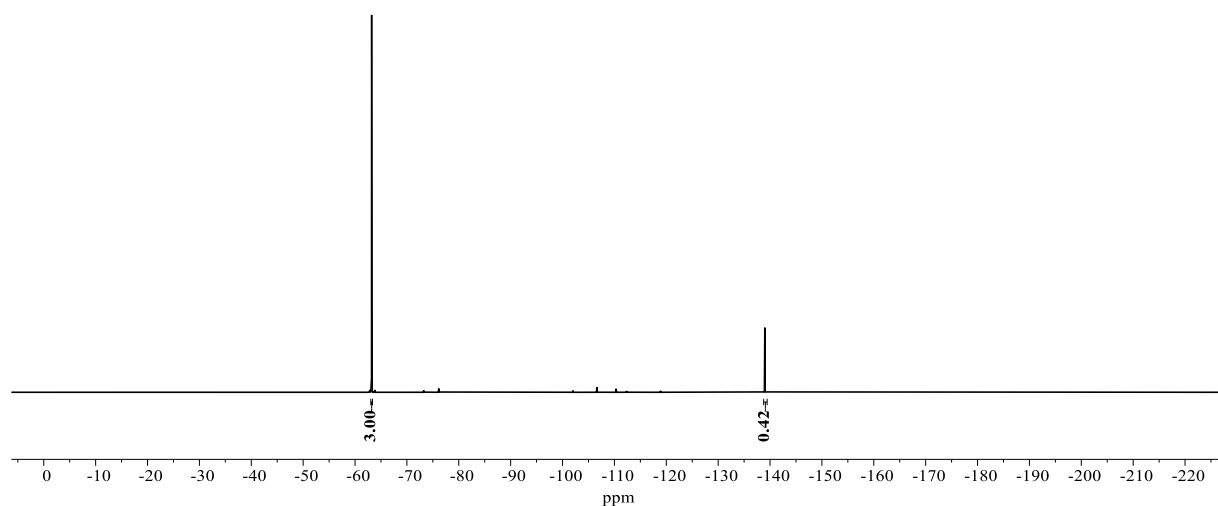
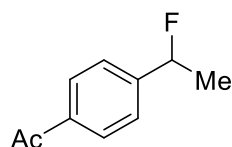


Figure 5.3-8 Crude $^{19}\text{F}\{^1\text{H}\}$ -NMR Spectrum (282 MHz, CD_2Cl_2) of the reaction mixture with PhCF_3 (62 μL , 0.50 mmol) as the internal standard (-63.2 ppm). The signals of the benzylic fluoride and the internal standard are integrated.



4-(1-fluoroethyl)acetophenone (60ao)

The general procedure A was followed using 4-ethylacetophenone **59ao** (81.3 mg, 0.50 mmol) at $-20\text{ }^\circ\text{C}$ with 4.0 F/mol total charge.

Benzyl Fluoride C–H Shift: $^1\text{H-NMR}$ (300 MHz, CD_2Cl_2) $\delta = 5.69$ (dq, $J = 47.7, 6.5$ Hz, 1H). Calibrated $^1\text{H-NMR}$ yield from benzylic proton: 17%. **Benzylic Fluoride Shift:** $^{19}\text{F}\{^1\text{H}\}\text{-NMR}$ (282 MHz, CD_2Cl_2) $\delta = -171.3$. Calibrated $^{19}\text{F}\{^1\text{H}\}\text{-NMR}$ yield from benzylic fluoride: 16%. **HR-MS** (EI) m/z calc. for $\text{C}_{10}\text{H}_{11}\text{FO}$ $[\text{M}]^+$: 166.0794, found: 166.0789. The spectral data are in accordance with those reported in literature.^[124b]

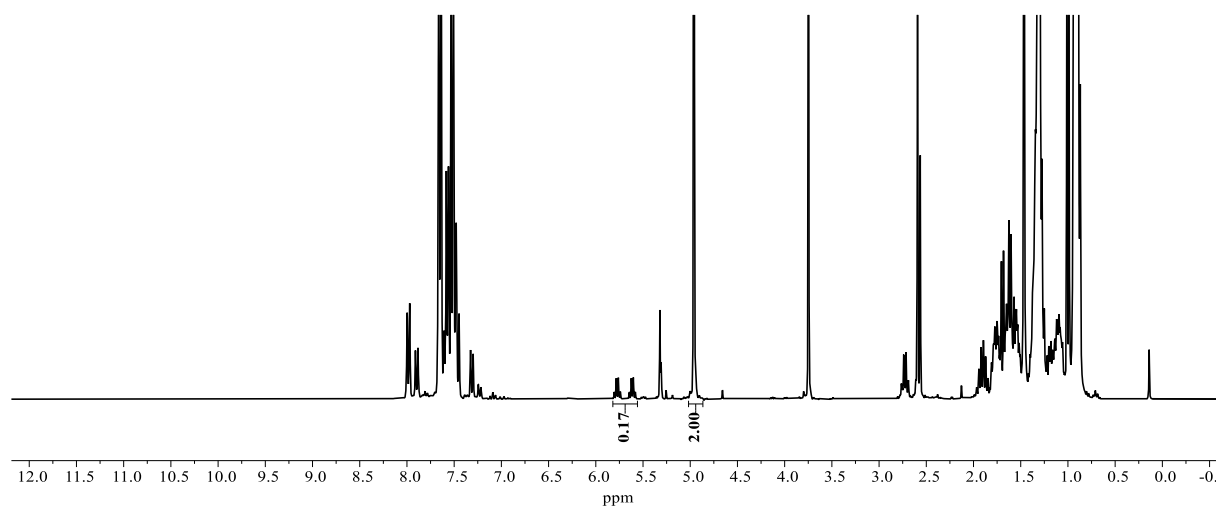


Figure 5.3-9 Crude $^1\text{H-NMR}$ Spectrum (300 MHz, CD_2Cl_2) of the reaction mixture with CH_2Br_2 (36 μL , 0.50 mmol) as the internal standard (4.96 ppm). The signals of the fluoroisopropyl group and the internal standard are integrated.

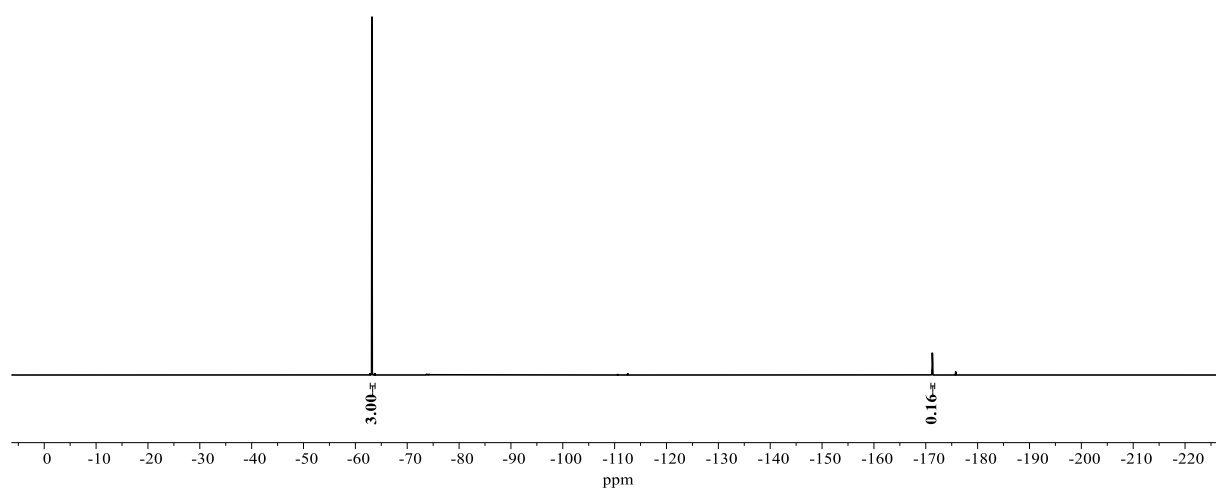
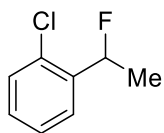


Figure 5.3-10 Crude $^{19}\text{F}\{^1\text{H}\}\text{-NMR}$ Spectrum (282 MHz, CD_2Cl_2) of the reaction mixture with PhCF_3 (62 μL , 0.50 mmol) as the internal standard (-63.2 ppm). The signals of the benzylic fluoride and the internal standard are integrated.



1-Chloro-2-(1-fluoroethyl)benzene (60ap)

The general procedure A was followed using 1-chloro-2-ethylbenzene **59ap** (70.5 mg, 0.50 mmol) at 0 °C.

Benzyl Fluoride C–H Shift: $^1\text{H-NMR}$ (300 MHz, CD_2Cl_2) $\delta = 6.01$ (dq, $J = 46.7, 6.4$ Hz). Calibrated $^1\text{H-NMR}$ yield from benzylic proton: 42%. **Benzylic Fluoride Shift:** $^{19}\text{F}\{^1\text{H}\}$ -NMR (282 MHz, CD_2Cl_2) $\delta = -175.5$. Calibrated $^{19}\text{F}\{^1\text{H}\}$ -NMR yield from benzylic fluoride: 37%. **HR-MS** (EI) m/z calc. for $\text{C}_8\text{H}_8^{35}\text{ClF} [\text{M}]^+$: 158.0299, found: 158.0293. The spectral data are in accordance with those reported in literature.^[124b]

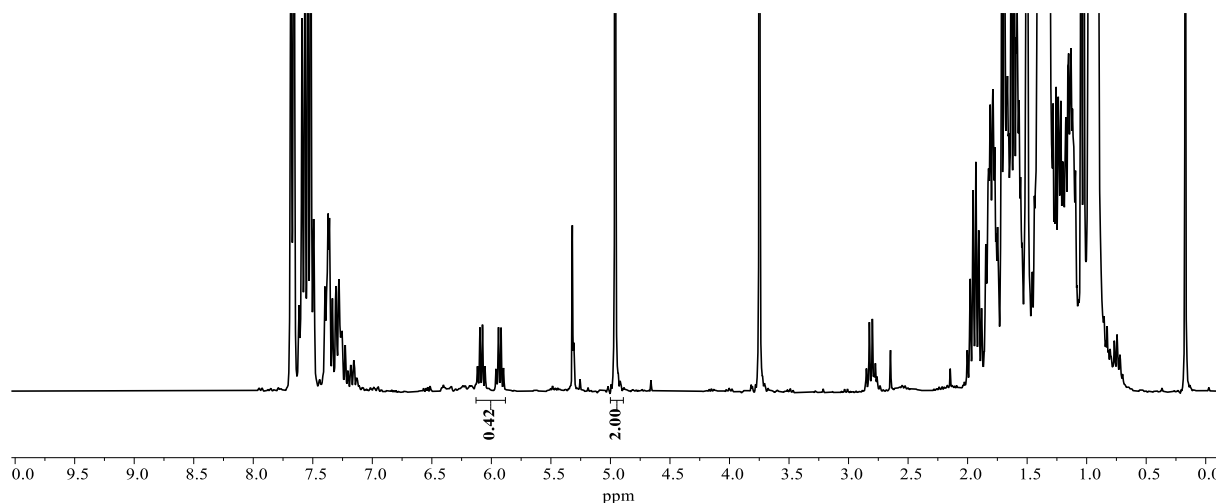


Figure 5.3-11 Crude $^1\text{H-NMR}$ Spectrum (300 MHz, CD_2Cl_2) of the reaction mixture with CH_2Br_2 (36 μL , 0.50 mmol) as the internal standard (4.96 ppm). The signals of the benzylic proton and the internal standard are integrated.

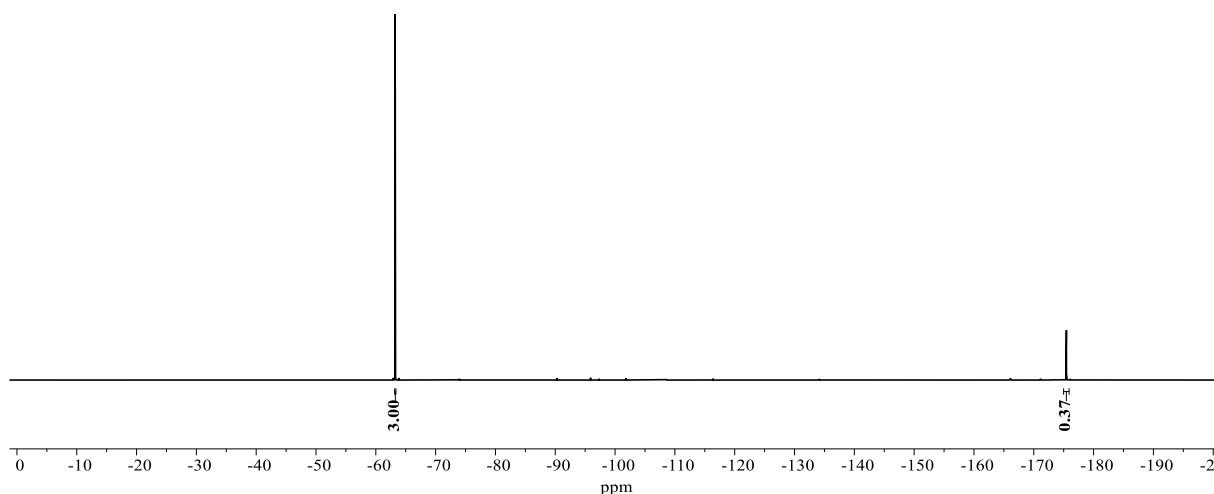
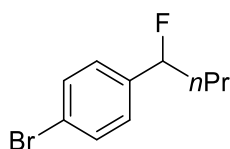


Figure 5.3-12 Crude $^{19}\text{F}\{^1\text{H}\}$ -NMR Spectrum (282 MHz, CD_2Cl_2) of the reaction mixture with PhCF_3 (62 μL , 0.50 mmol) as the internal standard (-63.2 ppm). The signals of the benzylic fluoride and the internal standard are integrated.



1-Bromo-4-(1-fluorobutyl)benzene (**60ar**)

The general procedure A was followed using 1-bromo-4-butylbenzene **59ar** (106.7 mg, 0.50 mmol) at 0°C . After conducting the NMR analysis, the solvents were removed in vacuo, and the residue was purified by FCC (*n*-hexane/EtOAc = 30:1) to obtain the product **60ar** as a colorless oil (63.6 mg, 0.28 mmol, 55%).

^1H -NMR (300 MHz, CDCl_3) δ = 7.50 (d, J = 7.8 Hz, 2H), 7.20 (d, J = 7.8 Hz, 2H), 5.39 (ddd, J = 47.7, 8.0, 4.9 Hz, 1H), 2.06–1.63 (m, 2H), 1.60–1.28 (m, 2H), 0.96 (t, J = 7.4 Hz, 3H). Calibrated ^1H -NMR (300 MHz, CD_2Cl_2) yield from benzylic proton: 87%. **$^{19}\text{F}\{^1\text{H}\}$ -NMR** (282 MHz, CDCl_3): δ = -175.5 . Calibrated $^{19}\text{F}\{^1\text{H}\}$ -NMR (282 MHz, CD_2Cl_2) yield from benzylic fluoride: 87%. **$^{13}\text{C}\{^1\text{H}\}$ -NMR** (75 MHz, CDCl_3) δ = 139.8 (d, $^2J_{\text{C-F}}$ = 20.3 Hz, C_q), 131.7 (CH), 127.4 (d, $^3J_{\text{C-F}}$ = 6.9 Hz), 122.2 (d, $^5J_{\text{C-F}}$ = 2.5 Hz, C_q), 93.9 (d, $^1J_{\text{C-F}}$ = 171.1 Hz, CH), 39.3 (d, $^2J_{\text{C-F}}$ = 23.2 Hz, CH_2), 18.4 (d, $^3J_{\text{C-F}}$ = 4.5 Hz, CH_2), 13.9 (CH_3). **IR** (ATR): $\tilde{\nu}$ = 2962, 2935, 2874, 1597, 1490, 1072, 1012, 954, 824, 543. **HR-MS** (EI) m/z calc. for $\text{C}_{10}\text{H}_{12}^{79}\text{BrF} [\text{M}]^+$: 230.0106, found: 230.0101.

EXPERIMENTAL PART

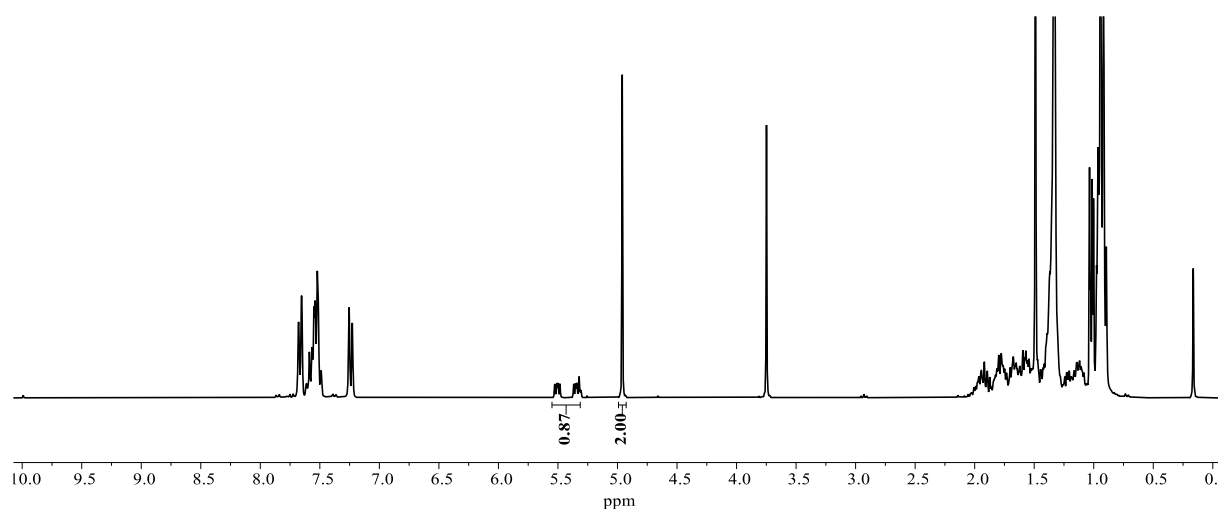


Figure 5.3-13 Crude ^1H -NMR Spectrum (300 MHz, CD_2Cl_2) of the reaction mixture with CH_2Br_2 (36 μL , 0.50 mmol) as the internal standard (4.96 ppm). The signals of the benzylic proton and the internal standard are integrated.

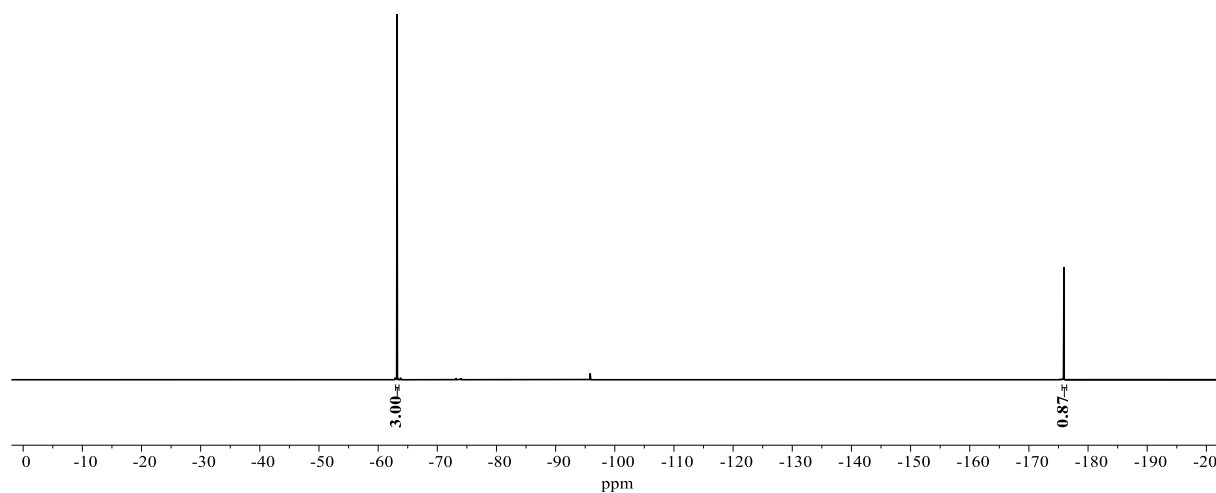
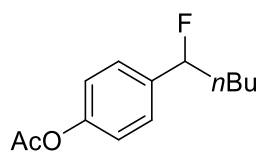


Figure 5.3-14 Crude $^{19}\text{F}\{^1\text{H}\}$ -NMR Spectrum (282 MHz, CD_2Cl_2) of the reaction mixture with PhCF_3 (62 μL , 0.50 mmol) as the internal standard (-63.2 ppm). The signals of the benzylic fluoride and the internal standard are integrated.



4-(1-fluoropentyl)phenyl acetate (**60at**)

The general procedure A was followed using 4-pentylphenyl acetate **59at** (103 mg, 0.50 mmol) at $-20\text{ }^\circ\text{C}$. After conducting the NMR analysis, the solvents were removed in vacuo, and the residue was purified by FCC on partially neutralized silica (*n*-hexane/EtOAc = 30:1) to obtain the product **60at** as a colorless oil (57.0 mg, 0.25 mmol, 50%).

EXPERIMENTAL PART

¹H-NMR (300 MHz, CDCl₃) δ = 7.34 (d, J = 8.4 Hz, 2H), 7.10 (d, J = 8.4 Hz, 2H), 5.41 (ddd, J = 47.7, 8.1, 4.9 Hz, 1H), 2.30 (s, 3H), 2.08–1.66 (m, 2H), 1.56–1.23 (m, 2H), 0.91 (t, J = 6.9 Hz, 3H). Calibrated ¹H-NMR yield from benzylic proton: 62%. **¹⁹F{¹H}-NMR** (282 MHz, CDCl₃): δ = -173.6. Calibrated ¹⁹F{¹H}-NMR yield from benzylic fluoride: 66%. **¹³C{¹H}-NMR** (101 MHz, CDCl₃) δ = 169.5 (C_q), 150.5 (d, $^5J_{C-F}$ = 2.2 Hz, C_q), 138.3 (d, $^2J_{C-F}$ = 20.3 Hz, C_q), 126.8 (d, $^3J_{C-F}$ = 6.8 Hz, CH), 121.7 (CH), 94.3 (d, $^1J_{C-F}$ = 170.5 Hz, CH), 37.0 (d, $^2J_{C-F}$ = 23.5 Hz, CH), 27.3 (d, $^3J_{C-F}$ = 4.2 Hz, CH₂), 22.6 (CH₂), 21.2 (CH₃), 14.0 (CH₃). **IR** (ATR): $\tilde{\nu}$ = 2958, 2936, 2867, 1760, 1510, 1369, 1190, 912, 851, 550. **HR-MS** (EI) m/z calc. for C₁₃H₁₇FO₂ [M]⁺: 224.1213, found: 224.1207.

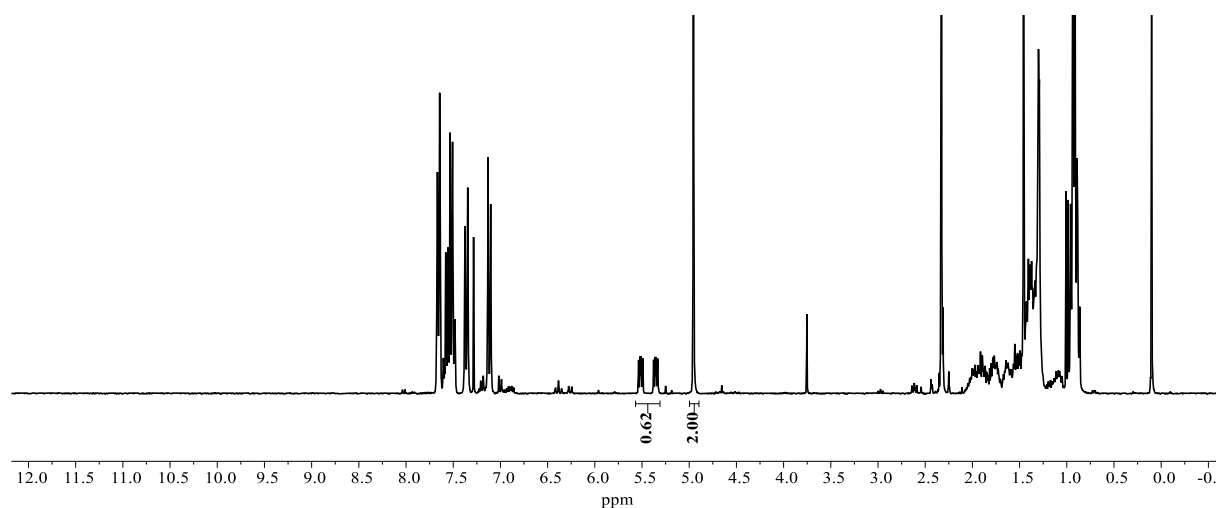


Figure 5.3-15 Crude ¹H-NMR Spectrum (300 MHz, CDCl₃) of the reaction mixture with CH₂Br₂ (36 μ L, 0.50 mmol) as the internal standard (4.93 ppm). The signals of the benzylic proton and the internal standard are integrated.

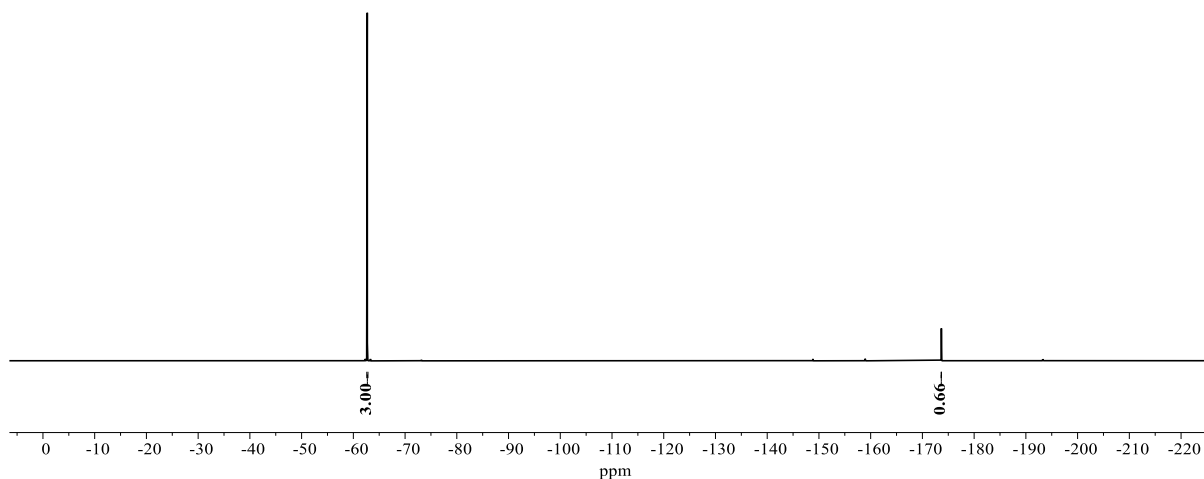
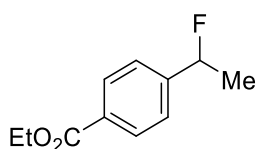


Figure 5.3-16 ^{19}F -NMR Spectrum (282 MHz, CDCl_3) of the reaction mixture with PhCF_3 (62 μL , 0.50 mmol) as the internal standard (-62.7 ppm). The signals of the benzylic fluoride and the internal standard are integrated.



Ethyl 4-(1-fluoroethyl)benzoate (**60au**)

The general procedure A was followed using ethyl 4-ethylbenzoate **59au** (89.3 mg, 0.50 mmol) at $-20\text{ }^\circ\text{C}$ with 4.0 F/mol total charge.

Benzyl Fluoride C–H Shift: ^1H -NMR (300 MHz, C_6D_6) $\delta = 5.19$ (dq, $J = 47.6, 6.4$ Hz). Calibrated ^1H -NMR yield from benzylic proton: 44%. **Benzylic Fluoride Shift:** $^{19}\text{F}\{^1\text{H}\}$ -NMR (282 MHz, C_6D_6) $\delta = -171.2$. Calibrated $^{19}\text{F}\{^1\text{H}\}$ -NMR yield from benzylic fluoride: 46%. **HR-MS** (EI) m/z calc. for $\text{C}_{11}\text{H}_{13}\text{FO}_2$ $[\text{M}]^+$: 196.0900, found: 196.0894.

The spectral data are in accordance with those reported in literature.^[252]

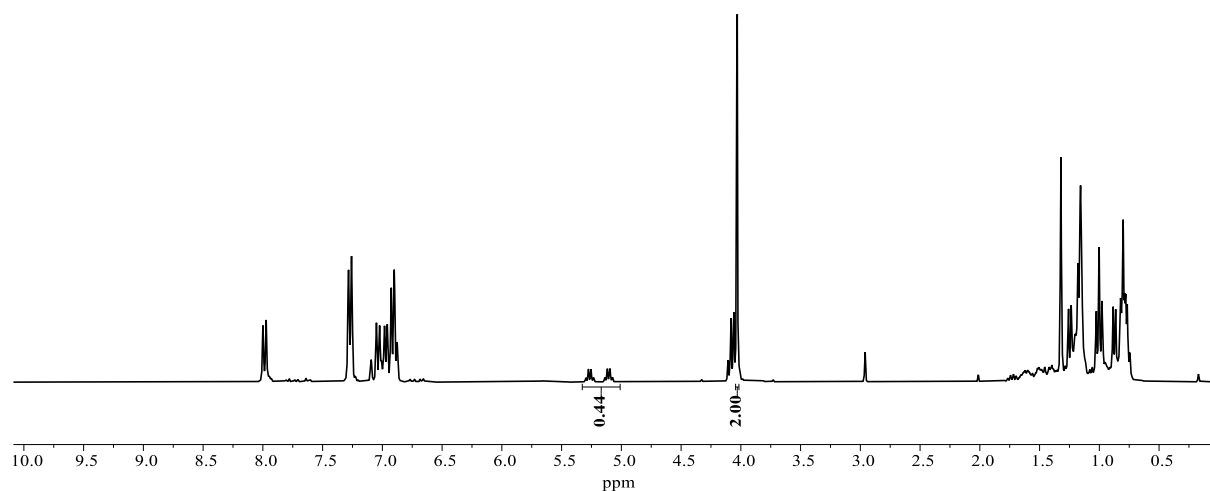


Figure 5.3-17 Crude ¹H-NMR Spectrum (300 MHz, C₆D₆) of the reaction mixture with CH₂Br₂ (36 μL, 0.50 mmol) as the internal standard (4.03 ppm). The signals of the benzylic proton and the internal standard are integrated.

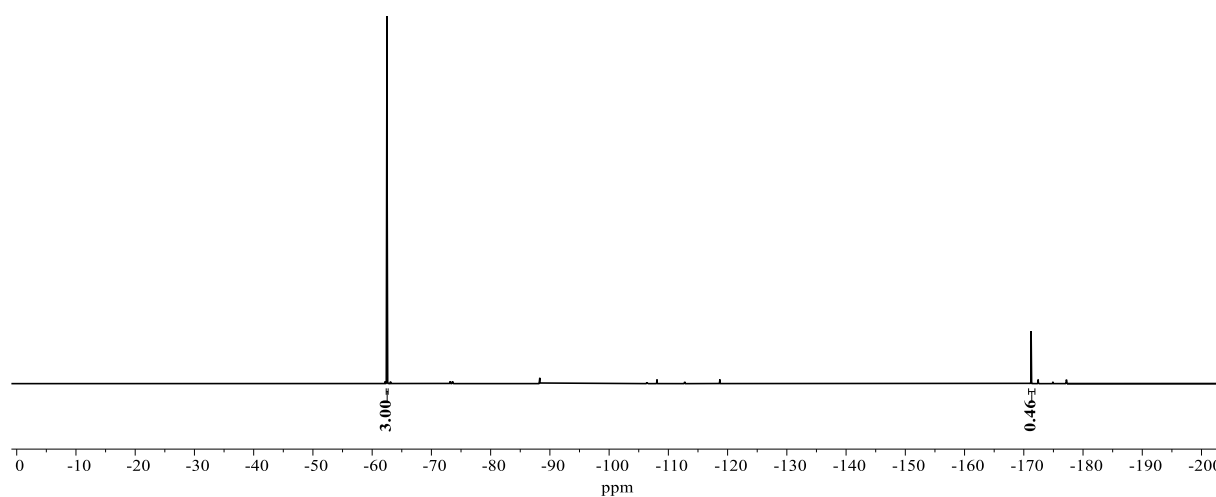
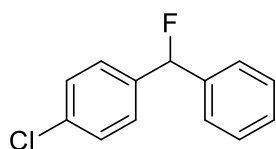


Figure 5.3-18 Crude ¹⁹F{¹H}-NMR Spectrum (282 MHz, C₆D₆) of the reaction mixture with PhCF₃ (62 μL, 0.50 mmol) as the internal standard (-63.5 ppm). The signals of the benzylic fluoride and the internal standard are integrated.



1-Chloro-4-(fluoro(phenyl)methyl)benzene (60av)

The general procedure A was followed using 4-chlorodiphenylmethane **59av** (81.3 mg, 0.50 mmol) at -20 °C with 3.0 F/mol total charge.

EXPERIMENTAL PART

Benzyl Fluoride C–H Shift: ^1H -NMR (300 MHz, CD_2Cl_2) $\delta = 6.47$ (d, $J = 47.3$ Hz). Calibrated ^1H -NMR yield from benzylic proton: 74%. **Benzylic Fluoride Shift:** $^{19}\text{F}\{^1\text{H}\}$ -NMR (282 MHz, CD_2Cl_2) $\delta = -167.4$. Calibrated $^{19}\text{F}\{^1\text{H}\}$ -NMR yield from benzylic fluoride: 74%. **HR-MS** (EI) m/z calc. for $\text{C}_{13}\text{H}_{10}^{35}\text{ClF} [\text{M}]^+$: 220.0455, found: 220.0450. The spectral data are in accordance with those reported in literature.^[286]

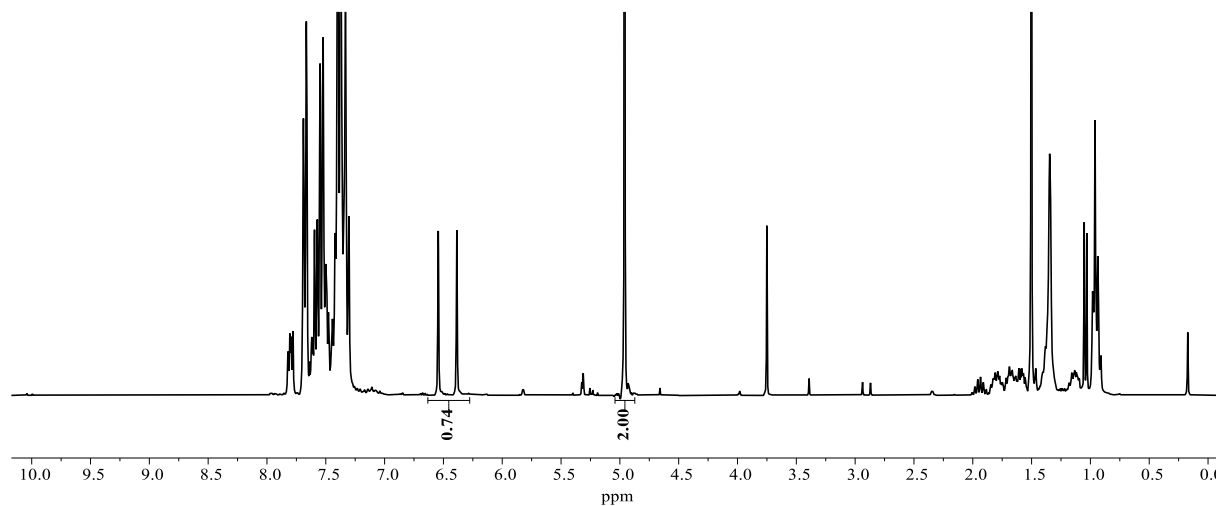


Figure 5.3-19 Crude ^1H -NMR Spectrum (300 MHz, CD_2Cl_2) of the reaction mixture with CH_2Br_2 (36 μL , 0.50 mmol) as the internal standard (4.96 ppm). The signals of the benzylic proton and the internal standard are integrated.

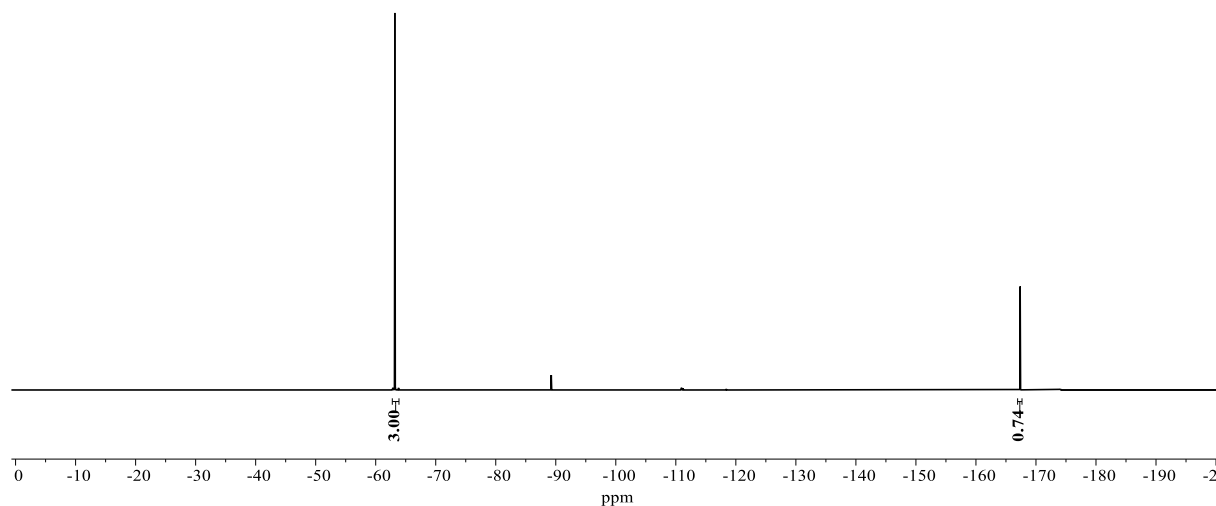
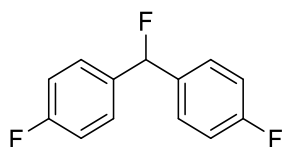


Figure 5.3-20 Crude $^{19}\text{F}\{^1\text{H}\}$ -NMR Spectrum (282 MHz, CD_2Cl_2) of the reaction mixture with PhCF_3 (62 μL , 0.50 mmol) as the internal standard (-63.2 ppm). The signals of the benzylic fluoride and the internal standard are integrated.

**4,4'-(fluoromethylene)bis(fluorobenzene) (60aw)**

The general procedure A was followed using 4,4'-difluorodiphenylmethane **59aw** (102 mg, 0.50 mmol) at $-20\text{ }^{\circ}\text{C}$ with 3.0 F/mol total charge.

Benzyl Fluoride C–H Shift: $^1\text{H-NMR}$ (300 MHz, CD_2Cl_2) $\delta = 6.45$ (d, $J = 47.4$ Hz). Calibrated $^1\text{H-NMR}$ yield from benzylic proton: 70%. **Benzylic Fluoride Shift:** $^{19}\text{F}\{^1\text{H}\}$ -NMR (282 MHz, CD_2Cl_2) $\delta = -164.0$ (t, $J = 3.6$ Hz). Calibrated $^{19}\text{F}\{^1\text{H}\}$ -NMR yield from benzylic fluoride: 70%. **HR-MS** (EI) m/z calc. for $\text{C}_{13}\text{H}_9\text{F}_3$ $[\text{M}]^+$: 222.0656, found: 222.0651. The spectral data are in accordance with those reported in literature.^[252]

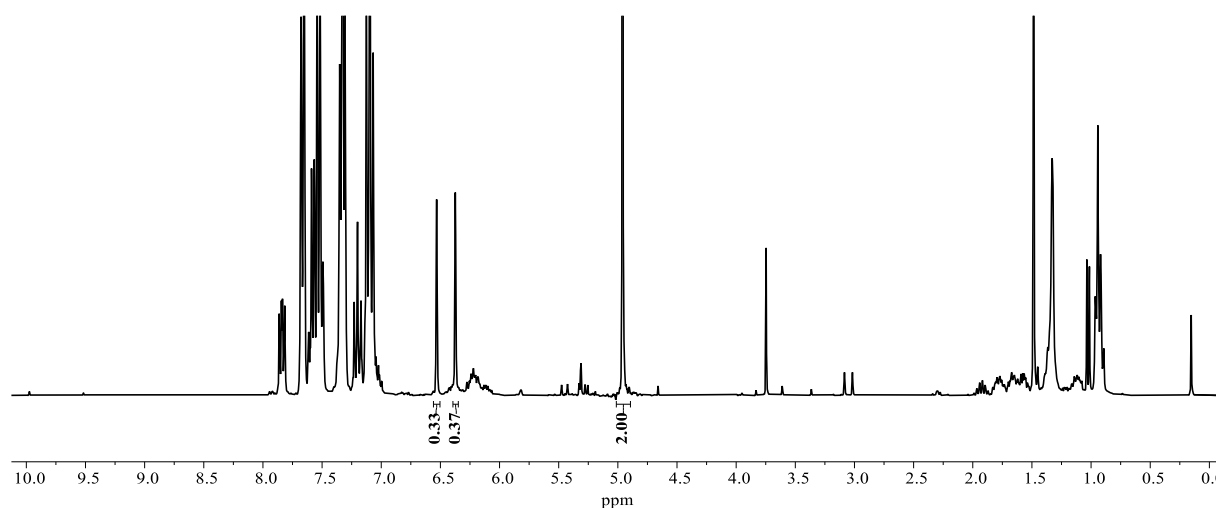


Figure 5.3-21 Crude $^1\text{H-NMR}$ Spectrum (300 MHz, CD_2Cl_2) of the reaction mixture with CH_2Br_2 (36 μL , 0.50 mmol) as the internal standard (4.96 ppm). The signals of the benzylic proton and the internal standard are integrated.

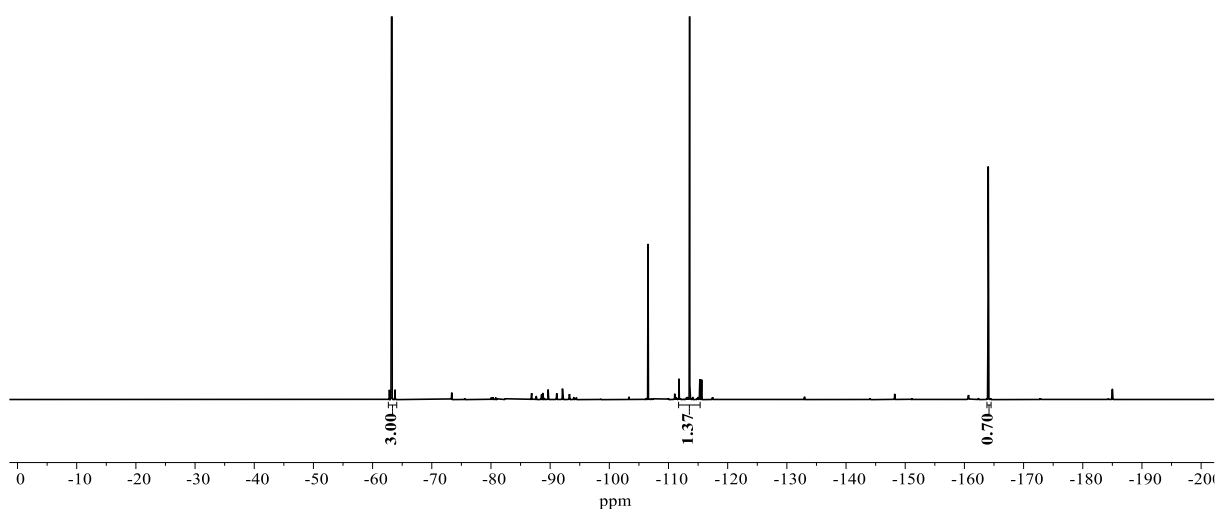
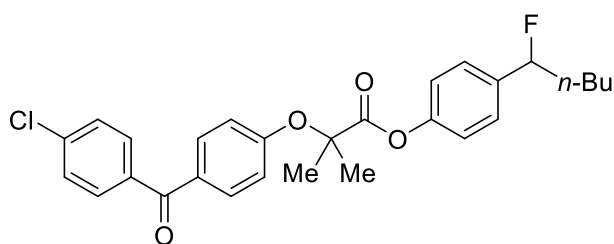


Figure 5.3-22 Crude $^{19}\text{F}\{^1\text{H}\}$ -NMR Spectrum (282 MHz, CD_2Cl_2) of the reaction mixture with PhCF_3 (62 μL , 0.50 mmol) as the internal standard (-63.2 ppm). The signals of the benzylic fluoride, aromatic fluoride and the internal standard are integrated.



4-(1-fluoropentyl)phenyl 2-(4-(4-chlorobenzoyl)phenoxy)-2-methylpropanoate (**60ax**)

The general procedure A was followed using ethyl 4-pentylphenyl 2-(4-(4-chlorobenzoyl)phenoxy)-2-methylpropanoate **59ax** (232 mg, 0.50 mmol) at $-20\text{ }^\circ\text{C}$ and 20 mA with 4.0 F/mol total charge. After conducting the crude NMR analysis, the solvents were removed in vacuo, and the residue was purified by FCC (*n*-hexane/EtOAc = 15:1), to obtain the product **60ax** (102 mg, 0.21 mmol, 42%) of a colorless solid.

M.p.: 64–66 $^\circ\text{C}$. ^1H -NMR (400 MHz, CDCl_3): δ = 7.81–7.76 (m, 2H), 7.74–7.70 (m, 2H), 7.48–7.44 (m, 2H), 7.35–7.30 (m, 2H), 7.02–6.97 (m, 4H), 5.41 (ddd, J = 47.7, 8.0, 4.9, 1H), 2.12–1.65 (m, 2H), 1.83 (s, 6H) 1.48–1.23 (m, 4H), 0.90 (t, J = 6.8, 3H). Calibrated ^1H -NMR yield from benzylic proton: 51%. $^{13}\text{C}\{^1\text{H}\}$ -NMR (126 MHz, CDCl_3): δ = 194.3 (C_q), 172.5 (C_q), 159.7 (C_q), 150.2 (C_q), 138.9 (d, $^2J_{\text{C-F}}$ = 20.2, C_q), 138.6 (C_q), 136.4 (C_q), 132.3 (CH), 131.3 (CH), 130.9 (C_q), 128.7 (CH), 126.9 (d, $^3J_{\text{C-F}}$ = 6.9, CH), 121.3 (CH), 117.5 (CH), 94.1 (d, $^1J_{\text{C-F}}$ = 171.1, CH), 79.6 (C_q), 37.1 (d, $^2J_{\text{C-F}}$ = 23.2, CH_2), 27.3 (d, $^3J_{\text{C-F}}$ = 4.2, CH_2), 25.6 (CH_3), 25.6 (CH_3), 22.6 (CH_2), 14.6 (CH_3). $^{19}\text{F}\{^1\text{H}\}$ -NMR (282

EXPERIMENTAL PART

MHz, CDCl_3): $\delta = -174.1$. Calibrated $^{19}\text{F}\{^1\text{H}\}$ -NMR yield from benzylic fluoride: 50%.
IR (ATR): $\tilde{\nu} = 2529, 2873, 1771, 1645, 1596, 1594, 1193, 1166, 1087, 853, 477$. **HR-MS**
(ESI) m/z calc. for $\text{C}_{28}\text{H}_{28}\text{ClFO}_4\text{Na}$ $[\text{M}+\text{Na}]^+$: 505.1558, found: 505.1552.

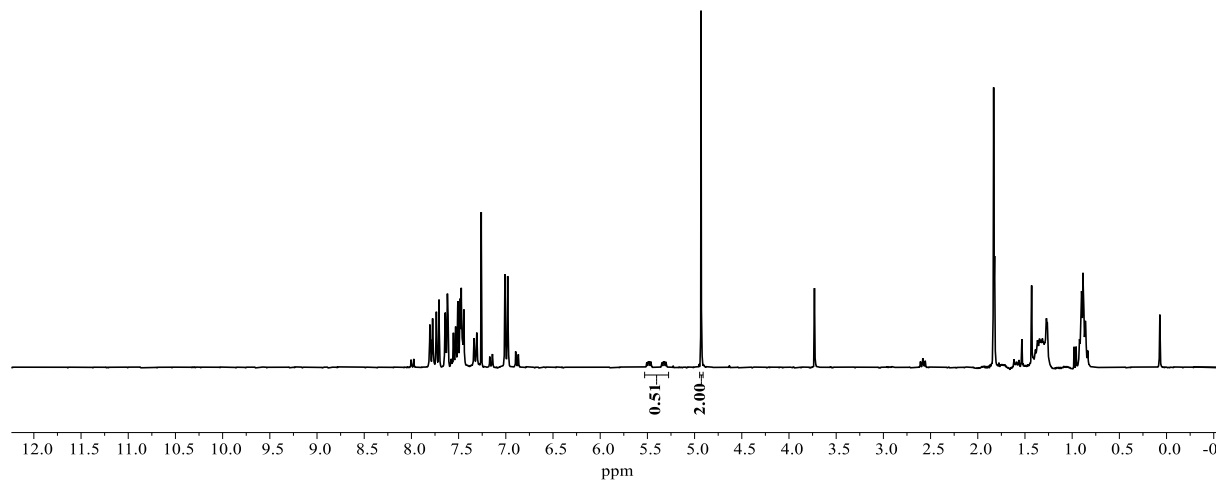


Figure 5.3-23 Crude ^1H -NMR Spectrum (300 MHz, CDCl_3) of the reaction mixture with CH_2Br_2 (36 μL , 0.50 mmol) as the internal standard (4.93 ppm). The signals of the benzylic proton and the internal standard are integrated.

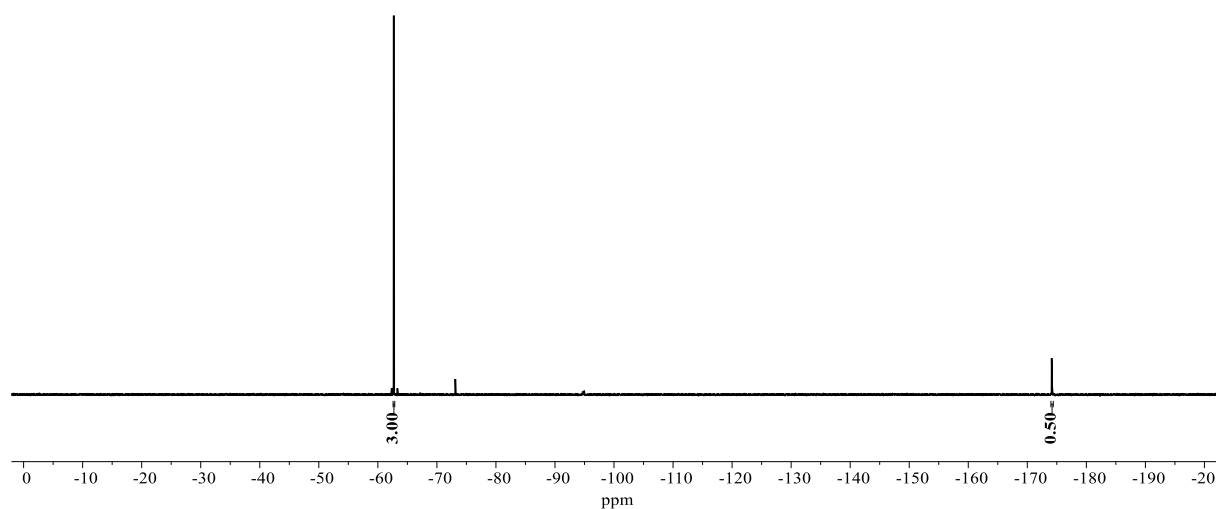
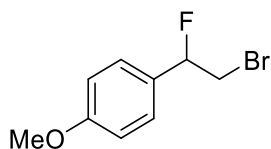


Figure 5.3-24 Crude $^{19}\text{F}\{^1\text{H}\}$ -NMR Spectrum (282 MHz, CDCl_3) of the reaction mixture with PhCF_3 (62 μL , 0.50 mmol) as the internal standard (-62.7 ppm). The signals of the benzylic fluoride and the internal standard are integrated.

**1-(2-bromo-1-fluoroethyl)-4-methoxybenzene (60ay)**

The general procedure A was followed using 1-(2-bromoethyl)-4-methoxybenzene **59ay** (107.5 mg, 0.50 mmol) at $-20\text{ }^{\circ}\text{C}$ and 10 mA with 2.5 F/mol total charge.

Benzylic Fluoride C–H Shift: $^1\text{H-NMR}$ (300 MHz, CD_2Cl_2) $\delta = 5.58$ (ddd, $J = 46.8, 8.0, 4.3$ Hz, 1H). Calibrated $^1\text{H-NMR}$ yield from benzylic proton: 24%. **Benzylic Fluoride Shift:** $^{19}\text{F}\{^1\text{H}\}\text{-NMR}$ (282 MHz, CD_2Cl_2) $\delta = -169.9$. Calibrated $^{19}\text{F}\{^1\text{H}\}\text{-NMR}$ yield from benzylic fluoride: 23%. **HR-MS** (EI) m/z calc. for $\text{C}_9\text{H}_{10}\text{BrFO}$ $[\text{M}]^+$: 231.9899, found: 231.9893. The spectral data are in accordance with those reported in literature.^[287]

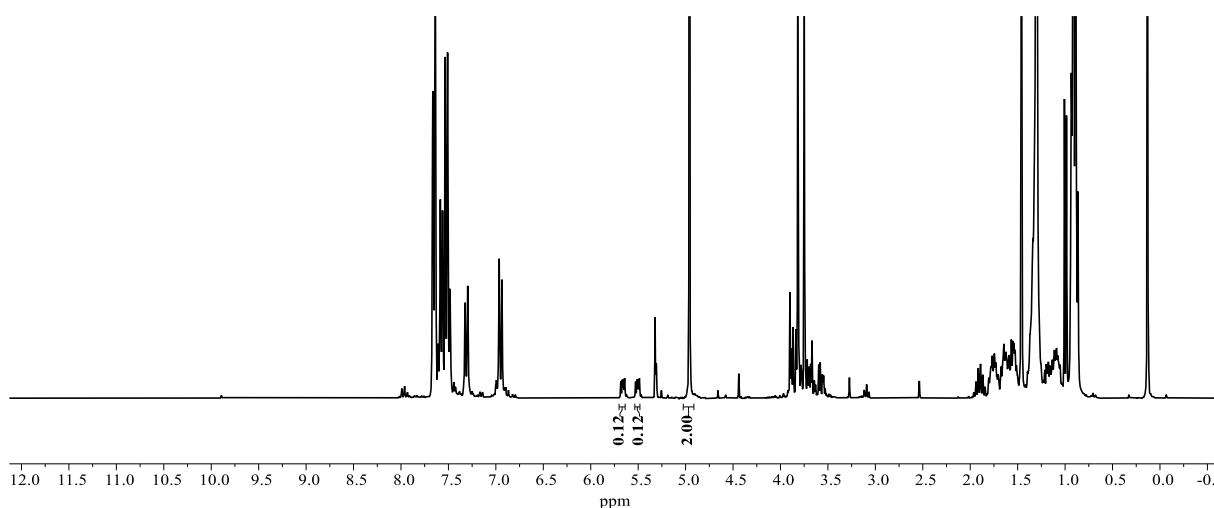


Figure 5.3-25 Crude $^1\text{H-NMR}$ Spectrum (300 MHz, CD_2Cl_2) of the reaction mixture with CH_2Br_2 (36 μL , 0.50 mmol) as the internal standard (4.96 ppm). The signals of the benzylic proton and the internal standard are integrated.

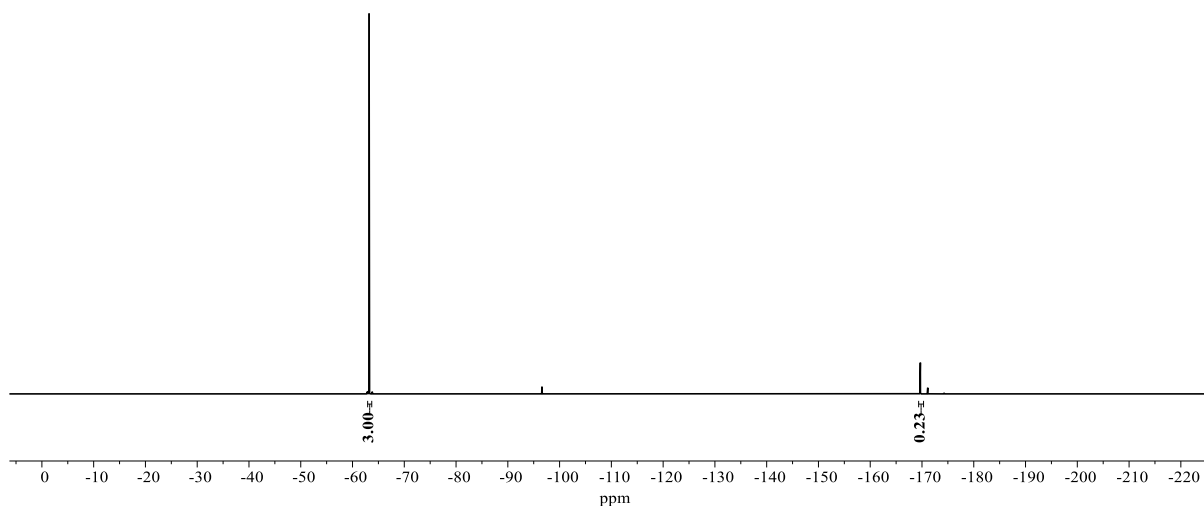
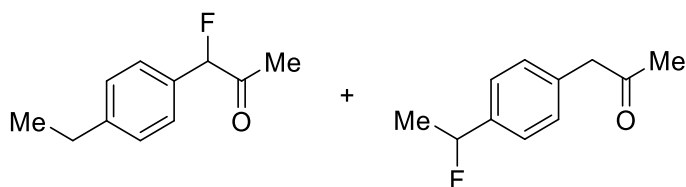


Figure 5.3-26 Crude $^{19}\text{F}\{^1\text{H}\}$ -NMR Spectrum (282 MHz, CD_2Cl_2) of the reaction mixture with PhCF_3 (62 μL , 0.50 mmol) as the internal standard (-63.2 ppm). The signals of the benzylic fluoride, aromatic fluoride and the internal standard are integrated.



1-(4-Ethylphenyl)-1-fluoropropan-2-one (**60az**) and 1-(4-(1-fluoroethyl)phenyl)propan-2-one (**60az'**)

The general procedure A was followed using 1-(4-ethylphenyl)-1-propan-2-one **59az** (81.4 mg, 0.50 mmol) at 0°C . After conducting the crude NMR analysis, the solvents were removed in vacuo, and the residue was purified by FCC on partially neutralized silica (*n*-hexane/EtOAc = 30:1), to obtain the product **60az** (23.5 mg, 0.13 mmol, 26%) of a colorless liquid.

Resonances of **60az**: ^1H -NMR (300 MHz, CDCl_3): $\delta = 7.32$ (d, $J = 8.1$ Hz, 2H), 7.24 (d, $J = 8.1$ Hz, 2H), 5.66 (d, $J = 48.6$ Hz, 1H), 2.66 (q, $J = 7.6$ Hz, 2H), 2.23 (d, $J = 3.8$ Hz, 3H), 1.24 (t, $J = 7.6$ Hz, 3H). Calibrated ^1H -NMR (300 MHz, C_6D_6) yield from benzylic protons of both isomers: 59%, consisting of $\delta = 5.27$ (d, $J = 48.9$ Hz, 35%) for **60az** and $\delta = 5.26$ (dq, $J = 47.7, 6.4$ Hz, 24%) for **60az'**. $^{13}\text{C}\{^1\text{H}\}$ -NMR (75 MHz, CDCl_3): $\delta = 204.8$ (d, $^2J_{\text{C-F}} = 26.6$ Hz, C_q), 145.9 (d, $^5J_{\text{C-F}} = 2.1$ Hz, C_q), 131.3 (d, $^2J_{\text{C-F}} = 20.7$ Hz, C_q), 128.6 (CH), 126.3 (d, $^3J_{\text{C-F}} = 6.5$ Hz, CH), 96.0 (d, $^1J_{\text{C-F}} = 187.1$ Hz, CH), 28.7 (CH_2), 25.3 (CH_3), 15.5 (CH_3). $^{19}\text{F}\{^1\text{H}\}$ -NMR (282 MHz, CDCl_3): $\delta = -180.8$. Calibrated $^{19}\text{F}\{^1\text{H}\}$ -NMR (282 MHz, C_6D_6) yield from benzylic fluoride: 59%, consisting of $\delta = -182.9$ (35%) for **60az**

and -168.9 (24%) for **60az'**. HR-MS (ESI) m/z calc. for $C_{11}H_{13}FONa$ $[M+Na]^+$: 203.0848, found: 203.0842.

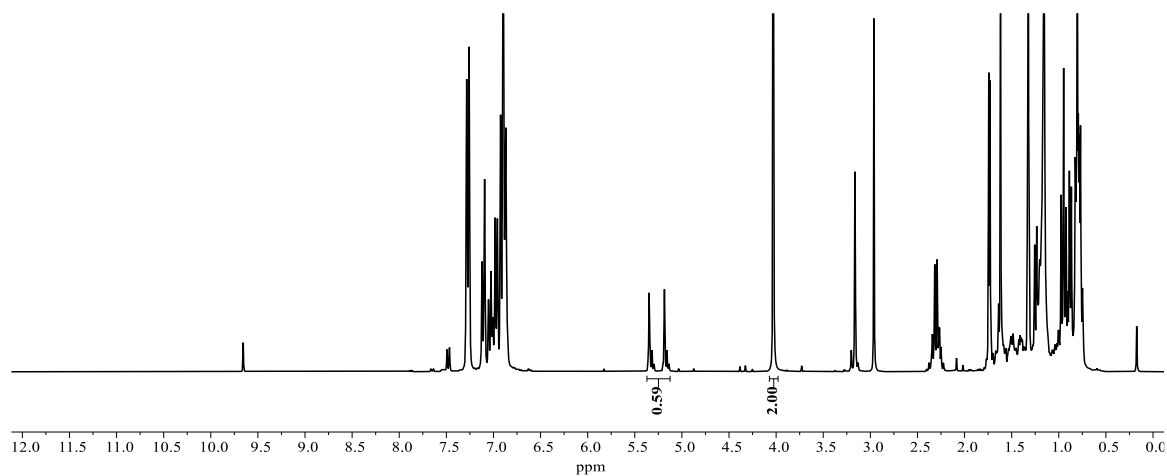


Figure 5.3-27 Crude 1H -NMR Spectrum (300 MHz, C_6D_6) of the reaction mixture with CH_2Br_2 (36 μL , 0.50 mmol) as the internal standard (4.03 ppm). The signals of the benzylic proton and the internal standard are integrated.

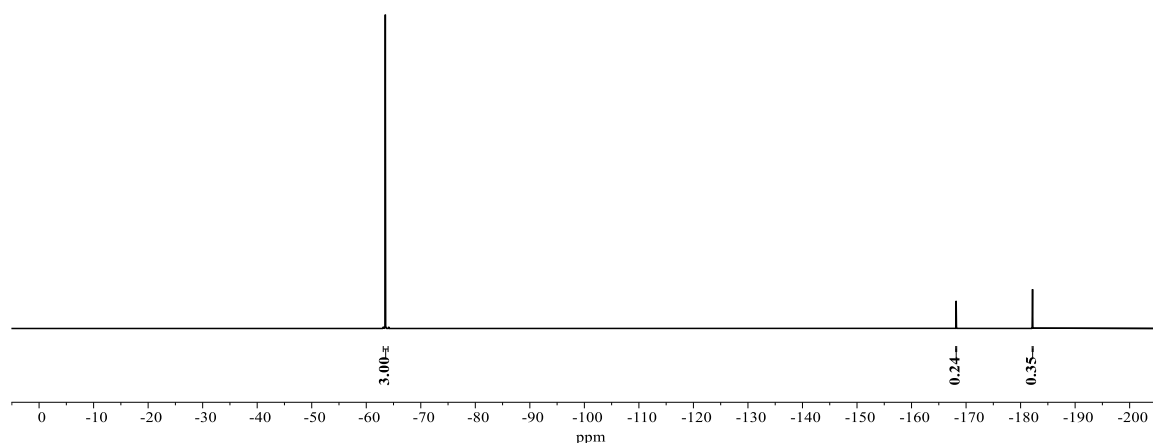
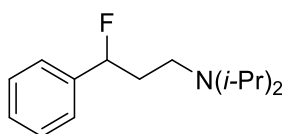


Figure 5.3-28 Crude $^{19}F\{^1H\}$ -NMR Spectrum (282 MHz, C_6D_6) of the reaction mixture with $PhCF_3$ (62 μL , 0.50 mmol) as the internal standard (-63.5 ppm). The signals of the benzylic fluoride and the internal standard are integrated.



3-Fluoro-*N,N*-diisopropyl-3-phenylpropan-1-amine (**60ba**)

The general procedure A was followed using *N,N*-diisopropyl-3-phenylpropan-1-amine **59ba** (110.0 mg, 0.50 mmol) at 0 $^{\circ}C$ and 10 mA with 4.0 F/mol total charge. The combined organic solutions were washed the first time with sat. aq. $NaHCO_3$ (20 mL) instead of water.

EXPERIMENTAL PART

After conducting the NMR analysis, the solvents were removed in vacuo, and the residue was purified by FCC on partially neutralized silica (*n*-hexane/EtOAc/NEt₃ = 35:4:1) to obtain the product **60ba** as a colorless oil (39.4 mg, 0.16 mmol, 33%).

¹H-NMR (300 MHz, CDCl₃) δ = 7.43–7.26 (m, 5H), 5.57 (ddd, J = 48.2, 8.8, 3.8 Hz, 1H), 3.01 (hept, J = 7.0 Hz, 2H), 2.61 (dd, J = 8.0, 6.2 Hz, 2H), 2.14 – 1.75 (m, 2H), 1.01 (t, J = 7.0 Hz, 12H). Calibrated **¹H-NMR** (300 MHz, C₆D₆) yield from benzylic proton: 49%. **¹⁹F{¹H}-NMR** (282 MHz, CDCl₃): δ = -176.4. Calibrated **¹⁹F{¹H}-NMR** (282 MHz, C₆D₆) yield from benzylic fluoride: 54%. **¹³C{¹H}-NMR** (101 MHz, CDCl₃): δ = 141.0 (d, $^2J_{C-F}$ = 19.7 Hz, C_q), 128.5 (CH), 128.2 (d, $^5J_{C-F}$ = 1.9 Hz, CH), 125.7 (d, $^3J_{C-F}$ = 6.8 Hz, CH), 93.0 (d, $^1J_{C-F}$ = 169.0 Hz, CH), 48.6 (CH), 41.0 (d, $^3J_{C-F}$ = 3.5 Hz), 39.0 (d, $^2J_{C-F}$ = 22.9 Hz), 21.4 (CH₃), 20.5 (CH₃). **IR** (ATR): $\tilde{\nu}$ = 2965, 2931, 2873, 1456, 1388, 1363, 1203, 1171, 1056, 910, 756, 699. **HR-MS** (EI) m/z calc. for C₁₅H₂₄FN [M]⁺: 237.1893, found: 237.1887.

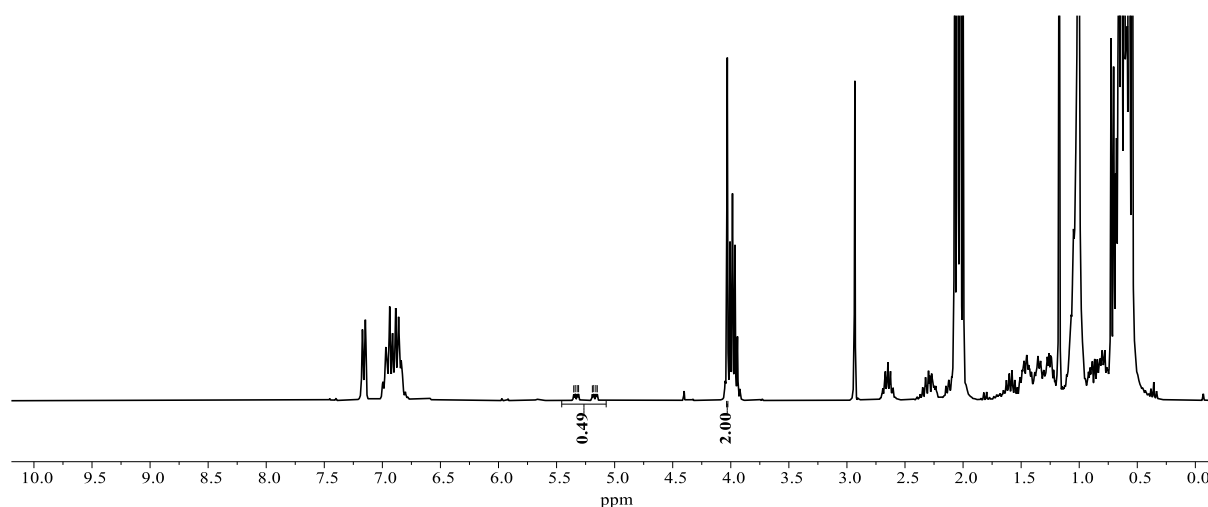


Figure 5.3-29 Crude ¹H-NMR Spectrum (300 MHz, C₆D₆) of the reaction mixture with CH₂Br₂ (36 μL, 0.50 mmol) as the internal standard (4.03 ppm). The signals of the benzylic proton and the internal standard are integrated.

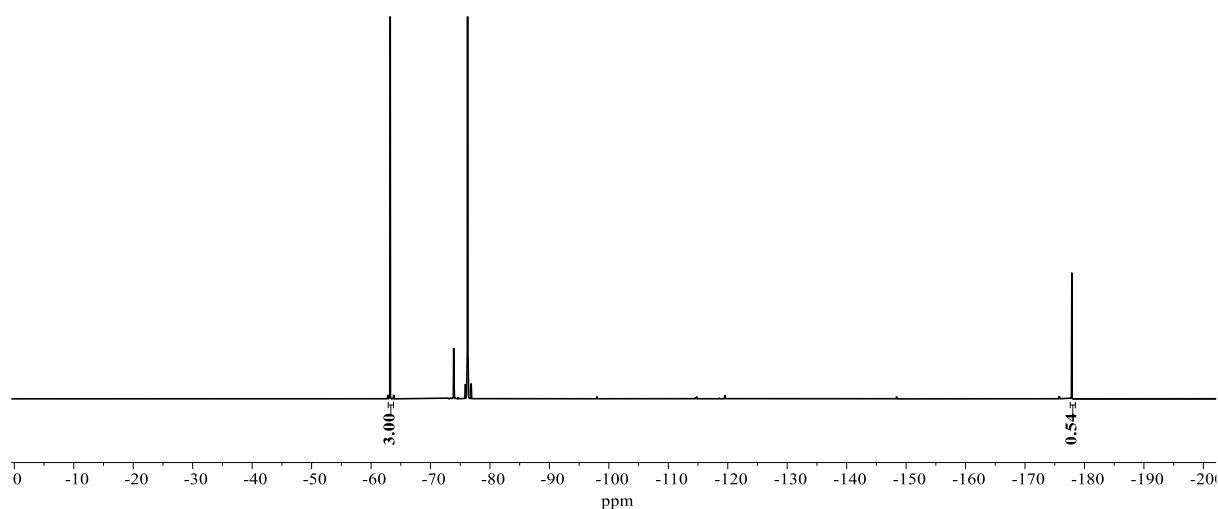
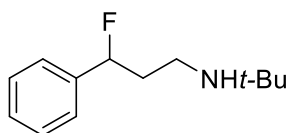


Figure 5.3-30 Crude $^{19}\text{F}\{^1\text{H}\}$ -NMR Spectrum (282 MHz, C_6D_6) of the reaction mixture with PhCF_3 (62 μL , 0.50 mmol) as the internal standard (-63.5 ppm). The signals of the benzylic fluoride and the internal standard are integrated.



***N*-(*tert*-butyl)-3-fluoro-3-phenylpropan-1-amine (60bb)**

The general procedure A was followed using *N*-(*tert*-butyl)-3-phenylpropan-1-amine **59bb** (95.9 mg, 0.50 mmol) at 0°C with 2.5 F/mol total charge. The combined organic solutions were washed the first time with sat. aq. NaHCO_3 (20 mL) instead of water. After conducting the NMR analysis, the solvents were removed in vacuo, and the residue was purified by FCC on partially neutralized silica (*n*-hexane/acetone/ NEt_3 = 30:4:1) to obtain the product **60bb** as a colorless oil (37.9 mg, 0.18 mmol, 36%).

^1H -NMR (400 MHz, CDCl_3) δ = Calibrated ^1H -NMR yield from benzylic proton: 48%.

$^{19}\text{F}\{^1\text{H}\}$ -NMR (282 MHz, CDCl_3): δ = -175.6 . Calibrated $^{19}\text{F}\{^1\text{H}\}$ -NMR yield from benzylic fluoride: 52%. $^{13}\text{C}\{^1\text{H}\}$ -NMR (101 MHz, CDCl_3): δ = 140.4 (d, $^2J_{\text{C-F}}$ = 19.7 Hz), 128.6 (CH), 128.4 (d, $^5J_{\text{C-F}}$ = 2.0 Hz, CH), 125.6 (d, $^3J_{\text{C-F}}$ = 6.9 Hz, CH), 93.5 (d, $^1J_{\text{C-F}}$ = 169.9 Hz, CH), 50.5 (C_q), 38.8 (d, $^3J_{\text{C-F}}$ = 4.0 Hz, CH_2), 38.6 (d, $^2J_{\text{C-F}}$ = 23.2 Hz, CH_2), 29.1 (CH_3). IR (ATR): $\tilde{\nu}$ = 2963, 2868, 1453, 1361, 1214, 1102, 972, 913, 758, 699, 552.

HR-MS (EI) m/z calc. for $\text{C}_{13}\text{H}_{21}\text{FN}$ $[\text{M}+\text{H}]^+$: 210.1653, found: 210.1653.

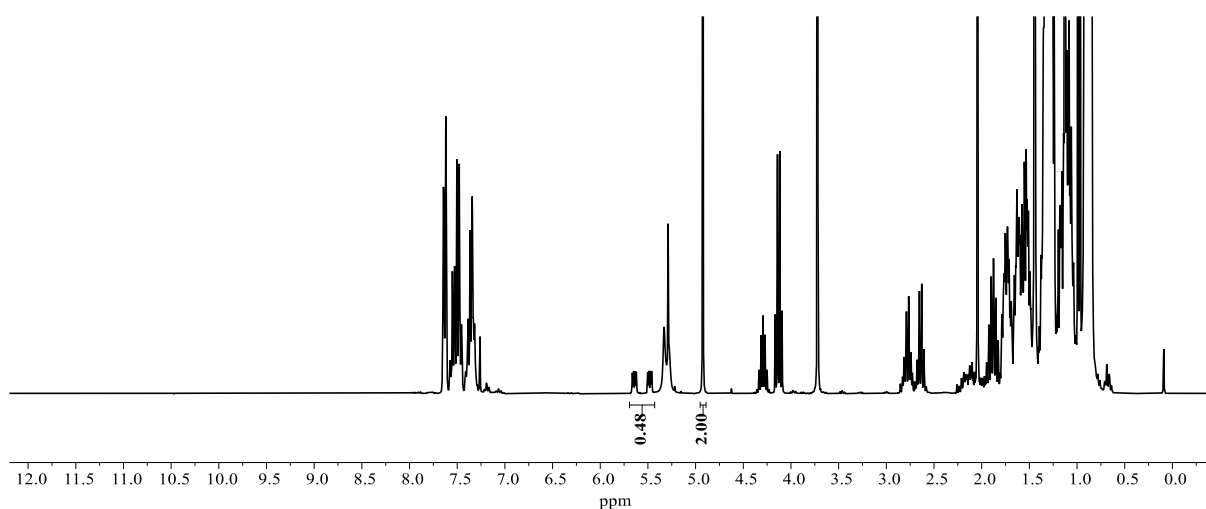


Figure 5.3-31 Crude ¹H-NMR Spectrum (300 MHz, CDCl₃) of the reaction mixture with CH₂Br₂ (36 μL, 0.50 mmol) as the internal standard (4.93 ppm). The signals of the benzylic proton and the internal standard are integrated.

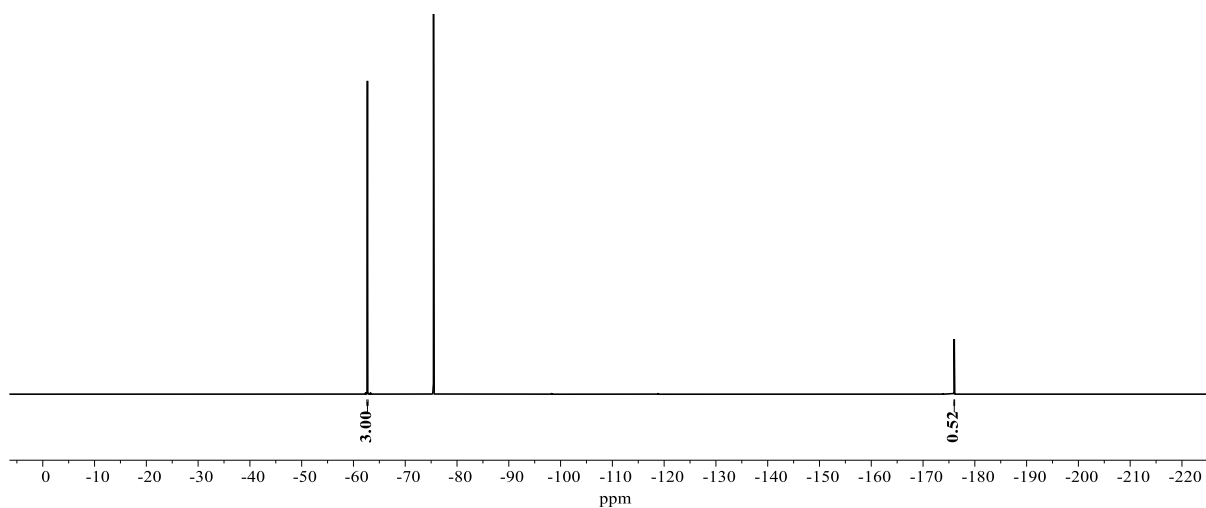
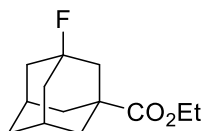


Figure 5.3-32 ¹⁹F-NMR Spectrum (282 MHz, CDCl₃) of the reaction mixture with PhCF₃ (62 μL, 0.50 mmol) as the internal standard (-62.7 ppm). The signals of the benzylic fluoride and the internal standard are integrated.



Ethyl 3-fluoroadamantane-1-carboxylate (**169**)

The general procedure A was followed using ethyl adamantane-1-carboxylate **168** (104 mg, 0.50 mmol) at -20 °C with 4.0 F/mol total charge. After conducting the NMR analysis, the solvents were removed in vacuo, and the residue was purified by FCC on partially

EXPERIMENTAL PART

neutralized silica (*n*-hexane/EtOAc = 25:1) to obtain the product **169** as a colorless oil (47.8 mg, 0.21 mmol, 42%).

¹H-NMR (300 MHz, CDCl₃): δ = 4.12 (q, *J* = 7.1 Hz, 2H), 2.39–2.29 (m, 2H), 2.02 (d, *J* = 5.8 Hz, 2H), 1.87 (dd, *J* = 5.7, 3.3 Hz, 4H), 1.83–1.73 (m, 4H), 1.60 (ddd, *J* = 3.0 Hz, 2H), 1.24 (t, *J* = 7.1 Hz, 3H). **¹⁹F{¹H}-NMR** (282 MHz, CDCl₃): δ = -132.3. Calibrated **¹⁹F{¹H}-NMR** (282 MHz, CD₂Cl₂) yield from aliphatic fluoride: 48%. **¹³C{¹H}-NMR** (101 MHz, CDCl₃): δ = 175.9 (d, ⁴*J*_{C-F} = 2.1 Hz, C_q), 92.4 (d, ¹*J*_{C-F} = 183.9 Hz, C_q), 60.6 (CH₂), 45.0 (d, ³*J*_{C-F} = 10.2 Hz, C_q), 43.8 (d, ²*J*_{C-F} = 19.9 Hz, CH₂), 42.0 (d, ²*J*_{C-F} = 17.4 Hz, CH₂), 37.7 (d, ⁴*J*_{C-F} = 2.0 Hz, CH₂), 35.0 (d, ⁴*J*_{C-F} = 2.1 Hz), 31.0 (d, ³*J*_{C-F} = 10.0 Hz, CH), 14.3 (CH₃). **IR** (ATR): $\tilde{\nu}$ = 2920, 2864, 1725, 1456, 1251, 1225, 1095, 1028, 939, 894, 548. **HR-MS** (EI) *m/z* calc. for C₁₃H₁₉FO₂ [M]⁺: 226.1369, found: 226.1364.

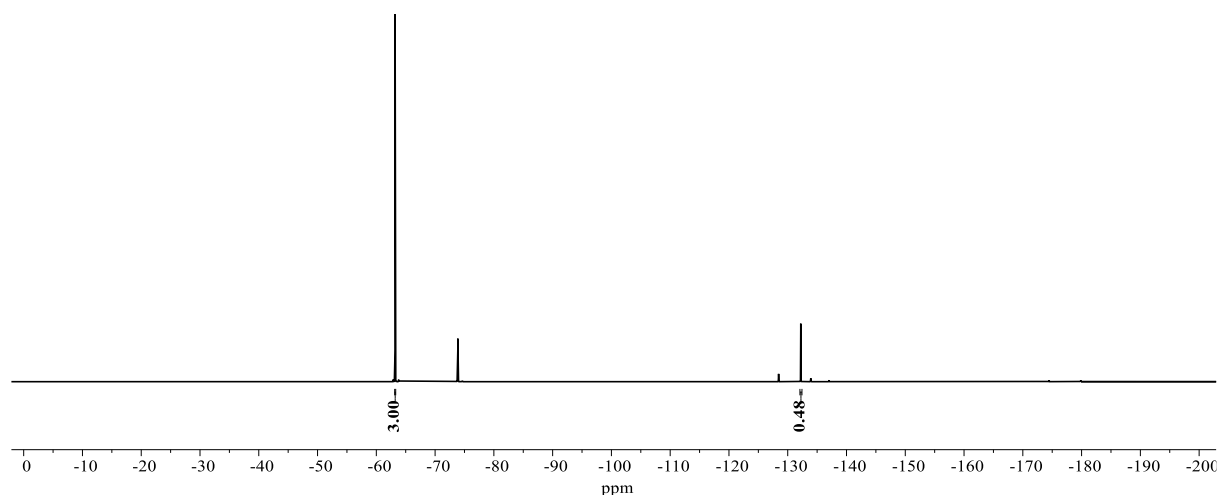
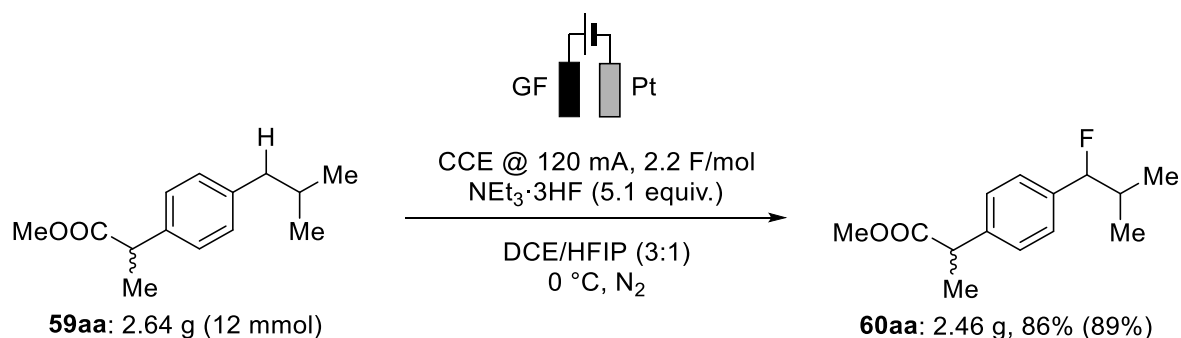


Figure 5.3-33 Crude ¹⁹F{¹H}-NMR Spectrum (282 MHz, CD₂Cl₂) of the reaction mixture with PhCF₃ (62 μL, 0.50 mmol) as the internal standard (-63.2 ppm). The signals of the benzylic fluoride and the internal standard are integrated.

5.3.2 Gram-Scale Reaction



Methyl 2-(4-(2-methylpropyl)phenyl)propanoate **59aa** (2.64 g, 12.0 mmol), DCE (24 mL), HFIP (8.0 mL) and $\text{NEt}_3 \cdot 3\text{HF}$ (8.0 mL) were placed in a 100 mL undivided cell under nitrogen atmosphere. A graphite felt (GF) anode (45 mm \times 25 mm \times 6.0 mm) and a platinum cathode (50 mm \times 25 mm \times 0.25 mm) were attached to an electrode holder which was assembled on the electrolysis cell. Electrocatalysis was performed at 0 °C with a constant current of 120 mA for 5.9 h (2.2 F/mol). After electrolysis, the platinum cathode and the graphite felt anode were washed with DCM (Pt: 1 \times 5.0 mL; C: 3 \times 15.0 mL). The solvents were combined with the reaction mixture and diluted with *n*-hexane (150 mL). The combined organic layers were washed three times with water (3 \times 75 mL) and dried over Na_2SO_4 . After adding silica gel (15 g), the mixture was filtered over celite, and the solvents were removed in vacuo. CH_2Br_2 (86 μL , 1.20 mmol) and PhCF_3 (148 μL , 1.20 mmol) were added to the residue and the mixture was submitted for NMR analyses. After conducting the crude NMR analysis, the solvents were removed in vacuo, and the residue was purified by FCC (*n*-hexane/EtOAc = 25/1), to obtain **60aa** (2.46 g, 86%) as a colorless oil.

^1H -NMR (400 MHz, CDCl_3 , mixture of diastereomers): δ = 7.34 (d, J = 8.2, 2H), 7.29 (d, J = 8.1, 2H), 5.12 (dd, J = 47.0, 6.8, 1H), 3.78 (q, J = 7.2, 1H), 3.71 (s, 3H), 2.23–2.05 (m, 1H), 1.55 (d, J = 7.2, 3H), 1.06 (d, J = 6.6, 3H), 0.90 (d, J = 6.9, 3H). Calibrated ^1H -NMR yield from benzylic proton: 89%. **$^{13}\text{C}\{^1\text{H}\}$ -NMR** (101 MHz, CDCl_3 , mixture of diastereomers): δ = 175.0 (C_q), 140.5 (d, $^5J_{\text{C-F}}$ = 1.8, C_q), 138.4 (d, $^2J_{\text{C-F}}$ = 20.6, C_q), 127.5 (CH), 126.6 (d, $^3J_{\text{C-F}}$ = 7.0, CH), 99.2 (d, $^1J_{\text{C-F}}$ = 173.5, CH), 52.2 (CH_3), 45.3 (CH), 34.4 (d, $^2J_{\text{C-F}}$ = 22.8, CH), 18.7 (CH_3) 18.5 (d, $^3J_{\text{C-F}}$ = 5.6, CH_3), 17.7 (d, $^3J_{\text{C-F}}$ = 5.2, CH_3). **$^{19}\text{F}\{^1\text{H}\}$ -NMR** (282 MHz, CDCl_3 , mixture of diastereomers) δ = -179.6, -179.6. Calibrated $^{19}\text{F}\{^1\text{H}\}$ -NMR yield from benzylic fluoride: 89%. **IR** (ATR): $\tilde{\nu}$ = 2978, 2876, 1736, 1514, 1207, 1161, 990, 840. **HR-MS** (EI) m/z calc. for $\text{C}_{14}\text{H}_{19}\text{FO}_2$ $[\text{M}]^+$: 238.1364, found: 238.1362. The spectral data are in accordance with those reported in literature. ^[5]

EXPERIMENTAL PART

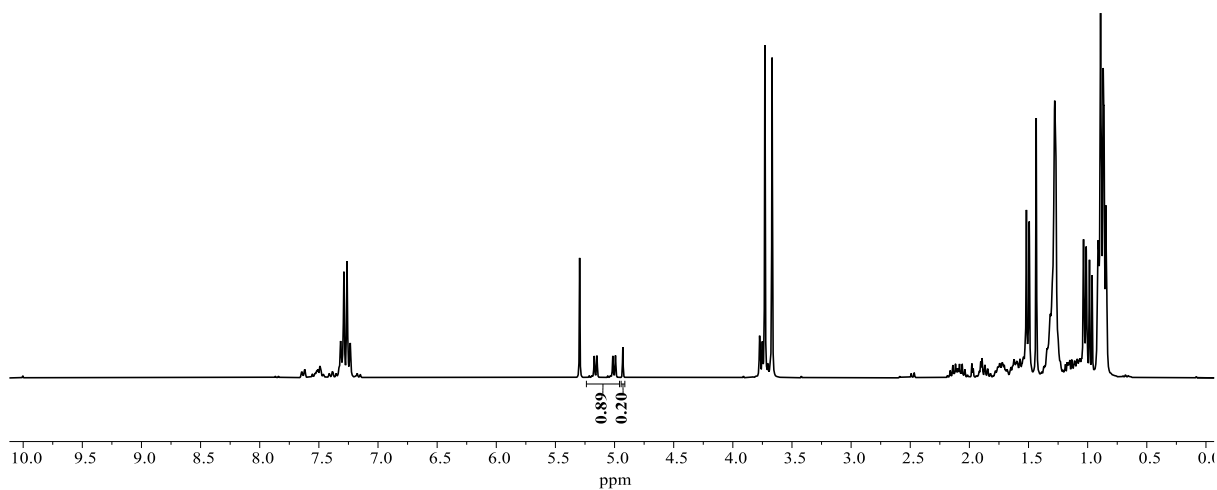


Figure 5.3-34 Crude ¹H-NMR Spectrum (300 MHz, CDCl₃) of the reaction mixture with CH₂Br₂ (86 μL, 1.20 mmol) as the internal standard (4.93 ppm).

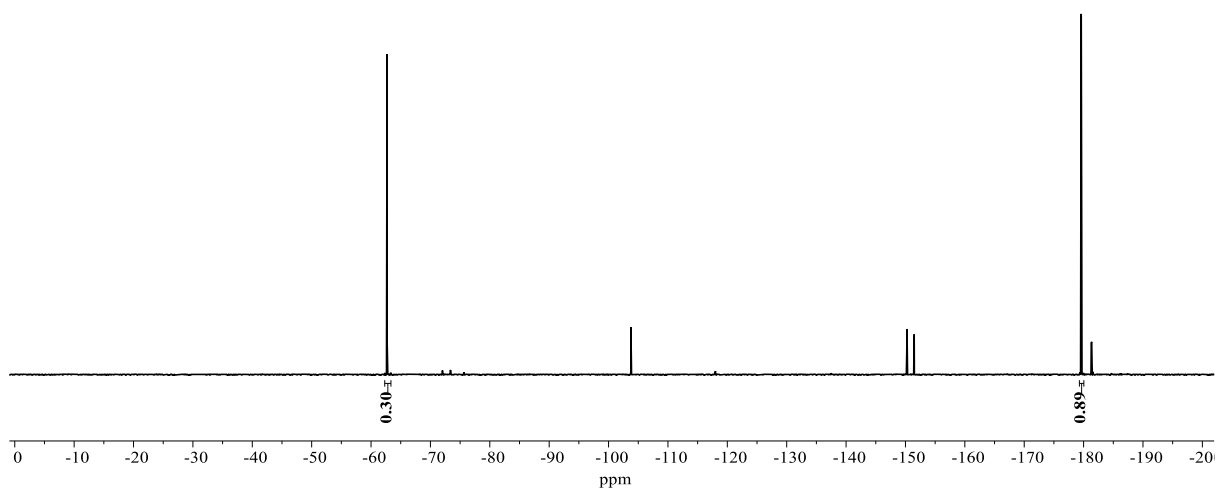
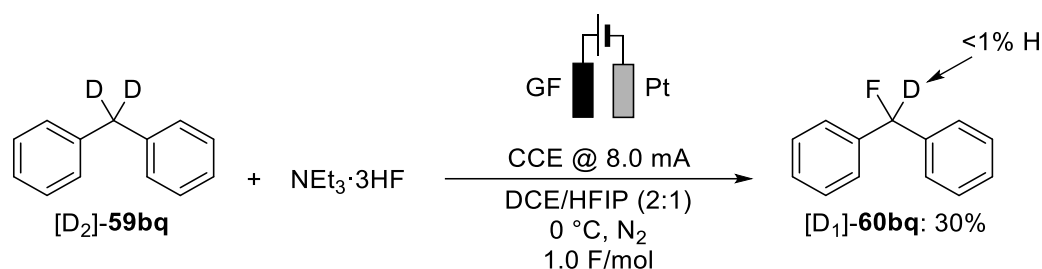


Figure 5.3-35 Crude ¹⁹F{¹H}-NMR Spectrum (282 MHz, CDCl₃) of the reaction mixture with PhCF₃ (148 μL, 1.20 mmol) as the internal standard (-62.7 ppm). The signals of the benzylic fluoride and the internal standard are integrated.

5.3.3 H/D Exchange Experiment



Diphenylmethane-*d*₂ [D₂]-59bq (85.0 mg, 0.50 mmol), DCE (2.0 mL), HFIP (1.0 mL) and NEt₃·3HF (1.0 mL) were placed in standard electrochemical cell. Electrocatalysis was performed at 0 °C with a constant current of 8.0 mA for 1.7 h (1.0 F/mol). After electrolysis, the platinum cathode and the graphite felt anode were washed with DCM (Pt: 1 × 2 mL; GF: 3 × 2 mL). The washings were combined with the reaction mixture and diluted with *n*-hexane (15 mL). The organic mixture was washed three times with water (3 × 15 mL) in a separatory funnel and dried over Na₂SO₄. After adding silica gel (2.0 g), the mixture was filtered over a pad of celite, and the solvents were removed in vacuo. CH₂Br₂ (36 μL, 0.50 mmol) and PhCF₃ (62 μL, 0.50 mmol) were added to the residue and the mixture was submitted for NMR analyses. The spectral data are in accordance with those reported in literature.^[124b]

Benzyl Fluoride C–H Shift: no benzylic proton incorporation was observed in the ¹H-NMR spectrum. **Benzyl Fluoride C–D Shift:** ²H-NMR (46 MHz, CHCl₃) δ = 6.55 (d, *J* = 7.4 Hz). Calibrated ²H-NMR yield from benzylic deuterium 30%. **Benzylic Fluoride Shift:** ¹⁹F{¹H}-NMR (282 MHz, CDCl₃) δ = -167.4 (t, *J* = 7.3 Hz). Calibrated ¹⁹F{¹H}-NMR yield from benzylic fluoride 32%. **HR-MS (EI)** *m/z* calc. for C₁₃H₁₀DF [M]⁺: 187.0908, found: 187.0902.

EXPERIMENTAL PART

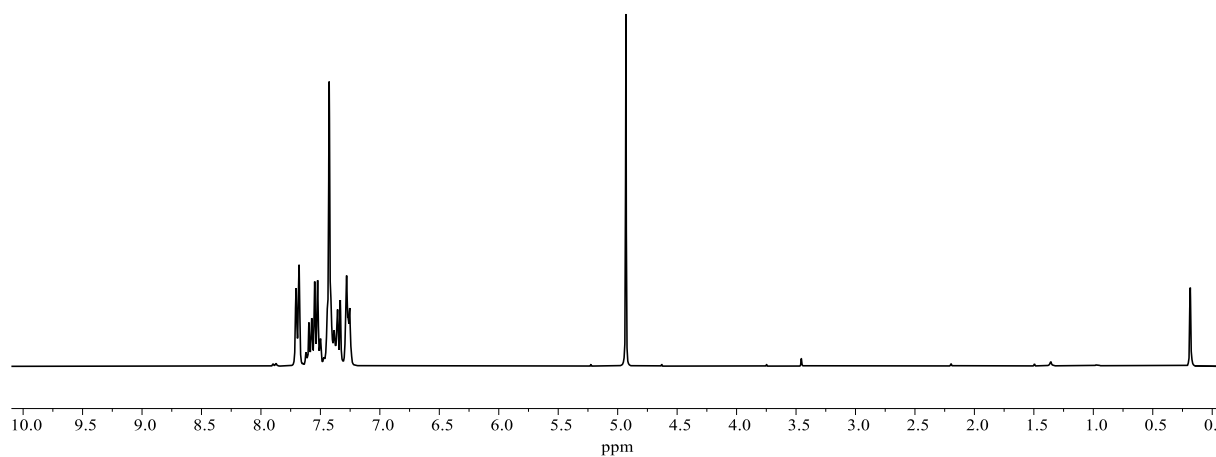


Figure 5.3-36 Crude ¹H-NMR Spectrum (300 MHz, CDCl₃) of the reaction mixture with CH₂Br₂ (36 μL, 0.50 mmol) as the internal standard (4.93 ppm).

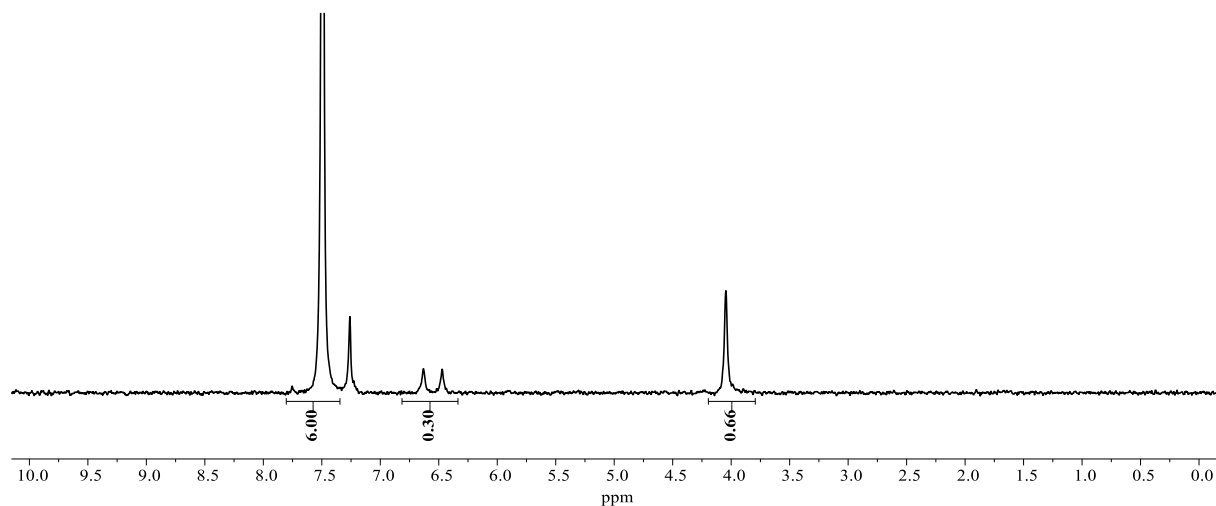


Figure 5.3-37 Crude ²H-NMR Spectrum (46 MHz, CHCl₃) of the reaction mixture with C₆D₆ (46 μL, 0.50 mmol) as the internal standard (7.49 ppm) and trace amounts of CDCl₃ (7.26 ppm). The signals of the benzylic deuterium of product and starting material and the internal standard are integrated.

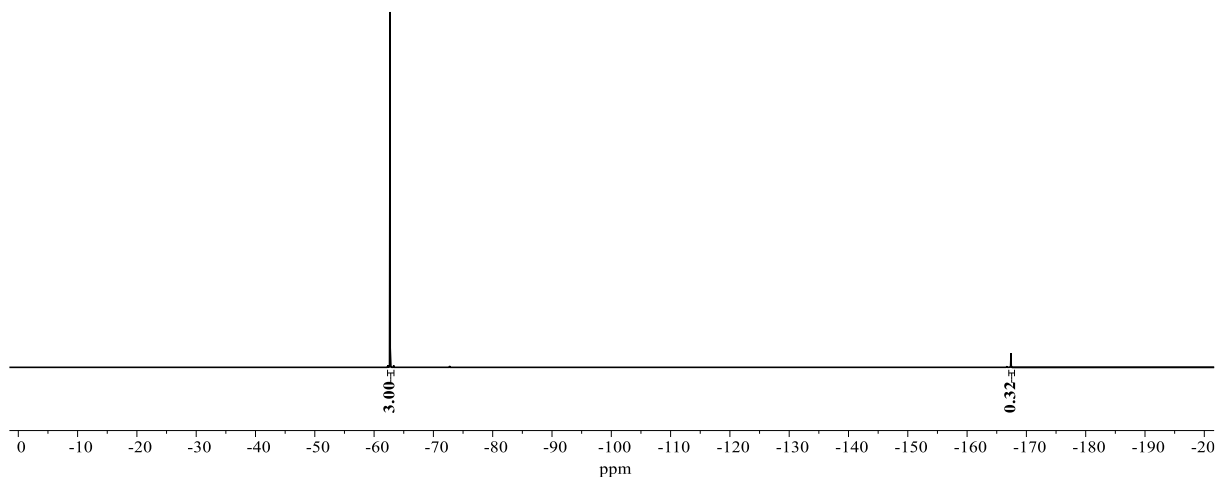
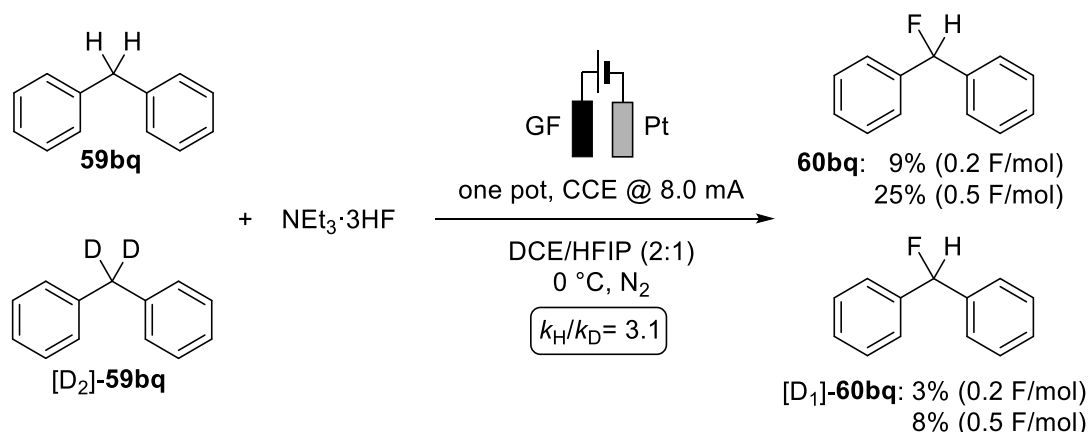


Figure 5.3-38 Crude $^{19}\text{F}\{^1\text{H}\}$ -NMR Spectrum (282 MHz, CDCl_3) of the reaction mixture with PhCF_3 (62 μL , 0.50 mmol) as the internal standard (-62.7 ppm). The signals of the benzylic fluoride and the internal standard are integrated.

5.3.4 Kinetic Isotope Effect Studies



The experiment was performed twice, with different reaction times. Diphenylmethane **59bq** (84.0 mg, 0.50 mmol) and diphenylmethane- d_2 $[\text{D}_2]\text{-59bq}$ (85.0 mg, 0.50 mmol), DCE (2.0 mL), HFIP (1.0 mL) and $\text{NEt}_3 \cdot 3\text{HF}$ (1.0 mL) were placed in a standard electrochemical cell. Electrocatalysis was performed at 0 °C with a constant current of 8.0 mA for 0.67 h (0.2 F/mol) and 1.67 h (0.5 F/mol), respectively. After electrolysis of each batch, the platinum cathode and the graphite felt anode were washed with DCM (Pt: 1 \times 5 mL; C: 3 \times 10.0 mL). The solvents were combined with the reaction mixture and diluted with *n*-hexane (25 mL). The organic layers were washed three times with water (3 \times 15 mL) in a separatory funnel and dried over Na_2SO_4 . After adding silica gel (2.0 g), the mixture was filtered over celite, and the solvents were removed in vacuo. CH_2Br_2 (36 μL ,

EXPERIMENTAL PART

0.50 mmol) and PhCF_3 (62 μL , 0.50 mmol) and C_6D_6 (46 μL , 0.50 mmol) were added to the residue and the mixture was submitted for NMR analyses.

Benzyl Fluoride C–H Shift: ^1H -NMR (300 MHz, CHCl_3) $\delta = 6.52$ (d, $J = 47.4$ Hz). Calibrated ^1H -NMR yield of **60bq** from benzylic proton: 9% (0.2 F/mol); 25% (0.5 F/mol).

Benzyl Fluoride C–D Shift: ^2H -NMR (46 MHz, CHCl_3) $\delta = 6.55$ (d, $J = 7.4$ Hz). Calibrated ^2H -NMR yield of $[\text{D}_1]$ -**60bq** from benzylic deuterium 3% (0.2 F/mol); 8% (0.5 F/mol): **Benzylic Fluoride Shift:** $^{19}\text{F}\{^1\text{H}\}$ -NMR (282 MHz, CDCl_3) $\delta = -166.7$ (s), -167.4 (t, $J = 7.3$ Hz). Calibrated $^{19}\text{F}\{^1\text{H}\}$ -NMR yields from benzylic fluorides: 9% for **60bq**, 3% for $[\text{D}_1]$ -**60bq** (0.2 F/mol); 26% for **60bq**, 8% for $[\text{D}_1]$ -**60bq** (0.5 F/mol). The spectral data are in accordance with those reported in literature.^[124b]

Accordingly, a KIE value of $k_{\text{H}}/k_{\text{D}} \approx 3.1$ was determined by the spectroscopic analyses.

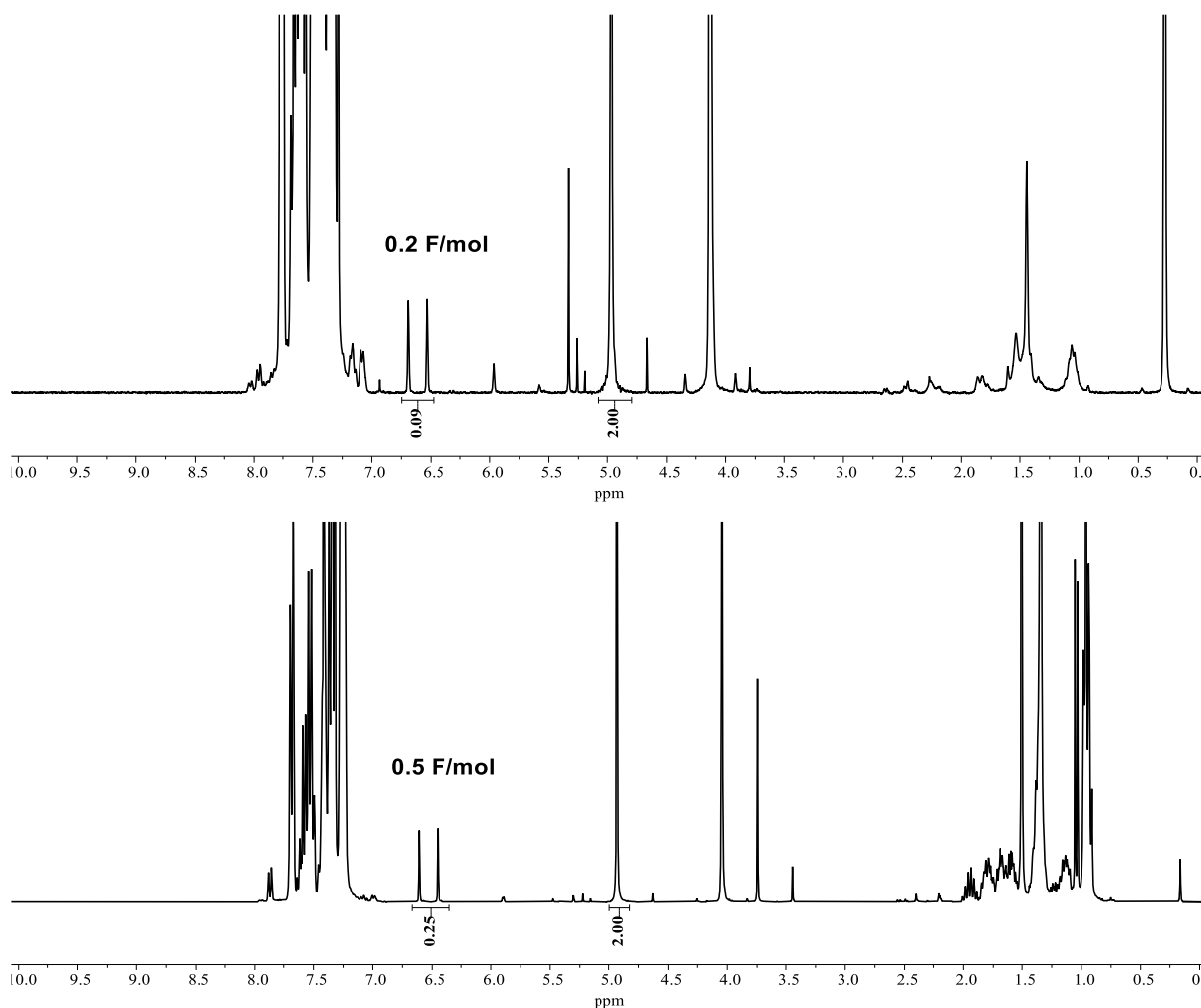


Figure 5.3-39 Crude ^1H -NMR Spectra (300 MHz, CDCl_3) of the reaction mixtures with CH_2Br_2 (36 μL , 0.50 mmol) as the internal standard (4.93 ppm). The signals of the benzylic deuterium of product and the internal standard are integrated.

EXPERIMENTAL PART

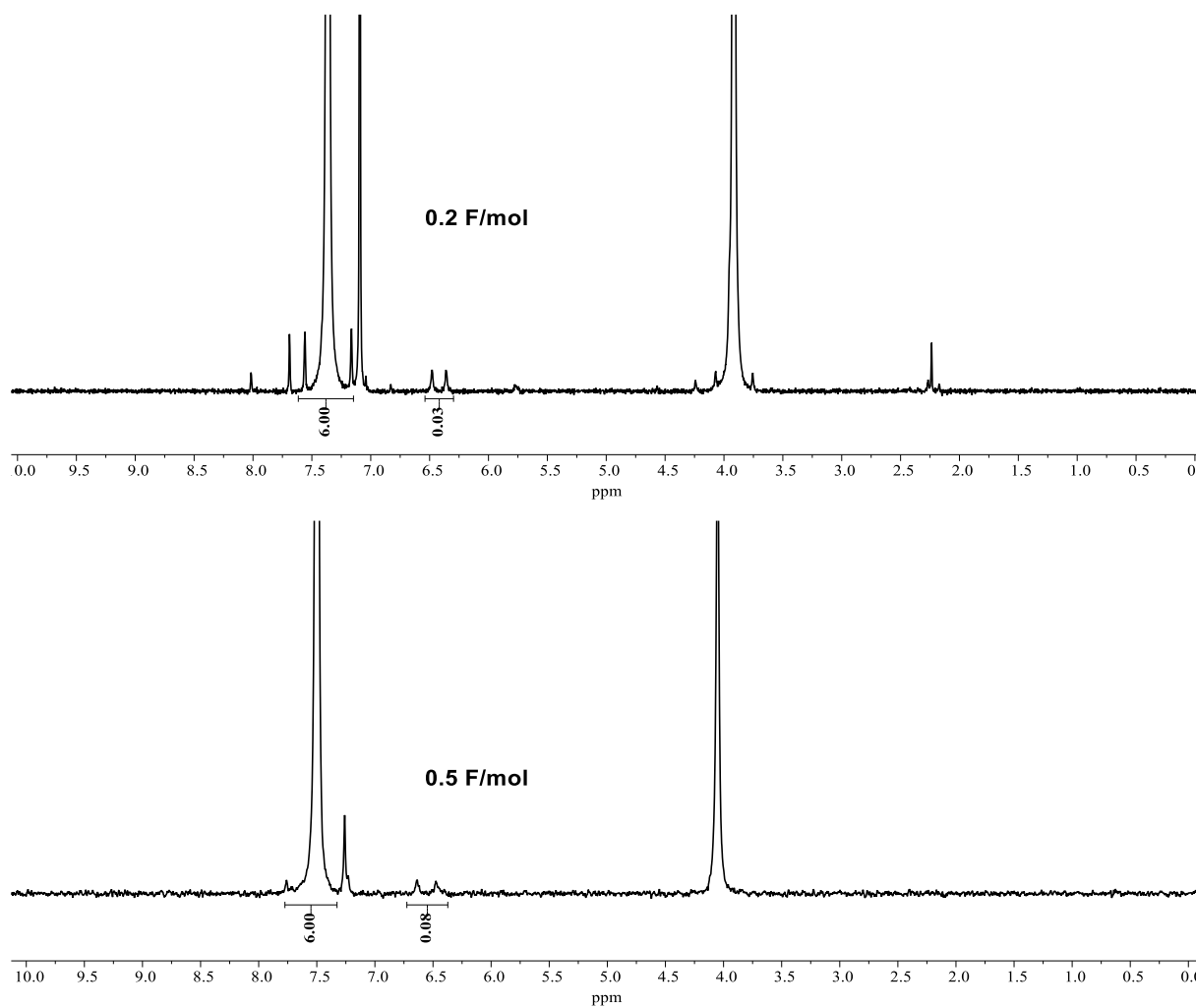


Figure 5.3-40 Crude ^2H -NMR Spectra (46 MHz, CHCl_3) of the reaction mixtures with C_6D_6 (46 μL , 0.50 mmol) as the internal standard (7.49 ppm) and trace amounts of CDCl_3 (7.26 ppm). The signals of the benzylic deuterium of product and the internal standard are integrated.

EXPERIMENTAL PART

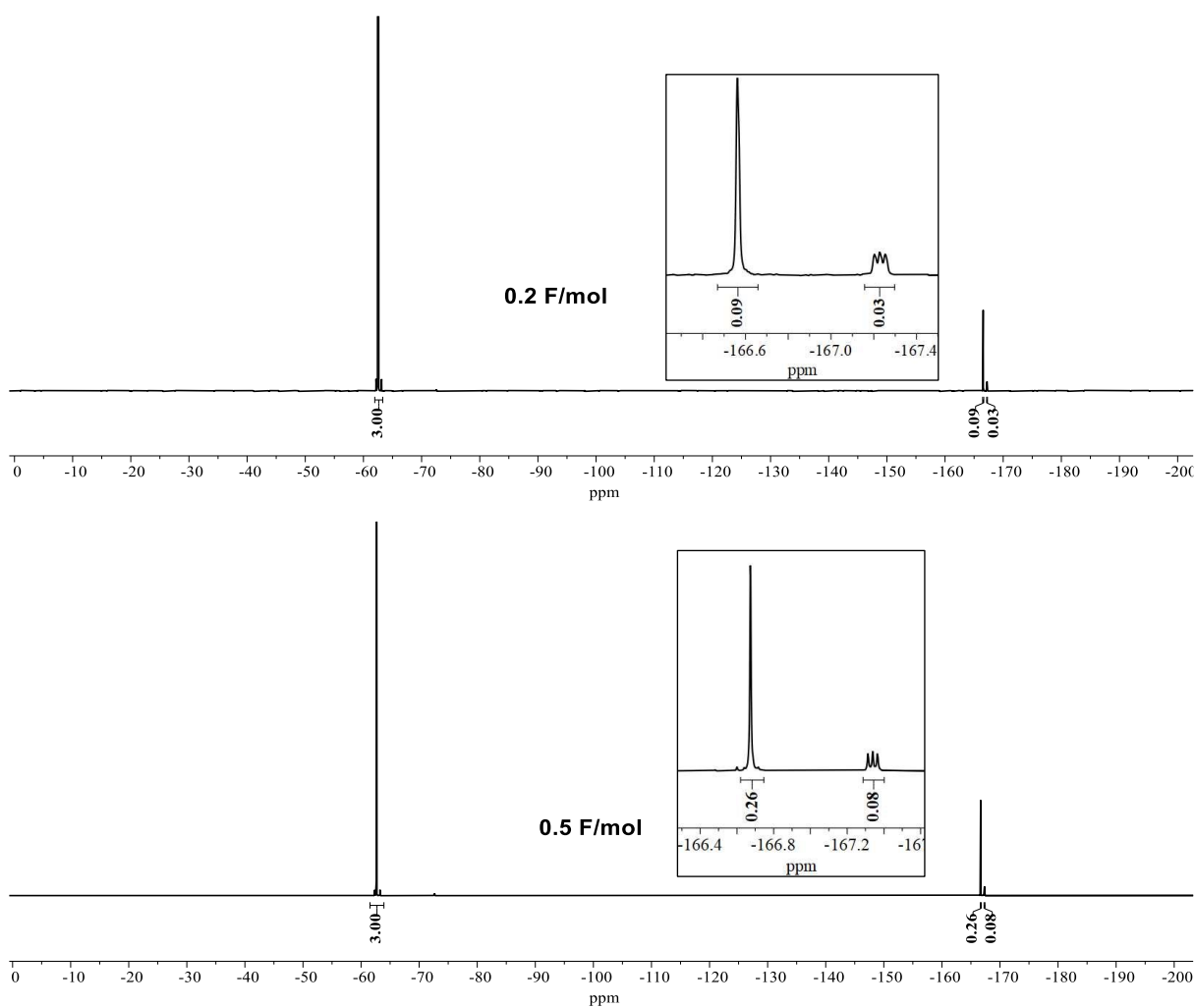
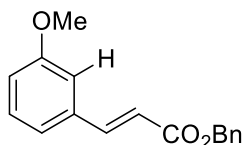


Figure 5.3-41 Crude $^{19}\text{F}\{^1\text{H}\}$ -NMR Spectra (282 MHz, CDCl_3) of the reaction mixtures with PhCF_3 (62 μL , 0.50 mmol) as the internal standard (-62.7 ppm). The signals of the benzylic fluoride and the internal standard are integrated.

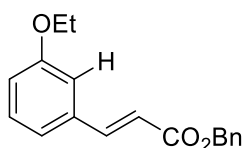
5.4 Ruthena-Electro-Catalyzed Decarboxylative Alkenylation

5.4.1 Characterization Data



Benzyl (*E*)-3-(3-methoxyphenyl)acrylate (**31aa**)

The general procedure B was followed using benzyl acrylate **11a** (65.0 mg, 0.40 mmol) and 2-methoxybenzoic acid **30a** (183.0 mg, 1.20 mmol). Isolation by FCC (*n*-hexane/EtOAc = 20:1→10:1) yielded **31aa** as a colorless oil (64.4 mg, 0.24 mmol, 60%). **¹H-NMR** (400 MHz, CDCl₃): δ = 7.70 (d, J = 16.0 Hz, 1H), 7.52–7.26 (m, 6H), 7.12 (d, J = 7.6 Hz, 1H), 7.04 (br, 1H), 6.94 (dd, J = 8.3, 2.6 Hz, 1H), 6.48 (d, J = 16.0 Hz, 1H), 5.26 (s, 2H), 3.83 (s, 3H). **¹³C{¹H}-NMR** (101 MHz, CDCl₃): δ = 166.9 (C_q), 160.0 (C_q), 145.2 (CH), 136.2 (C_q), 135.8 (C_q), 130.0 (CH), 128.7 (CH), 128.4 (CH), 128.4 (CH), 121.0 (CH), 118.3 (CH), 116.4 (CH), 113.0 (CH), 66.5 (CH₂), 55.4 (CH₃). **IR** (ATR): $\tilde{\nu}$ = 3038, 2950, 2837, 1708, 1636, 1580, 1248, 1155, 980, 736, 698, 679 cm⁻¹. **MS** (ESI): m/z (relative intensity) = 559.2 (66) [2M+Na]⁺, 291.1 (100) [M+Na]⁺. **HR-MS** (ESI): m/z calc. for C₁₇H₁₆O₃Na [M+Na]⁺: 291.0997; found: 291.0997. The analytical data are in accordance with those previously reported in literature.^[66c]

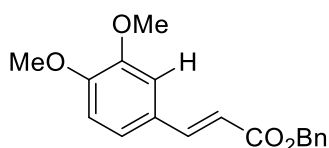


Benzyl (*E*)-3-(3-ethoxyphenyl)acrylate (**31ab**)

The general procedure B was followed using benzyl acrylate **11a** (65.1 mg, 0.40 mmol) and 2-ethoxybenzoic acid **30b** (200.3 mg, 1.20 mmol). Isolation by FCC (*n*-hexane/EtOAc = 24:1→10:1) yielded **31ab** as a colorless oil (49.9 mg, 0.17 mmol, 44%).

¹H-NMR (400 MHz, CDCl₃): δ = 7.69 (d, J = 16.0 Hz, 1H), 7.46–7.27 (m, 6H), 7.10 (d, J = 7.6 Hz, 1H), 7.03 (br, 1H), 6.92 (dd, J = 8.3, 2.5 Hz, 1H), 6.47 (d, J = 16.0 Hz, 1H), 5.25 (s, 2H), 4.05 (q, J = 7.0 Hz, 2H), 1.42 (t, J = 7.0 Hz, 3H). **¹³C{¹H}-NMR** (101 MHz,

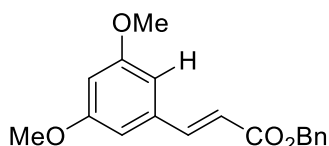
CDCl₃): δ = 166.9 (C_q), 159.4 (C_q), 145.3 (CH), 136.2 (C_q), 135.8 (C_q), 130.0 (CH), 128.7 (CH), 128.4 (CH), 128.4 (CH), 120.8 (CH), 118.2 (CH), 117.0 (CH), 113.6 (CH), 66.5 (CH₂), 63.7 (CH₂), 14.9 (CH₃). **IR** (ATR): $\tilde{\nu}$ = 3035, 2981, 2934, 1709, 1636, 1579, 1228, 1156, 1049, 980, 698, 679 cm⁻¹. **MS** (ESI): m/z (relative intensity) = 587.3 (82) [2M+Na]⁺, 305.1 (100) [M+Na]⁺. **HR-MS** (ESI): m/z calc. for C₁₈H₁₈O₃Na [M+Na]⁺: 305.1154; found: 305.1152. The analytical data are in accordance with those previously reported in literature.^[66c]



Benzyl (*E*)-3-(3,4-dimethoxyphenyl)acrylate (**31ac**)

The general procedure B was followed using benzyl acrylate **11a** (65.1 mg, 0.40 mmol) and 2,3-dimethoxybenzoic acid **30c** (218.0 mg, 1.20 mmol). Isolation by FCC (*n*-hexane/EtOAc = 12:1→6:1) yielded **31ac** as a colorless oil (41.7 mg, 0.14 mmol, 35%).

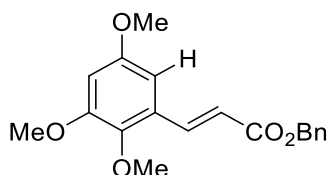
¹H-NMR (400 MHz, CDCl₃): δ = 7.67 (d, J = 15.9 Hz, 1H), 7.46–7.28 (m, 5H), 7.10 (dd, J = 8.3, 2.0 Hz, 1H), 7.05 (d, J = 2.0 Hz, 1H), 6.86 (d, J = 8.2 Hz, 1H), 6.36 (d, J = 16.0 Hz, 1H), 5.25 (s, 2H), 3.91 (s, 3H), 3.90 (s, 3H). **¹³C{¹H}-NMR** (101 MHz, CDCl₃): δ = 167.2 (C_q), 151.3 (C_q), 149.3 (C_q), 145.2 (CH), 136.3 (C_q), 128.7 (CH), 128.4 (CH), 128.4 (CH), 127.5 (C_q), 122.8 (CH), 115.7 (CH), 111.1 (CH), 109.7 (CH), 66.4 (CH₂), 56.1 (CH₃), 56.0 (CH₃). **IR** (ATR): $\tilde{\nu}$ = 2936, 2838, 1705, 1632, 1510, 1250, 1137, 1022, 805, 740, 698 cm⁻¹. **MS** (ESI): m/z (relative intensity) = 619.2 (64) [2M+Na]⁺, 321.1 (100) [M+Na]⁺. **HR-MS** (ESI): m/z calc. for C₁₈H₁₈O₄Na [M+Na]⁺: 321.1103; found: 321.1100. The analytical data are in accordance with those previously reported in literature.^[66c]



Benzyl (*E*)-3-(3,5-dimethoxyphenyl)acrylate (**31ad**)

The general procedure B was followed using benzyl acrylate **11a** (64.9 mg, 0.40 mmol) and 2,4-dimethoxybenzoic acid **30d** (217.0 mg, 1.20 mmol). Isolation by FCC (*n*-hexane/EtOAc = 12:1→6:1) yielded **31d** as a colorless oil (81.3 mg, 0.27 mmol, 68%).

¹H-NMR (400 MHz, CDCl₃): δ = 7.65 (d, J = 15.9 Hz, 1H), 7.47–7.30 (m, 5H), 6.66 (d, J = 2.2 Hz, 2H), 6.49 (dd, J = 2.4, 2.4 Hz, 1H), 6.46 (d, J = 16.0 Hz, 1H), 5.25 (s, 2H), 3.80 (s, 6H). **¹³C{¹H}-NMR** (101 MHz, CDCl₃): δ = 166.8 (C_q), 161.1 (2 C_q), 145.3 (CH), 136.4 (C_q), 136.1 (C_q), 128.7 (CH), 128.4 (CH), 128.4 (CH), 118.5 (CH), 106.1 (CH), 102.8 (CH), 66.6 (CH₂), 55.6 (CH₃). **IR** (ATR): $\tilde{\nu}$ = 2940, 2840, 1709, 1590, 1457, 1278, 1152, 1062, 977, 836, 733, 699 cm⁻¹. **MS** (ESI): m/z (relative intensity) = 619.2 (92) [2M+Na]⁺, 321.1 (100) [M+Na]⁺. **HR-MS** (ESI): m/z calc. for C₁₈H₁₈O₄Na [M+Na]⁺: 321.1103; found: 321.1097. The analytical data are in accordance with those previously reported in literature.^[66c]

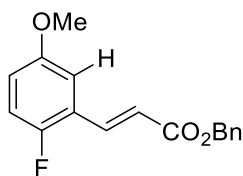


Benzyl (*E*)-3-(2,3,5-trimethoxyphenyl)acrylate (**31ae**)

The general procedure B was followed using benzyl acrylate **11a** (65.0 mg, 0.40 mmol) and 2,4,5-trimethoxybenzoic acid **30e** (255.0 mg, 1.20 mmol). Isolation by FCC (*n*-hexane/EtOAc = 10:1→5:1) yielded **31ae** as a colorless oil (80.1 mg, 0.27 mmol, 61%).

¹H-NMR (400 MHz, CDCl₃): δ = 8.04 (d, J = 16.2 Hz, 1H), 7.48–7.29 (m, 5H), 6.59 (d, J = 2.9 Hz, 1H), 6.54 (d, J = 2.9 Hz, 1H), 6.51 (d, J = 16.3 Hz, 1H), 5.26 (s, 2H), 3.85 (s, 3H), 3.80 (s, 3H), 3.79 (s, 3H). **¹³C{¹H}-NMR** (101 MHz, CDCl₃): δ = 167.0 (C_q), 156.2 (C_q), 154.0 (C_q), 143.1 (C_q), 140.1 (CH), 136.2 (C_q), 128.7 (CH), 128.4 (CH), 128.3 (CH), 128.3 (C_q), 119.2 (CH), 102.8 (CH), 100.9 (CH), 66.4 (CH₂), 61.7 (CH₃), 56.0 (CH₃), 55.7 (CH₃). **IR** (ATR): $\tilde{\nu}$ = 2935, 2841, 1712, 1484, 1278, 1156, 1057, 1000, 737, 699 cm⁻¹. **MS** (ESI): m/z (relative intensity) = 679.2 (100) [2M+Na]⁺, 351.1 (92) [M+Na]⁺. **HR-MS**

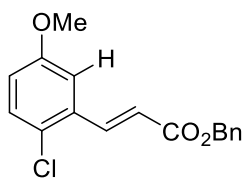
(ESI): m/z calc. for $C_{19}H_{20}O_5Na$ $[M+Na]^+$: 351.1208; found: 351.1206. The analytical data are in accordance with those previously reported in literature.^[66c]



Benzyl (*E*)-3-(2-fluoro-5-methoxyphenyl)acrylate (**31af**)

The general procedure B was followed using benzyl acrylate **11a** (65.2 mg, 0.40 mmol) and 5-fluoro-2-methoxybenzoic acid **30f** (204.9 mg, 1.20 mmol). Isolation by FCC (*n*-hexane/EtOAc = 24:1→12:1) yielded **31af** as a colorless oil (74.5 mg, 0.26 mmol, 65%).

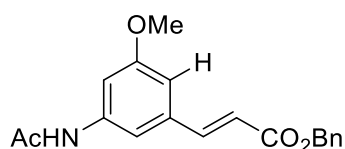
¹H-NMR (300 MHz, CDCl₃): δ = 7.82 (d, J = 16.2 Hz, 1H), 7.46–7.31 (m, 5H), 7.07–6.96 (m, 2H), 6.88 (ddd, J = 9.0, 4.1, 3.1 Hz, 1H), 6.56 (d, J = 16.2 Hz, 1H), 5.26 (s, 2H), 3.80 (s, 3H). **¹³C{¹H}-NMR** (101 MHz, CDCl₃): δ = 166.7 (C_q), 156.1 (d, $^1J_{C-F}$ = 247 Hz, C_q), 155.9 (d, $^4J_{C-F}$ = 2.1 Hz, C_q), 138.0 (d, $^3J_{C-F}$ = 2.6 Hz, CH), 136.1 (C_q), 128.8 (CH), 128.5 (CH), 128.4 (CH), 122.8 (d, $^2J_{C-F}$ = 13.3 Hz, C_q), 120.6 (d, $^3J_{C-F}$ = 6.5 Hz, CH), 117.7 (d, $^3J_{C-F}$ = 8.5 Hz, CH), 117.0 (d, $^2J_{C-F}$ = 24.0 Hz, CH), 112.8 (d, $^4J_{C-F}$ = 2.9 Hz, CH), 66.6 (CH₂), 55.9 (CH₃). **¹⁹F{¹H}-NMR** (282 MHz, CDCl₃): δ = -124.84. **IR** (ATR): $\tilde{\nu}$ = 2955, 2838, 1712, 1638, 1495, 1248, 1210, 1160, 980, 745, 695 cm⁻¹. **MS** (ESI): m/z (relative intensity) = 595.2 (69) $[2M+Na]^+$, 309.1 (100) $[M+Na]^+$. **HR-MS** (ESI): m/z calc. for $C_{17}H_{15}O_3FNa$ $[M+Na]^+$: 309.0903; found: 309.0900.



Benzyl (*E*)-3-(2-chloro-5-methoxyphenyl)acrylate (**31ag**)

The general procedure B was followed using benzyl acrylate **11a** (65.2 mg, 0.40 mmol) and 5-chloro-2-methoxybenzoic acid **30g** (204.9 mg, 1.20 mmol). Isolation by FCC (*n*-hexane/EtOAc = 20:1→10:1) yielded **31aa** as a colorless oil (58.5 mg, 0.19 mmol, 48%).

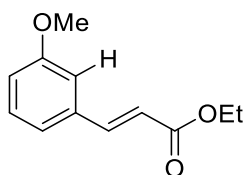
¹H-NMR (300 MHz, CDCl₃): δ = 8.10 (d, J = 16.2 Hz, 1H), 7.45–7.34 (m, 5H), 7.31 (d, J = 8.8 Hz, 1H), 7.10 (d, J = 3.0 Hz, 1H), 6.88 (dd, J = 8.8, 3.0 Hz, 1H), 6.46 (d, J = 16.0 Hz, 1H), 5.27 (s, 2H), 3.81 (s, 3H). **¹³C{¹H}-NMR** (75 MHz, CDCl₃): δ = 166.4 (C_q), 158.5 (C_q), 141.2 (CH), 136.1 (C_q), 133.4 (C_q), 131.0 (CH), 128.8 (CH), 128.5 (2 CH), 126.8 (C_q), 120.7 (CH), 117.7 (CH), 112.2 (CH), 66.7 (CH₂), 55.7 (CH₃). **IR** (ATR): $\tilde{\nu}$ = 2940, 2837, 1712, 1470, 1270, 1228, 1160, 1026, 978, 740, 698, 638 cm⁻¹. **MS** (ESI): m/z (relative intensity) = 627.2 (60) [2M+Na]⁺, 325.1 (100) [M+Na]⁺. **HR-MS** (ESI): m/z calc. for C₁₇H₁₅O₃ClNa [M+Na]⁺: 325.0607; found: 325.0607. The analytical data are in accordance with those previously reported in literature.^[66c]



Benzyl (*E*)-3-(3-acetamido-5-methoxyphenyl)acrylate (**31ah**)

The general procedure B was followed using benzyl acrylate **11a** (65.0 mg, 0.40 mmol) and 4-acetamido-2-methoxybenzoic acid **30h** (204.9 mg, 1.20 mmol). Isolation by FCC (1st run: *n*-hexane/EtOAc = 1:1→1:2; 2nd run: DCM/EtOAc = 5:1→1:3) yielded **31ah** as an off-white solid (69.0 mg, 0.21 mmol, 55%).

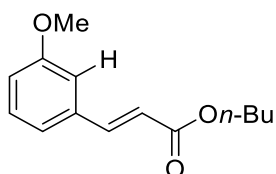
M.p.: 125–127 °C. **¹H-NMR** (400 MHz, CDCl₃): δ = 7.63 (d, J = 15.9 Hz, 1H), 7.45–7.31 (m, 6H), 7.29 (s, 1H), 7.16 (s, 1H), 6.79 (s, 1H), 6.45 (d, J = 15.9 Hz, 1H), 5.25 (s, 2H), 3.81 (s, 3H), 2.17 (s, 3H). **¹³C{¹H}-NMR** (101 MHz, CDCl₃): δ = 168.5 (C_q), 166.8 (C_q), 160.6 (C_q), 144.8 (CH), 139.6 (C_q), 136.1 (C_q), 128.8 (CH), 128.4 (CH), 128.4 (CH), 118.9 (CH), 112.0 (CH), 109.2 (CH), 107.7 (CH), 66.6 (CH₂), 55.6 (CH₃), 24.9 (CH₃). **IR** (ATR): $\tilde{\nu}$ = 3273, 3160, 3104, 3035, 2943, 1717, 1594, 1564, 1448, 1416, 1275, 1156, 969, 839, 744, 695, 521 cm⁻¹. **MS** (ESI): m/z (relative intensity) = 998.4 (55) [3M+Na]⁺, 673.3 (84) [2M+Na]⁺, 550.2 (86) [3M+2Na]⁺, 348.1 (100) [M+Na]⁺. **HR-MS** (ESI): m/z calc. for C₁₉H₁₉NO₄Na [M+Na]⁺: 348.1209; found: 348.1209.



Ethyl (*E*)-3-(3-methoxyphenyl)acrylate (**31ba**)

The general procedure B was followed using ethyl acrylate **11b** (40.4 mg, 0.40 mmol) and 2-methoxybenzoic acid **30a** (181.8 mg, 1.20 mmol). Isolation by FCC (*n*-hexane/EtOAc = 12:1→6:1) yielded **31ba** as a colorless oil (31.7 mg, 0.15 mmol, 38%).

¹H-NMR (400 MHz, CDCl₃): δ = 7.65 (d, *J* = 16.0 Hz, 1H), 7.30 (dd, *J* = 8.2, 7.6 Hz, 1H), 7.12 (d, *J* = 7.6 Hz, 1H), 7.04 (s, 1H), 6.93 (d, *J* = 8.2 Hz, 1H), 6.42 (d, *J* = 16.0 Hz, 1H), 4.27 (q, *J* = 7.1 Hz, 1H), 3.83 (s, 1H), 1.34 (t, *J* = 7.1 Hz, 1H). **¹³C{¹H}-NMR** (101 MHz, CDCl₃): δ = 167.1 (C_q), 160.0 (C_q), 144.6 (CH), 136.0 (C_q), 130.0 (CH), 120.9 (CH), 118.7 (CH), 116.3 (CH), 113.0 (CH), 60.7 (CH₃), 55.4 (CH₂), 14.5 (CH₃). **IR** (ATR): $\tilde{\nu}$ = 2982, 2940, 1709, 1639, 1586, 1250, 1164, 1037, 982, 855, 784, 680 cm⁻¹. **MS** (ESI): *m/z* (relative intensity) = 435.2 (83) [2M+Na]⁺, 229.1 (100) [M+Na]⁺. **HR-MS** (ESI): *m/z* calc. for C₁₂H₁₄O₃Na [M+Na]⁺: 229.0841; found: 229.0838. The analytical data are in accordance with those previously reported in literature.^[66c]

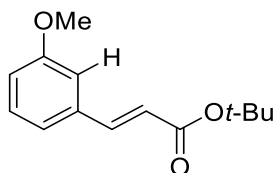


Butyl (*E*)-3-(3-methoxyphenyl)acrylate (**31ca**)

The general procedure B was followed using *n*-butyl acrylate **11c** (51.5 mg, 0.40 mmol) and 2-methoxybenzoic acid **30a** (182.0 mg, 1.20 mmol). Isolation by FCC (*n*-hexane/EtOAc = 15:1→7:1) yielded **31ca** as a colorless oil (41.3 mg, 0.18 mmol, 44%).

¹H-NMR (400 MHz, CDCl₃): δ = 7.65 (d, *J* = 16.0 Hz, 1H), 7.30 (dd, *J* = 7.9, 7.9 Hz, 1H), 7.12 (d, *J* = 7.7 Hz, 1H), 7.04 (dd, *J* = 2.0, 1.7 Hz, 1H), 6.93 (dd, *J* = 8.2, 2.3 Hz, 1H), 6.43 (d, *J* = 16.0 Hz, 1H), 4.21 (t, *J* = 6.7 Hz, 2H), 3.83 (s, 3H), 1.80–1.65 (m, 2H), 1.52–1.39 (m, 2H), 0.97 (t, *J* = 7.4 Hz, 3H). **¹³C{¹H}-NMR** (101 MHz, CDCl₃): δ = 167.2 (C_q), 160.0 (C_q), 144.6 (CH), 136.0 (C_q), 130.0 (CH), 120.9 (CH), 118.7 (CH), 116.3 (CH), 113.0 (CH), 64.6 (CH₂), 55.4 (CH₃), 30.9 (CH₂), 19.3 (CH₂), 13.9 (CH₃). **IR** (ATR): $\tilde{\nu}$ = 2958, 2874,

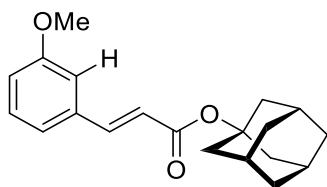
1710, 1638, 1586, 1252, 1164, 1042, 984, 783, 681 cm^{-1} . **MS** (ESI): m/z (relative intensity) = 491.3 (100) $[\text{2M}+\text{Na}]^+$, 257.1 (60) $[\text{M}+\text{Na}]^+$. **HR-MS** (ESI): m/z calc. for $\text{C}_{14}\text{H}_{18}\text{O}_3\text{Na}$ $[\text{M}+\text{Na}]^+$: 257.1154; found: 257.1148. The analytical data are in accordance with those previously reported in literature.^[66c]



***tert*-Butyl (*E*)-3-(3-methoxyphenyl)acrylate (**31da**)**

The general procedure B was followed using *tert*-butyl acrylate **11d** (51.7 mg, 0.40 mmol) and 2-methoxybenzoic acid **30a** (182.8 mg, 1.20 mmol). Isolation by FCC (*n*-hexane/EtOAc = 15:1→7:1) yielded **31da** as a colorless oil (33.1 mg, 0.14 mmol, 35%).

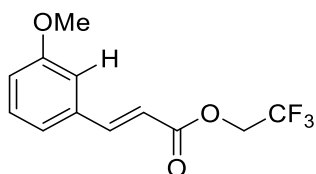
¹H-NMR (400 MHz, CDCl_3): δ = 7.55 (d, J = 16.0 Hz, 1H), 7.28 (dd, J = 8.2, 7.8 Hz, 1H), 7.10 (d, J = 7.8 Hz, 1H), 7.03 (dd, J = 2.0, 1.6 Hz, 1H), 6.91 (ddd, J = 8.2, 2.6, 0.8 Hz, 1H), 6.35 (d, J = 16.0 Hz, 1H), 3.83 (s, 3H), 1.54 (s, 9H). **¹³C{¹H}-NMR** (101 MHz, CDCl_3): δ = 166.4 (C_q), 160.0 (C_q), 143.6 (CH), 136.2 (C_q), 129.9 (CH), 120.9 (CH), 120.6 (CH), 116.0 (CH), 112.9 (CH), 80.7 (C_q), 55.4 (CH_3), 28.3 (CH_3). **IR** (ATR): $\tilde{\nu}$ = 2976, 2936, 1706, 1638, 1586, 1249, 1146, 1045, 980, 852, 784, 681 cm^{-1} . **MS** (ESI): m/z (relative intensity) = 491.3 (100) $[\text{2M}+\text{Na}]^+$, 257.1 (61) $[\text{M}+\text{Na}]^+$. **HR-MS** (ESI): m/z calc. for $\text{C}_{14}\text{H}_{18}\text{O}_3\text{Na}$ $[\text{M}+\text{Na}]^+$: 257.1154; found: 257.1155. The analytical data are in accordance with those previously reported in literature.^[66c]



1-Adamantyl (*E*)-3-(3-methoxyphenyl)acrylate (31ea**)**

The general procedure B was followed using 1-adamantyl acrylate **11e** (82.9 mg, 0.40 mmol) and 2-methoxybenzoic acid **30a** (183.0 mg, 1.20 mmol). Isolation by FCC (*n*-hexane/EtOAc = 15:1→7:1) yielded **31ea** as a colorless solid (48.0 mg, 0.15 mmol, 38%).

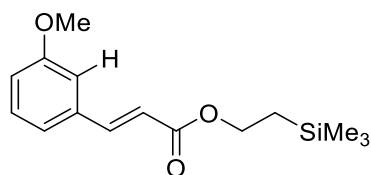
M.p.: 73–75 °C. **¹H-NMR** (300 MHz, CDCl₃): δ = 7.54 (d, *J* = 15.9 Hz, 1H), 7.28 (dd, *J* = 8.2, 7.6 Hz, 1H), 7.10 (d, *J* = 7.6 Hz, 1H), 7.03 (s, 1H), 6.91 (dd, *J* = 8.2, 2.6 Hz, 1H), 6.35 (d, *J* = 15.9 Hz, 1H), 3.83 (s, 3H), 2.20 (s, 9H), 1.70 (s, 6H). **¹³C{¹H}-NMR** (75 MHz, CDCl₃): δ = 166.1 (C_q), 160.0 (C_q), 143.5 (CH), 136.2 (C_q), 129.9 (CH), 120.9 (CH), 120.8 (CH), 116.0 (CH), 112.9 (CH), 80.8 (C_q), 55.4 (CH₃), 41.6 (CH₂), 36.4 (CH₂), 31.0 (CH). **IR** (ATR): $\tilde{\nu}$ = 2912, 2856, 1702, 1636, 1332, 1247, 1171, 1053, 1040, 841, 787, 676 cm⁻¹. **MS** (ESI): *m/z* (relative intensity) = 959.5 (100) [3M+Na]⁺, 647.4 (87) [2M+Na]⁺, 335.1 (27) [M+Na]⁺. **HR-MS** (ESI): *m/z* calc. for C₂₀H₂₄O₃Na [M+Na]⁺: 335.1623; found: 335.1618.



2,2,2-Trifluoroethyl (*E*)-3-(3-methoxyphenyl)acrylate (**31fa**)

The general procedure B was followed using 2,2,2-trifluoroethyl acrylate **11f** (62.0 mg, 0.40 mmol) and 2-methoxybenzoic acid **30a** (182.2 mg, 1.20 mmol). Isolation by FCC (*n*-hexane/EtOAc = 19:1→9:1) yielded **31fa** as a colorless oil (35.9 mg, 0.14 mmol, 34%).

¹H-NMR (400 MHz, CDCl₃): δ = 7.76 (d, *J* = 16.0 Hz, 1H), 7.32 (dd, *J* = 8.3, 7.9 Hz, 1H), 7.14 (d, *J* = 7.9 Hz, 1H), 7.06 (dd, *J* = 1.9, 1.7 Hz, 1H), 6.97 (dd, *J* = 8.3, 2.5 Hz, 1H), 6.48 (d, *J* = 16.0 Hz, 1H), 4.59 (q, *J* = 8.4 Hz, 2H), 3.84 (s, 3H). **¹³C{¹H}-NMR** (101 MHz, CDCl₃): δ = 165.3 (C_q), 160.1 (C_q), 147.3 (CH), 135.4 (C_q), 130.2 (CH), 123.2 (q, *J* = 277 Hz, C_q), 121.2 (CH), 117.0 (CH), 116.3 (CH), 113.3 (CH), 60.6 (q, *J* = 36.5 Hz, CH₂), 55.5 (CH₂). **¹⁹F{¹H}-NMR** (377 MHz, CDCl₃): δ = -73.7. **IR** (ATR): $\tilde{\nu}$ = 2966, 2843, 1731, 1637, 1281, 1252, 1144, 1046, 978, 851, 782, 679 cm⁻¹. **MS** (ESI): *m/z* (relative intensity) = 293.1 (70) [M+Na]⁺, 161.1 (100). **HR-MS** (ESI): *m/z* calc. for C₁₂H₁₁O₃F₃Na [M+Na]⁺: 283.0558; found: 283.0554.

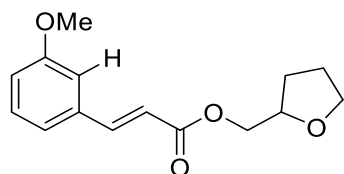


2-(Trimethylsilyl)ethyl (*E*)-3-(3-methoxyphenyl)acrylate (**31ga**)

The general procedure B was followed using 2-(trimethylsilyl)ethyl acrylate **11g** (82.9 mg, 0.40 mmol) and 2-methoxybenzoic acid **30a** (183.0 mg, 1.20 mmol). Isolation by FCC (*n*-hexane/EtOAc = 15:1→7:1) yielded **31ga** as a colorless oil (45.5 mg, 0.16 mmol, 41%).

¹H-NMR (400 MHz, CDCl₃): δ = 7.64 (d, J = 16.0 Hz, 1H), 7.30 (dd, J = 8.2, 7.6 Hz, 1H), 7.12 (d, J = 7.6 Hz, 1H), 7.04 (dd, J = 2.6, 1.6 Hz, 1H), 6.93 (ddd, J = 8.2, 2.6, 1.0 Hz, 1H), 6.41 (d, J = 16.0 Hz, 1H), 4.34–4.27 (m, 2H), 3.83 (s, 3H), 1.10–1.04 (m, 2H), 0.07 (s, 9H).

¹³C{¹H}-NMR (101 MHz, CDCl₃): δ = 167.2 (C_q), 160.0 (C_q), 144.5 (CH), 136.0 (C_q), 130.0 (CH), 120.9 (CH), 118.9 (CH), 116.2 (CH), 113.1 (CH), 62.9 (CH₂), 55.5 (CH₃), 17.6 (CH₂), -1.3 (CH₃). **IR** (ATR): $\tilde{\nu}$ = 2954, 2902, 1709, 1639, 1586, 1250, 1161, 1045, 985, 835, 781, 685 cm⁻¹. **MS** (ESI): m/z (relative intensity) = 857.4 (29) [3M+Na]⁺, 579.3 (100) [2M+Na]⁺, 301.1 (52) [M+Na]⁺. **HR-MS** (ESI): m/z calc. for C₁₅H₂₂O₃SiNa [M+Na]⁺: 301.1236; found: 301.1235.

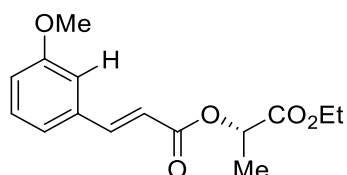


Tetrahydrofurfuryl (*E*)-3-(3-methoxyphenyl)acrylate (**31ha**)

The general procedure B was followed using tetrahydrofurfuryl acrylate **11h** (62.7 mg, 0.40 mmol) and 2-methoxybenzoic acid **30a** (182.5 mg, 1.20 mmol). Isolation by FCC (*n*-hexane/EtOAc = 4:1→3:2) yielded **31ha** as a yellow oil (36.0 mg, 0.14 mmol, 34%).

¹H-NMR (400 MHz, CDCl₃) δ = 7.68 (d, J = 16.0 Hz, 1H), 7.29 (dd, J = 8.1, 7.6 Hz, 1H), 7.11 (d, J = 7.6 Hz, 1H), 7.04 (s, 1H), 6.93 (d, J = 8.1 Hz, 1H), 6.48 (d, J = 16.0 Hz, 1H), 4.31 (dd, J = 11.2, 2.7 Hz, 1H), 4.24–4.16 (m, 1H), 4.16–4.09 (m, 1H), 3.93 (ddd, J = 7.7, 7.2, 7.2 Hz, 1H), 3.88–3.76 (m, 1H), 3.83 (s, 3H), 2.11–1.99 (m, 1H), 1.99–1.86 (m, 2H), 1.71–1.60 (m, 1H). **¹³C{¹H}-NMR** (101 MHz, CDCl₃) δ = 167.0 (C_q), 160.0 (C_q), 145.2 (CH), 135.9 (C_q), 130.0 (CH), 121.0 (CH), 118.3 (CH), 116.5 (CH), 113.0 (CH), 76.8 (CH),

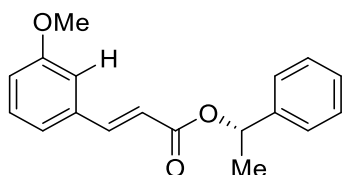
68.6 (CH₂), 66.8 (CH₂), 55.4 (CH₃), 28.2 (CH₂), 25.8 (CH₂). **IR** (ATR): $\tilde{\nu}$ = 2948, 2874, 1709, 1637, 1580, 1248, 1164, 1027, 981, 855, 783, 680 cm⁻¹. **MS** (ESI): *m/z* (relative intensity) = 547.2 (86) [2M+Na]⁺, 285.1 (100) [M+Na]⁺. **HR-MS** (ESI): *m/z* calc. for C₁₅H₁₈O₄Na [M+Na]⁺: 285.1103; found: 285.1103. The analytical data are in accordance with those previously reported in literature.^[66c]



(S)-1-ethoxy-1-oxopropan-2-yl (E)-3-(3-methoxyphenyl)acrylate (31ia)

The general procedure B was followed using (*S*)-1-ethoxy-1-oxopropan-2-yl acrylate **11i** (71.0 mg, 0.40 mmol) and 2-methoxybenzoic acid **30a** (182.7 mg, 1.20 mmol). Isolation by FCC (*n*-hexane/EtOAc = 5:1→2:1) yielded **31ia** as a brownish oil (47.9 mg, 0.17 mmol, 43%).

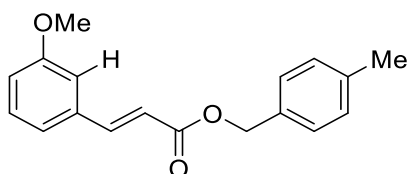
¹H-NMR (400 MHz, CDCl₃): δ = 7.72 (d, *J* = 16.0 Hz, 1H), 7.30 (dd, *J* = 8.2, 7.6 Hz, 1H), 7.13 (d, *J* = 7.6 Hz, 1H), 7.05 (s, 1H), 6.94 (dd, *J* = 8.2, 2.5 Hz, 1H), 6.50 (d, *J* = 16.0 Hz, 1H), 5.21 (q, *J* = 7.0 Hz, 1H), 4.23 (q, *J* = 7.1 Hz, 2H), 3.83 (s, 3H), 1.57 (d, *J* = 7.0 Hz, 3H), 1.29 (t, *J* = 7.1 Hz, 3H). **¹³C{¹H}-NMR** (101 MHz, CDCl₃): δ = 170.9 (C_q), 166.2 (C_q), 159.9 (C_q), 145.8 (CH), 135.6 (C_q), 129.9 (CH), 121.0 (CH), 117.5 (CH), 116.5 (CH), 112.9 (CH), 68.8 (CH), 61.4 (CH₂), 55.3 (CH₃), 17.1 (CH₃), 14.2 (CH₃). **IR** (ATR): $\tilde{\nu}$ = 2989, 2942, 1750, 1714, 1637, 1583, 1252, 1206, 1160, 1095, 1045, 981, 855, 784, 680 cm⁻¹. **MS** (ESI): *m/z* (relative intensity) = 579.2 (88) [2M+Na]⁺, 301.1 (100) [M+Na]⁺. **HR-MS** (ESI): *m/z* calc. for C₁₅H₁₈O₅Na [M+Na]⁺: 301.1052; found: 325.1046.



(*S*)-1-phenylethyl (*E*)-3-(3-methoxyphenyl)acrylate (31ja**)**

The general procedure B was followed using (*S*)-1-phenylethyl acrylate **11j** (71.0 mg, 0.40 mmol) and 2-methoxybenzoic acid **30a** (182.2 mg, 1.20 mmol). Isolation by FCC (*n*-hexane/EtOAc = 17:1→8:1) yielded **31ja** as a colorless oil (63.5 mg, 0.22 mmol, 56%).

¹H-NMR (300 MHz, CDCl₃): δ = 7.67 (d, *J* = 16.0 Hz, 1H), 7.50–7.24 (m, 6H), 7.12 (d, *J* = 7.6 Hz, 1H), 7.04 (br, 1H), 6.93 (dd, *J* = 8.2, 2.6 Hz, 1H), 6.46 (d, *J* = 16.0 Hz, 1H), 6.03 (q, *J* = 6.6 Hz, 1H), 3.83 (s, 3H), 1.62 (d, *J* = 6.6 Hz, 3H). **¹³C{¹H}-NMR** (75 MHz, CDCl₃): δ = 166.3 (C_q), 160.0 (C_q), 144.9 (CH), 141.9 (C_q), 135.9 (C_q), 130.0 (CH), 128.7 (CH), 128.0 (CH), 126.3 (CH), 121.0 (CH), 118.8 (CH), 116.4 (CH), 113.0 (CH), 72.6 (CH), 55.4 (CH₃), 22.4 (CH₃). **IR** (ATR): $\tilde{\nu}$ = 2981, 2937, 2837, 1708, 1637, 1581, 1248, 1164, 1050, 981, 852, 783, 760, 699, 680, 542 cm⁻¹. **MS** (ESI): *m/z* (relative intensity) = 587.3 (83) [2M+Na]⁺, 305.1 (100) [M+Na]⁺. **HR-MS** (ESI): *m/z* calc. for C₁₈H₁₈O₃Na [M+Na]⁺: 305.1154; found: 305.1156.

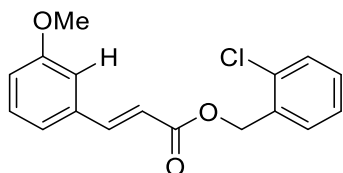


4-Methylbenzyl (*E*)-3-(3-methoxyphenyl)acrylate (31ka**)**

The general procedure B was followed using 4-methylbenzyl acrylate **11k** (70.9 mg, 0.40 mmol) and 2-methoxybenzoic acid **30a** (182.5 mg, 1.20 mmol). Isolation by FCC (*n*-hexane/EtOAc = 19:1→9:1) yielded **31ka** as a colorless oil (61.6 mg, 0.22 mmol, 54%).

¹H-NMR (400 MHz, CDCl₃): δ = 7.68 (d, *J* = 16.0 Hz, 1H), 7.34–7.27 (m, 3H), 7.20 (d, *J* = 7.6 Hz, 2H), 7.11 (d, *J* = 7.6 Hz, 1H), 7.03 (s, 1H), 6.93 (d, *J* = 8.2 Hz, 1H), 6.46 (d, *J* = 16.0 Hz, 1H), 5.21 (s, 2H), 3.82 (s, 3H), 2.37 (s, 3H). **¹³C{¹H}-NMR** (101 MHz, CDCl₃): δ = 166.9 (C_q), 160.0 (C_q), 145.1 (CH), 138.3 (C_q), 135.9 (C_q), 133.2 (C_q), 130.0 (CH), 129.4 (CH), 128.6 (CH), 121.0 (CH), 118.4 (CH), 116.4 (CH), 113.0 (CH), 66.5 (CH₂), 55.4 (CH₃), 21.4 (CH₃). **IR** (ATR): $\tilde{\nu}$ = 3008, 2951, 1709, 1638, 1586, 1254, 1160, 1043,

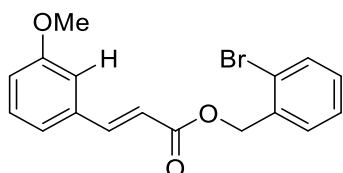
984, 851, 787, 680 cm^{-1} . **MS** (ESI): m/z (relative intensity) = 587.3 (100) $[2\text{M}+\text{Na}]^+$, 305.1 (92) $[\text{M}+\text{Na}]^+$. **HR-MS** (ESI): m/z calc. for $\text{C}_{18}\text{H}_{18}\text{O}_3\text{Na}$ $[\text{M}+\text{Na}]^+$: 305.1154; found: 305.1152.



2-Chlorobenzyl (*E*)-3-(3-methoxyphenyl)acrylate (**311a**)

The general procedure B was followed using 2-chlorobenzyl acrylate **11l** (71.0 mg, 0.40 mmol) and 2-methoxybenzoic acid **30a** (182.4 mg, 1.20 mmol). Isolation by FCC (*n*-hexane/EtOAc = 15:1→8:1) yielded **311a** as a colorless oil (50.4 mg, 0.16 mmol, 41%).

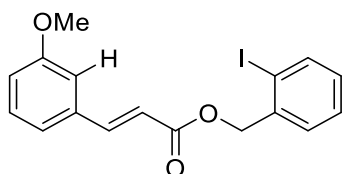
¹H-NMR (300 MHz, CDCl_3): δ = 7.72 (d, J = 16.0 Hz, 1H), 7.48 (dd, J = 5.7, 3.7 Hz, 1H), 7.45–7.38 (m, 1H), 7.35–7.27 (m, 3H), 7.13 (d, J = 7.6 Hz, 1H), 7.05 (s, 1H), 6.94 (dd, J = 8.2, 2.6 Hz, 1H), 6.50 (d, J = 16.0 Hz, 1H), 5.37 (s, 2H), 3.83 (s, 3H). **¹³C{¹H}-NMR** (75 MHz, CDCl_3): δ = 166.7 (C_q), 160.1 (C_q), 145.5 (CH), 135.8 (C_q), 133.9 (C_q), 130.0 (2 CH), 129.8 (CH), 129.7 (CH), 127.1 (CH), 121.0 (CH), 118.0 (CH), 116.5 (CH), 113.0 (CH), 63.8 (CH_2), 55.5 (CH_3), one C_q signal invisible due to concurrence with one of the CH signals. **IR** (ATR): $\tilde{\nu}$ = 3066, 2954, 2838, 1712, 1636, 1583, 1250, 1156, 1042, 980, 752, 679 cm^{-1} . **MS** (ESI): m/z (relative intensity) = 627.2 (80) $[2\text{M}+\text{Na}]^+$, 325.1 (100) $[\text{M}+\text{Na}]^+$. **HR-MS** (ESI): m/z calc. for $\text{C}_{17}\text{H}_{15}\text{O}_3\text{ClNa}$ $[\text{M}+\text{Na}]^+$: 325.0607; found: 325.0606.



2-Bromobenzyl (*E*)-3-(3-methoxyphenyl)acrylate (**311ma**)

The general procedure B was followed using 2-bromobenzyl acrylate **11m** (96.9 mg, 0.40 mmol) and 2-methoxybenzoic acid **30a** (182.9 mg, 1.20 mmol). Isolation by FCC (*n*-hexane/EtOAc = 15:1→8:1) yielded **311ma** as a colorless oil (38.0 mg, 0.11 mmol, 27%).

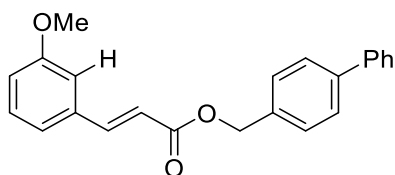
¹H-NMR (300 MHz, CDCl₃): δ = 7.88 (dd, J = 7.9, 1.2 Hz, 1H), 7.73 (d, J = 16.0 Hz, 1H), 7.49–7.23 (m, 3H), 7.13 (d, J = 7.6 Hz, 1H), 7.08–7.00 (m, 2H), 6.94 (dd, J = 8.2, 2.6 Hz, 1H), 6.51 (d, J = 16.0 Hz, 1H), 5.28 (s, 2H), 3.83 (s, 3H). **¹³C{¹H}-NMR** (75 MHz, CDCl₃): δ = 166.6 (C_q), 160.0 (C_q), 145.6 (CH), 139.7 (CH), 138.6 (C_q), 135.8 (C_q), 130.0 (CH), 130.0 (CH), 129.7 (CH), 128.5 (CH), 121.0 (CH), 118.0 (CH), 116.5 (CH), 113.1 (CH), 98.6 (C_q), 70.2 (CH₂), 55.5 (CH₃). **IR** (ATR): $\tilde{\nu}$ = 3065, 2940, 2839, 1712, 1637, 1583, 1250, 1153, 1035, 980, 750, 676 cm⁻¹. **MS** (ESI): m/z (relative intensity) = 717.1 (100) [⁷⁹M+⁸¹M+Na]⁺, 371.0 (85) [⁸¹M+Na]⁺. **HR-MS** (ESI): m/z calc. for C₁₇H₁₅O₃⁷⁹BrNa [M+Na]⁺: 369.0102; found: 369.0097.



2-iodobenzyl (*E*)-3-(3-methoxyphenyl)acrylate (**31na**)

The general procedure B was followed using 2-iodobenzyl acrylate **11n** (71.0 mg, 0.40 mmol) and 2-methoxybenzoic acid **30a** (183.3 mg, 1.20 mmol). Isolation by FCC (*n*-hexane/EtOAc = 17:1→8:1) yielded **31na** as a colorless oil (54.0 mg, 0.14 mmol, 34 %).

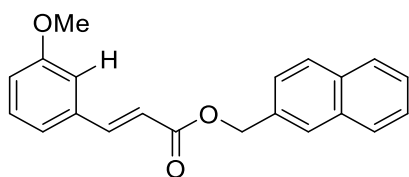
¹H-NMR (300 MHz, CDCl₃): δ = 7.73 (d, J = 16.0 Hz, 1H), 7.60 (dd, J = 7.9, 1.3 Hz, 1H), 7.47 (dd, J = 7.5, 1.8 Hz, 1H), 7.38–7.27 (m, 2H), 7.21 (ddd, J = 7.7, 7.7, 1.7, Hz 1H), 7.13 (d, J = 7.6 Hz, 1H), 7.05 (s, 1H), 6.94 (dd, J = 8.1, 2.5 Hz, 1H), 6.50 (d, J = 16.0 Hz, 1H), 5.34 (s, 2H), 3.83 (s, 3H). **¹³C{¹H}-NMR** (75 MHz, CDCl₃): δ = 166.6 (C_q), 160.1 (C_q), 145.6 (CH), 135.8 (C_q), 135.6 (C_q), 133.0 (CH), 130.1 (CH), 130.1 (CH), 129.9 (CH), 127.7 (CH), 123.7 (C_q), 121.0 (CH), 118.0 (CH), 116.5 (CH), 113.1 (CH), 66.0 (CH₂), 55.5 (CH₃). **IR** (ATR): $\tilde{\nu}$ = 3060, 2946, 1710, 1636, 1584, 1251, 1153, 1008, 978, 851, 748, 678 cm⁻¹. **MS** (ESI): m/z (relative intensity) = 1205.0 (24) [3M+Na]⁺, 811.0 (100) [2M+Na]⁺, 417.0 (80) [M+Na]⁺. **HR-MS** (ESI): m/z calc. for C₁₇H₁₅O₃I^{Na} [M+Na]⁺: 416.9964; found: 416.9958.



[1,1'-biphenyl]-4-ylmethyl (*E*)-3-(3-methoxyphenyl)acrylate (**310a**)

The general procedure B was followed using [1,1'-biphenyl]-4-ylmethyl acrylate **11o** (95.8 mg, 0.40 mmol) and 2-methoxybenzoic acid **30a** (182.1 mg, 1.20 mmol). Isolation by FCC (*n*-hexane/EtOAc = 17:1→9:1) yielded **310a** as a colorless solid (37.5 mg, 0.11 mmol, 27%).

M.p.: 82–84 °C. **¹H-NMR** (400 MHz, CDCl₃): δ = 7.72 (d, *J* = 16.0 Hz, 1H), 7.61 (d, *J* = 7.9, 7.9 Hz, 4H), 7.53–7.41 (m, 4H), 7.36 (dd, *J* = 7.4, 7.4 Hz, 1H), 7.30 (dd, *J* = 7.9, 7.9 Hz, 1H), 7.13 (d, *J* = 7.6 Hz, 1H), 7.05 (s, 1H), 6.94 (d, *J* = 8.2 Hz, 1H), 6.49 (d, *J* = 16.0 Hz, 1H), 5.30 (s, 2H), 3.83 (s, 3H). **¹³C{¹H}-NMR** (101 MHz, CDCl₃): δ = 166.9 (C_q), 160.0 (C_q), 145.3 (CH), 141.4 (C_q), 140.8 (C_q), 135.9 (C_q), 135.2 (C_q), 130.0 (CH), 129.0 (2 CH), 127.6 (CH), 127.5 (CH), 127.3 (CH), 121.0 (CH), 118.3 (CH), 116.5 (CH), 113.0 (CH), 66.3 (CH₂), 55.4 (CH₃). **IR** (ATR): $\tilde{\nu}$ = 3032, 2970, 2846, 1705, 1576, 1488, 1259, 1215, 1168, 980, 759, 680 cm⁻¹. **MS** (ESI): *m/z* (relative intensity) = 1055.4 (22) [3M+Na]⁺, 711.3 (100) [2M+Na]⁺, 367.1 (76) [M+Na]⁺. **HR-MS** (ESI): *m/z* calc. for C₂₃H₂₀O₃Na [M+Na]⁺: 367.1310; found: 367.1305.

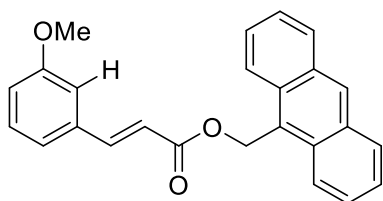


Naphthalen-2-ylmethyl (*E*)-3-(3-methoxyphenyl)acrylate (**31pa**)

The general procedure B was followed using naphthalen-2-ylmethyl acrylate **11p** (85.1 mg, 0.40 mmol) and 2-methoxybenzoic acid **30a** (182.8 mg, 1.20 mmol). Isolation by FCC (*n*-hexane/EtOAc = 17:1→9:1) yielded **31pa** as a colorless solid (37.1 mg, 0.12 mmol, 29%).

M.p.: 89–91 °C. **¹H-NMR** (400 MHz, CDCl₃): δ = 7.91–7.82 (m, 4H), 7.72 (d, *J* = 16.0 Hz, 1H), 7.55–7.46 (m, 3H), 7.30 (dd, *J* = 7.9, 7.9 Hz, 1H), 7.13 (d, *J* = 7.7 Hz, 1H), 7.05 (dd, *J* = 2.1, 1.8 Hz, 1H), 6.94 (dd, *J* = 8.3, 2.6 Hz, 1H), 6.51 (d, *J* = 16.0 Hz, 1H), 5.42 (s, 2H), 3.83 (s, 3H). **¹³C{¹H}-NMR** (101 MHz, CDCl₃): δ = 166.9 (C_q), 160.0 (C_q), 145.3

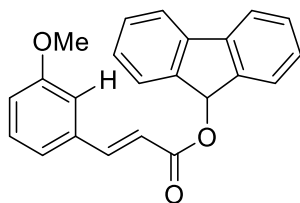
(CH), 135.9 (C_q), 133.6 (C_q), 133.4 (C_q), 133.3 (C_q), 130.0 (CH), 128.6 (CH), 128.1 (CH), 127.9 (CH), 127.6 (CH), 126.5 (CH), 126.4 (CH), 126.1 (CH), 121.0 (CH), 118.3 (CH), 116.5 (CH), 113.0 (CH), 66.7 (CH₂), 55.4 (CH₃). **IR** (ATR): $\tilde{\nu}$ = 3058, 2998, 2967, 2936, 1705, 1636, 1583, 1314, 1240, 1182, 992, 855, 832, 794, 683, 474 cm⁻¹. **MS** (ESI): *m/z* (relative intensity) = 977.4 (20) [3M+Na]⁺, 659.3 (100) [2M+Na]⁺, 341.1 (93) [M+Na]⁺. **HR-MS** (ESI): *m/z* calc. for C₂₁H₁₈O₃Na [M+Na]⁺: 341.1154; found: 341.1148



Anthracen-9-ylmethyl (*E*)-3-(3-methoxyphenyl)acrylate (**31qa**)

The general procedure B was followed using anthracene-9-ylmethyl acrylate **11q** (105.3 mg, 0.40 mmol) and 2-methoxybenzoic acid **30a** (182.5 mg, 1.20 mmol). Isolation by FCC (*n*-hexane/DCM/THF = 10:1:1→10:1:2) yielded **31qa** as a yellow solid (56.5 mg, 0.15 mmol, 38%).

M.p.: 95–96 °C. **¹H-NMR** (300 MHz, CDCl₃): δ = 8.54 (s, 1H), 8.40 (d, *J* = 8.9 Hz, 2H), 8.05 (d, *J* = 8.4 Hz, 2H), 7.68 (d, *J* = 16.0 Hz, 1H), 7.60 (ddd, *J* = 8.7, 6.6, 1.4 Hz, 2H), 7.51 (ddd, *J* = 7.8, 6.6, 1.2 Hz, 2H), 7.25 (dd, *J* = 7.9, 7.9 Hz, 1H), 7.05 (d, *J* = 7.9 Hz, 1H), 6.97 (dd, *J* = 1.8, 1.7 Hz, 1H), 6.90 (dd, *J* = 8.2, 2.4 Hz, 1H), 6.44 (d, *J* = 16.0 Hz, 1H), 6.29 (s, 2H), 3.77 (s, 3H). **¹³C{¹H}-NMR** (75 MHz, CDCl₃): δ = 167.3 (C_q), 160.0 (C_q), 145.4 (CH), 135.8 (C_q), 131.6 (C_q), 131.3 (C_q), 130.0 (CH), 129.4 (C_q), 129.3 (C_q), 126.9 (C_q), 126.4 (C_q), 125.3 (CH), 124.1 (CH), 121.0 (CH), 118.2 (CH), 116.5 (CH), 112.9 (CH), 59.1 (CH₂), 55.4 (CH₃). **IR** (ATR): $\tilde{\nu}$ = 3010, 2954, 2924, 1708, 1636, 1579, 1259, 1160, 980, 779, 680, 642 cm⁻¹. **MS** (ESI): *m/z* (relative intensity) = 1127.5 (17) [3M+Na]⁺, 759.3 (58) [2M+Na]⁺, 391.1 (53) [M+Na]⁺, 191 (100). **HR-MS** (ESI): *m/z* calc. for C₂₅H₂₀O₃Na [M+Na]⁺: 391.1310; found: 391.1305.

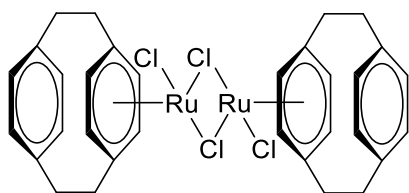


9H-fluoren-9-yl (*E*)-3-(3-methoxyphenyl)acrylate (**31ra**)

The general procedure B was followed using 9H-fluoren-9-yl acrylate **11r** (95.0 mg, 0.40 mmol) and 2-methoxybenzoic acid **30a** (182.3 mg, 1.20 mmol). Isolation by FCC (*n*-hexane/EtOAc = 17:1→9:1) yielded **31ra** as a yellowish oil (33.4 mg, 0.10 mmol, 24%).

¹H-NMR (400 MHz, CDCl₃): δ = 7.75 (d, J = 16.0 Hz, 1H), 7.70 (d, J = 7.6 Hz, 2H), 7.61 (d, J = 7.5 Hz, 2H), 7.43 (dd, J = 7.6, 7.6 Hz, 2H), 7.34–7.27 (m, 3H), 7.11 (d, J = 7.6 Hz, 1H), 7.03 (dd, J = 2.1, 2.1 Hz, 1H), 6.95 (s, 1H), 6.93 (dd, J = 8.3, 2.7 Hz, 1H), 6.52 (d, J = 16.0 Hz, 1H), 3.81 (s, 3H).

¹³C{¹H}-NMR (101 MHz, CDCl₃): δ = 167.7 (C_q), 160.0 (C_q), 145.7 (CH), 142.3 (C_q), 141.2 (C_q), 135.8 (C_q), 130.1 (CH), 129.7 (CH), 128.0 (CH), 126.2 (CH), 121.1 (CH), 120.2 (CH), 118.2 (CH), 116.6 (CH), 113.0 (CH), 75.3 (CH), 55.4 (CH₃). **IR** (ATR): $\tilde{\nu}$ = 3046, 2934, 2836, 1705, 1636, 1452, 1253, 1152, 1005, 977, 741, 678 cm⁻¹. **MS** (ESI): m/z (relative intensity) = 1049.4 (8) [3M+Na]⁺, 707.3 (95) [2M+Na]⁺, 365.1 (100) [M+Na]⁺. **HR-MS** (ESI): m/z calc. for C₂₃H₁₈O₃Na [M+Na]⁺: 365.1154; found: 365.1150.

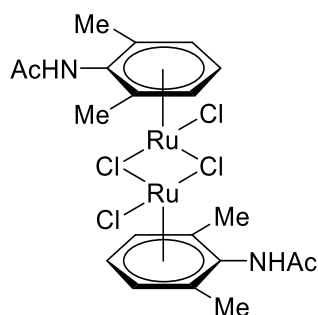


Dichloro (2.2-paracyclophane)ruthenium(II) dimer (**177a**)

The title complex was prepared by a variation of a known procedure,^[261] omitting the isolation of the air-sensitive [Ru⁰(pcp)(1,3-chd)] complex. In an oven-dried 20 mL Schlenk tube, [Ru(PhH)(pcp)](BF₄)₂ (112 mg, 0.20 mmol) was suspended in 4 mL of dry, O₂-free THF under an atmosphere of N₂. To the suspension was added Red-Al® (0.22 mL, 0.79 mmol, 70% solution in PhMe) and the resulting amber solution was stirred at room temperature for 2 h. The reaction was quenched by the addition of 50 μ L of O₂-free water, diluted with few mL of O₂-free hexane and dried by the addition of a small amount of

Na₂SO₄. Under N₂ atmosphere, the resulting black mixture was filtered over a pad of celite. The solid remains were washed with few mL of O₂-free hexane. To the combined filtrates, 4 mL of a degassed 1:1 mixture of acetone and conc. aq. HCl was added. A brown precipitate formed immediately. The mixture was stirred at room temperature for further 30 minutes and filtered. Washing with water, acetone and Et₂O with subsequent drying under vacuum yielded the target complex **177a** as a brown solid (43.5 mg, 57%). The complex is soluble in DMSO. However, it rapidly decomposes in solution to form pcp which is visible as a major impurity in the ¹H-NMR spectrum (δ = 6.46 (s, 8H), 3.01 (s, 8H)) and in the ¹³C{¹H}-NMR spectrum (δ = 139.2 (C_q), 132.9 (CH), 35.0 (CH₂)).

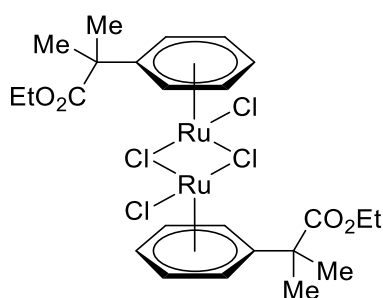
M.p.: > 250 °C (decomp.) °C. **¹H-NMR** (400 MHz, DMSO-*d*₆) δ = 6.85 (s, 4H), 5.21 (s, 4H), 3.18–3.10 (m, 4H), 2.82–2.73 (m, 4H). **¹³C{¹H}-NMR** (101 MHz, DMSO-*d*₆) δ = 139.3 (C_q), 133.3 (CH), 121.8 (C_q), 83.4 (CH), 32.8 (CH₂), 31.3 (CH₂). **IR** (ATR): $\tilde{\nu}$ = 3050 2929, 2852, 1712, 1500, 1374, 1234, 899, 820, 724, 656 572, 504 cm⁻¹. **MS** (ESI): *m/z* (relative intensity) = 713.1 (100) [M+Na]⁺, 761.9 (1) [M]⁺. **HR-MS** (ESI): *m/z* calc. for C₃₅H₄₁O₃¹⁰²Ru₂ [M+3MeO-4Cl]⁺: 713;1143 found: 713;1140. The analytical data are in accordance with those previously reported in literature.^[261]



Dichloro (2,6-dimethylacetanilide)ruthenium(II) dimer (**177b**)

[Ru(*p*-cymene)Cl₂]₂ (61.5 mg, 0.10 mmol) was heated to 230 °C for 25 min in presence of 2,6-dimethylacetanilide (326 mg, 2.0 mmol) and THTD (1.0 mL). after cooling down to r.t., the mixture was diluted with EtOH (2 mL) and filtered. The filter cake was suspended in acetone/EtOH (1:1, 2 mL) and filtered again. The last step was repeated until an orange filter cake without visible contamination of colorless solid remained. The solid was dissolved in CHCl₃, filtered through celite and re-precipitated by addition of Et₂O. Drying under vacuum gave the title compound as an orange solid (43.7 mg, 0.06 mmol, 65%)

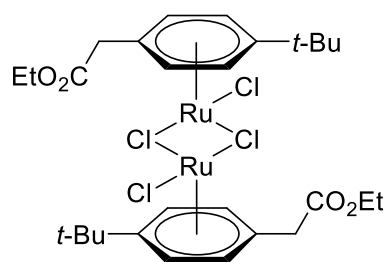
M.p.: > 280 °C (decomp.). **¹H-NMR** (300 MHz, CDCl₃) δ = 8.85 (s, 1H), 5.70 (t, *J* = 5.5 Hz, 1H), 5.11 (d, *J* = 5.5 Hz, 2H), 2.27 (s, 3H), 2.07 (s, 6H). **¹³C{¹H}-NMR** (75 MHz, CDCl₃) δ = 171.6 (C_q), 102.4 (C_q), 91.9 (C_q), 87.1 (CH), 75.6 (CH), 22.8 (CH₃), 17.0 (CH₃). **IR** (ATR): $\tilde{\nu}$ = 3230, 3050, 2980, 1684, 1492, 1440, 1270, 1024, 732, 576 cm⁻¹. **MS** (ESI): *m/z* (relative intensity) = 623.1 (100) [M+3MeO-4Cl]⁺, 672.9 (30) [M]⁺, 637.9 (16) [M-Cl]⁺. **HR-MS** (ESI): *m/z* calc. for C₂₃H₃₅N₂O₂¹⁰²Ru₂ [M+3MeO-4Cl]⁺: 623.0633; found: 633.0629.



Dichloro (ethyl 2-methyl-2-phenylpropanoate)ruthenium(II) dimer (177c)

To a solution of RuCl₃ hydrate (52.4 mg, 0.20 mmol) in EtOH (2.0 mL) was added dihydro 2-methyl-2-phenylpropanoic acid (65.0 mg, 0.40 mmol, isomer not specified). The mixture was stirred overnight at r.t. The precipitate was filtered and washed with EtOH and hexane. Drying under vacuum gave the title compound as a red solid (58.2 mg, 0.08 mmol, 80%)

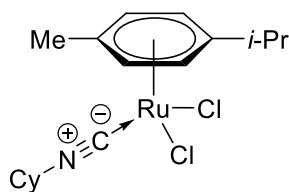
M.p.: > 200 °C (decomp.). **¹H-NMR** (400 MHz, CDCl₃) δ = 5.95 (d, *J* = 6.0 Hz, 2H), 5.80 (t, *J* = 5.5 Hz, 1H), 5.65 (dd, *J* = 6.0, 5.5 Hz, 2H), 4.05 (q, *J* = 7.1 Hz, 2H), 1.79 (s, 6H), 1.16 (t, *J* = 7.1 Hz, 3H). **¹³C{¹H}-NMR** (101 MHz, CDCl₃) δ = 174.3 (C_q), 96.8 (C_q), 86.7 (CH), 83.9 (CH), 78.7 (CH), 61.8 (CH₂), 45.4 (C_q), 24.7 (CH₃), 14.1 (CH₃). **IR** (ATR): $\tilde{\nu}$ = 3077, 2992, 1720, 1456, 1387, 1250, 1150, 1030, 853, 762, 672 cm⁻¹. **MS** (ESI): *m/z* (relative intensity) = 681.1 (100) [M+3MeO-4Cl]⁺, 729.9 (1) [M]⁺. **HR-MS** (ESI): *m/z* calc. for C₂₇H₄₁O₇¹⁰²Ru₂ [M+3MeO-4Cl]⁺: 681.0939; found: 681.0936.



Dichloro (ethyl 4-(*tert*-butyl)phenylacetate)ruthenium(II) dimer (177d)

To a solution of RuCl₃ hydrate (52.5 mg, 0.20 mmol) in EtOH (2.0 mL) was added dihydro 2-(4-(*tert*-butyl)phenyl)acetic acid (77.0 mg, 0.40 mmol, isomer not specified). The mixture was stirred overnight at r.t. The precipitate was filtered and washed with EtOH and hexane. Drying under vacuum gave the title compound as a red solid (29.2 mg, 0.04 mmol, 37%)

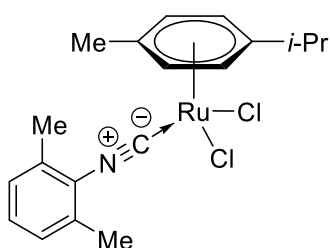
M.p.: > 200 °C (decomp.). **¹H-NMR** (400 MHz, CDCl₃) δ = 5.78 (d, J = 6.0 Hz, 2H), 5.44 (d, J = 6.0 Hz, 2H), 4.15 (q, J = 7.1 Hz, 2H), 3.57 (s, 2H), 1.42 (s, 9H), 1.26 (t, J = 7.1 Hz, 3H). **¹³C{¹H}-NMR** (101 MHz, CDCl₃) δ = 169.3 (C_q), 103.4 (C_q), 94.2 (C_q), 81.9 (CH), 79.6 (CH), 61.7 (CH₂), 39.5 (CH₂), 34.5 (C_q), 30.7 (CH₃), 14.3 (CH₃). **IR** (ATR): $\tilde{\nu}$ = 3060, 2960, 1728, 1464, 1369, 1248, 1138, 1022, 838, 666, 478 cm⁻¹. **MS** (ESI): m/z (relative intensity) = 741.1 (100) [M+2MeO-3Cl]⁺, 729.9 (1) [M]⁺. **HR-MS** (ESI): m/z calc. for C₃₀H₄₆O₆Cl¹⁰²Ru₂ [M+2MeO-3Cl]⁺: 741.1070; found: 741.1066.



Dichloro (*p*-cymene)(cyclohexylisocyanide)ruthenium(II) (178a)

The synthesis of the complex was adapted from from literature.^[288] To a solution of [Ru(*p*-cymene)Cl₂]₂ (61.3 mg, 0.10 mmol) in DCM (2.0 mL) was added cyclohexyl isocyanide (33.0 mg, 0.30 mmol). The mixture was stirred overnight at r.t. The solvent was removed under reduced pressure and hexane (2 mL) was added. The mixture was shaken vigorously. After separation and precipitation of the red oil, the colorless supernatant was removed with a pipette. The extraction step was repeated twice. Drying under vacuum gave the title compound as red solid (74.9 mg, 0.18 mmol, 90%)

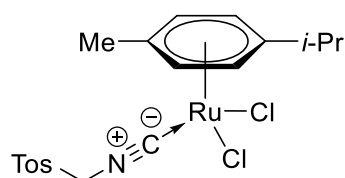
M.p.: 126–128 °C. **¹H-NMR** (400 MHz, CDCl₃) δ = 5.57 (d, J = 5.9 Hz, 2H), 5.40 (d, J = 5.9 Hz, 2H), 4.01 (dt, J = 8.7, 4.9 Hz, 1H), 2.86 (hept, J = 6.9 Hz, 1H), 2.29 (s, 3H), 2.03–1.89 (m, 2H), 1.85–1.73 (m, 4H), 1.53–1.34 (m, 4H), 1.31 (d, J = 6.9 Hz, 6H). **¹³C{¹H}-NMR** (101 MHz, CDCl₃) δ = 107.2 (C_q), 107.0 (C_q), 87.7 (CH), 87.5 (CH), 55.4 (CH), 32.8 (CH₂), 31.5 (CH), 25.0 (CH₂), 22.9 (CH₂), 22.7 (CH₃), 19.0 (CH₃). The signal of the isocyanide carbon is not well-resolved. **IR** (ATR): $\tilde{\nu}$ = 3057, 2934, 2862, 2192, 1450, 1362, 1323, 1030, 874, 660, 530 cm⁻¹. **MS** (ESI): m/z (relative intensity) = 380.1 (100) [M-Cl]⁺. **HR-MS** (ESI): m/z calc. for C₁₇H₂₅NCl¹⁰²Ru [M-Cl]⁺: 380.0719; found: 380.0719.



Dichloro (*p*-cymene)(2,6-dimethylphenylisocyanide)ruthenium(II) (178b)

The synthesis of the complex was adapted from literature.^[288] To a solution of [Ru(*p*-cymene)Cl₂]₂ (61.4 mg, 0.10 mmol) in DCM (2.0 mL) was added 2,6-dimethylphenyl isocyanide (39.8 mg, 0.30 mmol). The mixture was stirred overnight at r.t. The solvent was removed under reduced pressure and hexane (5 mL) was added. The red precipitate was filtered and washed with hexane. Drying under vacuum gave the title compound as a pale red solid (82.3 mg, 0.19 mmol, 94%)

M.p.: 150–151 °C. **¹H-NMR** (400 MHz, CDCl₃) δ = 7.17 (dd, J = 8.5, 6.6 Hz, 1H), 7.10 (d, J = 7.6 Hz, 2H), 5.70 (d, J = 6.0 Hz, 2H), 5.52 (d, J = 6.0 Hz, 2H), 2.94 (hept, J = 7.0 Hz, 1H), 2.48 (s, 6H), 2.36 (s, 3H), 1.34 (d, J = 6.9 Hz, 6H). **¹³C{¹H}-NMR** (101 MHz, CDCl₃) δ = 135.8 (C_q), 129.3 (CH), 128.0 (CH + C_q), 108.6 (C_q), 107.9 (C_q), 88.8 (CH), 88.3 (CH), 31.6 (CH), 22.7 (CH₃), 19.2 (CH₃), 19.1 (CH₃). The signal of the isocyanide carbon is not well resolved. **IR** (ATR): $\tilde{\nu}$ = 3050, 2962, 2925, 2872, 2157, 1470, 1380, 859, 785, 666, 508 cm⁻¹. **MS** (ESI): m/z (relative intensity) = 402.0 (100) [M-Cl]⁺, 437.0 (1) [M]⁺. **HR-MS** (ESI): m/z calc. for C₁₉H₂₃NCl¹⁰²Ru [M-Cl]⁺: 402.0563; found: 402.0563.



Dichloro (*p*-cymene)(*p*-toluenesulfonylmethylisocyanide)ruthenium(II) (178c)

The synthesis of the complex was adapted from literature.^[288] To a solution of [Ru(*p*-cymene)Cl₂]₂ (61.2 mg, 0.10 mmol) in DCM (2.0 mL) was added *p*-toluenesulfonylmethyl isocyanide (33.0 mg, 0.30 mmol). The mixture stirred overnight at r.t. The precipitate was filtered and washed with DCM. Drying under vacuum gave the title compound as a pale red solid (97.0 mg, 0.19 mmol, 95%)

M.p.: 178–180 °C. **¹H-NMR** (400 MHz, CDCl₃) δ = 7.90 (d, *J* = 7.6 Hz, 2H), 7.44 (d, *J* = 7.7 Hz, 2H), 5.74 (d, *J* = 5.9 Hz, 2H), 5.56 (d, *J* = 5.9 Hz, 2H), 4.97 (s, 2H), 2.96 (hept, *J* = 6.8 Hz, 1H), 2.46 (s, 3H), 2.33 (s, 3H), 1.33 (d, *J* = 6.8 Hz, 6H). **¹³C{¹H}-NMR** (101 MHz, CDCl₃) δ = 147.3 (C_q), 132.7 (C_q), 130.9 (CH), 129.3 (CH), 110.1 (C_q), 108.6 (C_q), 89.7 (CH), 89.5 (CH), 63.8 (CH₂), 31.4 (CH), 22.6 (CH₃), 22.0 (CH₃), 19.0 (CH₃). The signal of the isocyanide carbon is not well resolved. **IR** (ATR): $\tilde{\nu}$ = 3036, 2958, 2905, 2157, 1336, 1280, 1148, 1086, 898, 804, 734, 561, 512, 465 cm⁻¹. **MS** (ESI): *m/z* (relative intensity) = 524.0 (100) [M+Na]⁺, 466.0 (80) [M-Cl]⁺. **HR-MS** (ESI): *m/z* calc. for C₁₉H₂₃NO₂SCl¹⁰²RuNa [M+Na]⁺: 523.9768; found: 523.9768.

5.4.2 Electrolyte Activation Study

The conductivity was determined as an equivalent of the electrolysis rate of ferrocene under steady-state chronoamperometric conditions at a rotating ring disc electrode (RRDE).

Preparation of the electrolytes:

A uniform solid mixture of TBAPF₆ (3.875 g, 10.0 mmol) and ferrocene (93.0 mg, 0.50 mmol) was prepared (**EI-Fc**) by addition of Et₂O (20 mL) to the solids, followed by evaporation of the solvent and fine grinding.

An electrolyte (“polar”: **P-X**, “non-polar”: **NP-Y**) was prepared by addition of 2.00 mL of solvent to 79.4 mg of **EI-Fc** (0.20 mmol TBAPF₆ + 0.01 mmol ferrocene). Electrolytes of the following solvents were prepared: PGCC (**P-1**), THTD (**P-2**) and MeCN (**P-3**), PhMe (**NP-1**), *t*-AmOH (**NP-2**), 1,4-dioxane (**NP-3**) and PhOMe (**NP-4**).

Linear sweep voltammograms and chronoamperograms were recorded at 1000 rpm, with AgCl-coated silver wire as the pseudo-reference electrode and the RRDE being submerged approx. 1 mm below the electrolyte level. Prior to a measurement series of binary **P-X/NP-Y** mixtures, a positive linear sweep voltammogram of the respective **P-X/NP-Y** (1:3) sample was recorded. At the point, where steady state current was reached, 0.3 V was added to the respective voltage and the obtained value was applied for the chronoamperometric measurements (**Figure 5.4-1**).

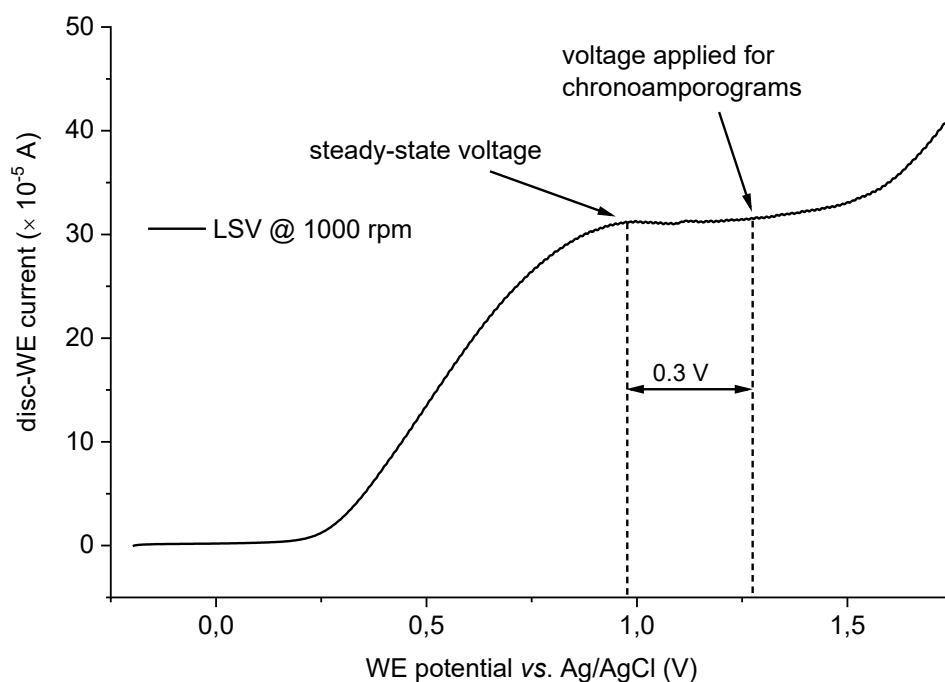


Figure 5.4-1 Representative LSV for chronoamperometry potential selection.

The measurement series of binary **P-X/NP-Y** mixtures started with the addition of **NP-Y** into the electrochemical cell and sonication for 1 min. Subsequently, the RRDE was placed into the electrolyte. The rotation of the RRDE prior to the measurement of each new composition was kept for 1 min to ensure mixing/equilibration. Three chronoamperograms of 10.0 s duration were recorded with a 1 min break in between for each composition, and the average WE current density values between 2.0 s and 10.0 s were taken (**Figure 5.4-2**) for one data point.

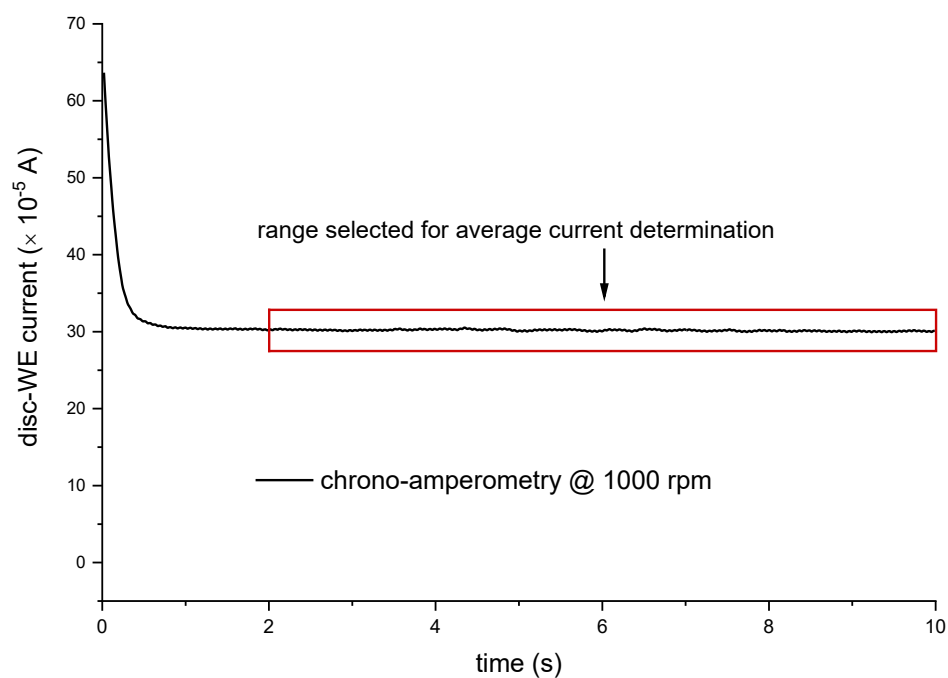


Figure 5.4-2 Representative chronoamperogram for average current (conductivity equivalent) determination.

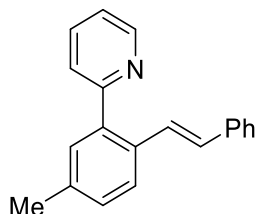
The **P-X/NP-Y** compositions were altered by direct injection of defined volumes Δ of **P-X** into the electrochemical cell to reach the desired volume percentage according to **Table 5.4-1**.

Table 5.4-1 Total added volume V_{add} and individual injection volumes Δ for the obtainment of a X -vol-% mixture of **P-X** and **NP-Y**, calculated for a starting volume of **NP-Y** $V_0 = 2.00$ mL.

X (%)	V_{add} (μL)	Δ (μL)	X (%)	V_{add} (μL)	Δ (μL)
0	0	0	16	381	55
2	41	41	18	439	58
4	83	42	20	500	61
6	128	45	25	667	167
8	174	46	30	857	190
10	222	48	40	1333	476
12	273	51	50	2000	667
14	326	53			

5.5 Rhoda-Electro-Catalyzed C–C Activation

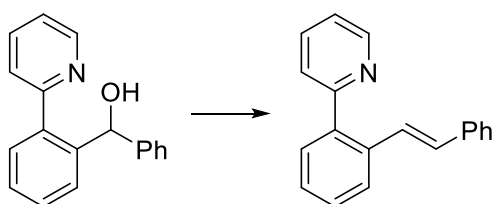
5.5.1 Characterization Data



(*E*)-2-(5-Methyl-2-styrylphenyl)pyridine (**52aa**)

The general procedure C was followed using **51a-I** (103 mg, 0.375 mmol) and **15a** (27 mg, 0.25 mmol) for 5 h. Purification by FCC (*n*-hexane/EtOAc = 14:1) yielded **52aa** (51 mg, 0.19 mmol, 75%) as a colorless oil.

¹H-NMR (600 MHz, CDCl₃): δ = 8.74 (d, *J* = 4.8 Hz, 1H), 7.71 (td, *J* = 7.7, 1.8 Hz, 1H), 7.65 (d, *J* = 8.0 Hz, 1H), 7.43 (d, *J* = 7.9 Hz, 1H), 7.39–7.34 (m, 3H), 7.31–7.16 (m, 6H), 7.01 (d, *J* = 16.1 Hz, 1H), 2.40 (s, 3H). ¹³C{¹H}-NMR (125 MHz, CDCl₃): δ = 159.0 (C_q), 149.6 (CH), 139.5 (C_q), 137.8 (C_q), 137.6 (C_q), 135.9 (CH), 132.9 (C_q), 130.8 (CH), 129.6 (CH), 129.3 (CH), 128.6 (CH), 127.5 (CH), 127.4 (CH), 126.6 (CH), 126.3 (CH), 125.2 (CH), 121.9 (CH), 21.4 (CH₃). IR (ATR): 3022, 1584, 1462, 963, 788, 750 cm⁻¹. MS (ESI) *m/z* (relative intensity): 272 (100) [M+H]⁺. HR-MS (ESI) *m/z* calc. for C₂₀H₁₈N [M+H]⁺: 272.1439, found: 272.1434. The analytical data correspond with those reported in the literature.^[102]

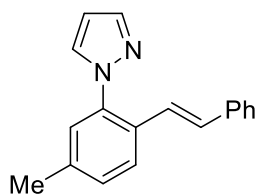


(*E*)-2-(2-Styrylphenyl)pyridine (**52ab**)

The general procedure C was followed using **51b-II** (98 mg, 0.375 mmol) and **15a** (26 mg, 0.25 mmol) for 4 h. Purification by FCC (*n*-hexane/EtOAc = 10:1) yielded **52ab** (50 mg, 0.19 mmol, 78%) as a colorless oil.

¹H-NMR (400 MHz, CDCl₃): δ = 8.75 (dt, *J* = 4.1, 1.2 Hz, 1H), 7.91–7.68 (m, 2H), 7.56 (dd, *J* = 7.6, 1.6 Hz, 1H), 7.50–7.34 (m, 5H), 7.34–7.16 (m, 5H), 7.05 (d, *J* = 16.2 Hz, 1H).

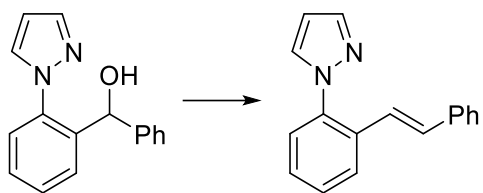
$^{13}\text{C}\{^1\text{H}\}$ -NMR (100 MHz, CDCl_3): δ = 158.8 (C_q), 149.5 (CH), 139.6 (C_q), 137.6 (C_q), 136.0 (CH), 135.7 (C_q), 130.2 (CH), 130.1 (CH), 128.6 (CH), 128.6 (CH), 127.6 (CH), 127.5 (CH), 127.5 (CH), 126.6 (CH), 126.2 (CH), 125.0 (CH), 121.8 (CH). IR (ATR): 3055, 3024, 1583, 1459, 1424, 1150, 1022, 961 cm^{-1} . MS (ESI) m/z (relative intensity): 280 (5) $[\text{M}+\text{Na}]^+$, 258 (100) $[\text{M}+\text{H}]^+$. HR-MS (ESI) m/z calc. for $\text{C}_{19}\text{H}_{16}\text{N}$ $[\text{M}+\text{H}]^+$: 258.1277, found: 258.1279. The analytical data correspond with those reported in the literature.^[102]



(E)-1-(5-Methyl-2-styrylphenyl)-1H-pyrazole (181aa)

The general procedure C was followed using **180a-I** (54 mg, 0.25 mmol) and **15a** (52 mg, 0.50 mmol) for 8 h. Purification by FCC (*n*-hexane/EtOAc = 20:1) yielded **181aa** (53 mg, 0.20 mmol, 82%) as a colorless oil.

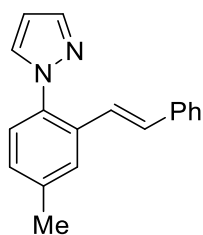
^1H -NMR (400 MHz, CDCl_3): δ = 7.76 (d, J = 1.8 Hz, 1H), 7.66–7.62 (m, 2H), 7.39–7.35 (m, 2H), 7.33–7.26 (m, 3H), 7.25–7.20 (m, 2H), 7.00 (d, J = 16.3 Hz, 1H), 6.91 (d, J = 16.3 Hz, 1H), 6.45 (dd, J = 2.4, 1.8 Hz, 1H), 2.39 (s, 3H). $^{13}\text{C}\{^1\text{H}\}$ -NMR (100 MHz, CDCl_3): δ = 140.6 (CH), 138.5 (C_q), 138.4 (C_q), 137.2 (C_q), 131.5 (CH), 130.3 (C_q), 130.0 (CH), 129.2 (CH), 128.6 (CH), 127.7 (CH), 126.8 (CH), 126.6 (CH), 126.4 (CH), 123.8 (CH), 106.4 (CH), 21.0 (CH_3). IR (ATR): 3050, 2981, 1597, 1516, 1264, 1098, 966 cm^{-1} . MS (ESI) m/z (relative intensity): 283 (40) $[\text{M}+\text{Na}]^+$, 261 (100) $[\text{M}+\text{H}]^+$. HR-MS (ESI) m/z calc. for $\text{C}_{18}\text{H}_{17}\text{O}_2$ $[\text{M}+\text{H}]^+$: 261.1386, found: 261.1384. The analytical data correspond with those reported in the literature.^[103]



(E)-1-(2-Styrylphenyl)-1H-pyrazole (181ab)

The general procedure C was followed using **180b-II** (94 mg, 0.375 mmol) and **15a** (26 mg, 0.25 mmol) for 4 h. Purification by FCC (*n*-hexane/EtOAc = 20:1) yielded **181ab** (44 mg, 0.18 mmol 72%) as a colorless oil.

¹H-NMR (600 MHz, CDCl₃): δ = 7.79–7.75 (m, 2H), 7.65 (d, J = 2.4 Hz, 1H), 7.44 (dd, J = 7.8, 1.5 Hz, 1H), 7.43–7.38 (m, 3H), 7.36 (td, J = 7.6, 1.5 Hz, 1H), 7.33–7.29 (m, 2H), 7.26–7.22 (m, 1H), 7.04 (d, J = 16.3 Hz, 1H), 6.95 (d, J = 16.3 Hz, 1H), 6.47 (dd, J = 2.1, 2.1 Hz, 1H). **¹³C{¹H}-NMR** (125 MHz, CDCl₃): δ = 140.7 (CH), 138.8 (C_q), 137.0 (C_q), 133.0 (C_q), 131.5 (CH), 131.2 (CH), 128.6 (CH), 128.4 (CH), 128.1 (CH), 127.9 (CH), 126.7 (CH), 126.6 (CH), 126.3 (CH), 123.9 (CH), 106.6 (CH). **IR** (ATR): 3045, 1599, 1517, 1495, 1393, 1265, 1044, 964 cm⁻¹. **MS** (ESI) m/z (relative intensity): 269 (45) [M+Na]⁺, 247 (100) [M+H]⁺. **HR-MS** (ESI) m/z calc. for C₁₇H₁₅N₂ [M+H]⁺: 247.1230, found: 247.1230. The analytical data correspond with those reported in the literature.^[102]

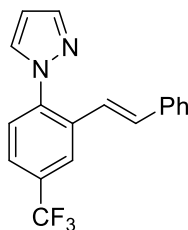


(E)-1-(4-Methyl-2-styrylphenyl)-1H-pyrazole (181ac)

The general procedure C was followed using **180c-I** (54 mg, 0.25 mmol) and **15a** (52 mg, 0.50 mmol) for 12 h. Purification by FCC (*n*-hexane/EtOAc = 20:1) yielded **181ac** (47.5 mg, 0.17 mmol, 71%) as a colorless oil.

¹H-NMR (400 MHz, CDCl₃): δ = 7.75 (d, J = 1.9 Hz, 1H), 7.61 (d, J = 2.4 Hz, 1H), 7.58–7.53 (m, 1H), 7.40–7.35 (m, 2H), 7.33–7.27 (m, 3H), 7.25–7.20 (m, 1H), 7.18–7.14 (m, 1H), 7.02 (d, J = 16.3 Hz, 1H), 6.89 (d, J = 16.3 Hz, 1H), 6.44 (dd, J = 2.4, 1.9 Hz, 1H), 2.44 (s, 3H). **¹³C{¹H}-NMR** (100 MHz, CDCl₃): δ = 140.5 (CH), 138.3 (C_q), 137.1 (C_q),

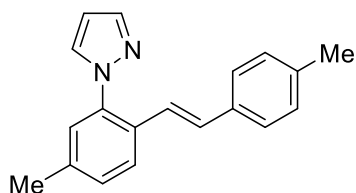
136.5 (C_q), 132.7 (C_q), 131.5 (CH), 130.9 (CH), 128.9 (CH), 128.6 (CH), 127.8 (CH), 126.9 (CH), 126.6 (CH), 126.2 (CH), 123.9 (CH), 106.4 (CH), 21.2 (CH₃). **IR** (ATR): 3025, 1598, 1517, 1498, 1393, 1265, 1044, 950 cm⁻¹. **MS** (ESI) *m/z* (relative intensity): 283 (50) [M+Na]⁺, 261 (100) [M+H]⁺. **HR-MS** (ESI) *m/z* calc. for C₁₈H₁₇N₂ [M+H]⁺: 261.1386, found: 261.1388.



(E)-1-[2-Styryl-5-(trifluoromethyl)phenyl]-1H-pyrazole (181ad)

The general procedure C was followed using **180d-I** (68 mg, 0.25 mmol) and **15a** (52 mg, 0.50 mmol) for 12 h. Purification by FCC (*n*-hexane/EtOAc = 20:1) yielded **181ad** (25 mg, 0.08 mmol, 32%) as a colorless oil.

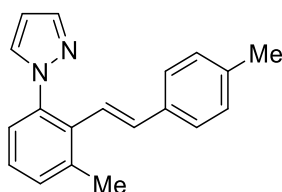
¹H-NMR (500 MHz, CDCl₃): δ = 8.01–7.96 (m, 1H), 7.81–7.78 (m, 1H), 7.70 (d, *J* = 2.4 Hz, 1H), 7.63–7.56 (m, 2H), 7.45–7.39 (m, 2H), 7.36–7.31 (m, 2H), 7.30–7.25 (m, 1H), 7.12 (d, *J* = 16.3 Hz, 1H), 7.01 (d, *J* = 16.3 Hz, 1H), 6.50 (dd, *J* = 2.1, 2.1 Hz, 1H). **¹³C{¹H}-NMR** (125 MHz, CDCl₃): δ = 141.5 (CH), 141.0 (C_q), 136.4 (C_q), 133.2 (C_q), 132.9 (CH), 131.5 (CH), 130.3 (q, ²*J*_{C-F} = 33.4 Hz, C_q), 128.8 (CH), 128.5 (CH), 126.9 (CH), 126.5 (CH), 124.7 (q, ³*J*_{C-F} = 3.6 Hz, CH), 124.0 (q, ³*J*_{C-F} = 3.8 Hz, CH), 123.8 (q, ¹*J*_{C-F} = 272.4 Hz, C_q), 122.9 (CH), 107.4 (CH). **¹⁹F{¹H}-NMR** (282 MHz, CDCl₃): δ = -62.6 (s). **IR** (ATR): 2958, 1765, 1732, 1486, 1365, 1125, 905 cm⁻¹. **MS** (ESI) *m/z* (relative intensity): 337 (100) [M+Na]⁺, 315 (80) [M+H]⁺. **HR-MS** (ESI) *m/z* calc. for C₁₈H₁₄F₃N₂ [M+H]⁺: 315.1104, found: 315.1106.



(E)-1-[5-Methyl-2-(4-methylstyryl)phenyl]-1H-pyrazole (181ba)

The general procedure C was followed using **181a-I** (81 mg, 0.375 mmol) and **15a** (30 mg, 0.25 mmol) for 5 h. Purification by FCC (*n*-hexane/EtOAc = 30:1) yielded **181ba** (49 mg, 0.18 mmol, 71%) as a white solid.

M. p.: 72–73 °C. **¹H-NMR** (400 MHz, CDCl₃): δ = 7.77 (d, *J* = 1.9 Hz, 1H), 7.67–7.63 (m, 2H), 7.30–7.27 (m, 3H), 7.22 (dd, *J* = 8.1, 1.9 Hz, 1H), 7.15–7.10 (m, 2H), 6.98 (d, *J* = 16.3 Hz, 1H), 6.86 (d, *J* = 16.3 Hz, 1H), 6.46 (dd, *J* = 2.4, 1.9 Hz, 1H), 2.40 (s, 3H), 2.34 (s, 3H). **¹³C{¹H}-NMR** (100 MHz, CDCl₃): δ = 140.7 (CH), 138.6 (C_q), 138.4 (C_q), 137.8 (C_q), 134.6 (C_q), 131.7 (CH), 130.5 (CH), 130.3 (C_q), 129.5 (CH), 129.3 (CH), 127.0 (CH), 126.7 (CH), 126.5 (CH), 123.0 (CH), 106.6 (CH), 21.4 (CH₃), 21.1 (CH₃). **IR** (ATR): 3023, 2917, 1515, 1455, 1037, 967, 950, 819, 799 cm⁻¹. **MS** (ESI) *m/z* (relative intensity): 297 (46) [M+Na]⁺, 275 (100) [M+H]⁺. **HR-MS** (ESI) *m/z* calc. for C₁₉H₁₉N₂ [M+H]⁺: 275.1543, found: 275.1543. The analytical data correspond with those reported in the literature.^[103]

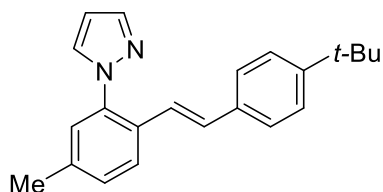


(E)-1-[3-Methyl-2-(4-methylstyryl)phenyl]-1H-pyrazole (181bg)

The general procedure C was followed using **180g-I** (27 mg, 0.125 mmol) and **15b** (74 mg, 0.625 mmol) for 8 h. Purification by FCC (*n*-hexane/EtOAc = 20:1) yielded **181bg** (21.2 mg, 0.15 mmol, 62%) as a colorless oil.

¹H-NMR (300 MHz, CDCl₃) δ = 7.72 (d, *J* = 1.8 Hz, 1H), 7.61 (d, *J* = 2.3 Hz, 1H), 7.37 – 7.22 (m, 5H), 7.14 (d, *J* = 8.0 Hz, 2H), 6.86 (d, *J* = 16.7 Hz, 1H), 6.38 (dd, *J* = 2.3, 1.8 Hz, 1H), 6.29 (d, *J* = 16.7 Hz, 1H), 2.51 (s, 3H), 2.36 (s, 3H). **¹³C{¹H}-NMR** (75 MHz, CDCl₃) δ = 140.1 (CH), 139.3 (C_q), 137.8 (C_q), 137.6 (C_q), 134.5 (C_q), 134.4 (CH), 133.3 (C_q), 131.5 (CH), 130.5 (CH), 129.3 (CH), 127.2 (CH), 126.3 (CH), 124.5 (CH), 122.2 (CH),

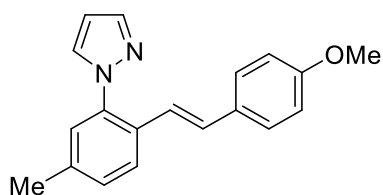
106.3 (CH), 21.2 (CH₃), 21.2 (CH₃). **IR** (ATR): 3023, 2920, 1514, 1474, 1394, 1329, 1192, 1045 cm⁻¹. **MS** (ESI) *m/z* (relative intensity) 297 (30) [M+Na]⁺, 275 (100) [M+H]⁺. **HR-MS** (ESI) *m/z* calc. for C₁₉H₁₉N₂ [M+H]⁺: 275.1543, found: 275.1544.



(E)-1-(2-[4-(tert-Butyl)styryl]-5-methylphenyl)-1H-pyrazole (181ca)

The general procedure C was followed using **180a-I** (54 mg, 0.25 mmol) and **15c** (73 mg, 0.50 mmol) for 9 h. Purification by FCC (*n*-hexane/EtOAc = 20:1) yielded **181ca** (58 mg, 0.18 mmol, 73%) as a colorless oil.

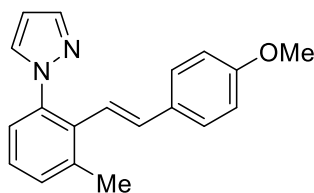
¹H-NMR (300 MHz, CDCl₃): δ = 7.83–7.76 (m, 1H), 7.72–7.63 (m, 2H), 7.41–7.22 (m, 6H), 7.03 (d, *J* = 16.3 Hz, 1H), 6.90 (d, *J* = 16.3 Hz, 1H), 6.48 (dd, *J* = 2.1, 2.1 Hz, 1H), 2.43 (s, 3H), 1.35 (s, 9H). **¹³C{¹H}-NMR** (75 MHz, CDCl₃): δ = 151.0 (C_q), 140.6 (CH), 138.5 (C_q), 138.3 (C_q), 134.5 (C_q), 131.6 (CH), 130.2 (CH), 130.2 (C_q), 129.2 (CH), 126.8 (CH), 126.4 (CH), 126.4 (CH), 125.6 (CH), 123.1 (CH), 106.4 (CH), 34.6 (C_q), 31.3 (CH₃), 21.0 (CH₃). **IR** (ATR): 3030, 2960, 2904, 1614, 1516, 1459, 1363, 1266, 1097, 967 cm⁻¹. **MS** (ESI) *m/z* (relative intensity): 339 (95) [M+Na]⁺, 317 (100) [M+H]⁺. **HR-MS** (ESI) *m/z* calc. for C₂₂H₂₅N₂ [M+H]⁺: 317.2012, found: 317.2013. The analytical data correspond with those reported in the literature.^[103]



(E)-1-(2-(4-methoxystyryl)-5-methylphenyl)-1H-pyrazole (181da)

The general procedure C was followed using **180a-I** (54 mg, 0.25 mmol) and **15d** (67 mg, 0.5 mmol) for 6 h. Purification by FCC (*n*-hexane/EtOAc = 10:1) yielded **181da** (42 mg, 0.14 mmol, 58%) as a white solid.

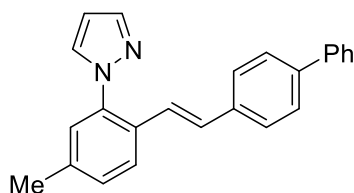
M. p.: 72–74 °C. **¹H-NMR** (400 MHz, CDCl₃): δ = 7.75 (d, J = 1.9 Hz, 1H), 7.65–7.58 (m, 2H), 7.33–7.27 (m, 2H), 7.26–7.23 (m, 1H), 7.22–7.18 (m, 1H), 6.94 (d, J = 16.2 Hz, 1H), 6.86–6.80 (m, 2H), 6.75 (d, J = 16.3 Hz, 1H), 6.44 (dd, J = 2.4, 1.9 Hz, 1H), 3.79 (s, 3H), 2.38 (s, 3H). **¹³C{¹H}-NMR** (100 MHz, CDCl₃): δ = 159.4 (C_q), 140.5 (CH), 138.3 (C_q), 138.0 (C_q), 131.5 (CH), 130.3 (C_q), 130.0 (C_q), 129.8 (CH), 129.2 (CH), 127.8 (CH), 126.8 (CH), 126.1 (CH), 121.6 (CH), 114.1 (CH), 106.4 (CH), 55.3 (CH₃), 20.9 (CH₃). **IR** (ATR): 3033, 2921, 1576, 1512, 1458, 1249, 1174, 1034, 951 cm⁻¹. **MS** (ESI) m/z (relative intensity): 313 (70) [M+Na]⁺, 291 (100) [M+H]⁺. **HR-MS** (ESI) m/z calc. for C₁₉H₁₉N₂O [M+H]⁺: 291.1492, found: 291.1491.



(E)-1-[2-(4-Methoxystyryl)-3-methylphenyl]-1H-pyrazole (181dg)

The general procedure C was followed using **180g-I** (27 mg, 0.125 mmol) and **15d** (84 mg, 0.625 mmol) for 8 h. Purification by FCC (*n*-hexane/EtOAc = 10:1) yielded **181dg** (20 mg, 0.14 mmol, 55%) as a colorless oil.

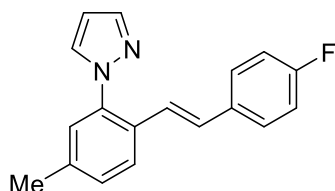
¹H-NMR (600 MHz, CDCl₃) δ = 7.70 (d, J = 1.9 Hz, 1H), 7.58 (d, J = 2.4 Hz, 1H), 7.34–7.30 (m, 1H), 7.29–7.27 (m, 1H), 7.26–7.23 (m, 3H), 6.86–6.83 (m, 2H), 6.74 (d, J = 16.7 Hz, 1H), 6.36 (dd, J = 2.4, 1.9 Hz, 1H), 6.23 (d, J = 16.7 Hz, 1H), 3.80 (s, 3H), 2.48 (s, 3H). **¹³C{¹H}-NMR** (75 MHz, CDCl₃) δ = 159.5 (C_q), 140.1 (CH), 139.2 (C_q), 137.6 (C_q), 133.9 (CH), 133.4 (C_q), 131.5 (CH), 130.6 (CH), 130.1 (C_q), 127.6 (CH), 127.0 (CH), 124.6 (CH), 121.0 (CH), 114.0 (CH), 106.3 (CH), 55.3 (CH₃), 21.2 (CH₃). **IR** (ATR): 2955, 2835, 1606, 1510, 1473, 1393, 1250, 1174, 1033, 972 cm⁻¹. **MS** (ESI) m/z (relative intensity) 313 (20) [M+Na]⁺, 291 (100) [M+H]⁺. **HR-MS** (ESI) m/z calc. for C₁₉H₁₉N₂O [M+H]⁺: 291.1492, found: 291.1491. The analytical data correspond with those reported in the literature.^[281]



(E)-1-(2-[2-([1,1'-Biphenyl]-4-yl)vinyl]-5-methylphenyl)-1H-pyrazole (181ea)

The general procedure C was followed using **180a-I** (81 mg, 0.375 mmol) and **15e** (45 mg, 0.25 mmol) for 6 h. Purification by FCC (*n*-hexane/EtOAc = 20:1) yielded **181ea** (60.5 mg, 0.18 mmol, 72%) as a white solid.

M. p.: 148–150 °C. **¹H-NMR** (400 MHz, CDCl₃): δ = 7.78 (d, *J* = 1.8 Hz, 1H), 7.69–7.64 (m, 2H), 7.61–7.53 (m, 4H), 7.47–7.39 (m, 4H), 7.36–7.31 (m, 1H), 7.29–7.26 (m, 1H), 7.26–7.21 (m, 1H), 7.03 (d, *J* = 16.3 Hz, 1H), 6.95 (d, *J* = 16.3 Hz, 1H), 6.50–6.44 (m, 1H), 2.40 (s, 3H). **¹³C{¹H}-NMR** (100 MHz, CDCl₃) δ = 140.6 (CH), 140.6 (C_q), 140.5 (C_q), 138.6 (C_q), 138.5 (C_q), 136.2 (C_q), 131.5 (CH), 130.0 (C_q), 129.8 (CH), 129.2 (CH), 128.8 (CH), 127.3 (CH), 127.3 (CH), 127.0 (CH), 126.9 (CH), 126.8 (CH), 126.4 (CH), 123.9 (CH), 106.5 (CH), 21.0 (CH₃). **IR** (ATR): 3053, 3032, 1614, 1599, 1518, 1486, 1329, 1264, 1044, 968 cm⁻¹. **MS** (ESI) *m/z* (relative intensity): 359 (90) [M+Na]⁺, 337 (100) [M+H]⁺. **HR-MS** (ESI) *m/z* calc. for C₂₄H₂₁N₂ [M+H]⁺: 337.1699, found: 337.1701.

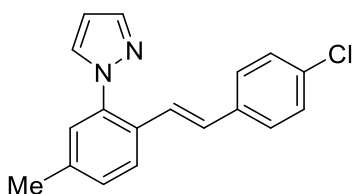


(E)-1-[2-(4-Fluorostyryl)-5-methylphenyl]-1H-pyrazole (181fa)

The general procedure C was followed using **180a-I** (54 mg, 0.25 mmol) and **15f** (61 mg, 0.50 mmol) for 8 h. Purification by FCC (*n*-hexane/EtOAc = 20:1) yielded **181fa** (43 mg, 0.15 mmol, 62%) as a colorless oil.

¹H-NMR (400 MHz, CDCl₃): δ = 7.75 (d, *J* = 1.8 Hz, 1H), 7.65–7.59 (m, 2H), 7.36–7.29 (m, 2H), 7.26–7.19 (m, 2H), 7.03–6.90 (m, 3H), 6.80 (d, *J* = 16.2 Hz, 1H), 6.45 (dd, *J* = 2.1, 2.1 Hz, 1H), 2.39 (s, 3H). **¹³C{¹H}-NMR** (100 MHz, CDCl₃) δ = 162.4 (d, ¹*J*_{C-F} = 247.5 Hz, C_q), 140.6 (CH), 138.5 (C_q), 138.5 (C_q), 133.4 (d, ⁴*J*_{C-F} = 3.3 Hz, C_q), 131.4 (CH), 129.9 (C_q), 129.3 (CH), 129.0 (CH), 128.1 (d, ³*J*_{C-F} = 8.0 Hz, CH), 126.9 (CH), 126.3 (CH), 123.6 (CH), 115.6 (d, ²*J*_{C-F} = 21.7 Hz, CH), 106.5 (CH), 21.0 (CH₃). **¹⁹F-NMR** (376 MHz,

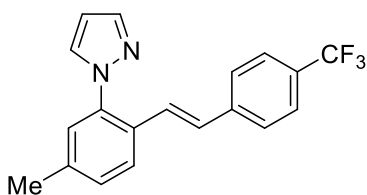
CDCl₃): $\delta = -113.9$ (s). **IR** (ATR): 3040, 2951, 1600, 1509, 1457, 1228, 1157, 1042, 951 cm⁻¹. **MS** (ESI) m/z (relative intensity): 301 (10) [M+Na]⁺, 279 (100) [M+H]⁺. **HR-MS** (ESI) m/z calc. for C₁₈H₁₆FN₂ [M+H]⁺: 279.1292, found: 279.1290. The analytical data correspond with those reported in the literature.^[103]



(E)-1-[5-Methyl-2-(4-chlorostyryl)phenyl]-1H-pyrazole (181ga)

The general procedure C was followed using **180a-I** (81 mg, 0.375 mmol) and **15g** (35 mg, 0.25 mmol) for 5 h. Purification by FCC (*n*-hexane/EtOAc = 14:1) yielded **181ga** (50 mg, 0.17 mmol, 68%) as a yellow solid.

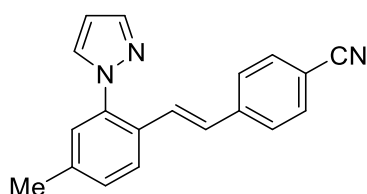
M. p.: 78–79 °C. **¹H-NMR** (400 MHz, CDCl₃): $\delta = 7.76$ (d, $J = 1.9$ Hz, 1H), 7.62 (d, $J = 8.0$ Hz, 1H), 7.62 (d, $J = 2.4$ Hz, 1H), 7.29–7.23 (m, 5H), 7.21 (dd, $J = 8.0, 1.9$ Hz, 1H), 6.92 (d, $J = 16.3$ Hz, 1H), 6.87 (d, $J = 16.3$ Hz, 1H), 6.45 (dd, $J = 2.4, 1.9$ Hz, 1H), 2.38 (s, 3H). **¹³C{¹H}-NMR** (100 MHz, CDCl₃): $\delta = 140.8$ (CH), 138.8 (C_q), 138.7 (C_q), 135.8 (C_q), 133.4 (C_q), 131.5 (CH), 129.9 (C_q), 129.4 (CH), 129.0 (CH), 128.9 (CH), 127.8 (CH), 127.0 (CH), 126.5 (CH), 124.6 (CH), 106.7 (CH), 21.1 (CH₃). **IR** (ATR): 3110, 2921, 1507, 1392, 953, 823, 763, 518 cm⁻¹. **MS** (ESI) m/z (relative intensity): 317 (50) [M+Na]⁺ (³⁵Cl), 295 (100) [M+H]⁺ (³⁵Cl). **HR-MS** (ESI) m/z calc. for C₁₈H₁₆N₂³⁵Cl [M+H]⁺: 295.1002, found: 295.0997. The analytical data correspond with those reported in the literature.^[102]



(E)-1-[5-Methyl-2-[4-(trifluoromethyl)styryl]phenyl]-1H-pyrazole (181ha)

The general procedure C was followed using **180a-I** (54 mg, 0.25 mmol) and **15h** (86 mg, 0.50 mmol) for 9 h. Purification by FCC (*n*-hexane/EtOAc = 20:1) yielded **181ha** (62 mg, 0.19 mmol, 76%) as a colorless oil.

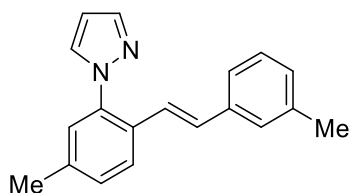
¹H-NMR (400 MHz, CDCl₃): δ = 7.77 (d, J = 1.9 Hz, 1H), 7.67–7.61 (m, 2H), 7.56–7.51 (m, 2H), 7.47–7.41 (m, 2H), 7.28–7.21 (m, 2H), 7.07–6.97 (m, 2H), 6.46 (dd, J = 2.4, 1.9 Hz, 1H), 2.40 (s, 3H). **¹³C{¹H}-NMR** (100 MHz, CDCl₃): δ = 140.8 (CH), 140.7 (C_q), 139.2 (C_q), 138.8 (C_q), 131.4 (CH), 129.4 (C_q), 129.3 (CH), 129.3 (q, $^2J_{C-F}$ = 32.4 Hz, C_q), 128.6 (CH), 126.9 (CH), 126.6 (CH), 126.5 (CH), 126.4 (CH), 125.5 (q, $^3J_{C-F}$ = 3.9 Hz, CH), 124.2 (q, $^1J_{C-F}$ = 271.7 Hz, C_q), 106.6 (CH), 21.0 (CH₃). **¹⁹F-NMR** (376 MHz, CDCl₃): δ = –62.5 (s). **IR** (ATR): 3045, 2925, 1612, 1517, 1322, 1163, 1120, 1066, 967 cm⁻¹. **MS** (ESI) m/z (relative intensity): 351 (30) [M+Na]⁺, 329 (100) [M+H]⁺. **HR-MS** (ESI) m/z calc. for C₁₉H₁₆F₃N₂ [M+H]⁺: 329.1260, found: 329.1262. The analytical data correspond with those reported in the literature.^[103]



(E)-1-[5-Methyl-2-(4-cyanostyryl)phenyl]-1H-pyrazole (181ia)

The general procedure C was followed using **180a-I** (81 mg, 0.375 mmol) and **15i** (33 mg, 0.25 mmol) for 5 h. Purification by FCC (*n*-hexane/EtOAc = 7:1) yielded **181ia** (51 mg, 0.18 mmol, 71%) as colorless needles.

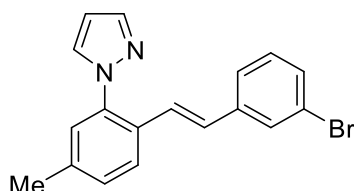
M. p.: 151–152 °C. **¹H-NMR** (300 MHz, CDCl₃): δ = 7.80 (d, J = 1.8 Hz, 1H), 7.68 (d, J = 8.7 Hz, 1H), 7.66 (d, J = 2.5 Hz, 1H), 7.59 (d, J = 8.4 Hz, 2H), 7.45 (d, J = 8.4 Hz, 2H), 7.34–7.22 (m, 2H), 7.08 (d, J = 16.3 Hz, 1H), 6.98 (d, J = 16.3 Hz, 1H), 6.50 (dd, J = 2.1, 2.1 Hz, 1H), 2.43 (s, 3H). **¹³C{¹H}-NMR** (125 MHz, CDCl₃): δ = 141.8 (C_q), 141.0 (CH), 139.7 (C_q), 139.0 (C_q), 132.5 (CH), 131.4 (CH), 129.5 (CH), 129.3 (C_q), 128.2 (CH), 127.8 (CH), 127.0 (CH), 127.0 (CH), 126.6 (CH), 119.0 (C_q), 110.8 (C_q), 106.9 (CH), 21.3 (CH₃). **IR** (ATR): 3108, 2223, 1598, 1334, 956, 822 cm⁻¹. **MS** (ESI) m/z (relative intensity): 308 (100) [M+Na]⁺, 286 (64) [M+H]⁺. **HR-MS** (ESI) m/z calc. for C₁₉H₁₆N₃ [M+H]⁺: 286.1344, found: 286.1339.



(E)-1-[5-methyl-2-(4-methylstyryl)phenyl]-1H-pyrazole (181ja)

The general procedure C was followed using **180a-I** (81 mg, 0.375 mmol) and **15j** (30 mg, 0.25 mmol) for 5 h. Purification by FCC (*n*-hexane/EtOAc = 30:1) and GPC (CHCl₃) yielded **181ja** (43 mg, 0.15 mmol, 62%) as a yellow oil.

¹H-NMR (300 MHz, CDCl₃): δ = 7.79 (d, *J* = 1.9 Hz, 1H), 7.70–7.61 (m, 2H), 7.34–7.26 (m, 1H), 7.26–7.18 (m, 4H), 7.11–7.05 (m, 1H), 7.00 (d, *J* = 16.3 Hz, 1H), 6.92 (d, *J* = 16.3 Hz, 1H), 6.48 (dd, *J* = 2.4, 1.8 Hz, 1H), 2.42 (s, 3H), 2.36 (s, 3H). **¹³C{¹H}-NMR** (125 MHz, CDCl₃): δ = 140.6 (CH), 138.6 (C_q), 138.4 (C_q), 138.2 (C_q), 137.2 (C_q), 131.6 (CH), 130.6 (CH), 130.1 (C_q), 129.2 (CH), 128.6 (CH), 128.6 (CH), 127.4 (CH), 126.8 (CH), 126.5 (CH), 123.7 (CH), 123.7 (CH), 106.5 (CH), 21.6 (CH₃), 21.2 (CH₃). **IR** (ATR): 3030, 2918, 1515, 1456, 1038, 951, 752, 690 cm⁻¹. **MS** (ESI) *m/z* (relative intensity): 297 (70) [M+Na]⁺, 275 (100) [M+H]⁺. **HR-MS** (ESI) *m/z* calc. for C₁₉H₁₉N₂ [M+H]⁺: 275.1543, found: 275.1543.

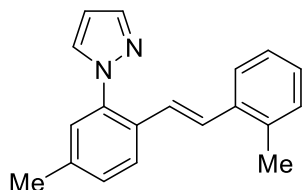


(E)-1-[5-Methyl-2-(3-bromostyryl)phenyl]-1H-pyrazole (181ka)

The general procedure C was followed using **180a-I** (81 mg, 0.375 mmol) and **15k** (46 mg, 0.25 mmol) for 5 h. Purification by FCC (*n*-hexane/EtOAc = 30:1) yielded **181ka** (79 mg, 0.23 mmol, 93%) as a yellow oil.

¹H-NMR (400 MHz, CDCl₃): δ = 7.79 (d, *J* = 1.9 Hz, 1H), 7.65–7.61 (m, 2H), 7.52–7.49 (m, 1H), 7.37–7.33 (m, 1H), 7.31–7.26 (m, 2H), 7.25–7.21 (m, 1H), 7.16 (t, *J* = 7.8, 1H), 6.94 (d, *J* = 16.3 Hz, 1H), 6.88 (d, *J* = 16.3 Hz, 1H), 6.48 (dd, *J* = 2.4, 1.9 Hz, 1H), 2.41 (s, 3H). **¹³C{¹H}-NMR** (100 MHz, CDCl₃): δ = 140.9 (CH), 139.5 (C_q), 139.0 (C_q), 138.8 (C_q), 131.5 (CH), 130.6 (CH), 130.2 (CH), 129.6 (C_q), 129.6 (CH), 129.4 (CH), 128.8 (CH),

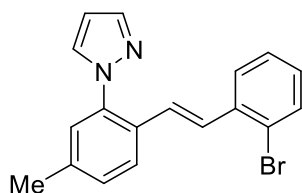
126.9 (CH), 126.6 (CH), 125.5 (CH), 125.1 (CH), 122.9 (C_q), 106.8 (CH), 21.1 (CH₃). **IR** (ATR): 3055, 2919, 1515, 1041, 950, 813, 750, 730, 677 cm⁻¹. **MS** (ESI) *m/z* (relative intensity): 363 (100) [M+Na]⁺ (⁸¹Br), 361 (100) [M+Na]⁺ (⁷⁹Br), 341 (65) [M+H]⁺ (⁸¹Br), 339 (65) [M+H]⁺ (⁷⁹Br). **HR-MS** (ESI) *m/z* calc. for C₁₈H₁₆N₂⁸¹Br [M+H]⁺: 341.0472, found: 341.0471, C₁₈H₁₆N₂⁷⁹Br [M+H]⁺: 339.0491, found: 339.0491.



(E)-1-[5-Methyl-2-(3-methylstyryl)phenyl]-1H-pyrazole (181la)

The general procedure C was followed using **180a-I** (81 mg, 0.375 mmol) and **2I** (30 mg, 0.25 mmol) for 5 h. Purification by FCC (*n*-hexane/EtOAc = 30:1) and GPC (CHCl₃) yielded **181la** (35 mg, 0.13 mmol, 51%) as a yellow oil.

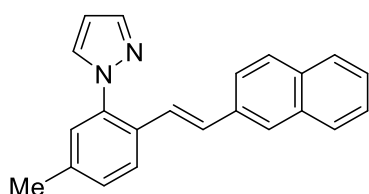
¹H-NMR (500 MHz, CDCl₃): δ = 7.76 (d, *J* = 1.9 Hz, 1H), 7.68–7.64 (m, 2H), 7.44–7.37 (m, 1H), 7.31–7.28 (m, 1H), 7.27–7.12 (m, 5H), 6.82 (d, *J* = 16.1 Hz, 1H), 6.45 (dd, *J* = 2.4, 1.9 Hz, 1H), 2.42 (s, 3H), 2.41 (s, 3H). **¹³C{¹H}-NMR** (125 MHz, CDCl₃): δ = 140.7 (CH), 138.7 (C_q), 138.5 (C_q), 136.2 (C_q), 135.9 (C_q), 131.5 (CH), 130.5 (C_q), 130.4 (CH), 129.3 (CH), 128.3 (CH), 127.7 (CH), 127.0 (CH), 126.8 (CH), 126.2 (CH), 125.6 (CH), 125.2 (CH), 106.6 (CH), 21.2 (CH₃), 20.1 (CH₃). **IR** (ATR): 3403, 2956, 1516, 1402, 1037, 950, 749, 618, 448 cm⁻¹. **MS** (ESI) *m/z* (relative intensity): 275 (100) [M+H]⁺, 297 (78) [M+Na]⁺. **HR-MS** (ESI) *m/z* calc. for C₁₉H₁₉N₂ [M+H]⁺: 275.1543, found: 275.1543. The analytical data correspond with those reported in the literature.^[103]



(E)-1-[5-methyl-2-(2-bromostyryl)phenyl]-1H-pyrazole (181ma)

The general procedure C was followed using **180a-I** (81 mg, 0.375 mmol) and **15m** (46 mg, 0.25 mmol) for 5 h. Purification by FCC (*n*-hexane/EtOAc = 30:1) yielded **181ma** (55 mg, 0.16 mmol, 64%) as a yellow oil.

¹H-NMR (400 MHz, CDCl₃): δ = 7.77 (d, *J* = 1.9 Hz, 1H), 7.72 (d, *J* = 7.9 Hz, 1H), 7.65 (d, *J* = 2.4 Hz, 1H), 7.56 (dd, *J* = 8.0, 1.3 Hz, 1H), 7.46 (dd, *J* = 7.9, 1.7 Hz, 1H), 7.40 (d, *J* = 16.2 Hz, 1H), 7.29–7.21 (m, 3H), 7.09 (ddd, *J* = 8.0, 7.3, 1.7 Hz, 1H), 6.88 (d, *J* = 16.2 Hz, 1H), 6.46 (dd, *J* = 2.4, 1.9 Hz, 1H), 2.42 (s, 3H). **¹³C{¹H}-NMR** (100 MHz, CDCl₃): δ = 140.9 (CH), 139.1 (C_q), 138.9 (C_q), 137.1 (C_q), 133.1 (CH), 131.6 (CH), 129.8 (C_q), 129.4 (CH), 129.0 (CH), 129.0 (CH), 127.7 (CH), 126.9 (CH), 126.9 (CH), 126.9 (CH), 126.7 (CH), 124.2 (C_q), 106.7 (CH), 21.2 (CH₃). **IR** (ATR): 3053, 2967, 1736, 1515, 1462, 1043, 1022, 811, 752 cm⁻¹. **MS** (EI) *m/z* (relative intensity): 363 (100) [M+Na]⁺ (⁸¹Br), 361 (100) [M+Na]⁺ (⁷⁹Br), 341 (40) [M+H]⁺ (⁸¹Br), 339 (40) [M+H]⁺ (⁷⁹Br). **HR-MS** (ESI) *m/z* calc. for C₁₈H₁₆N₂⁸¹Br [M+H]⁺: 341.0472, found: 341.0472, C₁₈H₁₆N₂⁷⁹Br [M+H]⁺: 339.0491, found: 339.0489.

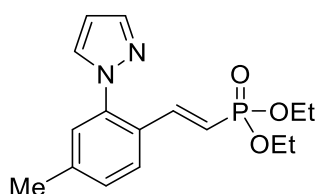


(E)-1-[5-methyl-2-[2-(naphthalen-2-yl)vinyl]phenyl]-1H-pyrazole (181na)

The general procedure C was followed using **180a-I** (81 mg, 0.375 mmol) and **15n** (39 mg, 0.25 mmol) for 5 h. Purification by FCC (*n*-hexane/EtOAc = 20:1) yielded **181na** (66 mg, 0.21 mmol, 85%) as a yellow solid.

M. p.: 99–101 °C. **¹H-NMR** (400 MHz, CDCl₃): δ = 7.84–7.75 (m, 5H), 7.72 (d, *J* = 8.0 Hz, 1H), 7.69 (d, *J* = 2.3 Hz, 1H), 7.57 (dd, *J* = 8.8, 1.7 Hz, 1H), 7.52–7.40 (m, 2H), 7.34–7.28 (m, 1H), 7.26 (dd, *J* = 8.0, 1.9 Hz, 1H), 7.18 (d, *J* = 16.3 Hz, 1H), 7.06 (d, *J* = 16.3

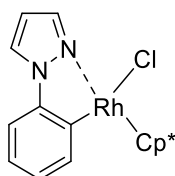
Hz, 1H), 6.50 (dd, $J = 2.4, 1.9$ Hz, 1H), 2.43 (s, 3H). $^{13}\text{C}\{^1\text{H}\}$ -NMR (100 MHz, CDCl_3): $\delta = 140.8$ (CH), 138.8 (C_q), 138.6 (C_q), 134.8 (C_q), 133.7 (C_q), 133.2 (C_q), 131.7 (CH), 130.6 (CH), 130.2 (C_q), 129.4 (CH), 128.4 (CH), 128.1 (CH), 127.8 (CH), 127.0 (CH), 126.9 (CH), 126.5 (CH), 126.4 (CH), 126.1 (CH), 124.3 (CH), 123.6 (CH), 106.7 (CH), 21.2 (CH_3). IR (ATR): 3054, 1513, 1390, 1042, 949, 811, 742 cm^{-1} . MS (ESI) m/z (relative intensity): 311 (100) $[\text{M}+\text{H}]^+$, 333 (65) $[\text{M}+\text{Na}]^+$. HR-MS (ESI) m/z calc. for $\text{C}_{22}\text{H}_{19}\text{N}_2$ $[\text{M}+\text{H}]^+$: 311.1548, found: 311.1543.



Diethyl (*E*)-[4-methyl-2-(1*H*-pyrazol-1-yl)styryl]phosphonate (**181pa**)

The general procedure C was followed using **180a-I** (81 mg, 0.375 mmol) and **15p** (41 mg, 0.25 mmol) for 5 h. Purification by FCC (EtOAc) yielded **181pa** (53 mg, 0.16 mmol, 66%) as a yellow oil.

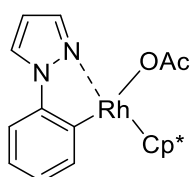
^1H -NMR (400 MHz, CDCl_3): $\delta = 7.70$ (d, $J = 1.9$ Hz, 1H), 7.57 (d, $J = 2.4$ Hz, 1H), 7.55 (d, $J = 8.0$, 1H), 7.34–7.19 (m, 3H), 6.44 (dd, $J = 2.4, 1.9$ Hz, 1H), 6.11 (dd, $J = 18.4, 17.6$ Hz, 1H), 4.11–3.99 (m, 4H), 2.38 (s, 3H), 1.28 (t, $J = 7.1$ Hz, 6H). $^{13}\text{C}\{^1\text{H}\}$ -NMR (100 MHz, CDCl_3): $\delta = 143.5$ (d, $^2J_{\text{C-P}} = 7.6$ Hz, CH), 141.3 (C_q), 141.1 (CH), 139.5 (C_q), 131.3 (CH), 129.4 (CH), 127.8 (d, $^3J_{\text{C-P}} = 23.5$ Hz, C_q), 127.1 (d, $^1J_{\text{C-P}} = 42.8$ Hz, CH), 116.9 (CH), 115.0 (CH), 107.1 (CH), 62.0 (d, $^2J_{\text{C-P}} = 5.6$ Hz, CH_2), 21.2 (CH_3), 16.4 (d, $^3J_{\text{C-P}} = 6.5$ Hz, CH_3). ^{31}P -NMR (162 MHz, CDCl_3) $\delta = 18.45$. IR (ATR): 3404, 2979, 1615, 1245, 1020, 948 cm^{-1} . MS (ESI) m/z (relative intensity): 321 (30) $[\text{M}+\text{H}]^+$, 343 (100) $[\text{M}+\text{Na}]^+$. HR-MS (ESI) m/z calc. for $\text{C}_{16}\text{H}_{22}\text{N}_2\text{O}_3\text{P}$ $[\text{M}+\text{H}]^+$: 321.1368, found: 321.1363.



[2-(1*H*-Pyrazol-1-yl)phenyl](pentamethylcyclopentadienyl)rhodium(III) chloride (190b-I)

[Cp*RhCl₂]₂ (37.1 mg, 0.06 mmol), 1-phenylpyrazole **148b-V** (26 mg, 0.18 mmol) and NaOAc (15 mg, 0.18 mmol) were stirred in DCM (6.0 mL, 0.1 M) for 6 h at r.t. The mixture was filtered through celite and concentrated *in vacuo*. Precipitation occurred upon addition of EtOAc (2 mL). The mixture was diluted with *n*-hexane (4 mL), and the solid was filtered and washed with *n*-hexane. **190b-I** was obtained as an orange solid (42 mg, 0.21 mmol, 84%).

¹H-NMR (300 MHz, CDCl₃) δ = 7.96 (d, *J* = 2.7 Hz, 1H), 7.82 (d, *J* = 2.1 Hz, 1H), 7.77 (dd, *J* = 7.4, 1.3 Hz, 1H), 7.22–7.12 (m, 2H), 7.06 (td, *J* = 7.4, 1.4 Hz, 1H), 6.52 (dd, *J* = 2.5, 2.5 Hz, 1H), 1.69 (s, 15H). ¹³C{¹H}-NMR (125 MHz, CDCl₃) δ = 159.3 (d, ²*J*_{C-Rh} = 32.4 Hz, C_q), 141.9 (C_q), 139.0 (CH), 137.6 (CH), 127.1 (CH), 125.1 (CH), 123.4 (CH), 111.1 (CH), 108.1 (CH), 95.8 (d, ²*J*_{C-Rh} = 6.7 Hz, C_q), 9.4 (CH₃). IR (ATR): 3083, 2918, 1475, 1405, 1071, 1024, 764, 390 cm⁻¹. MS (EI) *m/z* (relative intensity): 416 (20) [M]⁺, 381 (100) [M-Cl]⁺. HR-MS (ESI) *m/z* calc. for C₁₉H₂₂N₂Rh [M-Cl]⁺: 381.0838, found: 381.0833. The analytical data correspond with those reported in the literature.^[289]

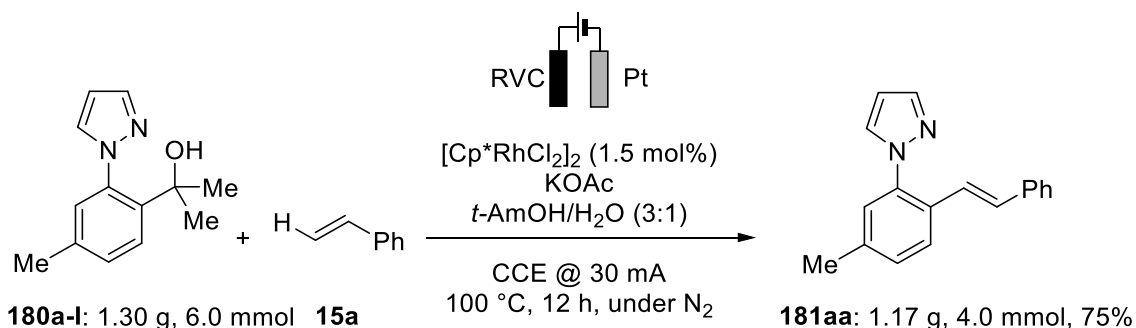


[2-(1*H*-Pyrazol-1-yl)phenyl](pentamethylcyclopentadienyl)rhodium(III) acetate (190b-II)

[Cp*RhCl₂]₂ (92.7 mg, 0.15 mmol), 1-phenylpyrazole **148b-V** (65 mg, 0.45 mmol) and AgOAc (151 mg, 0.90 mmol) were stirred in DCM (6 mL, 0.1 M) for 12 h at r.t. The mixture was filtered through celite and concentrated *in vacuo*. Precipitation occurred upon addition of EtOAc (2 mL) and sonication. The mixture was diluted with *n*-hexane (4 mL), and the solid was filtered and washed with Et₂O. **190b-II** was obtained as an orange solid (126 mg, 0.23 mmol, 94 %).

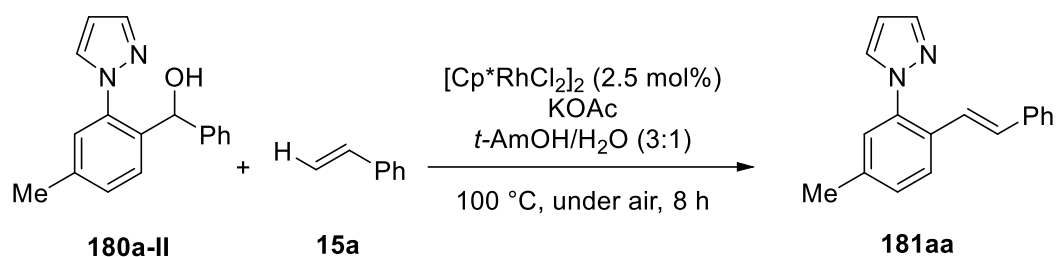
¹H-NMR (600 MHz, CDCl₃) δ = 8.05–8.01 (m, 2H), 7.91 (d, J = 2.6 Hz, 1H), 7.16 (dd, J = 7.1, 7.1 Hz, 2H), 7.07 (ddd, J = 7.7, 7.4, 1.4 Hz, 1H), 6.49 (d, J = 2.4, 2.4 Hz, 1H), 1.69 (s, 3H), 1.64 (s, 15H). **¹³C{¹H}-NMR** (125 MHz, CDCl₃) δ = 177.0 (C_q), 160.1 (d, $^1J_{C-Rh}$ = 34.3 Hz, C_q), 142.3 (C_q), 1.540 (CH), 137.3 (CH), 126.5 (CH), 124.2 (CH), 123.2 (CH), 110.6 (CH), 107.5 (CH), 94.5 (d, $^1J_{C-Rh}$ = 6.8 Hz, C_q), 24.7 (CH₃), 9.4 (CH₃). **IR** (ATR) 3076, 1580 1366, 1321, 1073, 747, 671, 389 cm⁻¹. **MS** (EI+) m/z (relative intensity): 441 (100) [M]⁺. **HR-MS** (ESI) m/z calc. for C₁₉H₂₂N₂Rh [M–OAc]⁺: 381.0838, found: 381.0833.

5.5.2 Gram-Scale Reaction



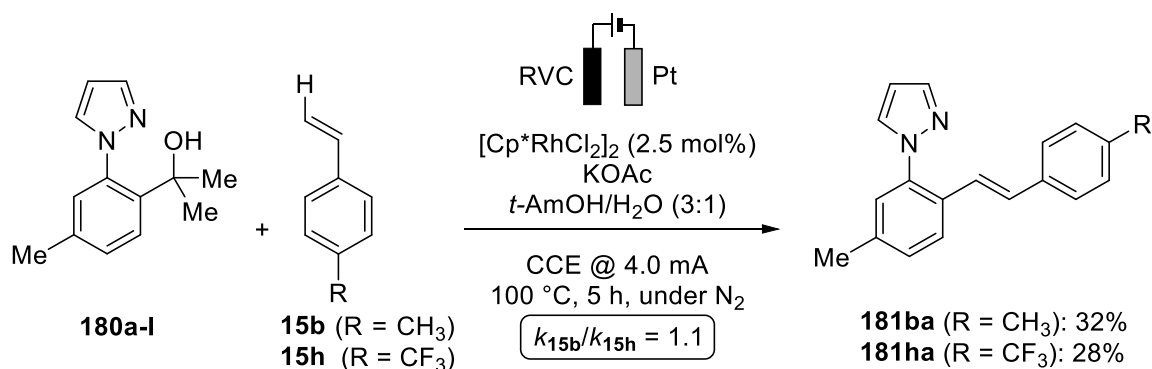
To an undivided two-necked flask (diameter: 40 mm; length: 130 mm; volume: 120 mL) equipped with a teflon-coated magnetic stirring bar and teflon cap, a RVC anode (25 mm × 50 mm × 6 mm) and a platinum cathode (25 mm × 50 mm × 0.25 mm) were added **180a-I** (1.30 g, 6.0 mol), **15a** (936 mg, 9.0 mmol), KOAc (1.18 g, 12 mmol), [Cp*RhCl₂]₂ (56 mg, 0.09 mmol) and *t*-AmOH/H₂O (3:1, 50 mL). Electrocatalysis was performed at T = 100 °C with a constant current of 30 mA, maintained for 12 h. The RVC anode was washed with EtOAc (3 × 30 mL) in an ultrasonic bath. Evaporation of the solvent and FCC (*n*-hexane/EtOAc = 15:1) yielded **181aa** (1.17g, 4.5 mmol, 75%) as a yellow oil.

5.5.3 C–C Alkenylation by Aerobic Oxidation



To a Schlenk tube were added **180a-II** (66 mg, 0.25 mmol), **15a** (52 mg, 0.50 mmol), KOAc (49 mg, 0.5 mmol), $[Cp^*RhCl_2]_2$ (3.9 mg, 2.5 mol%) and $t\text{-AmOH}/H_2O$ (3:1, 4.0 mL). The mixture was stirred for 8 h at 100 °C under air. Evaporation of the solvent and subsequent FCC ($n\text{-hexane}/EtOAc = 15:1$) yielded **181aa** (30.0 mg, 0.11 mmol, 46%) as a yellow oil.

5.5.4 Competition Experiment



The general procedure C was followed using **180a-I** (54 mg, 0.25 mmol), **15b** (30 mg, 0.25 mmol) and **15h** (43 mg, 0.25 mmol). The yields of **181ba** (32%) and **181ha** (28%) were determined by $^1H\text{-NMR}$ analysis of the crude mixture with CH_2Br_2 as the internal standard.

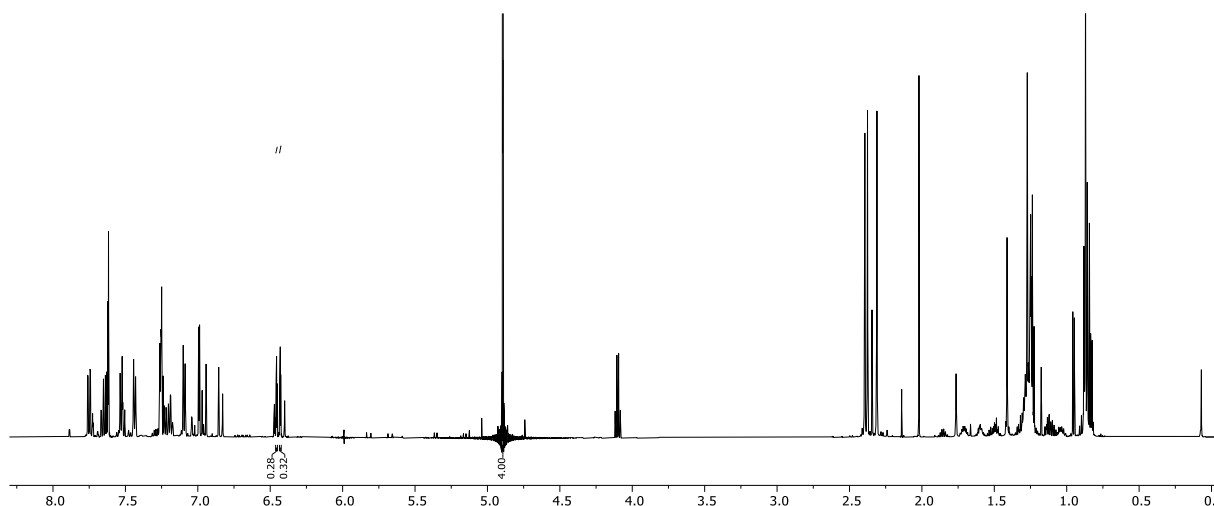
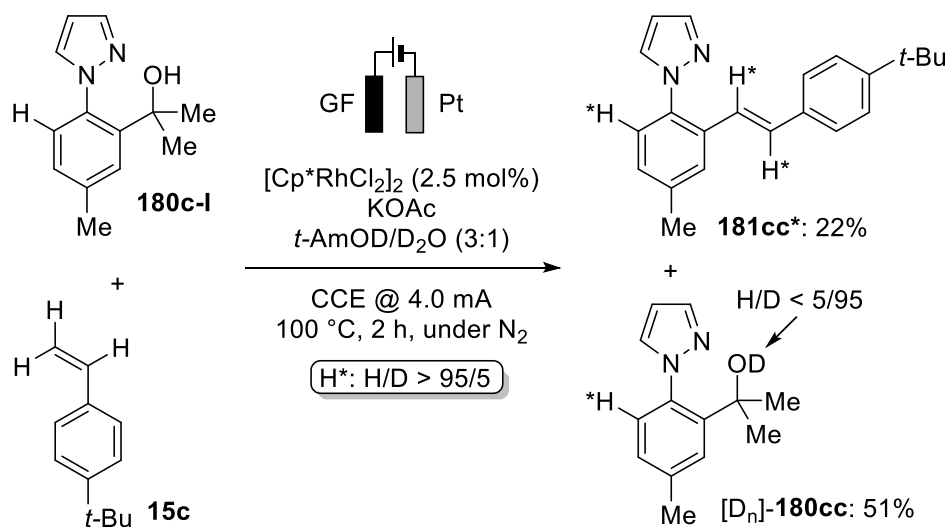


Figure 5.5-1 $^1\text{H-NMR}$ Spectrum (600 MHz, CDCl_3) of the reaction mixture with CH_2Br_2 (36 μL , 0.50 mmol) as the internal standard (4.96 ppm). The signals of the 4-pyrazolyl protons and the internal standard are integrated.

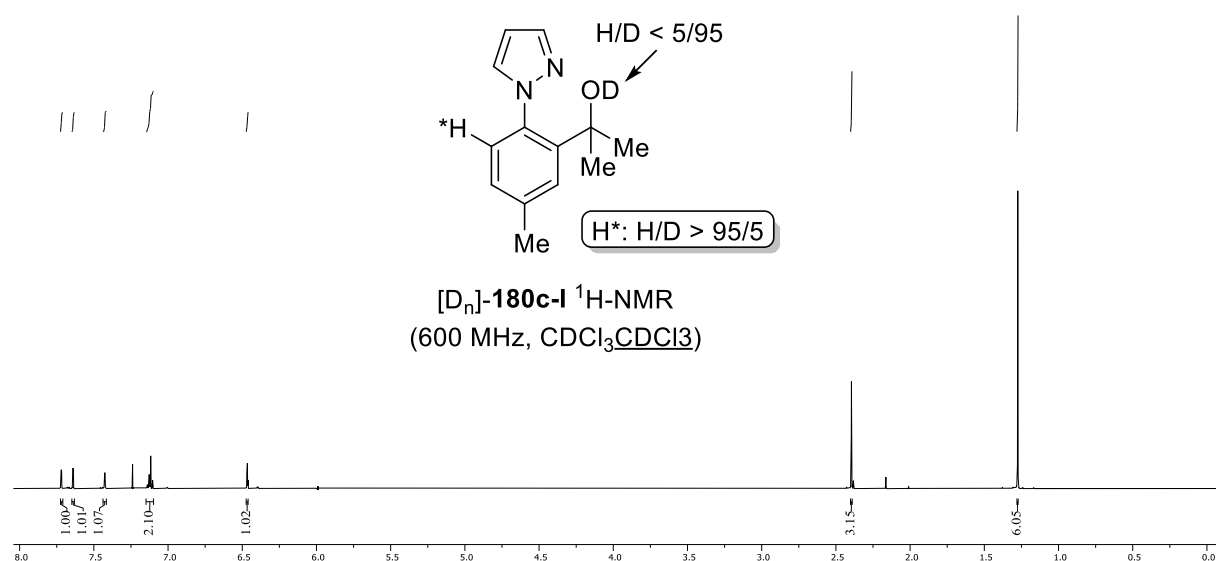
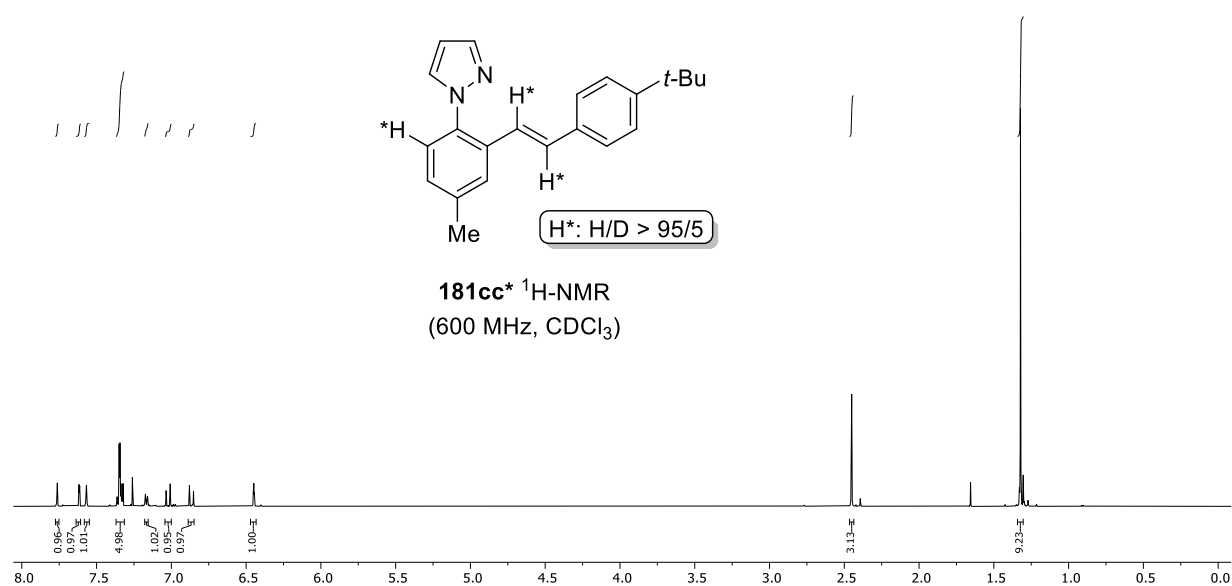
5.5.5 H/D Exchange Experiment



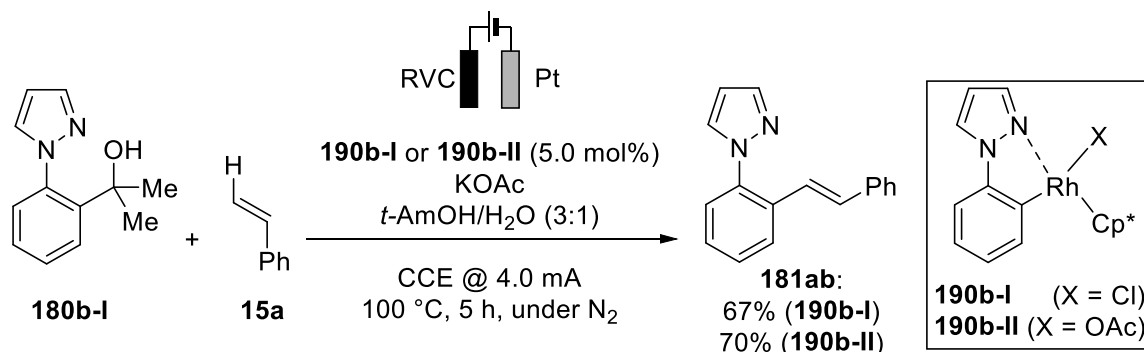
In a standard electrochemical cell, **180c-I** (81 mg, 0.375 mmol), **15c** (40 mg, 0.25 mmol), KOAc (49 mg, 0.50 mmol) and $[\text{Cp}^*\text{RhCl}_2]_2$ (3.9 mg, 2.5 mol%) were dissolved in $t\text{-AmOD}/\text{D}_2\text{O}$ (3:1, 4.0 mL). The atmosphere was exchanged to N_2 and electrocatalysis was performed at 100 °C with a constant current of 4.0 mA maintained for 2 h. The RVC anode was washed with EtOAc (3×10 mL). FCC ($n\text{-hexane}/\text{EtOAc} = 40:1 \rightarrow 10:1$) yielded **181cc*** (17 mg, 0.05 mmol, 22%) as a colorless oil and **[D_n]-180cc** (41 mg, 0.19 mmol, 51%) as a yellow oil. The D-incorporation was estimated by $^1\text{H-NMR}$ spectroscopy.

EXPERIMENTAL PART

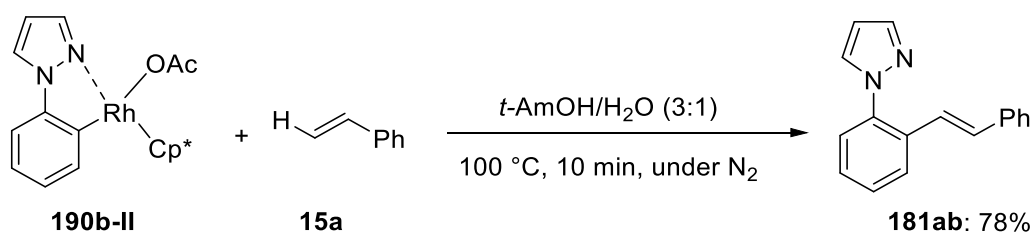
181cc*: $^1\text{H-NMR}$ (600 MHz, CDCl_3): $\delta = 7.78\text{--}7.75$ (m 1H), $7.63\text{--}7.61$ (m, 1H), $7.58\text{--}7.55$ (m, 1H), $7.37\text{--}7.31$ (m, 5H), $7.18\text{--}7.15$ (m, 1H), 7.02 (d, $J = 16.5$ Hz, 1H), 6.87 (d, $J = 16.5$ Hz, 1H), $6.47\text{--}6.43$ (m, 1H), 2.45 (s, 3H), 1.32 (s, 9H). $^{13}\text{C}\{^1\text{H}\}\text{-NMR}$ (125 MHz, CDCl_3): $\delta = 151.1$ (C_q), 140.6 (CH), 138.3 (C_q), 136.5 (C_q), 134.4 (C_q), 133.0 (C_q), 131.7 (CH), 130.9 (CH), 128.8 (CH), 126.9 (CH), 126.5 (CH), 126.3 (CH), 125.6 (CH), 123.3 (CH), 106.4 (CH), 34.8 (C_q), 31.5 (CH_3), 21.5 (CH_3). **IR** (ATR): $2960, 2930, 1614, 1517, 1393, 1256, 1013, 910$ cm^{-1} . **MS** (ESI) m/z (relative intensity): 339 (75) $[\text{M}+\text{Na}]^+$, 317 (100) $[\text{M}+\text{H}]^+$. **HR-MS** (ESI) m/z calc. for $\text{C}_{22}\text{H}_{25}\text{N}_2$ $[\text{M}+\text{H}]^+$: 317.2012 , found: 317.2013 .



5.5.6 Rhodium Complex **190b**-Catalyzed C–C Alkenylation and Product Release



In a standard electrochemical cell, **180b-I** (36.5 mg, 0.18 mmol), **15a** (13.0 mg, 0.125 mmol), KOAc (24.5 mg, 0.25 mmol), and **190b-I** (2.6 mg, 5.0 mol%) or **190b-II** (2.8 mg, 5.0 mol%) were dissolved in *t*-AmOH/H₂O (3:1, 4.0 mL). The atmosphere was exchanged to N₂ and electrocatalysis was performed at 100 °C with a constant current of 4.0 mA maintained for 5 h. The RVC anode was washed with EtOAc (3 × 10 mL). The combined organic phases were concentrated. Purification by FCC (*n*-hexane/EtOAc = 20:1) yielded **181ab** (20.6 mg, 0.08 mmol 67% for **190b-I**; 21.5 mg, 70% for **190b-II**).



In a 10 mL Schlenk tube, **190b-II** (33.0 mg, 75 μmol) and **15a** (15.7 mg, 0.15 mmol) were dissolved in degassed *t*-AmOH/H₂O (3:1, 2.0 mL). The mixture was stirred under N₂ at 100 °C for 10 min. Evaporation of solvents and subsequent FCC (*n*-hexane/EtOAc = 20:1) yielded **181ab** (14.3 mg, 78%).

6 REFERENCES

- [1] a) D. B. Newell, E. Tiesinga: *The international system of units (SI)*, National Institute of Standards and Technology Gaithersburg, MD, **2019**.; b) W. M. Haynes: *CRC Handbook of Chemistry and Physics, 95th Edition*, CRC Press Hoboken, **2015**.
- [2] a) N. Gaiand, A. Abbott, A. Witze, E. Gibney, J. Tollefson, A. Irwin, R. van Noorden, *Nature* **2022**, *607*, 440–443; b) R. Bleischwitz, R. Perincek, *Sicherheit und Frieden (S+F) / Security and Peace* **2017**, *35*, 129–133.
- [3] a) P. Anastas, N. Eghbali, *Chem. Soc. Rev.* **2010**, *39*, 301–312; b) P. T. Anastas, M. M. Kirchhoff, *Acc. Chem. Res.* **2002**, *35*, 686–694.
- [4] B. M. Trost, *Science* **1991**, *254*, 1471–1477.
- [5] E. J. Corey, X.-M. Cheng: *The logic of chemical synthesis*, Wiley New York, **1989**.
- [6] a) B. M. Trost, *Angew. Chem. Int. Ed.* **1995**, *34*, 259–281; b) B. M. Trost, *Science* **1983**, *219*, 245–250.
- [7] Y. Chen, C. Rosenkranz, S. Hirte, J. Kirchmair, *Nat. Prod. Rep.* **2022**, *39*, 1544–1556.
- [8] a) M. J. Buskes, M.-J. Blanco, *Molecules (Basel, Switzerland)* **2020**, *25*; b) A. de Meijere, S. Bräse, M. Oestreich: *Metal-Catalyzed Cross-Coupling Reactions and More*, Wiley Weinheim, Germany, **2014**.; c) Y. Nishihara: *Applied Cross-Coupling Reactions*, Springer Berlin, Heidelberg, **2013**.; d) N. Miyaura (Ed.) *Springer eBook Collection, Vol. 219*, Springer Berlin, **2002**.
- [9] a) R. F. Heck, *Acc. Chem. Res.* **1979**, *12*, 146–151; b) R. F. Heck, J. P. Nolley, *J. Org. Chem.* **1972**, *37*, 2320–2322; c) T. Mizoroki, K. Mori, A. Ozaki, *Bull. Chem. Soc. Jpn.* **1971**, *44*, 581.
- [10] a) J. K. Stille, *Angew. Chem. Int. Ed.* **1986**, *25*, 508–524; b) D. Milstein, J. K. Stille, *J. Am. Chem. Soc.* **1978**, *100*, 3636–3638; c) M. Kosugi, Y. Shimizu, T. Migita, *Chem. Lett.* **1977**, *6*, 1423–1424.
- [11] a) N. Miyaura, A. Suzuki, *Chem. Rev.* **1995**, *95*, 2457–2483; b) N. Miyaura, K. Yamada, A. Suzuki, *Tetrahedron Lett.* **1979**, *20*, 3437–3440.
- [12] a) R. J. P. Corriu, J. P. Masse, *J. Chem. Soc., Chem. Commun.* **1972**, 144a; b) K. Tamao, K. Sumitani, M. Kumada, *J. Am. Chem. Soc.* **1972**, *94*, 4374–4376.
- [13] Y. Hatanaka, T. Hiyama, *J. Org. Chem.* **1988**, *53*, 918–920.
- [14] a) K. Sonogashira, *J. Organomet. Chem.* **2002**, *653*, 46–49; b) K. Sonogashira, Y. Tohda, N. Hagihara, *Tetrahedron Lett.* **1975**, *16*, 4467–4470.
- [15] a) E. Negishi, *Acc. Chem. Res.* **1982**, *15*, 340–348; b) E. Negishi, A. O. King, N. Okukado, *J. Org. Chem.* **1977**, *42*, 1821–1823; c) S. Baba, E. Negishi, *J. Am. Chem. Soc.* **1976**, *98*, 6729–6731.
- [16] a) D. M. Chan, K. L. Monaco, R.-P. Wang, M. P. Winters, *Tetrahedron Lett.* **1998**, *39*, 2933–2936; b) D. A. Evans, J. L. Katz, T. R. West, *Tetrahedron Lett.* **1998**, *39*, 2937–2940; c) P. Y. Lam, C. G. Clark, S. Saubern, J. Adams, M. P. Winters, D. M. Chan, A. Combs, *Tetrahedron Lett.* **1998**, *39*, 2941–2944.
- [17] a) J. F. Hartwig, *Nature* **2008**, *455*, 314–322; b) J. F. Hartwig, *Angew. Chem. Int. Ed.* **1998**, *37*, 2046–2067; c) A. S. Guram, S. L. Buchwald, *J. Am. Chem. Soc.* **1994**, *116*, 7901–7902; d) F. Paul, J. Patt, J. F. Hartwig, *J. Am. Chem. Soc.* **1994**, *116*, 5969–5970.
- [18] a) H. Lin, D. Sun, *Org. Prep. Proced. Int.* **2013**, *45*; b) F. Monnier, M. Taillefer, *Angew. Chem. Int. Ed.* **2009**, *48*, 6954–6971; c) G. Evano, N. Blanchard, M. Toumi, *Chem. Rev.* **2008**, *108*, 3054–3131; d) W. R. H. Hurtley, *J. Chem. Soc.* **1929**, *0*, 1870–1873; e) I. Goldberg, *Ber. Dtsch. Chem. Ges.* **1906**, *39*, 1691–1692; f) F. Ullmann, *Ber. Dtsch. Chem. Ges.* **1903**, *36*, 2382–2384; g) F. Ullmann, J. Bielecki, *Ber. Dtsch. Chem. Ges.* **1901**, *34*, 2174–2185.
- [19] J. Halpern, *Acc. Chem. Res.* **1982**, *15*, 238–244.

REFERENCES

- [20] a) NobelPrize.org, "The Nobel Prize in Chemistry 2010", <https://www.nobelprize.org/prizes/chemistry/2010/summary/>, accessed on 01.10.2022; b) C. C. C. Johansson Seechurn, M. O. Kitching, T. J. Colacot, V. Snieckus, *Angew. Chem. Int. Ed.* **2012**, *51*, 5062–5085.
- [21] a) Wolf Foundation, "John F. Hartwig - Wolf Foundation", <https://wolffund.org.il/2019/01/22/john-f-hartwig/>, accessed on 01.10.2022; b) Wolf Foundation, "Stephen L. Buchwald - Wolf Foundation", <https://wolffund.org.il/2019/01/22/stephen-l-buchwald/>, accessed on 01.10.2022.
- [22] a) D. A. Everson, D. J. Weix, *J. Org. Chem.* **2014**, *79*, 4793–4798; b) C. E. I. Knappke, S. Grupe, D. Gärtner, M. Corpet, C. Gosmini, A. Jacobi von Wangelin, *Chem. – Eur. J.* **2014**, *20*, 6828–6842; c) T. Moragas, A. Correa, R. Martin, *Chem. – Eur. J.* **2014**, *20*, 8242–8258.
- [23] a) T. Dalton, T. Faber, F. Glorius, *ACS Cent. Sci.* **2021**, *7*, 245–261; b) L. Guillemard, N. Kaplaneris, L. Ackermann, M. J. Johansson, *Nat. Rev. Chem.* **2021**, *5*, 522–545; c) N. Y. S. Lam, K. Wu, J.-Q. Yu, *Angew. Chem. Int. Ed.* **2021**, *60*, 15767–15790; d) T. Rogge, N. Kaplaneris, N. Chatani, J. Kim, S. Chang, B. Punji, L. L. Schafer, D. G. Musaev, J. Wencel-Delord, C. A. Roberts et al., *Nat. Rev. Methods Primers* **2021**, *1*; e) P. Gandeepan, T. Müller, D. Zell, G. Cera, S. Warratz, L. Ackermann, *Chem. Rev.* **2019**, *119*, 2192–2452; f) Z. Nairoukh, M. Cormier, I. Marek, *Nat. Rev. Chem.* **2017**, *1*; g) T. Gensch, M. N. Hopkinson, F. Glorius, J. Wencel-Delord, *Chem. Soc. Rev.* **2016**, *45*, 2900–2936; h) X. Ribas: *C-H and C-X Bond Functionalization*, Royal Society of Chemistry Cambridge, **2013**; i) J. Wencel-Delord, T. Dröge, F. Liu, F. Glorius, *Chem. Soc. Rev.* **2011**, *40*, 4740–4761; j) R. G. Bergman, *Nature* **2007**, *446*, 391–393.
- [24] a) S. Murahashi, S. Horiie, *J. Am. Chem. Soc.* **1956**, *78*, 4816–4817; b) S. Murahashi, *J. Am. Chem. Soc.* **1955**, *77*, 6403–6404.
- [25] a) A. E. Shilov, G. B. Shul'pin, *Chem. Rev.* **1997**, *97*, 2879–2932; b) A. E. Shilov, *Pure Appl. Chem.* **1978**, *50*, 725–733.
- [26] a) R. G. Bergman, *Science* **1984**, *223*, 902–908; b) A. H. Janowicz, R. G. Bergman, *J. Am. Chem. Soc.* **1982**, *104*, 352–354.
- [27] a) J. Durrani, "Seeking out selective C–H activation", <https://www.chemistryworld.com/holy-grails/the-grails/c-h-bond-activation>, accessed on 12.10.2022; b) B. A. Arndtsen, R. G. Bergman, T. A. Mobley, T. H. Peterson, *Acc. Chem. Res.* **1995**, *28*, 154–162.
- [28] Wolf Foundation, "Robert G. Bergman - Wolf Foundation", <https://wolffund.org.il/2018/12/12/robert-bergman/>, accessed on 01.10.2022.
- [29] a) Y. Yang, J. Lan, J. You, *Chem. Rev.* **2017**, *117*, 8787–8863; b) S. A. Girard, T. Knauber, C.-J. Li, *Angew. Chem. Int. Ed.* **2014**, *53*, 74–100; c) S. I. Kozhushkov, L. Ackermann, *Chem. Sci.* **2013**, *4*, 886–896; d) S. H. Cho, J. Y. Kim, J. Kwak, S. Chang, *Chem. Soc. Rev.* **2011**, *40*, 5068–5083; e) C. S. Yeung, V. M. Dong, *Chem. Rev.* **2011**, *111*, 1215–1292; f) T. Satoh, M. Miura, *Chem. – Eur. J.* **2010**, *16*, 11212–11222.
- [30] a) S. Caron, R. W. Dugger, S. G. Ruggieri, J. A. Ragan, D. H. B. Ripin, *Chem. Rev.* **2006**, *106*, 2943–2989; b) N. G. Connelly, W. E. Geiger, *Chem. Rev.* **1996**, *96*, 877–910.
- [31] a) E. M. Simmons, J. F. Hartwig, *Angew. Chem. Int. Ed.* **2012**, *51*, 3066–3072; b) M. Gómez-Gallego, M. A. Sierra, *Chem. Rev.* **2011**, *111*, 4857–4963.
- [32] a) T. P. Pabst, P. J. Chirik, *Organometallics* **2021**, *40*, 813–831; b) S. R. Neufeldt, M. S. Sanford, *Acc. Chem. Res.* **2012**, *45*, 936–946; c) L. Ackermann, *Top. Organomet. Chem.* **2007**, *24*, 35–60.
- [33] a) I. V. Seregin, V. Gevorgyan, *Chem. Soc. Rev.* **2007**, *36*, 1173–1193; b) K. Shen, Y. Fu, J.-N. Li, L. Liu, Q.-X. Guo, *Tetrahedron* **2007**, *63*, 1568–1576.
- [34] a) K. Murali, L. A. Machado, R. L. Carvalho, L. F. Pedrosa, R. Mukherjee, E. N. Da Silva Júnior, D. Maiti, *Chem. – Eur. J.* **2021**, *27*, 12453–12508; b) C. Sambigioglio, D. Schönbauer, R. Blicke, T. Dao-Huy, G. Pototschnig, P. Schaaf, T. Wiesinger, M. F. Zia, J. Wencel-Delord, T. Besset et al., *Chem. Soc. Rev.* **2018**, *47*, 6603–6743.

REFERENCES

- [35] a) R. L. Carvalho, R. G. Almeida, K. Murali, L. A. Machado, L. F. Pedrosa, P. Dolui, D. Maiti, E. N. Da Silva Júnior, *Org. Biomol. Chem.* **2021**, *19*, 525–547; b) Y. Xia, G. Dong, *Nat. Rev. Chem.* **2020**, *4*, 600–614; c) P. Gandeepan, L. Ackermann, *Chem* **2018**, *4*, 199–222; d) W. Ma, P. Gandeepan, J. Li, L. Ackermann, *Org. Chem. Front.* **2017**, *4*, 1435–1467; e) G. Rousseau, B. Breit, *Angew. Chem. Int. Ed.* **2011**, *50*, 2450–2494.
- [36] M. C. Whisler, S. MacNeil, V. Snieckus, P. Beak, *Angewandte Chemie (International ed. in English)* **2004**, *43*, 2206–2225.
- [37] a) S. Rej, Y. Ano, N. Chatani, *Chem. Rev.* **2020**, *120*, 1788–1887; b) D. S. Timofeeva, D. M. Lindsay, W. J. Kerr, D. J. Nelson, *Catal. Sci. Technol.* **2020**, *10*, 7249–7255; c) A. Tomberg, M. É. Muratore, M. J. Johansson, I. Terstiege, C. Sköld, P.-O. Norrby, *iScience* **2019**, *20*, 373–391; d) S. De Sarkar, W. Liu, S. I. Kozhushkov, L. Ackermann, *Adv. Synth. Catal.* **2014**, *356*, 1461–1479; e) L. V. Desai, K. J. Stowers, M. S. Sanford, *J. Am. Chem. Soc.* **2008**, *130*, 13285–13293.
- [38] a) K. Korvorapun, R. C. Samanta, T. Rogge, L. Ackermann, *Synthesis* **2021**, *53*, 2911–2946; b) G. Meng, N. Y. S. Lam, E. L. Lucas, T. G. Saint-Denis, P. Verma, N. Chekshin, J.-Q. Yu, *J. Am. Chem. Soc.* **2020**, *142*, 10571–10591; c) A. Dey, S. K. Sinha, T. K. Achar, D. Maiti, *Angew. Chem. Int. Ed.* **2019**, *58*, 10820–10843; d) J. Li, S. de Sarkar, L. Ackermann, *Top. Organomet. Chem.* **2015**, *55*, 217–257; e) D. Tilly, J. Magolan, J. Mortier, *Chem. – Eur. J.* **2012**, *18*, 3804–3820.
- [39] a) K. M. Altus, J. A. Love, *Commun Chem* **2021**, *4*; b) C. Shan, L. Zhu, L.-B. Qu, R. Bai, Y. Lan, *Chem. Soc. Rev.* **2018**, *47*, 7552–7576; c) F. Roudesly, J. Oble, G. Poli, *J. Mol. Catal. A: Chem.* **2017**, *426*, 275–296; d) M. Albrecht, *Chem. Rev.* **2010**, *110*, 576–623; e) D. Balcells, E. Clot, O. Eisenstein, *Chem. Rev.* **2010**, *110*, 749–823; f) D. H. Ess, W. A. Goddard, R. A. Periana, *Organometallics* **2010**, *29*, 6459–6472; g) Y. Boutadla, D. L. Davies, S. A. Macgregor, A. I. Poblador-Bahamonde, *Dalton Trans.* **2009**, 5820–5831; h) J. A. Labinger, J. E. Bercaw, *Nature* **2002**, *417*, 507–514.
- [40] a) L. Ackermann, *Acc. Chem. Res.* **2014**, *47*, 281–295; b) L. Ackermann, *Chem. Rev.* **2011**, *111*, 1315–1345.
- [41] a) D. Lapointe, K. Fagnou, *Chem. Lett.* **2010**, *39*, 1118–1126; b) S. I. Gorelsky, D. Lapointe, K. Fagnou, *J. Am. Chem. Soc.* **2008**, *130*, 10848–10849.
- [42] D. L. Davies, S. A. Macgregor, C. L. McMullin, *Chem. Rev.* **2017**, *117*, 8649–8709.
- [43] a) T. Rogge, J. C. A. Oliveira, R. Kuniyil, L. Hu, L. Ackermann, *ACS Catal.* **2020**, *10*, 10551–10558; b) W. Ma, R. Mei, G. Tenti, L. Ackermann, *Chem. – Eur. J.* **2014**, *20*, 15248–15251.
- [44] R. A. Alharis, C. L. McMullin, D. L. Davies, K. Singh, S. A. Macgregor, *J. Am. Chem. Soc.* **2019**, *141*, 8896–8906.
- [45] a) B. Liu, A. M. Romine, C. Z. Rubel, K. M. Engle, B.-F. Shi, *Chem. Rev.* **2021**, *121*, 14957–15074; b) J. He, M. Wasa, K. S. L. Chan, Q. Shao, J.-Q. Yu, *Chem. Rev.* **2017**, *117*, 8754–8786; c) R. Jazzar, J. Hitce, A. Renaudat, J. Sofack-Kreutzer, O. Baudoin, *Chem. – Eur. J.* **2010**, *16*, 2654–2672.
- [46] a) O. Vyhivskiy, A. Kudashev, T. Miyakoshi, O. Baudoin, *Chem. – Eur. J.* **2021**, *27*, 1231–1257; b) T. Yoshino, S. Matsunaga, *ACS Catal.* **2021**, *11*, 6455–6466; c) F. Colobert, J. Wencel-Delord, *C-H Activation for Asymmetric Synthesis*, Wiley, **2019**.; d) J. Loup, U. Dhawa, F. Pesciaiolli, J. Wencel-Delord, L. Ackermann, *Angew. Chem. Int. Ed.* **2019**, *58*, 12803–12818; e) T. G. Saint-Denis, R.-Y. Zhu, G. Chen, Q.-F. Wu, J.-Q. Yu, *Science* **2018**, *359*; f) C. G. Newton, S.-G. Wang, C. C. Oliveira, N. Cramer, *Chem. Rev.* **2017**, *117*, 8908–8976; g) H. M. L. Davies, R. E. J. Beckwith, *Chem. Rev.* **2003**, *103*, 2861–2904.
- [47] a) O. Baudoin, *Angew. Chem. Int. Ed.* **2020**, *59*, 17798–17809; b) D. J. Abrams, P. A. Provencher, E. J. Sorensen, *Chem. Soc. Rev.* **2018**, *47*, 8925–8967; c) J. Yamaguchi, A. D. Yamaguchi, K. Itami, *Angew. Chem. Int. Ed.* **2012**, *51*, 8960–9009; d) W. R. Gutekunst, P. S. Baran, *Chem. Soc. Rev.* **2011**, *40*, 1976–1991; e) L. McMurray, F. O'Hara, M. J. Gaunt, *Chem. Soc. Rev.* **2011**, *40*, 1885–1898.
- [48] L. Zhang, T. Ritter, *J. Am. Chem. Soc.* **2022**, *144*, 2399–2414.

REFERENCES

- [49] a) H.-R. Tong, B. Li, G. Li, G. He, G. Chen, *CCS Chem.* **2021**, *3*, 1797–1820; b) W. Wang, M. M. Lorion, J. Shah, A. R. Kapdi, L. Ackermann, *Angew. Chem. Int. Ed.* **2018**, *57*, 14700–14717; c) A. F. M. Noisier, M. A. Brimble, *Chem. Rev.* **2014**, *114*, 8775–8806.
- [50] T. Cernak, K. D. Dykstra, S. Tyagarajan, P. Vachal, S. W. Krska, *Chem. Soc. Rev.* **2016**, *45*, 546–576.
- [51] a) M. D. R. Lutz, B. Morandi, *Chem. Rev.* **2021**, *121*, 300–326; b) B. Wang, M. A. Perea, R. Sarpong, *Angew. Chem. Int. Ed.* **2020**, *59*, 18898–18919; c) F. Song, T. Gou, B.-Q. Wang, Z.-J. Shi, *Chem. Soc. Rev.* **2018**, *47*, 7078–7115; d) P.-H. Chen, B. A. Billett, T. Tsukamoto, G. Dong, *ACS Catal.* **2017**, *7*, 1340–1360; e) G. Fumagalli, S. Stanton, J. F. Bower, *Chem. Rev.* **2017**, *117*, 9404–9432; f) D.-S. Kim, W.-J. Park, C.-H. Jun, *Chem. Rev.* **2017**, *117*, 8977–9015; g) M. Murakami, N. Ishida, *J. Am. Chem. Soc.* **2016**, *138*, 13759–13769; h) L. Souillart, N. Cramer, *Chem. Rev.* **2015**, *115*, 9410–9464; i) F. Chen, T. Wang, N. Jiao, *Chem. Rev.* **2014**, *114*, 8613–8661; j) K. Ruhland, *Eur. J. Org. Chem.* **2012**, *2012*, 2683–2706; k) M. Murakami, T. Matsuda, *Chem. Commun.* **2011**, *47*, 1100–1105; l) S. M. Bonesi, M. Fagnoni, *Chem. – Eur. J.* **2010**, *16*, 13572–13589.
- [52] A. Modak, D. Maiti, *Org. Biomol. Chem.* **2016**, *14*, 21–35.
- [53] a) W. D. Jones, *Top. Curr. Chem.* **2014**, *346*, 1–31; b) M. Murakami, Y. Ito, *Top. Organomet. Chem.* **1999**, *3*, 97–129; c) B. Rytchinski, D. Milstein, *Angew. Chem. Int. Ed.* **1999**, *38*, 870–883.
- [54] K. Nogi, H. Yorimitsu, *Chem. Rev.* **2021**, *121*, 345–364.
- [55] a) J. Kim, K. Shin, S. Jin, D. Kim, S. Chang, *J. Am. Chem. Soc.* **2019**, *141*, 4137–4146; b) M. P. Lanci, M. S. Remy, W. Kaminsky, J. M. Mayer, M. S. Sanford, *J. Am. Chem. Soc.* **2009**, *131*, 15618–15620.
- [56] a) I. Funes-Ardoiz, F. Maseras, *ACS Catal.* **2018**, *8*, 1161–1172; b) I. Funes-Ardoiz, F. Maseras, *Chem. – Eur. J.* **2018**, *24*, 12383–12388; c) I. Funes-Ardoiz, F. Maseras, *Angew. Chem.* **2016**, *128*, 2814–2817; d) S. V. Rosokha, J. K. Kochi, *Acc. Chem. Res.* **2008**, *41*, 641–653; e) J. K. Kochi, *Science* **1967**, *155*, 415–424.
- [57] "MINING.COM. Precious Metals", <https://www.mining.com/markets/commodity/group/precious-metals/>, accessed on 05.12.2022.
- [58] L. N. Lewis, J. F. Smith, *J. Am. Chem. Soc.* **1986**, *108*, 2728–2735.
- [59] S. Murai, F. Kakiuchi, S. Sekine, Y. Tanaka, A. Kamatani, M. Sonoda, N. Chatani, *Nature* **1993**, *366*, 529–531.
- [60] L. Ackermann, *Org. Lett.* **2005**, *7*, 3123–3125.
- [61] L. Ackermann, A. Althammer, R. Born, *Angew. Chem. Int. Ed.* **2006**, *45*, 2619–2622.
- [62] a) L. Ackermann, *Org. Process Res. Dev.* **2015**, *19*, 260–269; b) L. Ackermann, R. Vicente, H. K. Potukuchi, V. Pirovano, *Org. Lett.* **2010**, *12*, 5032–5035.
- [63] L. Ackermann, R. Vicente, A. Althammer, *Org. Lett.* **2008**, *10*, 2299–2302.
- [64] a) K. S. Singh, S. G. Sawant, P. H. Dixneuf, *ChemCatChem* **2016**, *8*, 1046–1050; b) Y. Zhao, Z. He, S. Li, J. Tang, G. Gao, J. Lan, J. You, *Chem. Commun.* **2016**, *52*, 4613–4616; c) R. Li, Y. Hu, R. Liu, R. Hu, B. Li, B. Wang, *Adv. Synth. Catal.* **2015**, *357*, 3885–3892; d) R. Manoharan, M. Jeganmohan, *Chem. Commun.* **2015**, *51*, 2929–2932; e) R. Prakash, K. Shekarrao, S. Gogoi, *Org. Lett.* **2015**, *17*, 5264–5267; f) Z. Zuo, X. Yang, J. Liu, J. Nan, L. Bai, Y. Wang, X. Luan, *J. Org. Chem.* **2015**, *80*, 3349–3356; g) C.-H. Hung, P. Gandeepan, C.-H. Cheng, *ChemCatChem* **2014**, *6*, 2692–2697; h) S. Nakanowatari, L. Ackermann, *Chem. – Eur. J.* **2014**, *20*, 5409–5413; i) L. Ackermann, J. Pospech, K. Graczyk, K. Rauch, *Org. Lett.* **2012**, *14*, 930–933; j) R. K. Chinnagolla, M. Jeganmohan, *Chem. Commun.* **2012**, *48*, 2030–2032; k) L. Ackermann, A. V. Lygin, N. Hofmann, *Angew. Chem. Int. Ed.* **2011**, *50*, 6379–6382.
- [65] S. Warratz, C. Kornhaab, A. Cajaraville, B. Niepötter, D. Stalke, L. Ackermann, *Angew. Chem. Int. Ed.* **2015**, *54*, 5513–5517.
- [66] a) Q. Bu, T. Rogge, V. Kotek, L. Ackermann, *Angew. Chem.* **2018**, *130*, 773–776; b) A. Bechtoldt, C. Tirlir, K. Raghuvanshi, S. Warratz, C. Kornhaab, L. Ackermann, *Angew. Chem. Int. Ed.* **2016**, *55*, 264–267; c) N. Y. P. Kumar, A. Bechtoldt, K. Raghuvanshi, L. Ackermann, *Angew. Chem. Int. Ed.* **2016**, *55*, 6929–6932; d) B. Li, J. Ma, Y. Liang, N. Wang, S. Xu, H. Song, B. Wang, *Eur. J. Org. Chem.* **2013**, *2013*, 1950–1962; e) M. C. Reddy,

REFERENCES

- M. Jeganmohan, *Eur. J. Org. Chem.* **2013**, *2013*, 1150–1157; f) L. Ackermann, L. Wang, R. Wolfram, A. V. Lygin, *Org. Lett.* **2012**, *14*, 728–731; g) J. Li, C. Kornhaas, L. Ackermann, *Chem. Commun.* **2012**, *48*, 11343–11345; h) L. Ackermann, J. Pospech, *Org. Lett.* **2011**, *13*, 4153–4155; i) K. Padala, M. Jeganmohan, *Org. Lett.* **2011**, *13*, 6144–6147; j) T. Ueyama, S. Mochida, T. Fukutani, K. Hirano, T. Satoh, M. Miura, *Org. Lett.* **2011**, *13*, 706–708.
- [67] a) T. Rogge, T. Müller, H. Simon, X. Hou, S. Wagschal, D. Broggini, L. Ackermann, *Synlett* **2022**, *33*, 346–350; b) L. Ackermann, E. Diers, A. Manvar, *Org. Lett.* **2012**, *14*, 1154–1157; c) L. Ackermann, P. Novák, R. Vicente, V. Pirovano, H. Potukuchi, *Synthesis* **2010**, *2010*, 2245–2253.
- [68] L. Ackermann, P. Novák, *Org. Lett.* **2009**, *11*, 4966–4969.
- [69] a) I. Choi, V. Müller, L. Ackermann, *Tetrahedron Lett.* **2021**, *72*, 153064; b) L. Ackermann, *Chem. Commun.* **2010**, *46*, 4866–4877; c) L. Ackermann, P. Novák, R. Vicente, N. Hofmann, *Angew. Chem. Int. Ed.* **2009**, *48*, 6045–6048.
- [70] S. Nakanowatari, L. Ackermann, *Chem. – Eur. J.* **2015**, *21*, 16246–16251.
- [71] a) K. Raghuvanshi, D. Zell, L. Ackermann, *Org. Lett.* **2017**, *19*, 1278–1281; b) V. S. Thirunavukkarasu, S. I. Kozhushkov, L. Ackermann, *Chem. Commun.* **2014**, *50*, 29–39; c) F. Yang, K. Rauch, K. Kettelhoit, L. Ackermann, *Angew. Chem. Int. Ed.* **2014**, *53*, 11285–11288; d) V. S. Thirunavukkarasu, J. Hubrich, L. Ackermann, *Org. Lett.* **2012**, *14*, 4210–4213.
- [72] a) M. Bhanuchandra, M. R. Yadav, R. K. Rit, M. Rao Kuram, A. K. Sahoo, *Chem. Commun.* **2013**, *49*, 5225–5227; b) J. Kim, J. Kim, S. Chang, *Chem. – Eur. J.* **2013**, *19*, 7328–7333; c) M. R. Yadav, R. K. Rit, A. K. Sahoo, *Org. Lett.* **2013**, *15*, 1638–1641; d) Q.-Z. Zheng, Y.-F. Liang, C. Qin, N. Jiao, *Chem. Commun.* **2013**, *49*, 5654–5656.
- [73] K. M. Engle, T.-S. Mei, M. Wasa, J.-Q. Yu, *Acc. Chem. Res.* **2012**, *45*, 788–802.
- [74] N. Kaplaneris, M. Vilches-Herrera, J. Wu, L. Ackermann, *ACS Sustainable Chem. Eng.* **2022**, *10*, 6871–6888.
- [75] A. Bechtoldt, M. E. Baumert, L. Vaccaro, L. Ackermann, *Green Chem.* **2018**, *20*, 398–402.
- [76] G. Rani, V. Luxami, K. Paul, *Chem. Commun.* **2020**, *56*, 12479–12521.
- [77] a) Z. Zeng, A. Feceu, N. Sivendran, L. J. Gooßen, *Adv. Synth. Catal.* **2021**, *363*, 2678–2722; b) J. Schwarz, B. König, *Green Chem.* **2018**, *20*, 323–361; c) F. Sandfort, M. J. O'Neill, J. Cornella, L. Wimmer, P. S. Baran, *Angew. Chem. Int. Ed.* **2017**, *56*, 3319–3323; d) N. Rodríguez, L. J. Goossen, *Chem. Soc. Rev.* **2011**, *40*, 5030–5048; e) R. Shang, L. Liu, *Sci. China Chem.* **2011**, *54*, 1670–1687; f) L. J. Goossen, F. Collet, K. Goossen, *Isr. J. Chem.* **2010**, *50*, 617–629.
- [78] M. Font, J. M. Quibell, G. J. P. Perry, I. Larrosa, *Chem. Commun.* **2017**, *53*, 5584–5597.
- [79] H. Chen, Y. A. Liu, X. Liao, *Synthesis* **2021**, *53*, 1–29.
- [80] A. Varenikov, E. Shapiro, M. Gandelman, *Chem. Rev.* **2021**, *121*, 412–484.
- [81] M. Nilsson, E. Kulonen, S. Sunner, V. Frank, J. Brunvoll, E. Bunnenberg, C. Djerassi, R. Records, *Acta Chem. Scand.* **1966**, *20*, 423–426.
- [82] A. G. Myers, D. Tanaka, M. R. Mannion, *J. Am. Chem. Soc.* **2002**, *124*, 11250–11251.
- [83] D. Tanaka, S. P. Romeril, A. G. Myers, *J. Am. Chem. Soc.* **2005**, *127*, 10323–10333.
- [84] L. J. Goossen, G. Deng, L. M. Levy, *Science* **2006**, *313*, 662–664.
- [85] H. A. Chiong, Q.-N. Pham, O. Daugulis, *J. Am. Chem. Soc.* **2007**, *129*, 9879–9884.
- [86] a) L. J. Gooßen, N. Rodríguez, C. Linder, P. P. Lange, A. Fromm, *ChemCatChem* **2010**, *2*, 430–442; b) J. Cornella, C. Sanchez, D. Banawa, I. Larrosa, *Chem. Commun.* **2009**, 7176–7178; c) L. J. Goossen, C. Linder, N. Rodríguez, P. P. Lange, A. Fromm, *Chem. Commun.* **2009**, 7173–7175; d) P. Lu, C. Sanchez, J. Cornella, I. Larrosa, *Org. Lett.* **2009**, *11*, 5710–5713.
- [87] J. Cornella, M. Rigbi, I. Larrosa, *Angew. Chem. Int. Ed.* **2011**, *50*, 9429–9432.
- [88] a) R. Schmitt, *J. Prakt. Chem.* **1885**, *31*, 397–411; b) H. Kolbe, *Ann. Chem. Pharm.* **1860**, *113*, 125–127.
- [89] J. Luo, S. Preciado, I. Larrosa, *J. Am. Chem. Soc.* **2014**, *136*, 4109–4112.
- [90] M. G. Organ, S. Avola, I. Dubovyk, N. Hadei, E. A. B. Kantchev, C. J. O'Brien, C. Valente, *Chem. – Eur. J.* **2006**, *12*, 4749–4755.

REFERENCES

- [91] N. Y. P. Kumar, T. Rogge, S. R. Yetra, A. Bechtoldt, E. Clot, L. Ackermann, *Chem. – Eur. J.* **2017**, *23*, 17449–17453.
- [92] a) J. W. Suggs, C. H. Jun, *J. Am. Chem. Soc.* **1986**, *108*, 4679–4681; b) J. W. Suggs, C. H. Jun, *J. Am. Chem. Soc.* **1984**, *106*, 3054–3056.
- [93] a) S.-Y. Liou, M. Gozin, D. Milstein, *J. Am. Chem. Soc.* **1995**, *117*, 9774–9775; b) M. Gozin, A. Weisman, Y. Ben-David, D. Milstein, *Nature* **1993**, *364*, 699–701.
- [94] M. Gandelman, A. Vigalok, L. J. W. Shimon, D. Milstein, *Organometallics* **1997**, *16*, 3981–3986.
- [95] M. Murakami, H. Amii, Y. Ito, *Nature* **1994**, *370*, 540–541.
- [96] H. F. Chow, C. W. Wan, K. H. Low, Y. Y. Yeung, *J. Org. Chem.* **2001**, *66*, 1910–1913.
- [97] Y. Terao, H. Wakui, T. Satoh, M. Miura, M. Nomura, *J. Am. Chem. Soc.* **2001**, *123*, 10407–10408.
- [98] T. Nishimura, H. Araki, Y. Maeda, S. Uemura, *Org. Lett.* **2003**, *5*, 2997–2999.
- [99] A. Horita, H. Tsurugi, A. Funayama, T. Satoh, M. Miura, *Org. Lett.* **2007**, *9*, 2231–2233.
- [100] A. Funayama, T. Satoh, M. Miura, *J. Am. Chem. Soc.* **2005**, *127*, 15354–15355.
- [101] T. Uto, M. Shimizu, K. Ueura, H. Tsurugi, T. Satoh, M. Miura, *J. Org. Chem.* **2008**, *73*, 298–300.
- [102] H. Li, Y. Li, X.-S. Zhang, K. Chen, X. Wang, Z.-J. Shi, *J. Am. Chem. Soc.* **2011**, *133*, 15244–15247.
- [103] S. Onodera, S. Ishikawa, T. Kochi, F. Kakiuchi, *J. Am. Chem. Soc.* **2018**, *140*, 9788–9792.
- [104] N. Ishida, S. Sawano, Y. Masuda, M. Murakami, *J. Am. Chem. Soc.* **2012**, *134*, 17502–17504.
- [105] "Q3D(R2) – Guideline for Elemental Impurities", <https://www.fda.gov/media/148474/download>, accessed on 05.10.2022.
- [106] a) J. D. Lasso, D. J. Castillo-Pazos, C.-J. Li, *Chem. Soc. Rev.* **2021**, *50*, 10955–10982; b) J. C. K. Chu, T. Rovis, *Angew. Chem. Int. Ed.* **2018**, *57*, 62–101; c) J. F. Hartwig, M. A. Larsen, *ACS Cent. Sci.* **2016**, *2*, 281–292; d) T. Brückl, R. D. Baxter, Y. Ishihara, P. S. Baran, *Acc. Chem. Res.* **2012**, *45*, 826–839.
- [107] a) S. Sarkar, K. P. S. Cheung, V. Gevorgyan, *Chem. Sci.* **2020**, *11*, 12974–12993; b) J. Robertson, J. Pillai, R. K. Lush, *Chem. Soc. Rev.* **2001**, *30*, 94–103.
- [108] a) P. R. D. Murray, J. H. Cox, N. D. Chiappini, C. B. Roos, E. A. McLoughlin, B. G. Hejna, S. T. Nguyen, H. H. Ripberger, J. M. Ganley, E. Tsui et al., *Chem. Rev.* **2022**, *122*, 2017–2291; b) H. Cao, X. Tang, H. Tang, Y. Yuan, J. Wu, *Chem Catalysis* **2021**, *1*, 523–598; c) R. Tyburski, T. Liu, S. D. Glover, L. Hammarström, *J. Am. Chem. Soc.* **2021**, *143*, 560–576; d) J. W. Darcy, B. Koronkiewicz, G. A. Parada, J. M. Mayer, *Acc. Chem. Res.* **2018**, *51*, 2391–2399; e) L. Capaldo, D. Ravelli, *Eur. J. Org. Chem.* **2017**, *2017*, 2056–2071.
- [109] a) D. L. Golden, S.-E. Suh, S. S. Stahl, *Nat. Rev. Chem.* **2022**, *6*, 405–427; b) H. Yi, G. Zhang, H. Wang, Z. Huang, J. Wang, A. K. Singh, A. Lei, *Chem. Rev.* **2017**, *117*, 9016–9085; c) M. P. Doyle, R. Duffy, M. Ratnikov, L. Zhou, *Chem. Rev.* **2010**, *110*, 704–724; d) H. M. L. Davies, J. R. Manning, *Nature* **2008**, *451*, 417–424.
- [110] H. M. L. Davies, D. Morton, *Chem. Soc. Rev.* **2011**, *40*, 1857–1869.
- [111] T. F. Markle, J. W. Darcy, J. M. Mayer, *Sci. Adv.* **2018**, *4*, eaat5776.
- [112] a) G. Tarantino, C. Hammond, *Green Chem.* **2020**, *22*, 5195–5209; b) R. Szpera, D. F. J. Moseley, L. B. Smith, A. J. Sterling, V. Gouverneur, *Angew. Chem. Int. Ed.* **2019**, *58*, 14824–14848; c) A. Koperniku, H. Liu, P. B. Hurley, *Eur. J. Org. Chem.* **2016**, *2016*, 871–886; d) T. Ahrens, J. Kohlmann, M. Ahrens, T. Braun, *Chem. Rev.* **2015**, *115*, 931–972; e) P. A. Champagne, J. Desroches, J.-D. Hamel, M. Vandamme, J.-F. Paquin, *Chem. Rev.* **2015**, *115*, 9073–9174; f) A. Lin, C. B. Huehls, J. Yang, *Org. Chem. Front.* **2014**, *1*, 434–438.
- [113] P. A. Champagne, Y. Benhassine, J. Desroches, J.-F. Paquin, *Angew. Chem. Int. Ed.* **2014**, *53*, 13835–13839.
- [114] a) A. R. A. Spencer, R. Grainger, A. Panigrahi, T. J. Lepper, K. Bentkowska, I. Larrosa, *Chem. Commun.* **2020**, *56*, 14479–14482; b) A. Vasilopoulos, D. L. Golden, J. A. Buss, S. S. Stahl, *Org. Lett.* **2020**, *22*, 5753–5757.
- [115] N. Rozatian, D. R. W. Hodgson, *Chem. Commun.* **2021**, *57*, 683–712.
- [116] G. A. Olah, J. G. Shih, G. Prakash, *J. Fluorine Chem.* **1986**, *33*, 377–396.

REFERENCES

- [117] a) S. Liang, G. B. Hammond, B. Xu, *Chem. – Eur. J.* **2017**, *23*, 17850–17861; b) O. E. Okoromoba, J. Han, G. B. Hammond, B. Xu, *J. Am. Chem. Soc.* **2014**, *136*, 14381–14384.
- [118] W. J. Middleton, *J. Org. Chem.* **1975**, *40*, 574–578.
- [119] a) J. Guo, C. Kuang, J. Rong, L. Li, C. Ni, J. Hu, *Chem. – Eur. J.* **2019**, *25*, 7259–7264; b) M. K. Nielsen, D. T. Ahneman, O. Riera, A. G. Doyle, *J. Am. Chem. Soc.* **2018**, *140*, 5004–5008; c) M. K. Nielsen, C. R. Ugaz, W. Li, A. G. Doyle, *J. Am. Chem. Soc.* **2015**, *137*, 9571–9574; d) T. Fujimoto, F. Becker, T. Ritter, *Org. Process Res. Dev.* **2014**, *18*, 1041–1044; e) F. Beaulieu, L.-P. Beauregard, G. Courchesne, M. Couturier, F. LaFlamme, A. L'Heureux, *Org. Lett.* **2009**, *11*, 5050–5053.
- [120] S. Bloom, C. R. Pitts, R. Woltornist, A. Griswold, M. G. Holl, T. Lectka, *Org. Lett.* **2013**, *15*, 1722–1724.
- [121] P. Xu, S. Guo, L. Wang, P. Tang, *Angew. Chem. Int. Ed.* **2014**, *53*, 5955–5958.
- [122] S. Bloom, C. R. Pitts, D. C. Miller, N. Haselton, M. G. Holl, E. Urheim, T. Lectka, *Angew. Chem. Int. Ed.* **2012**, *51*, 10580–10583.
- [123] M. B. Nodwell, A. Bagai, S. D. Halperin, R. E. Martin, H. Knust, R. Britton, *Chem. Commun.* **2015**, *51*, 11783–11786.
- [124] a) S. Bloom, M. McCann, T. Lectka, *Org. Lett.* **2014**, *16*, 6338–6341; b) J.-B. Xia, C. Zhu, C. Chen, *J. Am. Chem. Soc.* **2013**, *135*, 17494–17500.
- [125] W. Liu, J. T. Groves, *Angew. Chem. Int. Ed.* **2013**, *52*, 6024–6027.
- [126] C. Ni, F. Jiang, Y. Zeng, J. Hu, *J. Fluorine Chem.* **2015**, *179*, 3–13.
- [127] A. Volta, *Phil. Trans. R. Soc.* **1800**, *90*, 403–431.
- [128] V. Petrov: *Announcements on galvanic-voltaic experiments*,. Conducted by the Professor of Physics Vasily Petrov, Based on an enormous battery, consisting at times of 4200 copper and zinc disks, located at St. Petersburg's Medical and Surgical Academy., State Medical College Press St. Petersburg, **1803**.
- [129] a) M. Faraday, *Phil. Trans. R. Soc.* **1834**, *124*, 77–122; b) M. Faraday, *Phil. Trans. R. Soc.* **1832**, *122*, 125–162.
- [130] a) H. Kolbe, *Ann. Chem. Pharm.* **1849**, *69*, 257–294; b) H. Kolbe, *Ann. Chem. Pharm.* **1848**, *64*, 339–341.
- [131] M. C. Leech, K. Lam, *Acc. Chem. Res.* **2020**, *53*, 121–134.
- [132] a) M. C. Leech, A. D. Garcia, A. Petti, A. P. Dobbs, K. Lam, *React. Chem. Eng.* **2020**, *5*, 977–990; b) D. S. P. Cardoso, B. Šljukić, D. M. F. Santos, C. A. C. Sequeira, *Org. Process Res. Dev.* **2017**, *21*, 1213–1226; c) C. A. C. Sequeira, D. M. F. Santos, *J. Braz. Chem. Soc.* **2009**, *20*, 387–406.
- [133] a) K. Li, Q. Fan, H. Chuai, H. Liu, S. Zhang, X. Ma, *Trans. Tianjin Univ.* **2021**, *27*, 202–216; b) R. K. B. Karlsson, A. Cornell, *Chem. Rev.* **2016**, *116*, 2982–3028; c) S. Lakshmanan, T. Murugesan, *Clean Techn. Environ. Policy* **2014**, *16*, 225–234; d) I. Moussallem, J. Jörissen, U. Kunz, S. Pinnow, T. Turek, *J. Appl. Electrochem.* **2008**, *38*, 1177–1194; e) T. F. O'Brien, T. V. Bommaraju, F. Hine: *Handbook of chlor-alkali technology*, Springer New York, **2005**.
- [134] G. E. Totten (Ed.) *Handbook of aluminum*, Dekker New York, **2003**.
- [135] a) J. H. Simons, *J. Electrochem. Soc.* **1949**, *95*, 47; b) J. H. Simons, R. D. Dresdner, *J. Electrochem. Soc.* **1949**, *95*, 64; c) J. H. Simons, H. T. Francis, J. A. Hogg, *J. Electrochem. Soc.* **1949**, *95*, 53; d) J. H. Simons, W. J. Harland, *J. Electrochem. Soc.* **1949**, *95*, 55; e) J. H. Simons, W. H. Pearlson, T. J. Brice, W. A. Wilson, R. D. Dresdner, *J. Electrochem. Soc.* **1949**, *95*, 59.
- [136] S. Möhle, M. Zirbes, E. Rodrigo, T. Gieshoff, A. Wiebe, S. R. Waldvogel, *Angew. Chem. Int. Ed.* **2018**, *57*, 6018–6041.
- [137] a) B. Fritz, L. Hans, W. Karl, G. Harald, US3477923 (A), **1966**.; b) M. M. Baizer, *J. Electrochem. Soc.* **1964**, *111*, 215; c) M. M. Baizer, US3193481 (A), **1963**.
- [138] a) K. Scott: *Sustainable and green electrochemical science and technology*, Wiley Hoboken, NJ, Chichester, West Sussex, **2017**.; b) E. J. Horn, B. R. Rosen, P. S. Baran, *ACS Cent. Sci.* **2016**, *2*, 302–308; c) H. J. Schäfer, *C. R. Chim.* **2011**, *14*, 745–765; d) C. Comminellis, G. Chen (Eds.) *Electrochemistry for the environment*, Springer New

REFERENCES

- York, NY, **2010**.; e) B. A. Frontana-Uribe, R. D. Little, J. G. Ibanez, A. Palma, R. Vasquez-Medrano, *Green Chem.* **2010**, *12*, 2099.
- [139] a) M. C. Leech, K. Lam, *Nat. Rev. Chem.* **2022**, *6*, 275–286; b) E. C. R. McKenzie, S. Hosseini, A. G. C. Petro, K. K. Rudman, B. H. R. Gerroll, M. S. Mubarak, L. A. Baker, R. D. Little, *Chem. Rev.* **2022**, *122*, 3292–3335; c) A. Scheremetjew, T. H. Meyer, Z. Lin, L. Massignan, L. Ackermann in *Science of Synthesis* (Ed.: L. Ackermann), Thieme, Stuttgart, **2022**, pp. 3–32; d) C. Kingston, M. D. Palkowitz, Y. Takahira, J. C. Vantourout, B. K. Peters, Y. Kawamata, P. S. Baran, *Acc. Chem. Res.* **2020**, *53*, 72–83; e) R. D. Little, *J. Org. Chem.* **2020**, *85*, 13375–13390; f) S. D. Minter, P. Baran, *Acc. Chem. Res.* **2020**, *53*, 545–546; g) C. Schotten, T. P. Nicholls, R. A. Bourne, N. Kapur, B. N. Nguyen, C. E. Willans, *Green Chem.* **2020**, *22*, 3358–3375; h) C. Sandford, M. A. Edwards, K. J. Klunder, D. P. Hickey, M. Li, K. Barman, M. S. Sigman, H. S. White, S. D. Minter, *Chem. Sci.* **2019**, *10*, 6404–6422; i) N. Elgrishi, K. J. Rountree, B. D. McCarthy, E. S. Rountree, T. T. Eisenhart, J. L. Dempsey, *J. Chem. Educ.* **2018**, *95*, 197–206; j) A. Wiebe, T. Gieshoff, S. Möhle, E. Rodrigo, M. Zirbes, S. R. Waldvogel, *Angew. Chem. Int. Ed.* **2018**, *57*, 5594–5619.
- [140] a) IKA, "Electrasyn. Fundamentals", <https://www.ika.com/electrasyn/Fundamentals.html>, accessed on 01.06.2021; b) P. S. Baran, E. Horn, D. Waldmann, US2018217096 (A1), **2017**.
- [141] a) S. B. Beil, D. Pollok, S. R. Waldvogel, *Angew. Chem. Int. Ed.* **2021**; b) M. Yan, Y. Kawamata, P. S. Baran, *Angew. Chem. Int. Ed.* **2018**, *57*, 4149–4155.
- [142] a) L. Ackermann (Ed.) *Science of Synthesis*, 2021/5, Georg Thieme Verlag Stuttgart, New York, Delhi, Rio de Janeiro, Beijing, **2022**.; b) L. F. T. Novaes, J. Liu, Y. Shen, L. Lu, J. M. Meinhardt, S. Lin, *Chem. Soc. Rev.* **2021**, *50*, 7941–8002; c) C. Zhu, N. W. J. Ang, T. H. Meyer, Y. Qiu, L. Ackermann, *ACS Cent. Sci.* **2021**, *7*, 415–431; d) L. Ackermann, *Acc. Chem. Res.* **2020**, *53*, 84–104; e) A. Shatskiy, H. Lundberg, M. D. Kärkäs, *ChemElectroChem* **2019**, *6*, 4067–4092; f) Y. Jiang, K. Xu, C. Zeng, *Chem. Rev.* **2018**, *118*, 4485–4540; g) M. Yan, Y. Kawamata, P. S. Baran, *Chem. Rev.* **2017**, *117*, 13230–13319; h) O. Hammerich, B. Speiser (Eds.) *Organic electrochemistry*, CRC Press Boca Raton, Fla., **2016**.; i) A. Jutand, *Chem. Rev.* **2008**, *108*, 2300–2347.
- [143] C. Kittel: *Introduction to solid state physics*, Wiley Hoboken, NJ, **2018**.
- [144] J.-M. Savéant, *Chem. Rev.* **2008**, *108*, 2348–2378.
- [145] K. J. Lee, B. D. McCarthy, J. L. Dempsey, *Chem. Soc. Rev.* **2019**, *48*, 2927–2945.
- [146] a) L. Buglioni, F. Raymenants, A. Slattery, S. D. A. Zondag, T. Noël, *Chem. Rev.* **2022**, *122*, 2752–2906; b) T. Hardwick, N. Ahmed, *ACS Sustainable Chem. Eng.* **2021**, *9*, 4324–4340; c) J. P. Barham, B. König, *Angew. Chem. Int. Ed.* **2020**, *59*, 11732–11747; d) A. J. Bard, *Science* **1980**, *207*, 139–144.
- [147] a) R. A. Marcus, "Nobel Lecture. Electron Transfer Reactions in Chemistry: Theory and Experiment", <https://www.nobelprize.org/prizes/chemistry/1992/marcus/lecture/>, accessed on 28.05.2021; b) R. A. Marcus, *Electrochim. Acta* **1968**, *13*, 995–1004; c) R. A. Marcus, *Can. J. Chem.* **1959**, *37*, 155–163; d) R. A. Marcus, *J. Chem. Phys.* **1956**, *24*, 966–978.
- [148] A. J. Bard, *J. Am. Chem. Soc.* **2010**, *132*, 7559–7567.
- [149] a) D. M. Heard, A. J. J. Lennox, *Angew. Chem.* **2020**, *132*, 19026–19044; b) D. Bélanger, J. Pinson, *Chem. Soc. Rev.* **2011**, *40*, 3995–4048.
- [150] a) F. Wang, S. S. Stahl, *Acc. Chem. Res.* **2020**, *53*, 561–574; b) R. Francke, R. D. Little, *Chem. Soc. Rev.* **2014**, *43*, 2492–2521; c) E. Steckhan, *Angew. Chem. Int. Ed.* **1986**, *25*, 683–701.
- [151] a) M. Elsherbini, T. Wirth, *Acc. Chem. Res.* **2019**, *52*, 3287–3296; b) T. Noël, Y. Cao, G. Laudadio, *Acc. Chem. Res.* **2019**, *52*, 2858–2869; c) D. Pletcher, R. A. Green, R. C. D. Brown, *Chem. Rev.* **2018**, *118*, 4573–4591.
- [152] a) N. Shida, Y. Zhou, S. Inagi, *Acc. Chem. Res.* **2019**, *52*, 2598–2608; b) K.-F. Chow, F. Mavré, J. A. Crooks, B.-Y. Chang, R. M. Crooks, *J. Am. Chem. Soc.* **2009**, *131*, 8364–8365.
- [153] a) K. Hayashi, J. Griffin, K. C. Harper, Y. Kawamata, P. S. Baran, *J. Am. Chem. Soc.* **2022**, *144*, 5762–5768; b) Y. Kawamata, K. Hayashi, E. Carlson, S. Shaji, D. Waldmann, B. J. Simmons, J. T. Edwards, C. W. Zapf, M. Saito,

REFERENCES

- P. S. Baran, *J. Am. Chem. Soc.* **2021**, *143*, 16580–16588; c) A. G. Wills, D. L. Poole, C. M. Alder, M. Reid, *ChemElectroChem* **2020**, *7*, 2771–2776.
- [154] a) M. Rafiee, M. N. Mayer, B. T. Punchedhewa, M. R. Mumau, *J. Org. Chem.* **2021**, *86*, 15866–15874; b) K. D. Moeller, *Chem. Rev.* **2018**, *118*, 4817–4833.
- [155] a) J. C. Oliveira, J. Frey, S.-Q. Zhang, L.-C. Xu, X. Li, S.-W. Li, X. Hong, L. Ackermann, *Trends Chem.* **2022**, *4*, 863–885; b) S.-Q. Zhang, L.-C. Xu, S.-W. Li, J. C. A. Oliveira, X. Li, L. Ackermann, X. Hong, *Chem. – Eur. J.* **2022**; c) K. Jorner, A. Tomberg, C. Bauer, C. Sköld, P.-O. Norrby, *Nat. Rev. Chem.* **2021**, *5*, 240–255; d) A. Mistry, A. A. Franco, S. J. Cooper, S. A. Roberts, V. Viswanathan, *ACS Energy Lett.* **2021**, *6*, 1422–1431; e) J. Rein, J. R. Annand, M. K. Wismer, J. Fu, J. C. Siu, A. Klapars, N. A. Strotman, D. Kalyani, D. Lehnerr, S. Lin, *ACS Cent. Sci.* **2021**, *7*, 1347–1355; f) A. G. Wills, S. Charvet, C. Battilocchio, C. C. Scarborough, K. M. P. Wheelhouse, D. L. Poole, N. Carson, J. C. Vantourout, *Org. Process Res. Dev.* **2021**, *25*, 2587–2600; g) C. B. Santiago, J.-Y. Guo, M. S. Sigman, *Chem. Sci.* **2018**, *9*, 2398–2412.
- [156] S. Mattsson, G. Senges, S. Riedel, B. Paulus, *Chem. – Eur. J.* **2020**, *26*, 10781–10786.
- [157] L. Ebersson, K. Nyberg, *J. Am. Chem. Soc.* **1966**, *88*, 1686–1691.
- [158] L. Ebersson, K. Nyberg, *Tetrahedron Lett.* **1966**, *7*, 2389–2393.
- [159] a) J. Yoshida, A. Shimizu, R. Hayashi, *Chem. Rev.* **2018**, *118*, 4702–4730; b) R. Hayashi, A. Shimizu, Y. Song, Y. Ashikari, T. Nokami, J. Yoshida, *Chem. – Eur. J.* **2017**, *23*, 61–64; c) R. Hayashi, A. Shimizu, J. Yoshida, *J. Am. Chem. Soc.* **2016**, *138*, 8400–8403; d) T. Morofuji, A. Shimizu, J. Yoshida, *J. Am. Chem. Soc.* **2014**, *136*, 4496–4499.
- [160] Z.-W. Hou, D.-J. Liu, P. Xiong, X.-L. Lai, J. Song, H.-C. Xu, *Angew. Chem. Int. Ed.* **2021**, *60*, 2943–2947.
- [161] S. Zhang, Y. Li, T. Wang, M. Li, L. Wen, W. Guo, *Org. Lett.* **2022**, *24*, 1742–1746.
- [162] M. Rafiee, F. Wang, D. P. Hruszkewycz, S. S. Stahl, *J. Am. Chem. Soc.* **2018**, *140*, 22–25.
- [163] H. Wang, K. Liang, W. Xiong, S. Samanta, W. Li, A. Lei, *Sci. Adv.* **2020**, *6*, eaaz0590.
- [164] A. P. Atkins, A. C. Rowett, D. M. Heard, J. A. Tate, A. J. J. Lennox, *Org. Lett.* **2022**, *24*, 5105–5108.
- [165] S. Tang, R. Guillot, L. Grimaud, M. R. Vitale, G. Vincent, *Org. Lett.* **2022**, *24*, 2125–2130.
- [166] a) C. Nolte, J. Ammer, H. Mayr, *J. Org. Chem.* **2012**, *77*, 3325–3335; b) D. Landini, A. Maia, A. Rampoldi, *J. Org. Chem.* **1989**, *54*, 328–332.
- [167] M. Noel, V. Suryanarayanan, S. Chellammal, *J. Fluorine Chem.* **1997**, *83*, 31–40.
- [168] a) T. Tajima, H. Kurihara, A. Nakajima, T. Fuchigami, *J. Electroanal. Chem.* **2005**, *580*, 155–160; b) T. Tajima, H. Ishii, T. Fuchigami, *Electrochem. Commun.* **2002**, *4*, 589–592.
- [169] E. Laurent, B. Marquet, R. Tardivel, *J. Fluorine Chem.* **1990**, *49*, 115–126.
- [170] S. M. Lee, J. M. Roseman, C. Blair Zartman, E. P. Morrison, S. J. Harrison, C. A. Stankiewicz, W. J. Middleton, *J. Fluorine Chem.* **1996**, *77*, 65–70.
- [171] K. Momota, K. Mukai, K. Tako, M. Morita, *Electrochim. Acta* **1998**, *43*, 2503–2514.
- [172] Y. Hou, S. Higashiya, T. Fuchigami, *Electrochim. Acta* **2000**, *45*, 3005–3010.
- [173] a) T. Fuchigami, S. Inagi, *Acc. Chem. Res.* **2020**, *53*, 322–334; b) T. Fuchigami, S. Inagi, *Chem. Commun.* **2011**, *47*, 10211–10223; c) V. Suryanarayanan, M. Noel, *J. Fluorine Chem.* **1998**, *92*, 177–180.
- [174] V. Dinoiu, T. Fukuhara, K. Miura, N. Yoneda, *J. Fluorine Chem.* **2003**, *121*, 227–231.
- [175] T. Sawamura, K. Takahashi, S. Inagi, T. Fuchigami, *Angew. Chem. Int. Ed.* **2012**, *51*, 4413–4416.
- [176] N. Shida, H. Takenaka, A. Gotou, T. Isogai, A. Yamauchi, Y. Kishikawa, Y. Nagata, I. Tomita, T. Fuchigami, S. Inagi, *J. Org. Chem.* **2021**, *86*, 16128–16133.
- [177] a) C. A. Malapit, M. B. Prater, J. R. Cabrera-Pardo, M. Li, T. D. Pham, T. P. McFadden, S. Blank, S. D. Minter, *Chem. Rev.* **2022**, *122*, 3180–3218; b) P. Gandeepan, L. H. Finger, T. H. Meyer, L. Ackermann, *Chem. Soc. Rev.* **2020**, *49*, 4254–4272; c) T. H. Meyer, L. H. Finger, P. Gandeepan, L. Ackermann, *Trends Chem.* **2019**, *1*, 63–76.
- [178] C. Amatore, C. Cammoun, A. Jutand, *Adv. Synth. Catal.* **2007**, *349*, 292–296.

REFERENCES

- [179] a) L. Zhou, W. Lu, *Chem. – Eur. J.* **2014**, *20*, 634–642; b) Y. Fujiwara, I. Moritani, S. Danno, R. Asano, S. Teranishi, *J. Am. Chem. Soc.* **1969**, *91*, 7166–7169; c) I. Moritanl, Y. Fujiwara, *Tetrahedron Lett.* **1967**, *8*, 1119–1122.
- [180] F. Kakiuchi, T. Kochi, H. Mutsutani, N. Kobayashi, S. Urano, M. Sato, S. Nishiyama, T. Tanabe, *J. Am. Chem. Soc.* **2009**, *131*, 11310–11311.
- [181] H. Aiso, T. Kochi, H. Mutsutani, T. Tanabe, S. Nishiyama, F. Kakiuchi, *J. Org. Chem.* **2012**, *77*, 7718–7724.
- [182] Q.-L. Yang, Y.-Q. Li, C. Ma, P. Fang, X.-J. Zhang, T.-S. Mei, *J. Am. Chem. Soc.* **2017**, *139*, 3293–3298.
- [183] Y.-Q. Li, Q.-L. Yang, P. Fang, T.-S. Mei, D. Zhang, *Org. Lett.* **2017**, *19*, 2905–2908.
- [184] a) Q.-L. Yang, C.-Z. Li, L.-W. Zhang, Y.-Y. Li, X. Tong, X.-Y. Wu, T.-S. Mei, *Organometallics* **2019**, *38*, 1208–1212; b) C. Ma, C.-Q. Zhao, Y.-Q. Li, L.-P. Zhang, X.-T. Xu, K. Zhang, T.-S. Mei, *Chem. Commun.* **2017**, *53*, 12189–12192.
- [185] T. V. Grayaznova, Y. Dudkina, D. R. Islamov, O. N. Kataeva, O. G. Sinyashin, D. A. Vicic, Y. Budnikova, *J. Organomet. Chem.* **2015**, *785*, 68–71.
- [186] Z. Duan, L. Zhang, W. Zhang, L. Lu, L. Zeng, R. Shi, A. Lei, *ACS Catal.* **2020**, *10*, 3828–3831.
- [187] Y. Qiu, W.-J. Kong, J. Struwe, N. Saueremann, T. Rogge, A. Scheremetjew, L. Ackermann, *Angew. Chem. Int. Ed.* **2018**, *57*, 5828–5832.
- [188] Y. Qiu, M. Stangier, T. H. Meyer, J. C. A. Oliveira, L. Ackermann, *Angew. Chem. Int. Ed.* **2018**, *57*, 14179–14183.
- [189] Q.-L. Yang, Y.-K. Xing, X.-Y. Wang, H.-X. Ma, X.-J. Weng, X. Yang, H.-M. Guo, T.-S. Mei, *J. Am. Chem. Soc.* **2019**, *141*, 18970–18976.
- [190] Y.-K. Xing, X.-R. Chen, Q.-L. Yang, S.-Q. Zhang, H.-M. Guo, X. Hong, T.-S. Mei, *Nat. Commun.* **2021**, *12*, 930.
- [191] Y. Qiu, A. Scheremetjew, L. Ackermann, *J. Am. Chem. Soc.* **2019**, *141*, 2731–2738.
- [192] Y. Zhang, J. Struwe, L. Ackermann, *Angew. Chem. Int. Ed.* **2020**, *59*, 15076–15080.
- [193] W.-J. Kong, L. H. Finger, J. C. A. Oliveira, L. Ackermann, *Angew. Chem.* **2019**, *131*, 6408–6412.
- [194] W.-J. Kong, Z. Shen, L. H. Finger, L. Ackermann, *Angew. Chem. Int. Ed.* **2020**, *59*, 5551–5556.
- [195] M. Stangier, A. M. Messinis, J. C. A. Oliveira, H. Yu, L. Ackermann, *Nat. Commun.* **2021**, *12*, 4736.
- [196] Y. Wang, J. C. A. Oliveira, Z. Lin, L. Ackermann, *Angew. Chem. Int. Ed.* **2021**, *60*, 6419–6424.
- [197] W.-J. Kong, L. H. Finger, A. M. Messinis, R. Kuniyil, J. C. A. Oliveira, L. Ackermann, *J. Am. Chem. Soc.* **2019**, *141*, 17198–17206.
- [198] Z.-J. Wu, F. Su, W. Lin, J. Song, T.-B. Wen, H.-J. Zhang, H.-C. Xu, *Angew. Chem. Int. Ed.* **2019**, *58*, 16770–16774.
- [199] X. Tan, L. Massignan, X. Hou, J. Frey, J. C. A. Oliveira, M. N. Hussain, L. Ackermann, *Angew. Chem. Int. Ed.* **2021**, *60*, 13264–13270.
- [200] a) A. M. Jones, C. E. Banks, *Beilstein J. Org. Chem.* **2014**, *10*, 3056–3072; b) T. Shono, Y. Matsumura, K. Tsubata, *J. Am. Chem. Soc.* **1981**, *103*, 1172–1176.
- [201] Y. Qiu, C. Tian, L. Massignan, T. Rogge, L. Ackermann, *Angew. Chem. Int. Ed.* **2018**, *57*, 5818–5822.
- [202] F. Xu, Y.-J. Li, C. Huang, H.-C. Xu, *ACS Catal.* **2018**, *8*, 3820–3824.
- [203] M.-J. Luo, M. Hu, R.-J. Song, D.-L. He, J.-H. Li, *Chem. Commun.* **2019**, *55*, 1124–1127.
- [204] M.-J. Luo, T.-T. Zhang, F.-J. Cai, J.-H. Li, D.-L. He, *Chem. Commun.* **2019**, *55*, 7251–7254.
- [205] Z.-Q. Wang, C. Hou, Y.-F. Zhong, Y.-X. Lu, Z.-Y. Mo, Y.-M. Pan, H.-T. Tang, *Org. Lett.* **2019**, *21*, 9841–9845.
- [206] R. Mei, J. Koeller, L. Ackermann, *Chem. Commun.* **2018**, *54*, 12879–12882.
- [207] X. Tan, X. Hou, T. Rogge, L. Ackermann, *Angew. Chem. Int. Ed.* **2021**, *60*, 4619–4624.
- [208] L. Yang, R. Steinbock, A. Scheremetjew, R. Kuniyil, L. H. Finger, A. M. Messinis, L. Ackermann, *Angew. Chem. Int. Ed.* **2020**, *59*, 11130–11135.
- [209] L. Massignan, X. Tan, T. H. Meyer, R. Kuniyil, A. M. Messinis, L. Ackermann, *Angew. Chem. Int. Ed.* **2020**, *59*, 3184–3189.

REFERENCES

- [210] X. Hou, N. Kaplaneris, B. Yuan, J. Frey, T. Ohyama, A. M. Messinis, L. Ackermann, *Chem. Sci.* **2022**, *13*, 3461–3467.
- [211] a) F. Kakiuchi, T. Kochi, *Chem. Rec.* **2021**, *21*, 2320–2331; b) Y. Qiu, C. Zhu, M. Stangier, J. Struwe, L. Ackermann, *CCS Chem.* **2021**, *3*, 1529–1552.
- [212] N. Sauermann, T. H. Meyer, C. Tian, L. Ackermann, *J. Am. Chem. Soc.* **2017**, *139*, 18452–18455.
- [213] a) X. Gao, P. Wang, L. Zeng, S. Tang, A. Lei, *J. Am. Chem. Soc.* **2018**, *140*, 4195–4199; b) N. Sauermann, R. Mei, L. Ackermann, *Angew. Chem. Int. Ed.* **2018**, *57*, 5090–5094.
- [214] C. Tian, U. Dhawa, J. Struwe, L. Ackermann, *Chin. J. Chem.* **2019**, *37*, 552–556.
- [215] C. Tian, L. Massignan, T. H. Meyer, L. Ackermann, *Angew. Chem. Int. Ed.* **2018**, *57*, 2383–2387.
- [216] R. Mei, N. Sauermann, J. C. A. Oliveira, L. Ackermann, *J. Am. Chem. Soc.* **2018**, *140*, 7913–7921.
- [217] R. Mei, W. Ma, Y. Zhang, X. Guo, L. Ackermann, *Org. Lett.* **2019**, *21*, 6534–6538.
- [218] S. Tang, D. Wang, Y. Liu, L. Zeng, A. Lei, *Nat. Commun.* **2018**, *9*, 798.
- [219] a) R. Mei, X. Fang, L. He, J. Sun, L. Zou, W. Ma, L. Ackermann, *Chem. Commun.* **2020**, *56*, 1393–1396; b) T. H. Meyer, J. C. A. Oliveira, S. C. Sau, N. W. J. Ang, L. Ackermann, *ACS Catal.* **2018**, *8*, 9140–9147.
- [220] L. Zeng, H. Li, S. Tang, X. Gao, Y. Deng, G. Zhang, C.-W. Pao, J.-L. Chen, J.-F. Lee, A. Lei, *ACS Catal.* **2018**, *8*, 5448–5453.
- [221] S. C. Sau, R. Mei, J. Struwe, L. Ackermann, *ChemSusChem* **2019**, *12*, 3023–3027.
- [222] U. Dhawa, C. Tian, W. Li, L. Ackermann, *ACS Catal.* **2020**, *10*, 6457–6462.
- [223] Q.-L. Yang, X.-Y. Wang, J.-Y. Lu, L.-P. Zhang, P. Fang, T.-S. Mei, *J. Am. Chem. Soc.* **2018**, *140*, 11487–11494.
- [224] S. Kathiravan, S. Suriyanarayanan, I. A. Nicholls, *Org. Lett.* **2019**, *21*, 1968–1972.
- [225] C. Tian, U. Dhawa, A. Scheremetjew, L. Ackermann, *ACS Catal.* **2019**, *9*, 7690–7696.
- [226] S.-K. Zhang, R. C. Samanta, N. Sauermann, L. Ackermann, *Chem. – Eur. J.* **2018**, *24*, 19166–19170.
- [227] S.-K. Zhang, J. Struwe, L. Hu, L. Ackermann, *Angew. Chem. Int. Ed.* **2020**, *59*, 3178–3183.
- [228] S.-K. Zhang, A. Del Vecchio, R. Kuniyil, A. M. Messinis, Z. Lin, L. Ackermann, *Chem* **2021**, *7*, 1379–1392.
- [229] C. Zhu, M. Stangier, J. C. A. Oliveira, L. Massignan, L. Ackermann, *Chem. – Eur. J.* **2019**, *25*, 16382–16389.
- [230] L. Massignan, C. Zhu, X. Hou, J. C. A. Oliveira, A. Salamé, L. Ackermann, *ACS Catal.* **2021**, *11*, 11639–11649.
- [231] a) A. N. Campbell, S. S. Stahl, *Acc. Chem. Res.* **2012**, *45*, 851–863; b) K. M. Gligorich, M. S. Sigman, *Angew. Chem. Int. Ed.* **2006**, *45*, 6612–6615; c) A. Bielanski, J. Haber: *Oxygen in Catalysis*, CRC Press, **1990**.
- [232] T. Sato, Y. Hamada, M. Sumikawa, S. Araki, H. Yamamoto, *Ind. Eng. Chem. Res.* **2014**, *53*, 19331–19337.
- [233] P. M. Osterberg, J. K. Niemeier, C. J. Welch, J. M. Hawkins, J. R. Martinelli, T. E. Johnson, T. W. Root, S. S. Stahl, *Org. Process Res. Dev.* **2015**, *19*, 1537–1543.
- [234] G. R. Astbury, *Org. Process Res. Dev.* **2002**, *6*, 893–895.
- [235] a) C. Bottecchia, D. Lehnerr, F. Lévesque, M. Reibarkh, Y. Ji, V. L. Rodrigues, H. Wang, Y. Lam, T. P. Vickery, B. M. Armstrong et al., *Org. Process Res. Dev.* **2022**, *26*, 2423–2437; b) G. Laudadio, W. de Smet, L. Struik, Y. Cao, T. Noël, *J. Flow Chem.* **2018**, *8*, 157–165.
- [236] M. Stangier, A. Scheremetjew, L. Ackermann, *Chem. – Eur. J.* **2022**, e202201654.
- [237] a) M. Inoue, Y. Sumii, N. Shibata, *ACS omega* **2020**, *5*, 10633–10640; b) N. A. Meanwell, *J. Med. Chem.* **2018**, *61*, 5822–5880; c) J. Wang, M. Sánchez-Roselló, J. L. Aceña, C. Del Pozo, A. E. Sorochinsky, S. Fustero, V. A. Soloshonok, H. Liu, *Chem. Rev.* **2014**, *114*, 2432–2506; d) W. K. Hagmann, *J. Med. Chem.* **2008**, *51*, 4359–4369; e) S. Purser, P. R. Moore, S. Swallow, V. Gouverneur, *Chem. Soc. Rev.* **2008**, *37*, 320–330; f) K. Müller, C. Fach, F. Diederich, *Science* **2007**, *317*, 1881–1886; g) J.-P. Bégué, D. Bonnet-Delpon, *J. Fluorine Chem.* **2006**, *127*, 992–1012.
- [238] a) R. Berger, G. Resnati, P. Metrangolo, E. Weber, J. Hulliger, *Chem. Soc. Rev.* **2011**, *40*, 3496–3508; b) F. Babudri, G. M. Farinola, F. Naso, R. Ragni, *Chem. Commun.* **2007**, 1003–1022.

REFERENCES

- [239] a) Y. Ogawa, E. Tokunaga, O. Kobayashi, K. Hirai, N. Shibata, *iScience* **2020**, *23*, 101467; b) P. Jeschke, *ChemBioChem* **2004**, *5*, 571–589.
- [240] a) K. L. Kirk, *Org. Process Res. Dev.* **2008**, *12*, 305–321; b) D. O'Hagan, *Chem. Soc. Rev.* **2008**, *37*, 308–319.
- [241] a) B. M. Johnson, Y.-Z. Shu, X. Zhuo, N. A. Meanwell, *J. Med. Chem.* **2020**, *63*, 6315–6386; b) K. C. Lee, S.-Y. Lee, S. C. Yearn, Y. C. Dae, *Bull. Korean Chem. Soc.* **2004**, *25*, 1225–1230; c) B Kevin Park, Neil R Kitteringham, Paul M O'Neill.
- [242] a) S. Preshlock, M. Tredwell, V. Gouverneur, *Chem. Rev.* **2016**, *116*, 719–766; b) Y. Magata, L. Lang, D. O. Kiesewetter, E. M. Jagoda, M. A. Channing, W. C. Eckelman, *Nucl. Med. Biol.* **2000**, *27*, 163–168.
- [243] M. D. Stangier, *Dissertation: C–H Activation via Iridium and Rhodium Electrocatalysis and Undirected Electrochemical Fluorination*, Georg-August-Universität Göttingen, **2022**.
- [244] J.-W. Lee, M. T. Oliveira, H. B. Jang, S. Lee, D. Y. Chi, D. W. Kim, C. E. Song, *Chem. Soc. Rev.* **2016**, *45*, 4638–4650.
- [245] a) "Authorisation List - ECHA", <https://echa.europa.eu/authorisation-list>, accessed on 11.01.2023; b) J. Sherwood, *Angew. Chem. Int. Ed.* **2018**, *57*, 14286–14290.
- [246] a) A. W. Black, P. N. Bartlett, *Phys. Chem. Chem. Phys.* **2022**, *24*, 8093–8103; b) M. H. Abraham, A. F. D. de Namor, *J. Chem. Soc., Faraday Trans. 1* **1976**, *72*, 955.
- [247] a) P. G. Jessop, *Green Chem.* **2011**, *13*, 1391; b) C. Capello, U. Fischer, K. Hungerbühler, *Green Chem.* **2007**, *9*, 927.
- [248] a) G. A. O. Tiago, I. A. S. Matias, A. P. C. Ribeiro, L. M. D. R. S. Martins, *Molecules (Basel, Switzerland)* **2020**, *25*; b) W. L. F. Armarego: *Purification of laboratory chemicals*, Butterworth-Heinemann Amsterdam, Boston, Heidelberg, London, New York, Oxford, Paris, San Diego, San Francisco, Singapore, Sydney, Tokyo, **2017**.
- [249] a) K. Spilovska, F. Zemek, J. Korabecny, E. Nepovimova, O. Soukup, M. Windisch, K. Kuca, *Curr. Med. Chem.* **2016**, *23*, 3245–3266; b) G. Lamoureux, G. Artavia, *Curr. Med. Chem.* **2010**, *17*, 2967–2978.
- [250] a) L. Wanka, K. Iqbal, P. R. Schreiner, *Chem. Rev.* **2013**, *113*, 3516–3604; b) M. Aoyama, T. Fukuhara, S. Hara, *J. Org. Chem.* **2008**, *73*, 4186–4189.
- [251] a) E. Baciocchi, M. Bietti, O. Lanzalunga, *Acc. Chem. Res.* **2000**, *33*, 243–251; b) E. Baciocchi, F. D'Acunzo, C. Galli, O. Lanzalunga, *J. Chem. Soc., Perkin Trans. 2* **1996**, 133–140; c) E. Baciocchi, M. Mattioli, R. Romano, R. Ruzziconi, *J. Org. Chem.* **1991**, *56*, 7154–7160.
- [252] I. N.-M. Leibler, M. A. Tekle-Smith, A. G. Doyle, *Nat. Commun.* **2021**, *12*, 6950.
- [253] a) J. M. Ramos-Villaseñor, E. Rodríguez-Cárdenas, C. E. Barrera Díaz, B. A. Frontana-Uribe, *J. Electrochem. Soc.* **2020**, *167*, 155509; b) I. Colomer, A. E. R. Chamberlain, M. B. Haughey, T. J. Donohoe, *Nat. Rev. Chem.* **2017**, *1*; c) B. Elsler, A. Wiebe, D. Schollmeyer, K. M. Dyballa, R. Franke, S. R. Waldvogel, *Chem. – Eur. J.* **2015**, *21*, 12321–12325.
- [254] M. Hasegawa, T. Fuchigami, *Electrochim. Acta* **2004**, *49*, 3367–3372.
- [255] a) M. Fingas (Ed.) *De Gruyter STEM*, De Gruyter Berlin, Boston, **2022**.; b) S. Faramawy, T. Zaki, A.-E. Sakr, *J. Nat. Gas Sci. Eng.* **2016**, *34*, 34–54; c) H. H. Schobert: *Chemistry of fossil fuels and biofuels*, Cambridge Univ. Press Cambridge, **2013**.
- [256] a) C. Zhang, F. Wang, *Acc. Chem. Res.* **2020**, *53*, 470–484; b) C. Chio, M. Sain, W. Qin, *Renew. Sust. Energ. Rev.* **2019**, *107*, 232–249; c) Z. Sun, B. Fridrich, A. de Santi, S. Elangovan, K. Barta, *Chem. Rev.* **2018**, *118*, 614–678; d) M. Verziu, A. Tirsoaga, B. Cojocar, C. Bucur, B. Tudora, A. Richel, M. Aguedo, A. Samikannu, J. P. Mikkola, *Mol. Catal.* **2018**, *450*, 65–76; e) T. vom Stein, T. den Hartog, J. Buendia, S. Stoychev, J. Mottweiler, C. Bolm, J. Klankermayer, W. Leitner, *Angew. Chem.* **2015**, *127*, 5957–5961; f) J. Zakzeski, P. C. A. Bruijninx, A. L. Jongerius, B. M. Weckhuysen, *Chem. Rev.* **2010**, *110*, 3552–3599.
- [257] P. B. Arockiam, C. Bruneau, P. H. Dixneuf, *Chem. Rev.* **2012**, *112*, 5879–5918.

REFERENCES

- [258] a) L. Ackermann (Ed.) *Science of Synthesis*, Thieme Stuttgart, **2022.**; b) K. Gong, Q. Fang, S. Gu, S. F. Y. Li, Y. Yan, *Energy Environ. Sci.* **2015**, *8*, 3515–3530.
- [259] a) F. Martínez-Peña, S. Infante-Tadeo, A. Habtemariam, A. M. Pizarro, *Inorg. Chem.* **2018**, *57*, 5657–5668; b) B. Therrien, *Coord. Chem. Rev.* **2009**, *253*, 493–519.
- [260] P. O. Nubel, C. L. Hunt, D. S. Choi, T. J. Marks, WO9740934 (A1), **1997**.
- [261] R. T. Swann, A. W. Hanson, V. Boekelheide, *J. Am. Chem. Soc.* **1986**, *108*, 3324–3334.
- [262] R. Stodt, S. Gencaslan, I. M. Müller, W. S. Sheldrick, *Eur. J. Inorg. Chem.* **2003**, *2003*, 1873–1882.
- [263] D. Zell, S. Warratz, D. Gelman, S. J. Garden, L. Ackermann, *Chem. – Eur. J.* **2016**, *22*, 1248–1252.
- [264] C. Lo, R. Cariou, C. Fischmeister, P. H. Dixneuf, *Adv. Synth. Catal.* **2007**, *349*, 546–550.
- [265] M. T. Huynh, C. W. Anson, A. C. Cavell, S. S. Stahl, S. Hammes-Schiffer, *J. Am. Chem. Soc.* **2016**, *138*, 15903–15910.
- [266] a) M. M. Amer, R. Hommelsheim, C. Schumacher, D. Kong, C. Bolm, *Faraday Discuss.* **2023**, *241*, 79–90; b) J. Ayarza, Z. Wang, J. Wang, C.-W. Huang, A. P. Esser-Kahn, *ACS Macro Lett.* **2020**, *9*, 1237–1248; c) Y. Pang, J. W. Lee, K. Kubota, H. Ito, *Angew. Chem. Int. Ed.* **2020**, *59*, 22570–22576; d) C. Schumacher, J. G. Hernández, C. Bolm, *Angew. Chem. Int. Ed.* **2020**, *59*, 16357–16360; e) S. Tu, Y. Guo, Y. Zhang, C. Hu, T. Zhang, T. Ma, H. Huang, *Adv. Funct. Mater.* **2020**, *30*, 2005158; f) K. Kubota, Y. Pang, A. Miura, H. Ito, *Science* **2019**, *366*, 1500–1504; g) M. B. Starr, J. Shi, X. Wang, *Angew. Chem. Int. Ed.* **2012**, *51*, 5962–5966.
- [267] a) J. S. Jaworski, M. Cembor, M. Orlik, *J. Electroanal. Chem.* **2005**, *582*, 165–170; b) N. L. Cox, C. A. Kraus, R. M. Fuoss, *Trans. Faraday Soc.* **1935**, *31*, 749–761.
- [268] V. Chaban, *J. Mol. Model.* **2015**, *21*, 172.
- [269] P. Wang, A. Anderko, *Fluid Phase Equilib.* **2001**, *186*, 103–122.
- [270] P. Wang, A. Anderko, R. D. Young, *Ind. Eng. Chem. Res.* **2004**, *43*, 8083–8092.
- [271] C. M. Hansen: *Hansen Solubility Parameters*, CRC Press, **2007**.
- [272] R. Sala, G. Kiala, L. F. Veiros, G. Broggini, G. Poli, J. Oble, *J. Org. Chem.* **2022**, *87*, 4640–4648.
- [273] R. Grainger, J. Cornella, D. C. Blakemore, I. Larrosa, J. M. Campanera, *Chem. – Eur. J.* **2014**, *20*, 16680–16687.
- [274] a) G. T. Whiteker, C. J. Copley, *Top. Organomet. Chem.* **2012**, *42*, 35–46; b) J. R. Zoeller, V. H. Agreda, S. L. Cook, N. L. Lafferty, S. W. Polichnowski, D. M. Pond, *Catalysis Today* **1992**, *13*, 73–91; c) W. U. Knox, J. U. Roth, F. U. Paulik, A. U. Hershman, US3769329 (A), **1970**.
- [275] a) V. S. Shende, V. B. Saptal, B. M. Bhanage, *Chem. Rec.* **2019**, *19*, 2022–2043; b) B. Gupta, I. Singh, *Hydrometallurgy* **2013**, *134-135*, 11–18; c) C. Nowotny, W. Halwachs, K. Schügerl, *Sep. Purif. Technol.* **1997**, *12*, 135–144.
- [276] a) K. Tanaka: *Rhodium Catalysis in Organic Synthesis*, Wiley, **2019.**; b) P. A. Evans (Ed.) *Modern rhodium-catalyzed organic reactions*, Wiley-VCH Weinheim, **2005**.
- [277] a) W. Zhu, T. B. Gunnoe, *Acc. Chem. Res.* **2020**, *53*, 920–936; b) D. A. Colby, A. S. Tsai, R. G. Bergman, J. A. Ellman, *Acc. Chem. Res.* **2012**, *45*, 814–825; c) G. Song, F. Wang, X. Li, *Chem. Soc. Rev.* **2012**, *41*, 3651–3678; d) D. A. Colby, R. G. Bergman, J. A. Ellman, *Chem. Rev.* **2010**, *110*, 624–655.
- [278] A. Korotvicka, D. Necas, M. Katora, *COC* **2012**, *16*, 1170–1214.
- [279] a) L. Brammer, *Faraday Discuss.* **2017**, *203*, 485–507; b) C. C. Robertson, J. S. Wright, E. J. Carrington, R. N. Perutz, C. A. Hunter, L. Brammer, *Chem. Sci.* **2017**, *8*, 5392–5398.
- [280] N. V. Belkova, L. M. Epstein, O. A. Filippov, E. S. Shubina, *Chem. Rev.* **2016**, *116*, 8545–8587.
- [281] H. Wang, I. Choi, T. Rogge, N. Kaplaneris, L. Ackermann, *Nat. Catal.* **2018**, *1*, 993–1001.
- [282] G. R. Fulmer, A. J. M. Miller, N. H. Sherden, H. E. Gottlieb, A. Nudelman, B. M. Stoltz, J. E. Bercaw, K. I. Goldberg, *Organometallics* **2010**, *29*, 2176–2179.
- [283] Jack Bernstein/Jay S. Roth/William T. Miller Jr.
- [284] D. Cantillo, O. de Frutos, J. A. Rincón, C. Mateos, C. O. Kappe, *J. Org. Chem.* **2014**, *79*, 8486–8490.

REFERENCES

- [285] M. Haerter, H. Beck, P. Ellinghaus, K. Berhoerster, S. Greschat, K. H. Thierauch, DE102008057344 (A1), **2008**.
- [286] Q. Zhang, J. C. Mixdorf, G. J. Reynders, H. M. Nguyen, *Tetrahedron* **2015**, *71*, 5932–5938.
- [287] S. Liang, F. J. Barrios, O. E. Okoromoba, Z. Hetman, B. Xu, G. B. Hammond, *J. Fluorine Chem.* **2017**, *203*, 136–139.
- [288] G. Albertin, S. Antoniutti, J. Castro, S. Paganelli, *J. Organomet. Chem.* **2010**, *695*, 2142–2152.
- [289] Y. Boutadla, D. L. Davies, R. C. Jones, K. Singh, *Chem. – Eur. J.* **2011**, *17*, 3438–3448.

ACKNOWLEDGEMENTS

First and foremost, I want to express my gratitude to my supervisor *Prof. Lutz Ackermann*. Thank you for giving me the opportunity to experience this fascinating journey in your laboratories. You have built a flourishing scientific microcosmos in Göttingen, and I feel privileged to have learned from you personally and the big international community of scientists, that you have gathered. I feel inspired by your devotion to science and model work ethics. Your professional guidance and kind support motivated me even in the most challenging periods.

Furthermore, I want to thank my second supervisor *Prof. Shoubhik Das* for the valuable ideas and suggestions for my PhD projects. Of course, I want to also thank the other members of my thesis committee – *Prof. Dietmar Stalke*, *Jun-Prof. Nadja Simeth*, *Jun.-Prof. Johannes Walker* and *Dr. Daniel Janßen-Müller* – for taking their time to evaluate my research and assist in my graduation.

The mighty Ackermann group! On a professional level, I am grateful to have had the possibility to work with so many great chemists. I could see what passion for science means every day, and I learned a lot from experienced, reflective, humble and knowledgeable researchers. For all the fruitful discussions, as well as the technical and moral support, I especially want to thank Youai Qiu, Lars Finger, Tjark Meyer, Shou-Kun Zhang, Nikolaos Kaplaneris, João Oliveira, Antonis Messinis, Zhipeng Lin, Maximilian Stangier and Leonardo Massignan. I had the pleasure to collaborate with many awesome scientists on exciting projects and I want to thank all of them for their trust into my expertise. Big thanks to the careful proofreaders, who made this thesis a bit more bearable (or even enjoyable) for me, as well as other readers (whether involuntary or indeed interested): João Oliveira, Philipp Boos, Hendrik Simon, Simon Homöller and Tsuyoshi Ohyama. It is hard to interact equally with everyone in such a big and heterogeneous group of people, but despite our size and outside crises of the past years, we managed to keep a sense of family, and I always look back smiling when I think of all the dinners, barbecues, legendary parties, group outings etc. I will really miss our awesome football sessions, where we, as “Lutzifers” and “Ackermaniacs”, experienced the power of teamwork on another level.

Shout-out to our fantastic laboratory staff, that never gave up to deal with the sometimes frightening impracticality of an academic researcher, and have kept the lab running smoothly: Stefan Beusshausen and Karsten Rauch. To our helpful secretaries and scientific

ACKNOWLEDGEMENTS

coordinator, who are responsible for the warm welcome of newcomers and who bring order into in the administrative section of a scientist's busy and at times chaotic mind: Gabriele Keil-Knepel, Bianca Spitalieri, Sabine Schacht and Svenja Warratz. To the analytical department. All the work is worth nothing without solid data on what we fabricate. Gladly, we can count on your expertise and pleasant cooperation! Much appreciation to our institute's glass construction, mechanical and electrical workshops, who masterfully materialized our wild and creative ideas, but also troubleshot the results of occasional clumsiness and, admittedly, negligence.

The challenging part of this journey would have been hard to cope with, if it wasn't for my faithful friends from Potsdam: Luise Trogisch, Tobias Rindfleisch, Boris Zühlke, Boris Silbermann, Alexander v. Berlepsch and Margaryta Paliy. Whether I was in the mood for laughing or crying, or complaining, or talking nonsense, I could always count on you as people, with whom I could share my personal concerns. A very special tribute goes to my kind-hearted friend Alexander Ghorbani, who passionately supported me from Toronto. A new chapter in life also opens the door to new friendships, and I am grateful to have met open-hearted, sincere, funny, compassionate and intelligent people here in Göttingen. Thank you: Leonardo Massignan, Nate Ang, Renato Lúcio de Carvalho, Elena Cotroneo and Valentina Pelliccioli! I had unforgettable times with you, and you helped me to let off a lot of steam. You really boosted my happiness here, and strengthened my confidence.

The beginning and the end of the day has been mostly marked with a lovely greeting from an awesome flatmate. Thank you all – Shih-Ju Lee, Jasmin Oster, Christian Scheulen Sophie Teichmann, Felix Alebrand, Michael Neuwirt and Benedikt Bader – for the many interesting chats, the insights into different cuisines, and for just the fact that thanks to you I enjoyed coming back home after work!

My bike. I know you are just an assemblage of inanimate metal and polymer, but your everyday service was vital for me, and I really appreciate that you didn't leave with someone else, despite spending the nights outside, even in winter.

Finally, I want to sincerely thank for the support of my family. My grandmother Zilja Leschinskaja זיליא, who was my big teacher in life, and someone I could always look up to. And of course my mother Uljana Scheremetjewa, who continues to encourage me to work for a greater cause and whose unconditional, heartwarming love I have felt every day.

CURRICULUM VITAE

Personal Information

Name: Alexej Scheremetjew
Date of birth: 20/03/1993
Place of birth: Bernau b. Berlin (Germany)
Citizenship: German

Education

04/2018 – present: **Ph.D. student**, *Prof. Dr. Lutz Ackermann* research group, Institute of Organic and Biomolecular Chemistry, Georg-August-University Göttingen, Germany. Research focus: Electrochemical C–C and C–H Functionalizations

10/2015 – 01/2018: **M.Sc. student** in chemistry, Universität Potsdam, Germany (final grade: 1.1/with distinction). Master thesis: “Development of Molecular Probes for the Study of the HDAC6 Zinc-Finger Ubiquitin Binding Domain” (supervised by *Prof. Dr. Mark Lautens*, University of Toronto, Canada; grade: 1.0)

10/2012 – 11/2015: **B.Sc. student** in chemistry, Universität Potsdam, Germany (final grade: 1.9/good). Bachelor thesis: “Development of an electrospun polymeric matrix as a collector material for a microfluidic chemical sensor” (supervised by *Prof. Dr. Israel Schechter*, Technion – Israel Institute of Technology, Haifa, Israel; grade: 1.5)

06/2012: **Abitur** (A-level), Humboldt-Gymnasium, Potsdam, Germany (final grade: 1.0)

Fellowships

- 09/2012 – present: Member of the Gesellschaft Deutscher Chemiker e.V. (GDCh, German Chemical Society)
- 10/2012 – 01/2018: Fellow of the Ernst-Ludwig-Ehrlich Studienwerk e.V (ELES)

Publications

- 1) Present Thesis. Available online under DOI: 10.53846/goediss-9793
- 2) M. Stangier, A. Scheremetjew, L. Ackermann, "Chemo- and Site-Selective Electrooxidative Alkane Fluorination by C(sp³)-H Cleavage" *Chem. Eur. J.* **2022**, 28, e202201654.
- 3) W. Wei, A. Scheremetjew, L. Ackermann, "Electrooxidative Palladium- and Enantioselective Rhodium-Catalyzed [3+2] Spiroannulations" *Chem. Sci.* **2022**, 13, 2783–2788.
- 4) A. Scheremetjew, T. H. Meyer, Z. Lin, L. Massignan, L. Ackermann, "Fundamental Principles of Organic Electrochemistry" In *Science of Synthesis: Electrochemistry in Organic Synthesis*, Ackermann, L., Ed.; Thieme: Stuttgart, **2021**, 3–32.
- 5) L. Yang, B. B. Jei, A. Scheremetjew, B. Yuan, C. Stückl, L. Ackermann, "Electrooxidative o-Carborane Chalcogenations Without Directing Groups: Cage Activation by Copper Catalysis at Room Temperature" *Chem. Sci.* **2021**, 12, 12971–12976.
- 6) L. Yang, B. B. Jei, A. Scheremetjew, R. Kuniyil, L. Ackermann, "Electrochemical B–H Nitrogenation: Access to Amino Acid and BODIPY-Labeled nido-Carboranes" *Angew. Chem. Int. Ed.* **2021**, 60, 1482–1487.
- 7) L. Yang, R. Steinbock, A. Scheremetjew, R. Kuniyil, L. H. Finger, A. M. Messinis, L. Ackermann, "Aza-Ruthena(II)-Bicyclo-[3.2.0]-Heptadiene: Key Intermediate for Ruthenaelectro(II/III/I)-Catalyzed Alkyne Annulations" *Angew. Chem. Int. Ed.* **2020**, 59, 11130–11135.
- 8) Y. Qiu, A. Scheremetjew, L. H. Finger, L. Ackermann, "Electrophotocatalytic Undirected C–H Trifluoromethylations of (Het)Arenes" *Chem. Eur. J.* **2020**, 26, 3241–3246.
- 9) C. Tian, U. Dhawa, A. Scheremetjew, L. Ackermann, "Cupraelectro-Catalyzed Alkyne Annulation: Evidence for Distinct C–H Alkynylation and Decarboxylative C–H/C–C Manifolds" *ACS Catal.* **2019**, 9, 7690–7696.
- 10) Y. Qiu, A. Scheremetjew, L. Ackermann, "Electrooxidative C–C Alkenylation by Rhodium(III) Catalysis" *J. Am. Chem. Soc.* **2019**, 141, 2731–2738.
- 11) Y. Qiu, W.-J. Kong, J. Struwe, N. Sauermann, T. Rogge, A. Scheremetjew, L. Ackermann, "Electrooxidative Rhodium-Catalyzed C–H/C–H Activation: Electricity as Oxidant for Cross-Dehydrogenative Alkenylation" *Angew. Chem. Int. Ed.* **2018**, 57, 5828–5832.

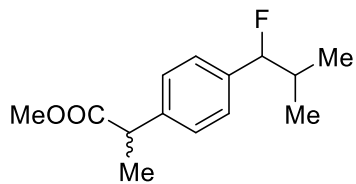
’ These authors contributed equally to the published work.

ZUSAMMENFASSUNG

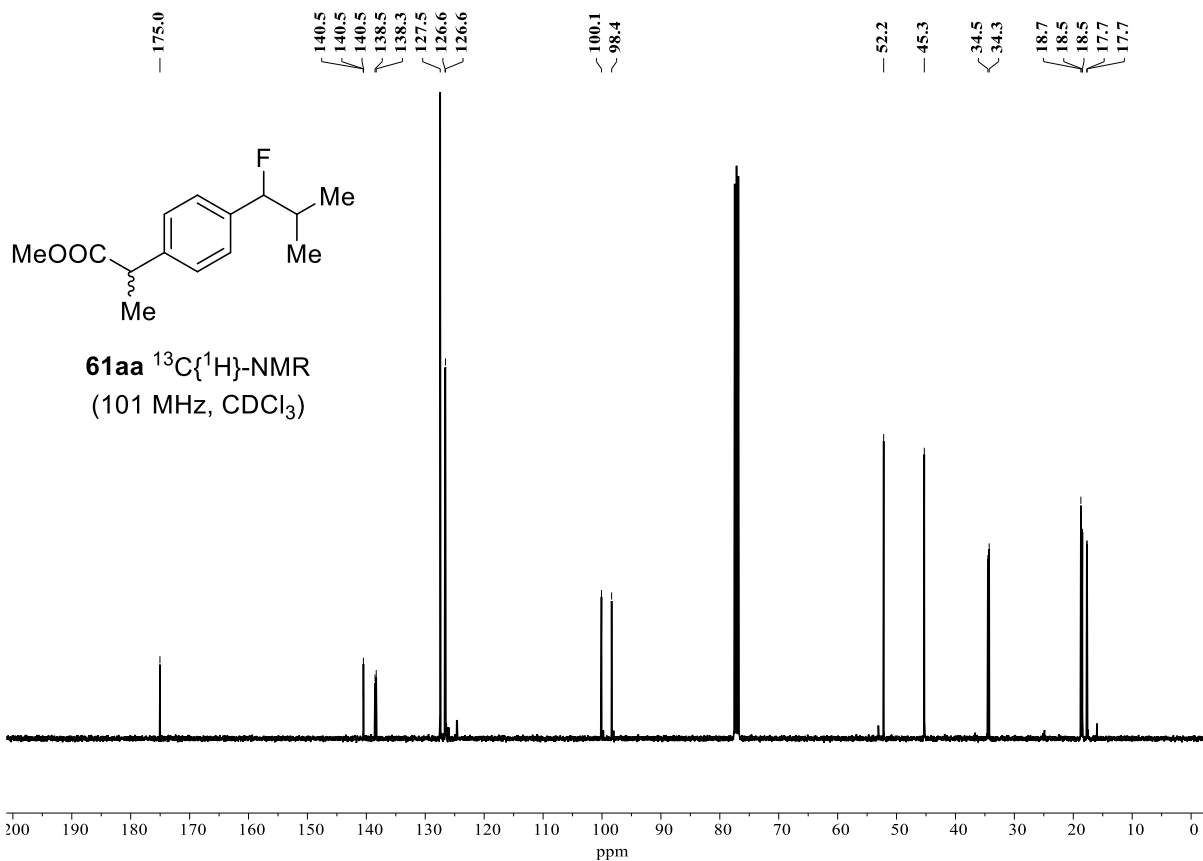
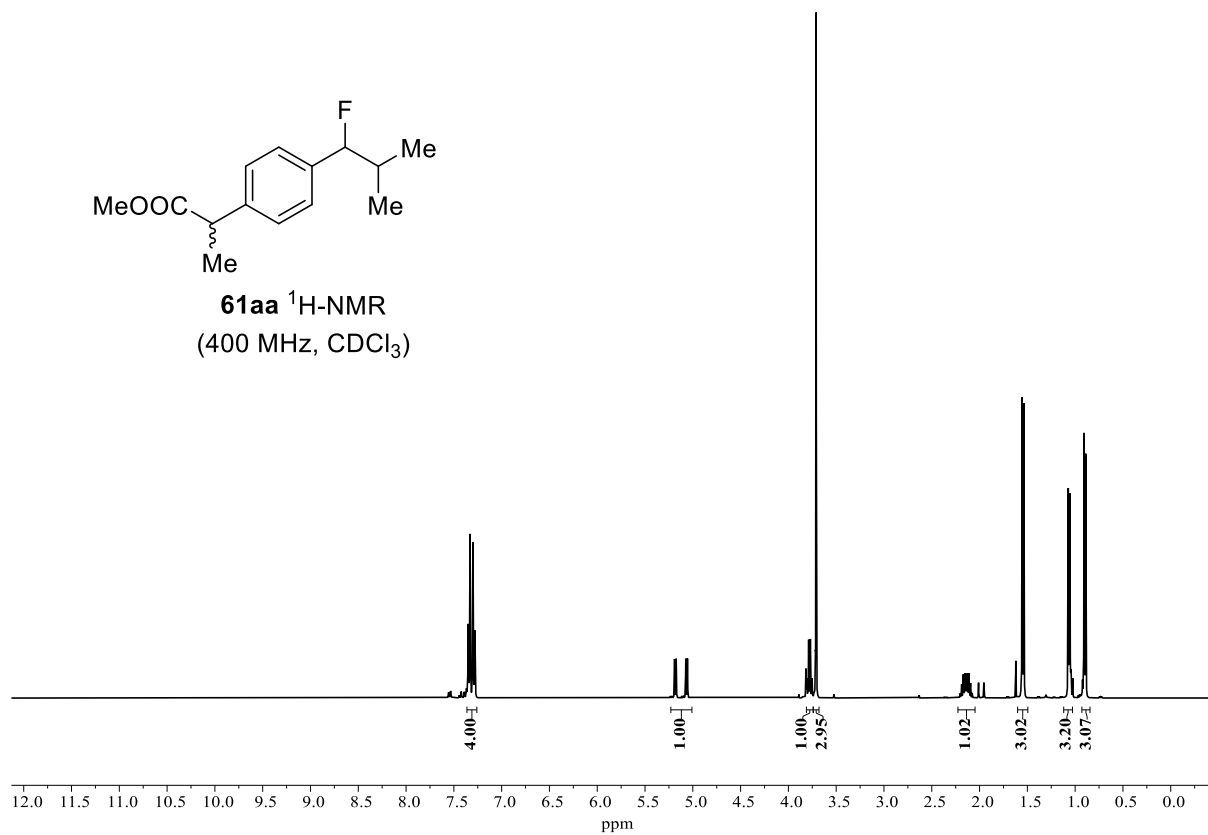
Direkte Funktionalisierungen von C–H- und C–C-Bindungen haben sich als zeitsparende und kostengünstige Alternativen zu etablierten Kreuzkupplungsreaktionen etabliert. Für oxidative Kupplungsvarianten werden allerdings stöchiometrische Mengen an Oxidationsmitteln benötigt, sodass üblicherweise entweder auf ökologisch und ökonomisch bedenkliche Reagenzien, wie Edelmetallsalze, oder auf brandfördernden Sauerstoff zurückgegriffen wird. Für diesen nachteiligen Aspekt ist Elektrochemie ein attraktiver Lösungsansatz, da die Stöchiometrie der Redoxreaktion auf ihre Quintessenz reduziert werden kann: den Elektronentransfer. Die Produktions- und Abfallbehandlungskosten können dadurch erheblich gesenkt werden. Darüber hinaus könnte das Arbeiten bei minimalen Überspannungen auch zu einer breiteren Anwendbarkeit einer vergleichbaren Reaktion mit chemischen Oxidationsmitteln beitragen. In Anbetracht dieser vorteilhaften Eigenschaften wird die Einbindung der Elektrolyse auf dem Gebiet der C–H- und C–C-Funktionalisierungen anhand von drei verschiedenen Reaktionen untersucht. Für jede der Reaktionen wurde beabsichtigt, die ökologische Bilanz zu verbessern, indem schädliche und teure chemische Oxidationsmittel durch preiswerten, leicht verfügbaren und umweltfreundlichen Strom ersetzt werden. Besonderes Augenmerk wurde auf die Untersuchung der Toleranz von funktionellen Gruppen gelegt. Im ersten Projekt wurde eine ungerichtete und metallfreie elektrochemische Fluorierung von benzyllischen C–H-Bindungen entwickelt. Die Reaktion funktionierte unter Verwendung von kostengünstigem $\text{NEt}_3 \cdot 3\text{HF}$ als Quelle für nukleophiles Fluorid, welches praktischerweise auch die elektrische Leitfähigkeit des Systems sicherstellt. Der Schlüsselfaktor für die bemerkenswerte Toleranz gegenüber funktionellen Gruppen und die ausgezeichnete Chemoselektivität war die Verwendung von HFIP als Cosolvens. Im zweiten Projekt wurde die Elektrifizierung einer Ruthenium-katalysierten decarboxylativen C–H-Alkenylierung versucht. Trotz einer Reihe von Beispielen mit vergleichbarer Effizienz, wie bei chemisch-oxidierender Reaktionsführung, lieferte diese spezielle Umwandlung im Allgemeinen eher mäßige Ausbeuten und zeigte eine begrenzte Toleranz gegenüber funktionellen Gruppen. Aufgrund der Notwendigkeit von unpolaren Reaktionsmedien, die für Elektrolysen gemeinhin ungünstig sind, wurde die Aktivierung von Elektrolyten mit hohem unpolarem Lösungsmittelanteil untersucht. Schließlich wurde eine elektrochemische netto-dehydrierende C–C/C–H-Kopplung durch Rhodiumkatalyse und Zuhilfenahme einer entfernbaren dirigierenden Gruppe erreicht. Die optimierten

Bedingungen ermöglichten die Synthese von Diaryl-substituierten *E*-Alkenen in einer benutzerfreundlichen ungeteilten elektrochemischen Zelle. Die Reaktion wies eine ausgezeichnete Regioselektivität auf, sodass sogar sterisch überlastete 1,2,3-substituierte Arene in guter Ausbeute gewonnen wurden.

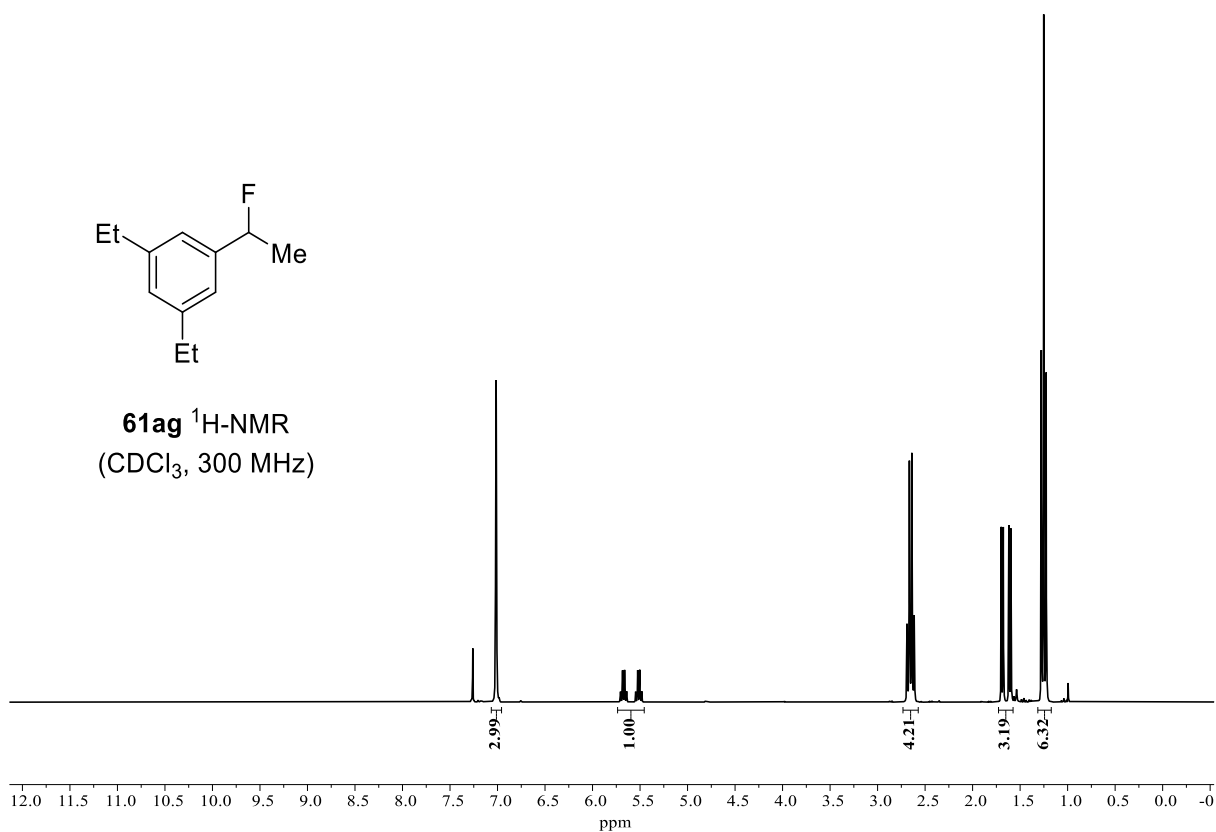
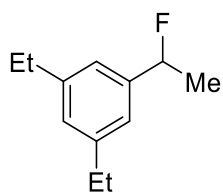
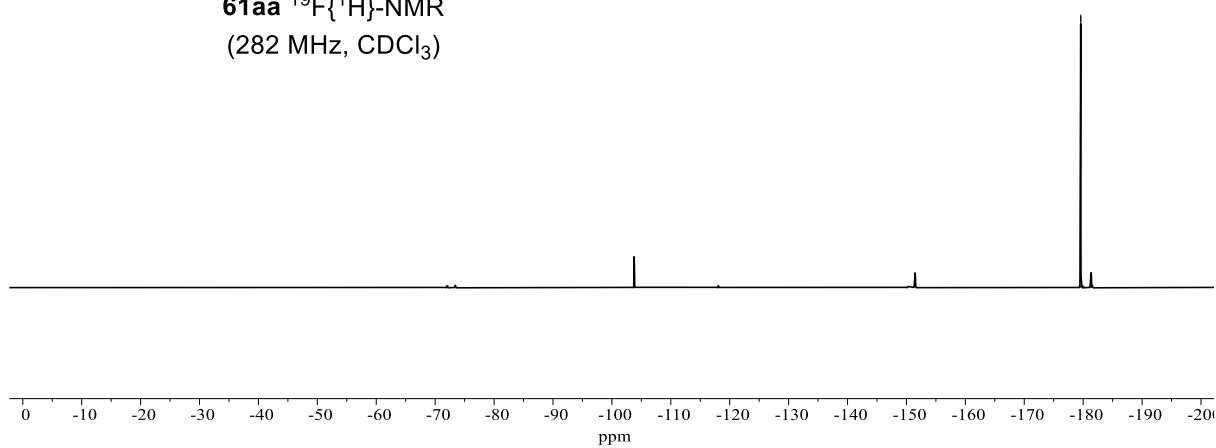
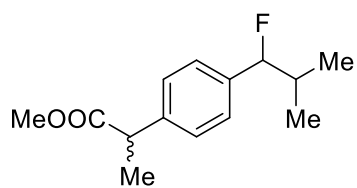
NMR SPECTRA



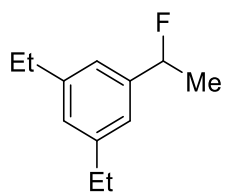
61aa $^1\text{H-NMR}$
(400 MHz, CDCl_3)



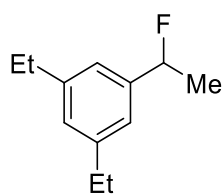
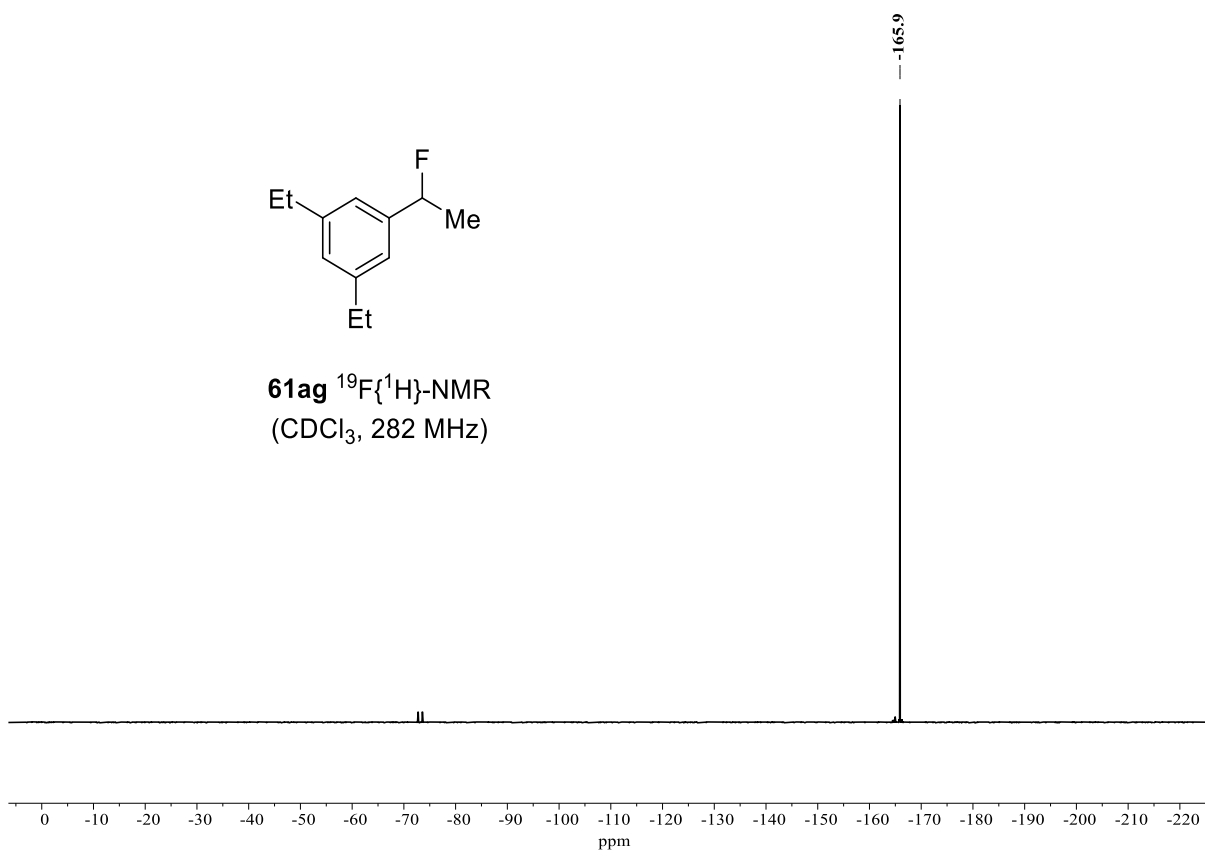
NMR SPECTRA



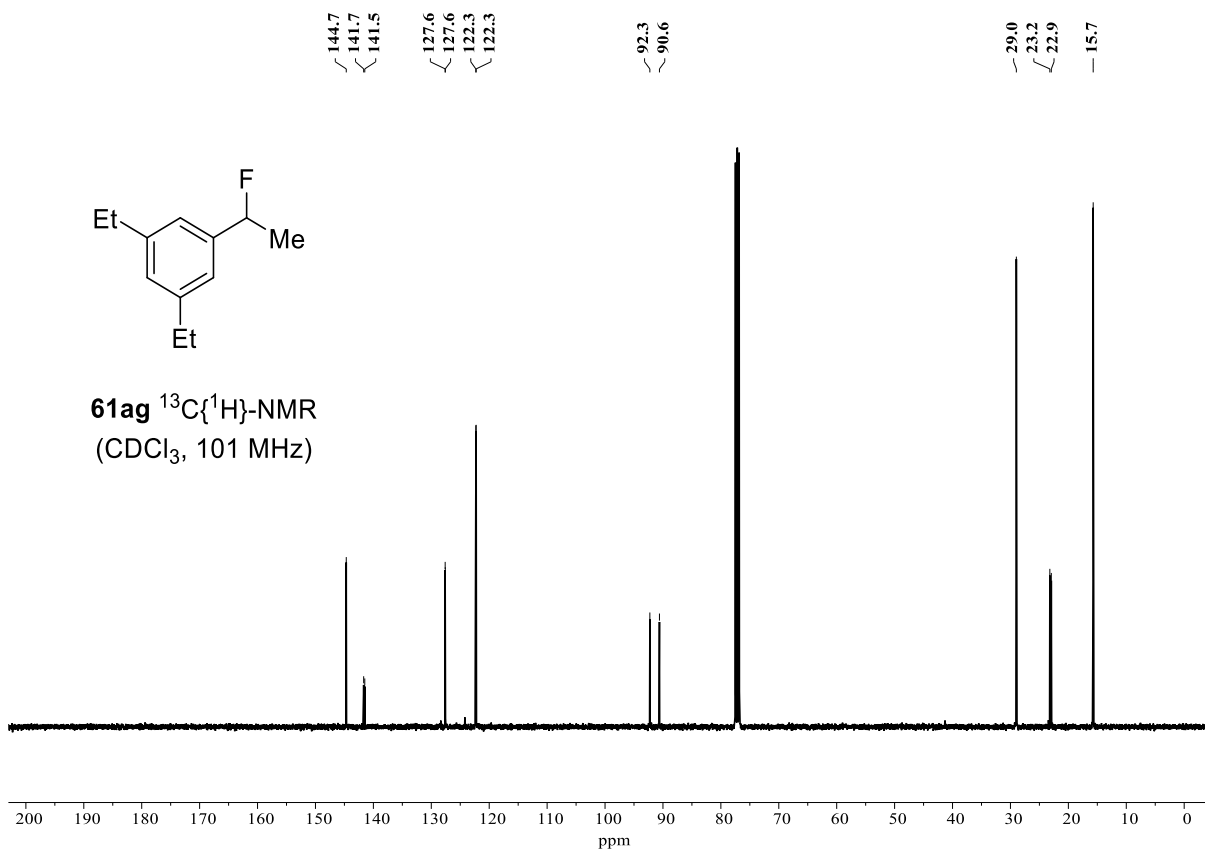
NMR SPECTRA



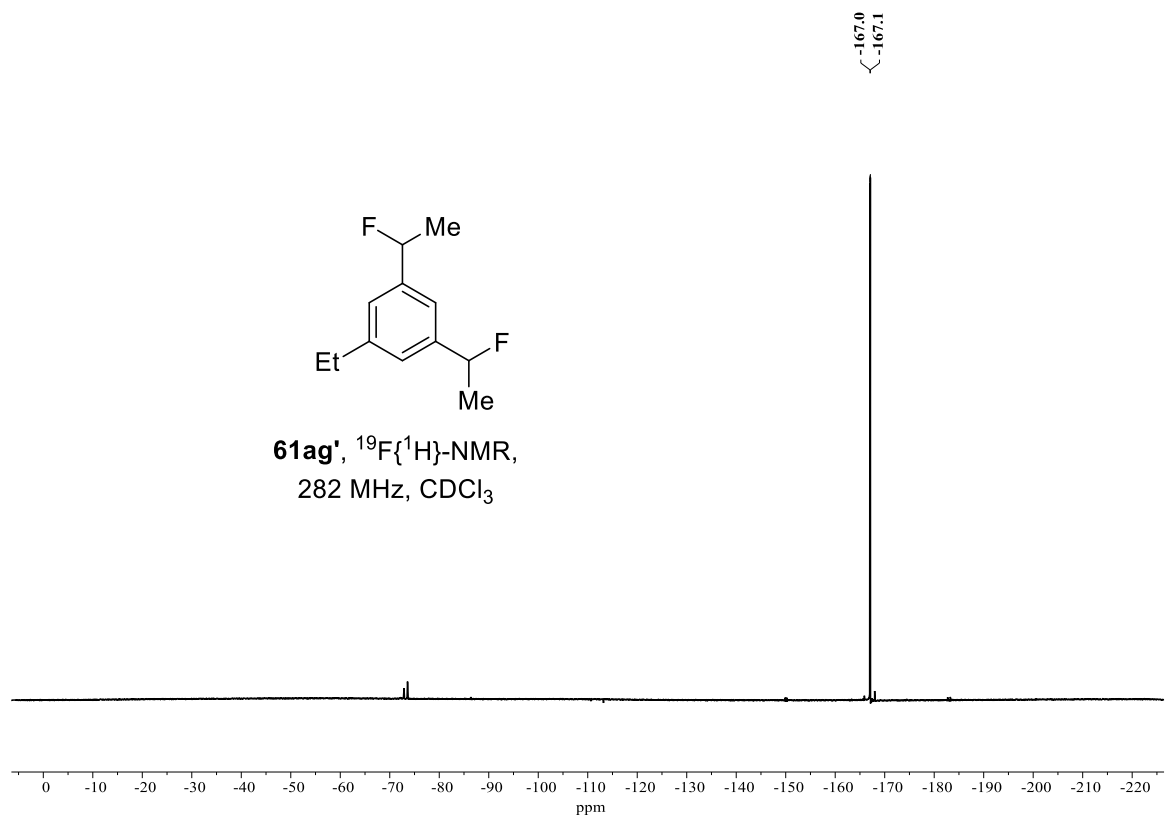
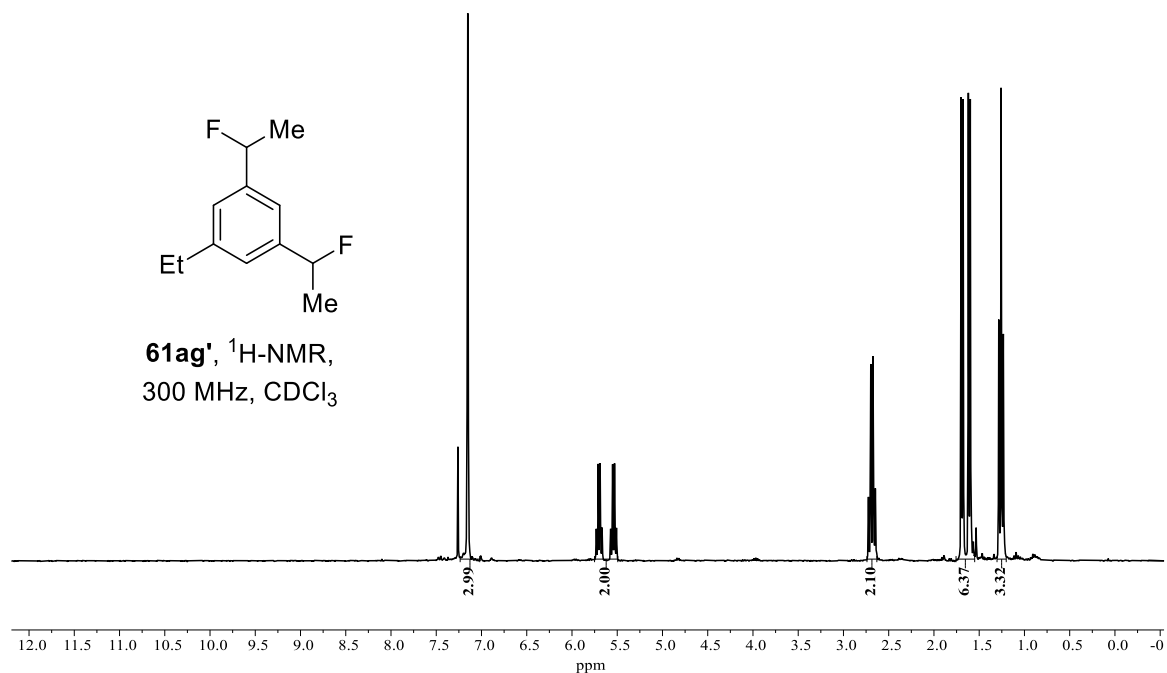
61ag $^{19}\text{F}\{^1\text{H}\}$ -NMR
(CDCl_3 , 282 MHz)



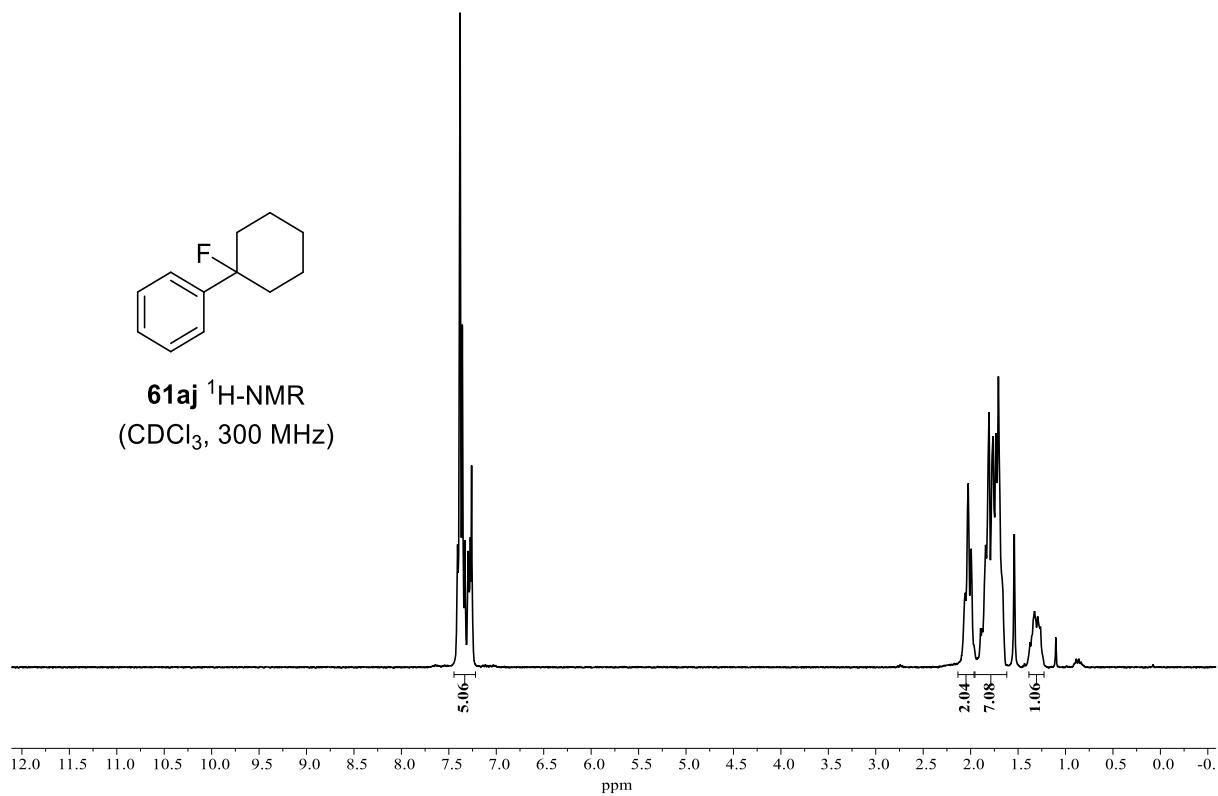
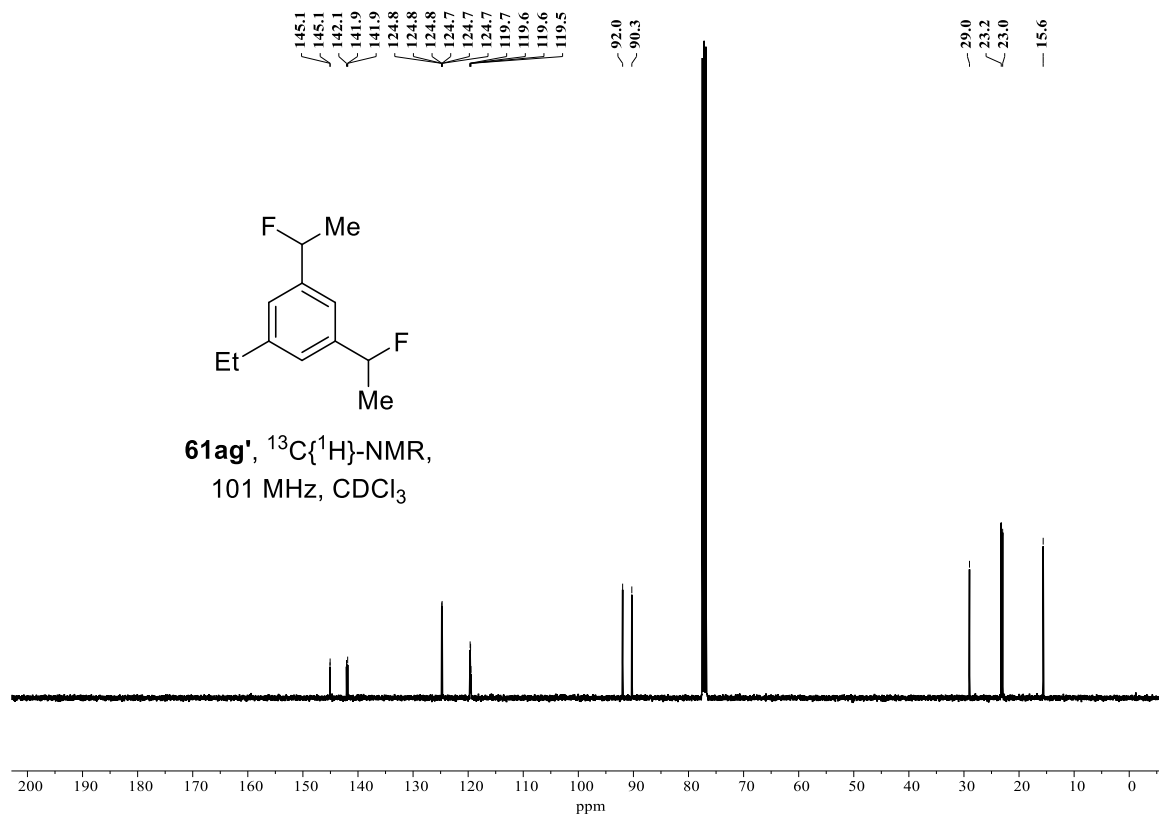
61ag $^{13}\text{C}\{^1\text{H}\}$ -NMR
(CDCl_3 , 101 MHz)



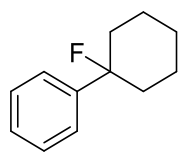
NMR SPECTRA



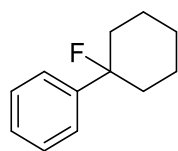
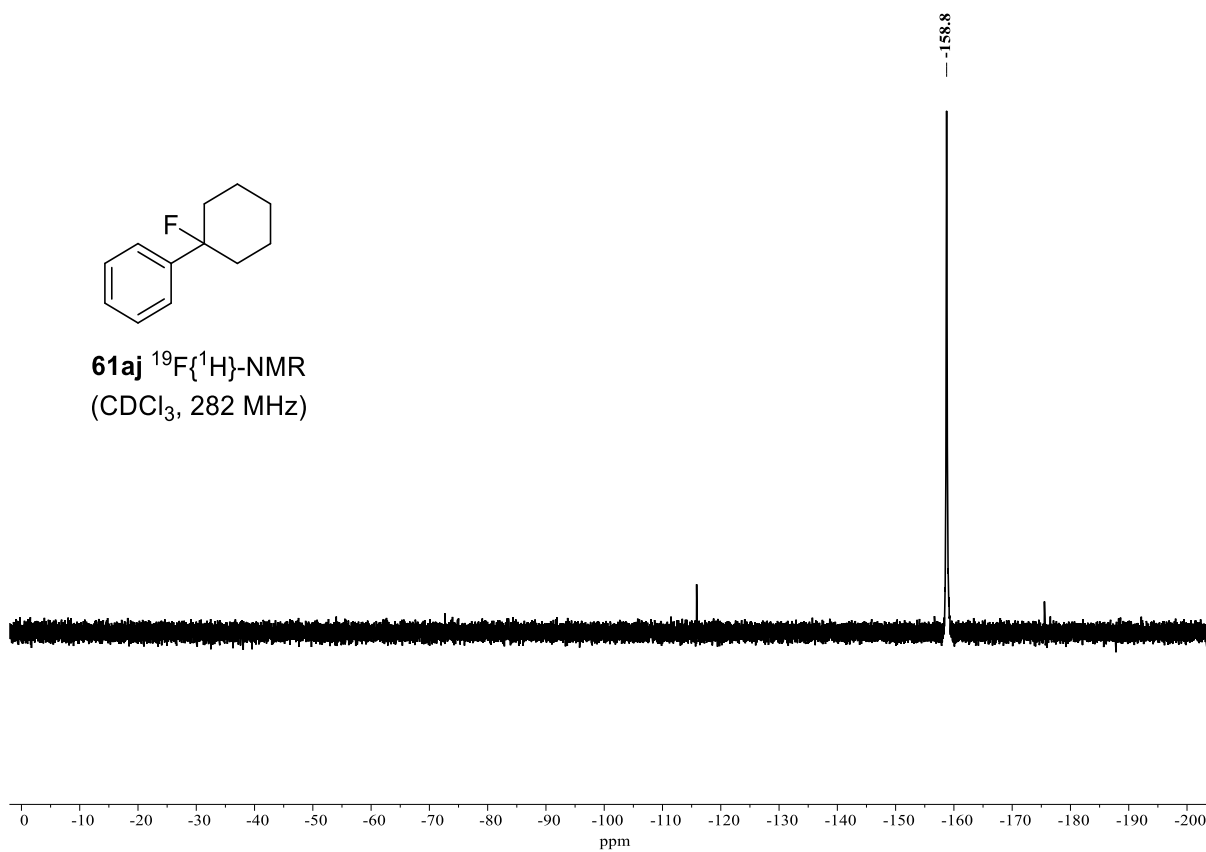
NMR SPECTRA



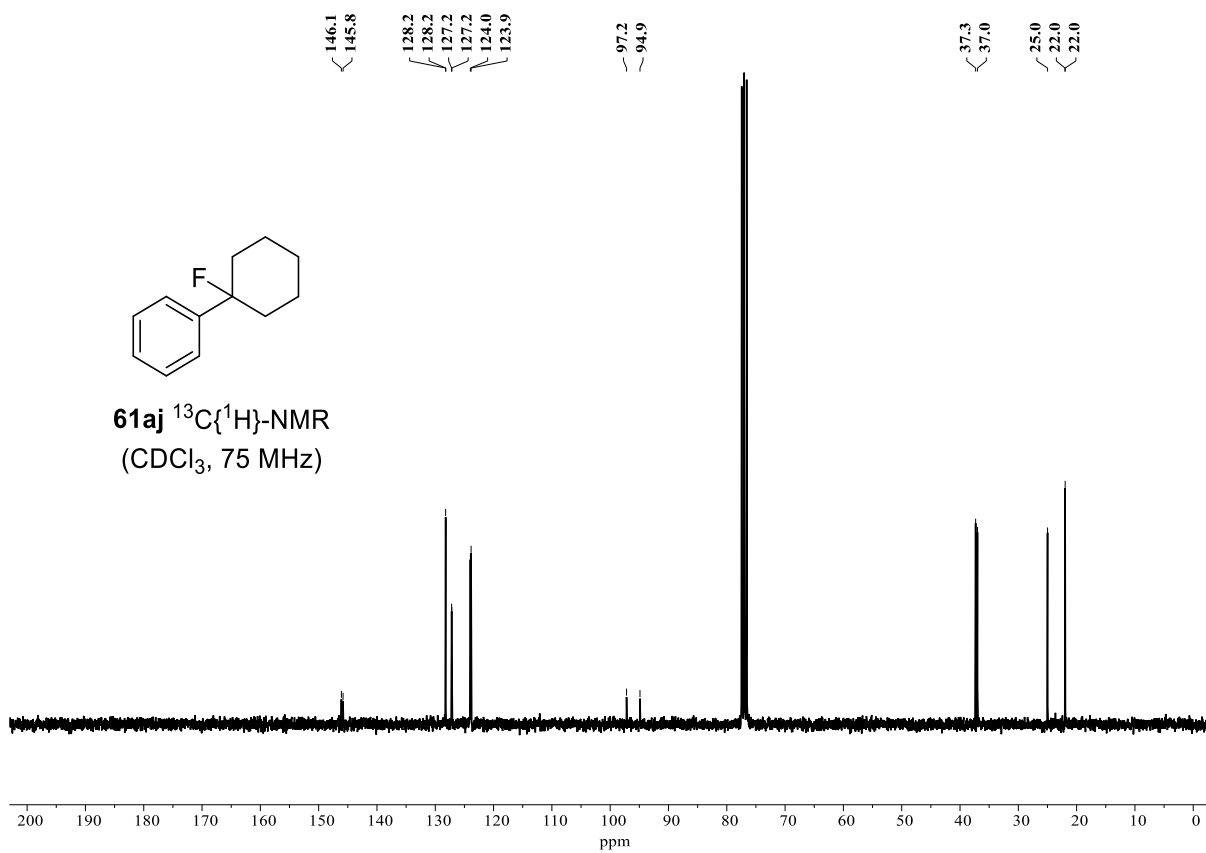
NMR SPECTRA



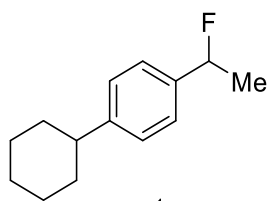
61aj $^{19}\text{F}\{^1\text{H}\}$ -NMR
(CDCl_3 , 282 MHz)



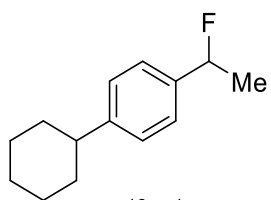
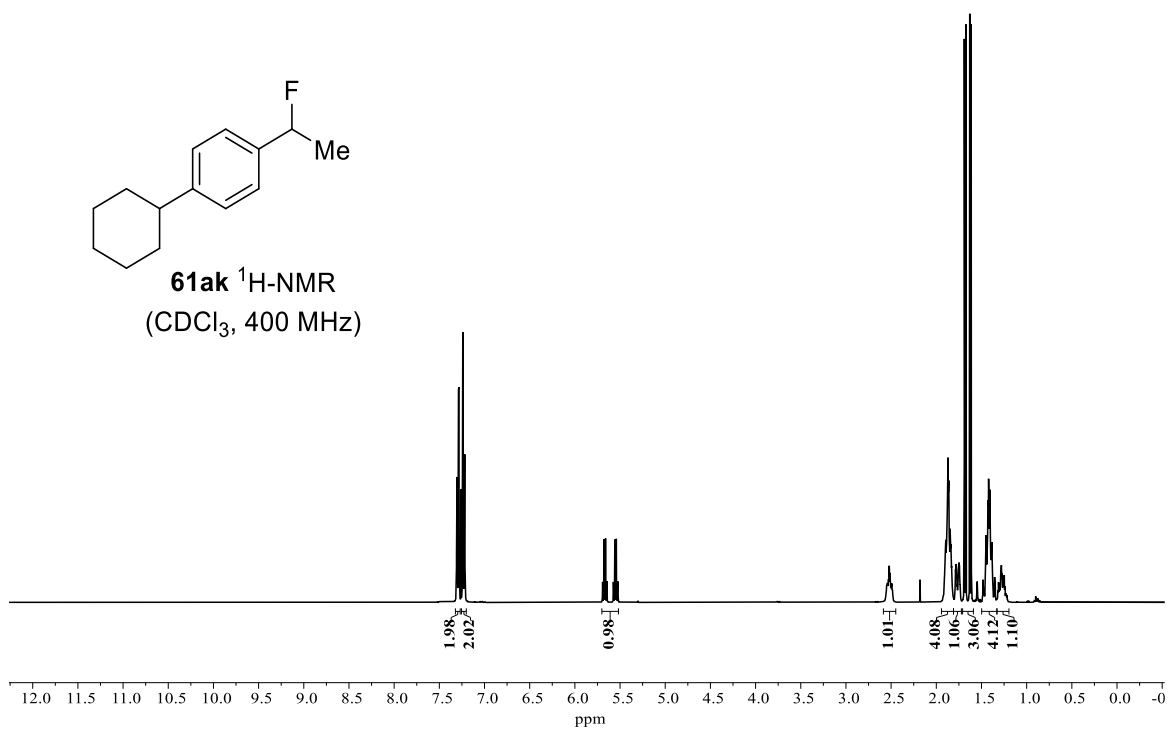
61aj $^{13}\text{C}\{^1\text{H}\}$ -NMR
(CDCl_3 , 75 MHz)



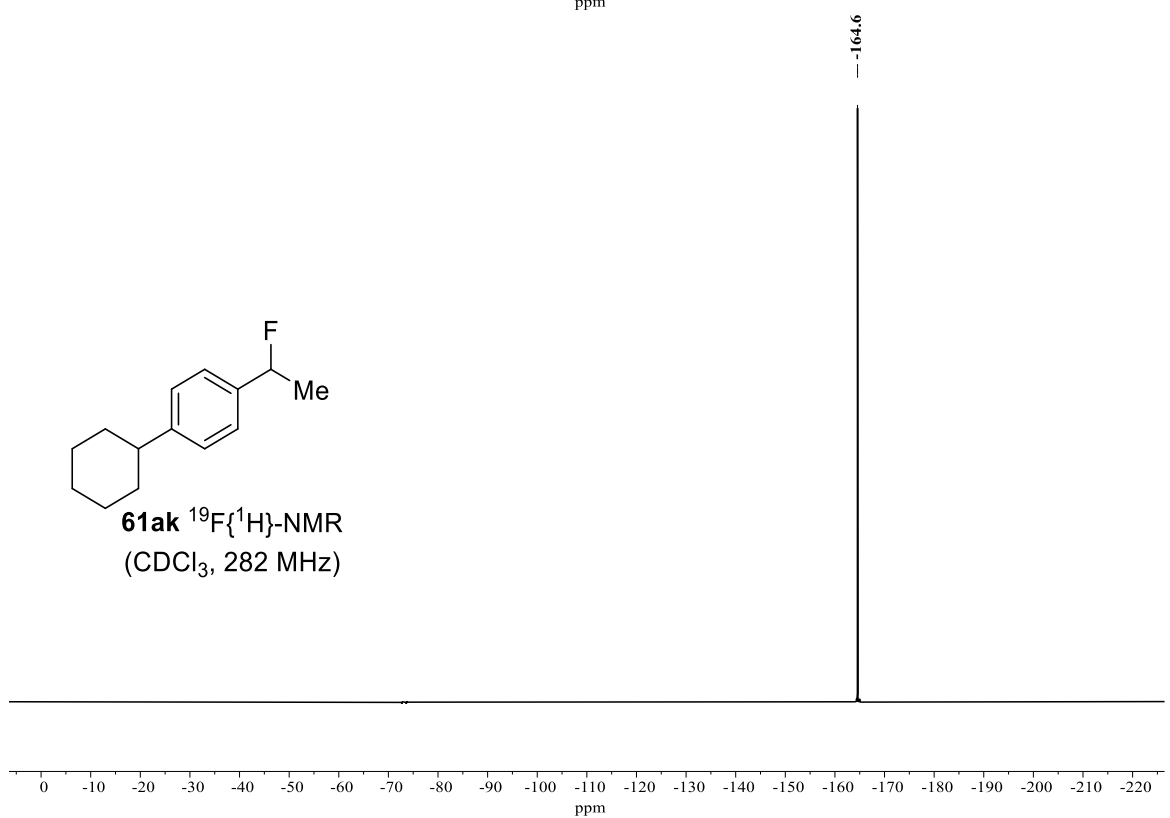
NMR SPECTRA



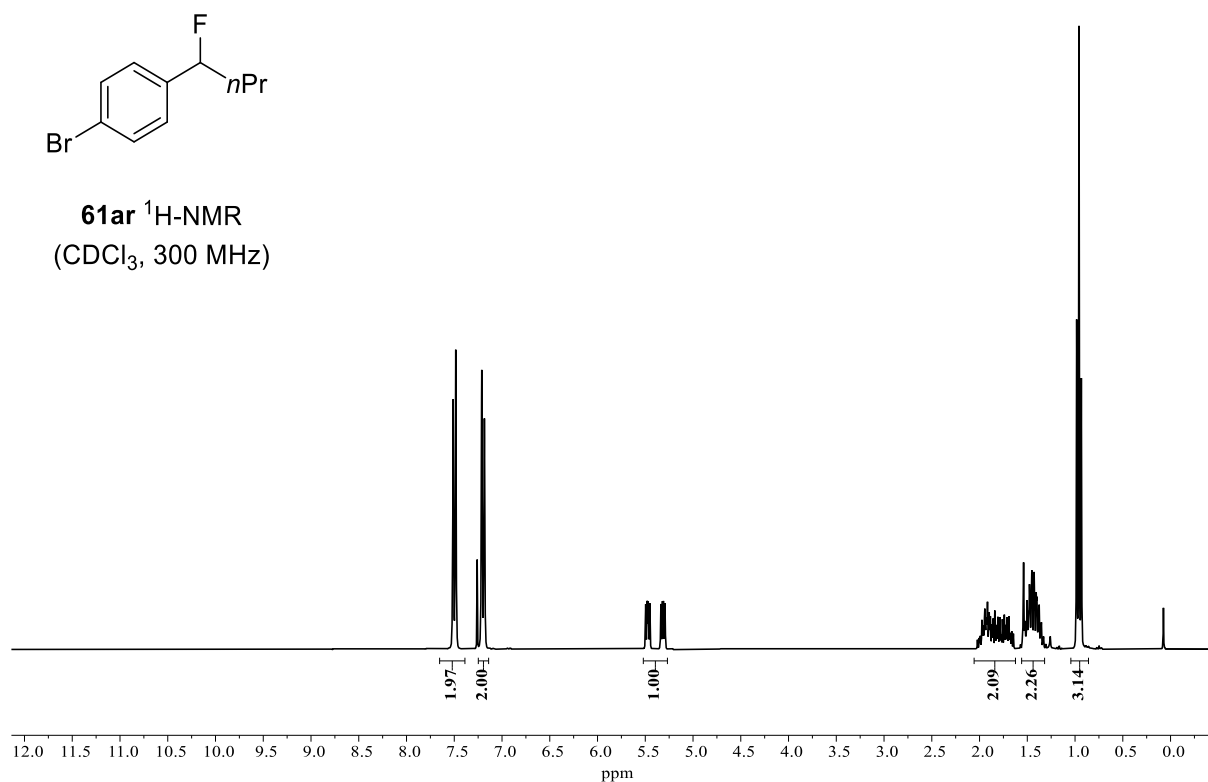
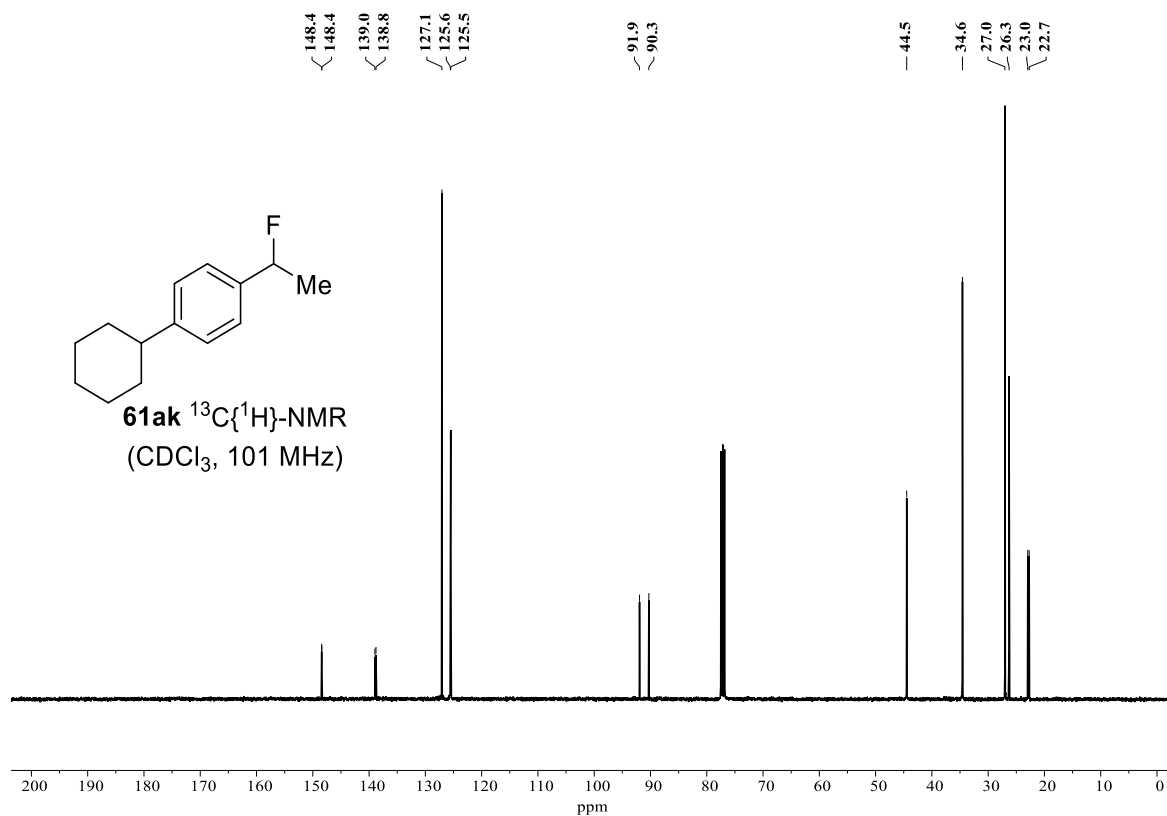
61ak $^1\text{H-NMR}$
(CDCl_3 , 400 MHz)



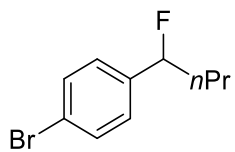
61ak $^{19}\text{F}\{^1\text{H}\}\text{-NMR}$
(CDCl_3 , 282 MHz)



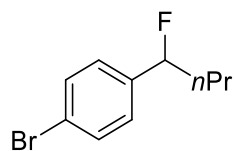
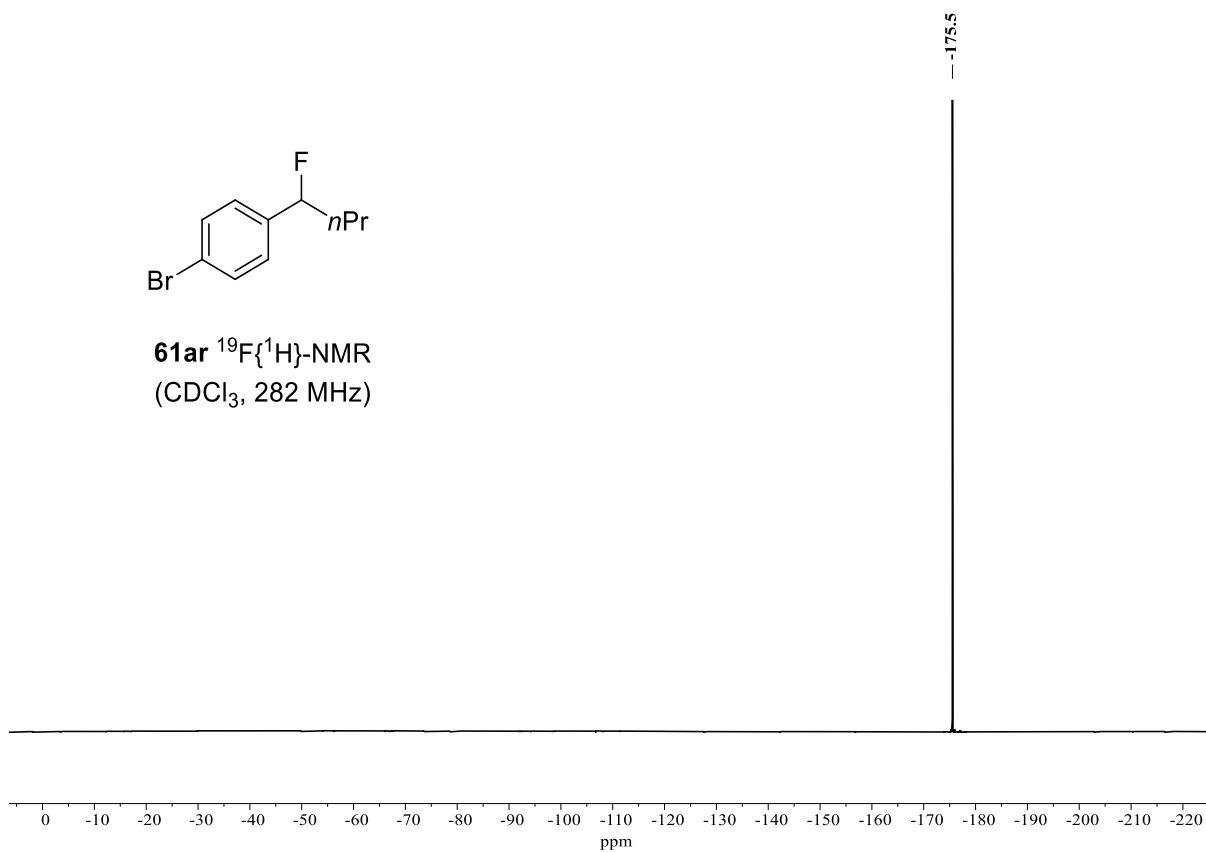
NMR SPECTRA



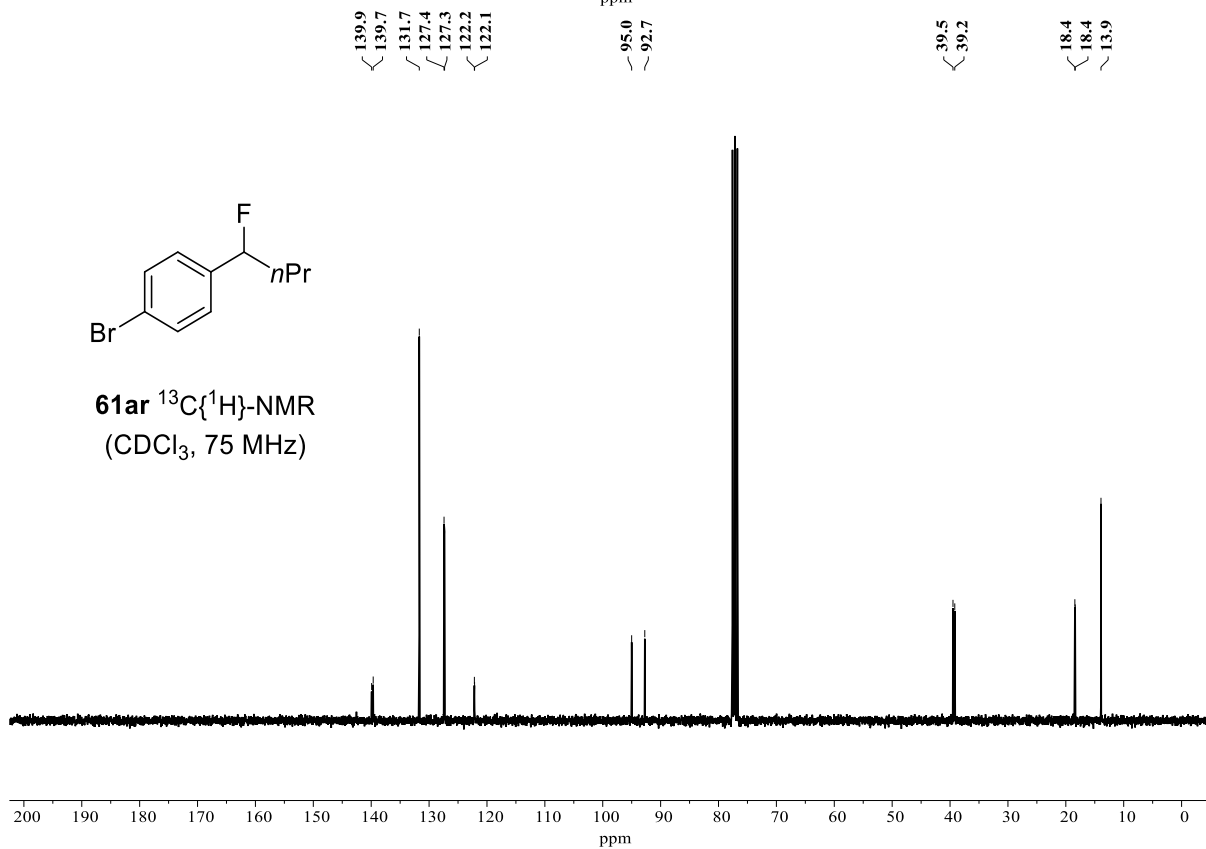
NMR SPECTRA



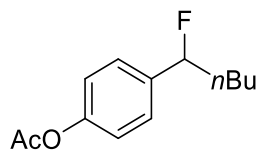
61ar $^{19}\text{F}\{^1\text{H}\}$ -NMR
(CDCl_3 , 282 MHz)



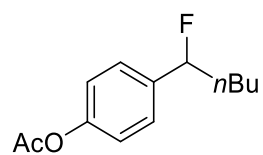
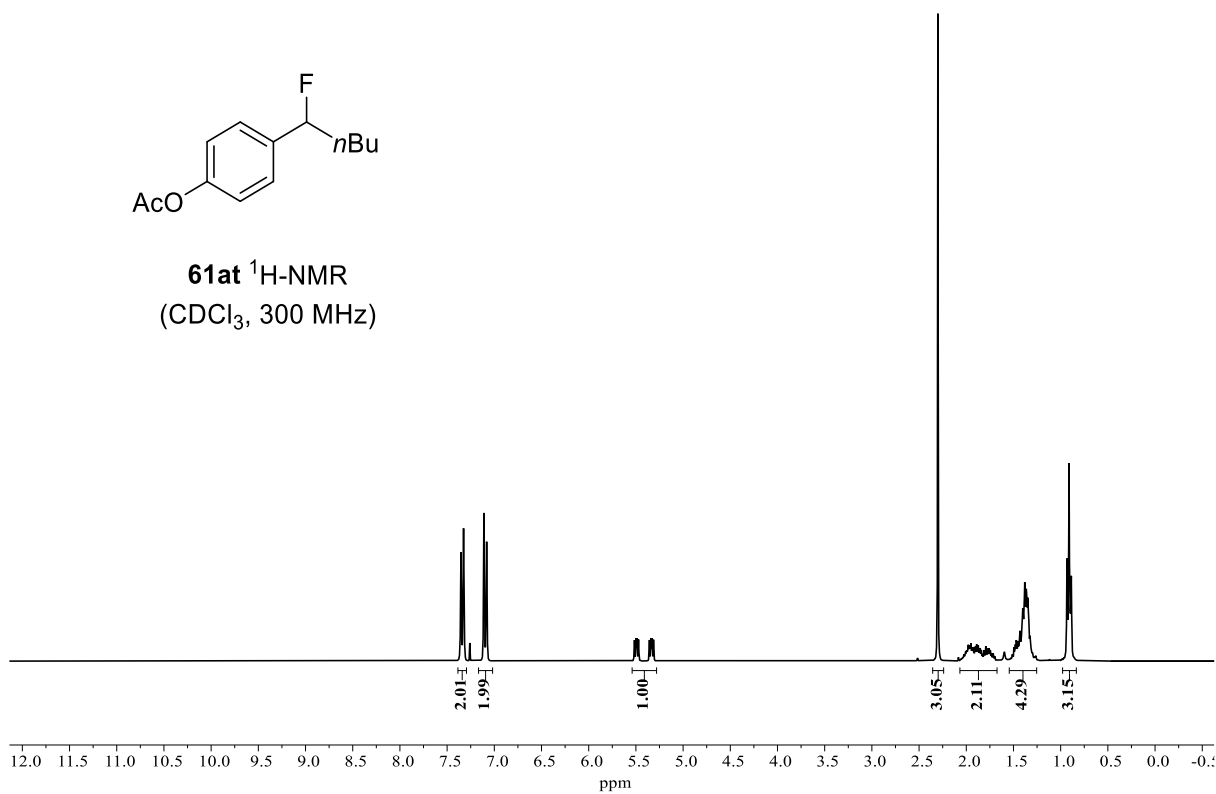
61ar $^{13}\text{C}\{^1\text{H}\}$ -NMR
(CDCl_3 , 75 MHz)



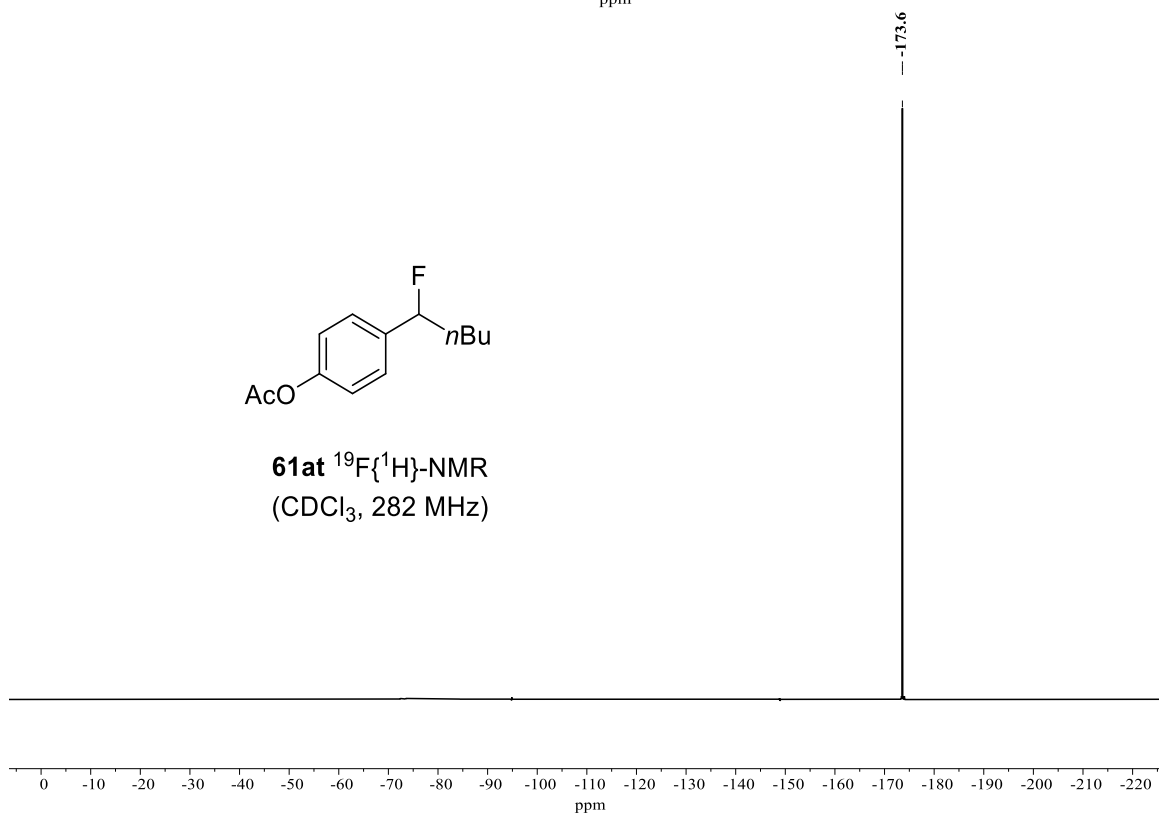
NMR SPECTRA



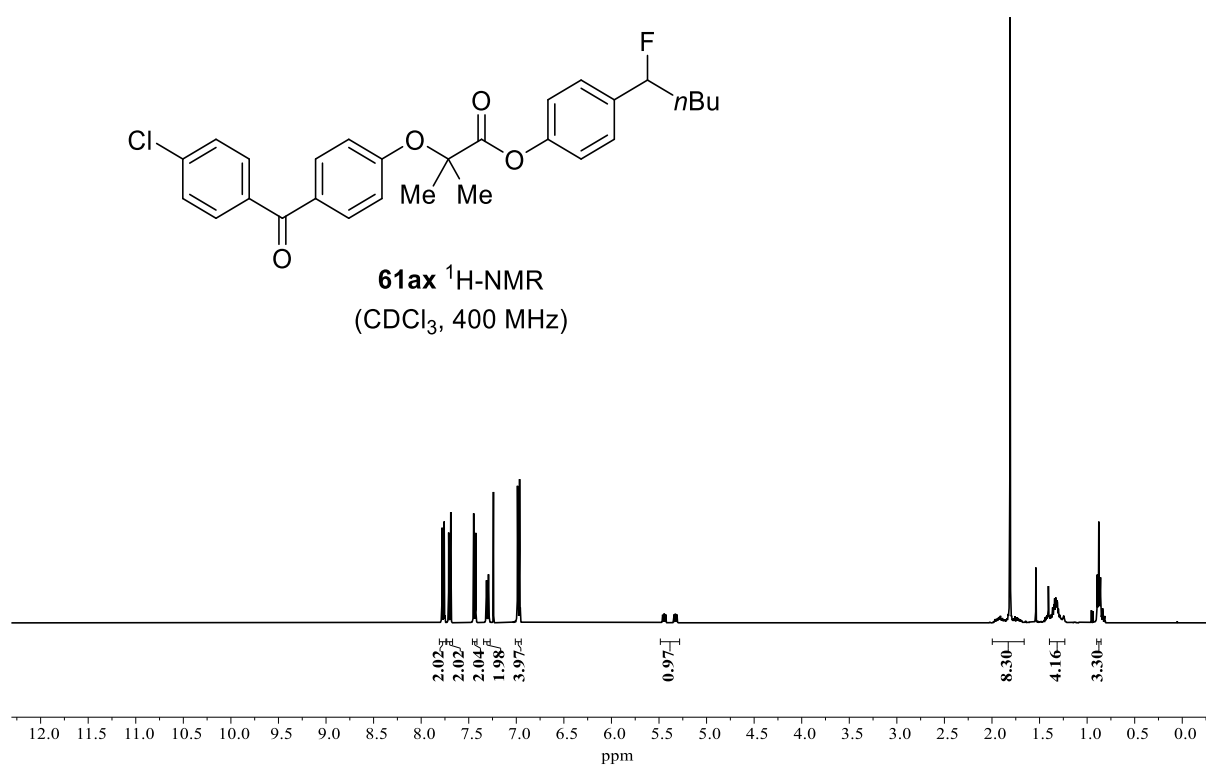
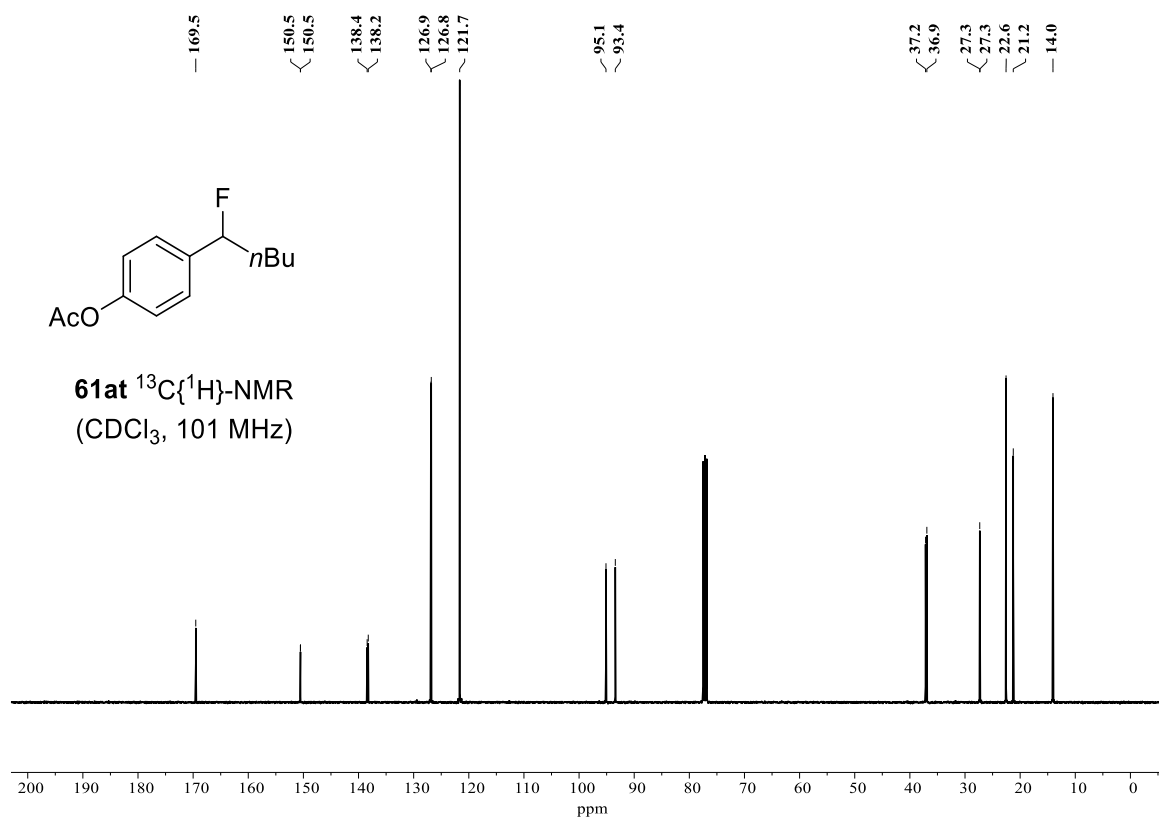
61at ^1H -NMR
(CDCl_3 , 300 MHz)



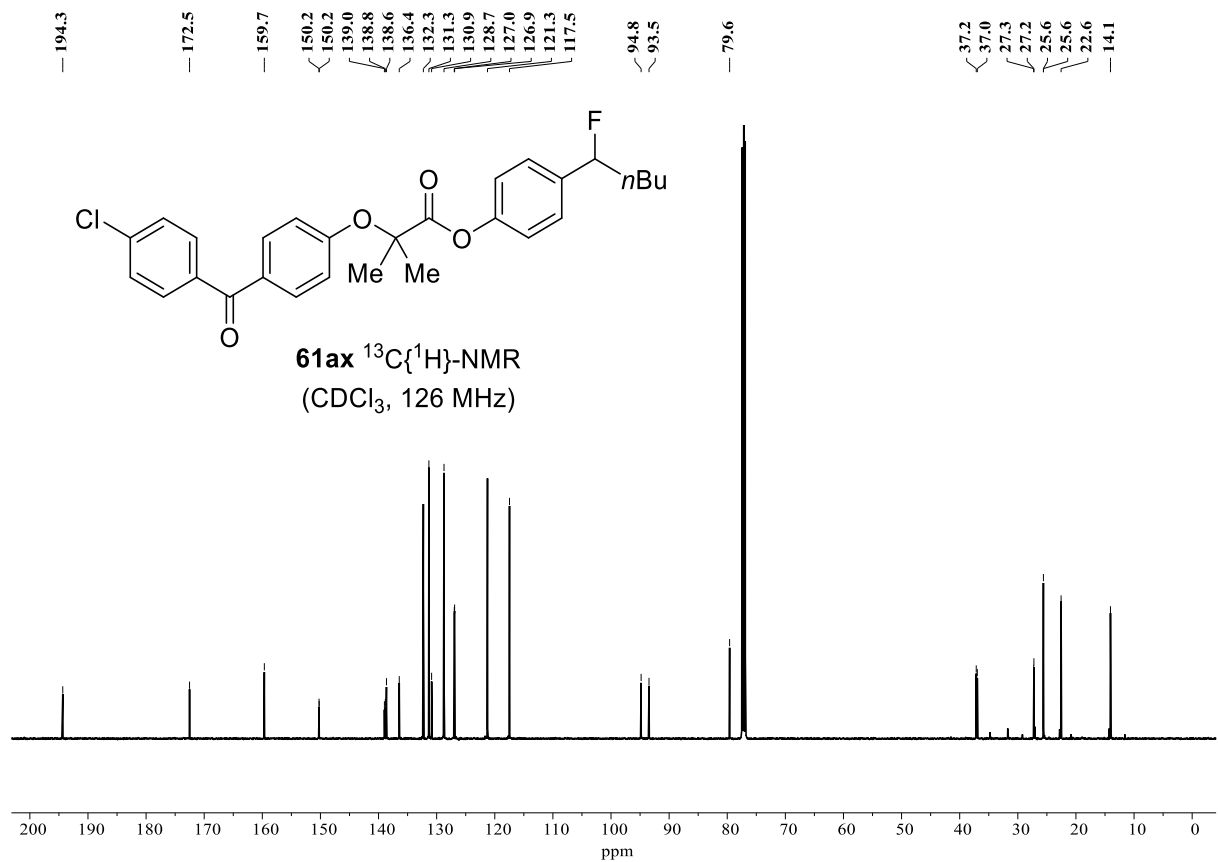
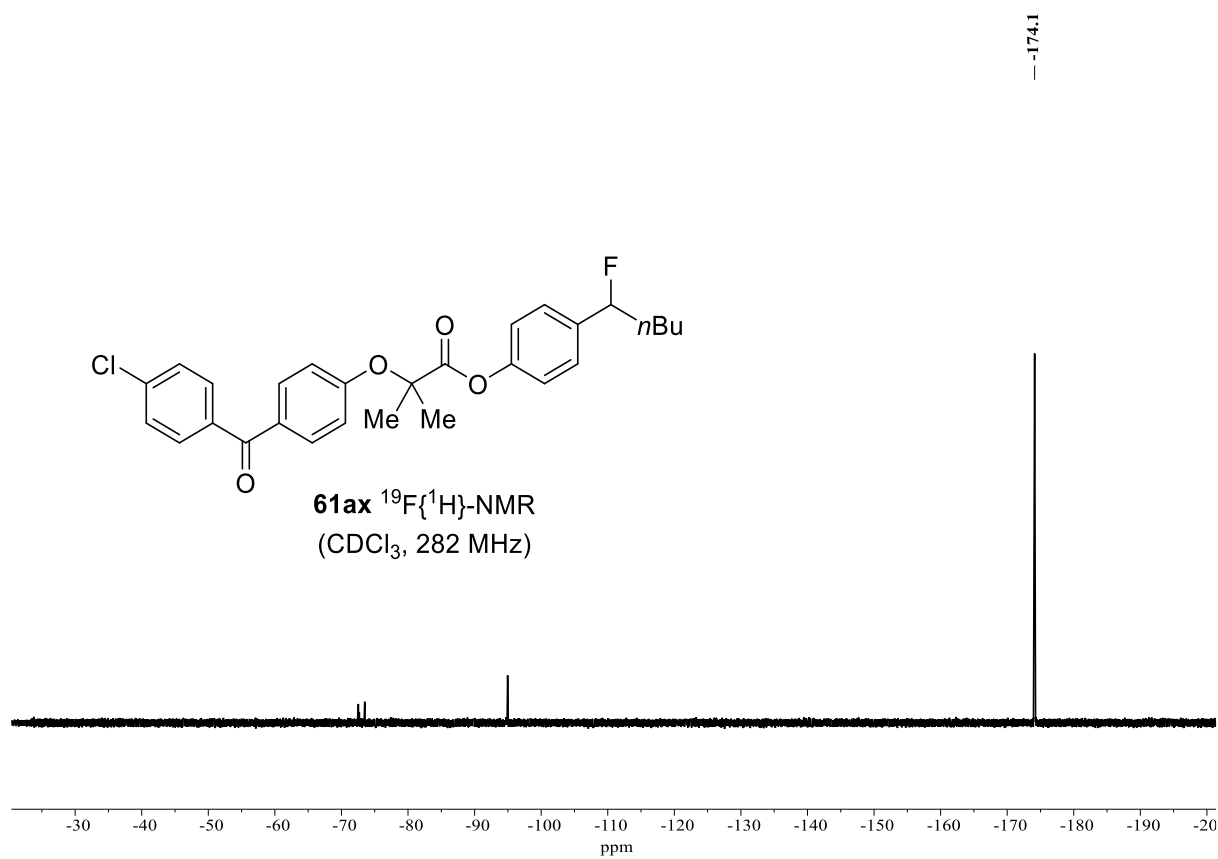
61at $^{19}\text{F}\{^1\text{H}\}$ -NMR
(CDCl_3 , 282 MHz)



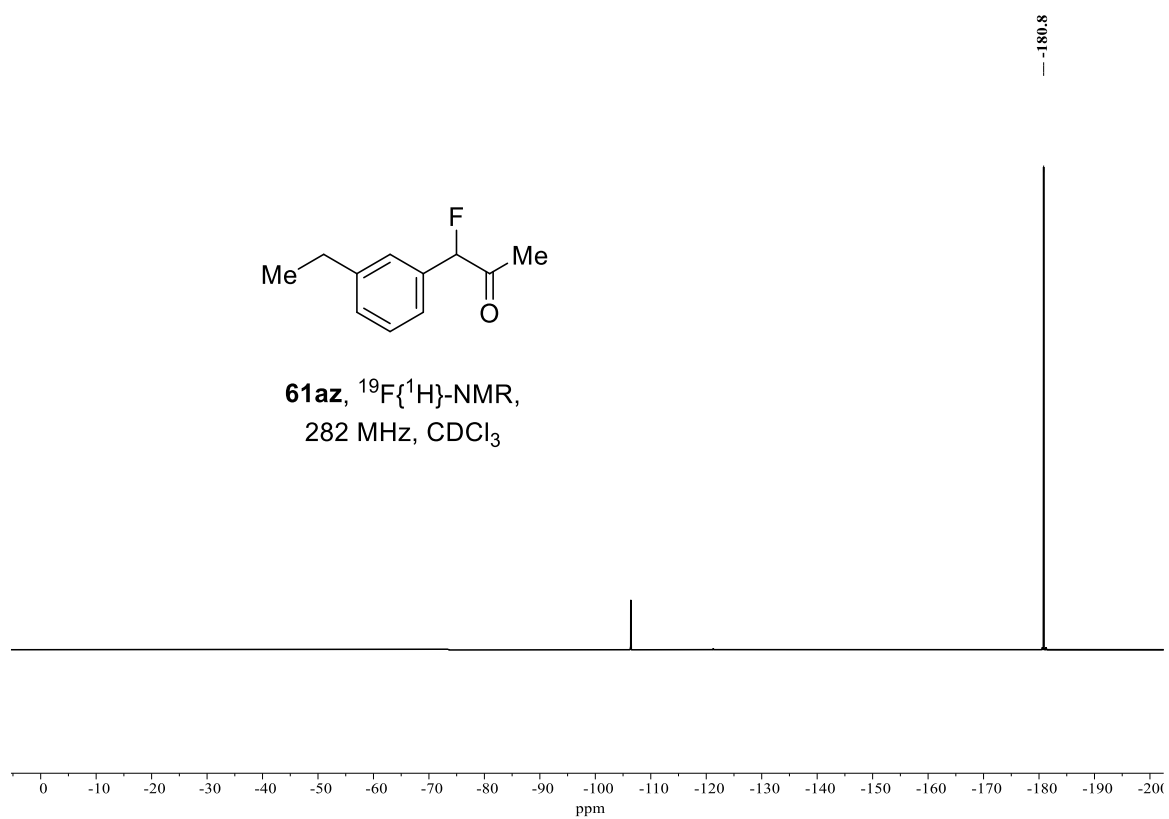
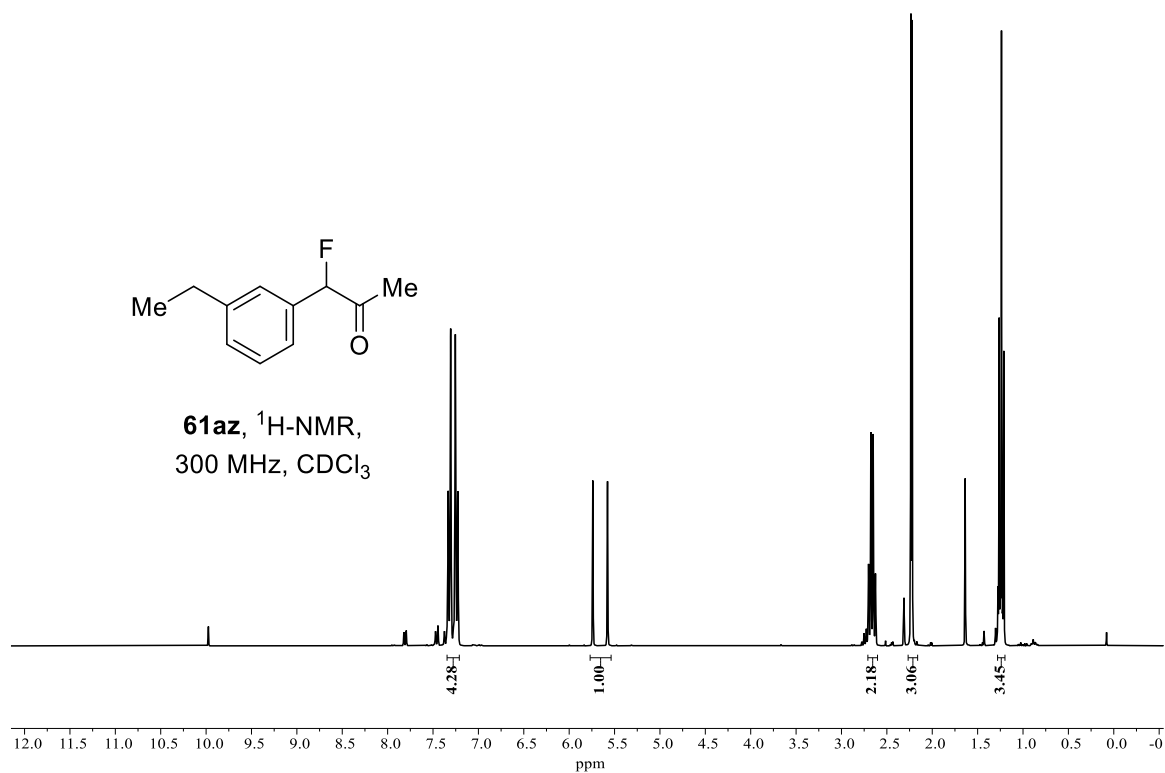
NMR SPECTRA



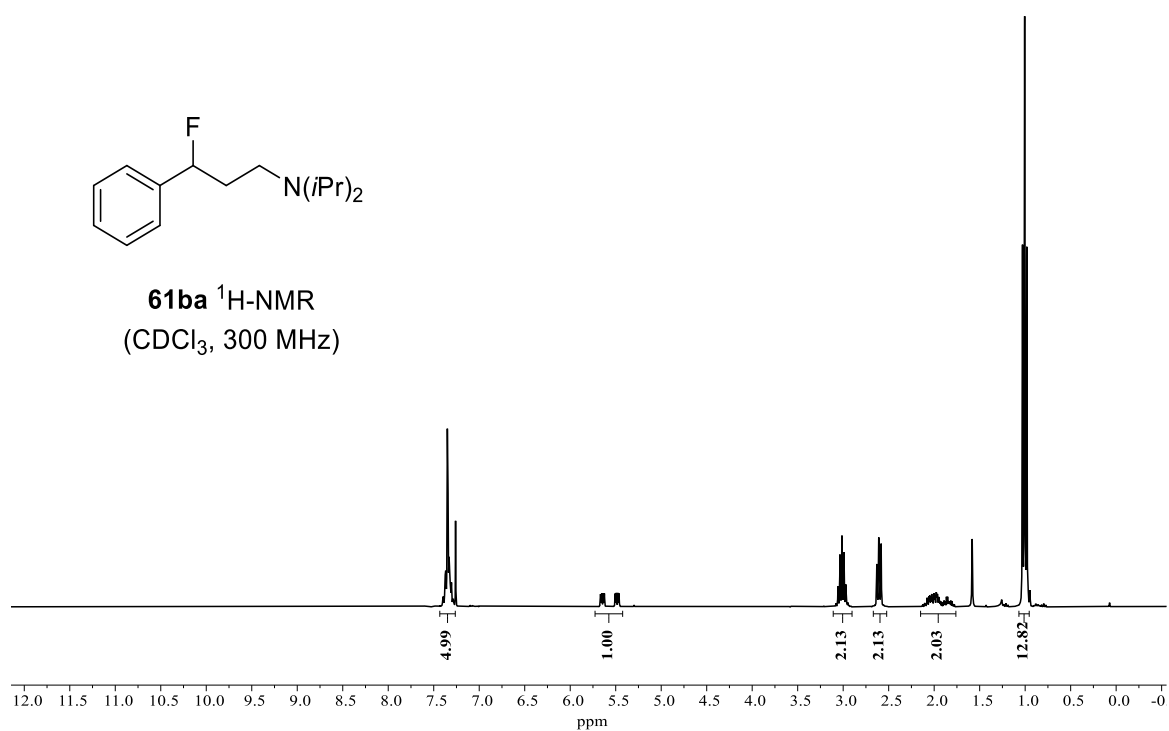
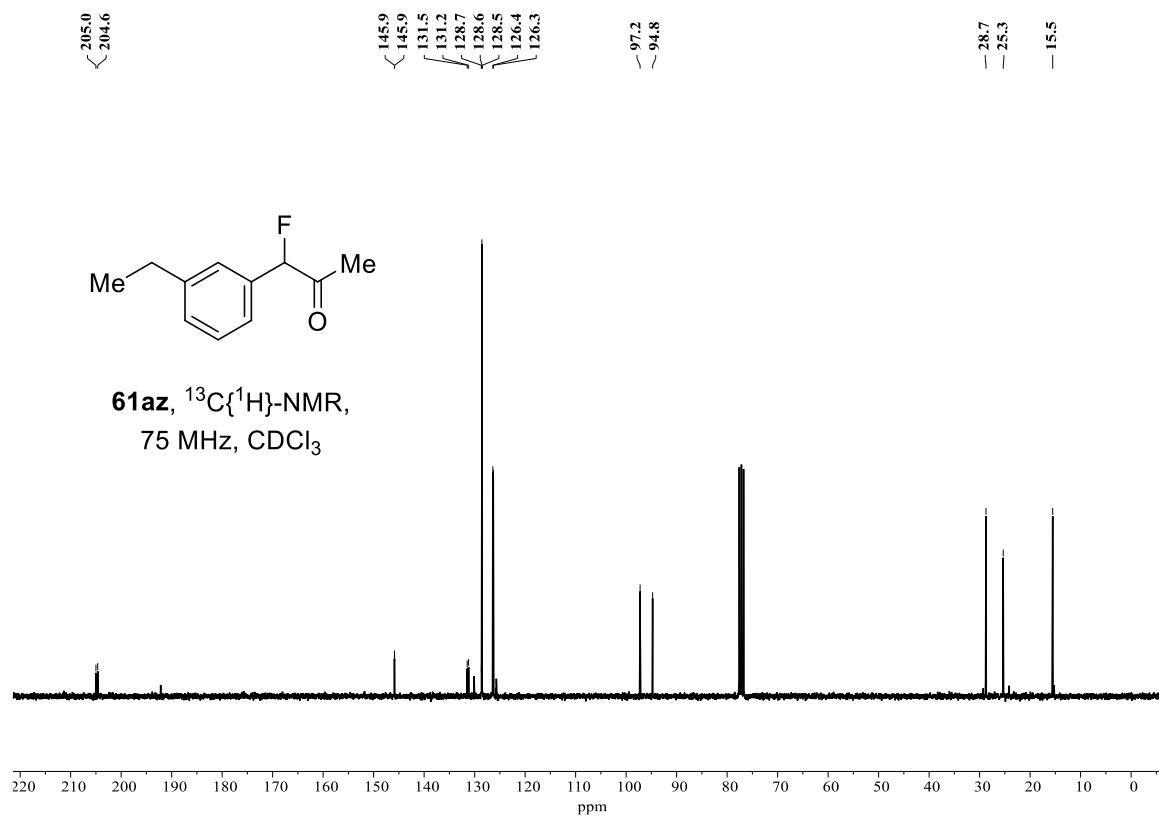
NMR SPECTRA



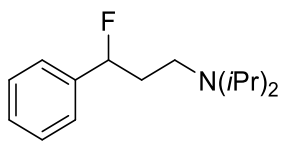
NMR SPECTRA



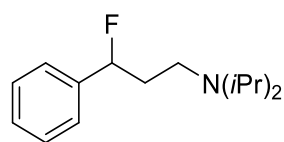
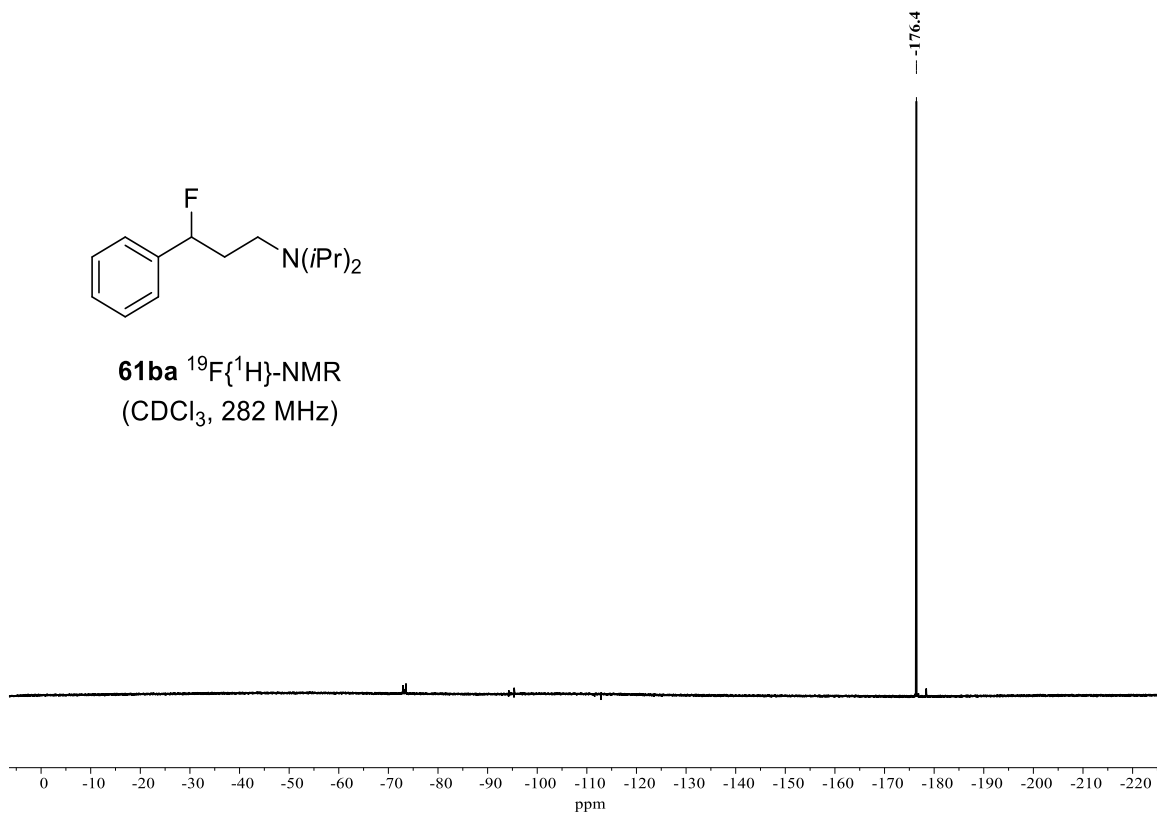
NMR SPECTRA



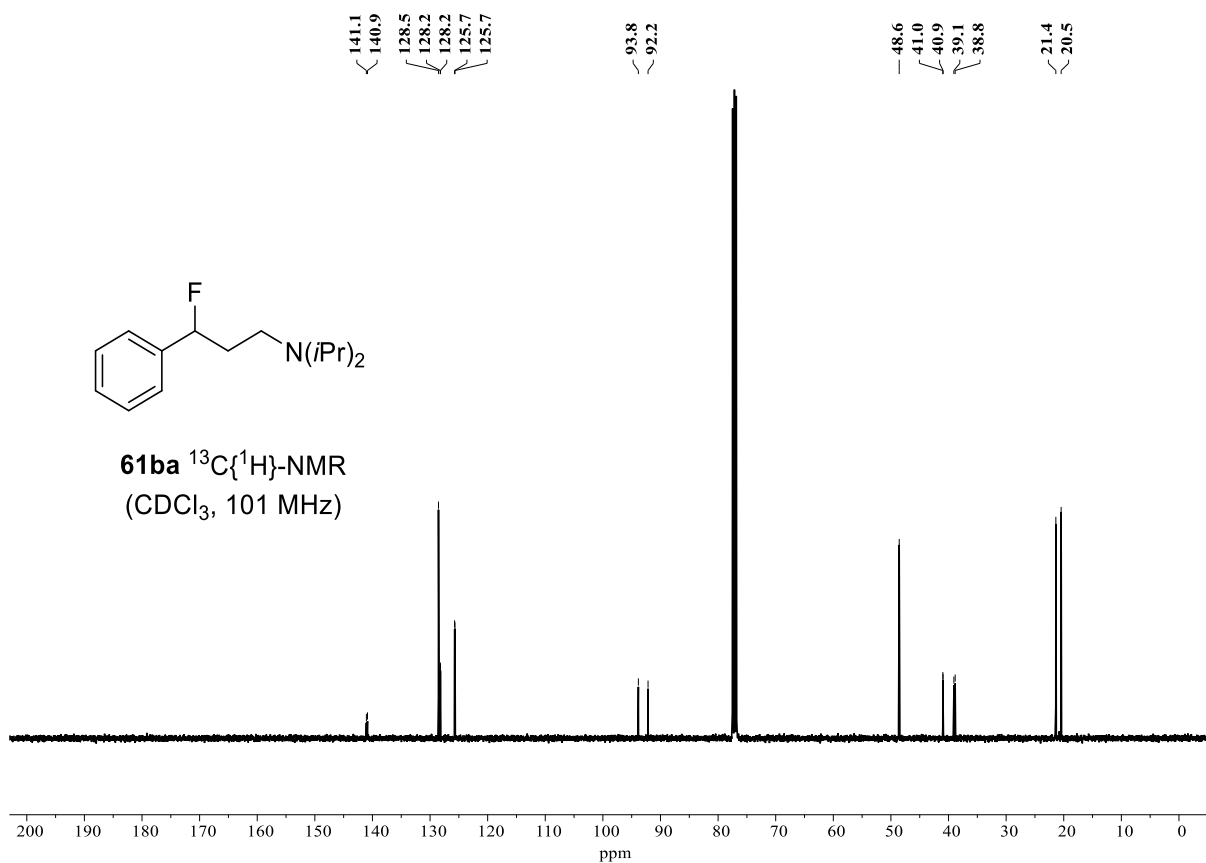
NMR SPECTRA



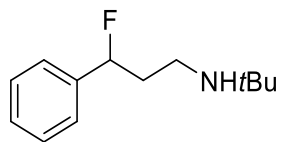
61ba $^{19}\text{F}\{^1\text{H}\}$ -NMR
(CDCl_3 , 282 MHz)



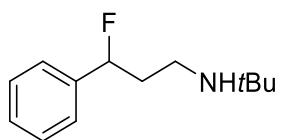
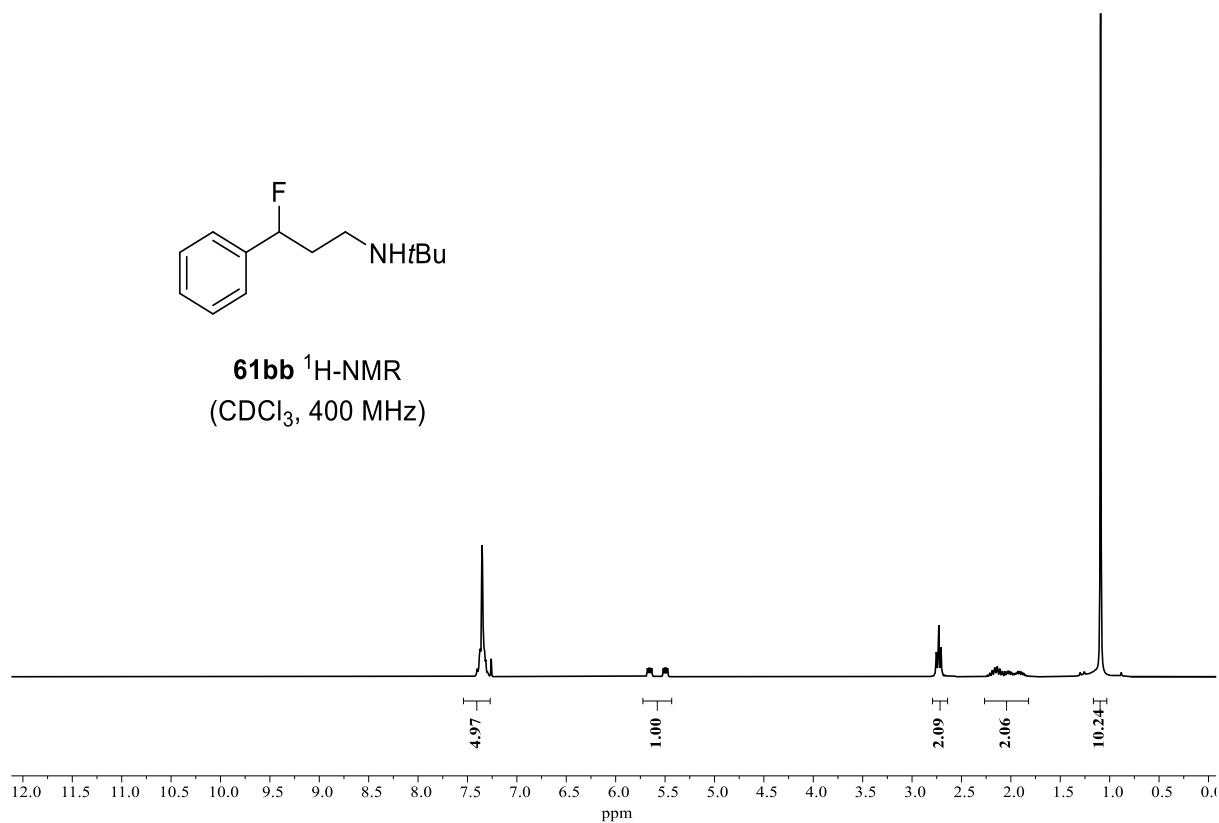
61ba $^{13}\text{C}\{^1\text{H}\}$ -NMR
(CDCl_3 , 101 MHz)



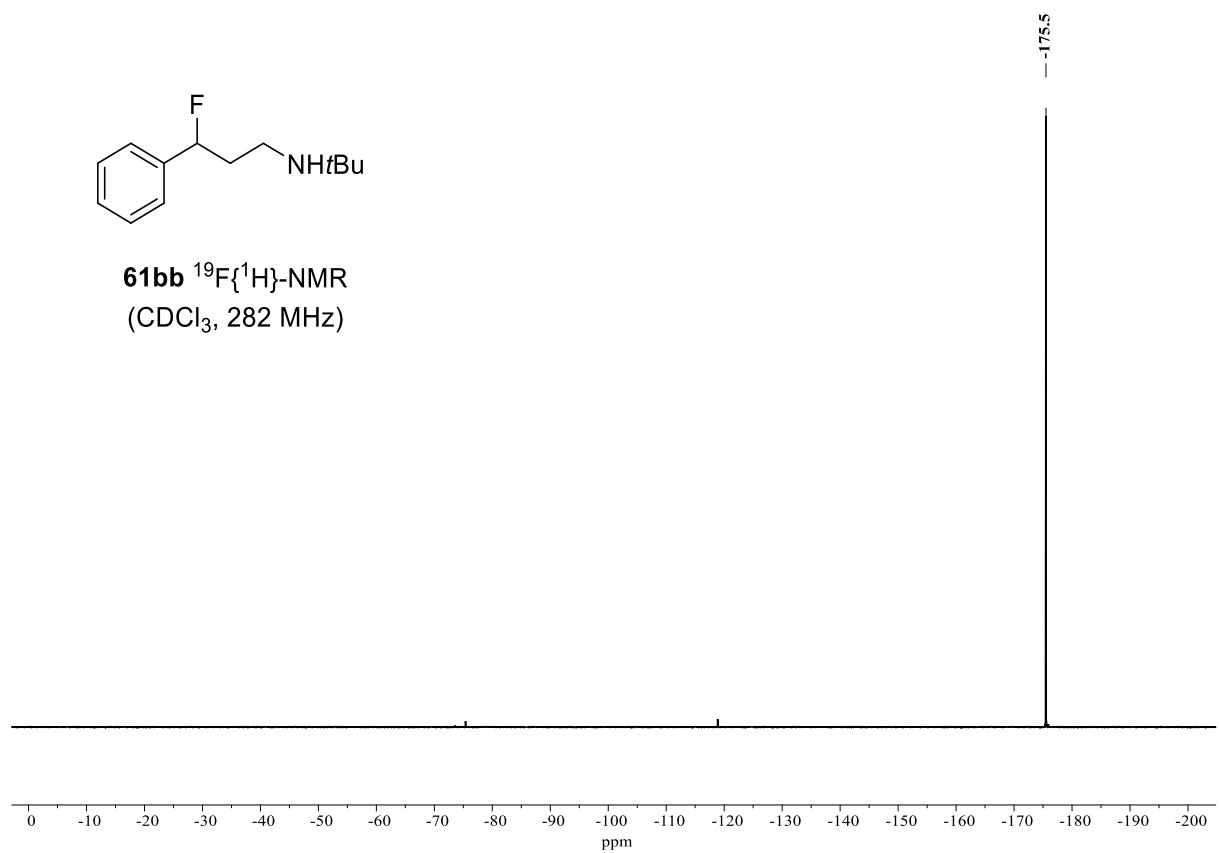
NMR SPECTRA



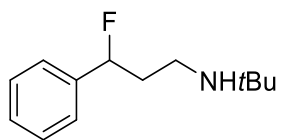
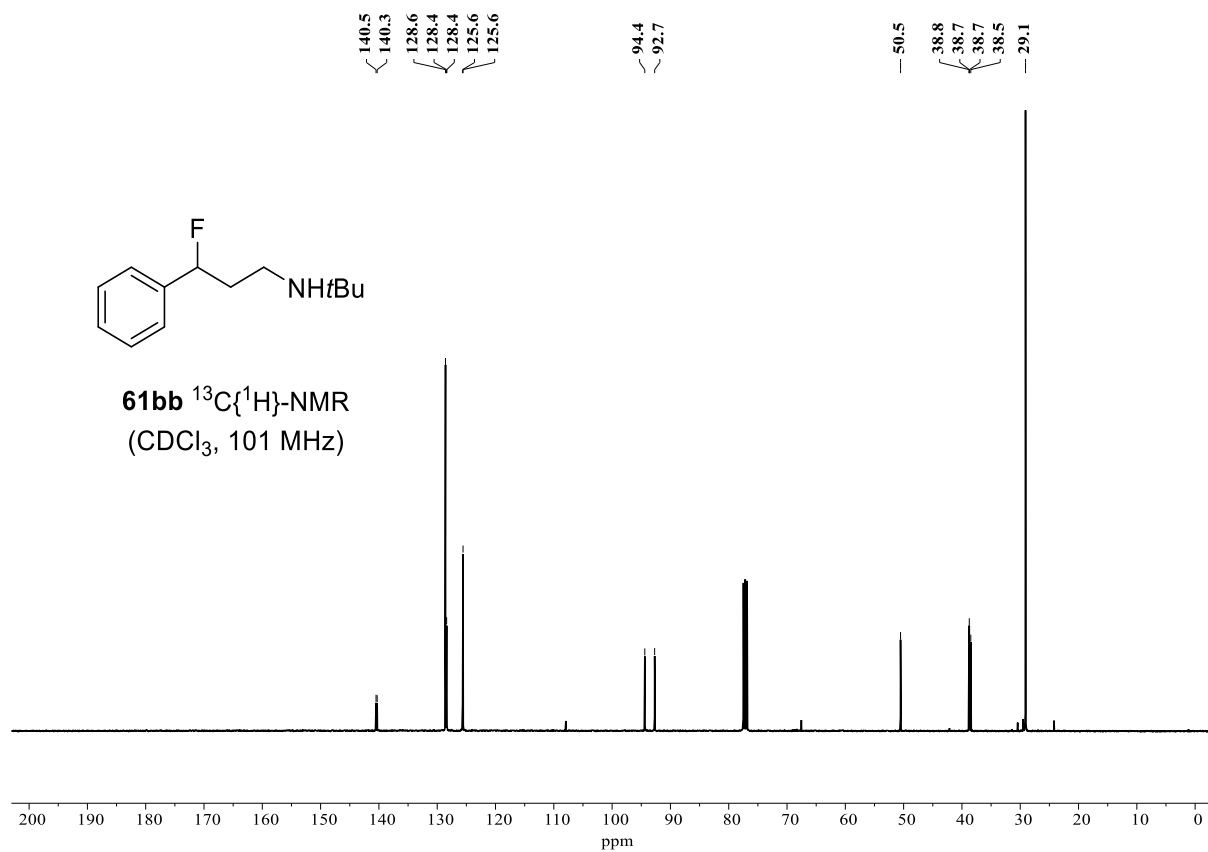
61bb ^1H -NMR
(CDCl_3 , 400 MHz)



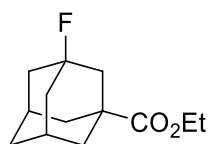
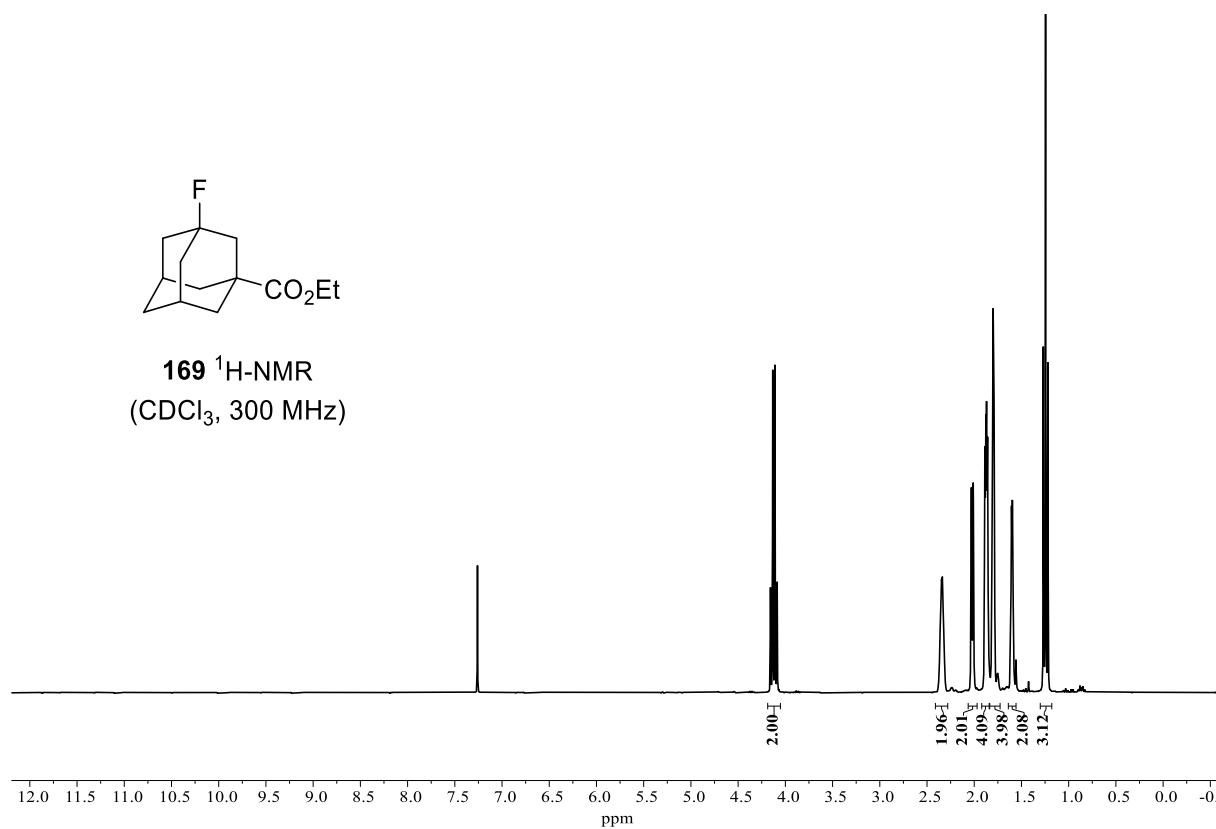
61bb $^{19}\text{F}\{^1\text{H}\}$ -NMR
(CDCl_3 , 282 MHz)



NMR SPECTRA

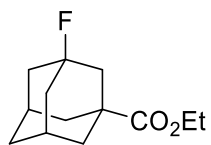


61bb $^{13}\text{C}\{^1\text{H}\}$ -NMR
 (CDCl₃, 101 MHz)

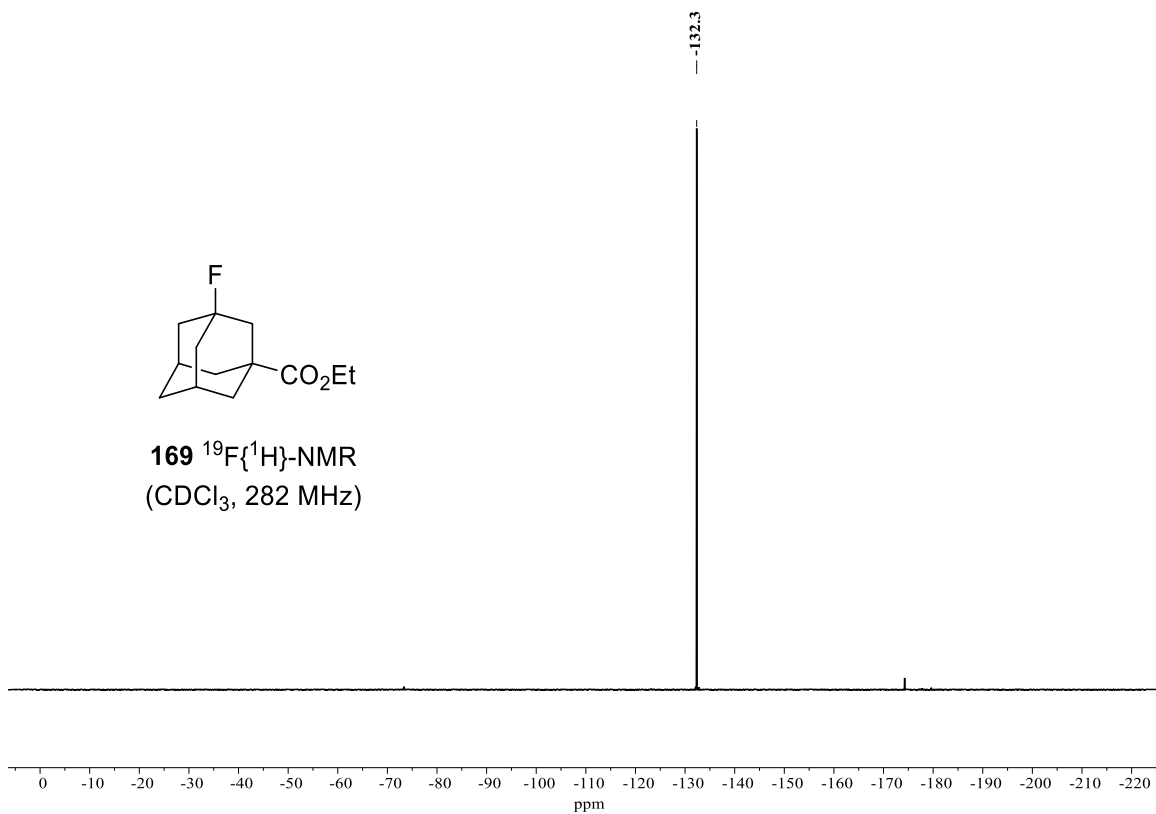


169 ^1H -NMR
 (CDCl₃, 300 MHz)

NMR SPECTRA



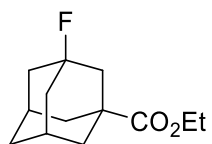
169 $^{19}\text{F}\{^1\text{H}\}$ -NMR
(CDCl_3 , 282 MHz)



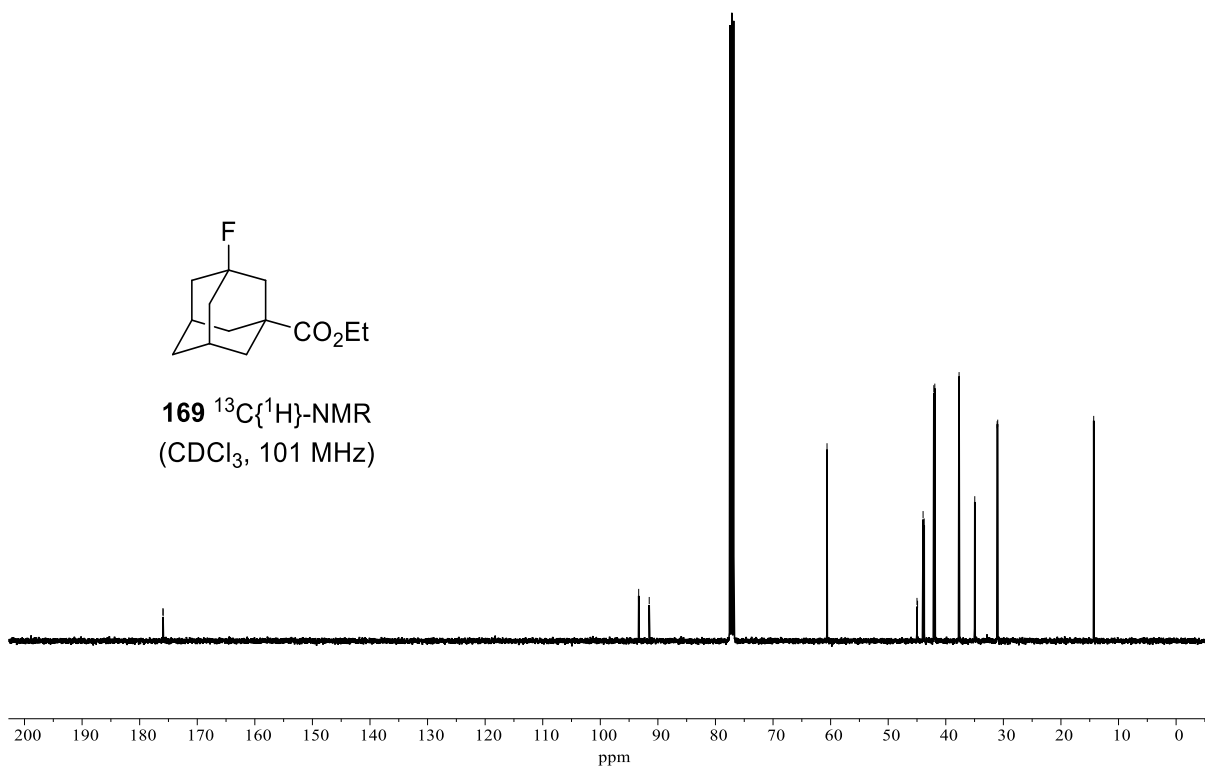
176.0
175.9

93.3
91.5

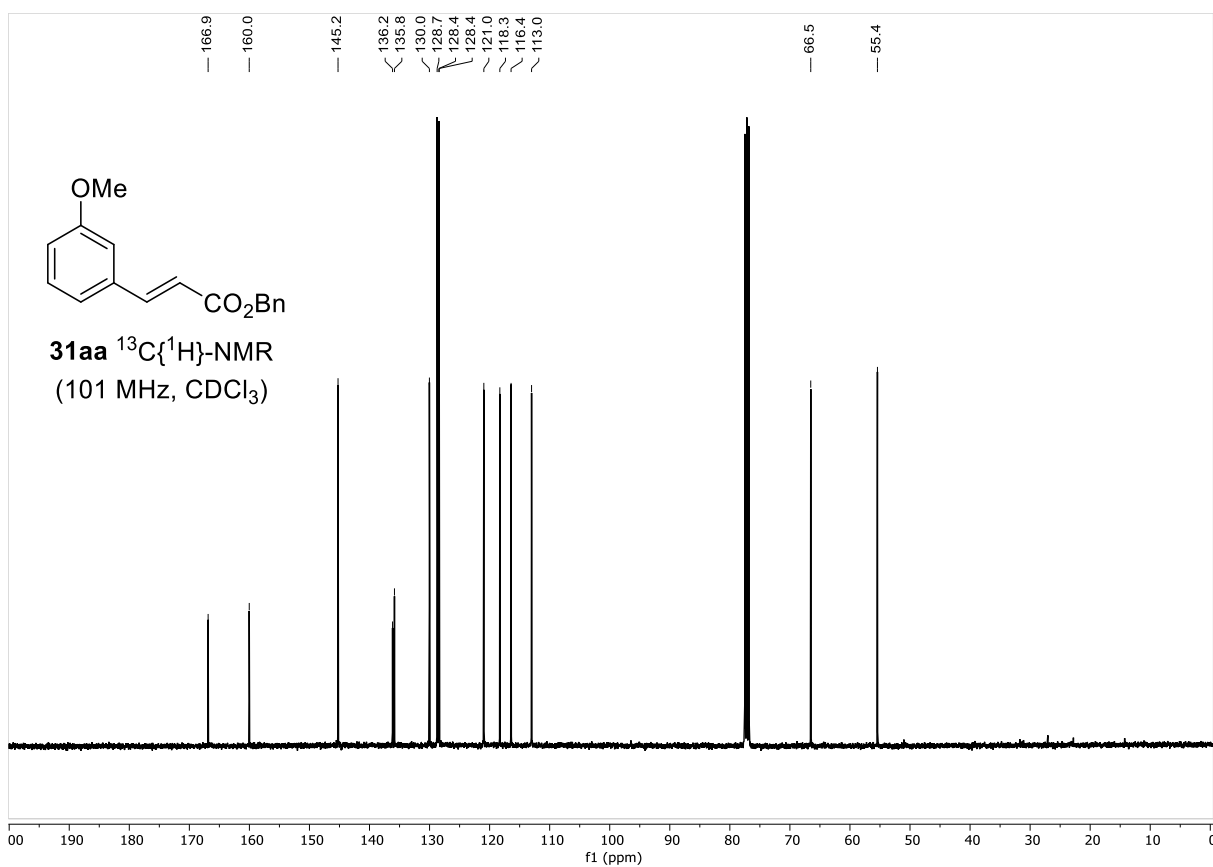
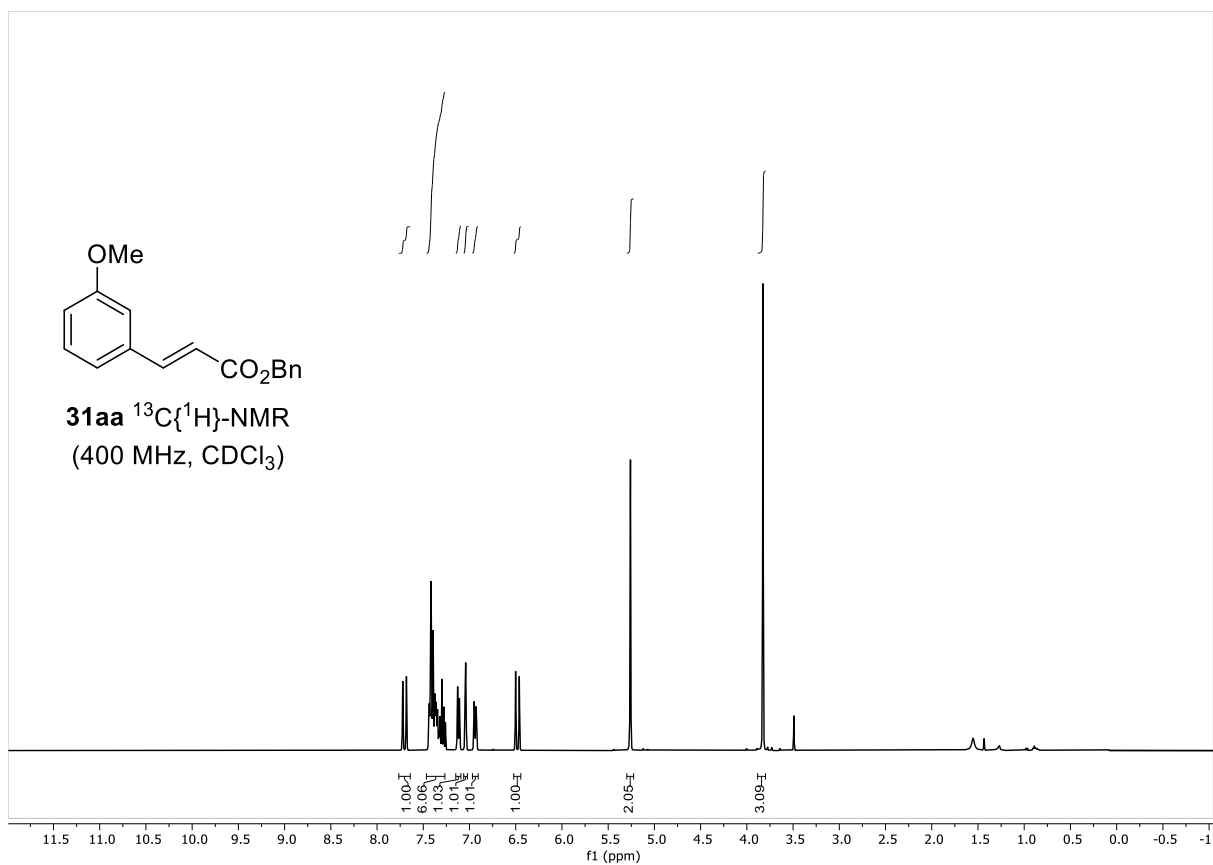
60.6
45.0
44.9
43.9
43.7
42.1
41.9
37.7
37.7
35.0
35.0
31.1
31.0
14.3



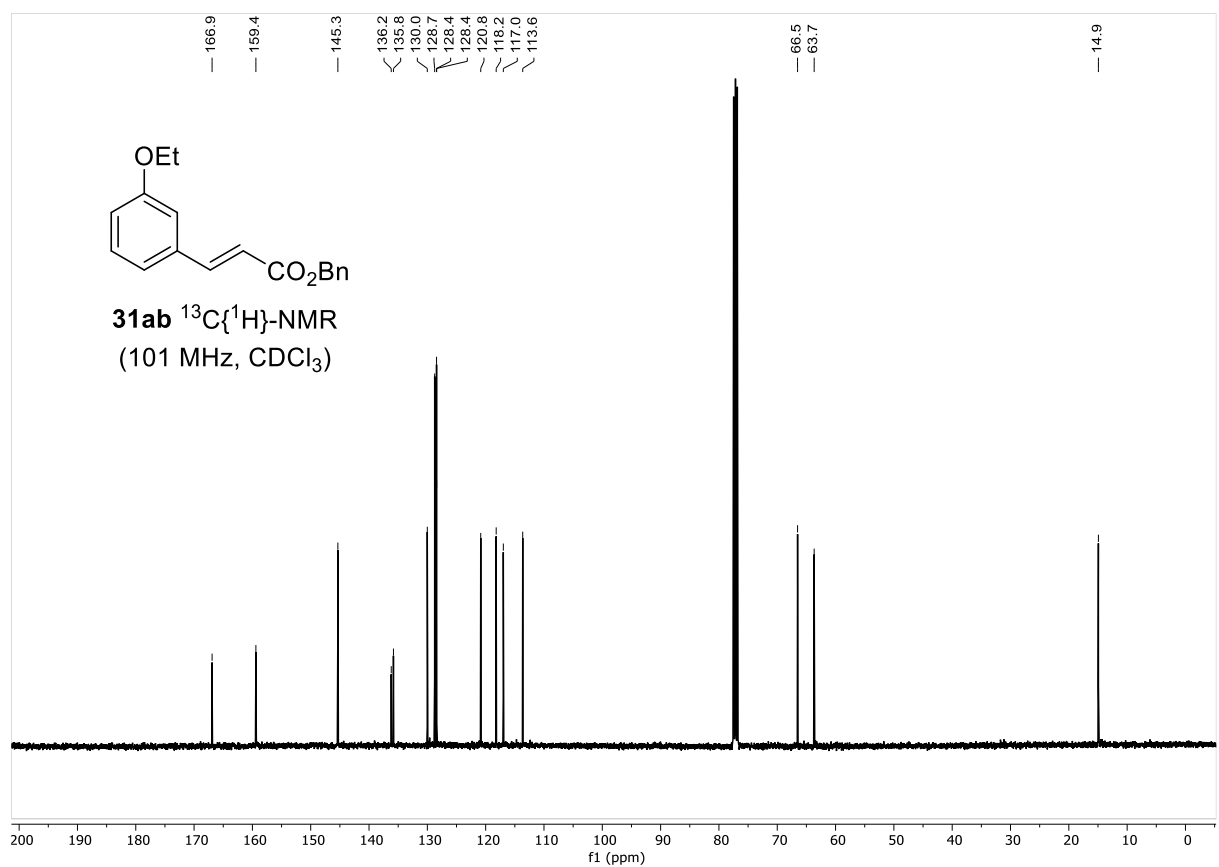
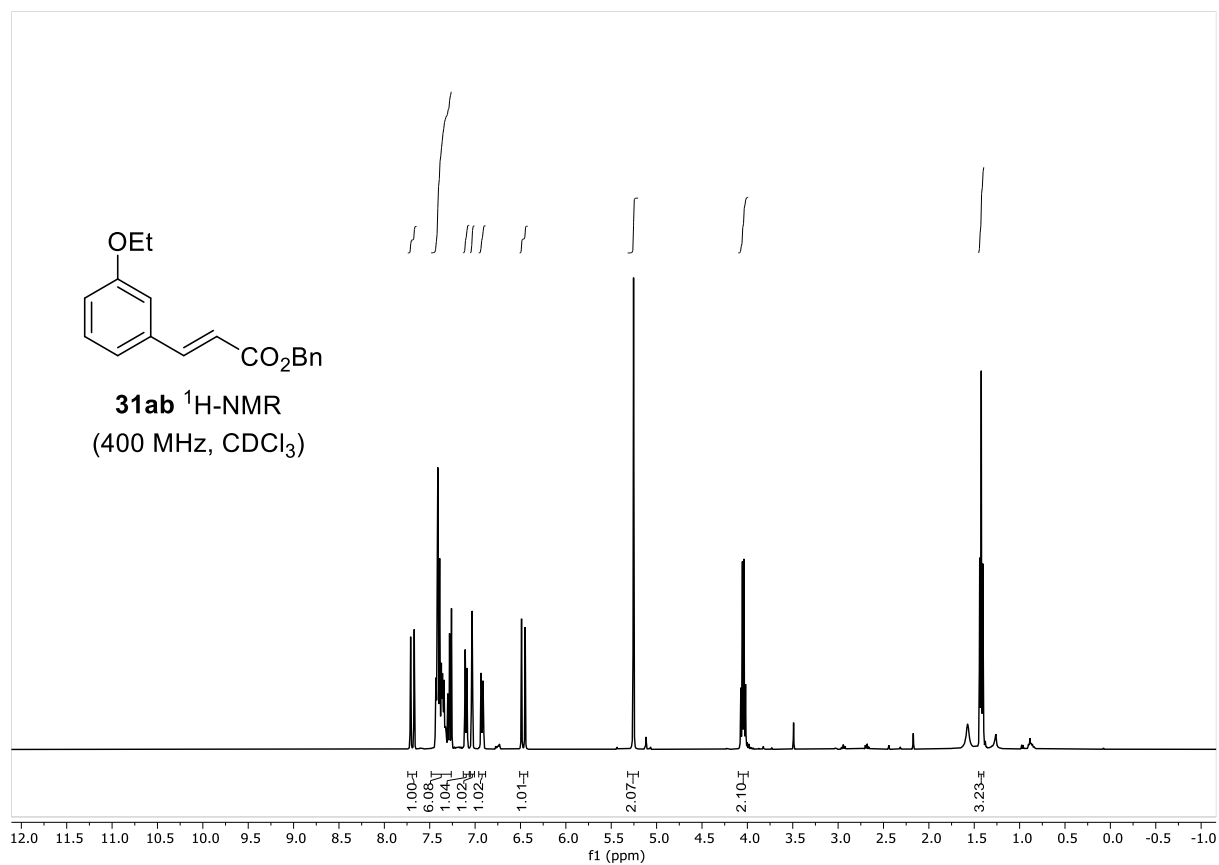
169 $^{13}\text{C}\{^1\text{H}\}$ -NMR
(CDCl_3 , 101 MHz)



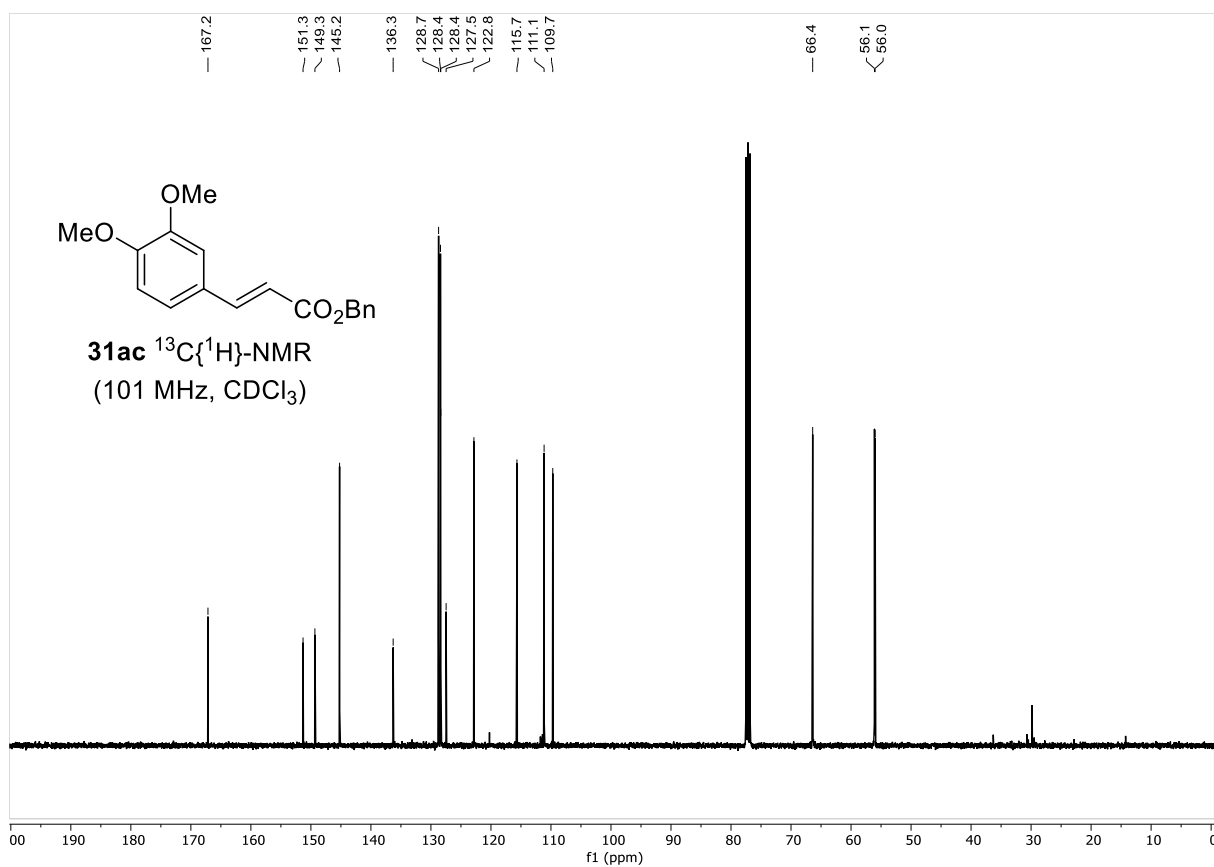
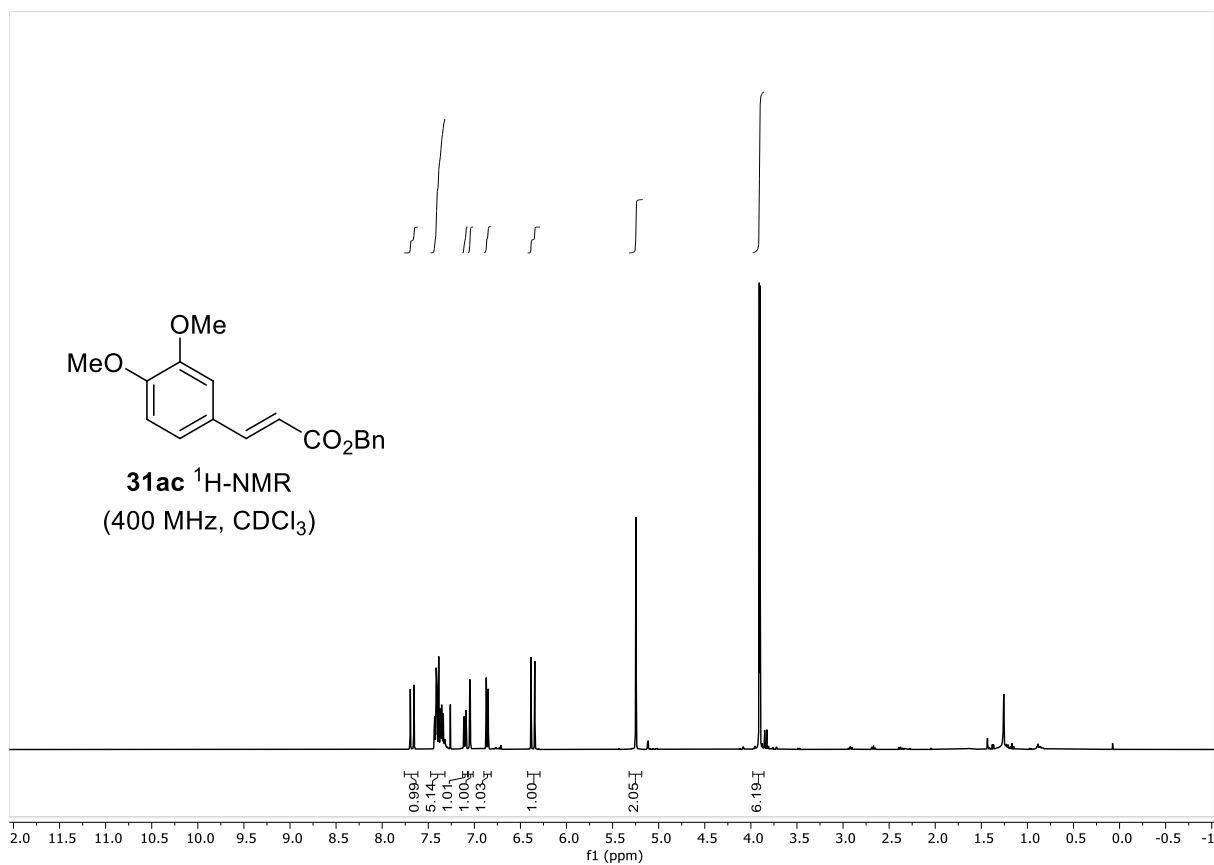
NMR SPECTRA



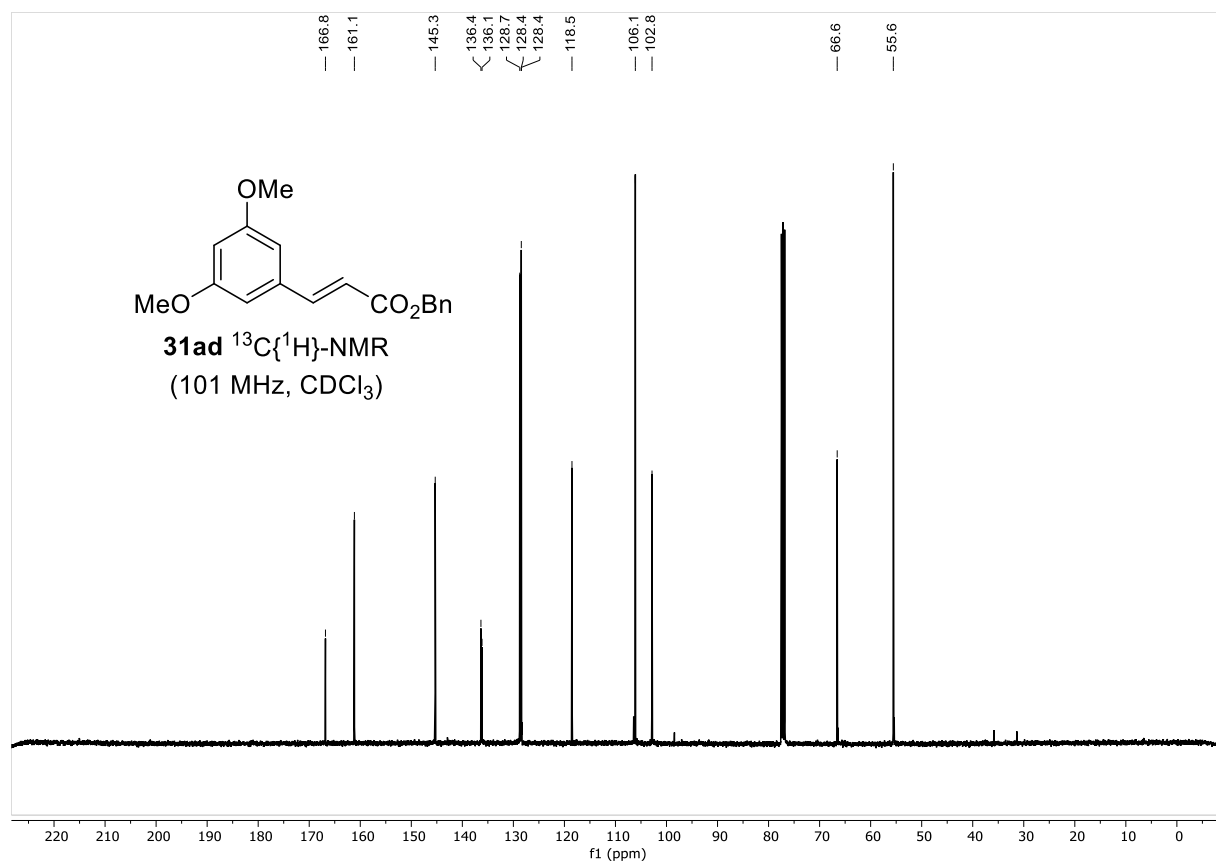
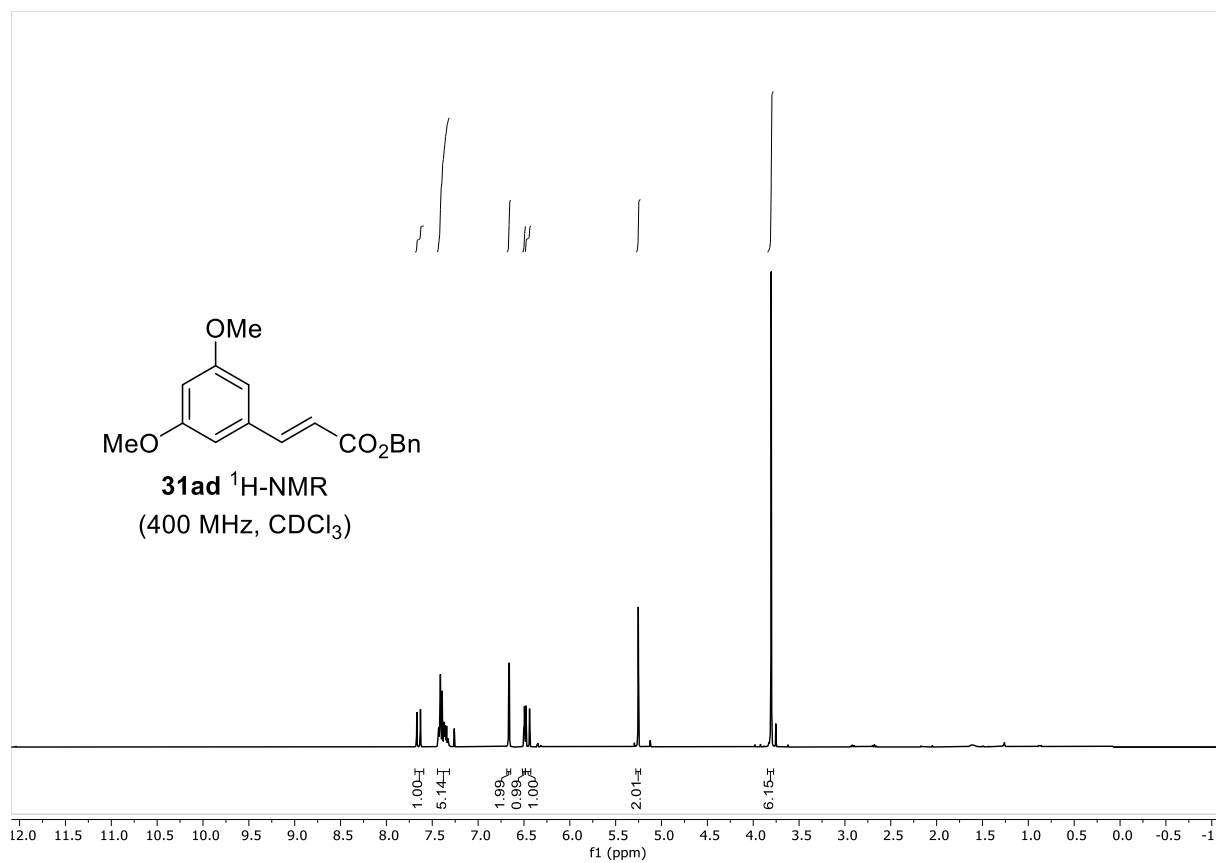
NMR SPECTRA



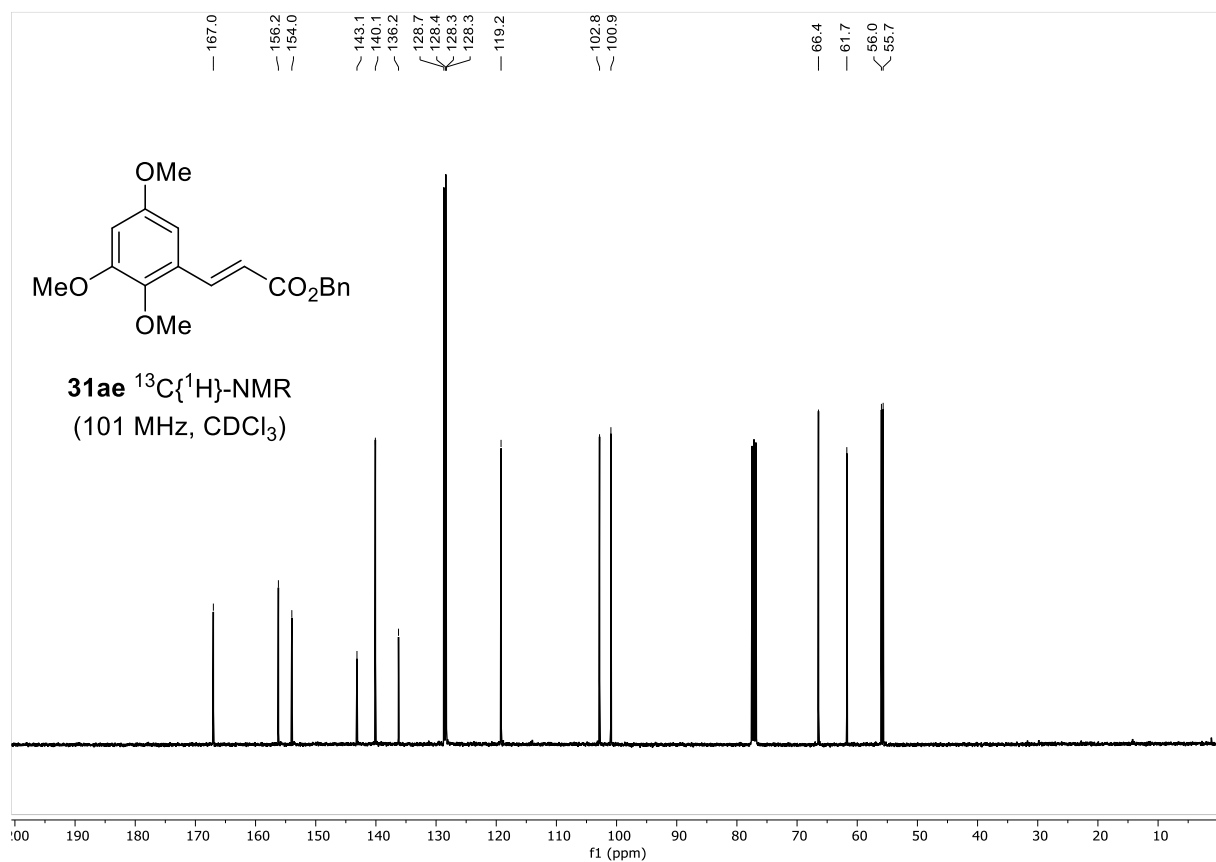
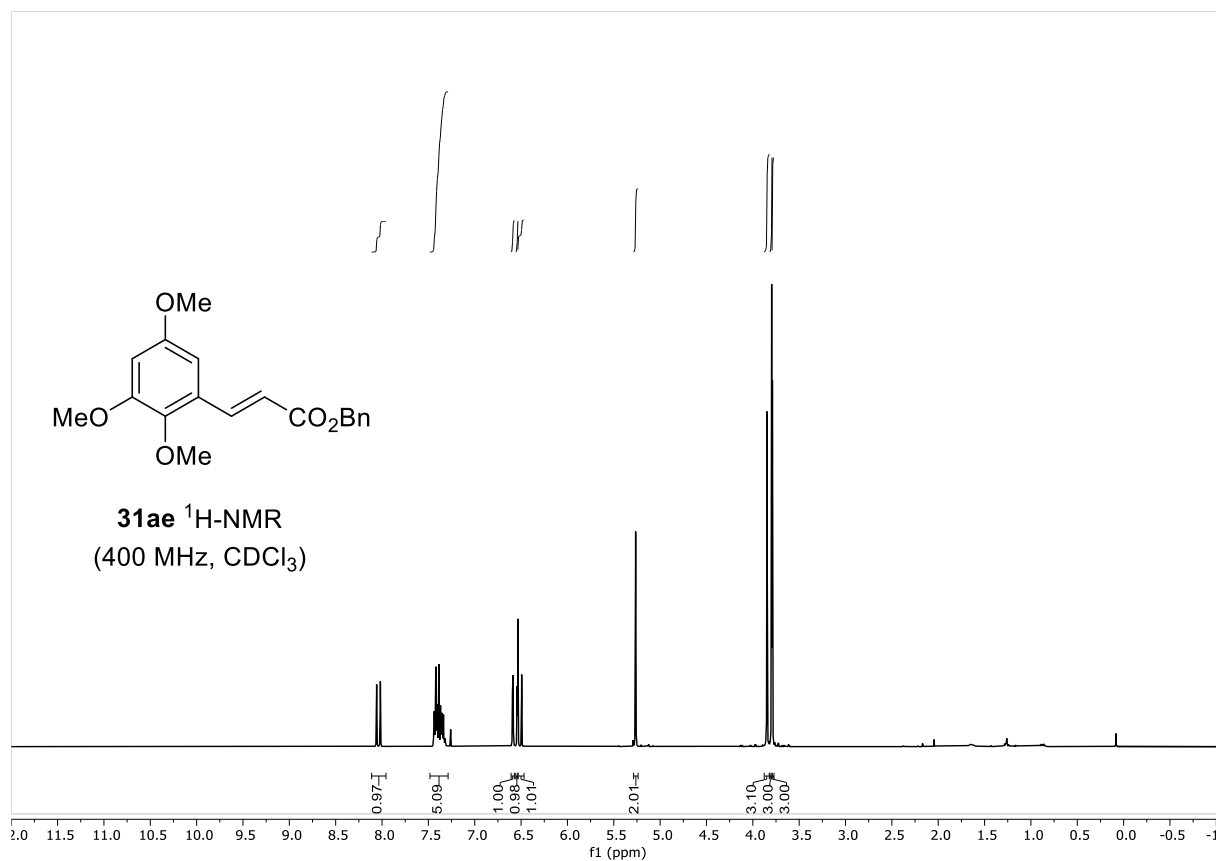
NMR SPECTRA



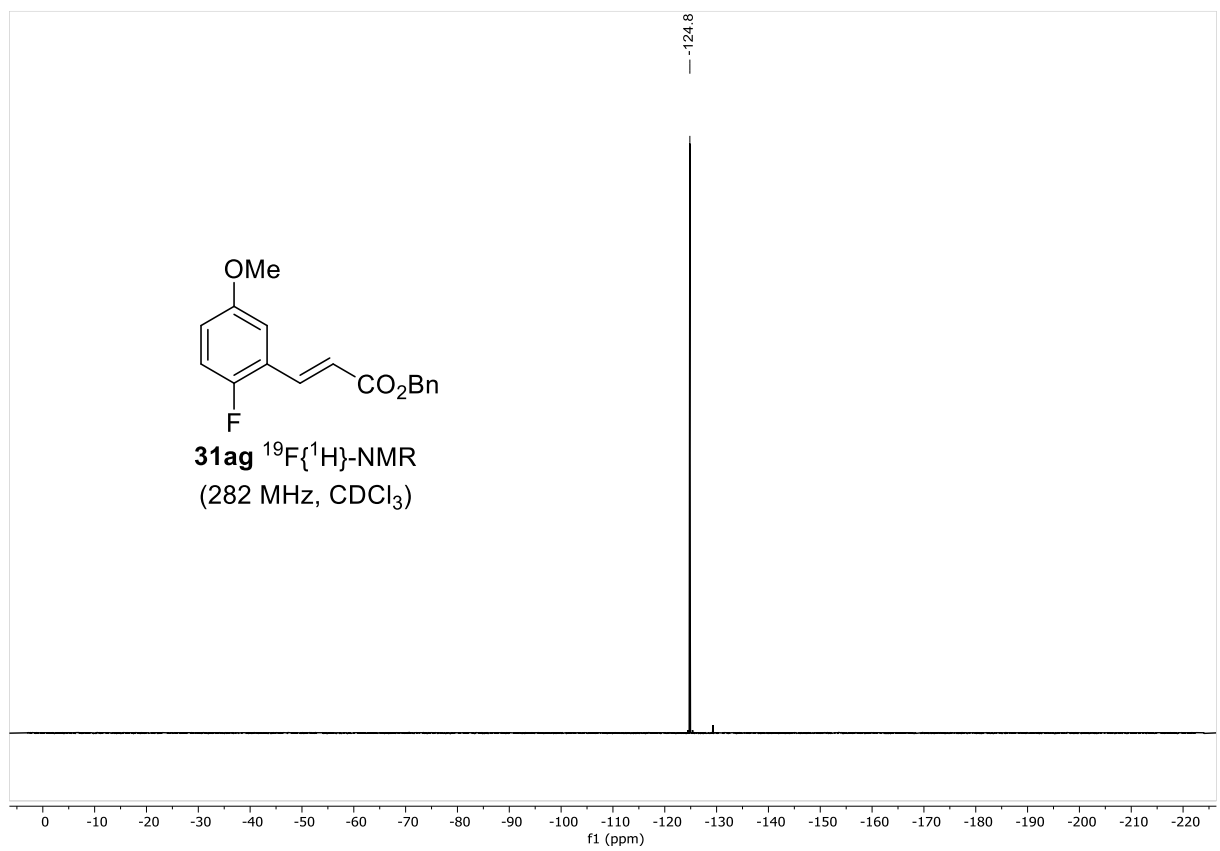
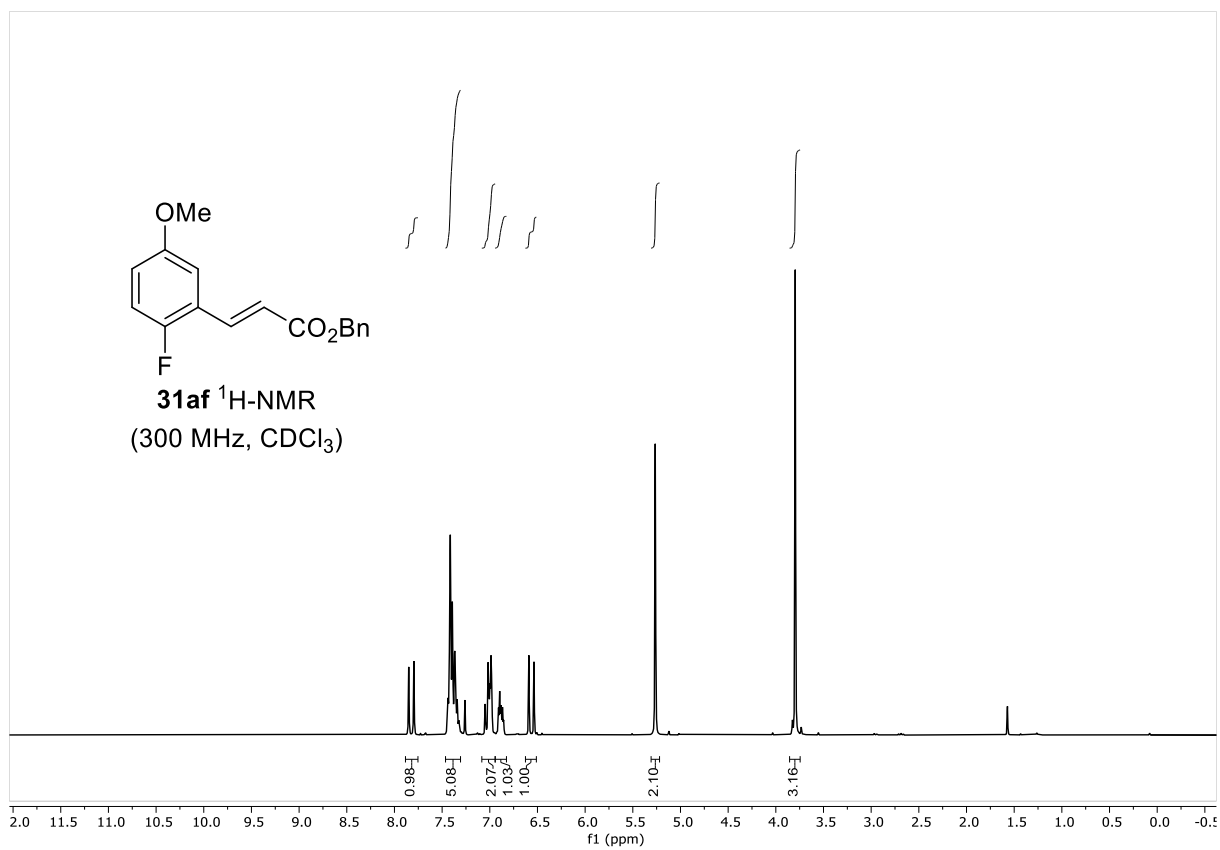
NMR SPECTRA



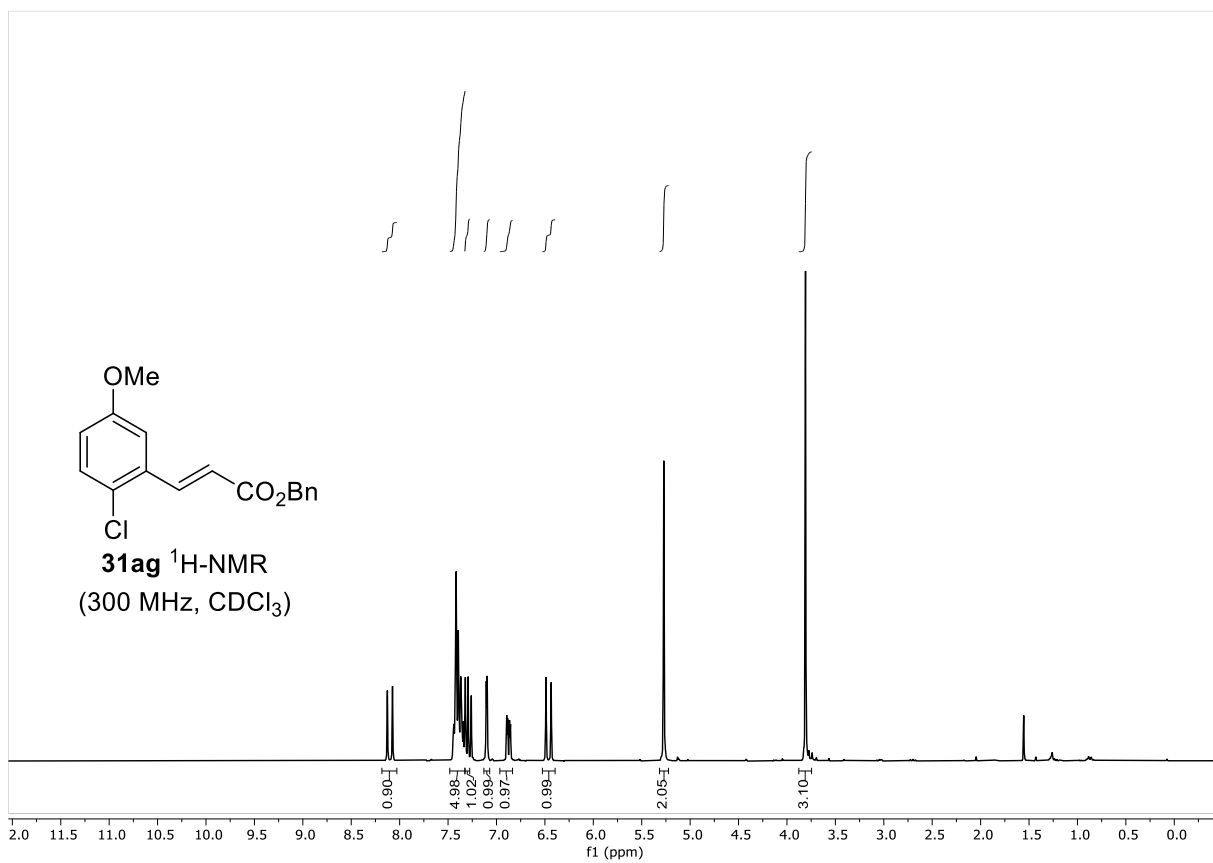
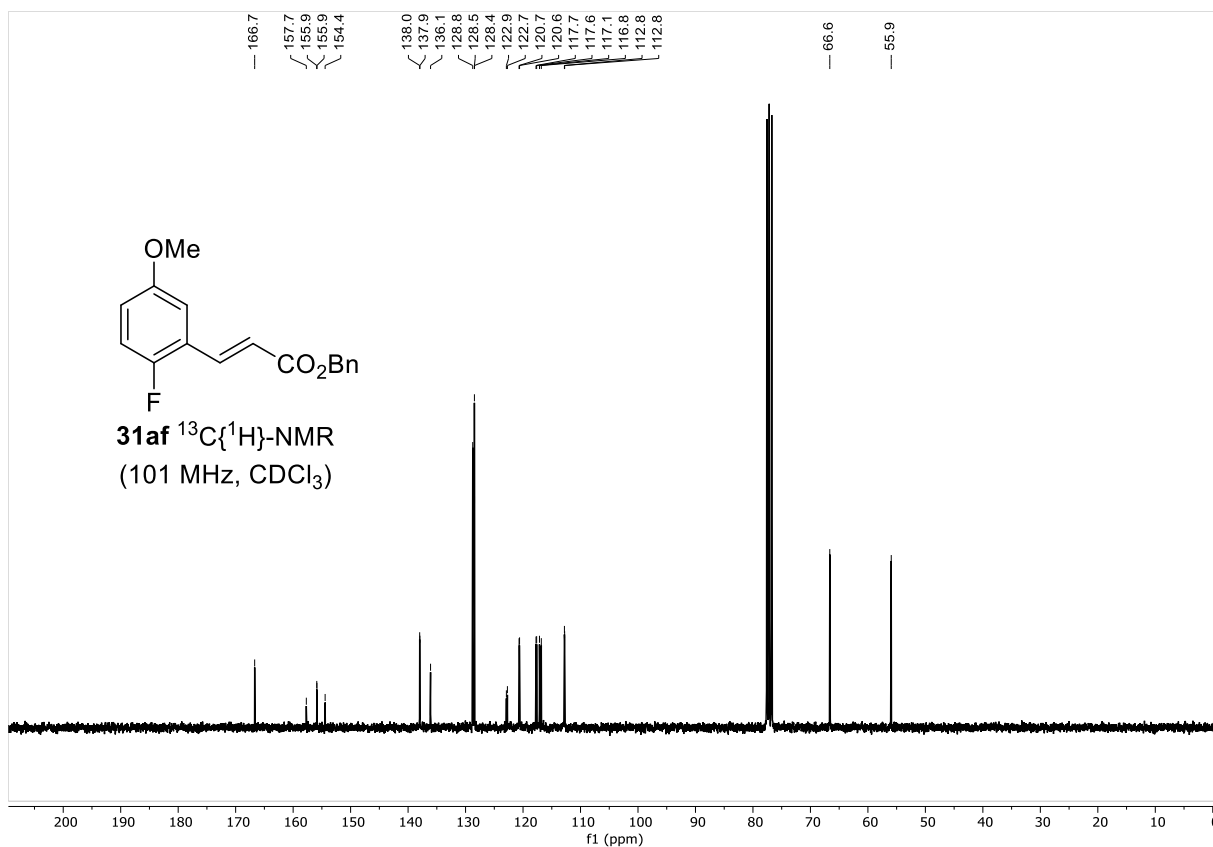
NMR SPECTRA



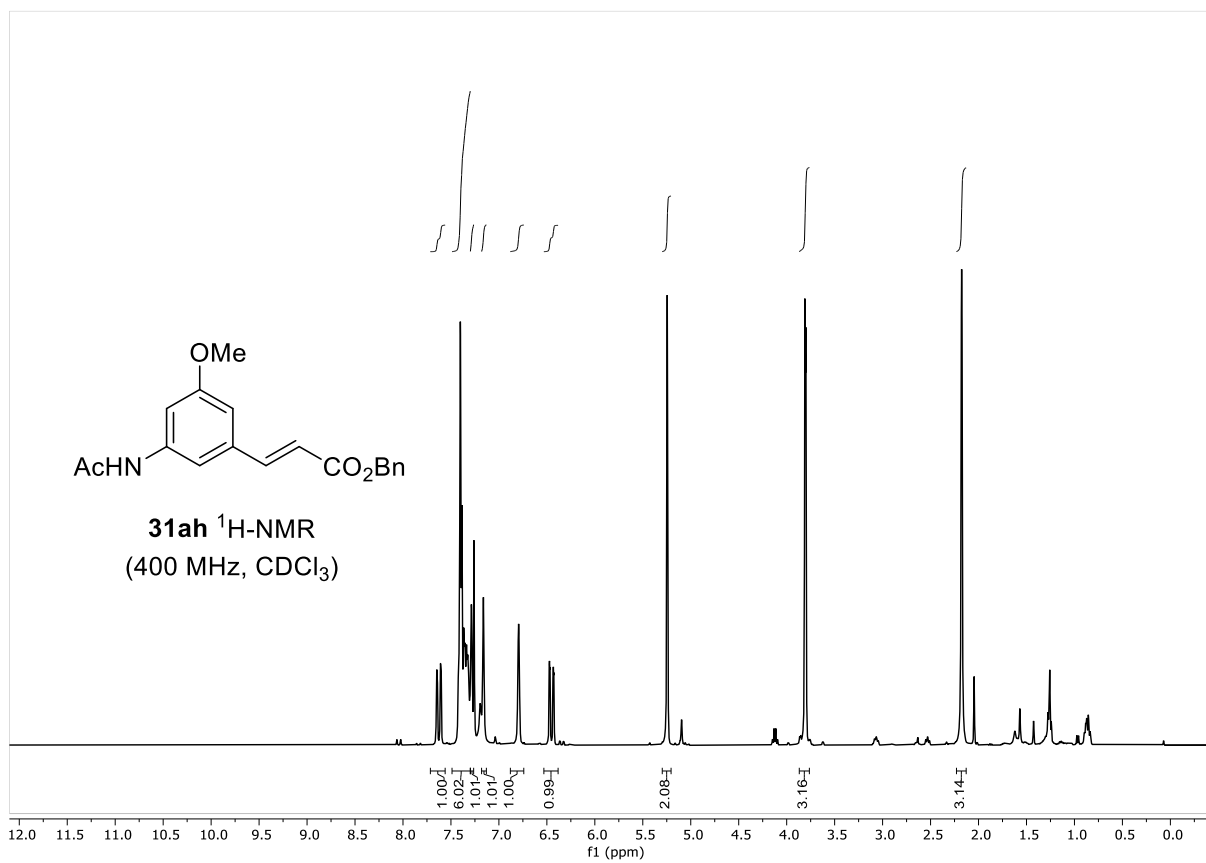
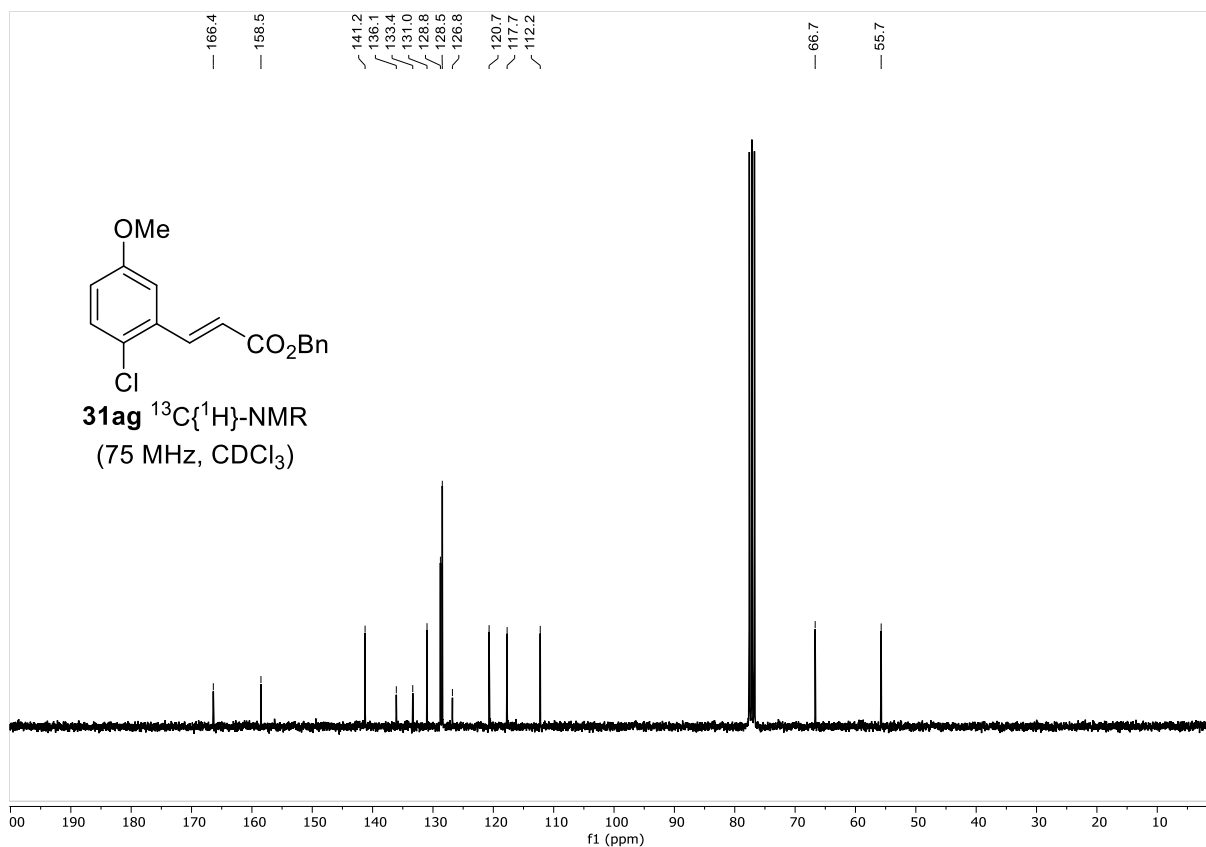
NMR SPECTRA



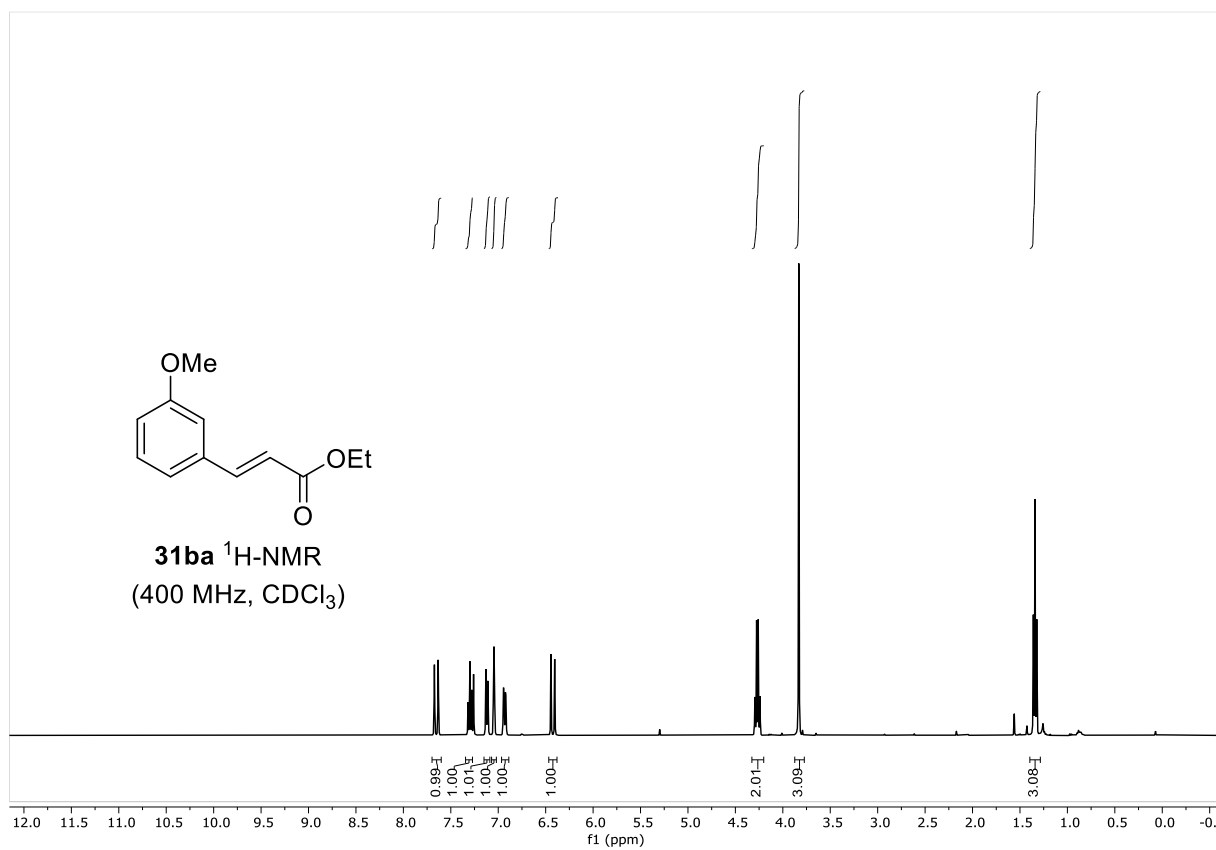
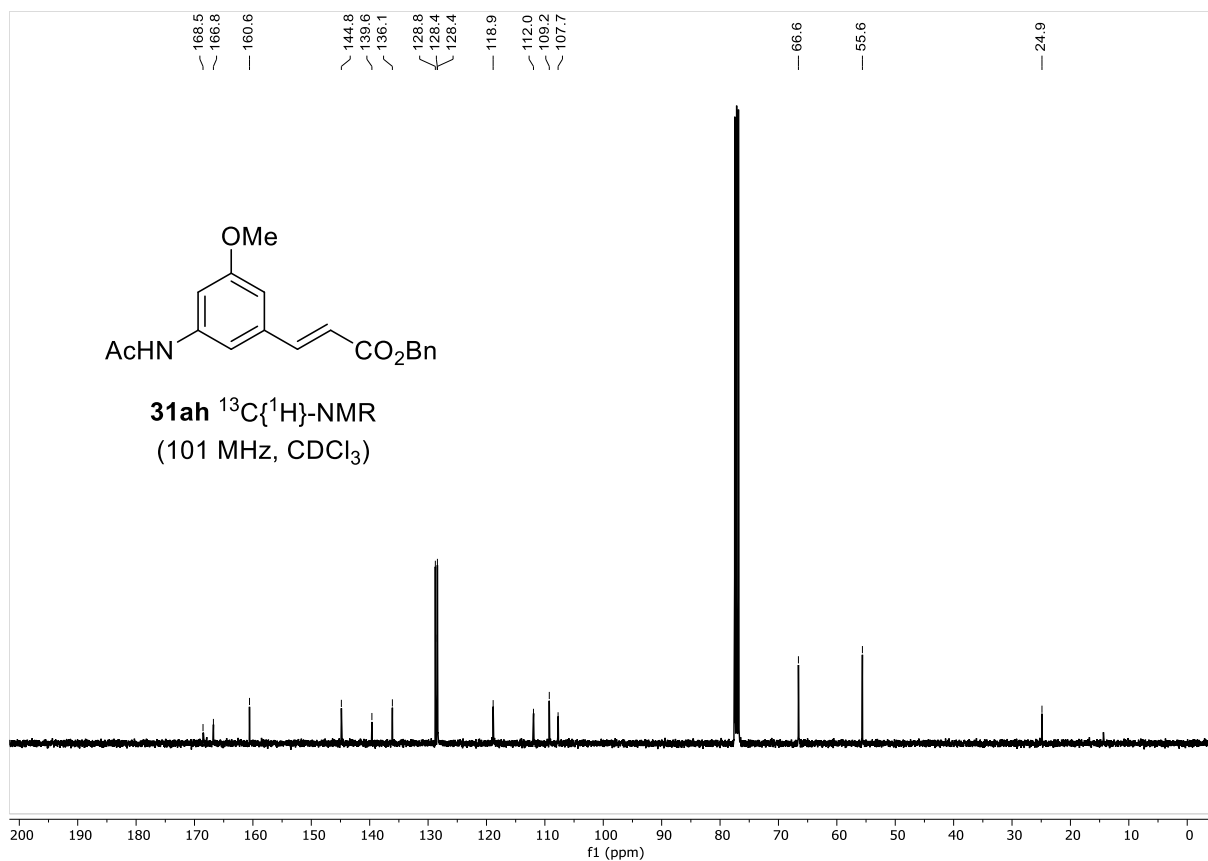
NMR SPECTRA



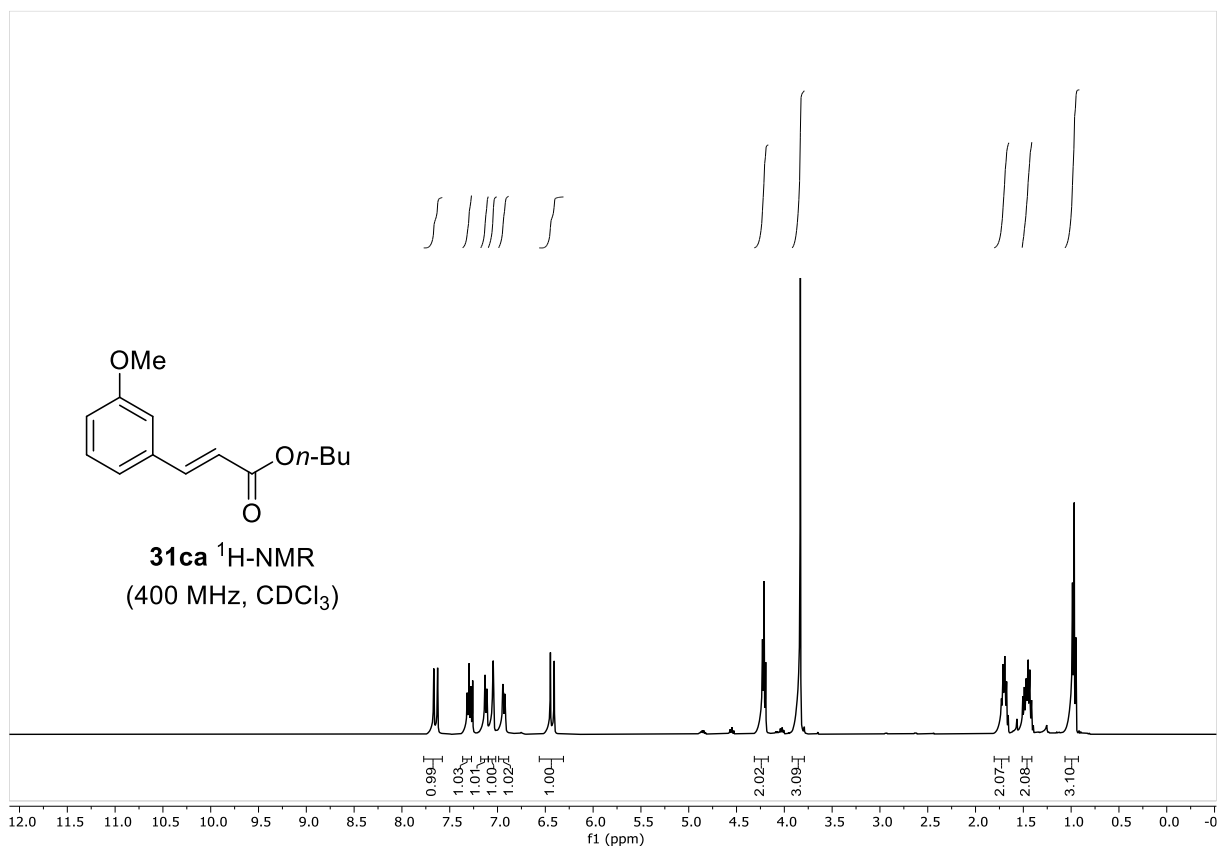
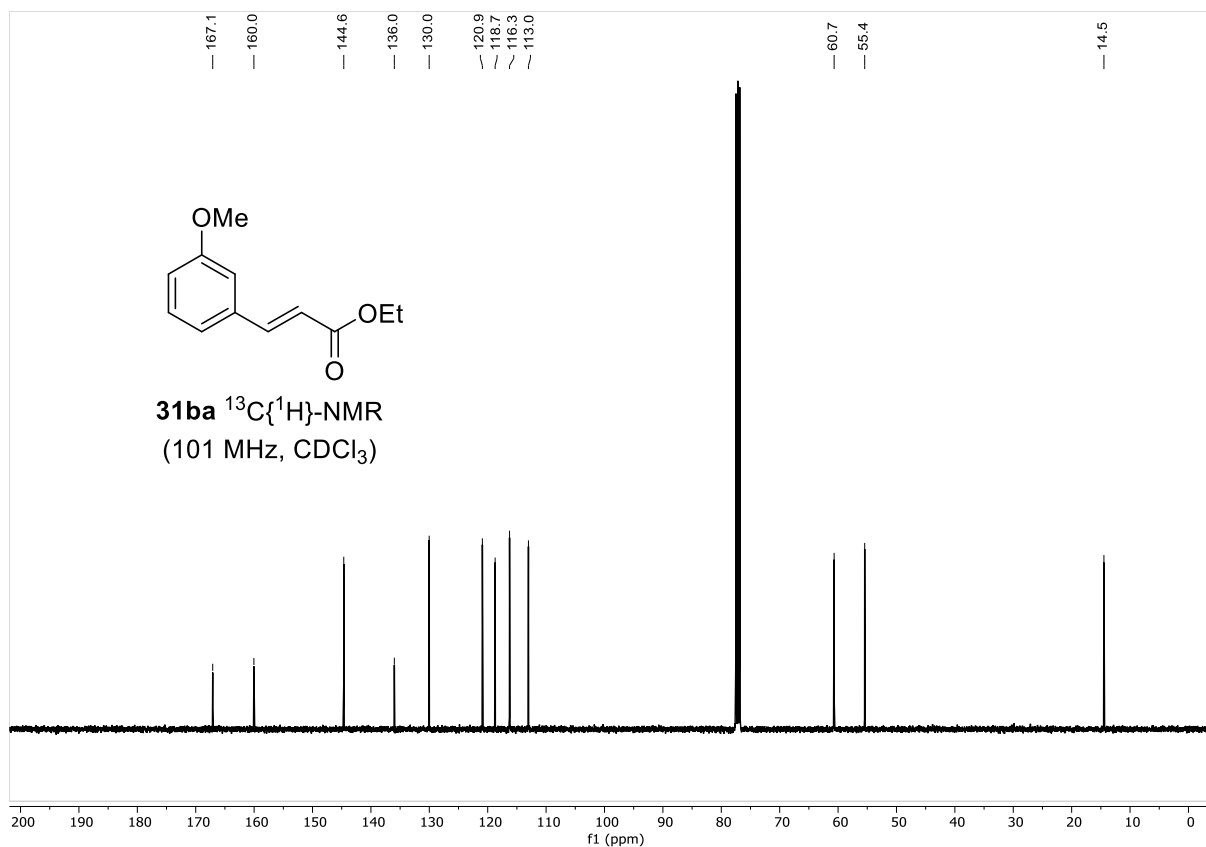
NMR SPECTRA



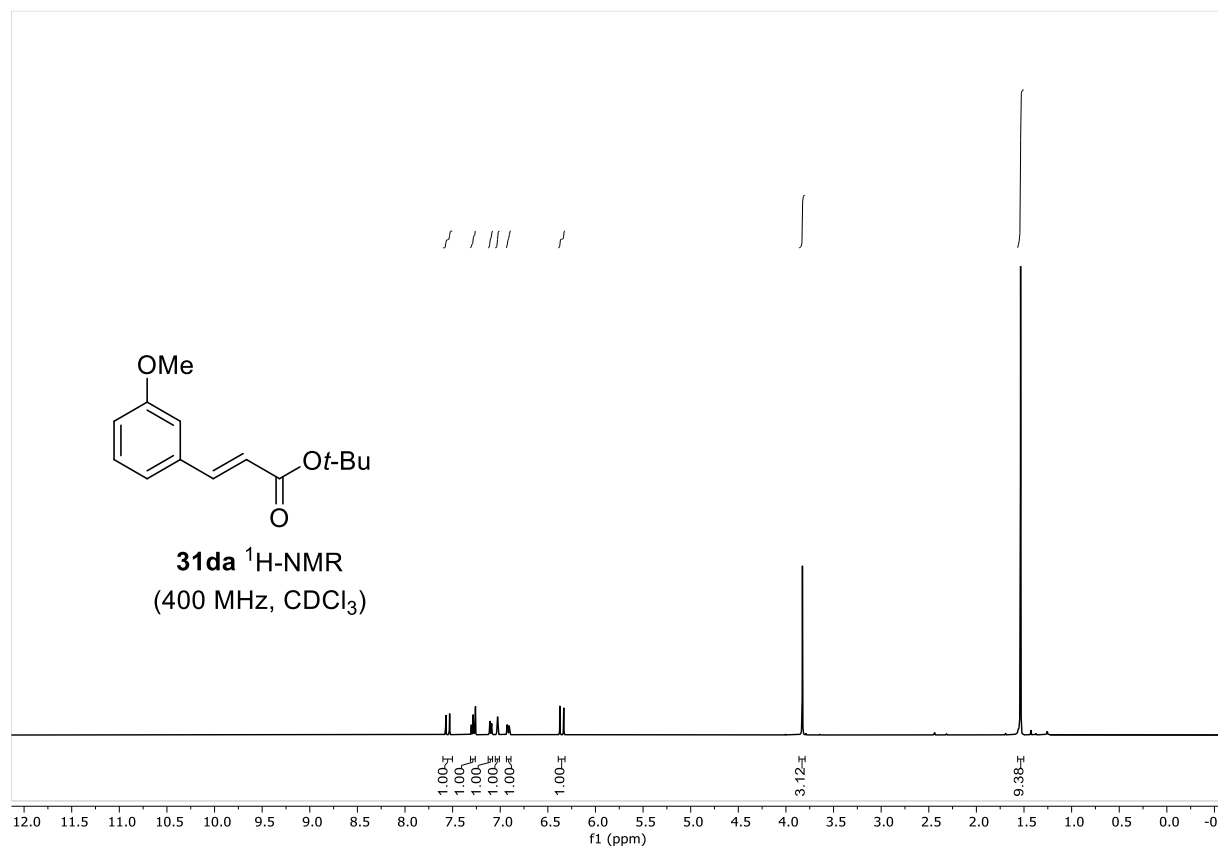
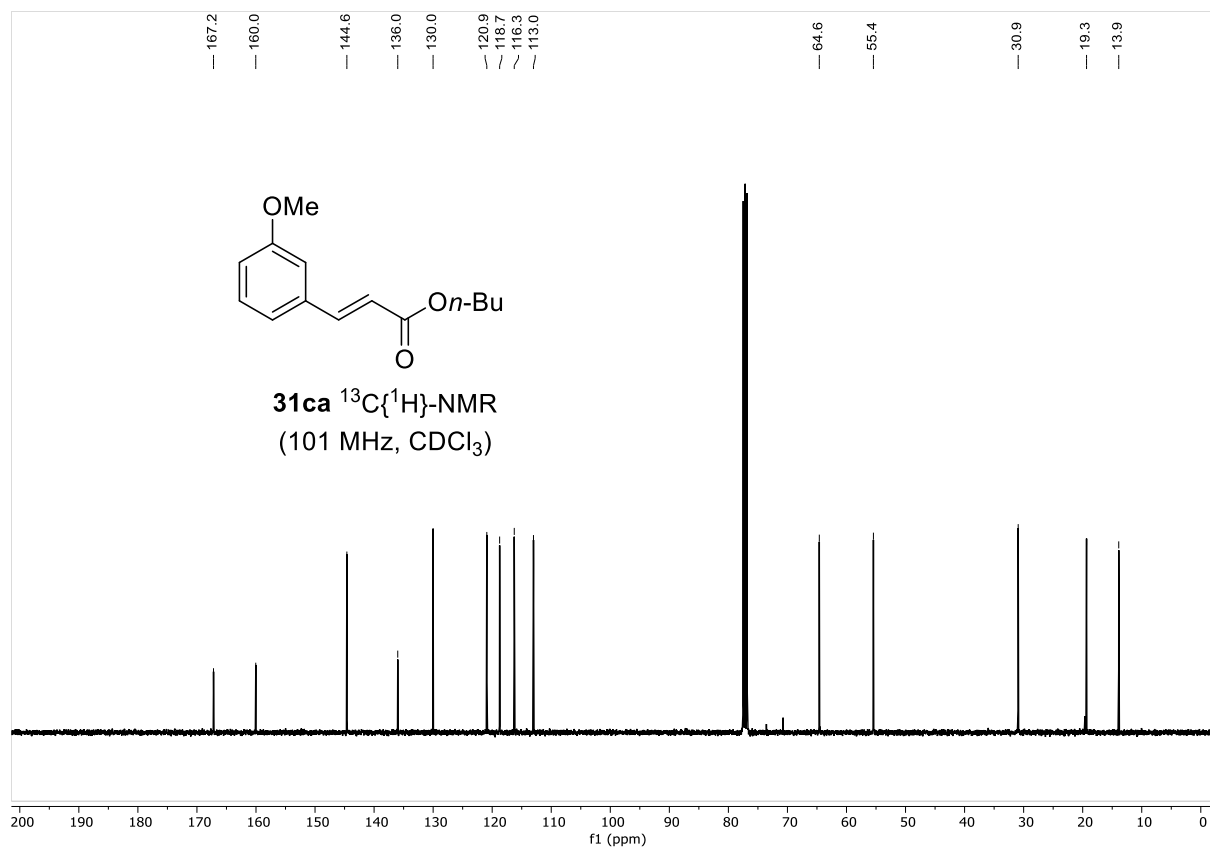
NMR SPECTRA



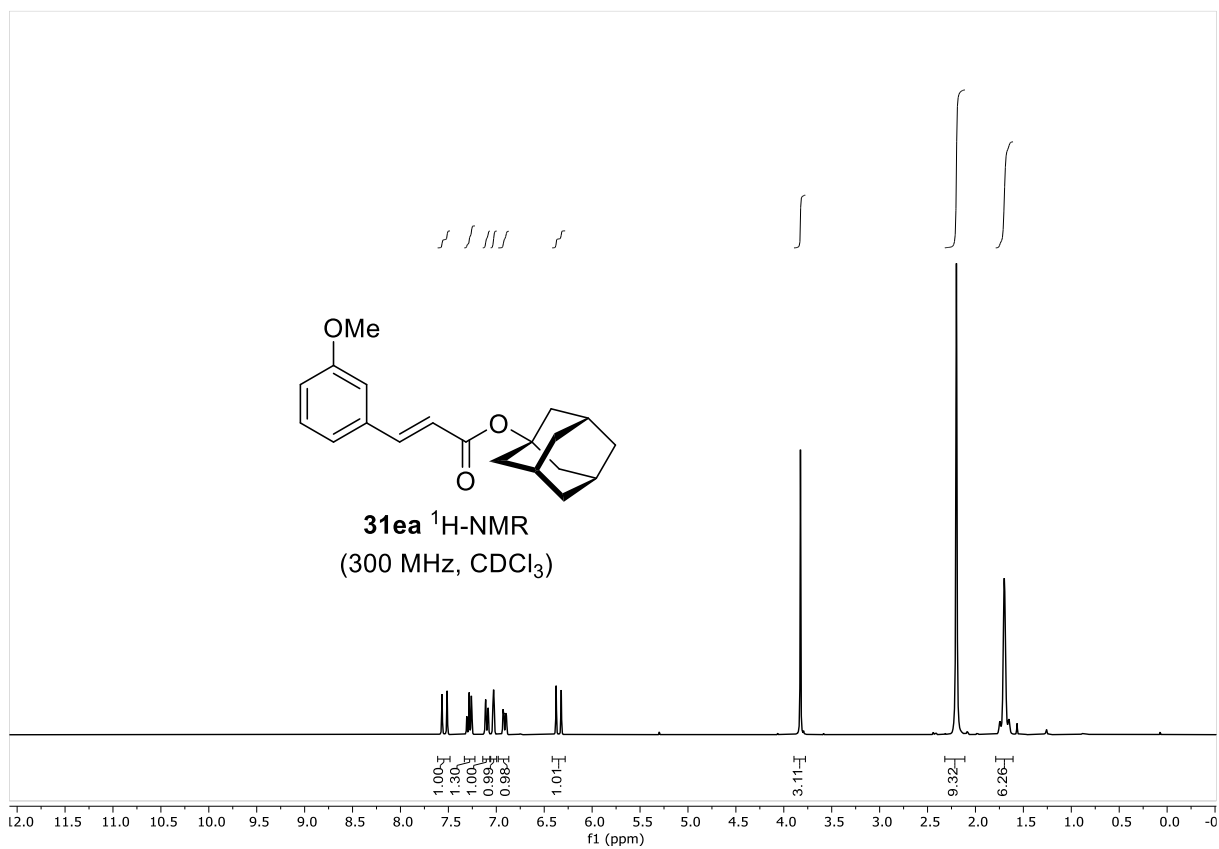
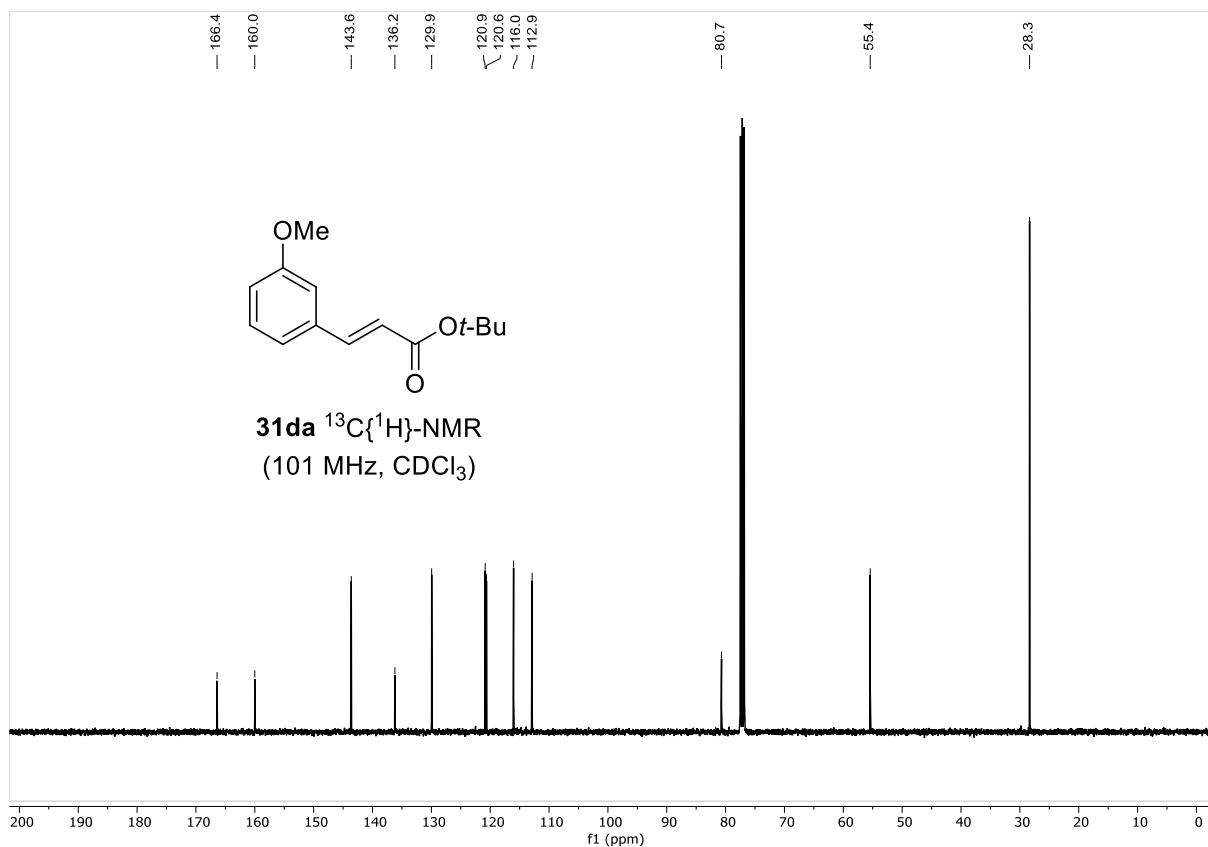
NMR SPECTRA



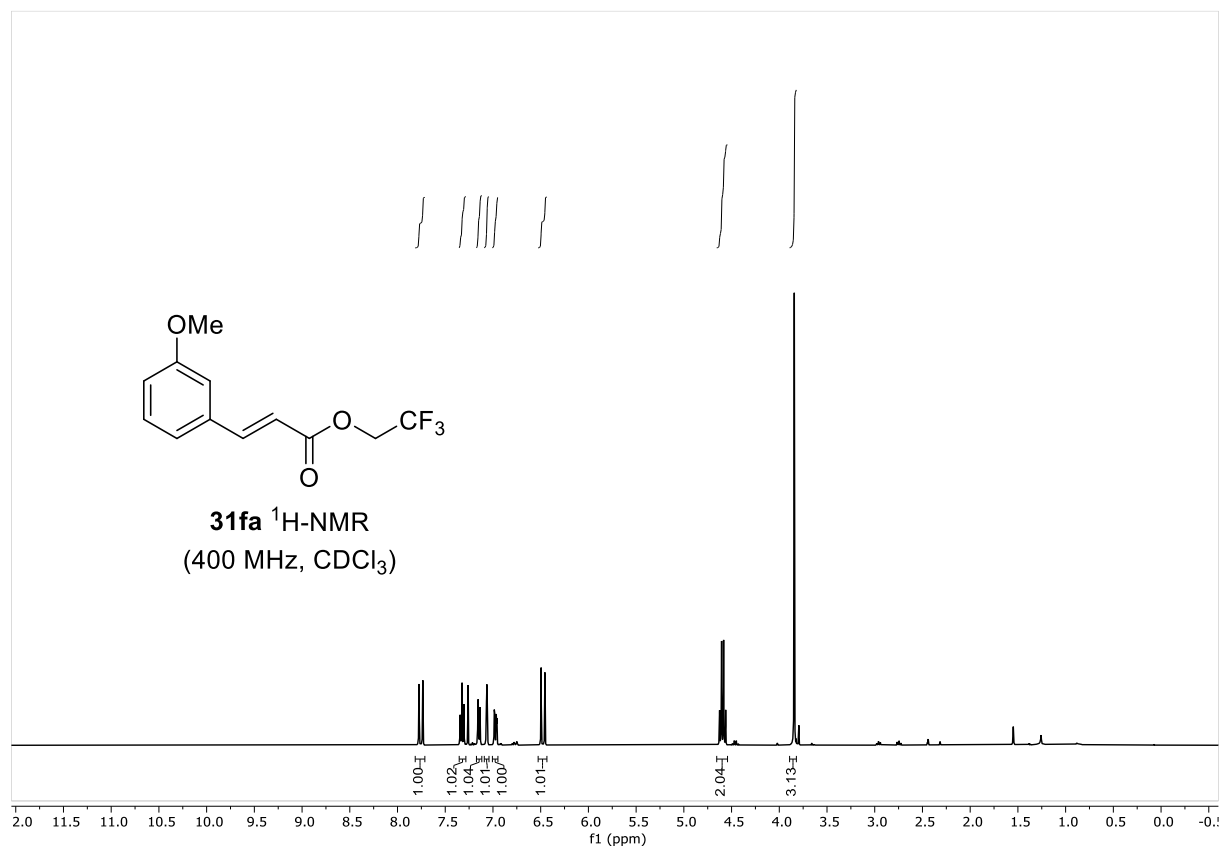
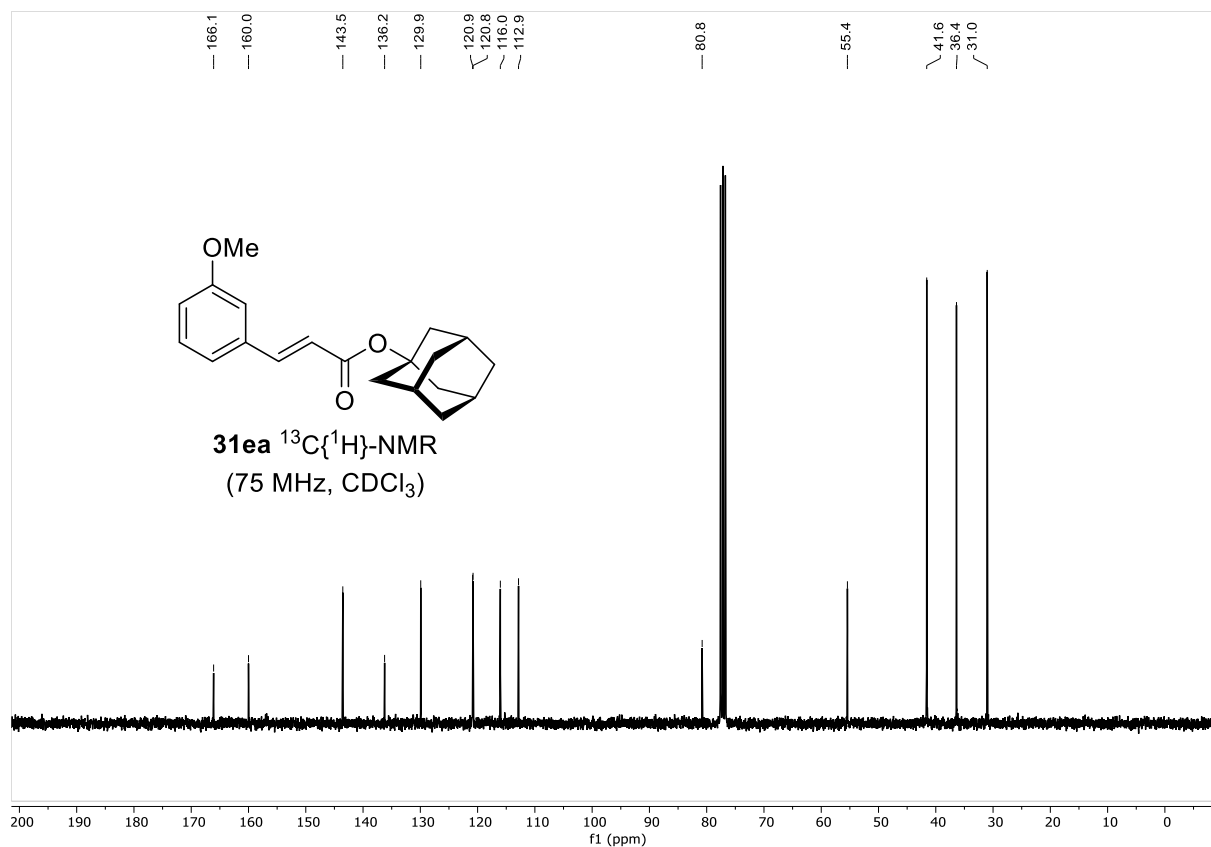
NMR SPECTRA



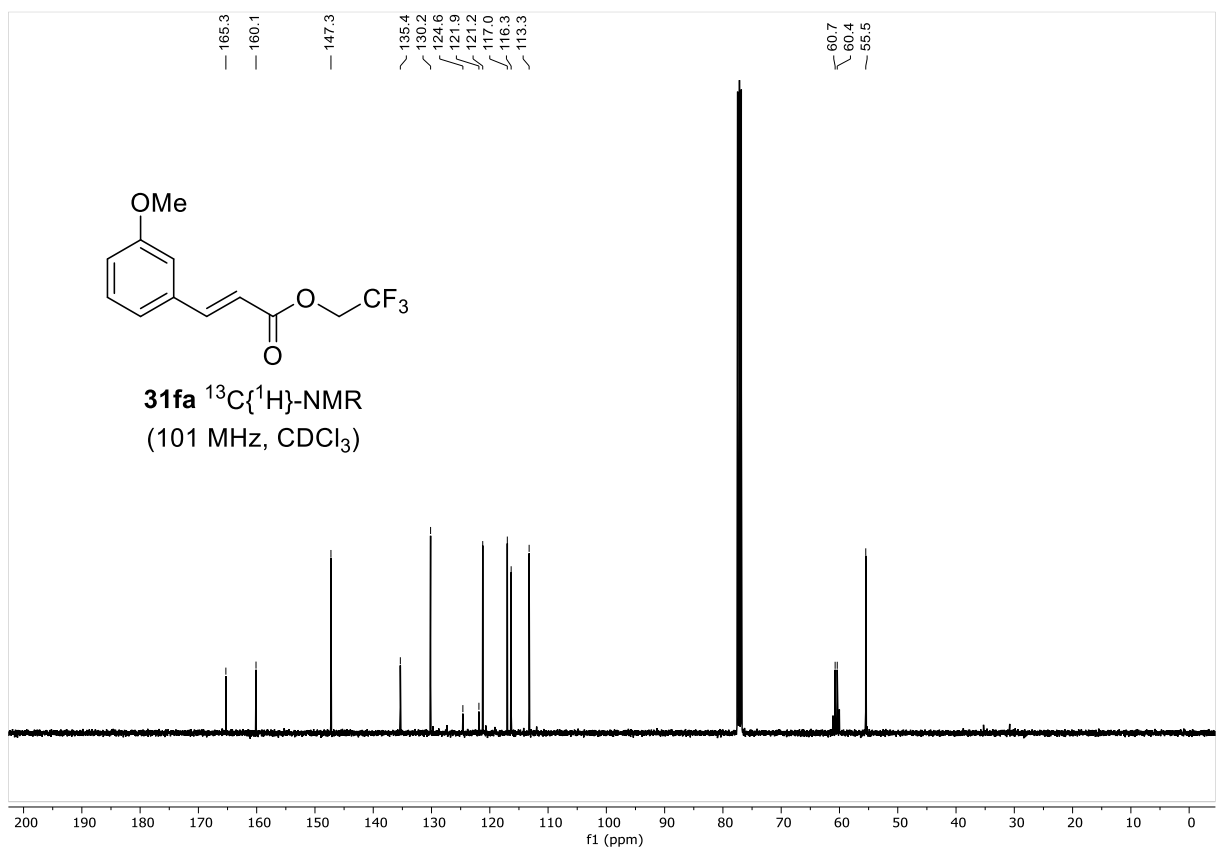
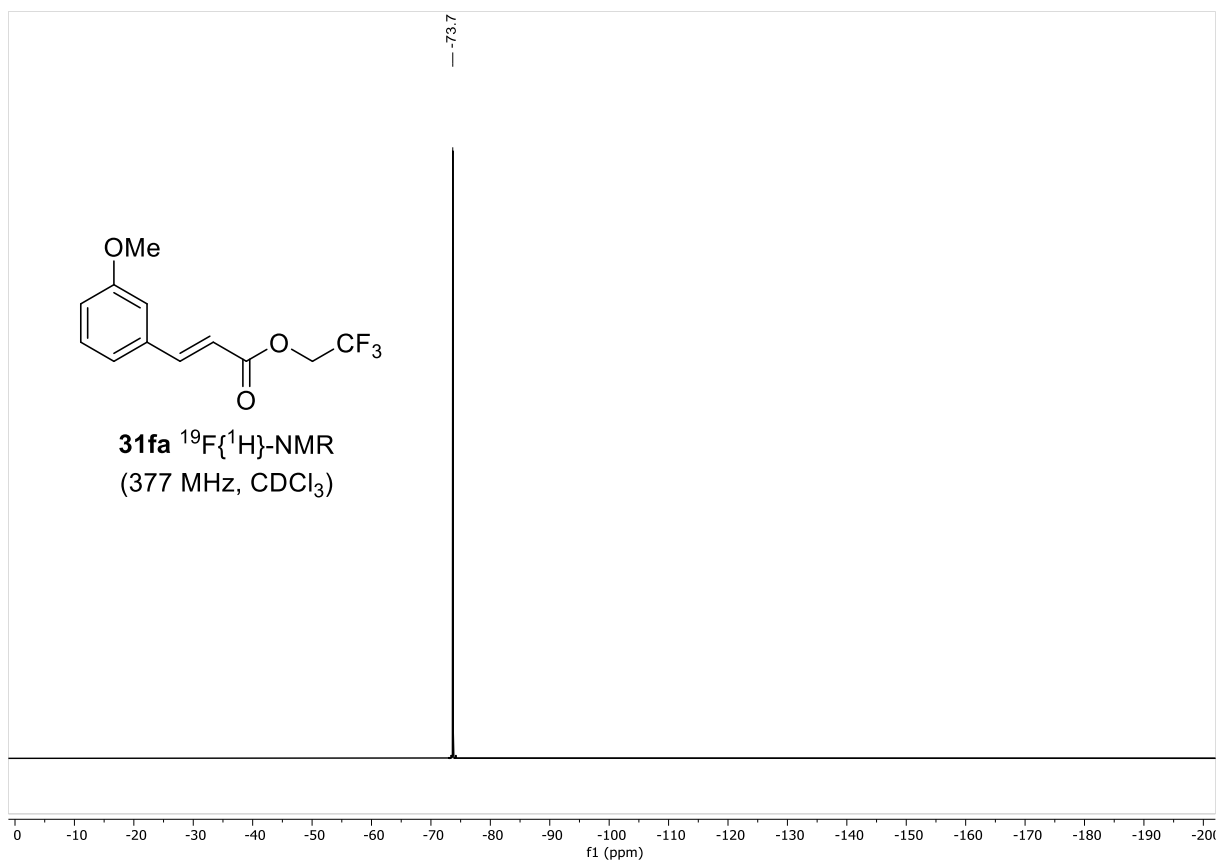
NMR SPECTRA



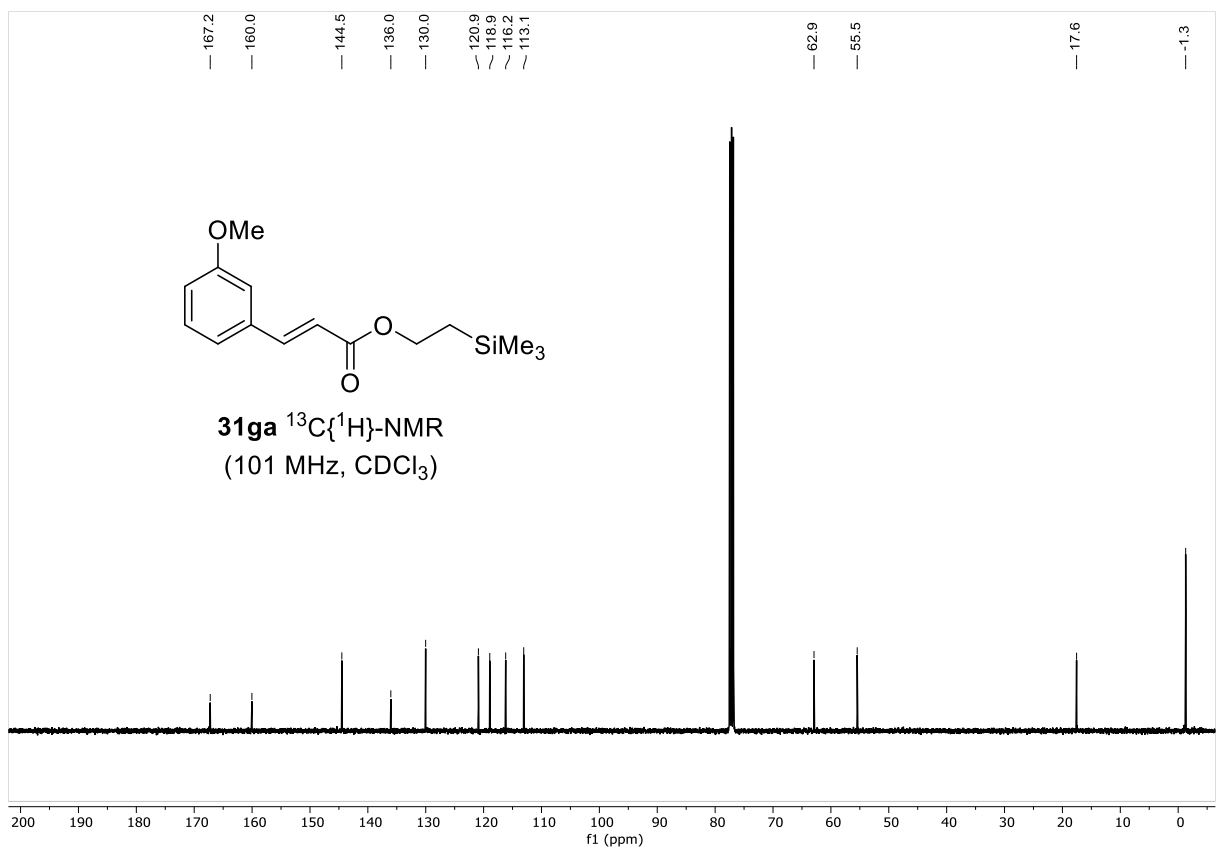
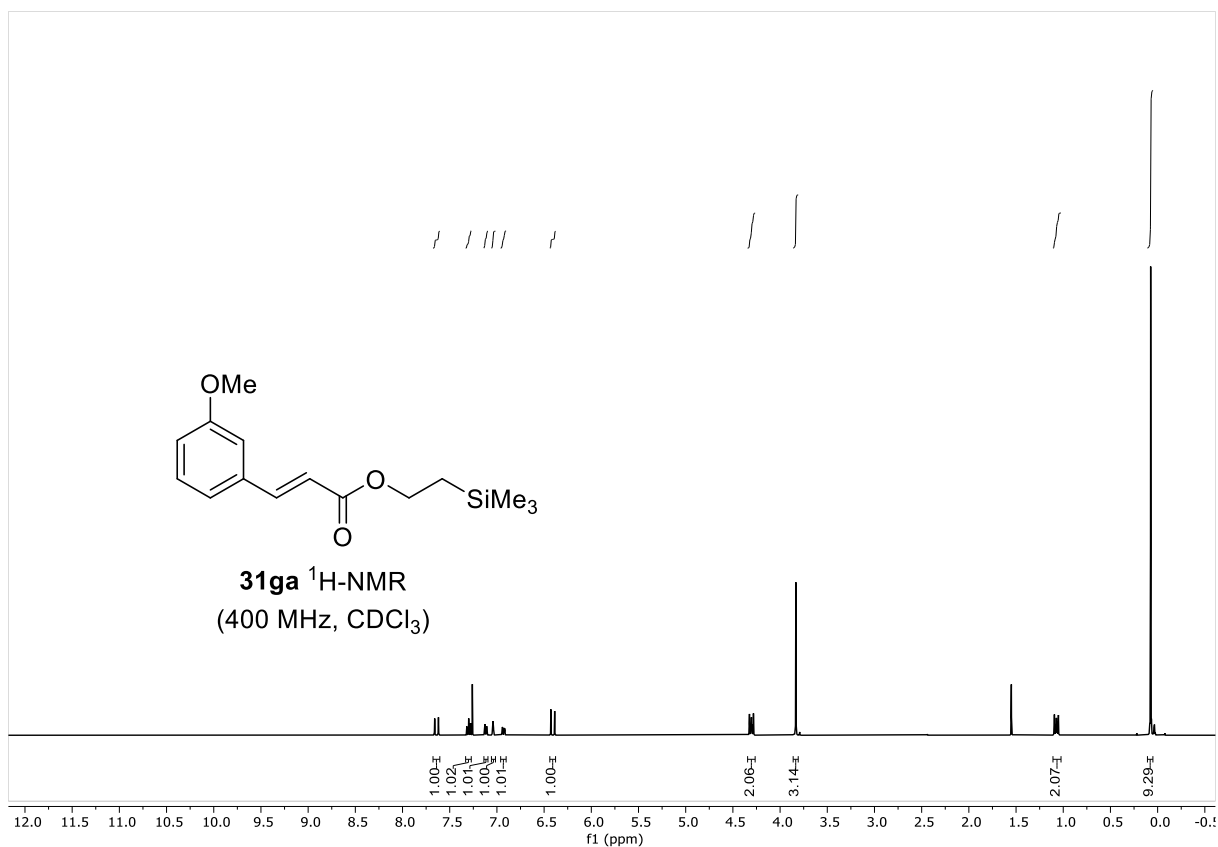
NMR SPECTRA



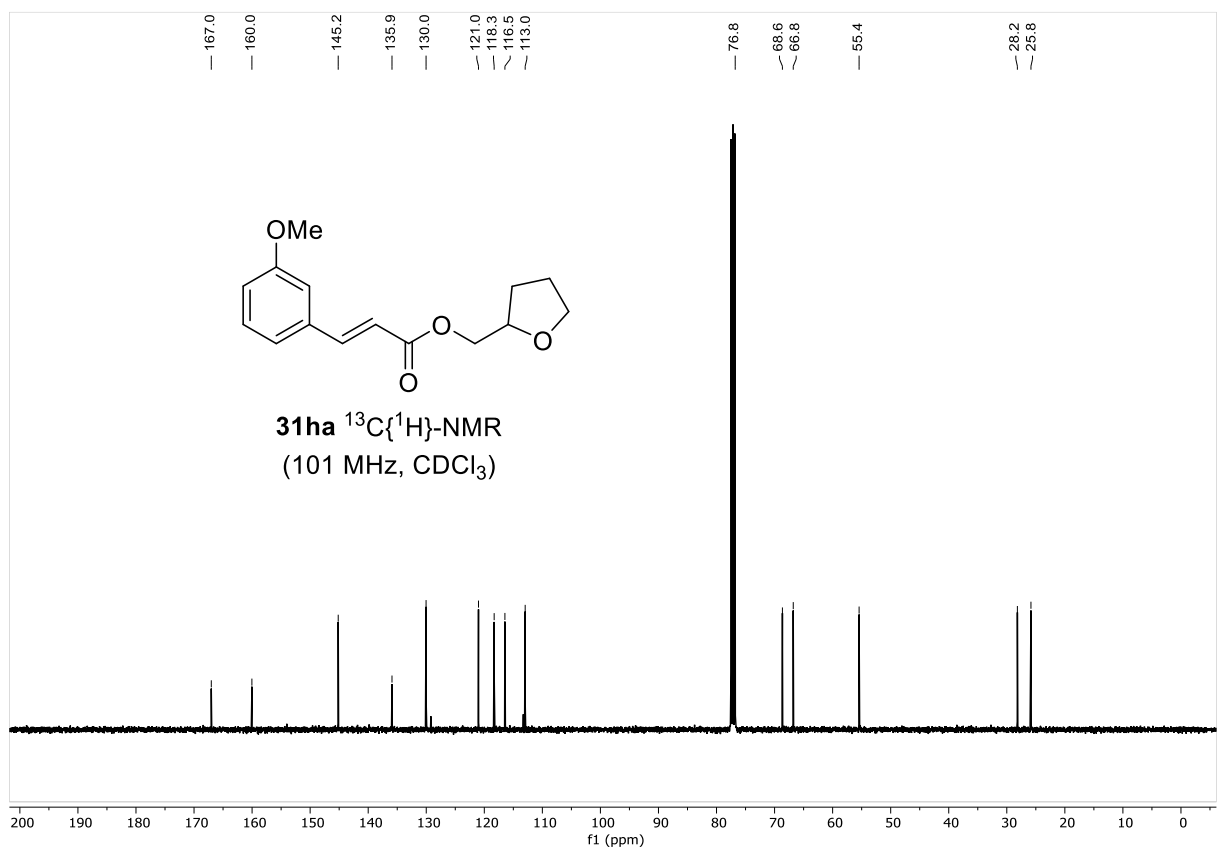
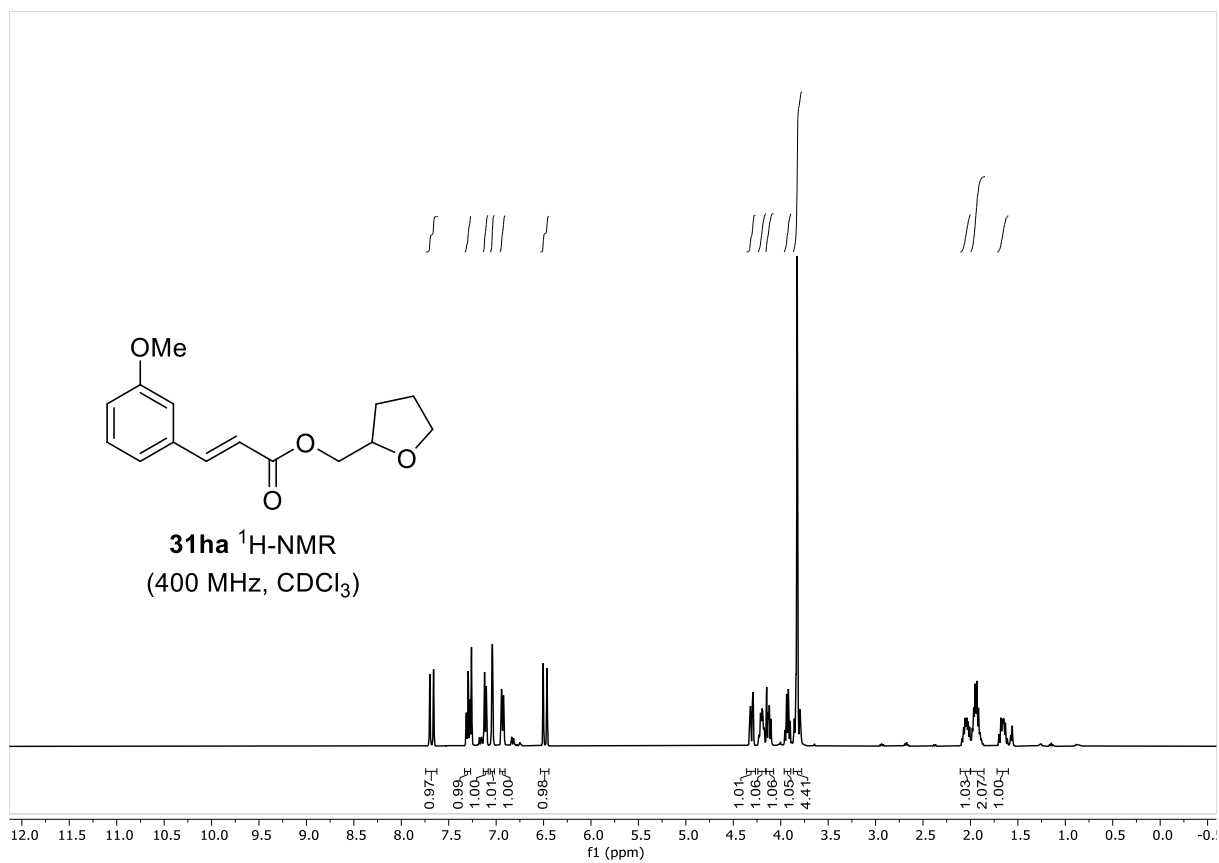
NMR SPECTRA



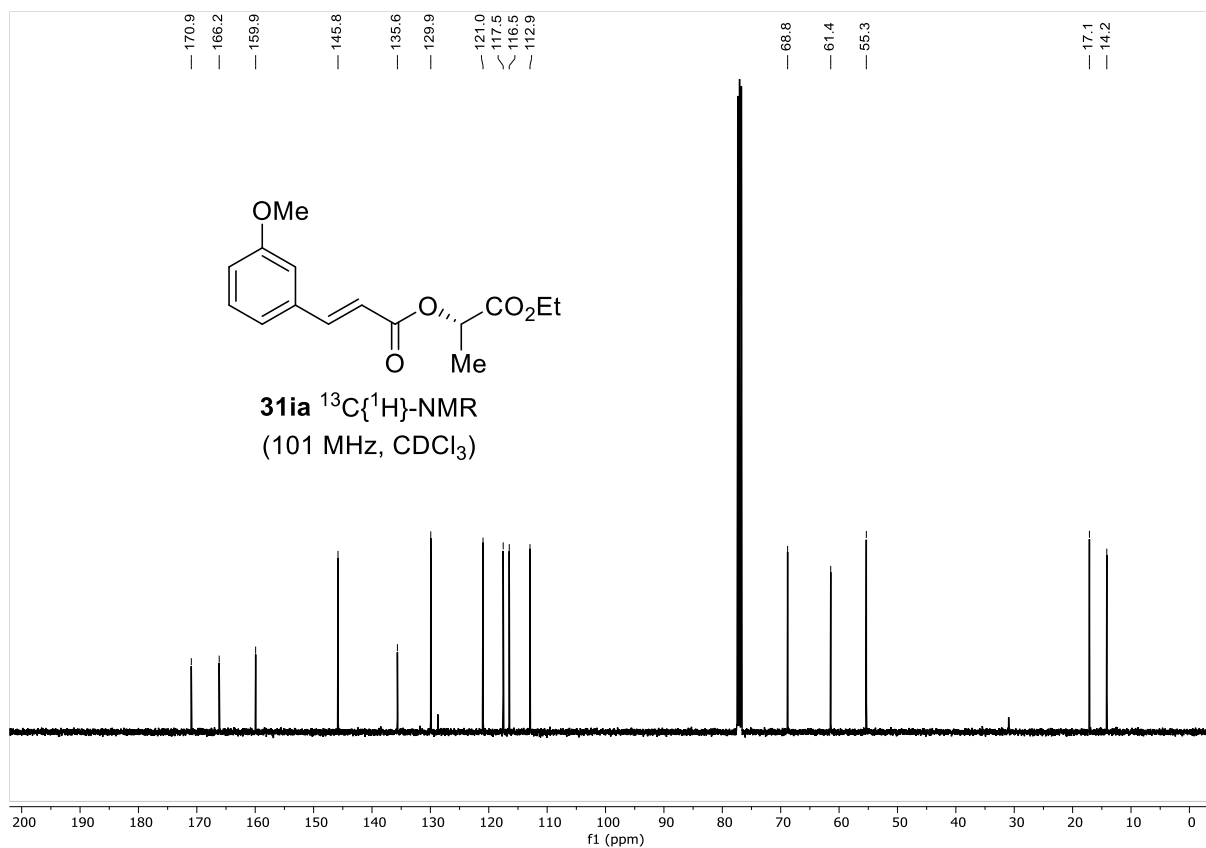
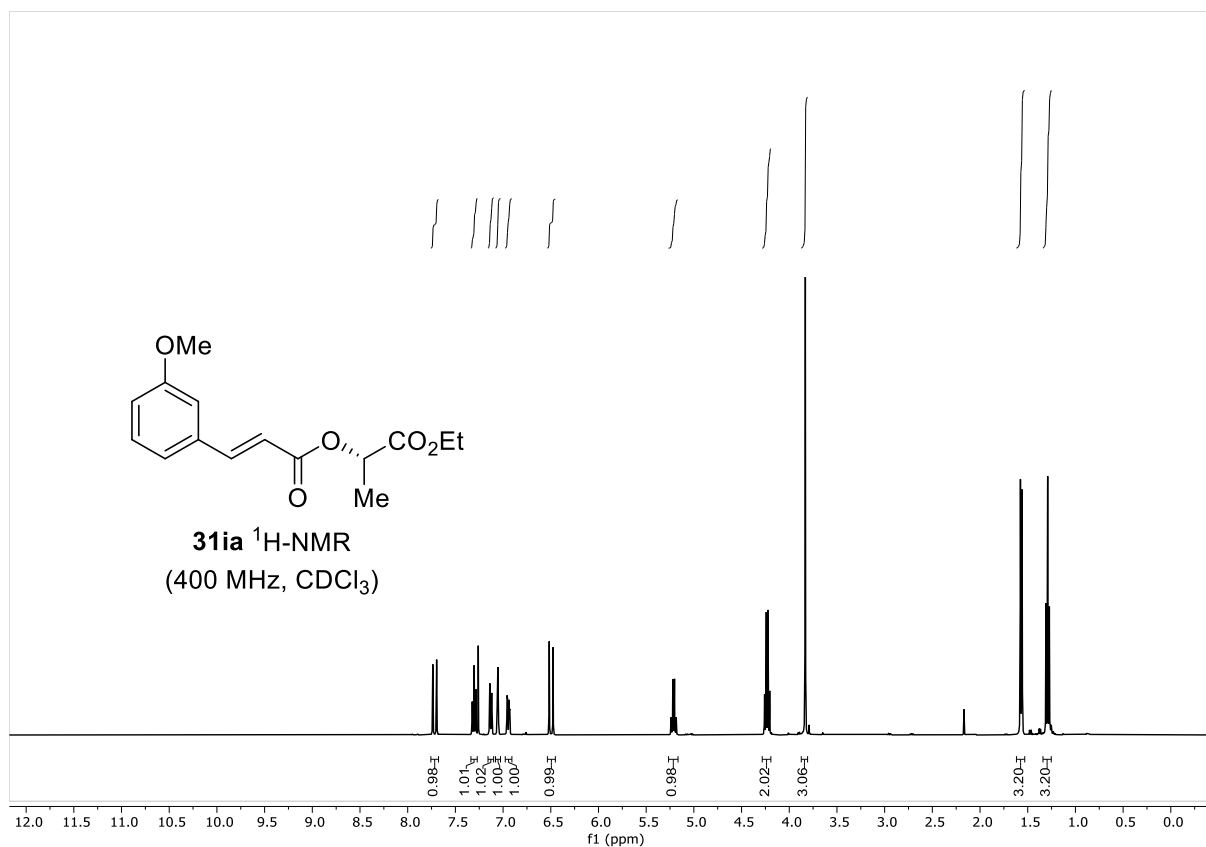
NMR SPECTRA



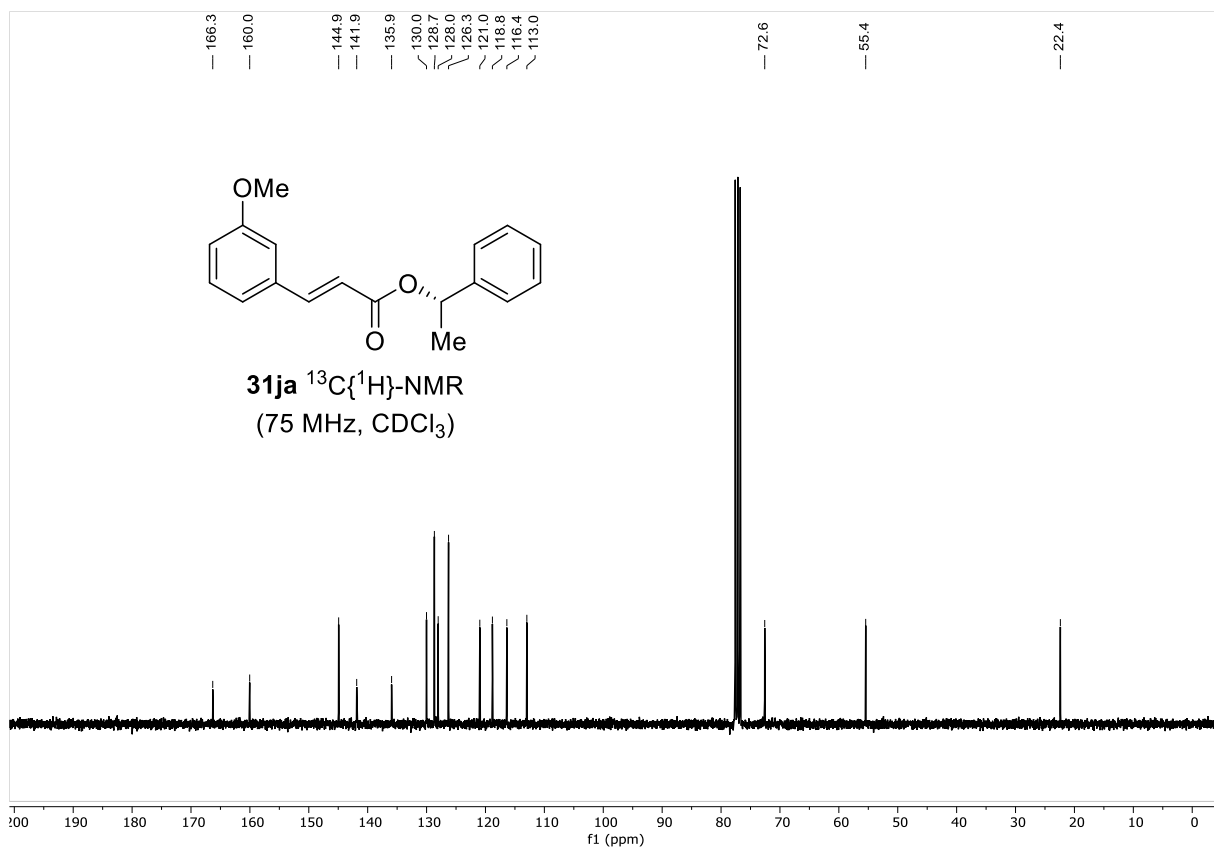
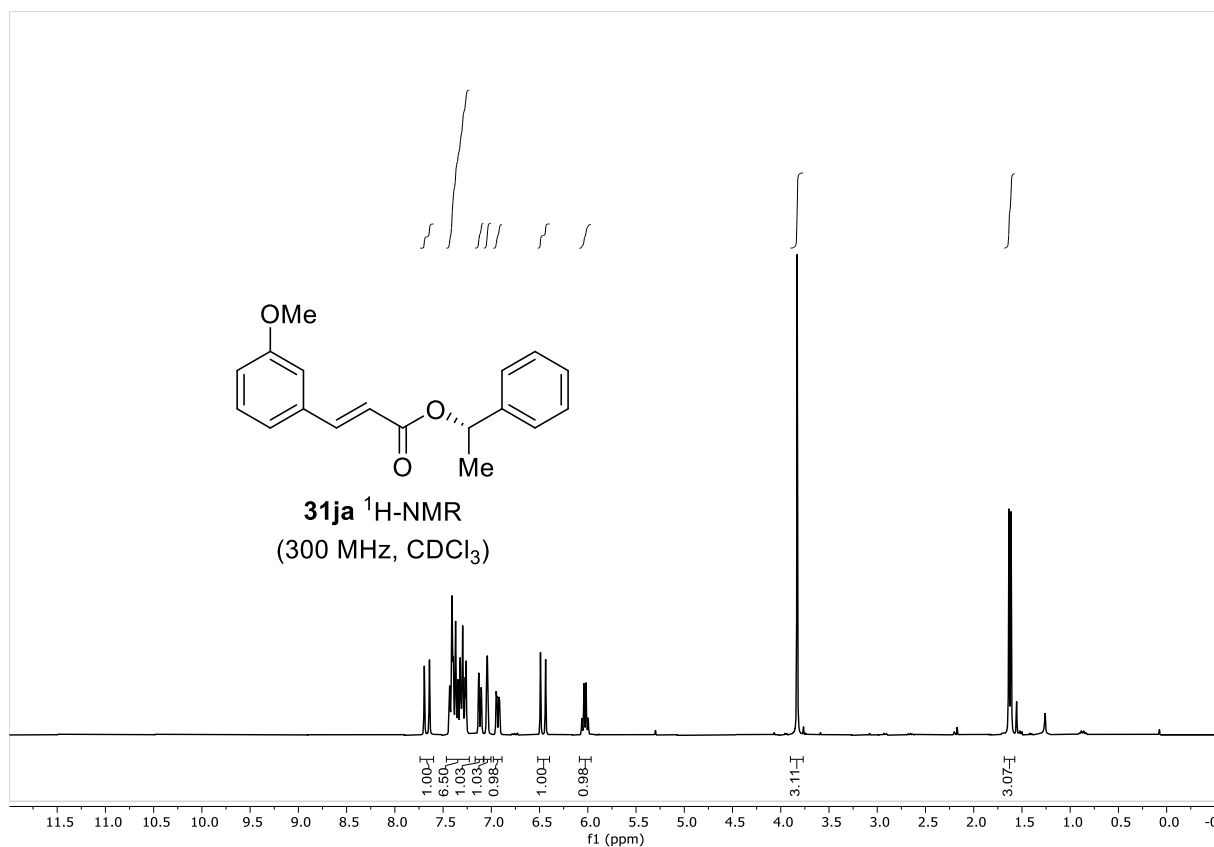
NMR SPECTRA



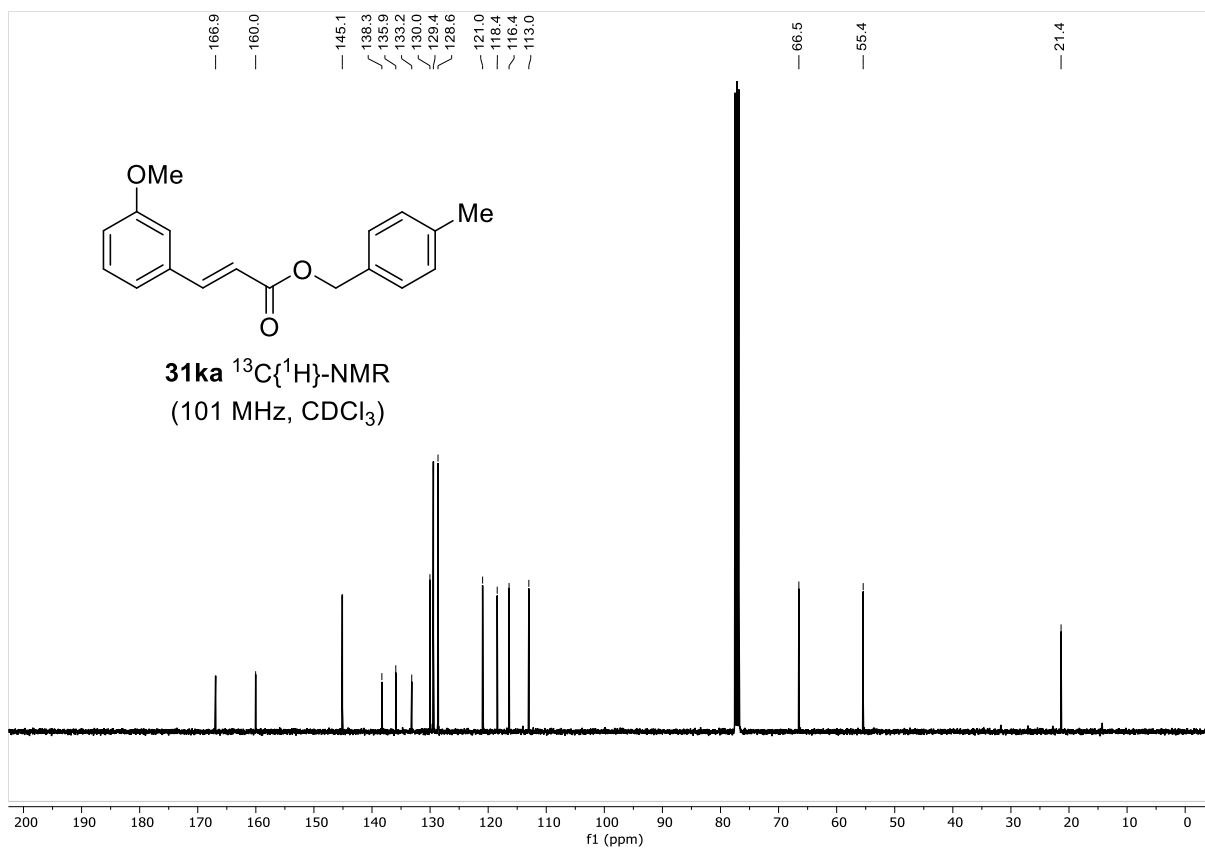
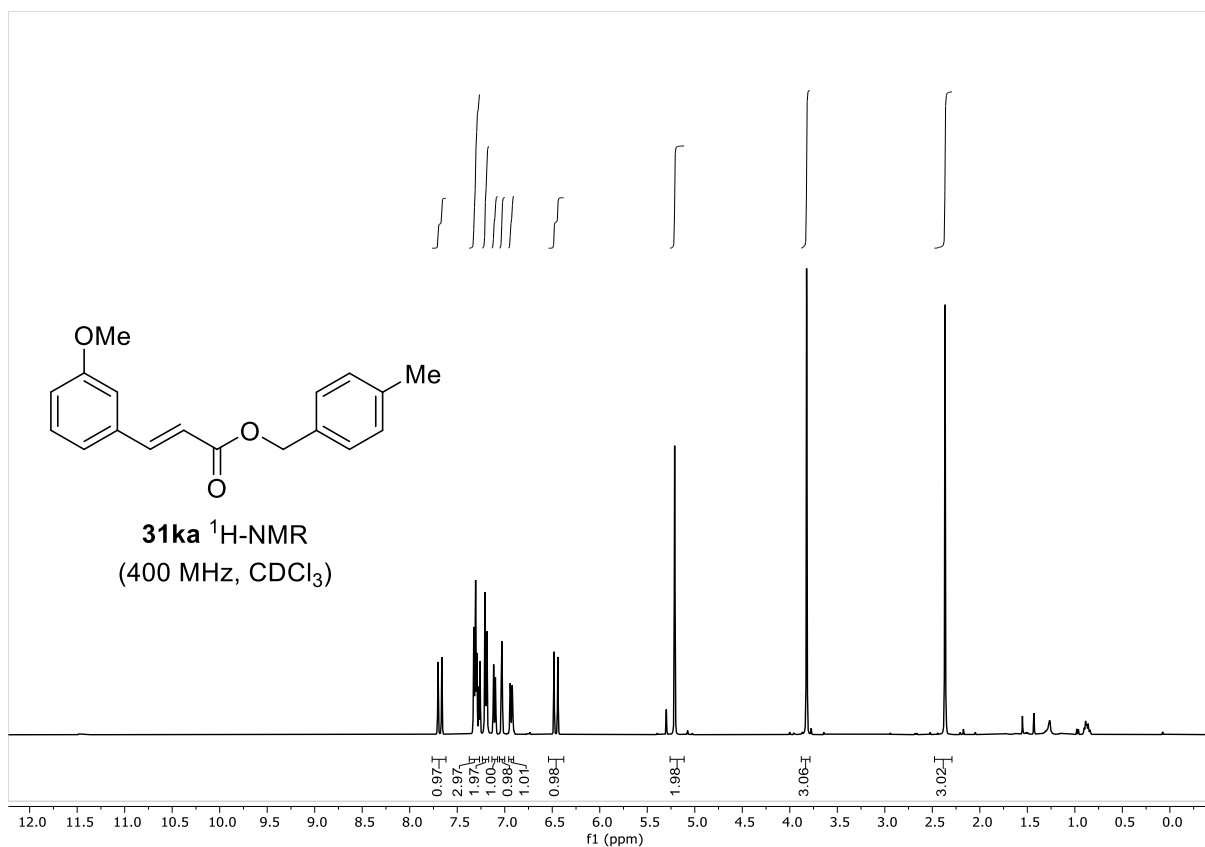
NMR SPECTRA



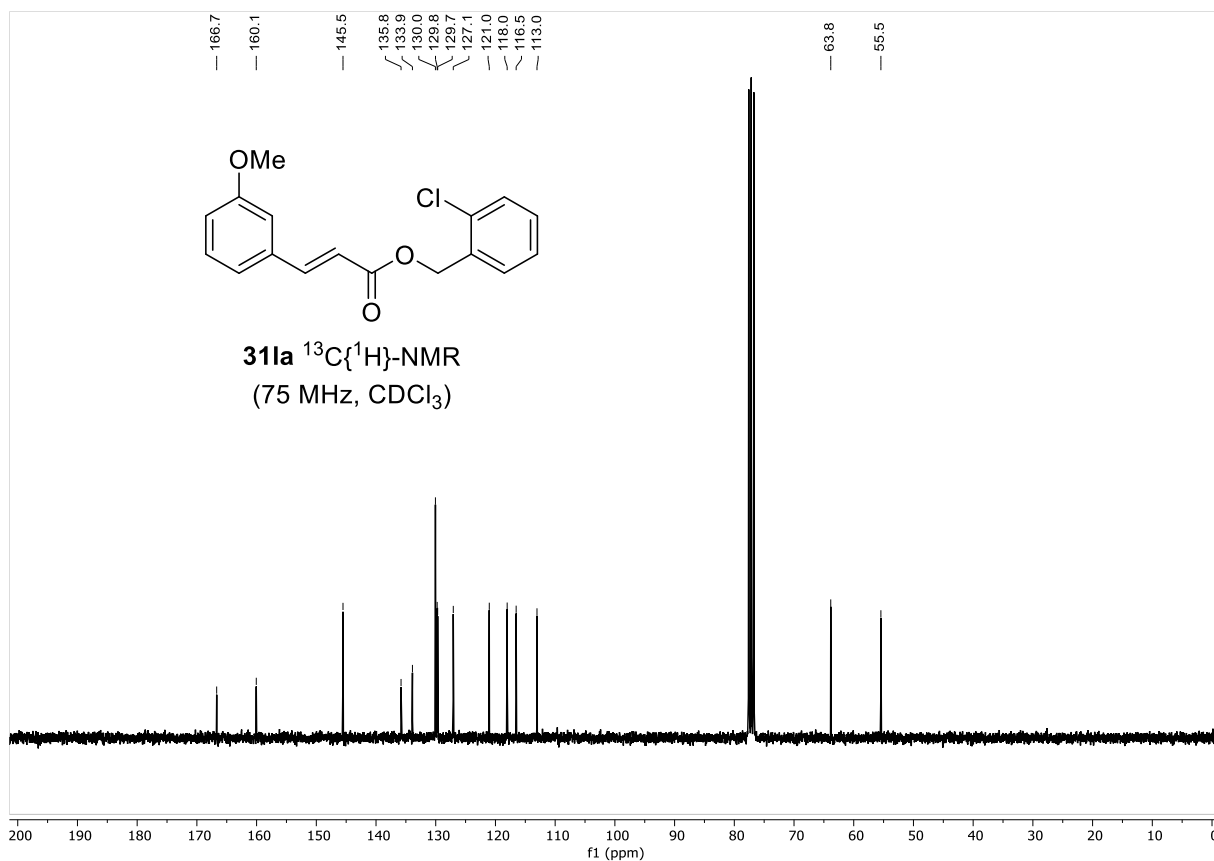
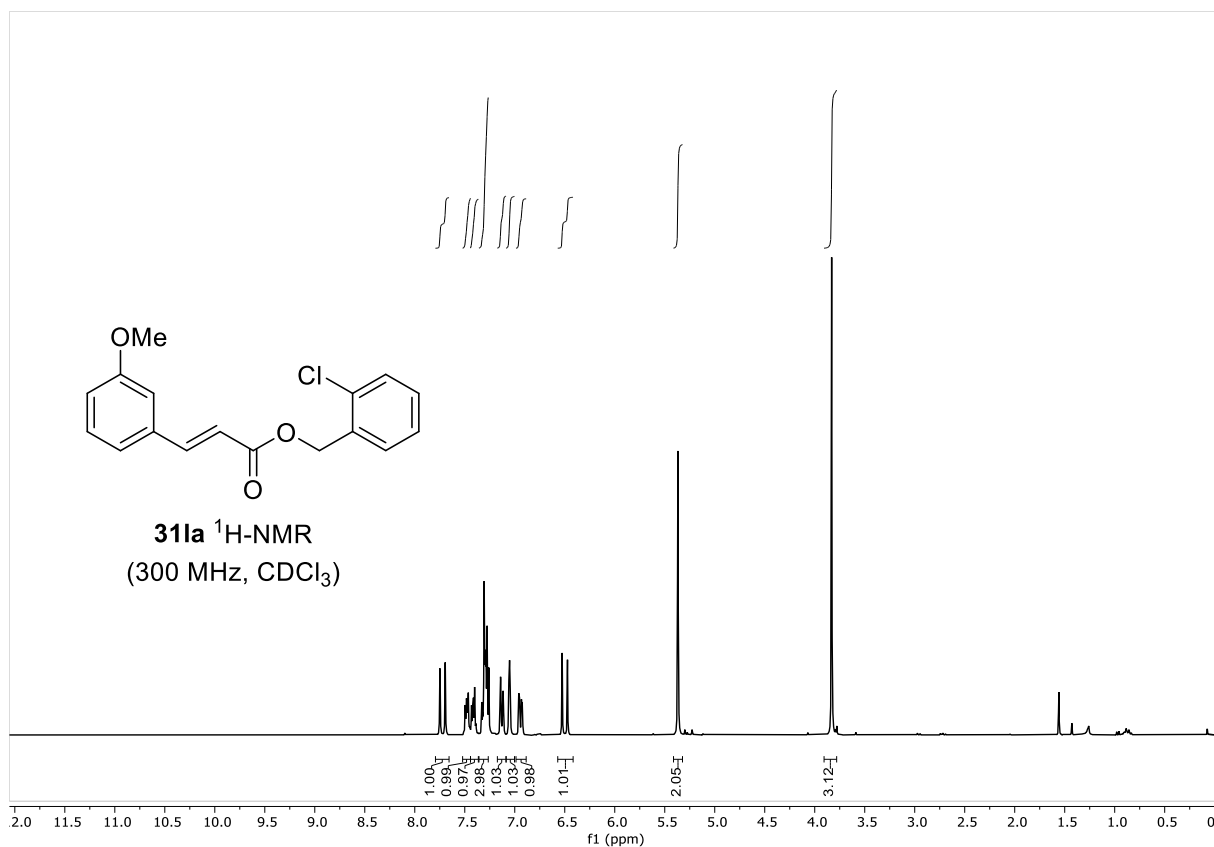
NMR SPECTRA



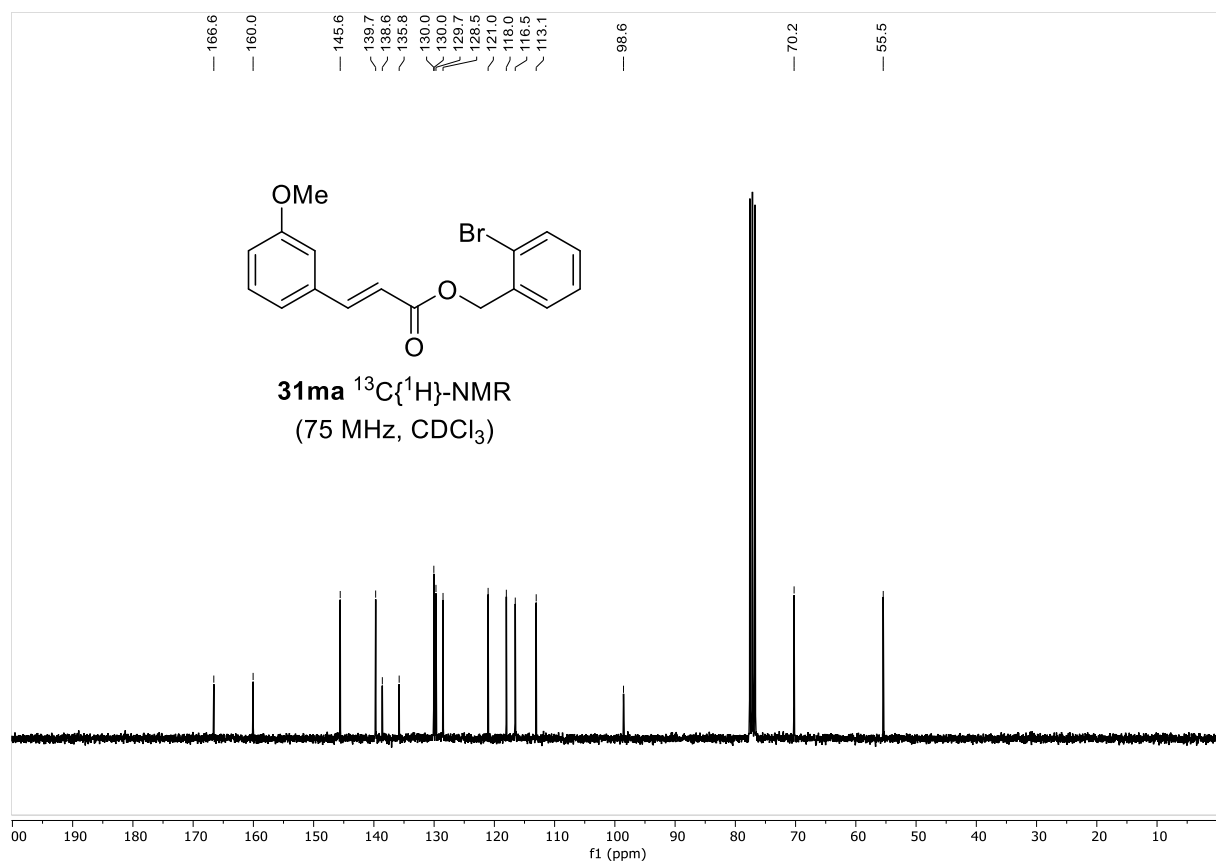
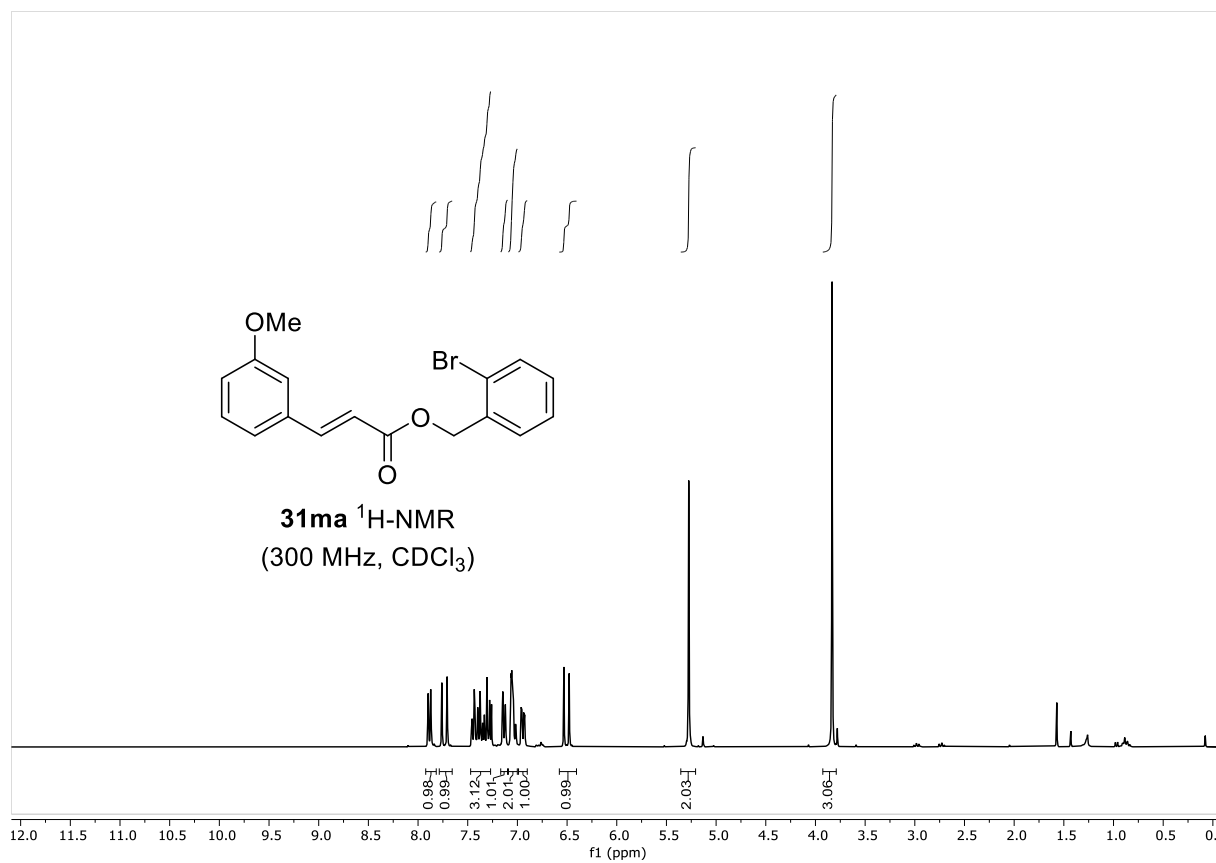
NMR SPECTRA



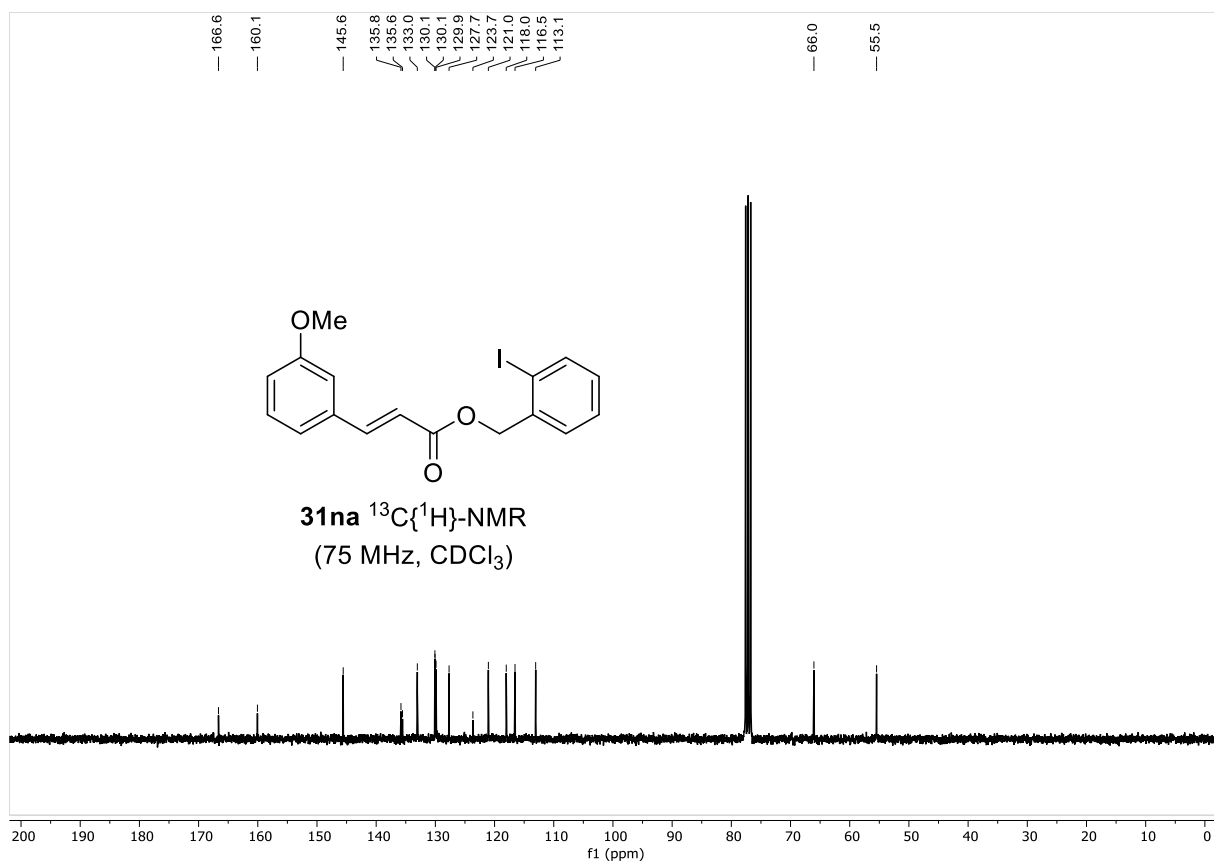
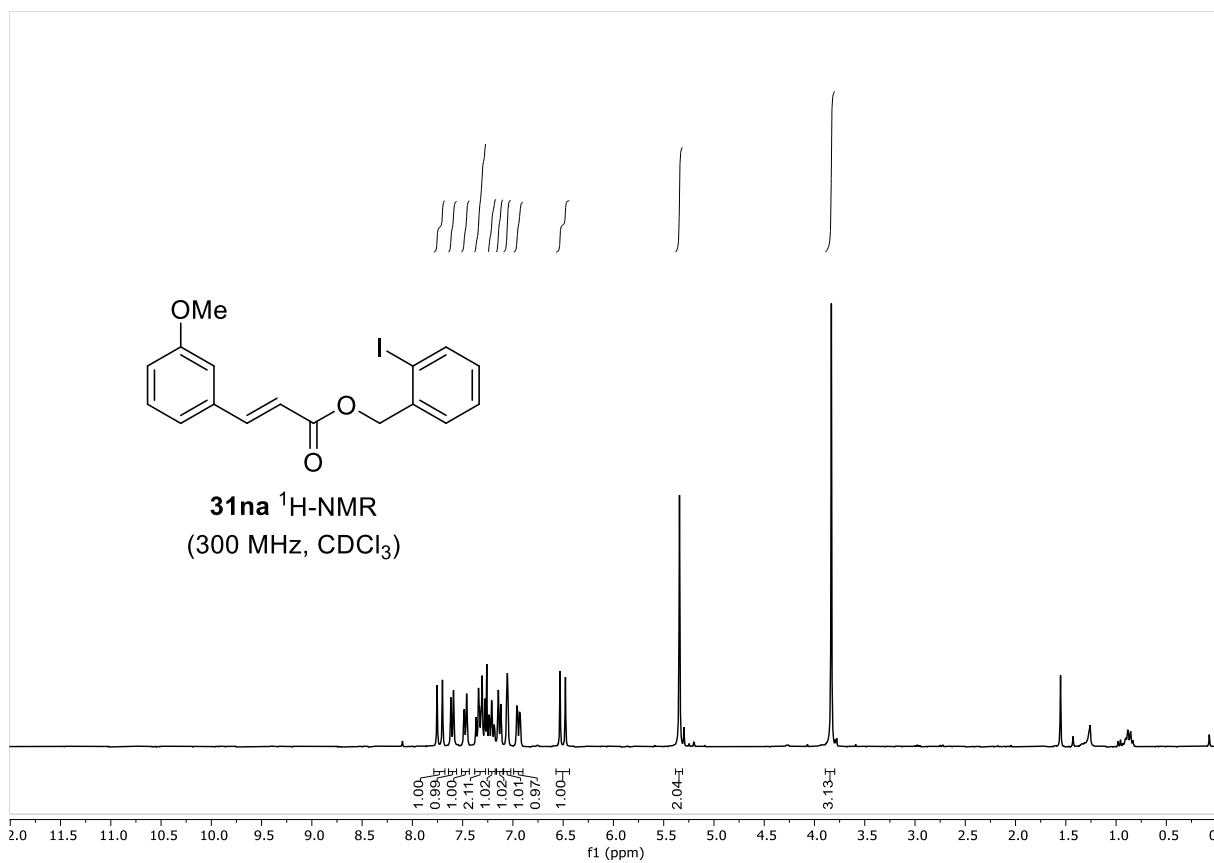
NMR SPECTRA



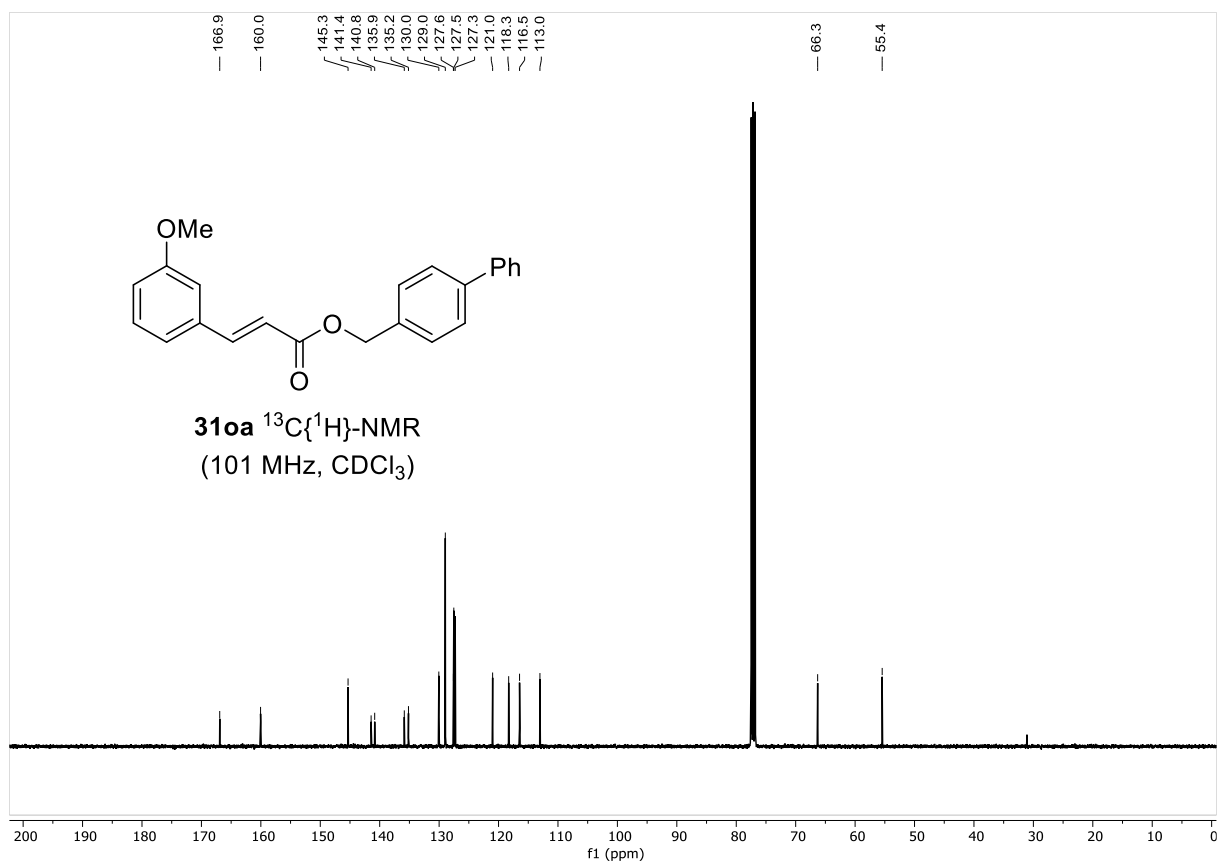
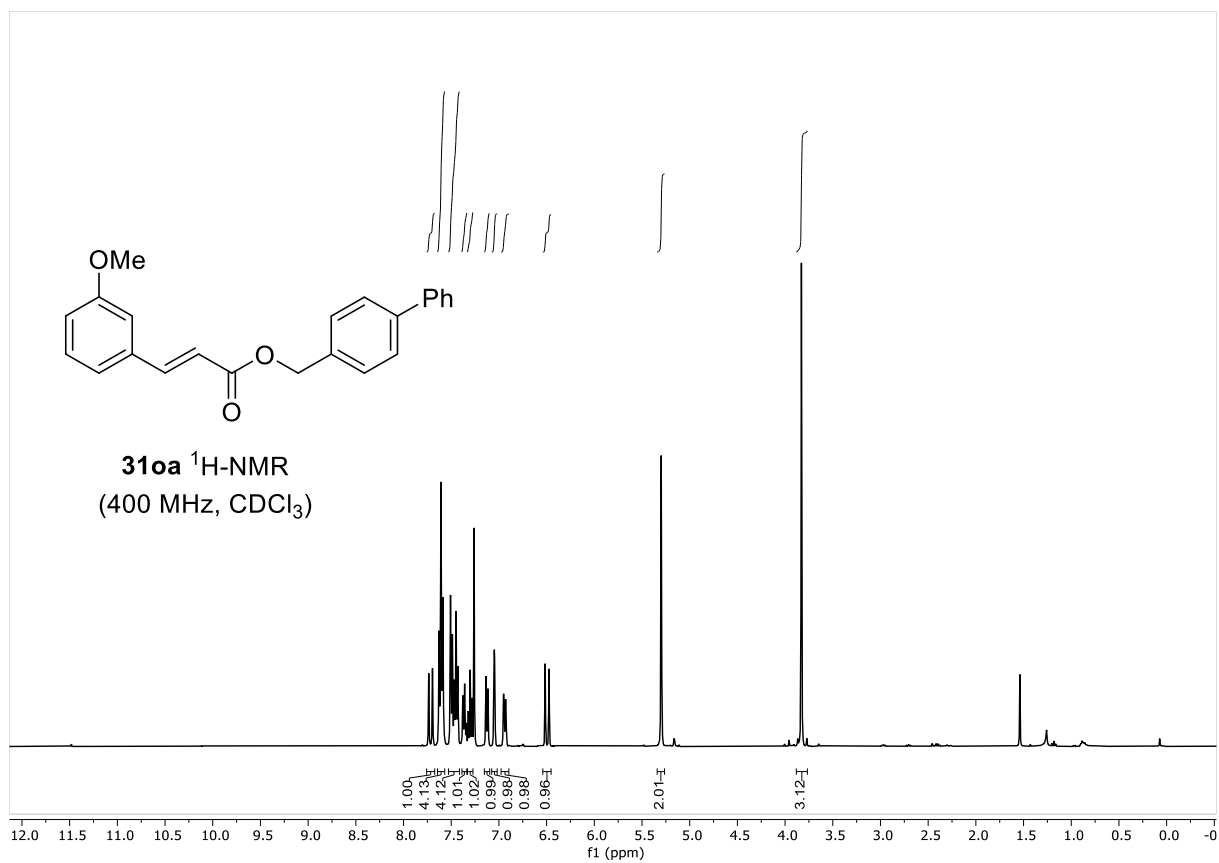
NMR SPECTRA



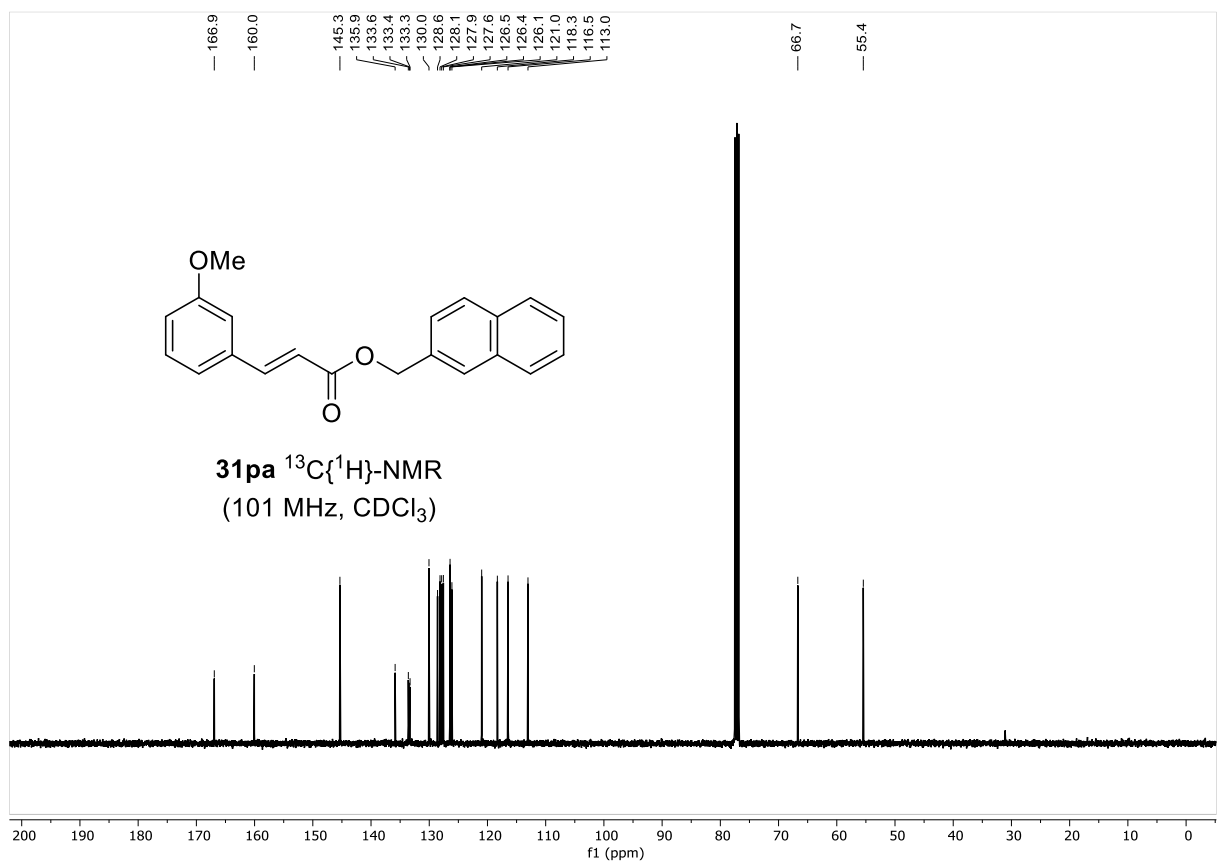
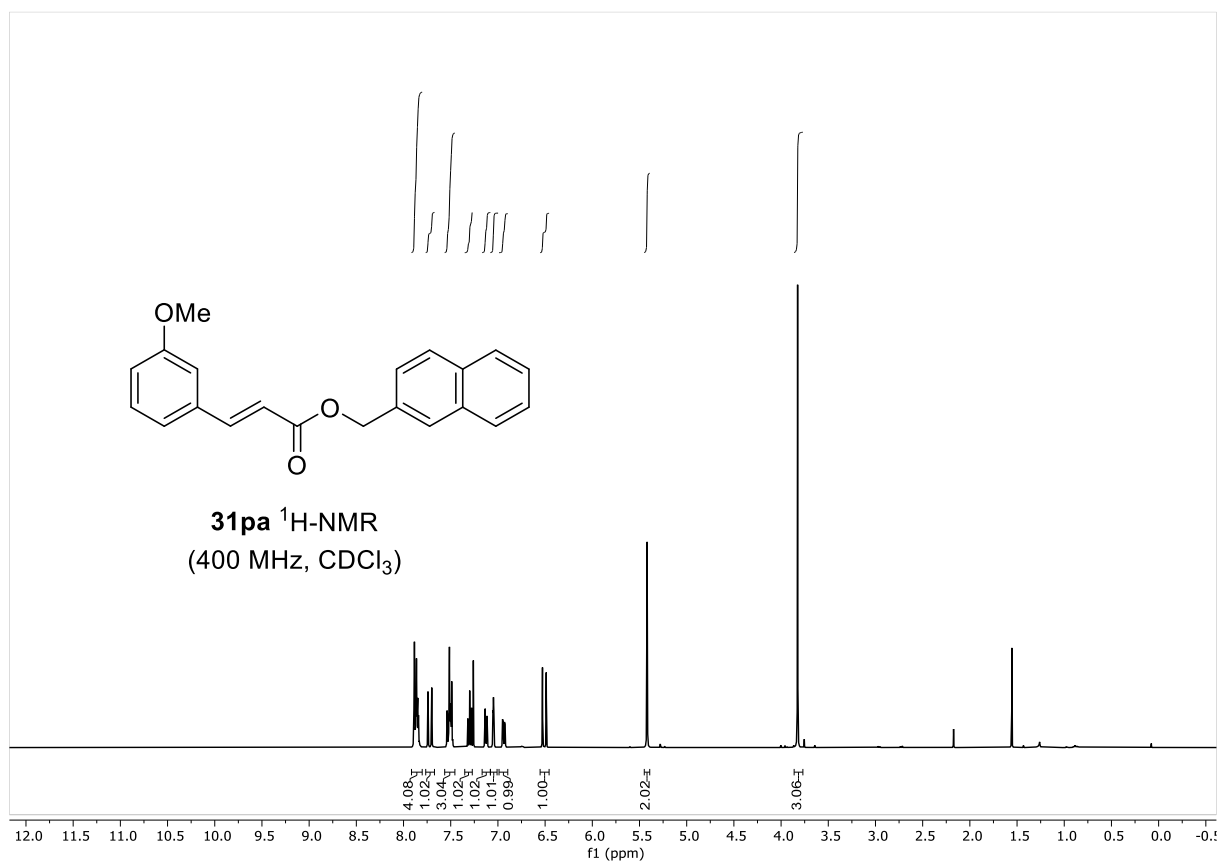
NMR SPECTRA



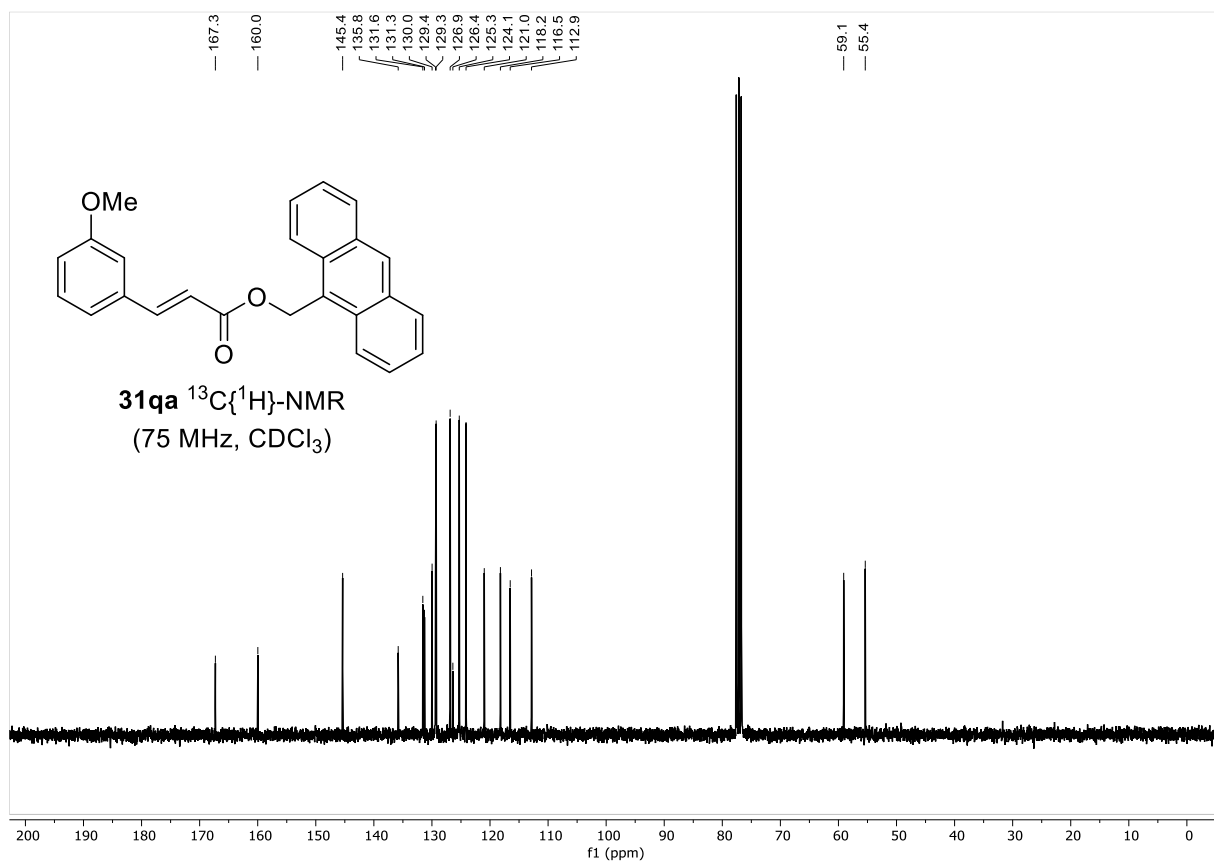
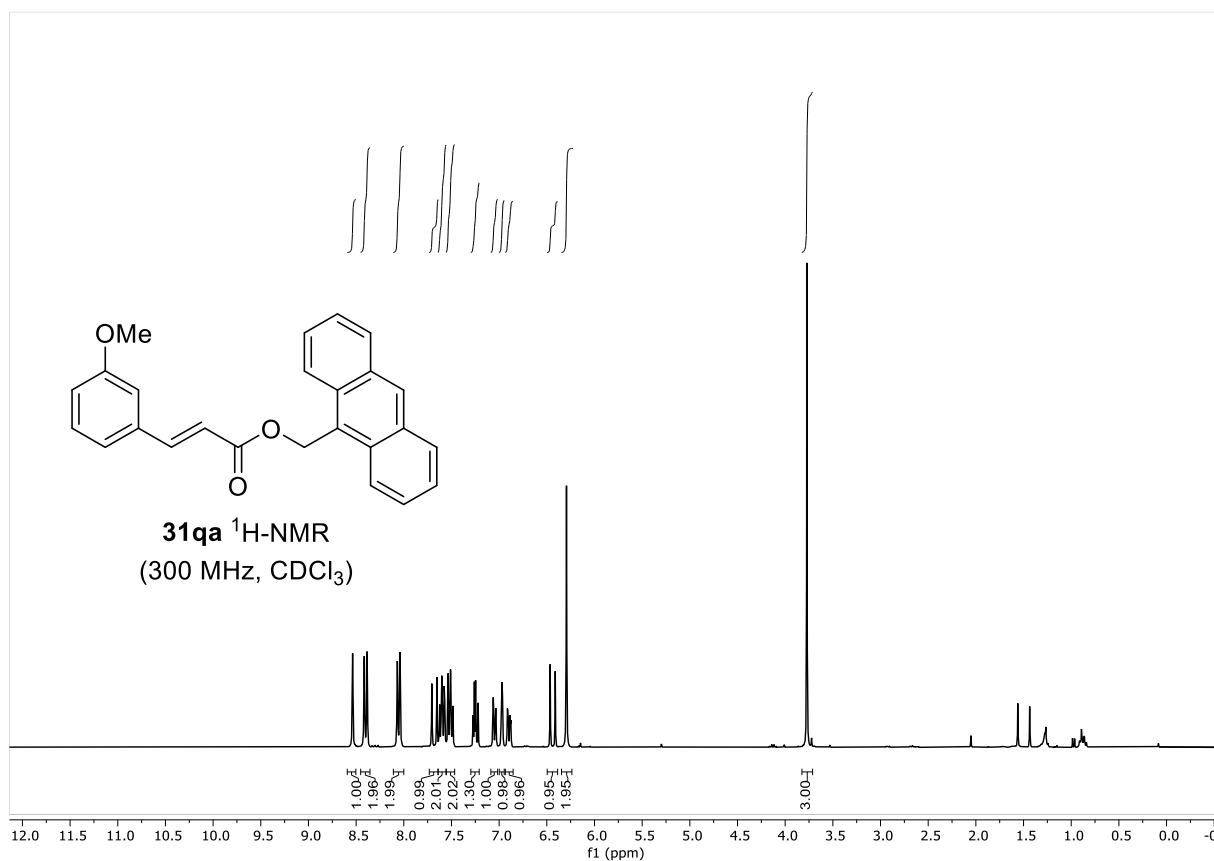
NMR SPECTRA



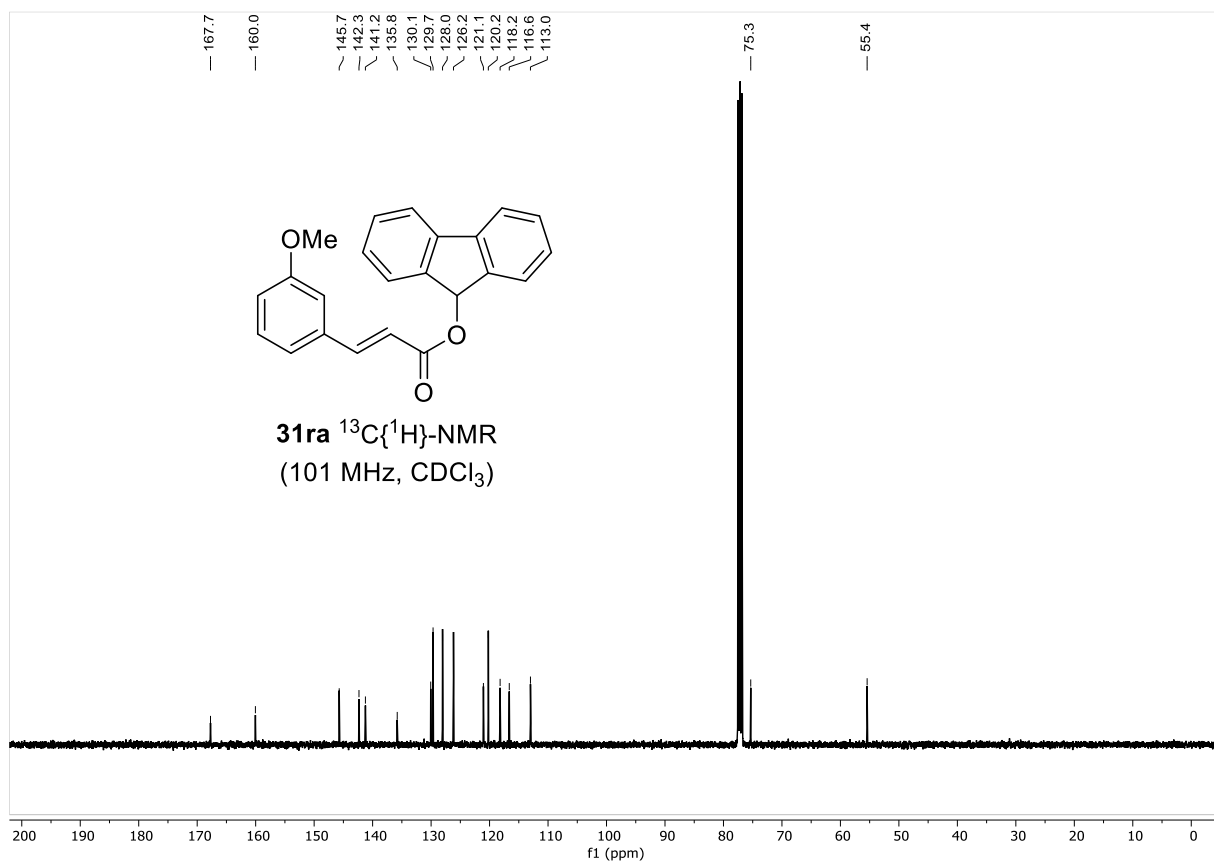
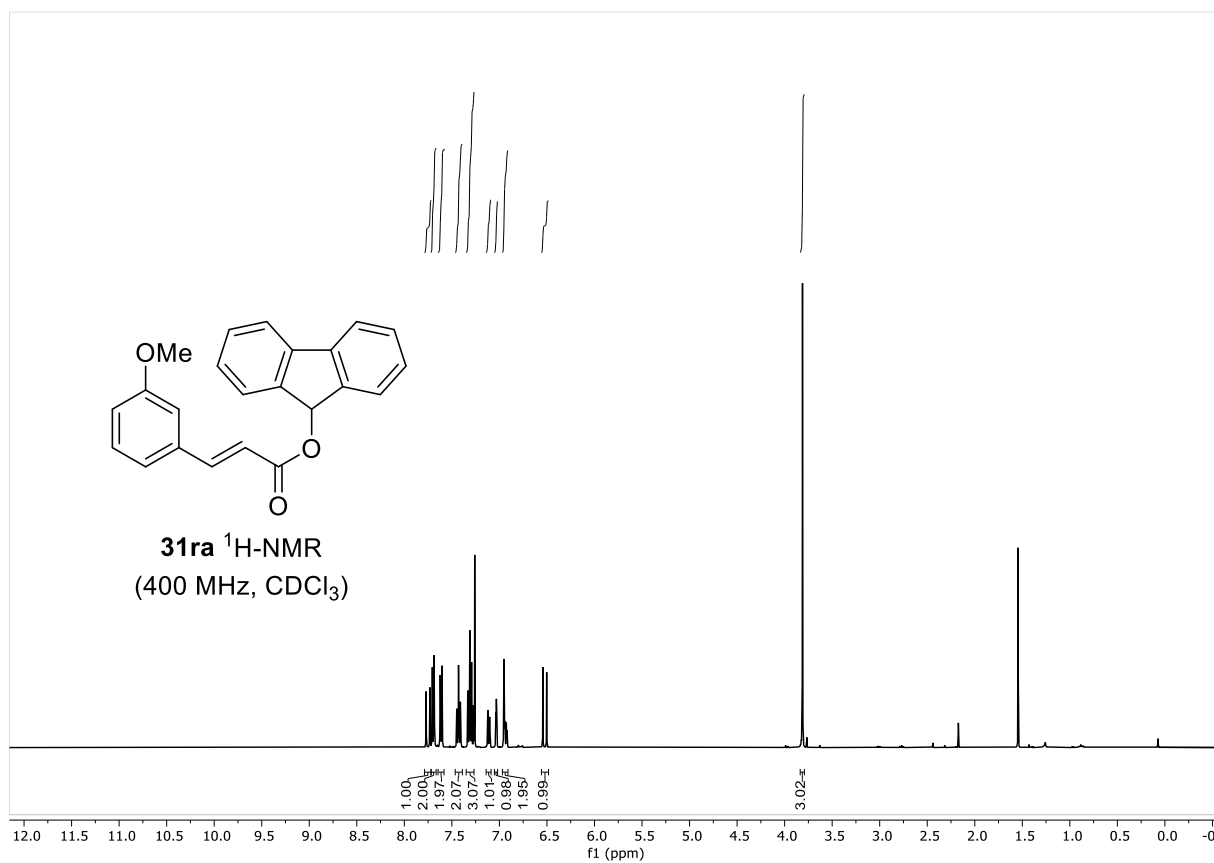
NMR SPECTRA



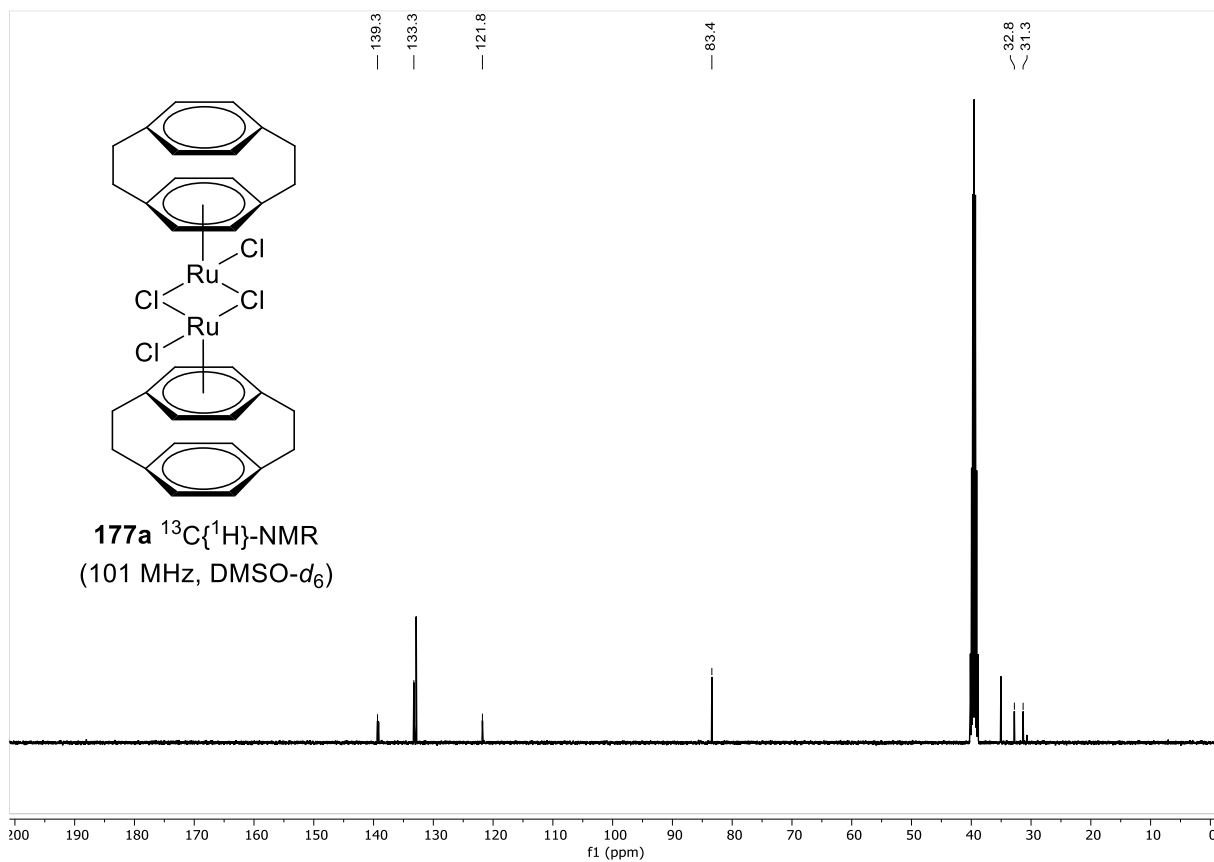
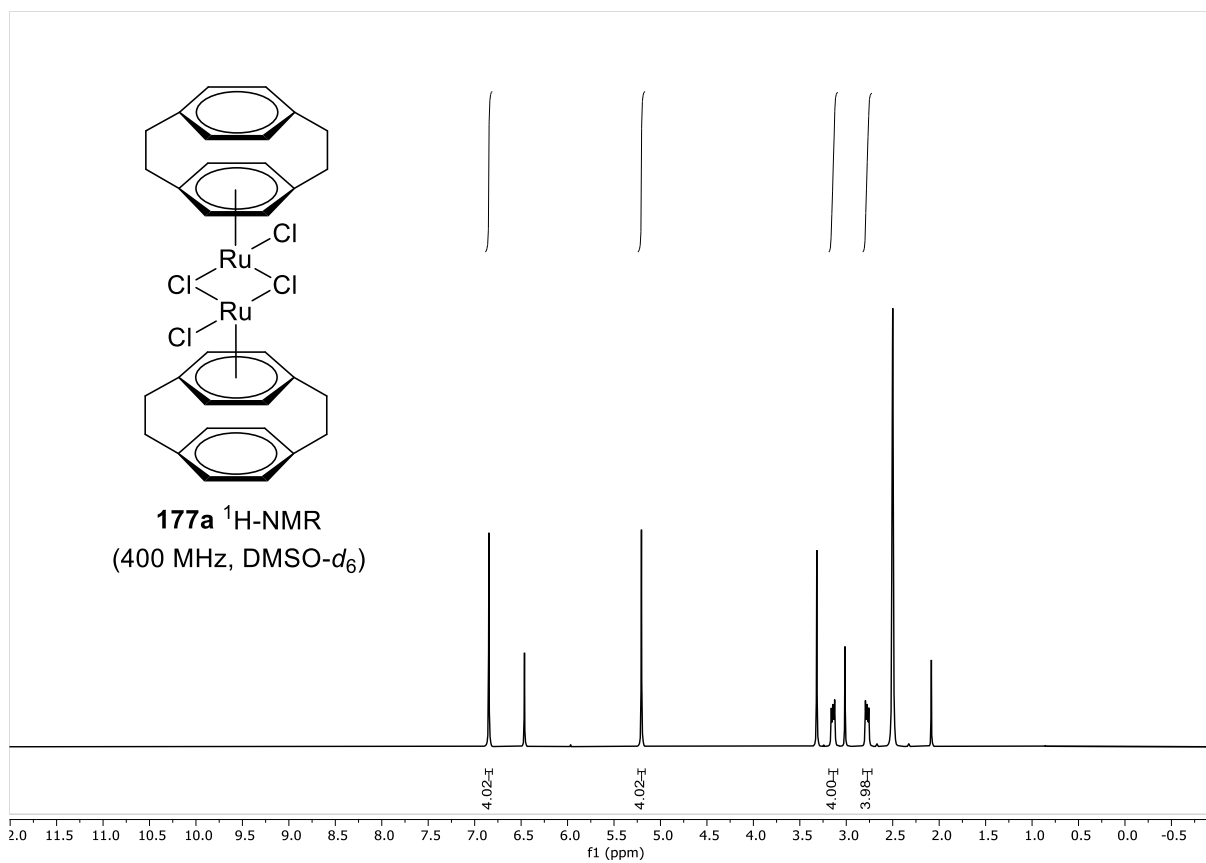
NMR SPECTRA



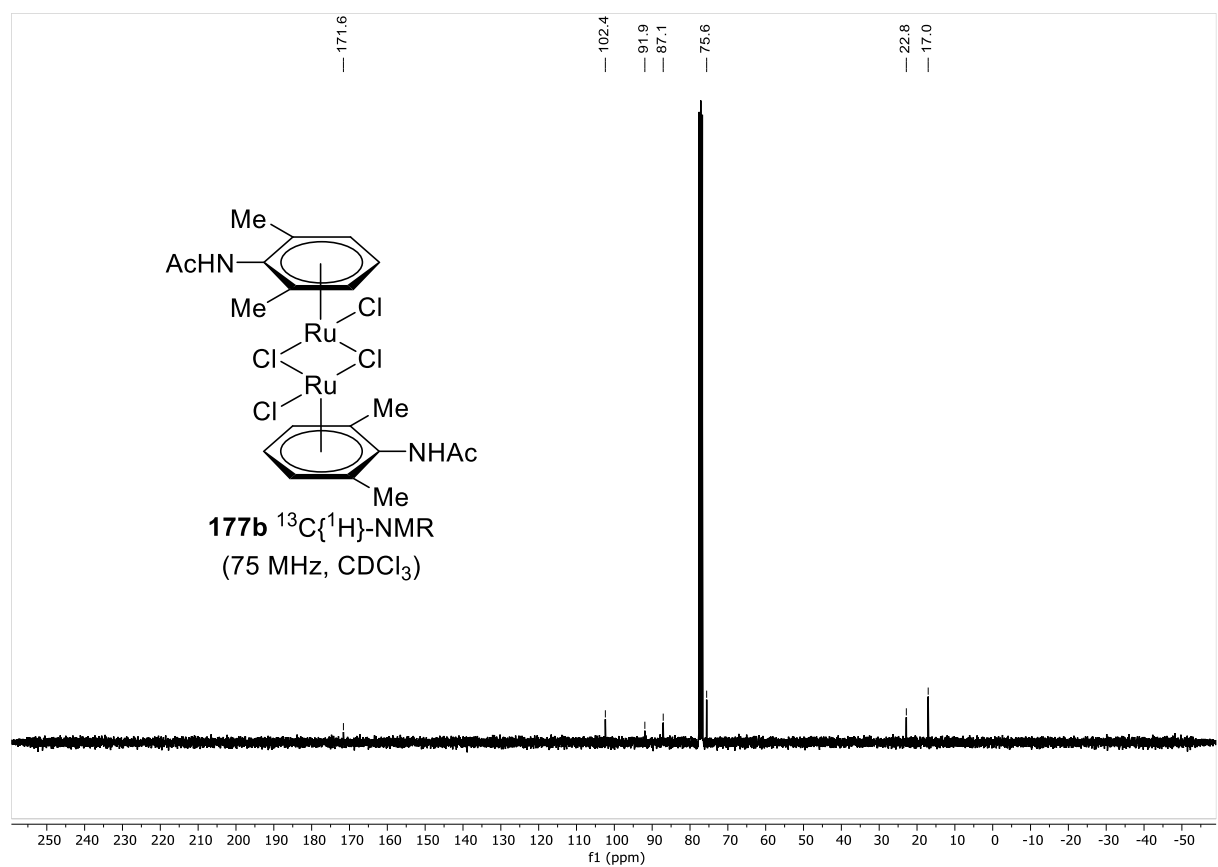
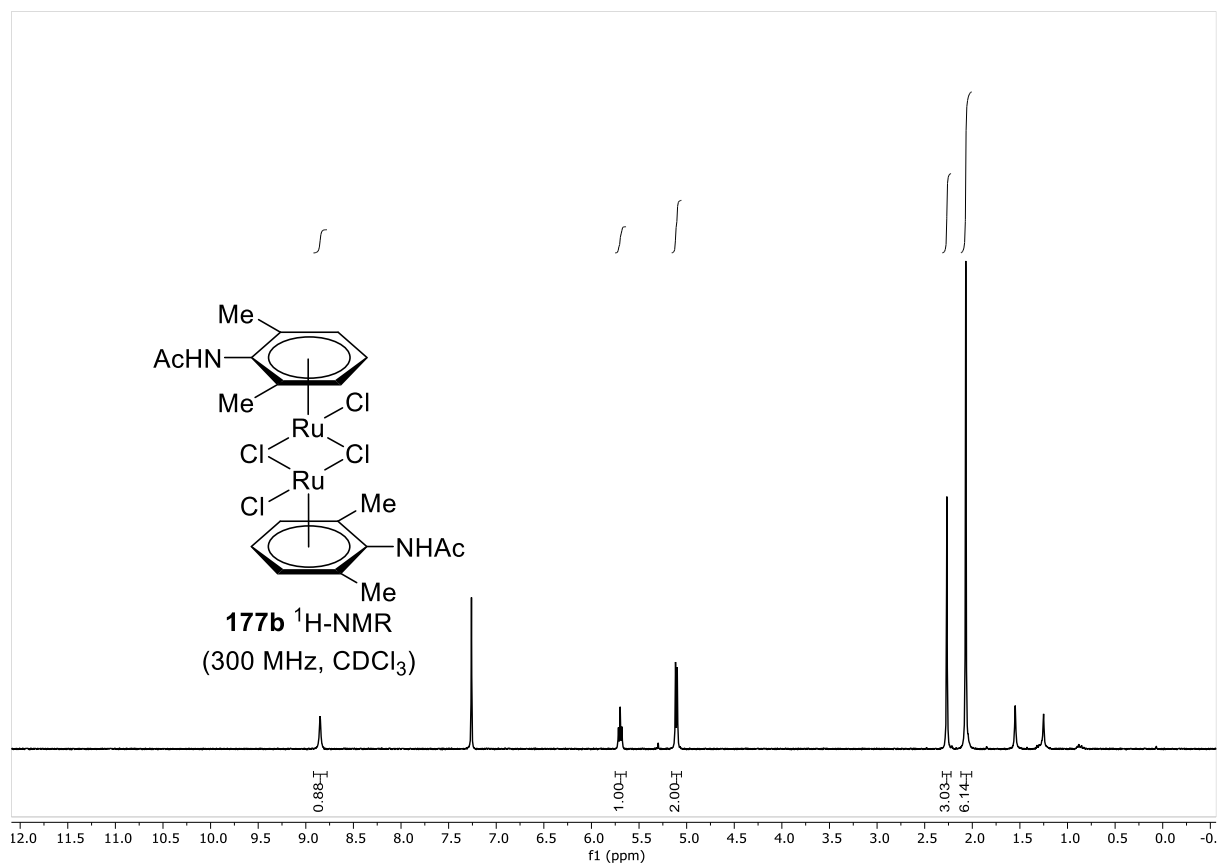
NMR SPECTRA



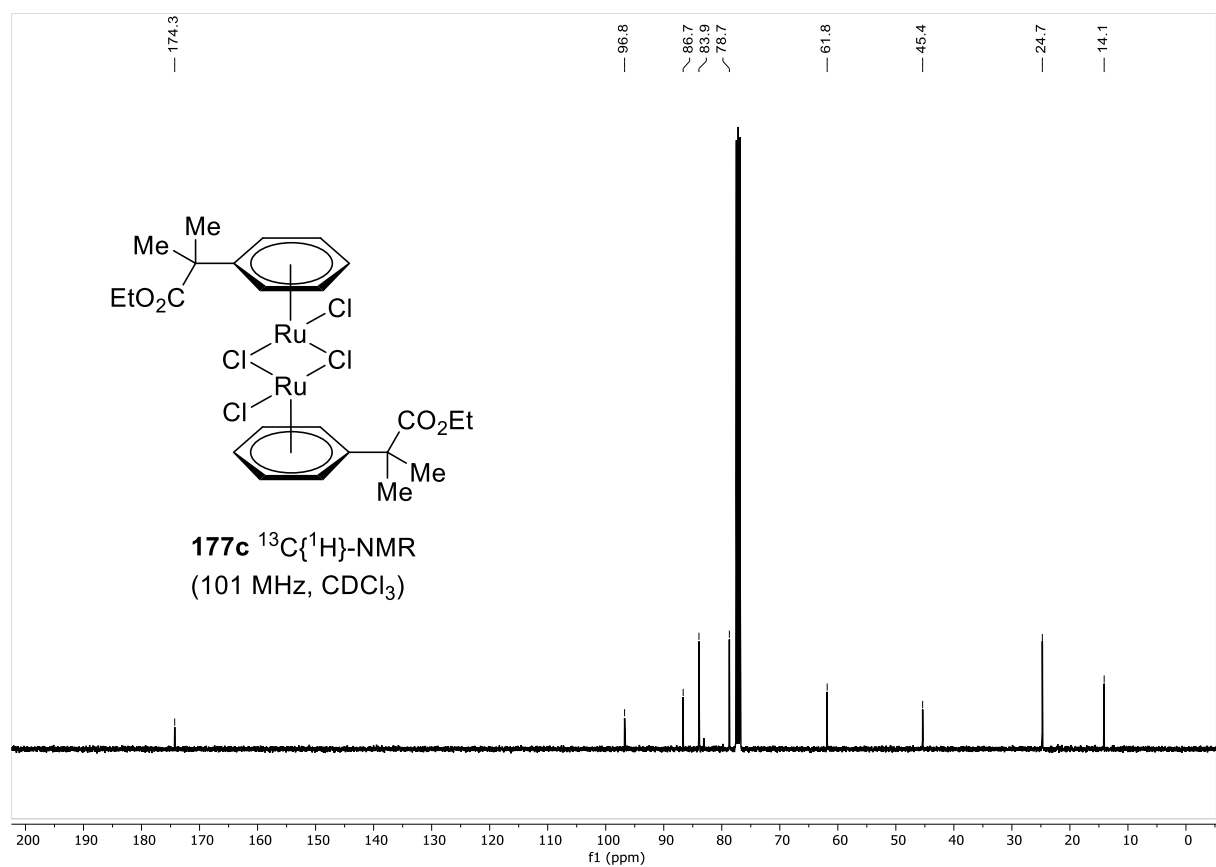
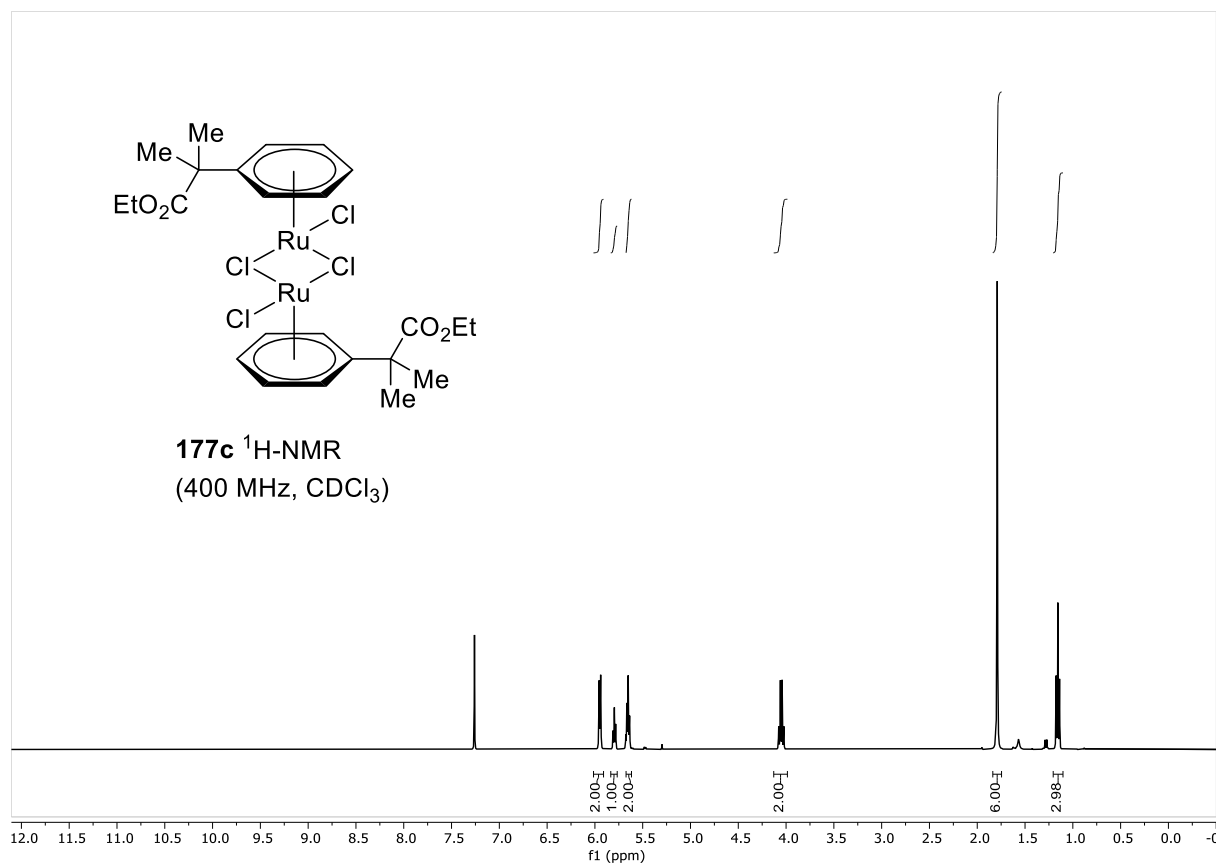
NMR SPECTRA



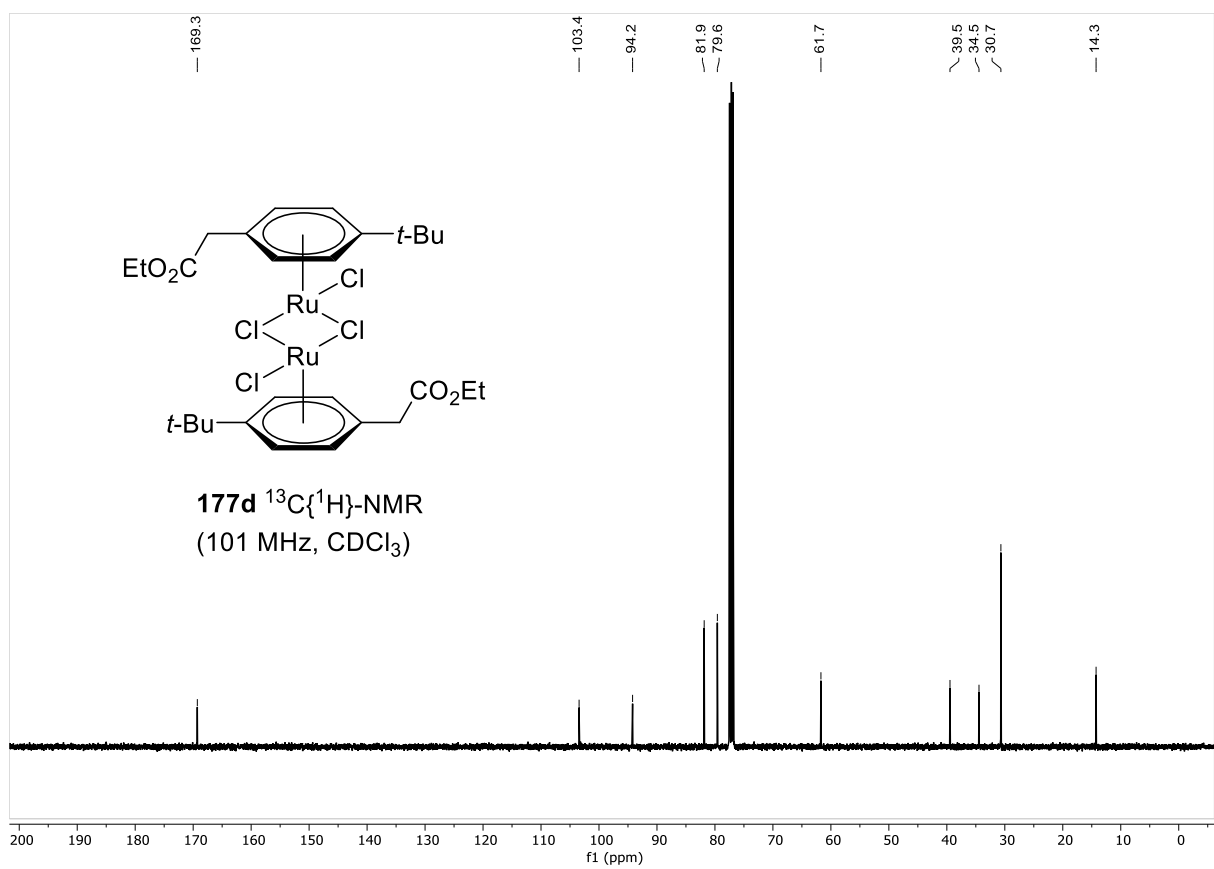
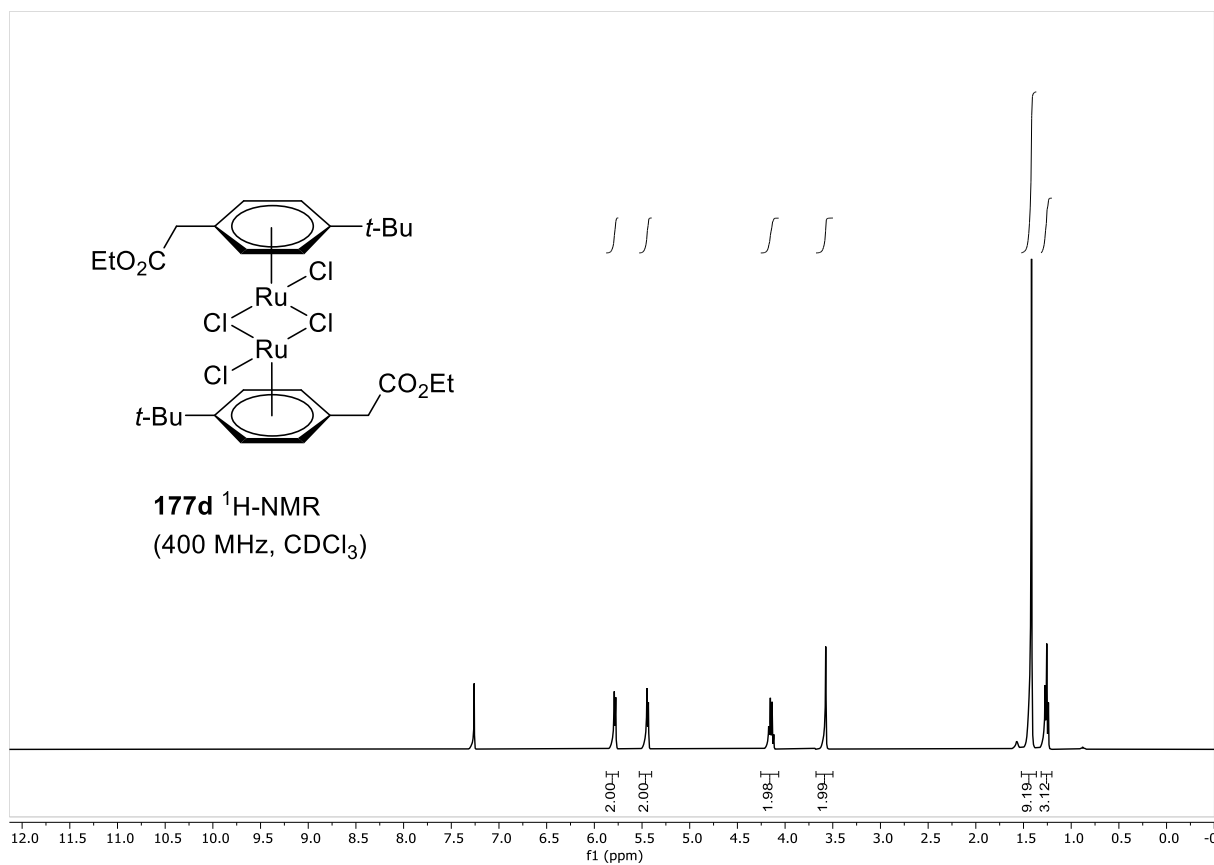
NMR SPECTRA



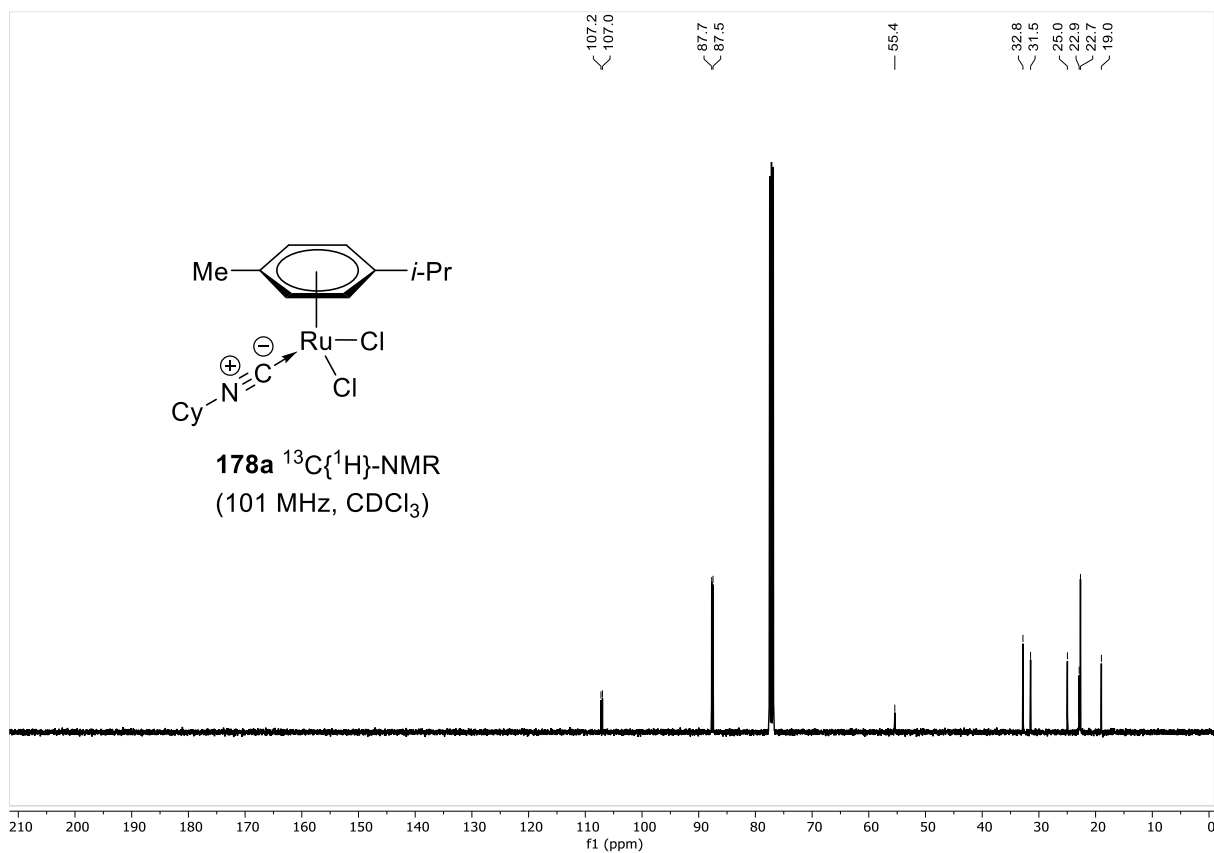
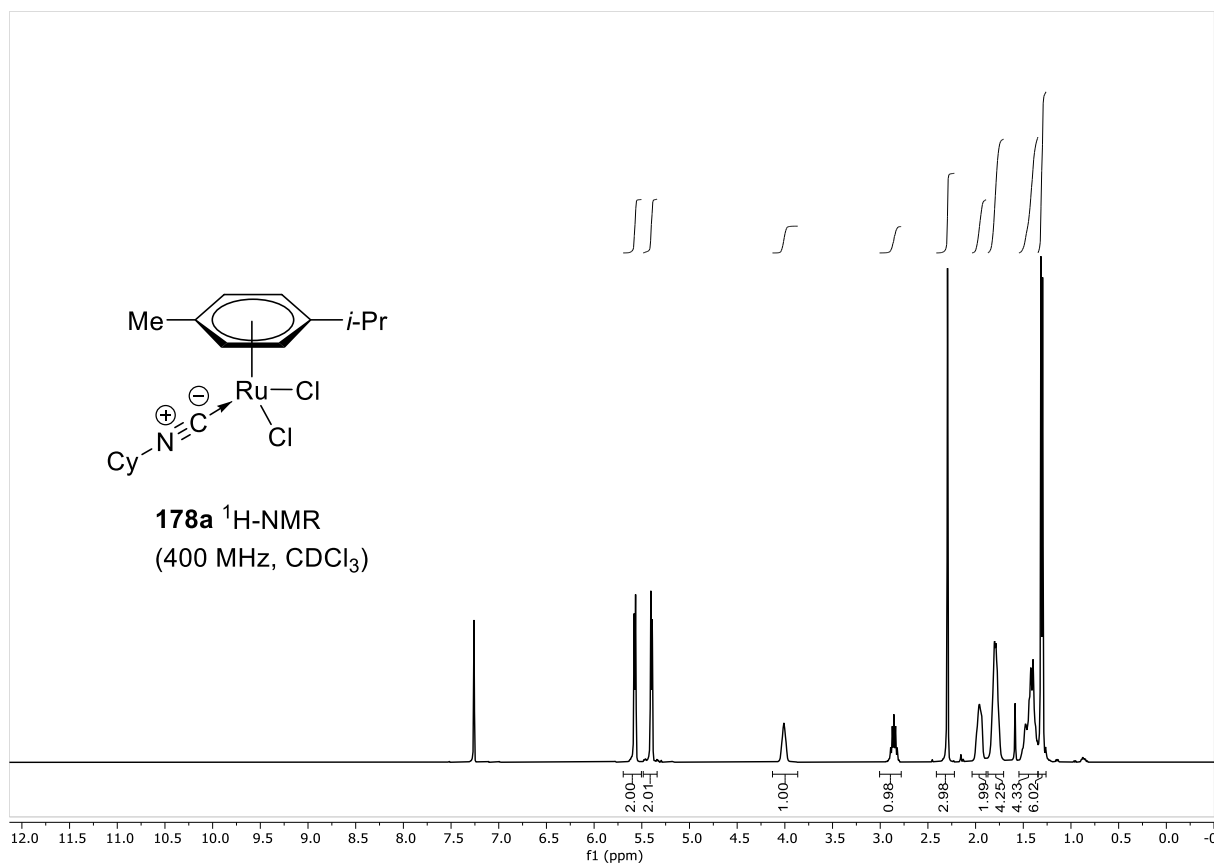
NMR SPECTRA



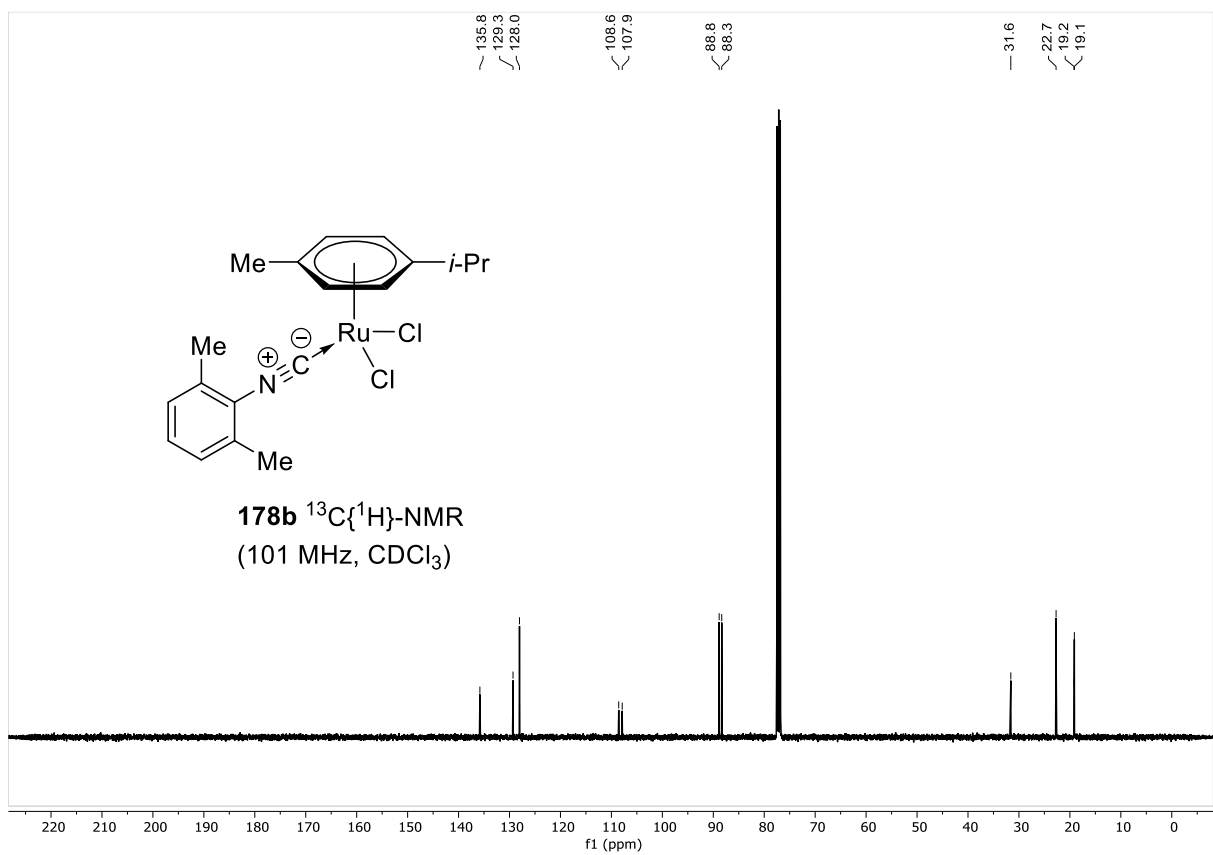
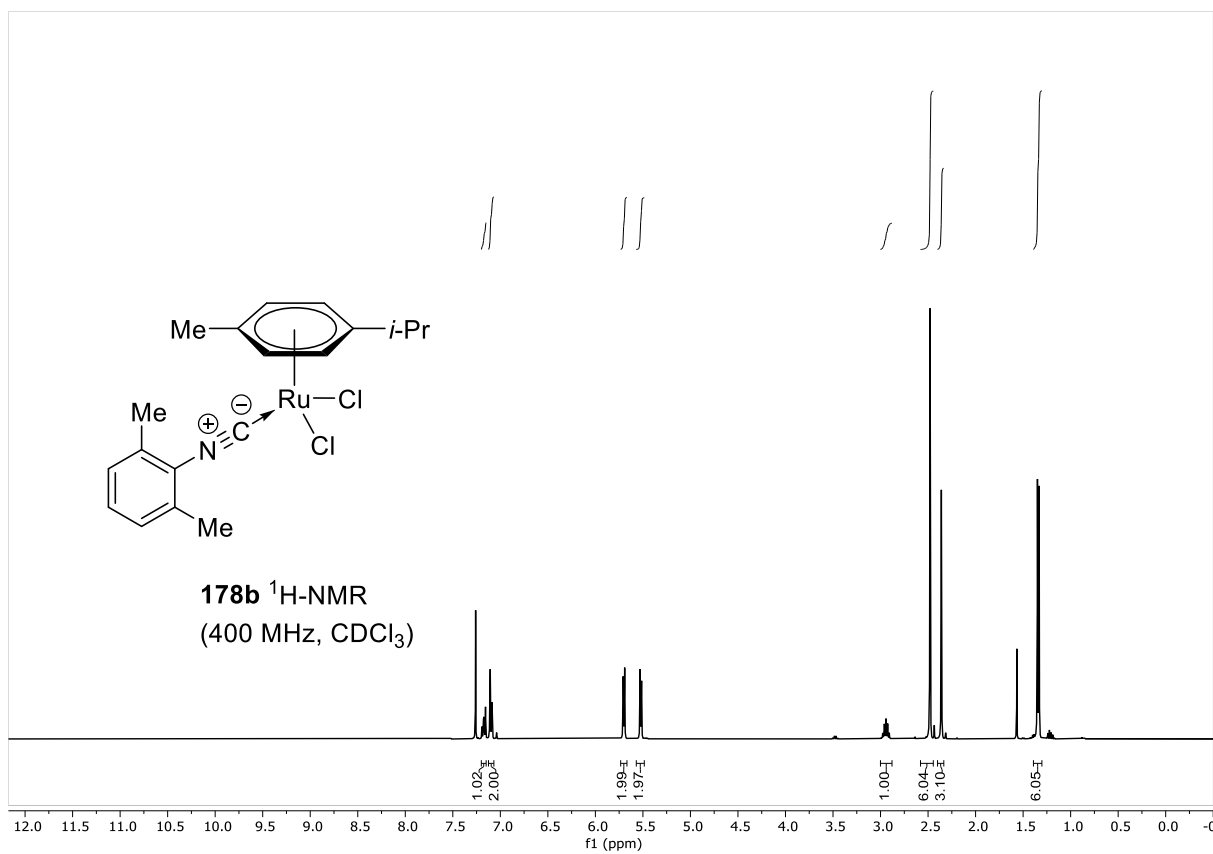
NMR SPECTRA



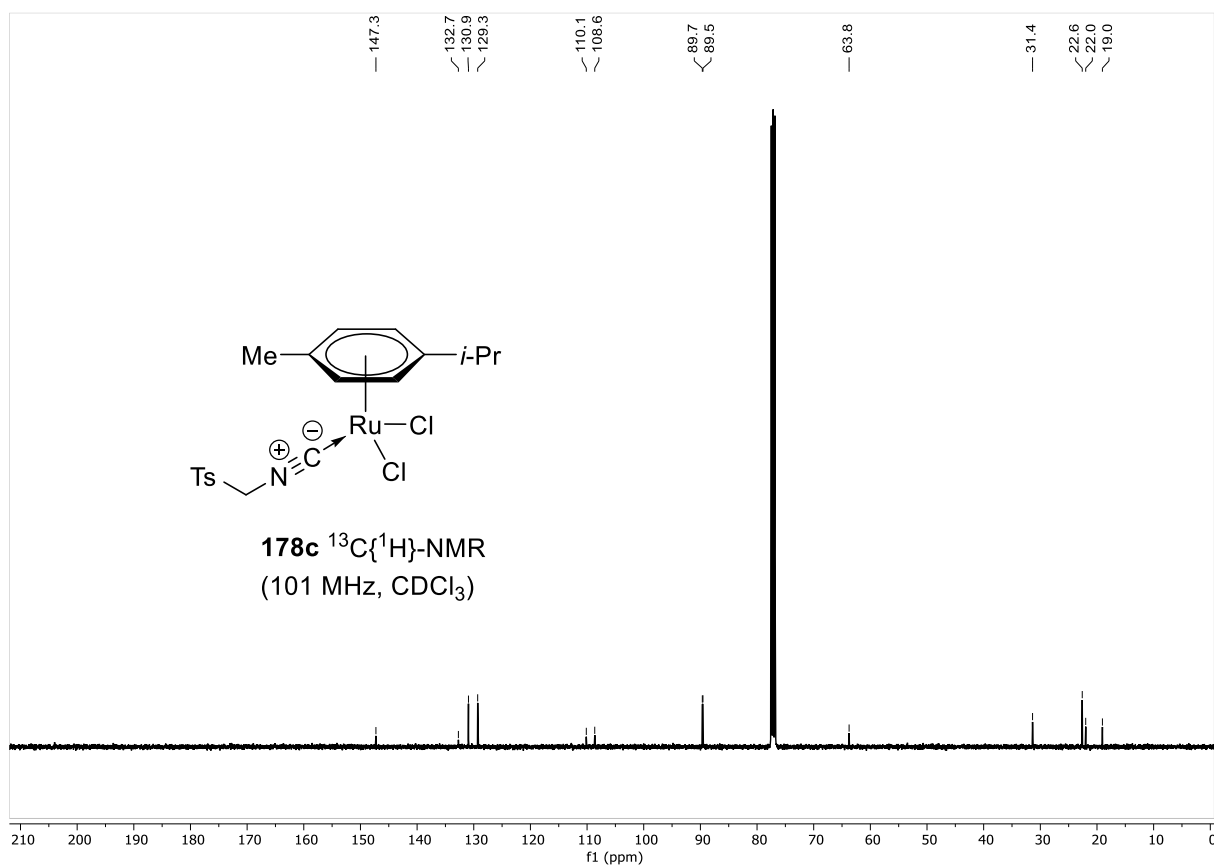
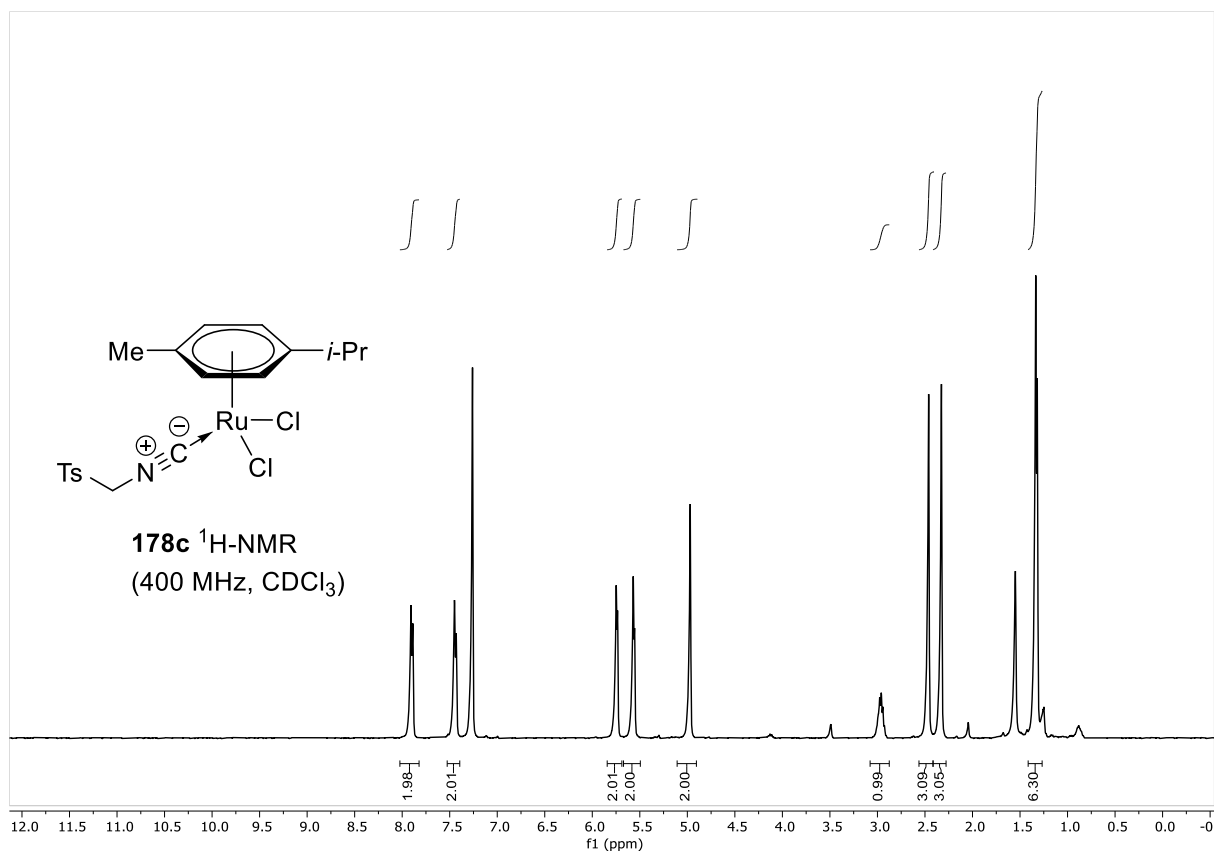
NMR SPECTRA



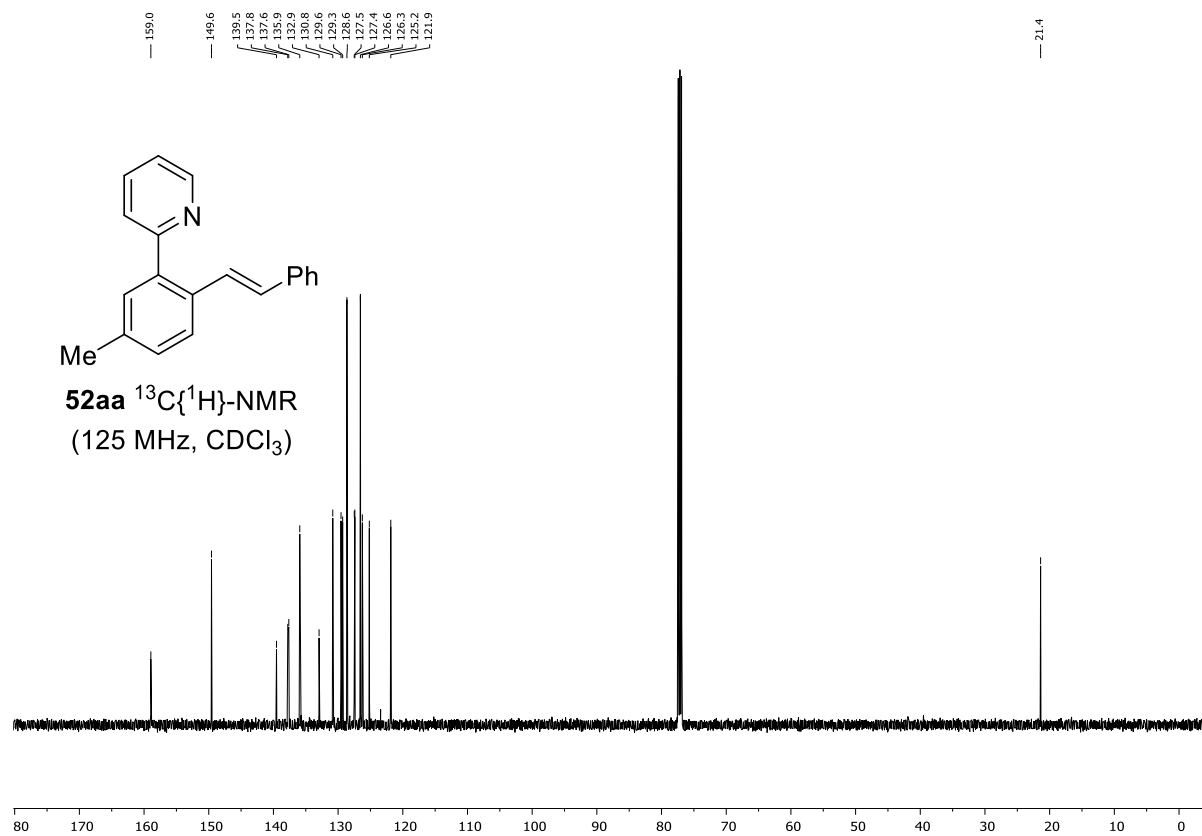
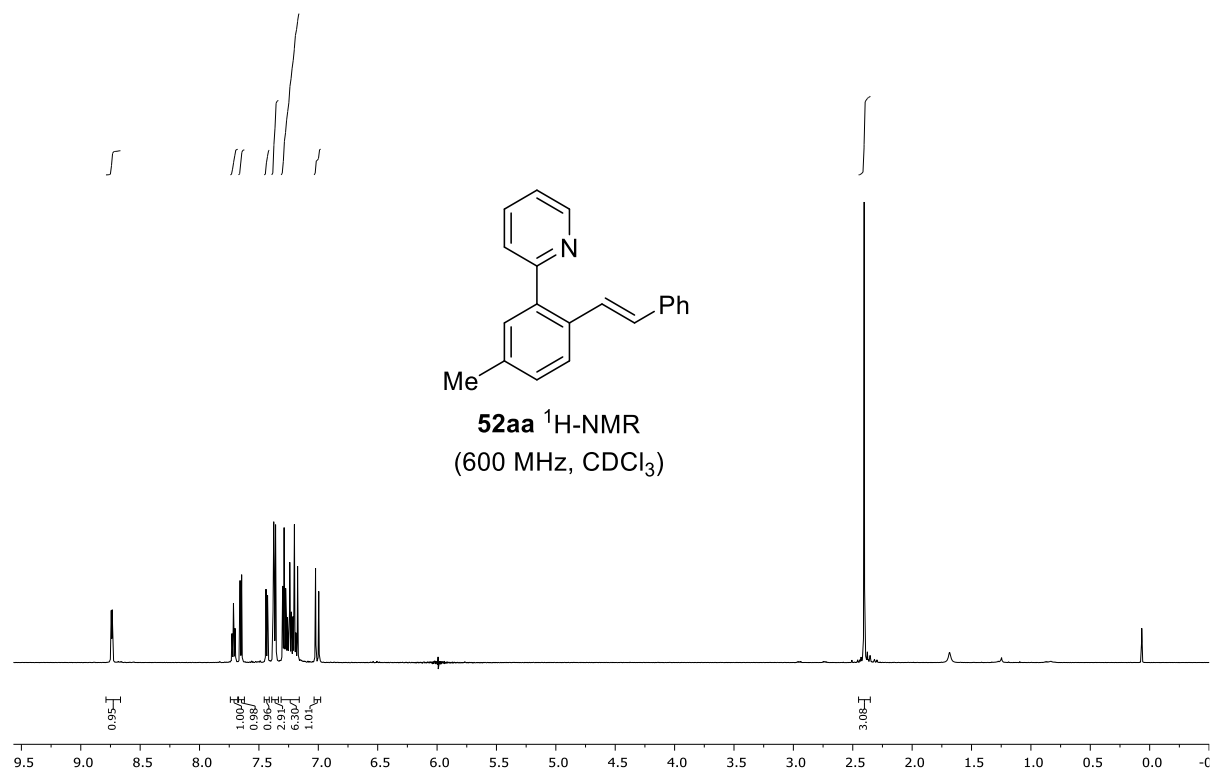
NMR SPECTRA



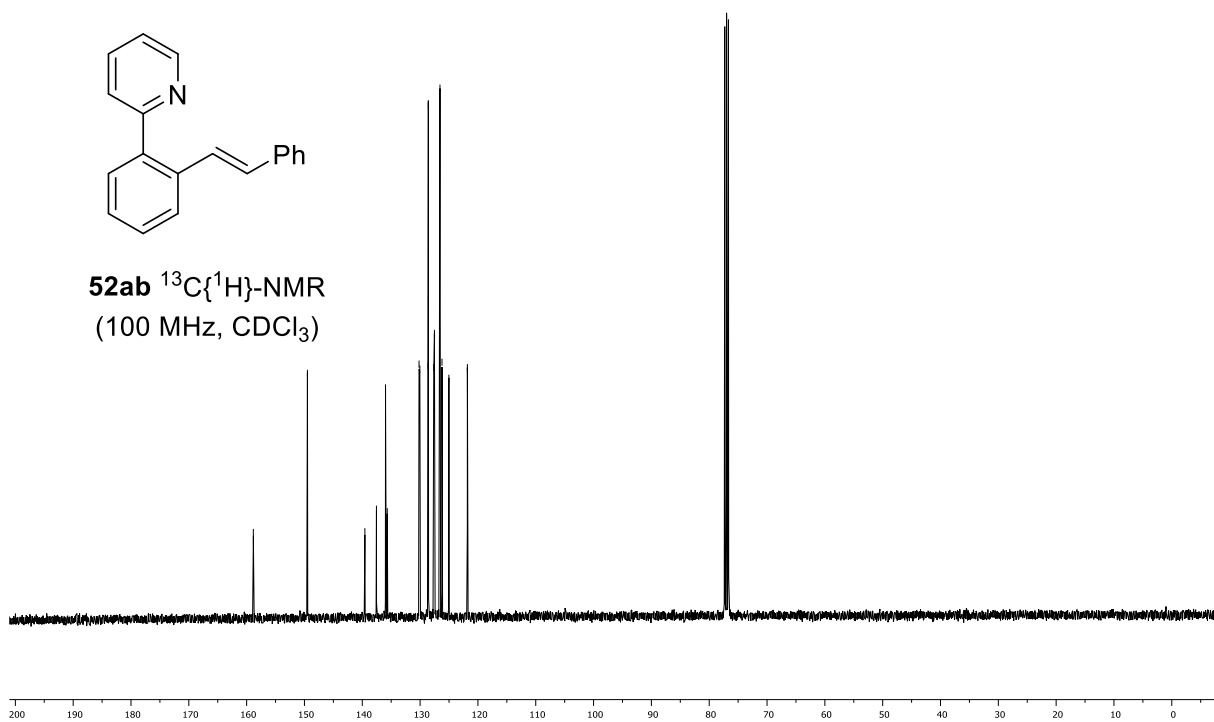
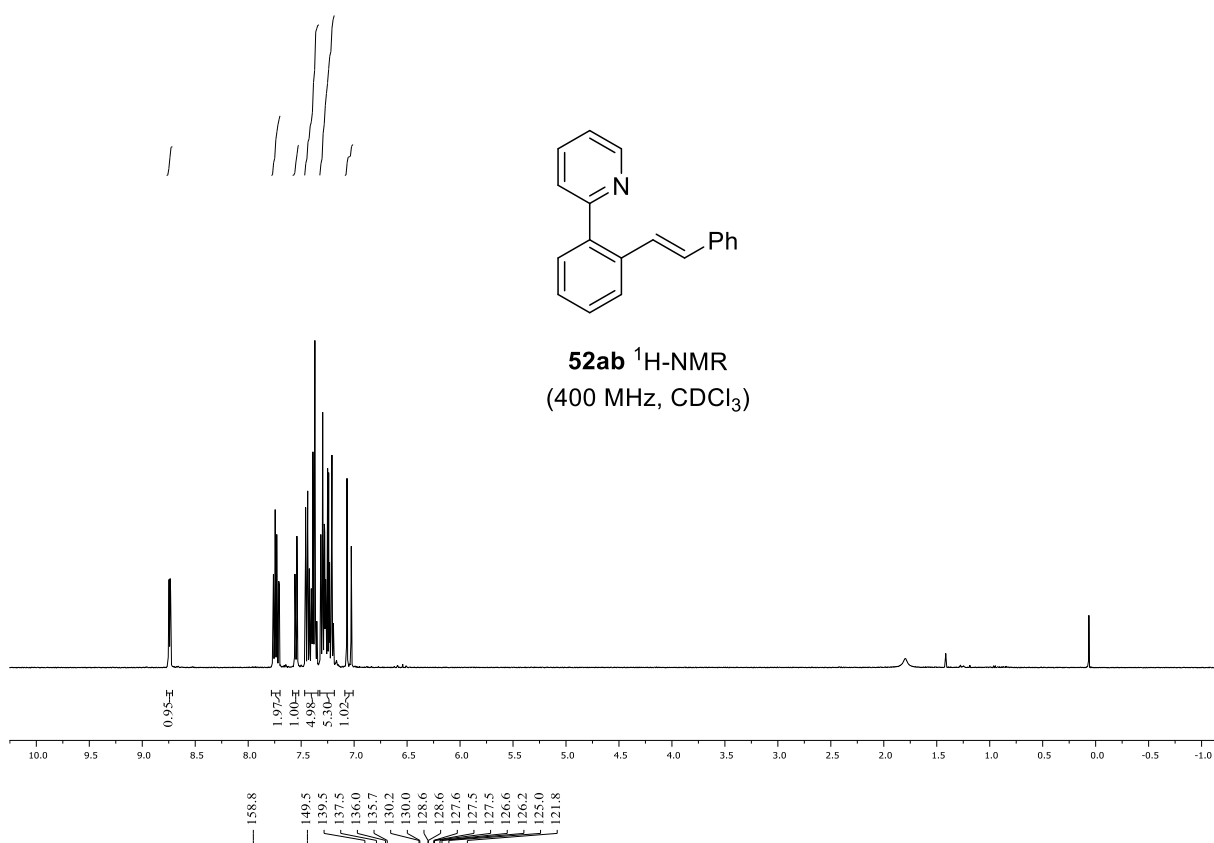
NMR SPECTRA



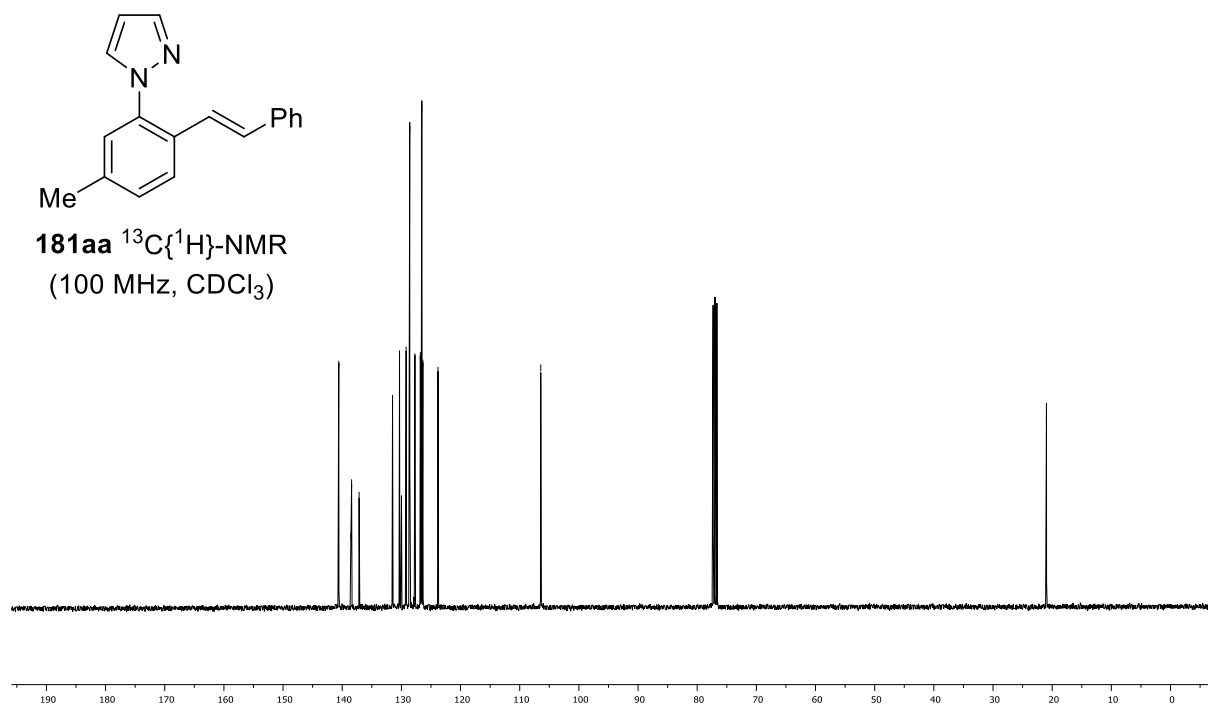
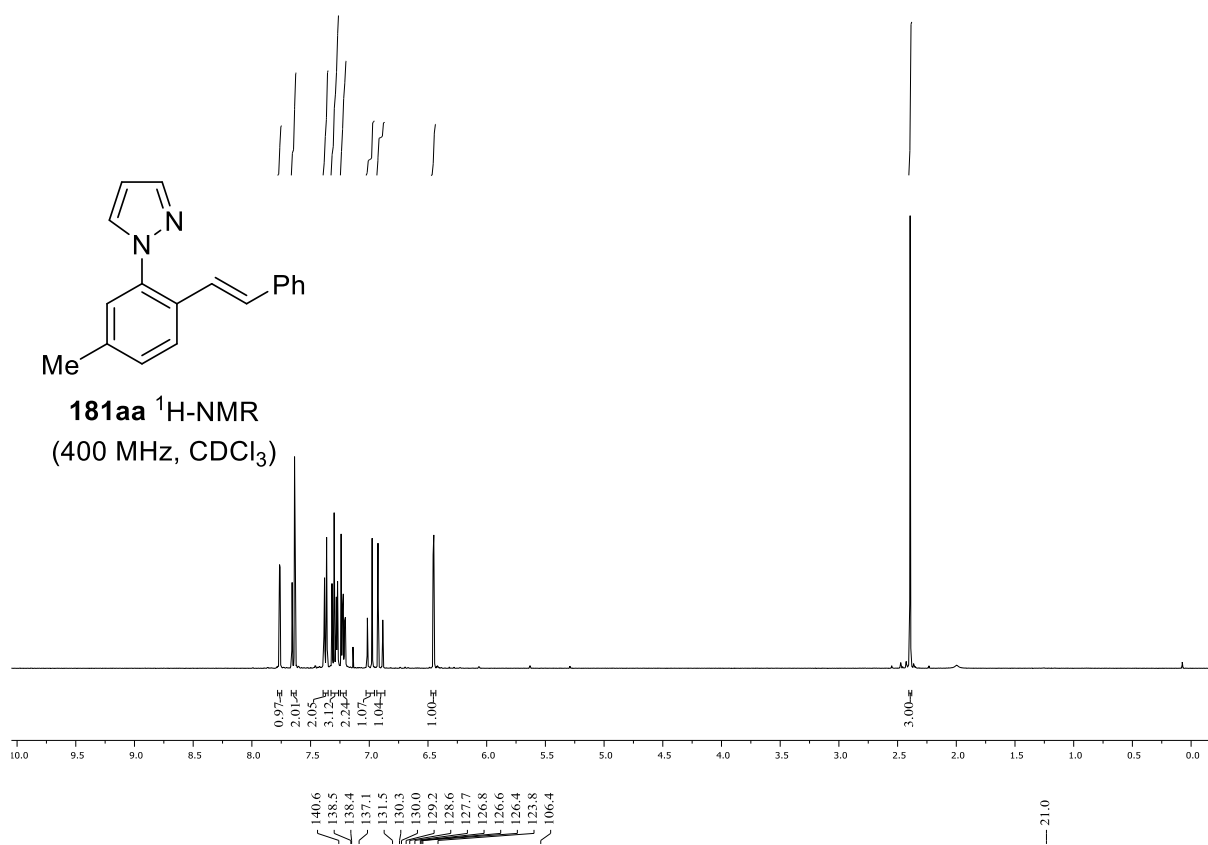
NMR SPECTRA



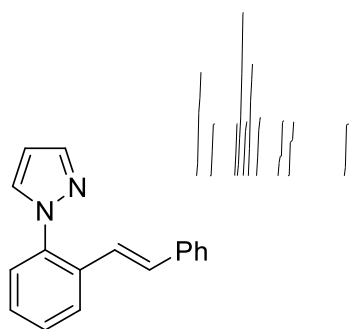
NMR SPECTRA



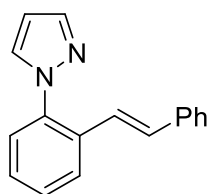
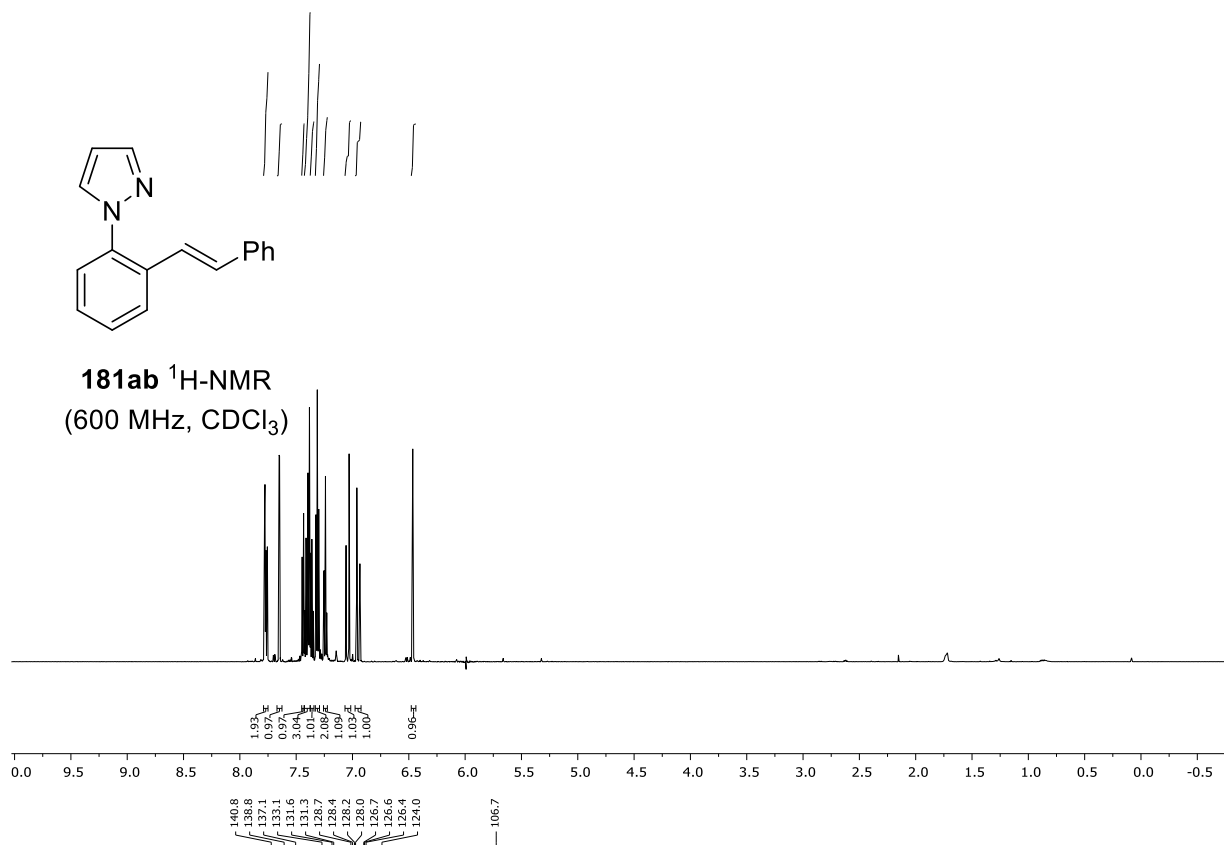
NMR SPECTRA



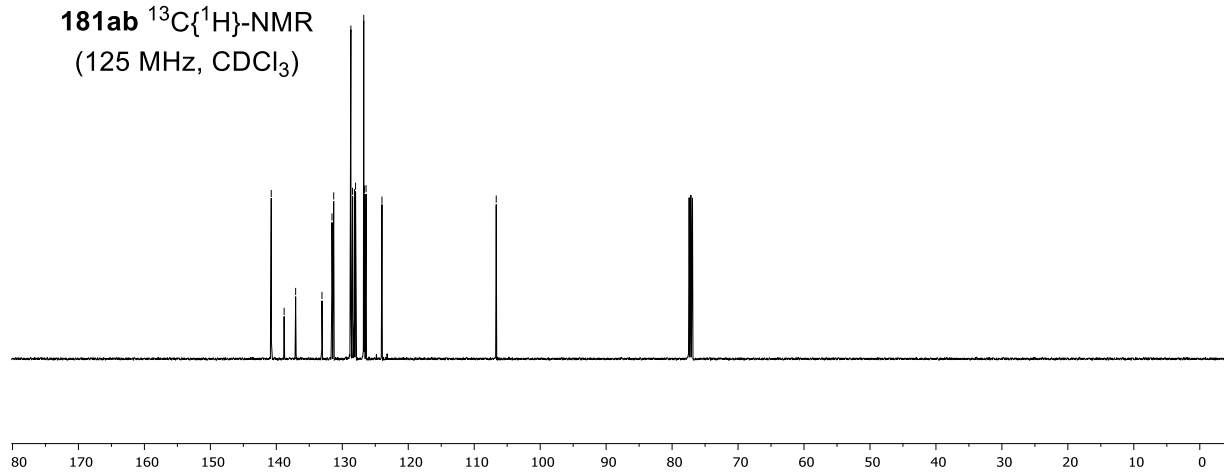
NMR SPECTRA



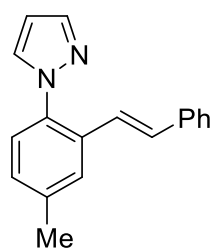
181ab $^1\text{H-NMR}$
(600 MHz, CDCl_3)



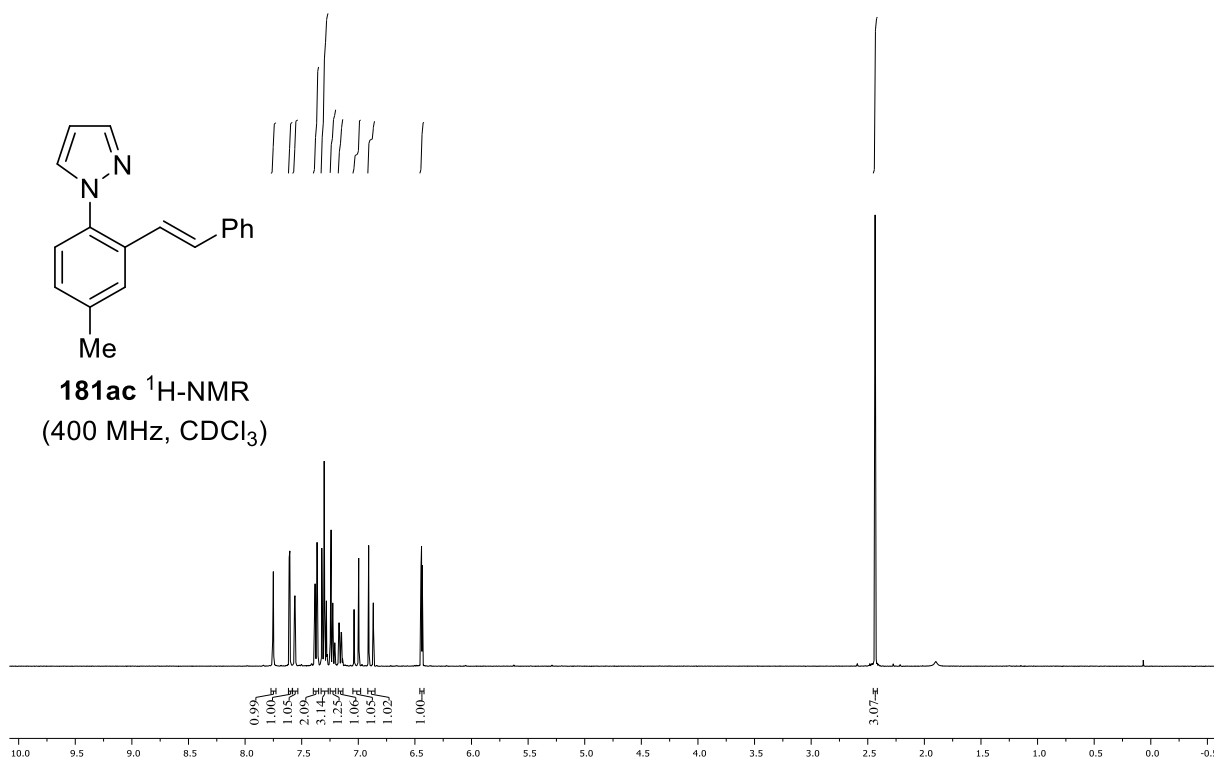
181ab $^{13}\text{C}\{^1\text{H}\}\text{-NMR}$
(125 MHz, CDCl_3)



NMR SPECTRA



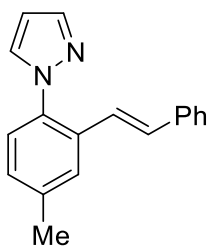
181ac $^1\text{H-NMR}$
(400 MHz, CDCl_3)



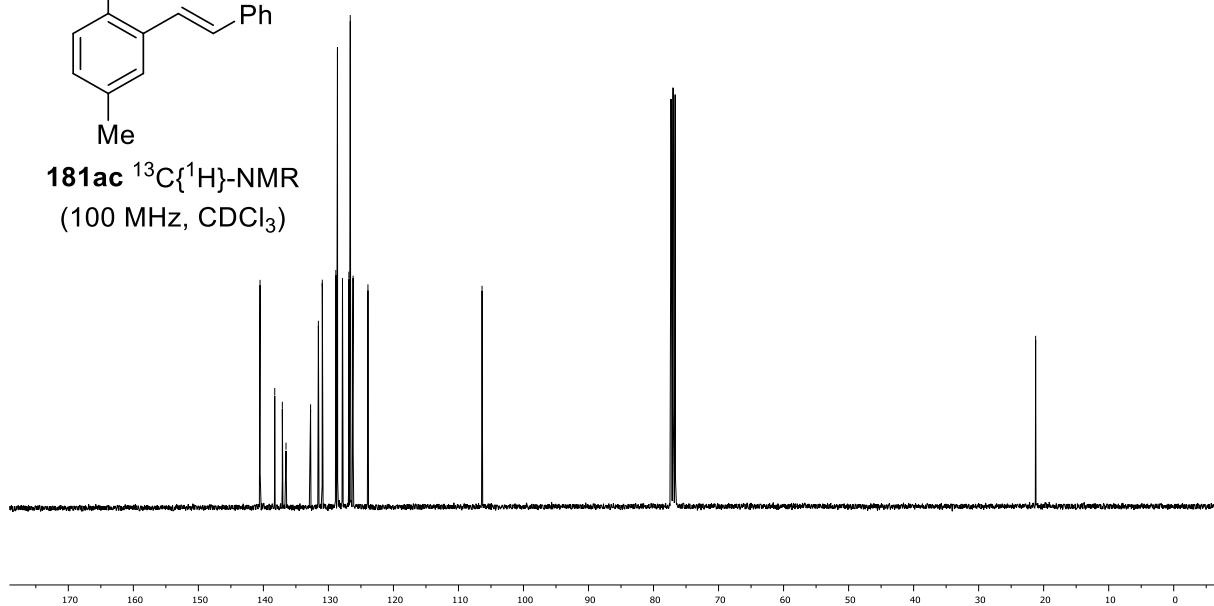
140.5
138.3
137.1
136.5
132.7
131.5
130.9
128.9
128.6
127.8
126.9
126.6
126.2
123.9

106.4

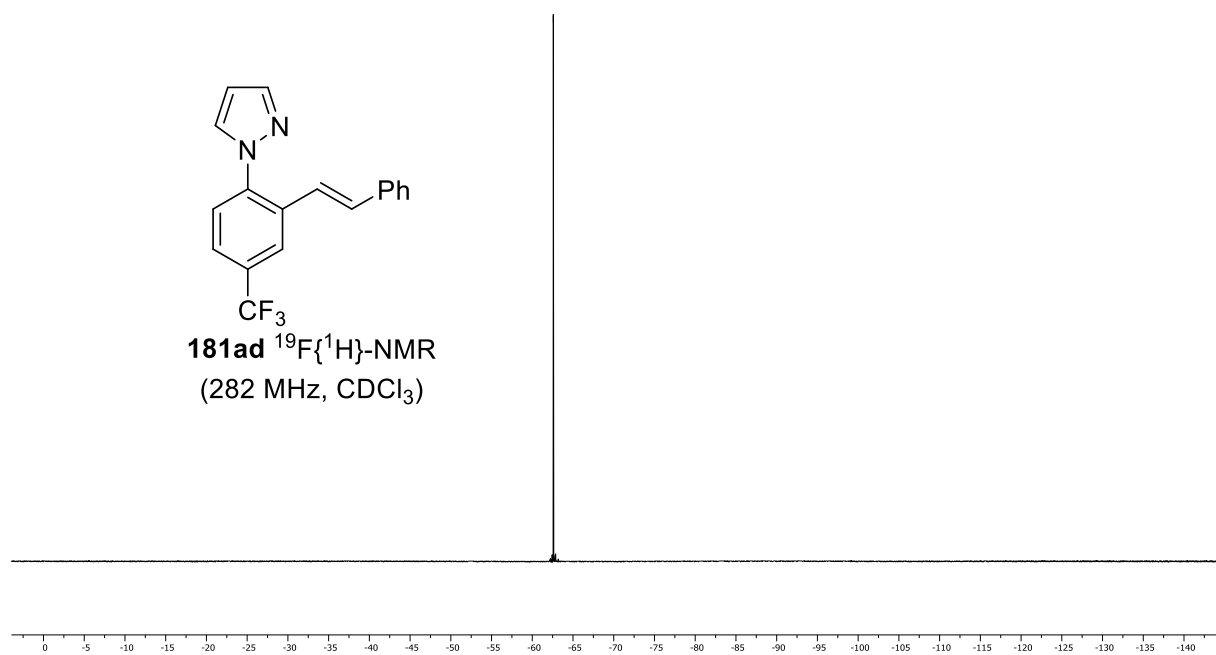
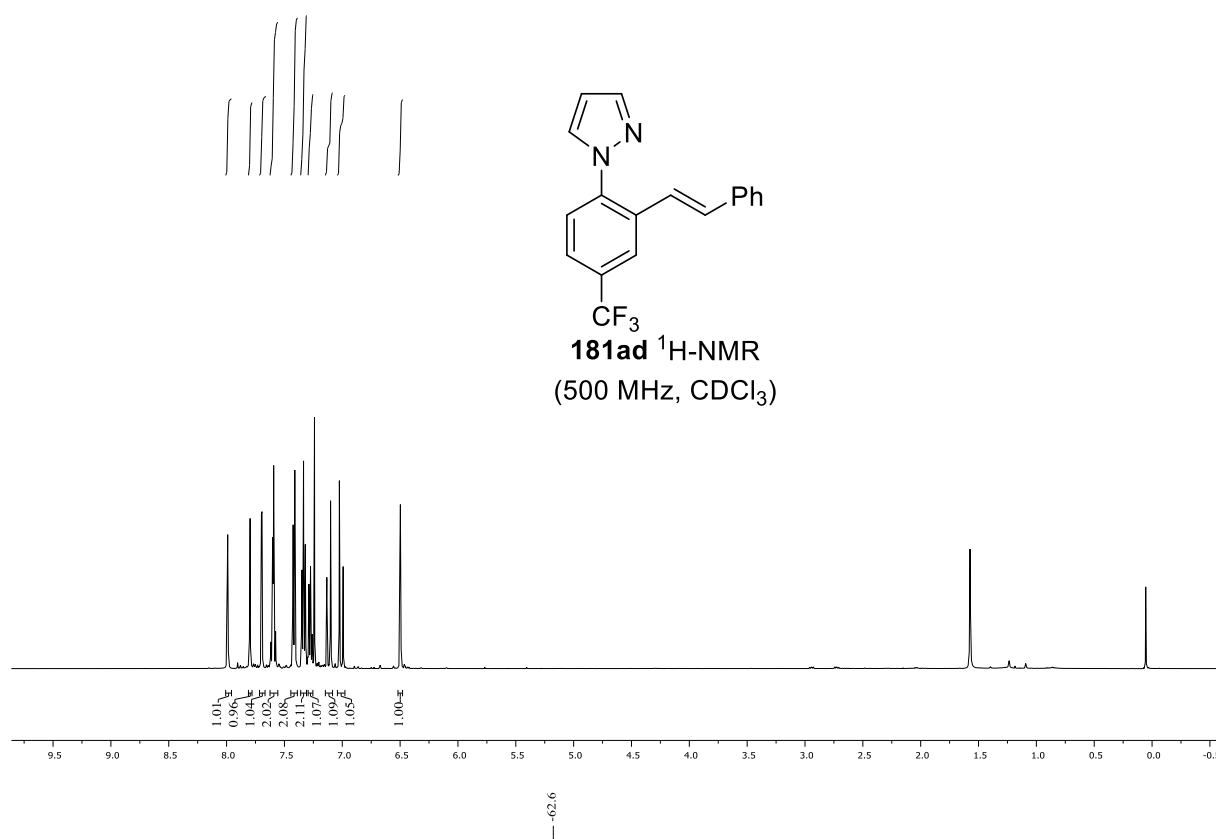
21.2



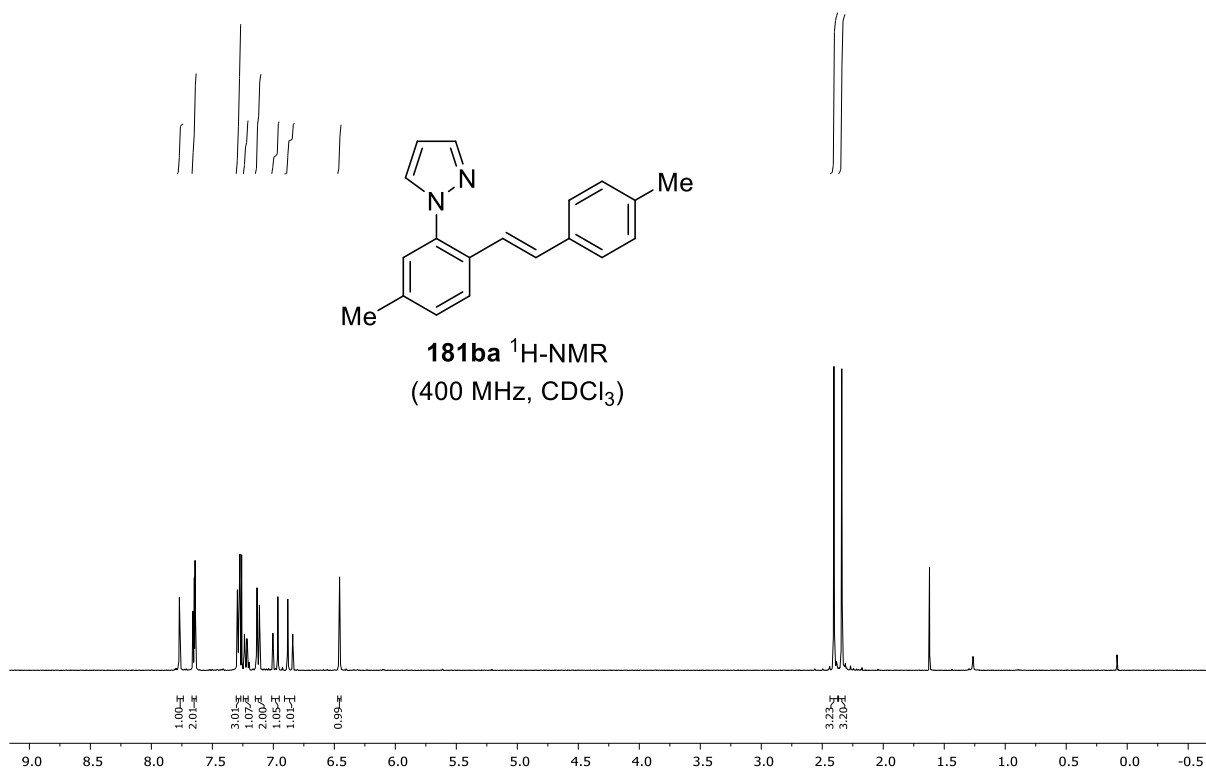
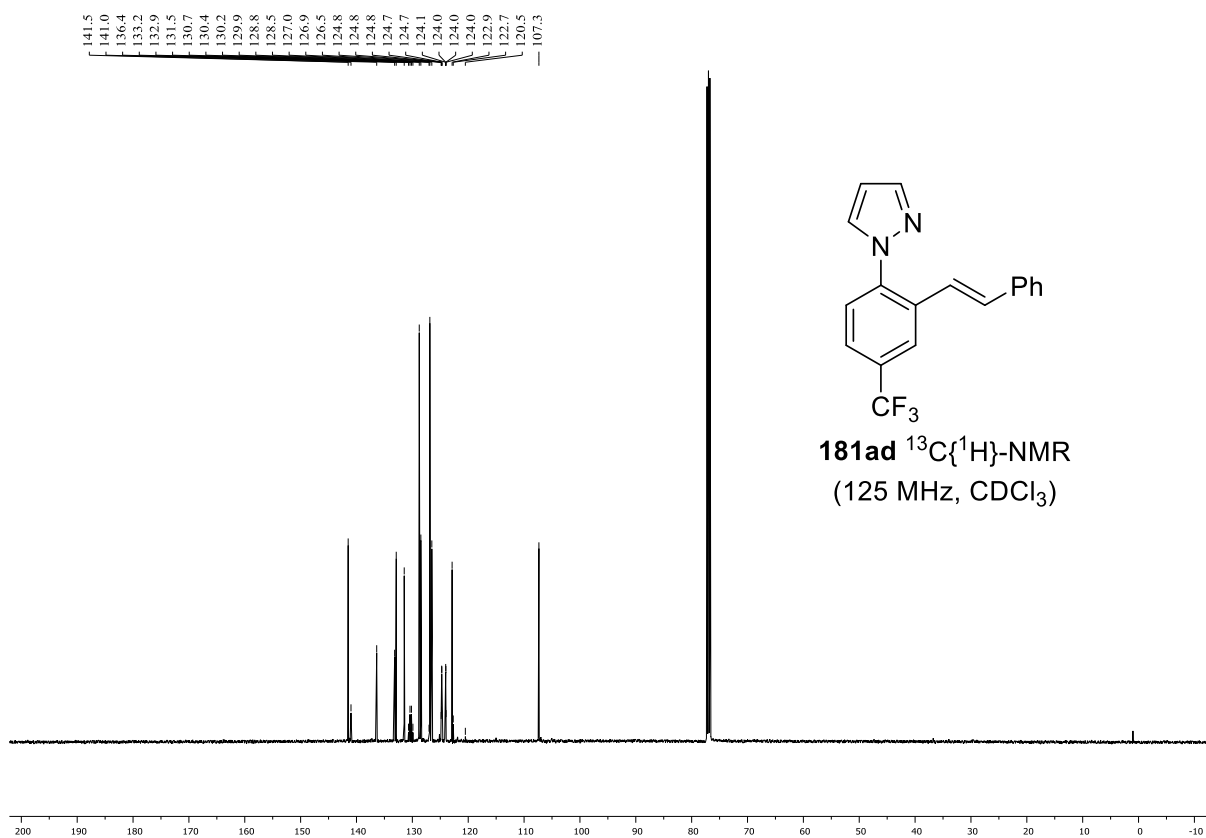
181ac $^{13}\text{C}\{^1\text{H}\}\text{-NMR}$
(100 MHz, CDCl_3)



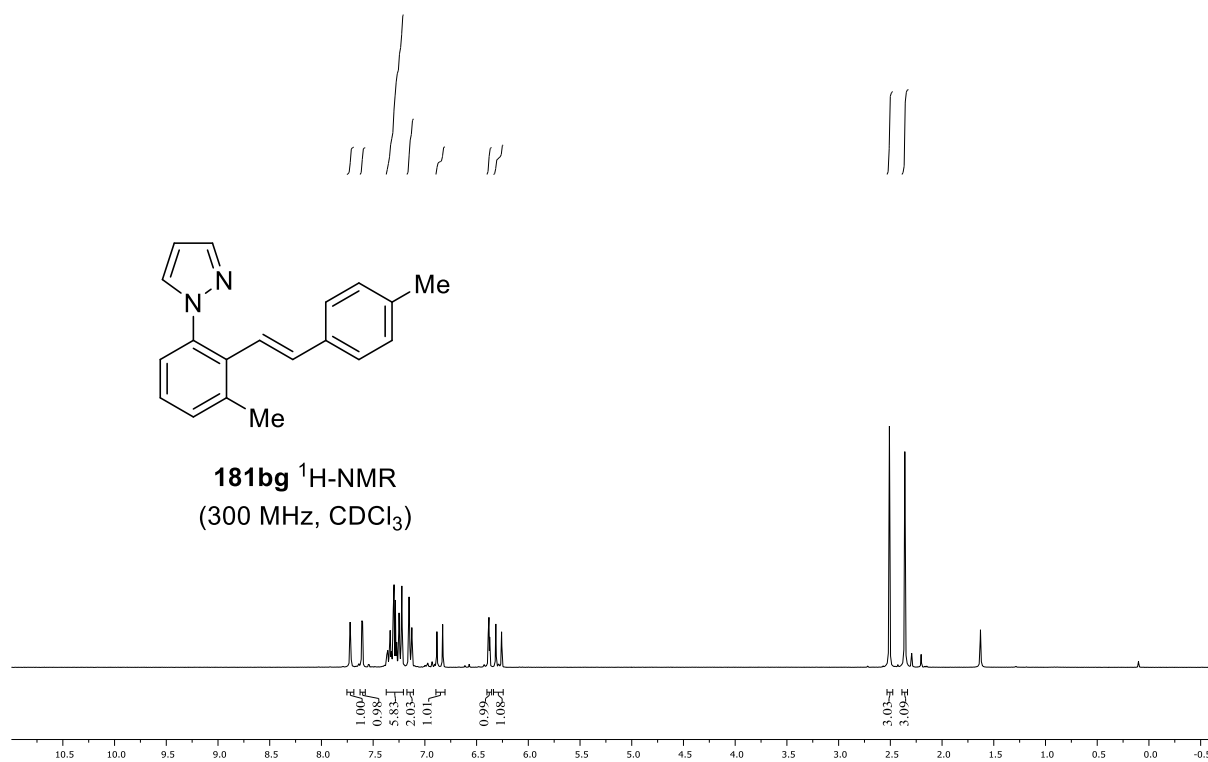
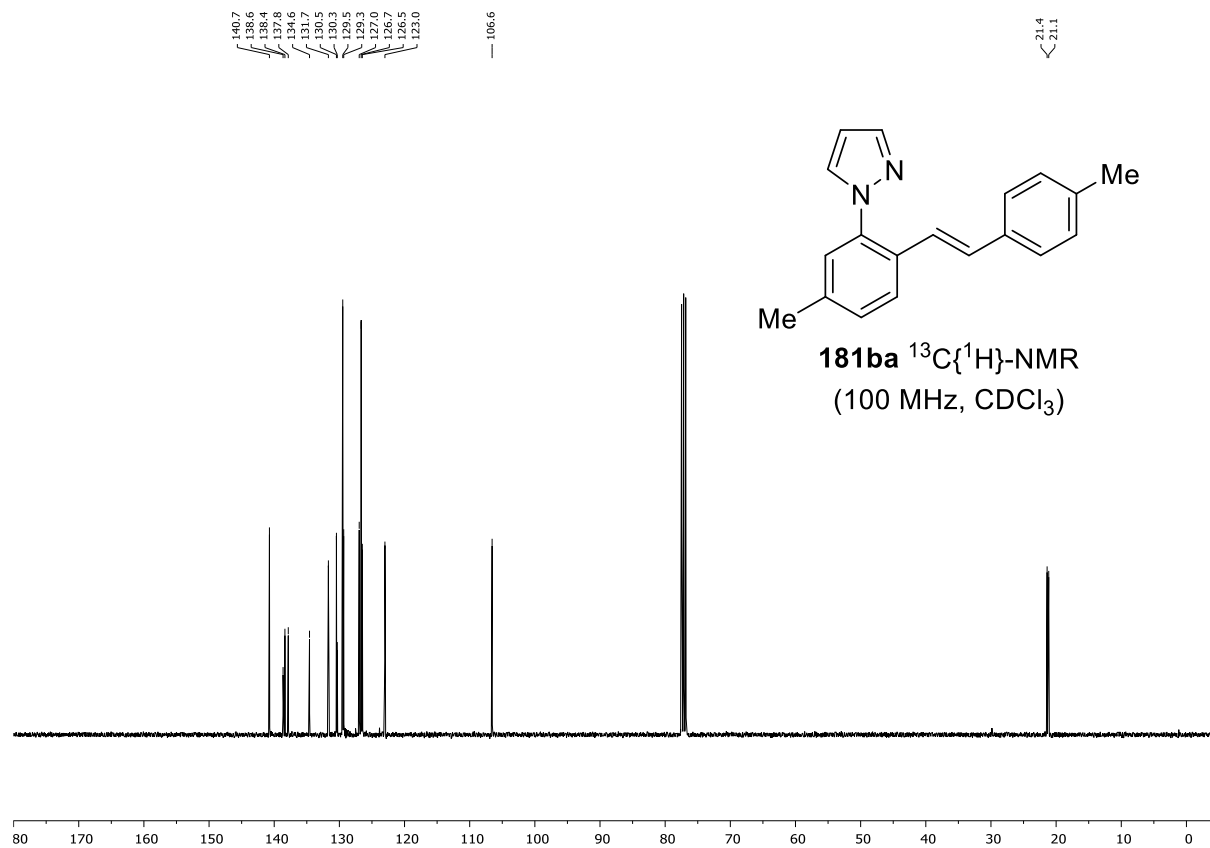
NMR SPECTRA



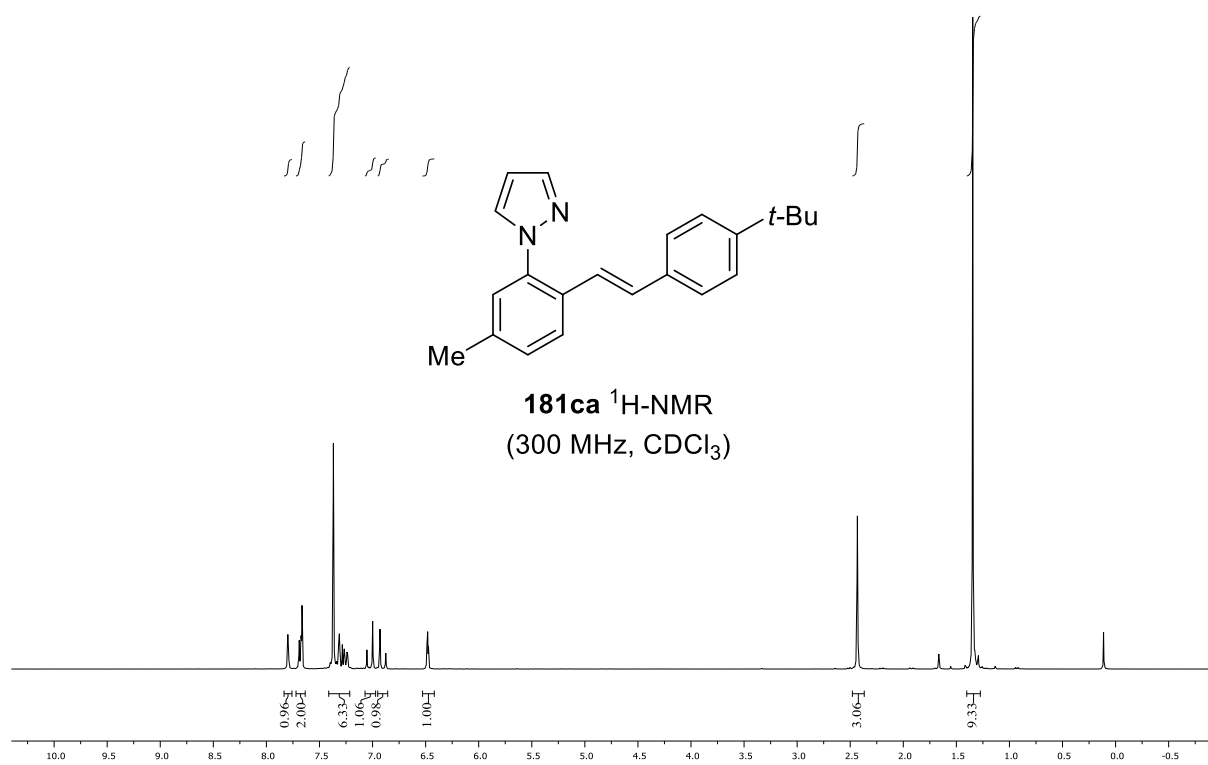
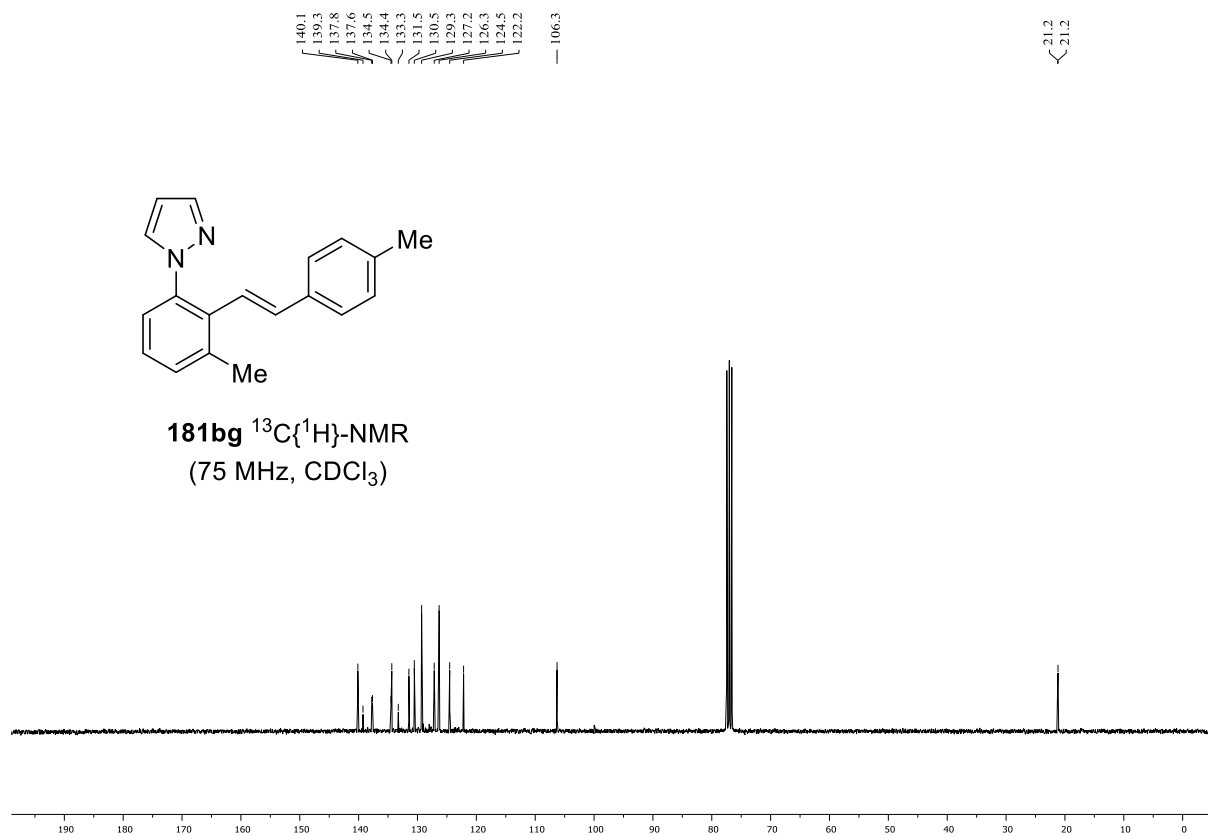
NMR SPECTRA



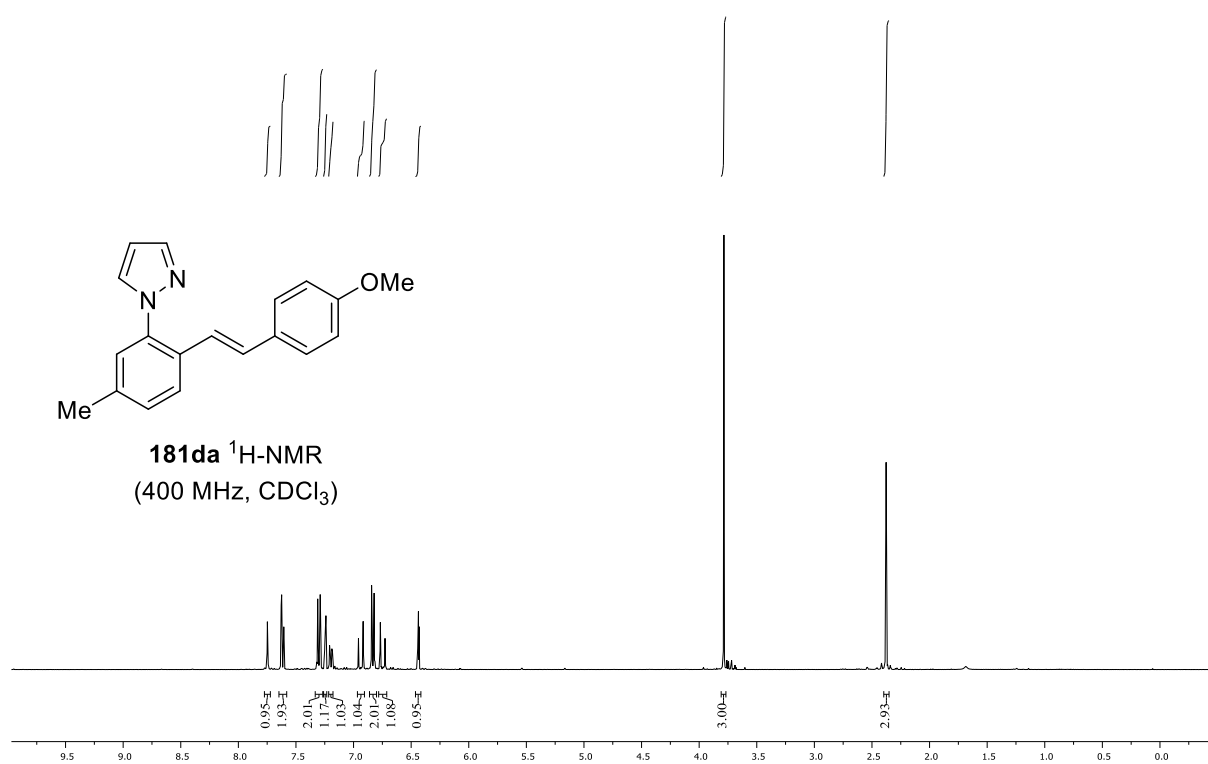
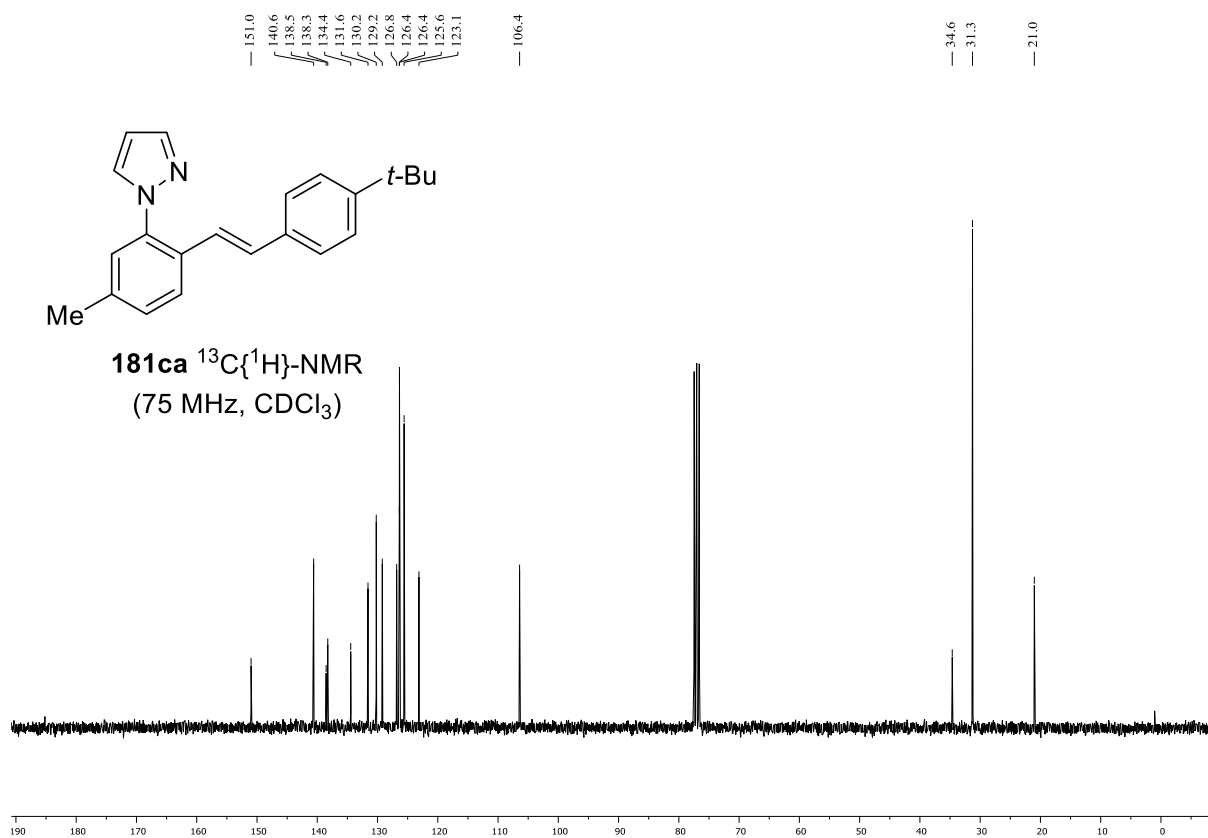
NMR SPECTRA



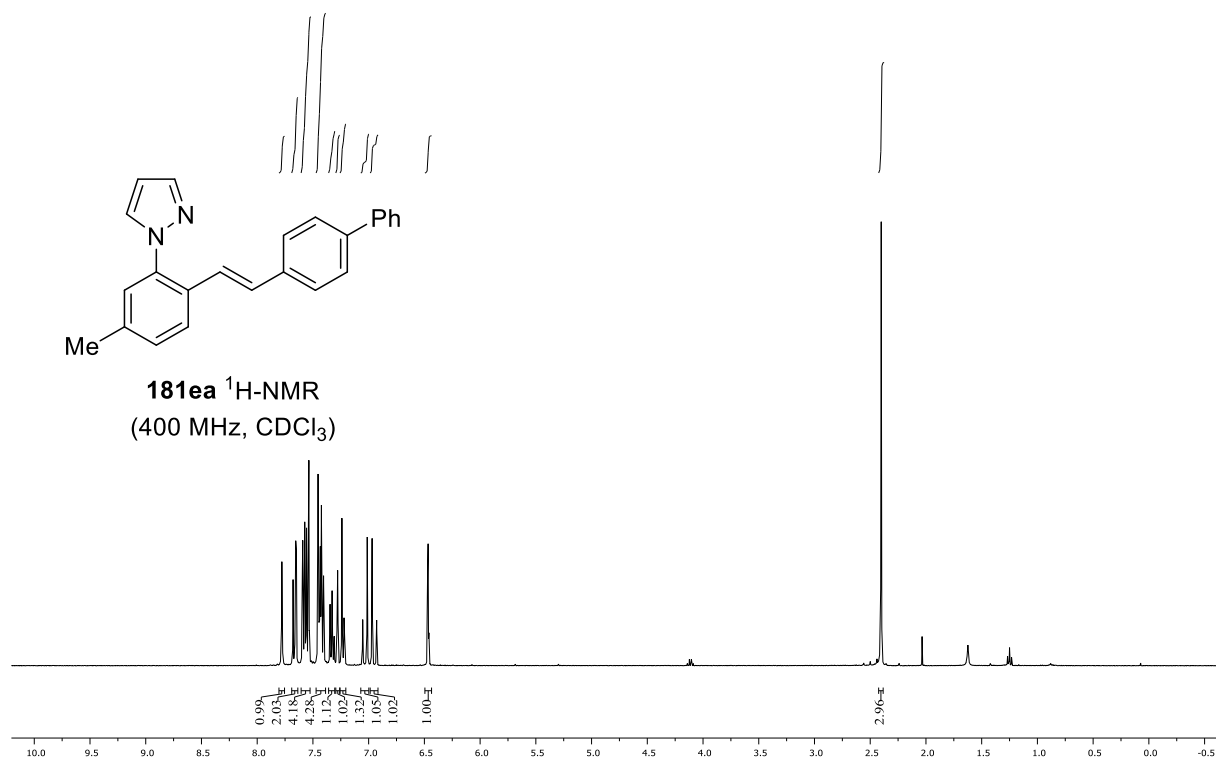
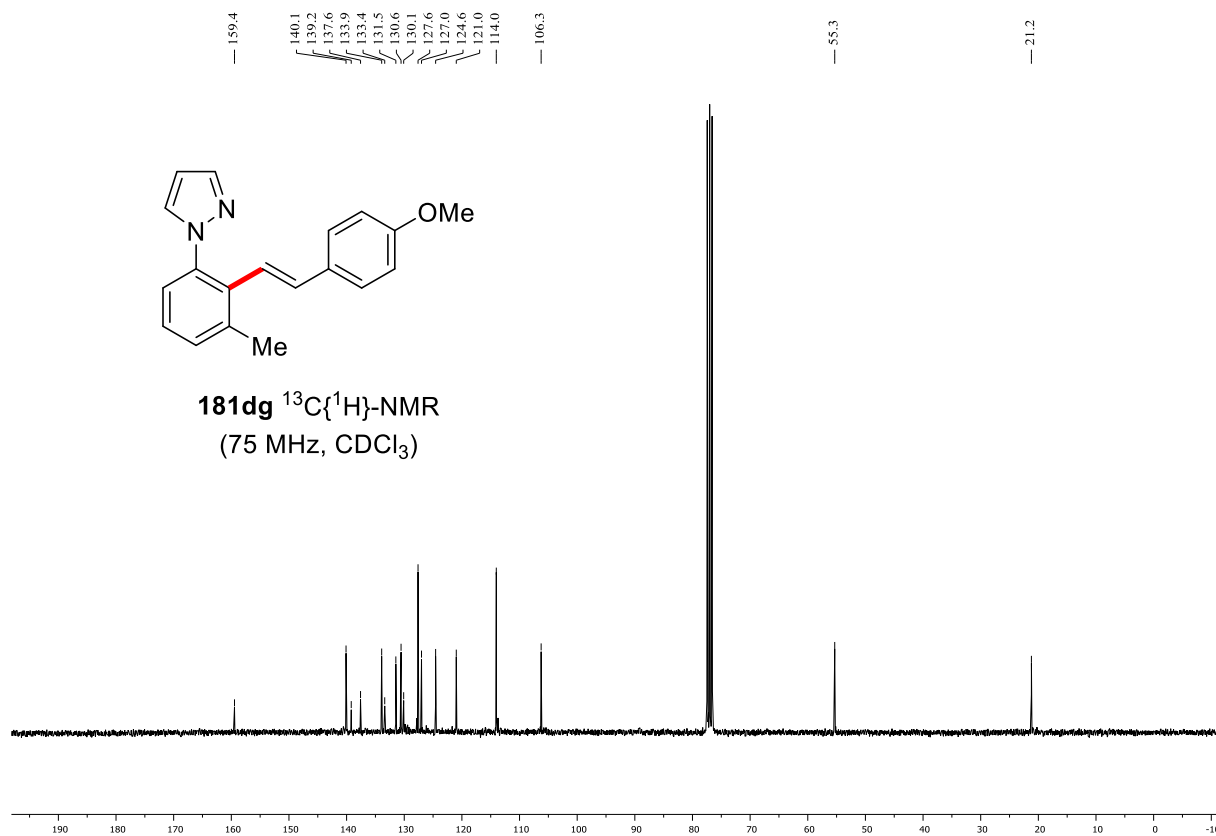
NMR SPECTRA



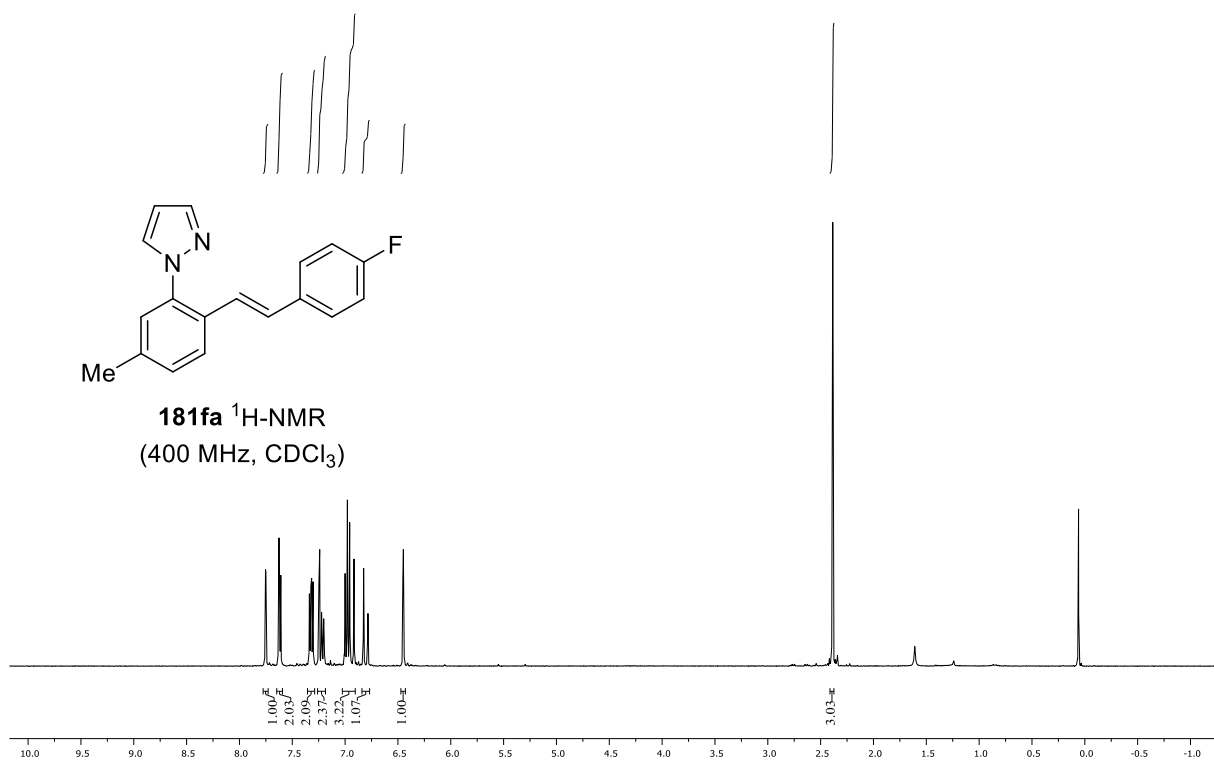
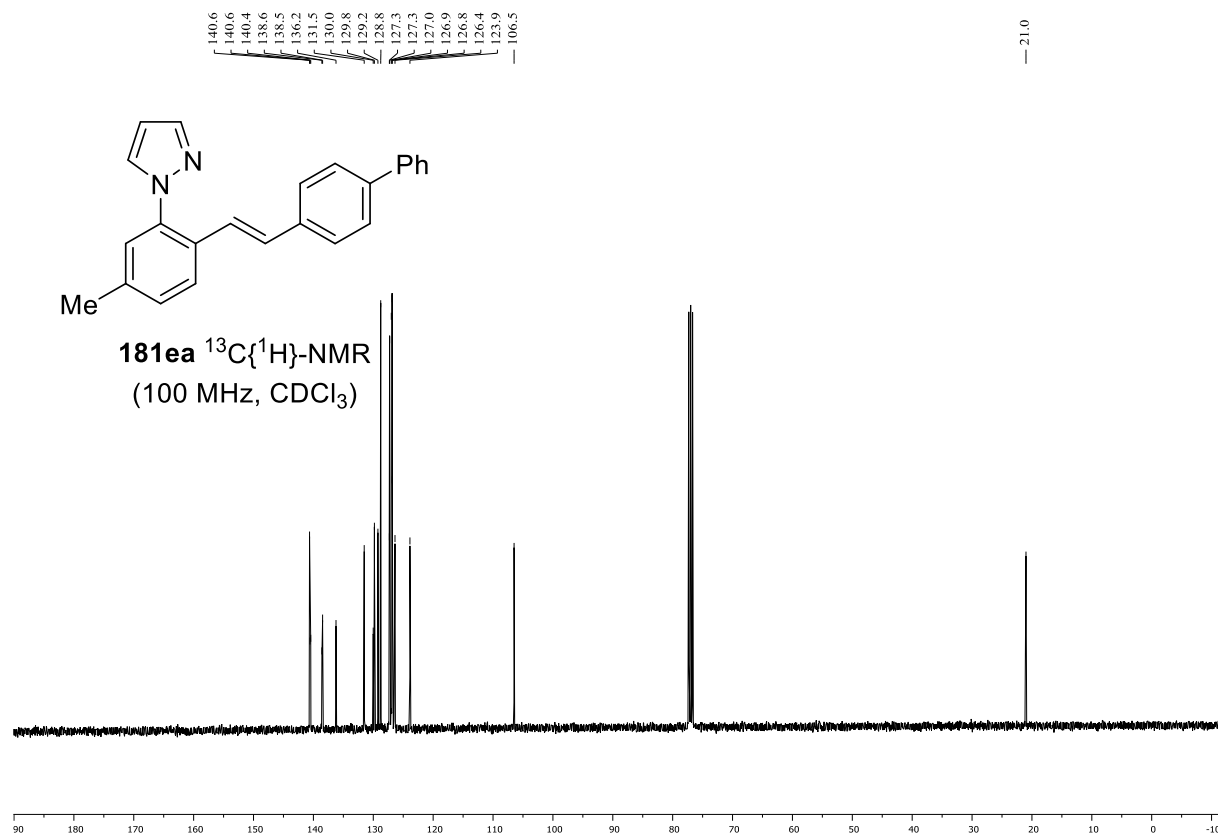
NMR SPECTRA



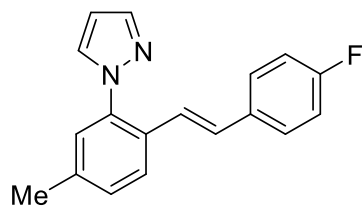
NMR SPECTRA



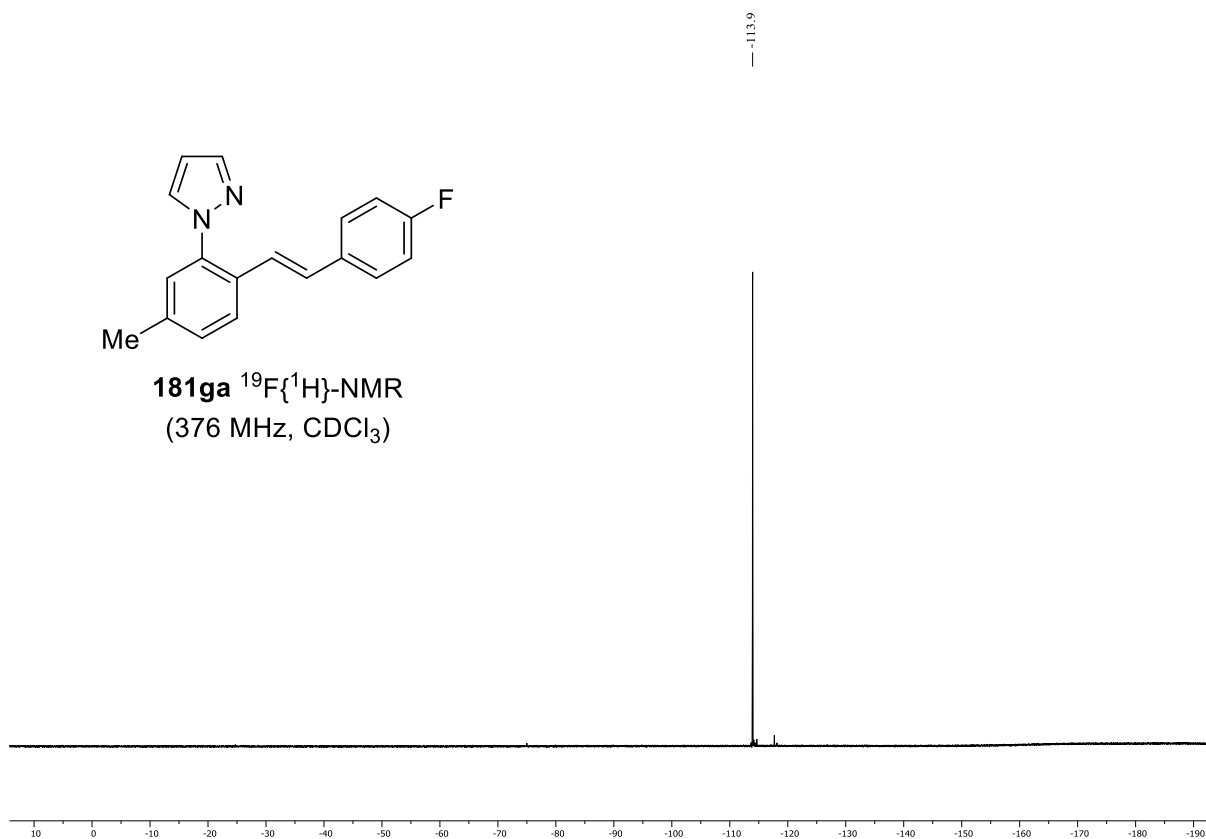
NMR SPECTRA



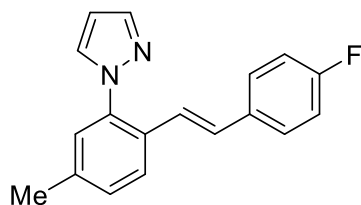
NMR SPECTRA



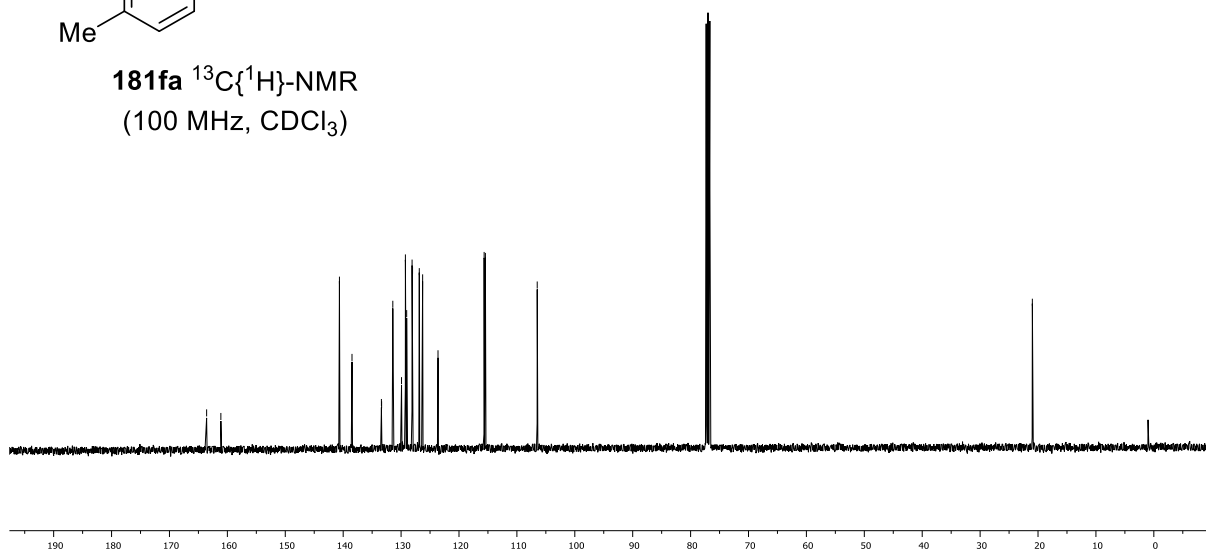
181ga $^{19}\text{F}\{^1\text{H}\}$ -NMR
(376 MHz, CDCl_3)



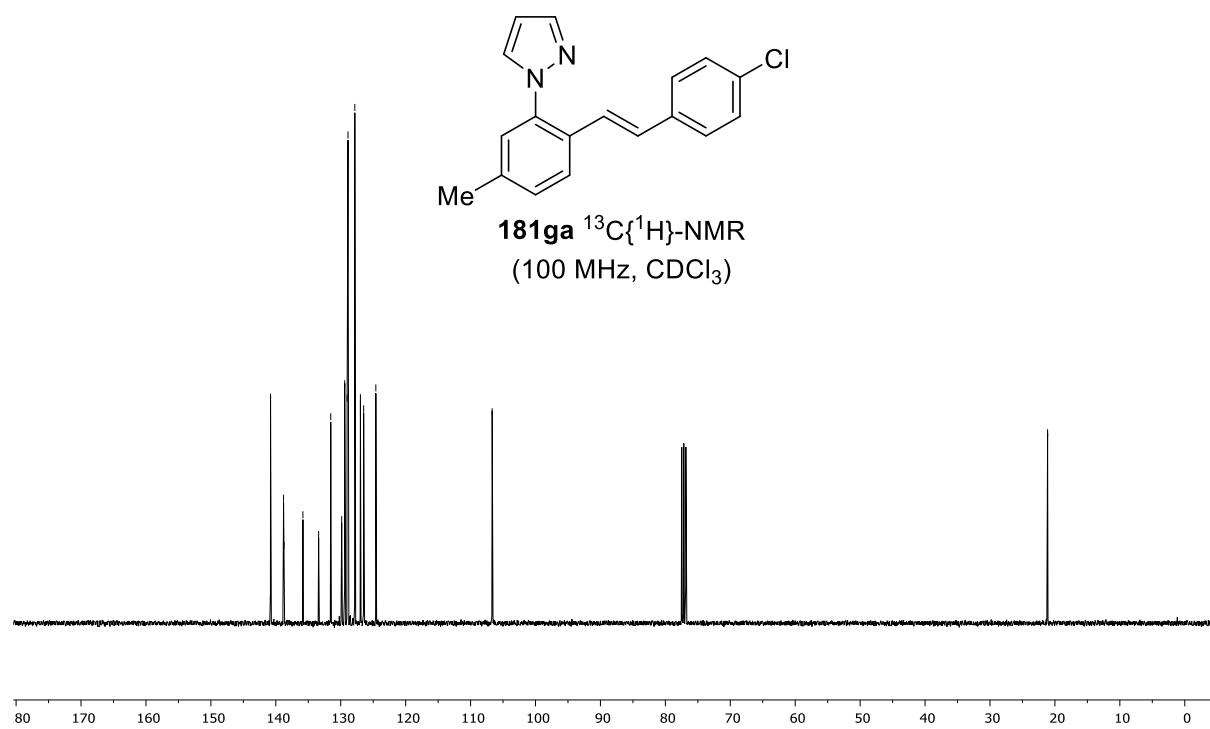
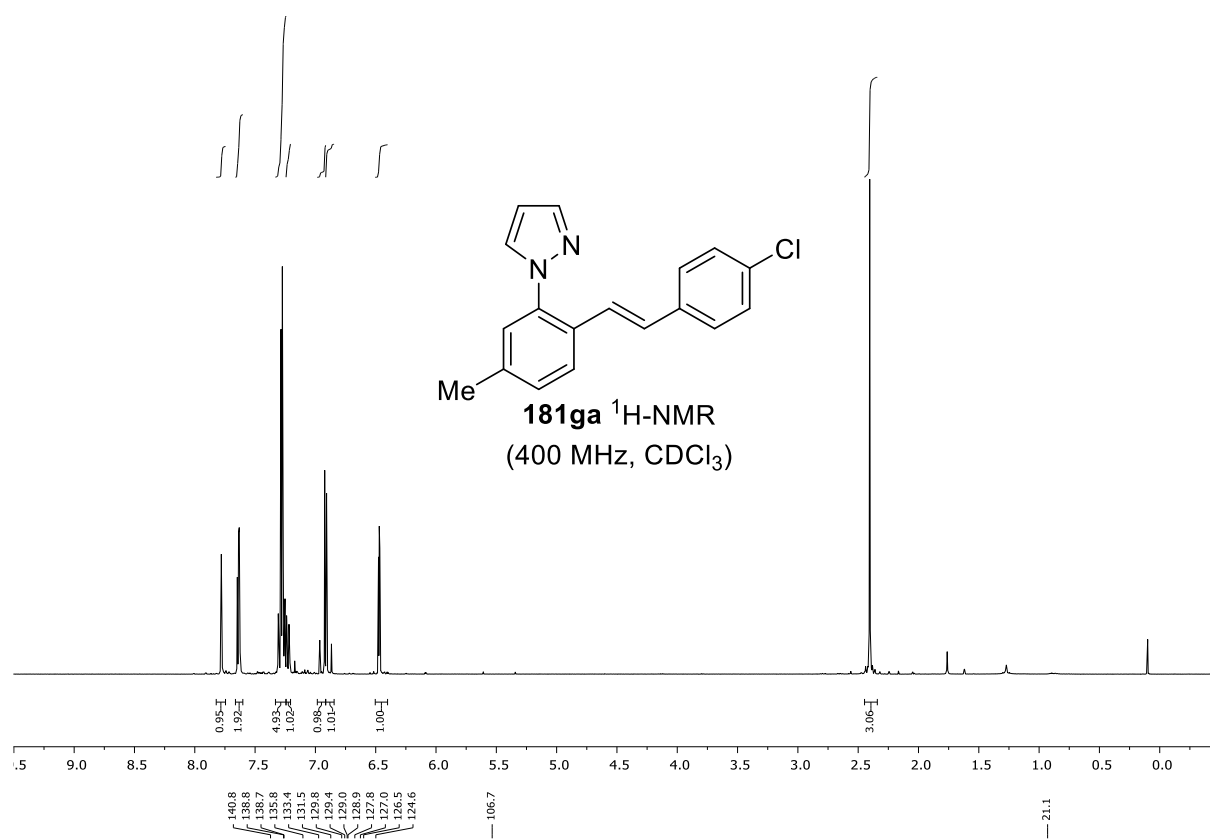
163.6
 161.1
 140.6
 138.5
 138.5
 133.4
 133.4
 131.4
 129.9
 129.3
 129.0
 128.1
 128.0
 126.9
 126.3
 123.6
 115.7
 115.4
 106.5



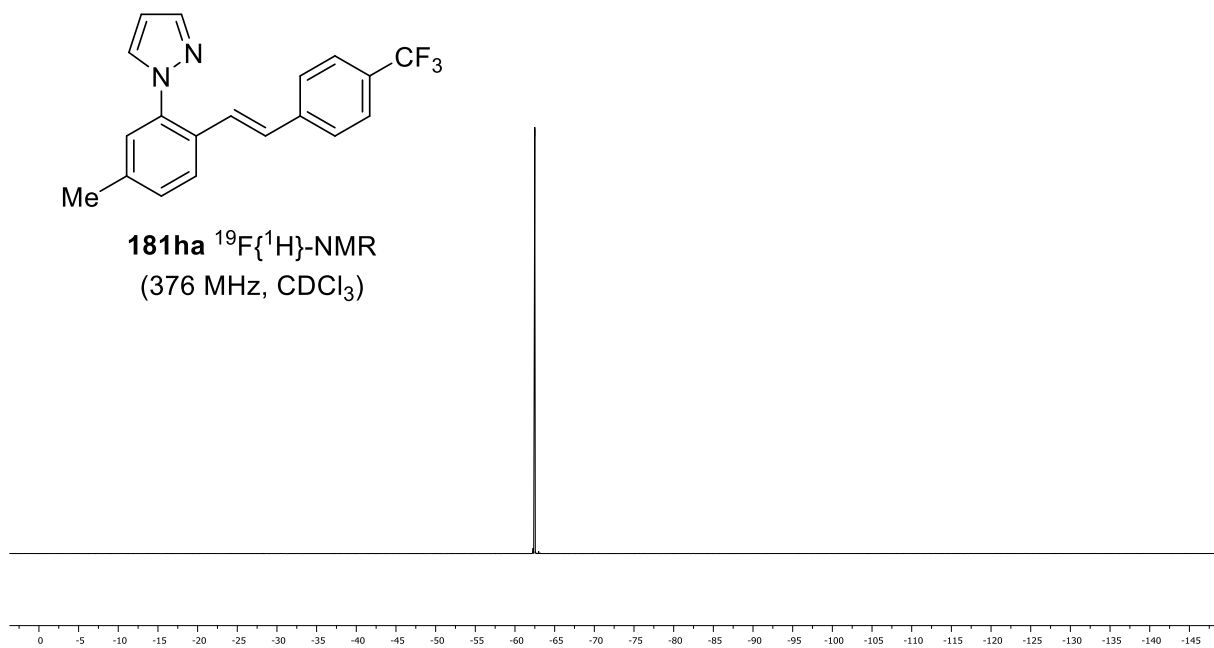
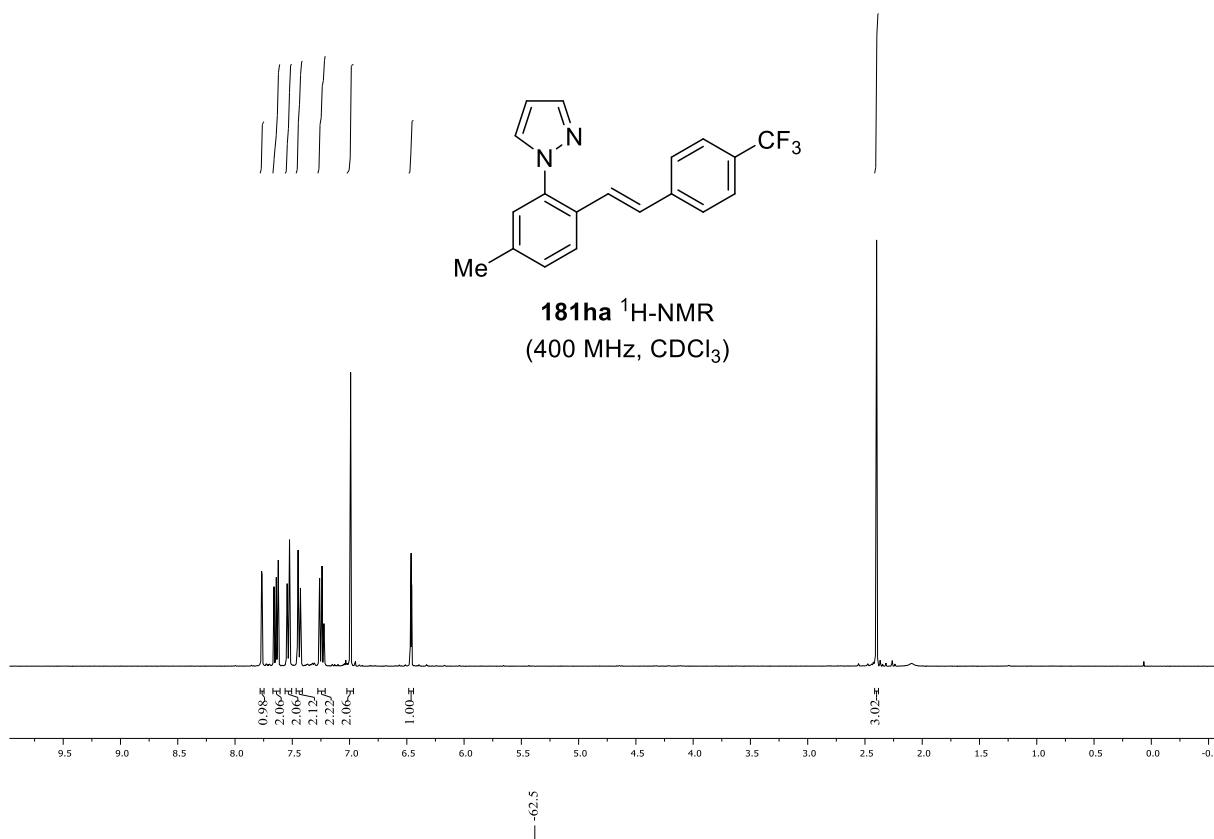
181fa $^{13}\text{C}\{^1\text{H}\}$ -NMR
(100 MHz, CDCl_3)



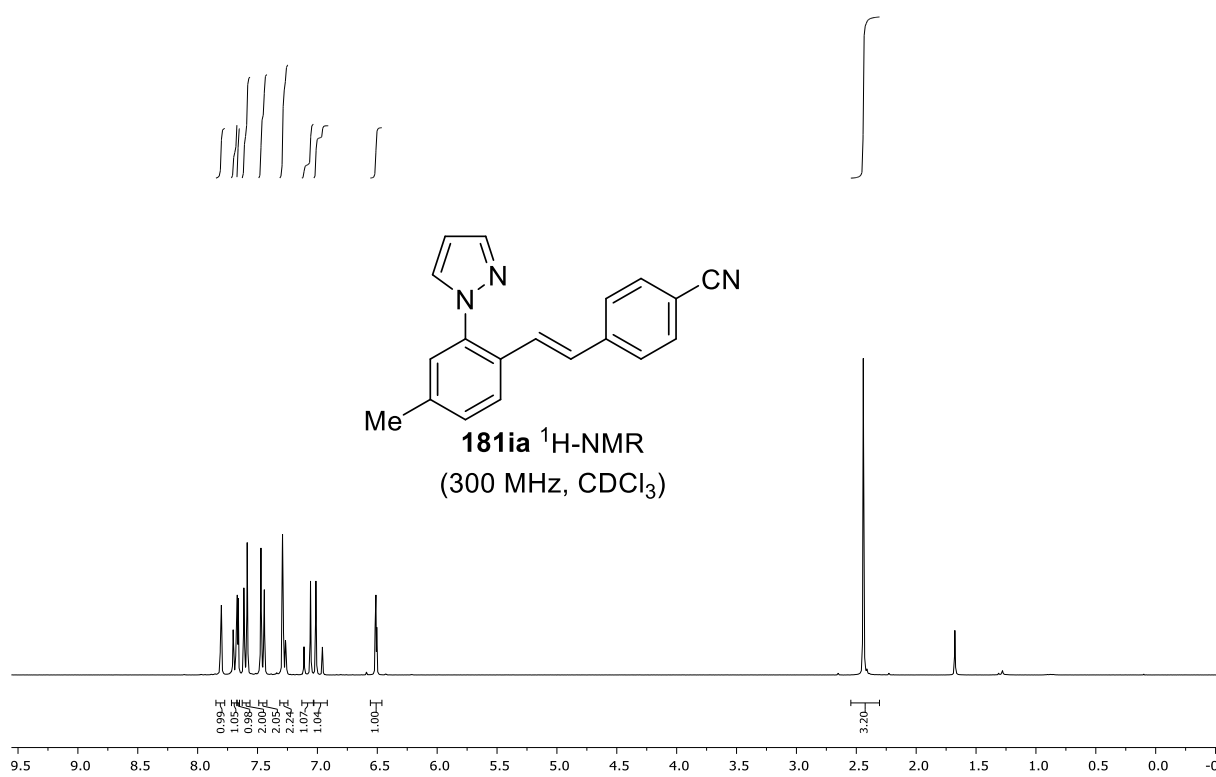
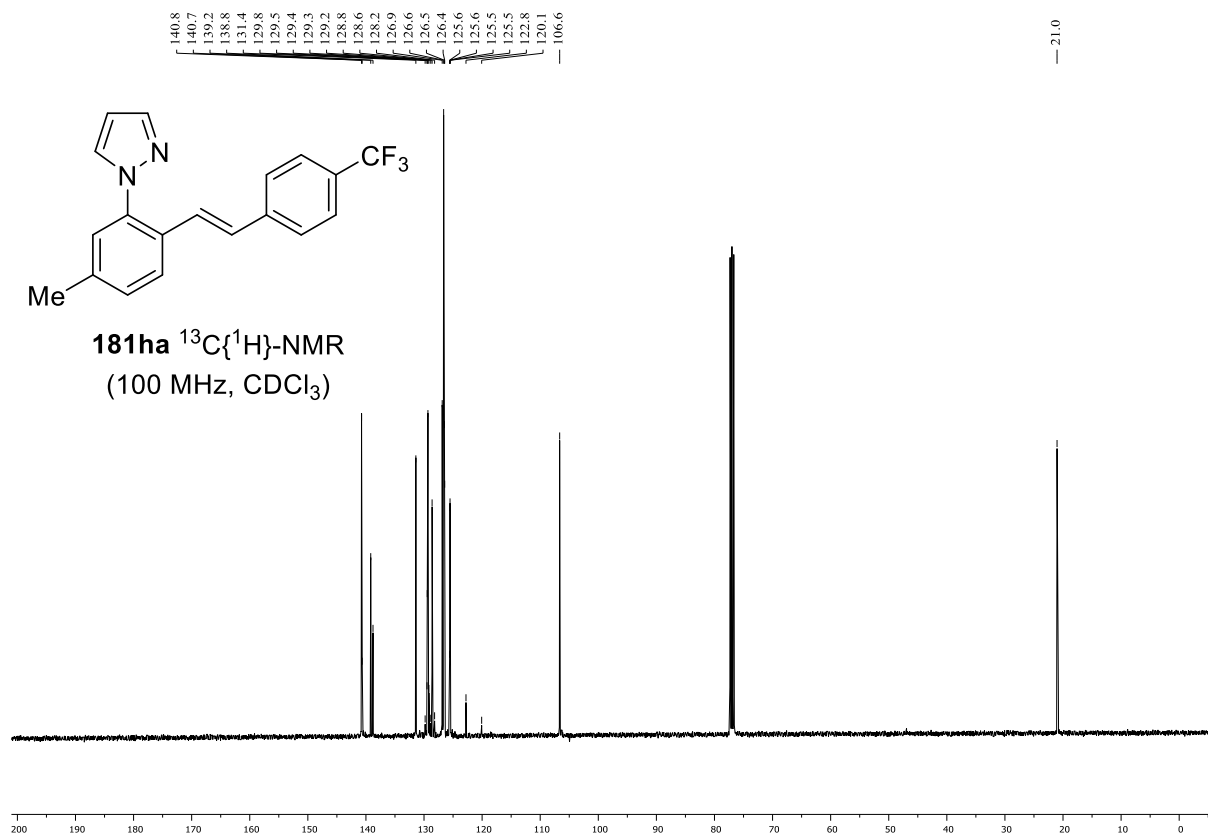
NMR SPECTRA



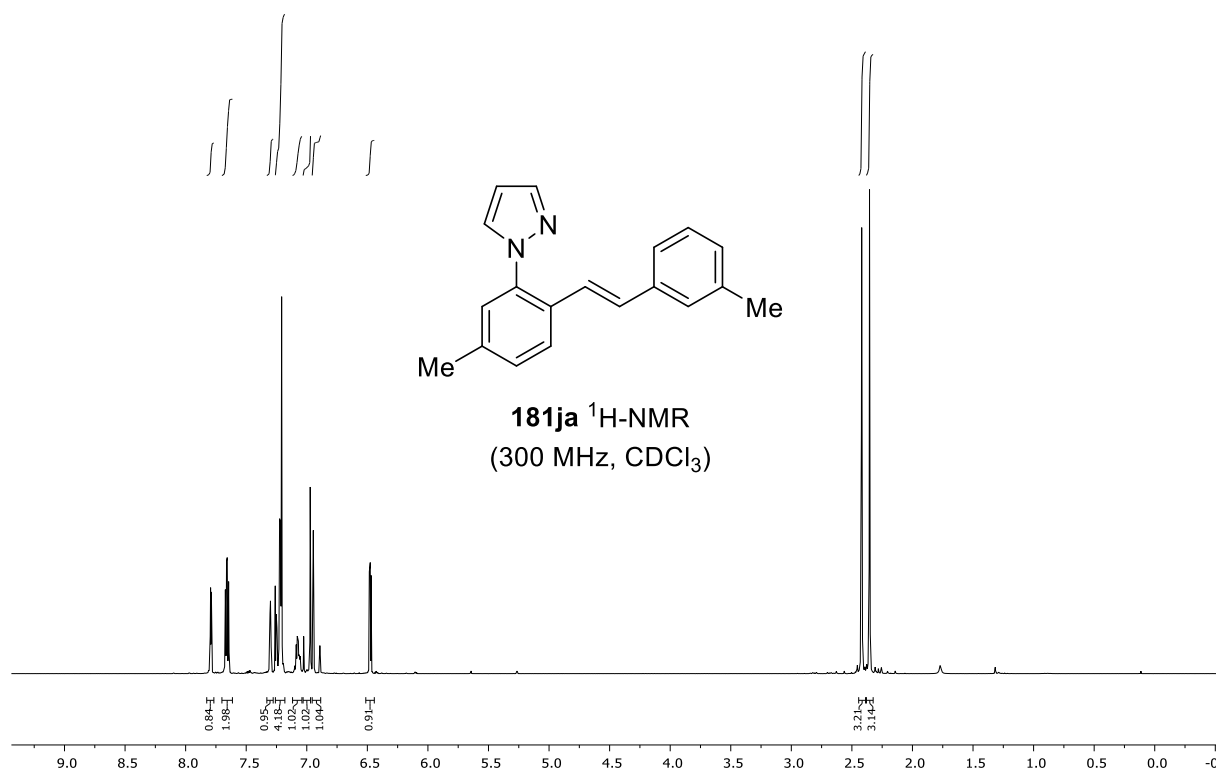
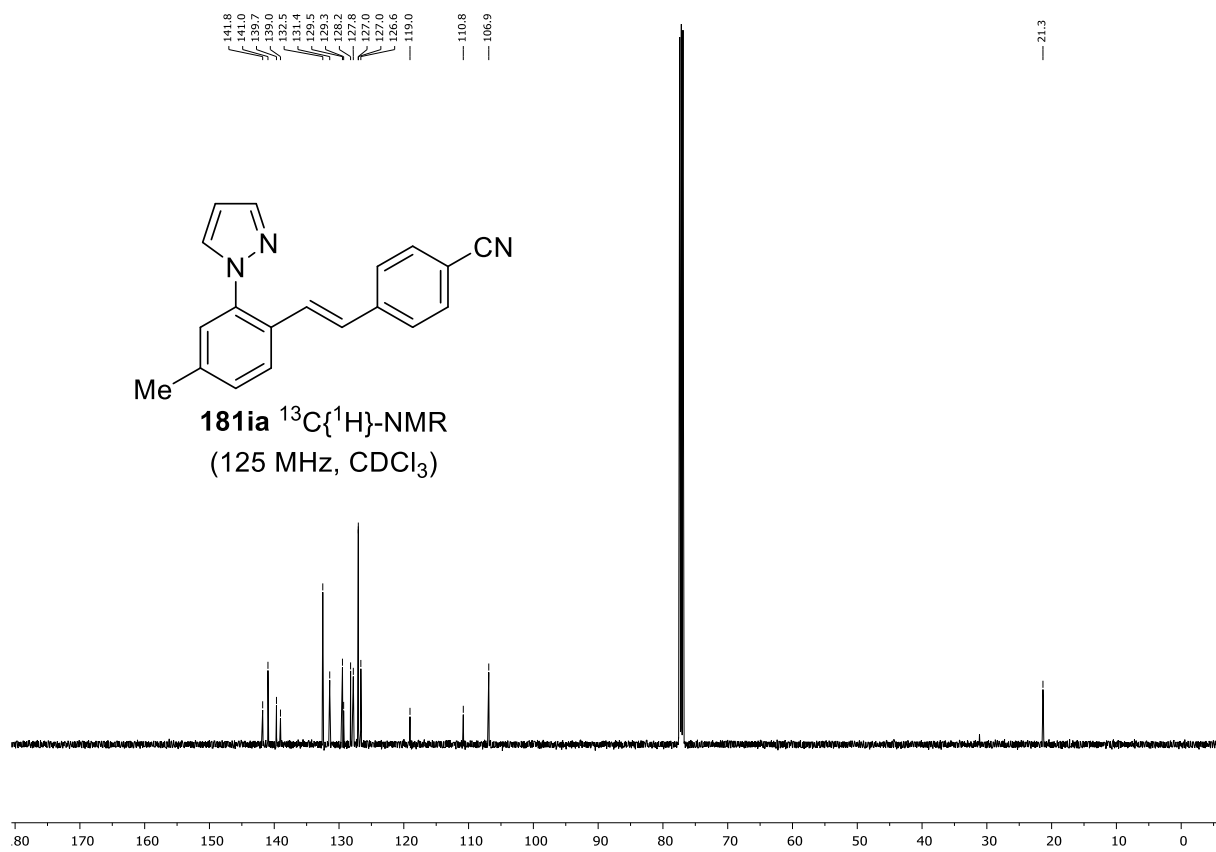
NMR SPECTRA



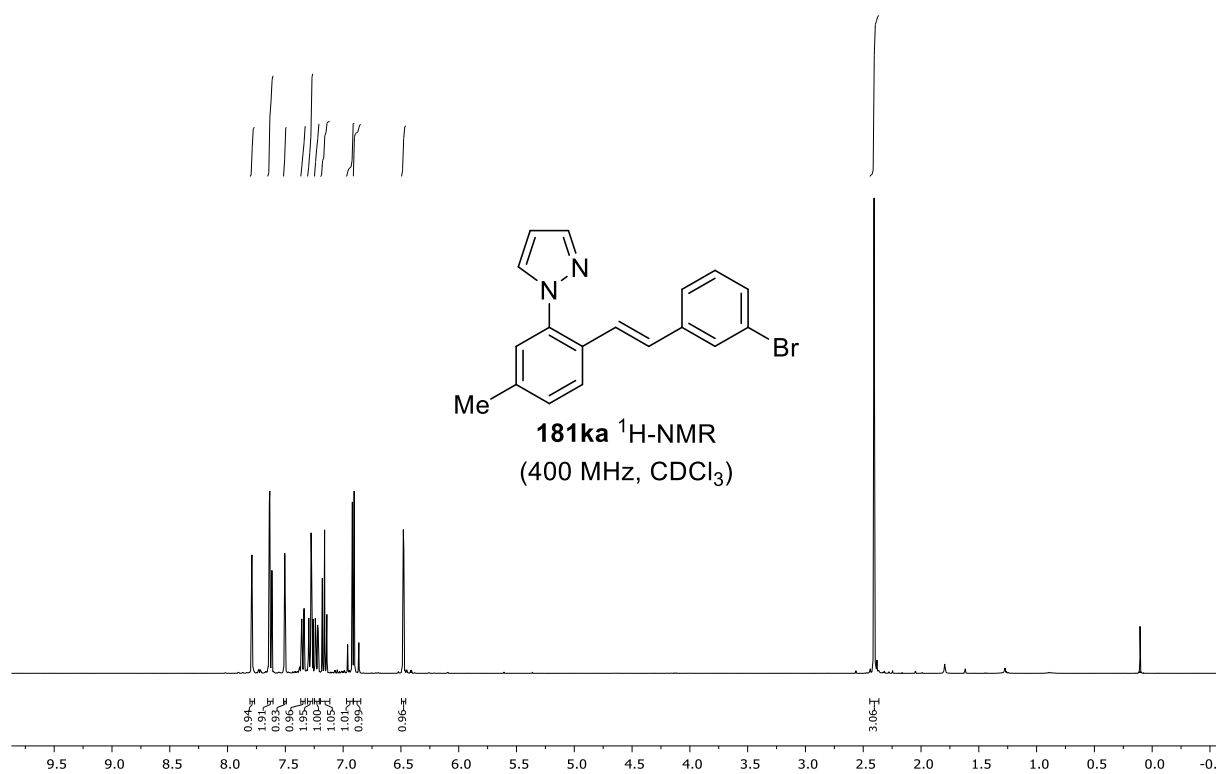
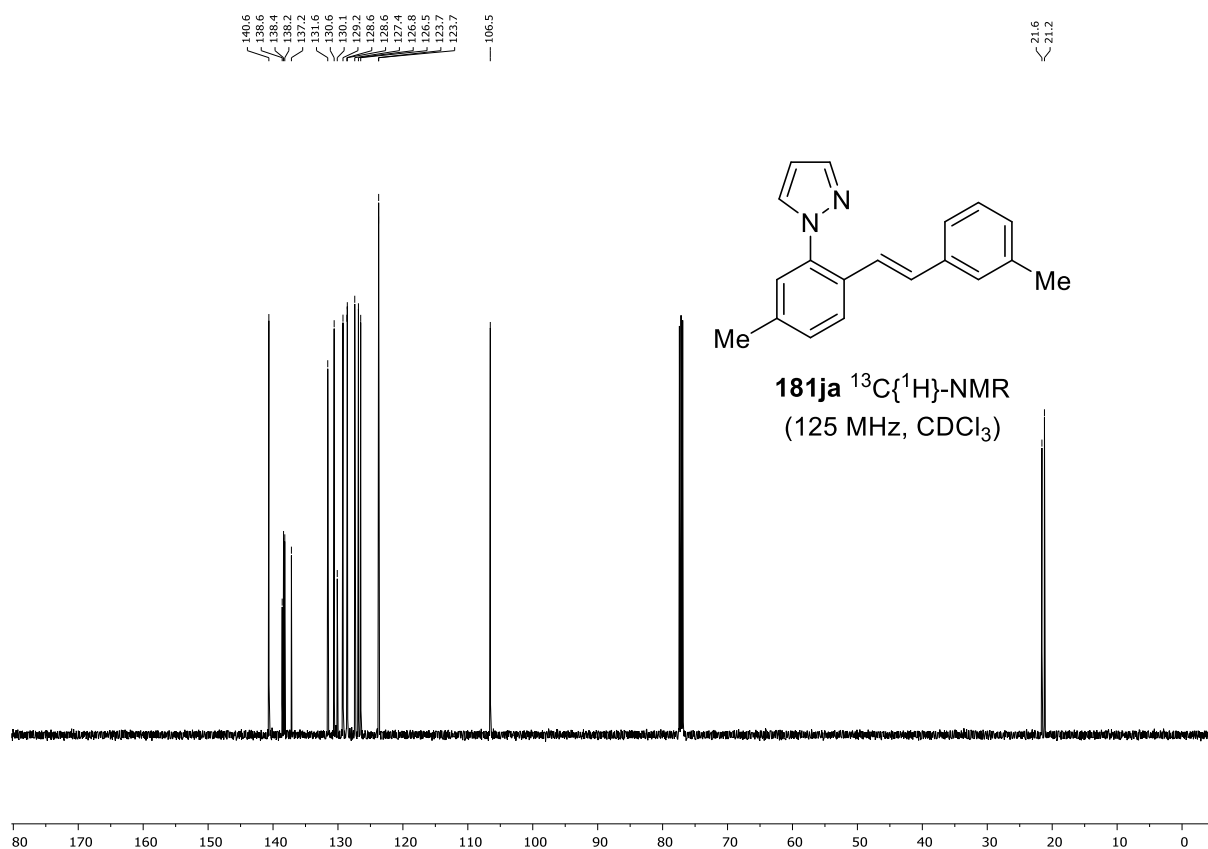
NMR SPECTRA



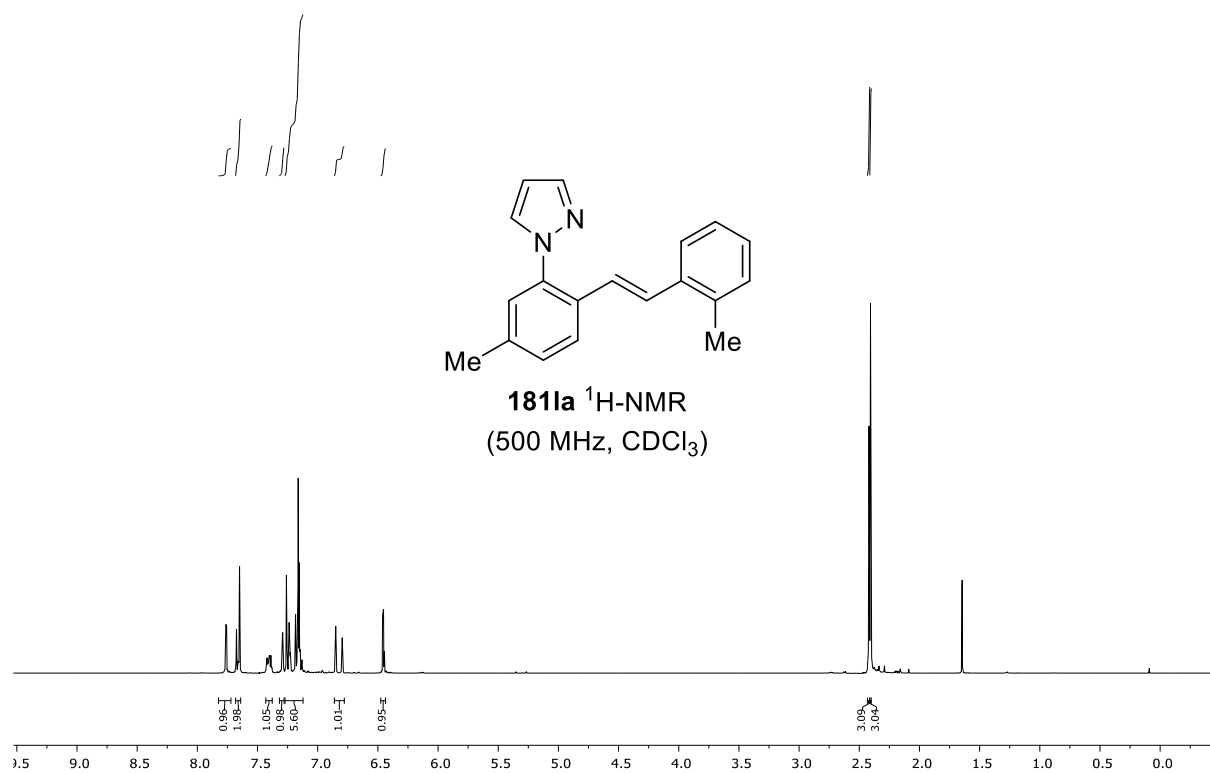
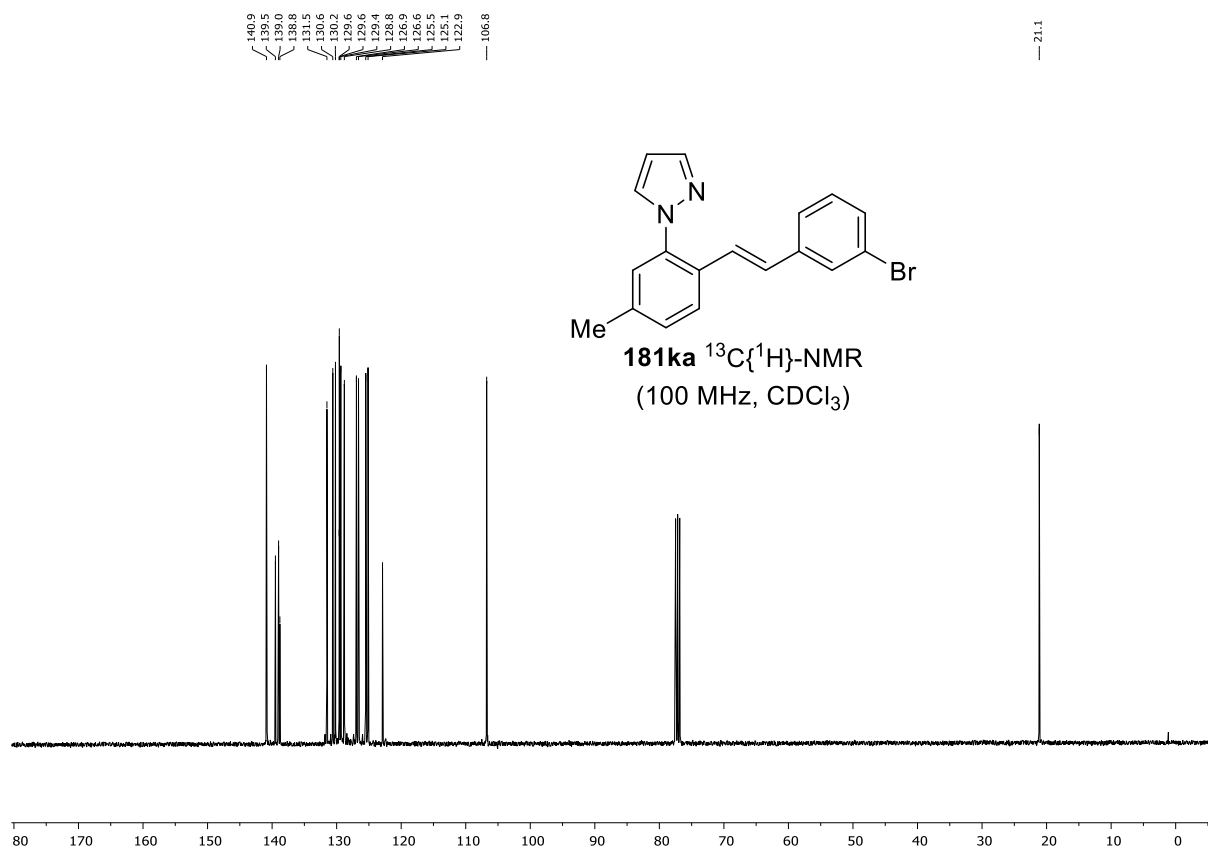
NMR SPECTRA



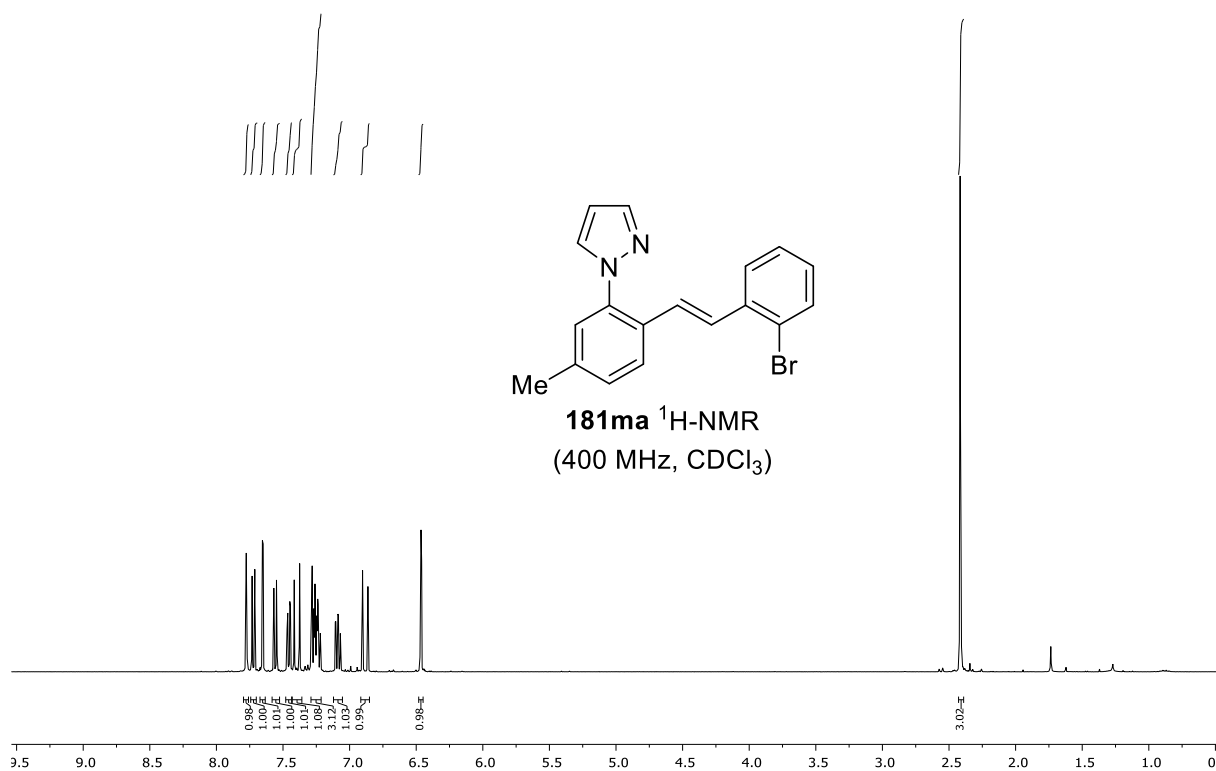
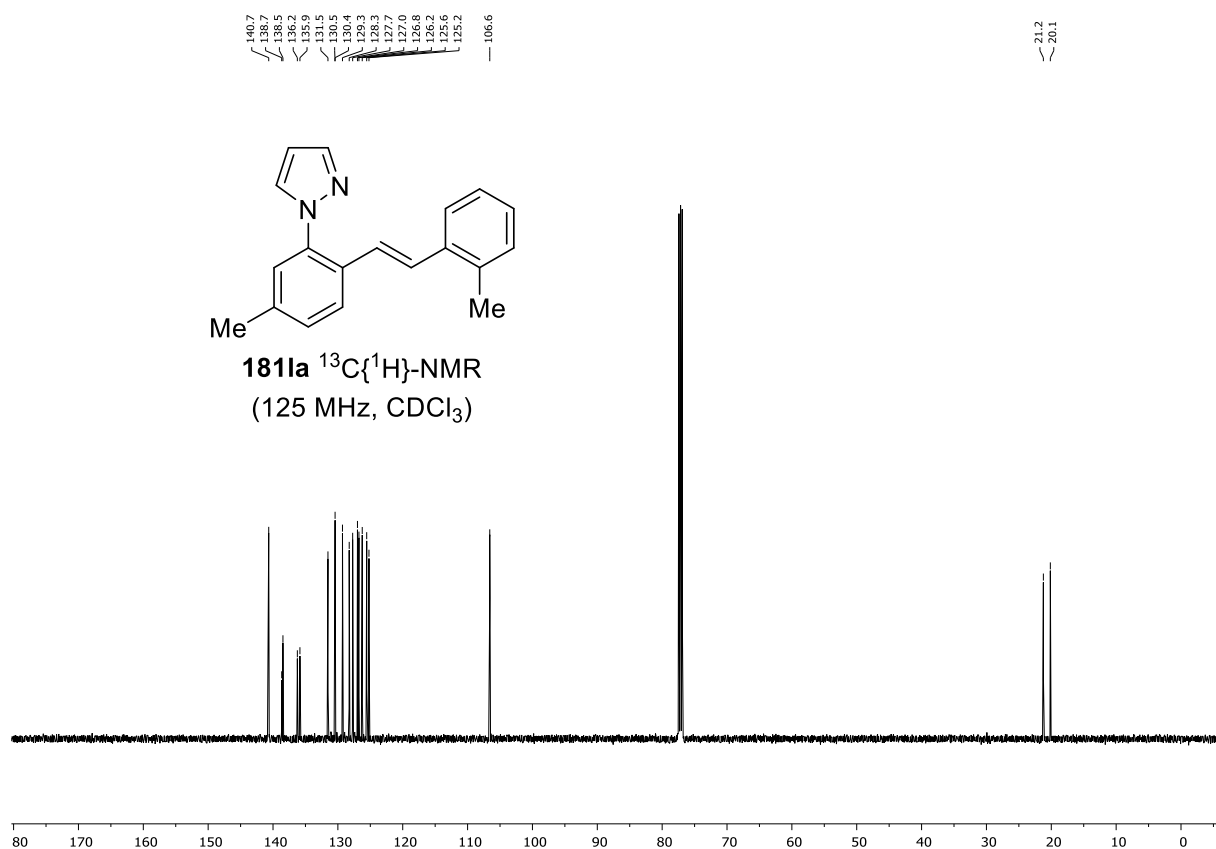
NMR SPECTRA



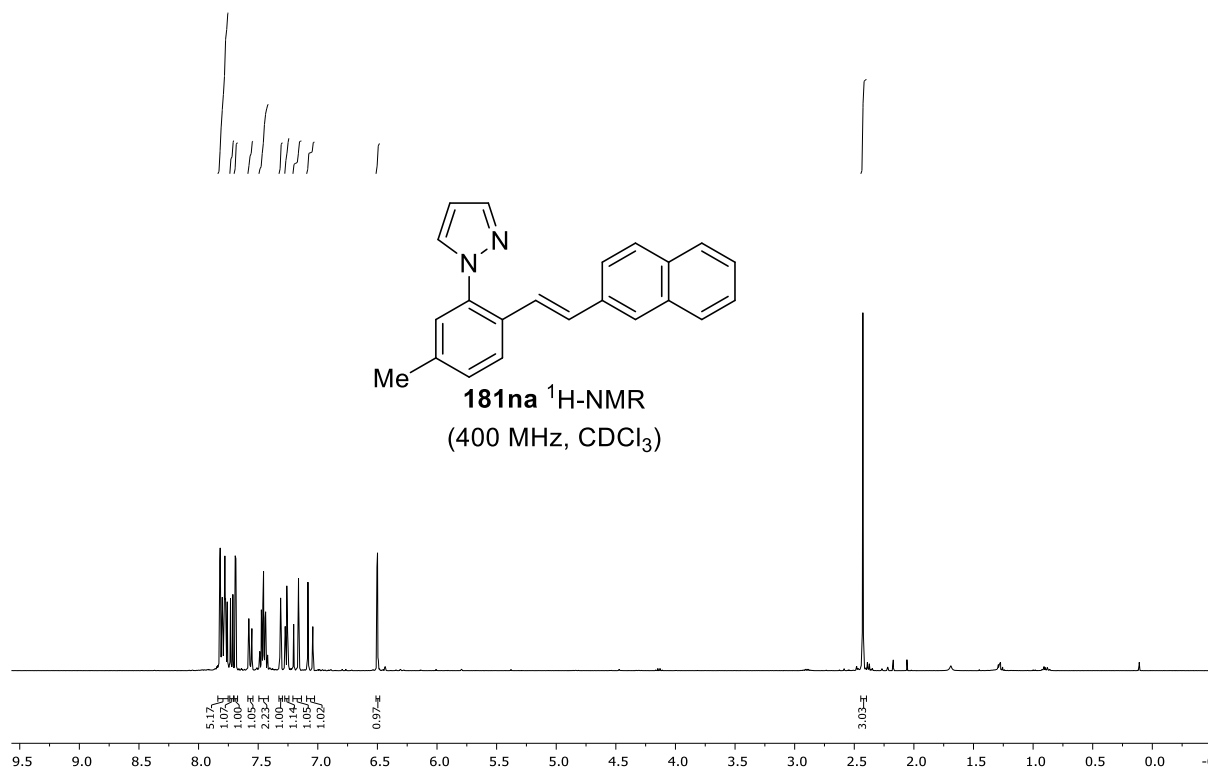
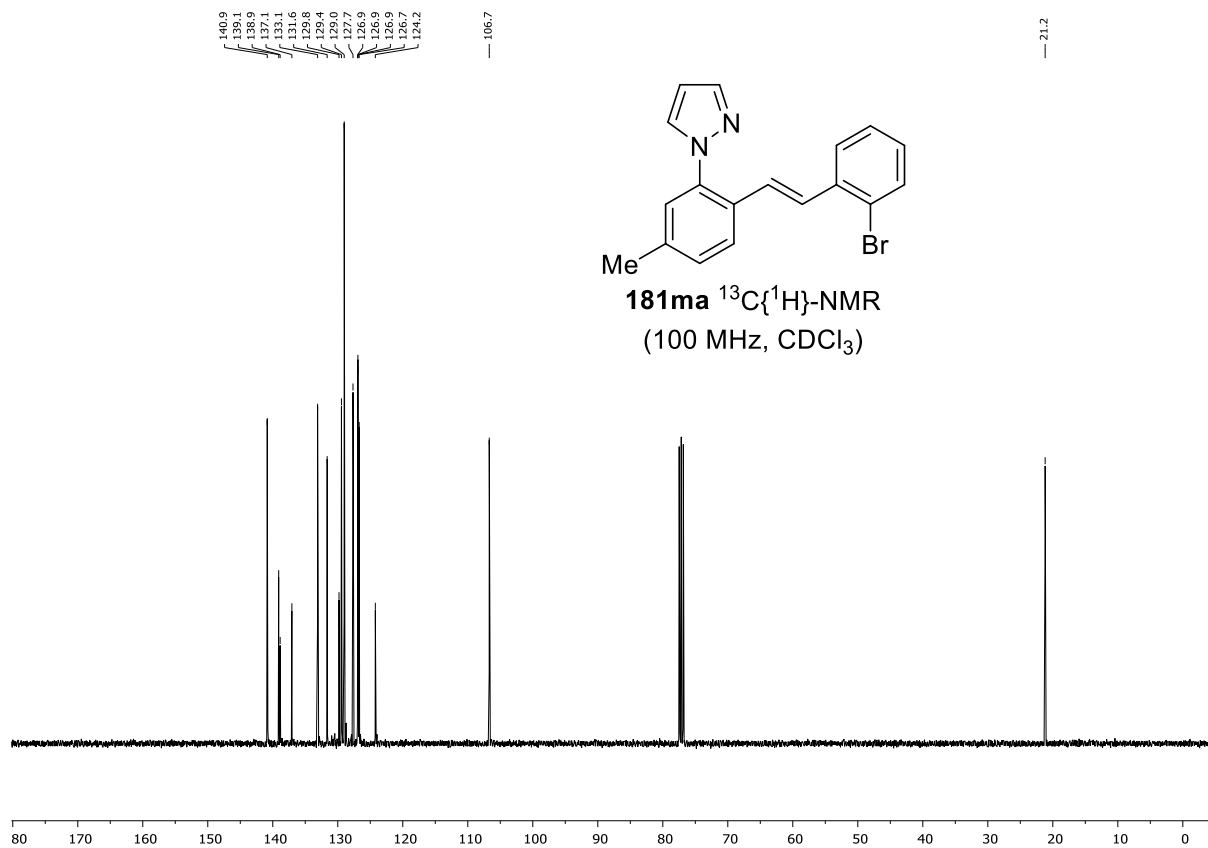
NMR SPECTRA



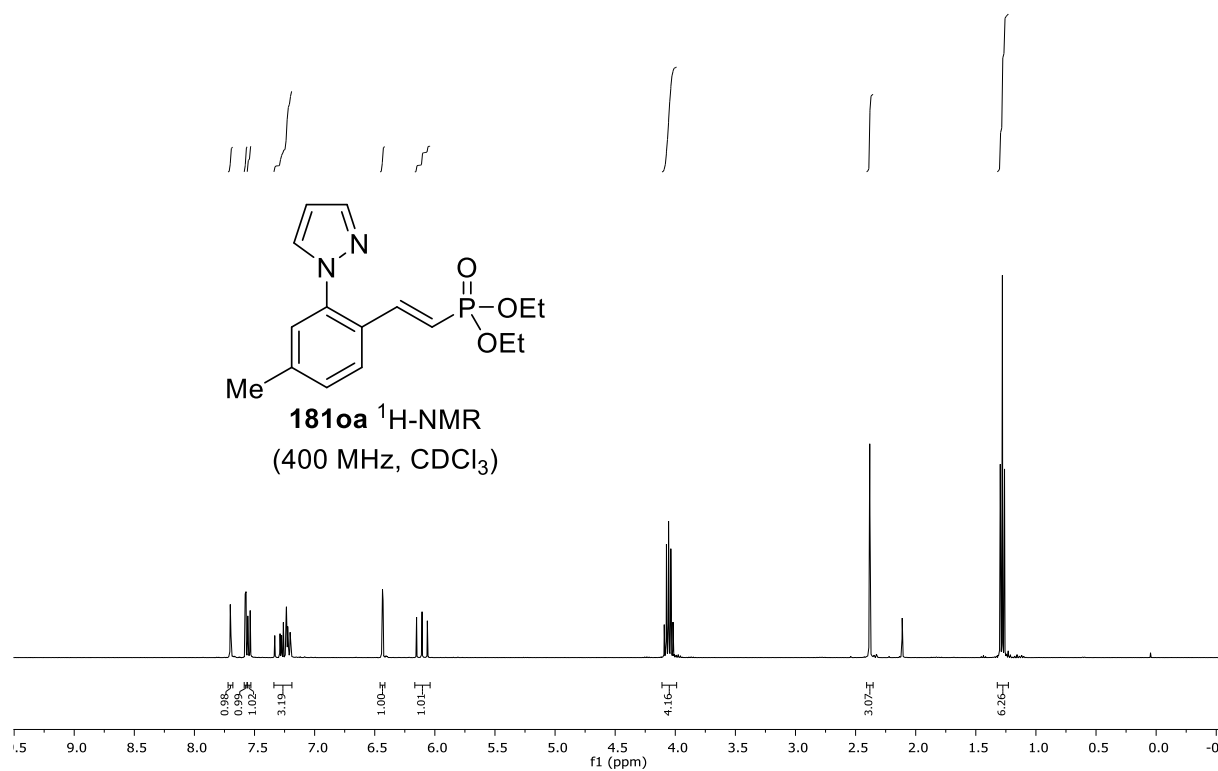
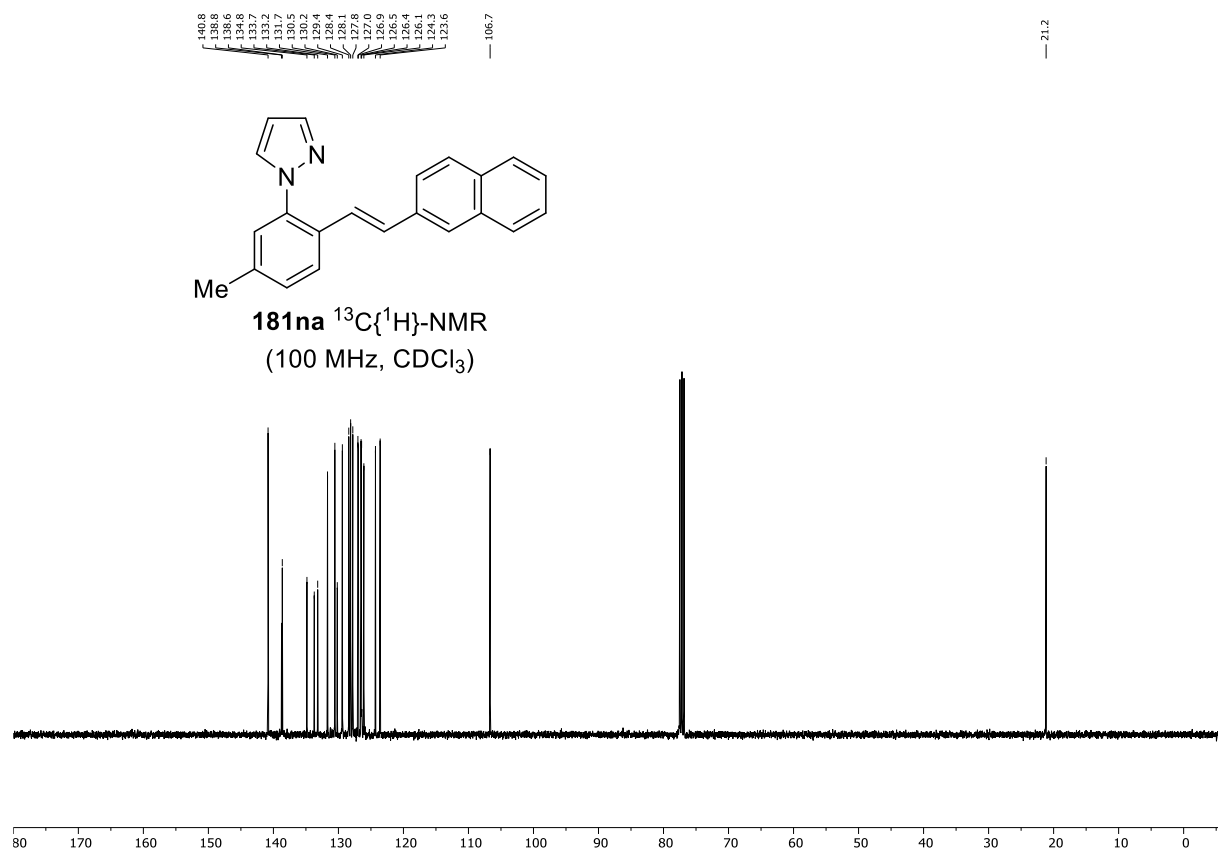
NMR SPECTRA



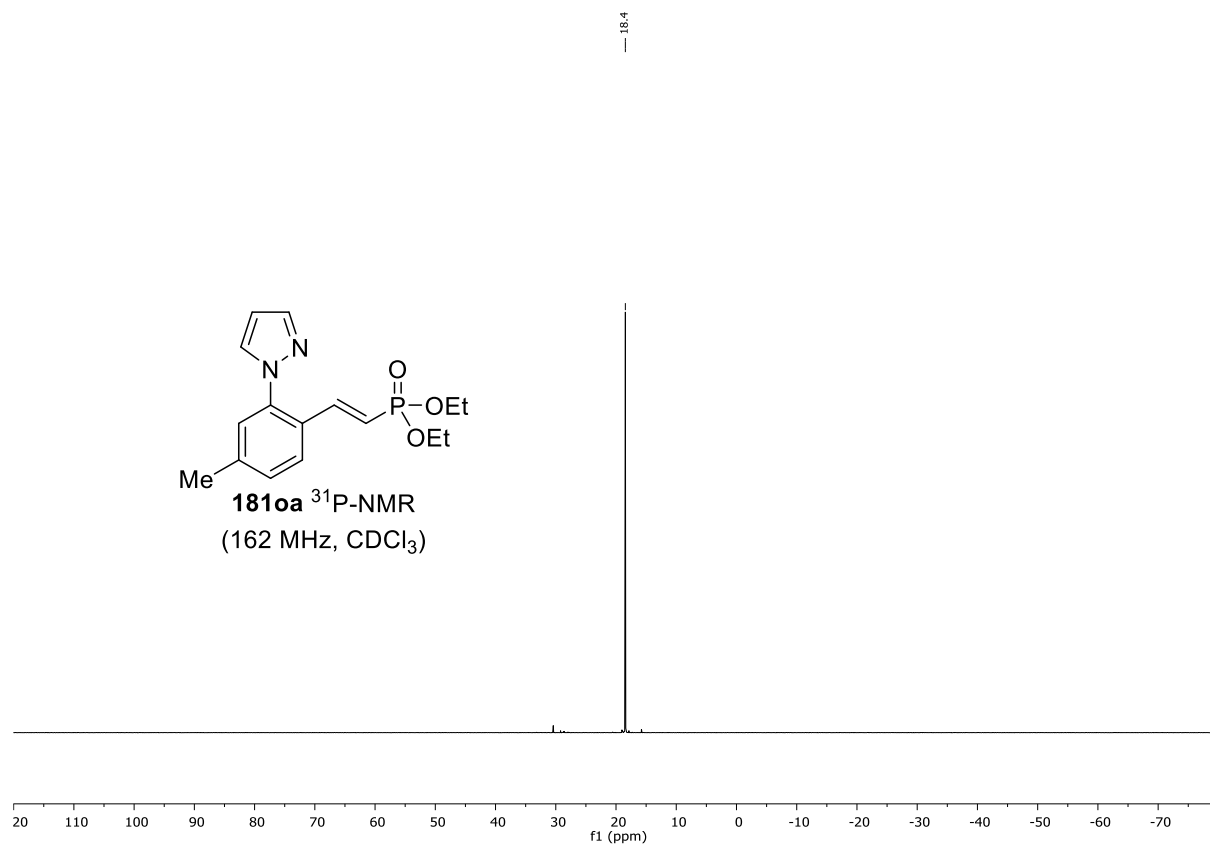
NMR SPECTRA



NMR SPECTRA



NMR SPECTRA



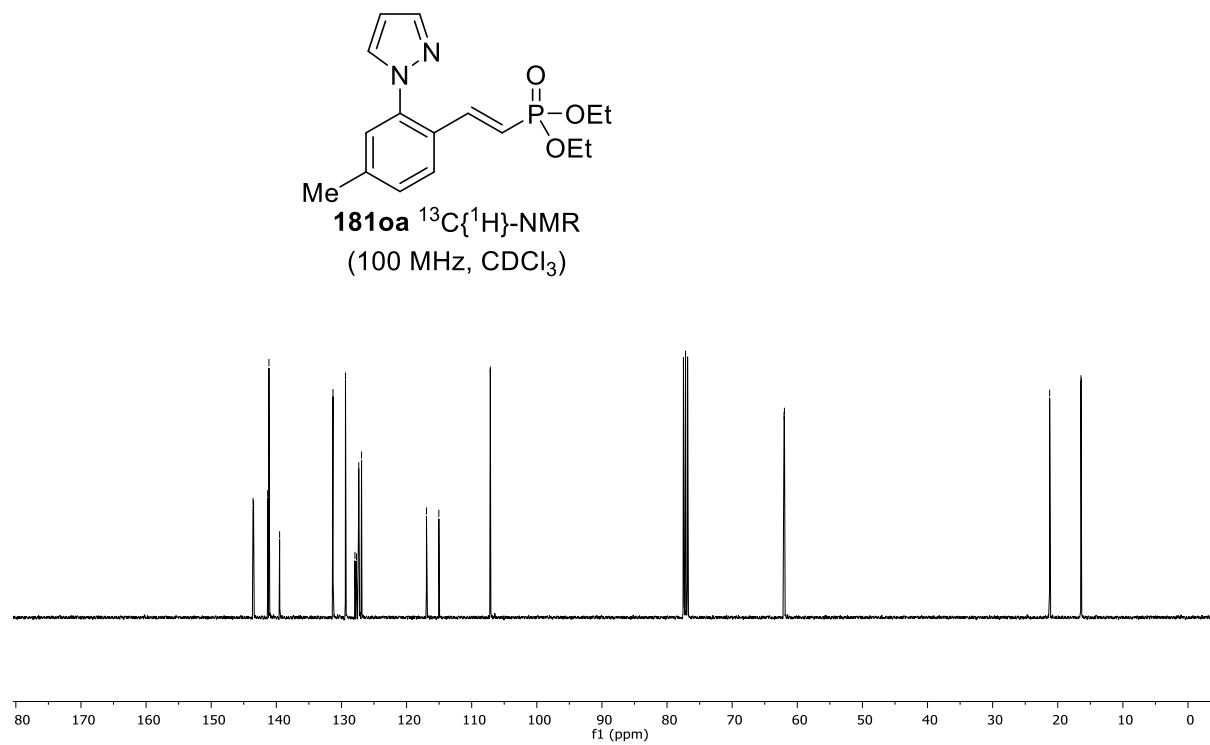
\swarrow 143.6
 \swarrow 143.5
 \swarrow 141.3
 \swarrow 141.1
 \swarrow 139.5
 \swarrow 131.3
 \swarrow 129.4
 \swarrow 127.9
 \swarrow 127.7
 \swarrow 127.3
 \swarrow 126.9

 \swarrow 116.9
 \swarrow 115.0

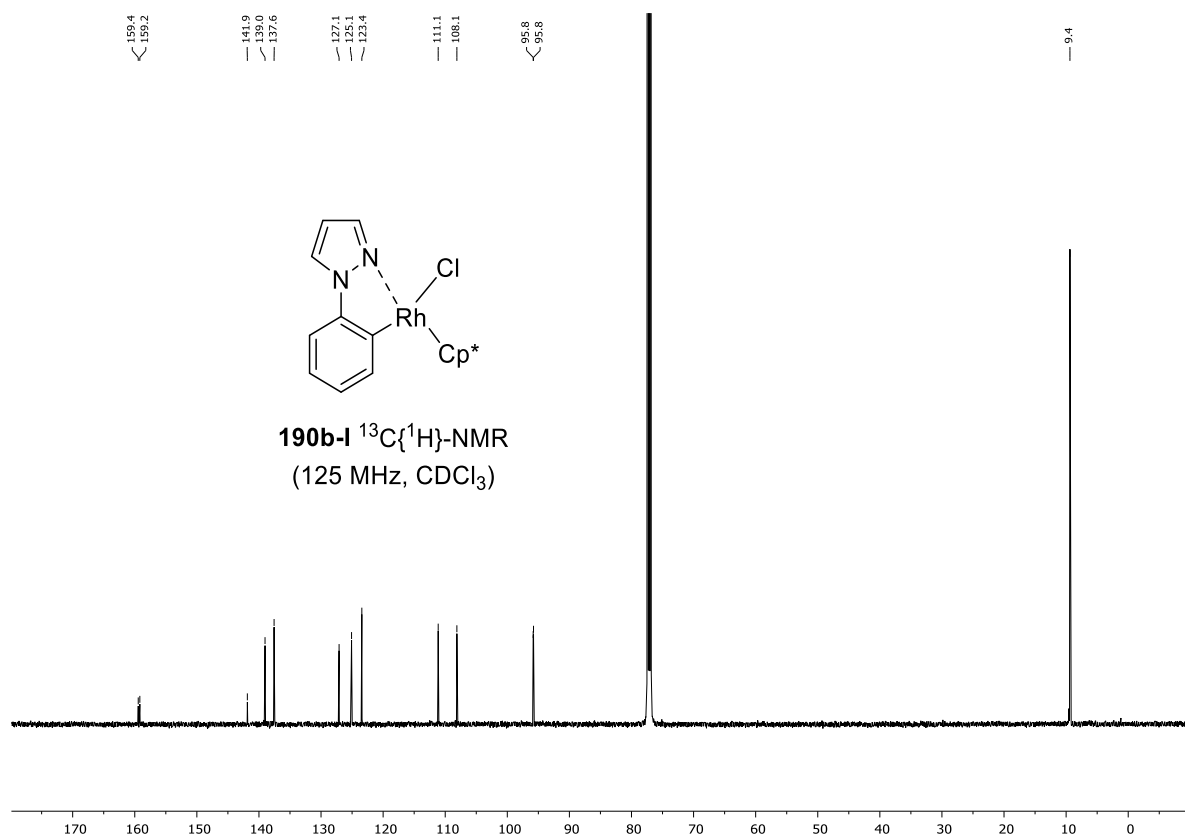
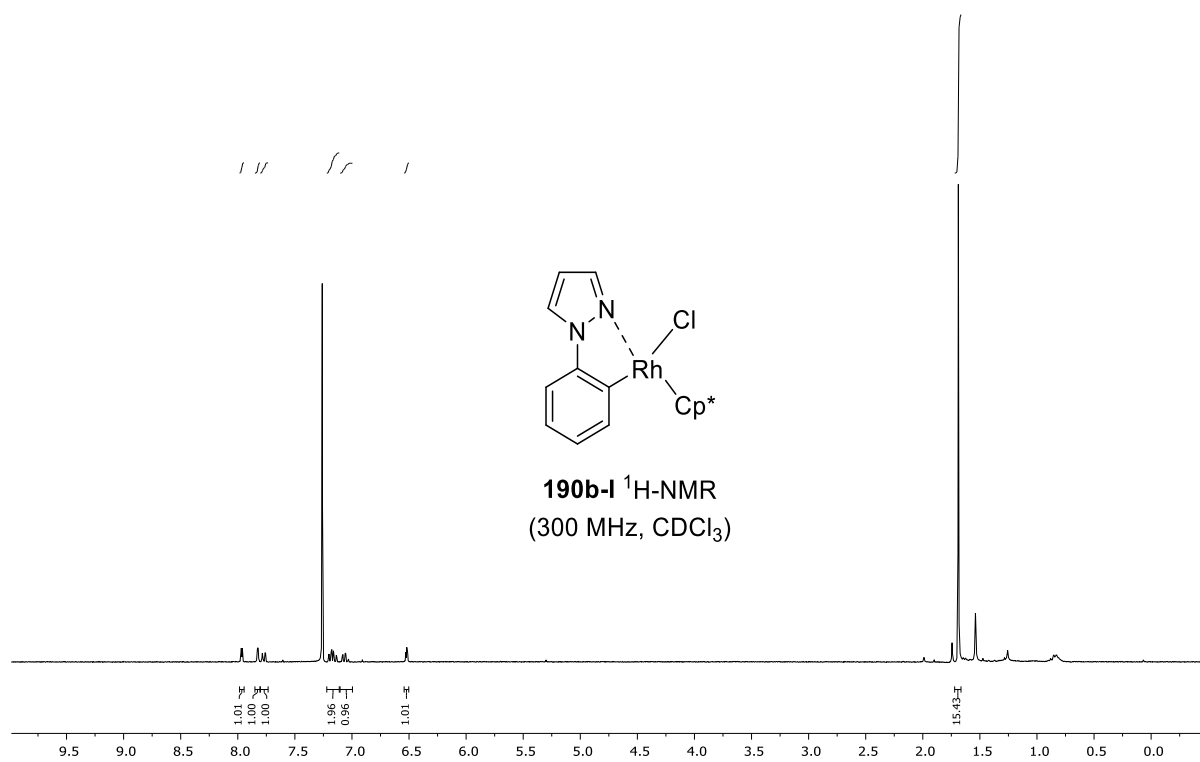
 \swarrow 107.1

 \swarrow 62.0
 \swarrow 62.0

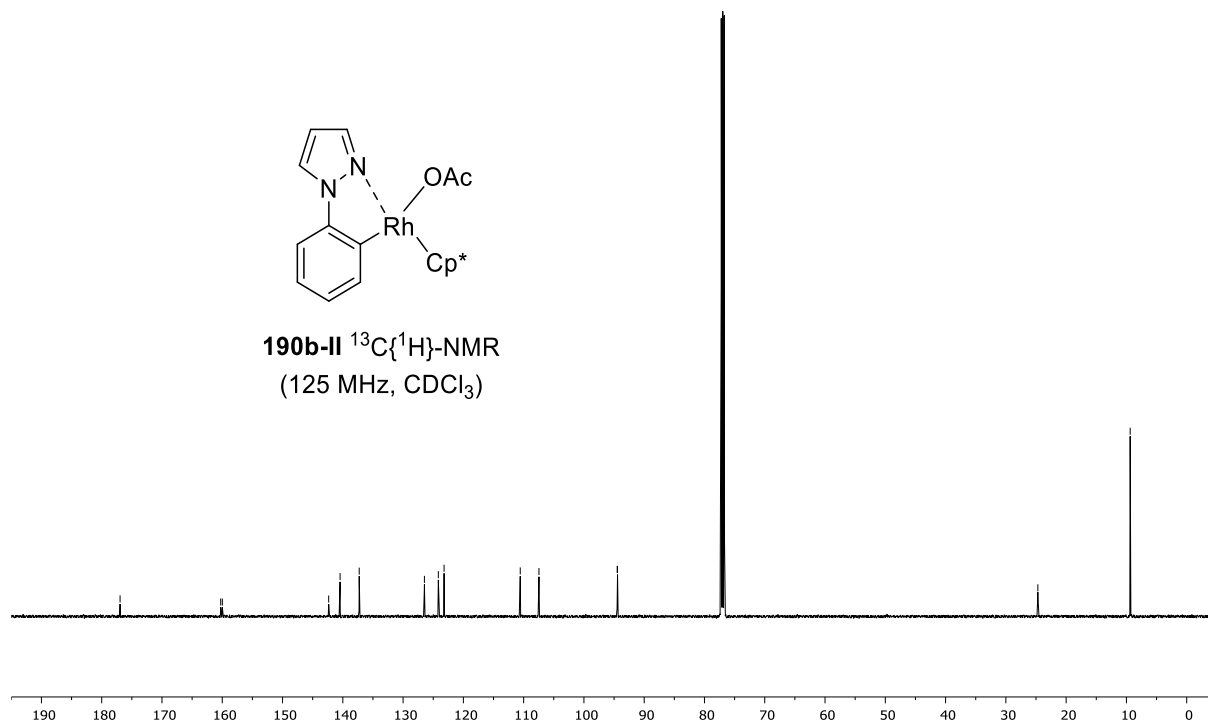
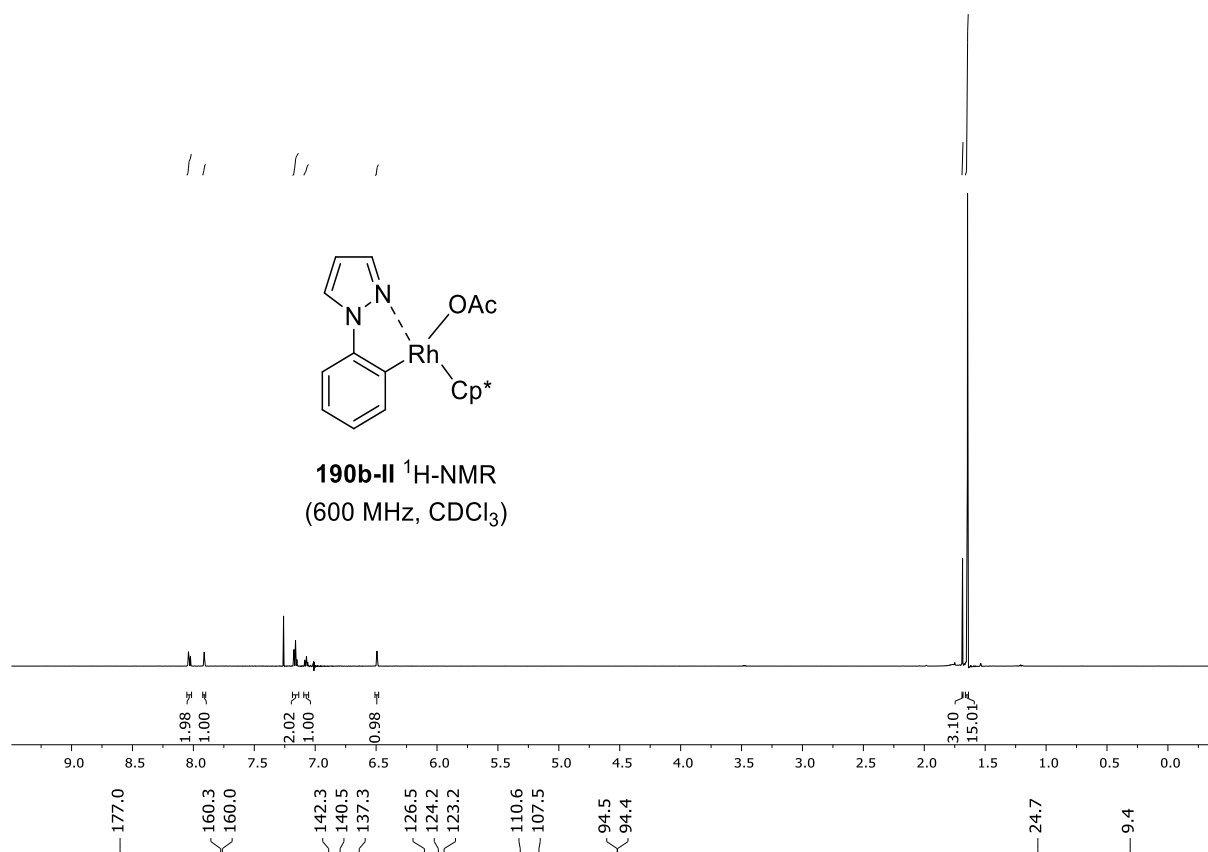
 \swarrow 21.2
 \swarrow 16.4
 \swarrow 16.4



NMR SPECTRA



NMR SPECTRA



NMR SPECTRA

